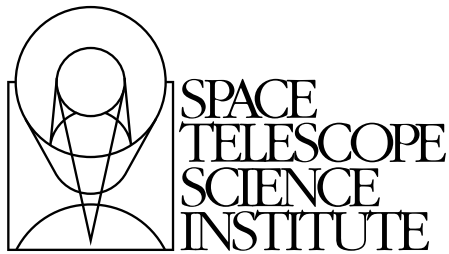

Version 8.0
October 2004

Space Telescope Imaging Spectrograph Instrument Handbook for Cycle 14



Space Telescope Science Institute
3700 San Martin Drive
Baltimore, Maryland 21218
help@stsci.edu

User Support

For prompt answers to any question, please contact the STScI Help Desk.

- **E-mail:** help@stsci.edu
- **Phone:** (410) 338-1082

World Wide Web

Information and other resources are available on the STIS WWW site:

<http://www.stsci.edu/hst/stis/>

Revision History

Version	Date	Editor
1.0	June 1996	Stefi Baum
2.0	June 1998	Nolan Walborn and Stefi Baum
3.0	June 1999	Kailash Sahu
4.0	June 2000	Claus Leitherer
4.1	July 2000	Claus Leitherer
5.0	June 2001	Claus Leitherer
5.1	July 2001	Claus Leitherer
6.0	October 2002	Charles Proffitt
7.0	October 2003	Jessica Kim Quijano and Bahram Mobasher
8.0	October 2004	Jesús Maíz-Apellániz and Jessica Kim Quijano

Authorship

This document is written and maintained by the Spectrographs Group in the Instruments Division of STScI. At the time of the writing of this manual the Group includes the following members, all of whom contributed directly to the writing of this Handbook: Tom Brown (honorary), Ivo Busko (honorary), James Davies, Rosa Díaz-Miller, Linda Dressel, Paul Goudfrooij, Phil Hodge (honorary), Jessica Kim Quijano, Jesús Maíz-Apellániz, Bahram Mobasher (honorary), Charles Proffitt, Kailash Sahu (honorary), David Stys (honorary), and Nolan Walborn.

Citation

In publications, refer to this document as:

Maíz-Apellániz, J. and Kim Quijano, J., et al. 2004, "STIS Instrument Handbook", Version 8.0, (Baltimore: STScI).

Send comments or corrections to:
Space Telescope Science Institute
3700 San Martin Drive
Baltimore, Maryland 21218
E-mail: help@stsci.edu



Acknowledgments

It is with pleasure that we thank the ST-ECF, in particular Michael Rosa and Jeremy Walsh, for their numerous contributions, and the STIS Instrument Definition Team at GSFC, in particular Bruce Woodgate (PI), Randy Kimble, Chuck Bowers, Ted Gull, and Mary Beth Kaiser, for ongoing technical interaction, for material provided in support of this Handbook. We also thank Don Lindler (Sigma Space Corporation) for his technical contributions and many illuminating discussions. We are particularly grateful to Susan Rose for cheerfully supporting the editing of this handbook.

Table of Contents

Acknowledgments	iii
------------------------------	-----

Part I: Introduction	1
-----------------------------------	---

Chapter 1: Introduction	3
--------------------------------------	---

1.1 Purpose	3
-------------------	---

1.1.1 Document Conventions	4
----------------------------------	---

1.1.2 Examples Used in this Handbook.....	4
---	---

1.2 Handbook Layout.....	5
--------------------------	---

1.3 Proposal Preparations and Observations with STIS.....	8
--	---

1.3.1 The Spectrographs Group at STScI	9
--	---

1.4 The Help Desk at STScI.....	9
---------------------------------	---

1.5 The STIS Web Pages and Support Information.....	10
--	----

1.6 Nonproprietary STIS Data.....	12
-----------------------------------	----

Chapter 2: Special Considerations for Cycle 14	13
---	----

2.1 STIS Unlikely to be Available During Cycle 14....	13
---	----

2.2 HST Two-Gyro Science Mode	14
-------------------------------------	----

2.3 New versions of STIS Exposure Time Calculators	15
---	----

Differences and improvements with respect to CGI ETCs.....	15
---	----

Significant changes since the Phase I version of the APT Spectroscopic ETC.....	16
--	----

2.4 Use of Available-but-unsupported Capabilities	17
--	----

2.5 Scheduling Efficiency and Visit Orbit Limits	18
2.6 MAMA Scheduling Policies.....	19
2.7 Prime and Parallel Observing: MAMA Bright Object Constraints	19
2.8 STIS Snapshot Policies	20

Chapter 3: Introduction to STIS..... 23

3.1 Instrument Capabilities	23
3.2 Instrument Design.....	24
3.2.1 Detectors	25
3.2.2 STIS Physical Configuration	26
3.3 Basic Instrument Operations.....	28
3.3.1 Typical STIS Observing Sequence.....	30
3.4 Designing STIS Observations.....	31
3.4.1 Identify Science Requirements and Define STIS Configuration.....	31
3.4.2 Determine Exposure Time and Check Feasibility.....	34
3.4.3 Identify Need for Non-Science Exposures and Constraints	35
3.4.4 Determine Total Orbit Request.....	36

Part II: User's Guide..... 37

Chapter 4: Spectroscopy..... 39

4.1 Overview	39
4.1.1 Throughputs.....	42
4.1.2 STIS vs. ACS Spectroscopy	43
4.1.3 Limiting Magnitudes.....	45
4.1.4 Saturation	46
4.1.5 MAMA Bright-Object Limits.....	46
4.1.6 Scanned Gratings: Prime and Secondary (Tilt) Positions.....	47
4.1.7 Cross-Over Regions	48
4.2 First-Order Long-Slit Spectroscopy	49
4.2.1 Gratings for First-Order Spectroscopy.....	49
4.2.2 Slits for First-Order Spectroscopy.....	50
4.2.3 STIS Pseudo-aperture Positions	52
4.2.4 Detailed First-Order Spectroscopic Information.....	56

4.3 Echelle Spectroscopy in the Ultraviolet	56
4.3.1 Echelle Gratings	57
4.3.2 Slits for Echelle Spectroscopy	58
4.3.3 Detailed Echelle Information.....	58
4.4 Objective-Prism Spectroscopy.....	58

Chapter 5: Imaging..... 63

5.1 Imaging Overview	63
5.1.1 STIS versus ACS Imaging.....	65
5.1.2 STIS vs. WFPC2 Imaging.....	69
5.1.3 Caveats for STIS Imaging.....	70
5.1.4 Throughputs and Limiting Magnitudes.....	71
5.1.5 Signal-To-Noise Ratios.....	74
5.1.6 Saturation	74
5.2 Optical CCD Imaging.....	74
5.2.1 Effect of the optical baffles on STIS CCD imaging	75
5.2.2 Unfiltered (Clear) CCD Imaging—50CCD	76
5.2.3 Optical Longpass—F28X50LP	76
5.2.4 [O III]—F28X50OIII	76
5.2.5 [O II]—F28X50OII	77
5.3 Ultraviolet Imaging with the MAMA Detectors.....	78
5.3.1 Bright-Object Limits	79
5.3.2 Optical Performance	79
5.3.3 Unfiltered (Clear) MAMA Imaging—25MAMA	80
5.3.4 Longpass-Filtered MAMA Imaging— F25SRF2 and F25QTZ.....	81
5.3.5 MAMA Narrow-band-Filtered Imaging	82
5.4 Neutral-Density Filters	86

Chapter 6: Exposure Time Calculations..... 87

6.1 Overview	87
6.1.1 The STIS Exposure Time Calculators	87
6.2 Determining Count Rates from Sensitivities.....	88
6.2.1 Spectroscopy	89
6.2.2 Imaging	92
6.3 Throughput and Sensitivity	93

6.4 Computing Exposure Times	94
6.4.1 Calculating Exposure Times for a Given Signal-to-Noise	95
6.5 Detector and Sky Backgrounds	96
6.5.1 Detector Backgrounds	97
6.5.2 Sky Background.....	97
6.6 Tabular Sky Backgrounds	103
6.7 Extinction Correction	105
6.8 Exposure Time Examples	106
6.8.1 Spectroscopy of Diffuse Source (M86)	106
6.8.2 Spectroscopy of Solar-Analog Star P041-C	107
6.8.3 Extended Source with Flux in cgs units (NGC 6543): Imaging and Spectroscopy	109
6.8.4 Echelle Spectroscopy of a Bright Star with Large Extinction (Sk -69° 215).....	111
6.8.5 Imaging a Faint Stellar Source	112
6.8.6 Time-Tag Observations of a Flare Star (AU Mic)	113
Chapter 7: Feasibility and Detector Performance	115
7.1 The CCD	115
7.1.1 Detector Properties.....	115
7.1.2 Effects of the Change to STIS Side-2 Electronics on CCD Performance	116
7.1.3 CCD Spectral Response.....	117
7.1.4 CCD Sensitivity.....	117
7.1.5 CCD Long-Wavelength Fringing.....	120
7.1.6 Fringing due to the Order Sorter Filters	122
7.1.7 Optical Performance	124
7.1.8 Readout Format.....	127
7.1.9 Analog-to-Digital Conversion: Selecting the CCDGAIN.....	127
7.2 CCD Operation and Feasibility Considerations.....	129
7.2.1 CCD Saturation.....	129
7.2.2 CCD Shutter Effects	130
7.2.3 Cosmic Rays.....	130
7.2.4 Hot Pixels.....	131
7.2.5 CCD Bias Subtraction and Amplifier Non-Linearity.....	133

7.2.6 Charge Transfer Efficiency	134
7.2.7 Mitigation of CTE Loss for Long-slit Spectroscopy.....	136
7.2.8 UV Light and the STIS CCD	139
7.3 The MAMA Detectors.....	140
7.3.1 MAMA Properties.....	140
7.3.2 MAMA Spectral Response.....	142
7.3.3 MAMA Sensitivity.....	142
7.3.4 Optical Performance.....	144
7.4 MAMA Operation and Feasibility Considerations.....	147
7.4.1 MAMA Saturation—Overflowing the 16 Bit Buffer.....	147
7.4.2 MAMA Darks.....	147
7.4.3 MAMA Signal-to-Noise Ratio Limitations.....	151
7.4.4 MAMA Non-linearity.....	152
7.5 MAMA Spectral Offsetting.....	153
7.6 MAMA Bright-Object Limits.....	154
7.6.1 Overview.....	154
7.6.2 Observational Limits	154
7.6.3 How Do You Determine if You Violate a Bright Object Limit?.....	155
7.6.4 Policy and Observers' Responsibility in Phase I and Phase II.....	156
7.6.5 Policy on Observations That Fail Because they Exceed Bright-Object Limits	158
7.6.6 What To Do If Your Source is Too Bright for Your Chosen Configuration?.....	159
7.6.7 Bright-Object Protection for Solar System Observations	159
7.6.8 Jupiter and Saturn	161
Chapter 8: Target Acquisition.....	163
8.1 Introduction.....	163
8.1.1 Initial Pointing	164
8.1.2 Acquisitions.....	165
8.1.3 Peakups.....	165
8.1.4 Drift Rates.....	166
8.2 STIS Onboard CCD Target Acquisitions (ACQ).....	169
8.2.1 How it Works.....	169

8.2.2 Target-Location Algorithms.....	171
8.2.3 Selecting Target Acquisition Parameters.....	174
8.2.4 Specifying Acquisitions in Phase II.....	181
8.2.5 Solar-System Acquisitions.....	182
8.3 Onboard Target Acquisition	
Peakups (ACQ/PEAK)	183
8.3.1 Selecting Peakup Parameters	187
8.3.2 Specifying Acquisition Peakups in Phase II.....	189
8.4 Determining the PLATE-ID of HST	
Observations	189
8.5 Acquisition Examples	190
8.5.1 Point source Acquisition of an Isolated Object	190
8.5.2 Point Source Acquisition of Bright, Isolated Object with CCD Dispersed Light Peakup.....	191
8.5.3 Diffuse-Source Acquisition of a Spiral Galaxy	193
8.5.4 Point Source Acquisition in a Crowded Field.....	194
8.5.5 Point Source Acquisition of a QSO with Fuzz Behind the Fiduciary Bar	196
8.5.6 Point Source Acquisition of a Bright, Isolated Star Into the Wedge	198
8.6 STIS Post-Observation Target Acquisition	
Analysis	200
8.6.1 Paper Products—Coarse Centering	200
8.6.2 TAS—Fine Centering.....	200
8.6.3 Did the Acquisition Succeed?	200

Chapter 9: Overheads and Orbit-Time Determination

9.1 Overview	201
9.2 STIS Exposure Overheads	202
9.3 Orbit Use Determination Examples	205
9.3.1 Sample Orbit Calculation 1: Long-Slit Spectroscopy of the Galaxy M86	206
9.3.2 Sample Orbit Calculation 2: Low-Dispersion Spectroscopy of Solar-Analog Star P041-C	208
9.3.3 Sample Orbit Calculation 3: Imaging and Spectroscopy of the Cat’s Eye Planetary Nebula, NGC 6543	209
9.3.4 Sample Orbit Calculation 4: MAMA Echelle Spectroscopic Exposures in the CVZ.....	211
9.3.5 Sample Orbit Calculation 5: Faint CCD Imaging.....	213

Chapter 10: Summary and Checklist	215
10.1 Phase I Proposing	215
10.1.1 Phase I Orbit-Allocation Examples	217
10.2 Phase II—Scheduling Approved Observations	217

Part III: Supporting Material

Chapter 11: Data Taking	221
11.1 Basic Operating Modes	221
11.1.1 CCD ACCUM Mode	222
11.1.2 MAMA ACCUM Mode	226
11.1.3 MAMA TIME-TAG Mode	229
11.2 Exposure Sequences and Contemporaneous Calibrations	232
11.2.1 Auto-Wavecal	233
11.2.2 CR-SPLIT	235
11.2.3 Fringe Flat Fields	235
11.2.4 Repeat Exposures	239
11.3 Patterns and Dithering	239
11.3.1 STIS Imaging Patterns	240
11.3.2 STIS Spectroscopic Patterns	240
11.3.3 Generic Patterns	240
11.3.4 Combining Patterns	241
11.3.5 Dither Strategies	244
11.4 Fixing Orientation on the Sky	248

Chapter 12: Special Uses of STIS	253
12.1 Slitless First-Order Spectroscopy	253
12.2 Long-Slit Echelle Spectroscopy	256
12.3 Time-Resolved Observations	257
12.4 Observing Too-Bright Objects with STIS	259
12.5 High Signal-to-Noise Ratio Observations	261
12.5.1 Dithering	262
12.5.2 FP-SPLIT Slits for Echelle Observations	262
12.6 Improving the Sampling of the Line-Spread Function	265

12.7 Considerations for Observing Planetary Targets.....	266
12.7.1 Long-Slit Spectroscopy.....	266
12.8 Parallel Observing with STIS	267
12.8.1 Using STIS in Parallel with Other Instruments.....	268
12.8.2 The STIS Archival Pure Parallel Program	268
12.9 Coronagraphic Spectroscopy	270
12.10 Coronagraphic Imaging—50CORON	273

Chapter 13: Spectroscopic

Reference Material	279
13.1 Introduction.....	279
13.2 Using the Information in this Chapter	280
13.2.1 Wavelength Ranges	280
13.2.2 Grating Sensitivities and Throughputs.....	281
13.2.3 Signal-To-Noise Plots	282
13.2.4 Plate Scales.....	284
13.2.5 Apertures	285
13.2.6 Fiducials on Bars	285
13.2.7 Spatial Profiles.....	286
13.2.8 Line-Spread Functions (Instrumental Profiles)	286
13.3 Gratings.....	289
13.4 Apertures	337
13.5 Spatial Profiles.....	362
13.6 Line-Spread Functions	368
13.7 Spectral Purity, Order Confusion, and Peculiarities	373
13.7.1 Recommendations for stellar observations with narrow slits.....	374
13.7.2 Order Overlap and Scattered Light for Echelle Gratings.....	375
13.7.3 Spectroscopic Mode Peculiarities.....	378
13.7.4 Railroad Tracks.....	382
13.8 MAMA Spectroscopic Bright-Object Limits.....	383

Chapter 14: Imaging Reference

Material	387
14.1 Introduction.....	387
14.2 Using the Information in this Chapter	388
14.2.1 Sensitivity Units and Conversions	388
14.2.2 Signal-To-Noise	390
14.2.3 Point Spread Functions	391
14.3 CCD.....	394
14.4 NUV MAMA	408
14.5 FUV MAMA	435
14.6 Image-Mode Geometric Distortion.....	457
14.7 Spatial Dependence of the STIS PSF	458
14.8 MAMA Imaging Bright Object Limits	461

Part IV: Calibration..... 463

Chapter 15: Overview of Pipeline

Calibration	465
15.1 Pipeline Processing Overview	465
15.2 How Phase II parameter choices affect calibration.....	471
15.3 More Detailed Information	472

Chapter 16: Accuracies

16.1 Summary of Accuracies	473
16.1.1 Flats	476

Chapter 17: Calibration Status and Plans.....

17.1 Introduction.....	477
17.2 Ground Testing and Calibration	478
17.3 SMOV2 Testing and Calibration.....	478
17.4 Cycle 7 Calibration	480
17.4.1 Calibration Priorities.....	480
17.4.2 Calibration Status	482
17.5 Cycle 8 Calibration	482

17.6 Cycle 9 Calibration 483
17.7 Cycle 10 Calibration 484
17.8 Cycle 11 Calibration 484
17.9 Cycle 12 Calibration 485
17.10 Cycle 13 Calibration 486

Appendix A: Available-But-Unsupported Spectroscopic Capabilities 489

A.1 Introduction 489
A.2 Full Aperture Complement 490
A.3 Central Wavelength Settings 494

Glossary 495

Index 499



PART I:

Introduction

The chapters in this part explain how to use this Handbook, where to go for help, and special considerations for using STIS in Cycle 14.

Introduction

In this chapter. . .

1.1 Purpose / 3
1.2 Handbook Layout / 5
1.3 Proposal Preparations and Observations with STIS / 8
1.4 The Help Desk at STScI / 9
1.5 The STIS Web Pages and Support Information / 10
1.6 Nonproprietary STIS Data / 12

STIS is a versatile imaging spectrograph. The instrument provides spatially resolved spectroscopy from 1150 to 10,300 Å at low to medium spectral resolution, echelle spectroscopy in the ultraviolet, solar-blind imaging in the ultraviolet, time tagging of photons in the ultraviolet for high time resolution, and direct and coronagraphic imaging in the optical. This Handbook provides instrument-specific information you need to propose for STIS observations (Phase I), design accepted programs (Phase II), and understand STIS in detail.

This chapter explains the layout of the Handbook and describes how to use the [Help Desk](#) at STScI and the STScI [STIS World Wide Web \(WWW\) site](#) to get help and further information. Instrument and operating updates will be posted on the [STIS web site](#).

1.1 Purpose

The *STIS Instrument Handbook* is the basic reference manual for the Space Telescope Imaging Spectrograph; it describes the instrument's properties, performance, operations, and calibration. The Handbook is maintained by the Spectrographs Group at STScI. Wherever possible, the

most recent operational data have been incorporated into this revised edition.

We have designed the document to serve three purposes:

- To provide instrument-specific information for preparing Phase I STIS observing proposals.
- To provide instrument-specific information to support the design of Phase II proposals for accepted STIS programs.
- To provide technical information about the performance and operation of the instrument that can help in the understanding of problems and in the interpretation of data acquired with STIS.

This Handbook is not meant to serve as a manual for the reduction and analysis of data taken with STIS. The [HST Data Handbook](#) (available from the STScI [Help Desk](#) or the [STIS World Wide Web site](#)) describes how to work with STIS data.

1.1.1 Document Conventions

This document follows the usual STScI convention in which terms, words, and phrases which are to be entered by the user in a literal way on an HST proposal are shown in a typewriter font (e.g., `STIS/CCD`, `SHADOW`). Names of software packages or commands (e.g., **calstis**) are given in boldface.

Wavelengths in this Handbook and in STIS data products are always measured in vacuum conditions. Wavelength units in this Handbook are in Angstroms (Å).

1.1.2 Examples Used in this Handbook

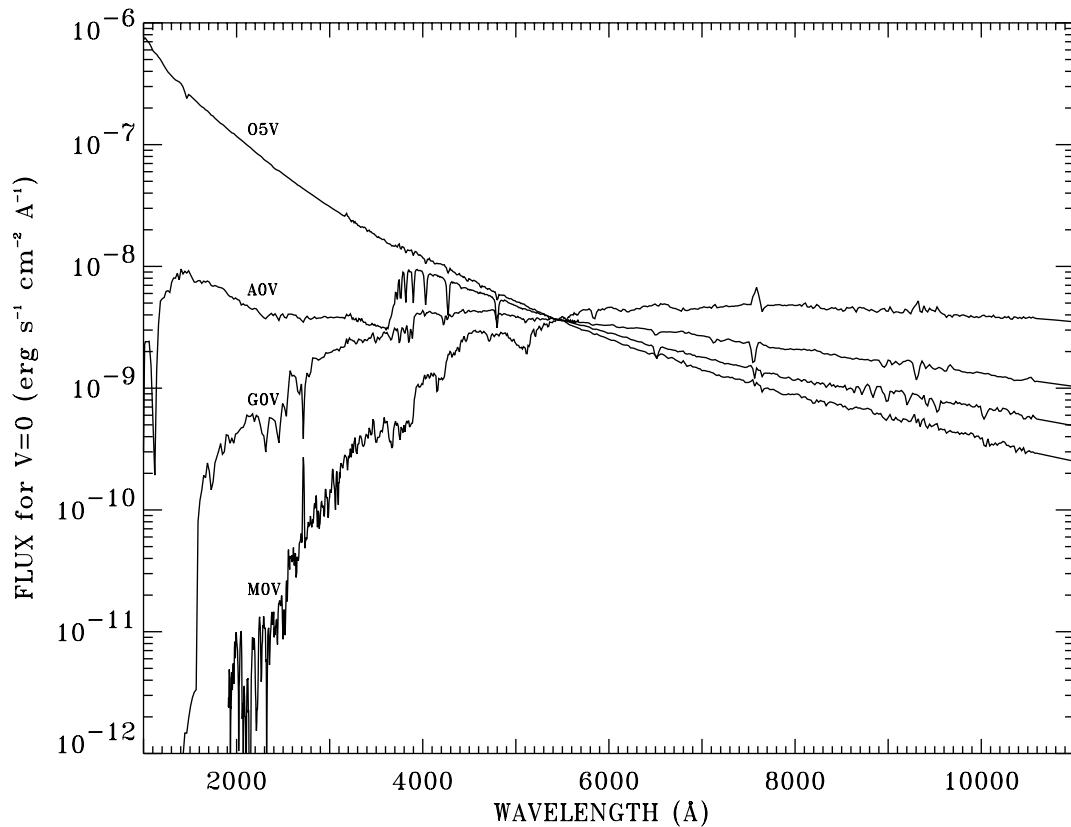
The Handbook uses six observational examples to illustrate various scenarios such as calculation of exposure times, estimation of overheads, etc. throughout the text. The examples are:

- Long-slit optical spectroscopy of the nearby galaxy NGC 4406 (M86).
- Long-slit optical and ultraviolet spectroscopy and optical imaging of NGC 6543, the Cat's Eye planetary nebula.
- First-order low-resolution spectroscopy covering STIS's full wavelength range from 1,150 Å in the UV to 10,300 Å in the near-IR of the continuous viewing zone (CVZ) solar analog star P041-C.
- Echelle spectroscopy of the O-type star Sk-69°215 in the Large Magellanic Cloud (LMC), a target in the CVZ.

- Deep optical imaging of a random field.
- Time-resolved ultraviolet spectroscopy of the flare star AU Mic.

In addition, we use stellar spectra throughout the Handbook to illustrate signal-to-noise ratio calculations and derive limiting magnitudes. Figure 1.1 shows the normalized spectra of O, A, G, and M stars from an observed catalog of stars (for details, see Buser, 1978, *A&A*, 62, 411) which are used in the Handbook examples.

Figure 1.1: Spectra of O5V, A0V, G0V, and M0V stars normalized at 5550 Å used throughout the Handbook. Note the dramatic differences in the UV properties.



1.2 Handbook Layout

To guide you through STIS's capabilities and help optimize your scientific use of the instrument we have divided this Handbook into four parts:

- Part 1 - Introduction
- Part 2 - User's Guide

- Part 3 - Supporting Material
- Part 4 - Calibration

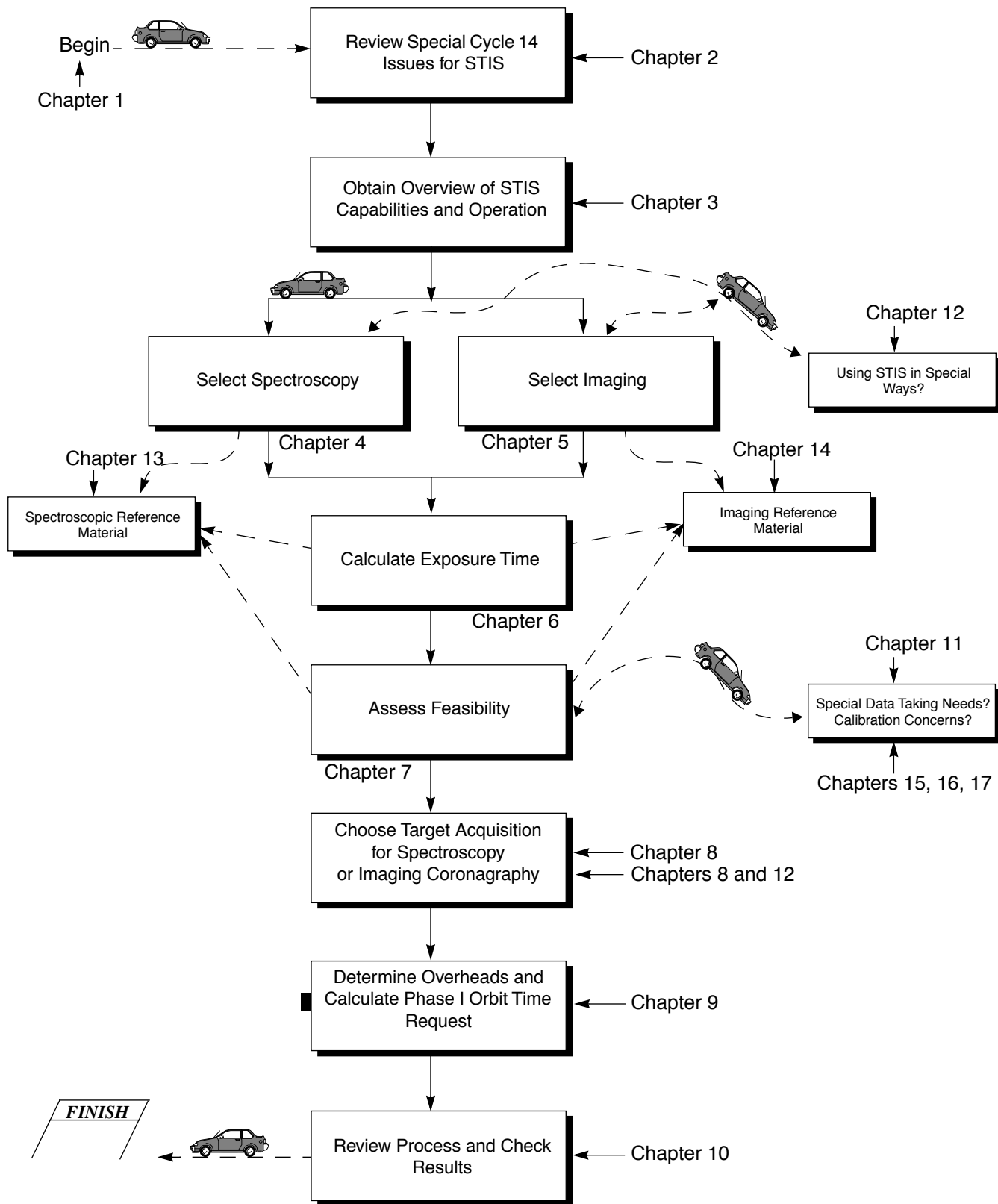
Figure 1.2 provides a road map to the use of this Handbook.

The Supporting Material and Calibration sections contain technical information which supports the material found in the User's Guide; readers are referred to the information at appropriate points in the User's Guide.

The chapters in this Handbook are as follows:

- Part 1 - Introduction
 - Chapter 1, *Introduction*, includes information about getting help and where to find additional information about STIS.
 - Chapter 2, *Special Considerations for Cycle 14*, describes special policy considerations for using STIS during Cycle 14.
- Part 2 - User's Guide
 - Chapter 3, *Introduction to STIS*, provides an overview of STIS's full capabilities. Discussion is provided to help guide you through the technical details you need to consider in choosing the optimum STIS configuration and in determining the number of orbits to request.
 - Chapter 4, *Spectroscopy*, provides a detailed, grating-by-grating description of STIS's spectroscopic capabilities, including spectral resolutions, throughputs, and descriptions of the slits and apertures.
 - Chapter 5, *Imaging*, provides a detailed, filter-by-filter description of STIS's imaging capabilities. A comparison is provided between STIS, ACS, and WFPC2 capabilities.
 - Chapter 6, *Exposure Time Calculations*, describes how to perform signal-to-noise and exposure time calculations, either by using pencil and paper, or by using the software tools provided on the STIS World Wide Web site.
 - Chapter 7, *Feasibility and Detector Performance*, provides a description of the three detectors and their physical characteristics, capabilities, and limitations, including saturation, linearity, and bright-object limits.
 - Chapter 8, *Target Acquisition*, helps you select the optimum target acquisition sequence needed to place the target in the desired science aperture.
 - Chapter 9, *Overheads and Orbit-Time Determination*, provides information needed to convert a series of planned science exposures to an estimated number of orbits, including spacecraft and STIS overheads. This chapter applies principally to the planning of Phase I proposals.

Figure 1.2: Handbook Roadmap



- Chapter 10, *Summary and Checklist*, presents a summary and a checklist you should use to assure that there are no major omissions in your Phase I and Phase II proposals.
- Part 3 - Supporting Material
 - Chapter 11 describes data-taking with STIS, including the instrument operating modes (ACCUM, TIME-TAG), the use of subarrays and binning, and the various types of “associated” observations and contemporaneous calibrations (WAVECALs, CCDFLATS, CR-SPLIT, PATTERNS). This chapter also discusses dithering and how to orient the long slits.
 - Chapter 12, *Special Uses of STIS*, provides information on special science uses of STIS, including slitless spectroscopy, long-slit echelle spectroscopy, time-resolved spectroscopy and imaging, observations of very bright targets, techniques for obtaining higher signal-to-noise and spectral sampling, observations of planetary objects, parallel observing, and coronagraphic spectroscopy and imaging.
 - Chapter 13, *Spectroscopic Reference Material*, contains the detailed plots of sensitivities, line-spread functions, aperture throughputs, and the tables of bright-object limits referred to in Chapter 4.
 - Chapter 14, *Imaging Reference Material*, contains the detailed plots of sensitivities and tables of bright-object limits referred to in Chapter 5.
- Part 4 - Calibration
 - Chapter 15, *Overview of Pipeline Calibration*, briefly describes the processing of STIS data by the STScI pipeline and the products that are sent to observers.
 - Chapter 16, *Accuracies*, summarizes the accuracies for STIS data calibrated by the STScI pipeline.
 - Chapter 17, *Calibration Status and Plans*, provides an overview of the current state of STIS calibration and development plans for the immediate future.

1.3 Proposal Preparations and Observations with STIS

Use the STIS Instrument Handbook together with the [Cycle 14 Call for Proposals \(CP\)](#) and [HST Primer](#) when assembling your STIS Phase I proposal. The CP provides policy and instructions for proposing. The HST

Primer provides a basic introduction to the technical aspects of HST and its instruments, and explains how to calculate the appropriate number of orbits for your Phase I observing time requests. The *STIS Instrument Handbook* contains technical information about STIS describing its expected performance and presenting suggestions for use. Chapter 2 in the Handbook describes special considerations for Cycle 14.

If your Phase I proposal is accepted, you will be asked to submit a Phase II proposal in which you specify the exact configurations, exposure times, and sequences of observations that STIS and the telescope should perform. To assemble your Phase II proposal, use the *STIS Instrument Handbook* in conjunction with the *Phase II Proposal Instructions*. These instructions describe the exact rules and syntax that apply to the planning and scheduling of STIS observations and provide relevant observatory information.¹

1.3.1 The Spectrographs Group at STScI

STScI has a team of Instrument Scientists, Scientific Programmers, and Data Analysts who support the development, operation, and calibration of STIS. The team is also responsible for supporting STIS users. Furthermore, the Spectrographs Branch provides archival support for the heritage instruments FOS and GHRS.

1.4 The Help Desk at STScI

STScI has a Help Desk whose staff quickly provide answers on any HST-related topic, including questions regarding STIS and the proposal process. The Help Desk staff have access to all of the resources available at the Institute, and they maintain a database of answers so that frequently asked questions can be immediately answered. (FAQs are also posted on the STIS web site.) The Help Desk staff also provide hard copies of STScI documentation, including *Instrument Science Reports* and *Instrument Handbooks*. Electronic copies of documents are available via the web. Questions sent to the Help Desk are answered within two working days. Usually, the Help Desk staff will reply with the answer to a question, but occasionally they will need more time to investigate the answer. In these cases, they will reply with an estimate of the time needed to prepare a full answer.

We ask that you please send *all* initial inquiries to the Help Desk. If your question requires a STIS Instrument Scientist to answer it, the Help Desk

1. You should also check the [STIS web site](#) for any updates relevant to the current proposal cycle

staff will put one in contact with you. By sending your request to the Help Desk, you are guaranteed that someone will provide you with a timely response.



Note: *File attachments to email messages should not be sent directly to the Help Desk. Instead, please make a note in your message, and the Help Desk staff will let you know how to deliver the attachments to us.*

To contact the Help Desk at STScI:

- **E-mail:** help@stsci.edu
- **Phone:** 1-410-338-1082
Toll-free in the U.S.: 1-800-544-8125

The Space Telescope European Coordinating Facility (ST-ECF) also maintains a Help Desk. European users should generally contact the ST-ECF for help; all other users should contact STScI. To contact the ST-ECF Help Desk:

- **E-mail:** stdesk@eso.org

As always, if you need help, just send E-mail to help@stsci.edu.

1.5 The STIS Web Pages and Support Information

The Spectrographs Branch at STScI maintains World Wide Web pages (Figure 1.3 on page 12) as part of STScI's web service. The URL for the top level STScI STIS web site is:

<http://www.stsci.edu/hst/stis>

The STIS web pages include up-to-date information about STIS operations and performance. Links to this information are organized into categories and sub-categories which are listed in a menu on the left hand side of all STIS group web pages. In addition to these main categories, a “shortcuts” list of links to frequently used resources is displayed on the right hand side of most STIS web pages. You can also search for specific information, as all STIS documentation is indexed on STIS-specific keywords.

The categories are:


- ***Instrument Design:*** A high-level summary of the basic design and operation of the Space Telescope Imaging Spectrograph (STIS), including summary information on the [detectors](#), [gratings](#), [apertures](#), and [filters](#) available for use.
- ***Performance:*** More detailed information on actual on-orbit performance of the STIS. Sub-categories are [image quality](#), [sensitivity](#), [spectral resolution](#), [throughput](#), [background](#), [accuracy](#), [monitoring](#), and [anomalies](#).
- ***Observing Strategy:*** Discussions of [target acquisitions](#), [pushing the limits](#), and other aspects of the design of [imaging](#) and [spectroscopic](#) observations with STIS.
- ***Proposing:*** Things you need to know in order to successfully construct and submit [Phase I](#) and [Phase II](#) proposals for STIS observations, and how to monitor the status of your observing program.
- ***Data Analysis:*** Resources describing STIS data characteristics and analysis, including the [HST Data Handbook](#).
- ***Software Tools:*** Software tools that can be retrieved (e.g., an IRAF script for creating daily dark reference files) or run directly over the network (e.g., the [Exposure Time Calculators](#) and the [Target Acquisition Simulator](#)).
- ***Document Archive:*** Electronic versions of the Instrument and Data Handbooks as well as detailed technical information concerning the development, performance, testing, operation, and calibration of the STIS as documented in a series of [STIS Instrument Science Reports \(ISRs\)](#) and [STSci Analysis Newsletters \(STANs\)](#). These reports can be downloaded directly from the WWW.

Figure 1.3: STIS Web Page

The screenshot shows the STIS web page with a navigation bar at the top containing links for Astronomy Resources, Data Archives, HST (selected), JWST, Partners, and The Institute. The main header is 'SPACE TELESCOPE IMAGING SPECTROGRAPH' with a search, help, and FAQ menu. The left sidebar contains a table of contents with categories like Instrument Design, Performance, Observing Strategy, Proposing, Data Analysis, Software Tools, and Document Archive. The main content area features a 'STIS Post-SM3B Report' with a detailed text block about the instrument's performance and a 'STIS Shortcuts' box with links to various resources. Below the report is a 'New in the Last 45 Days' section with a link to an ISR document. A 'Program Status' box includes a 'Prop ID' input field and a 'Go' button. The footer contains 'Copyright Notice' and 'Printable Page' links.

1.6 Nonproprietary STIS Data

There is a large amount of existing, nonproprietary STIS data available for retrieval from the HST Data Archive. They include observations obtained in the Second Servicing Mission Early Release programs (EROs—see *Ap.J. Letters*, Vol. 492, No. 2, 1998), the [STIS Archival Pure Parallel Program](#) (Section 12.8.2), the ongoing calibration programs (see Chapter 17), data taken in connection with the Hubble Deep Fields ([North](#), [South](#), and [Ultra Deep Fields](#)), and early GTO and GO observations that are no longer proprietary. You can use either the [HST Archive web interface](#) or [StarView](#) to search for such data directly. Any such data may be freely acquired, as described in the *HST Data Handbook*, for technical or scientific use. Examples of nonproprietary STIS science data are shown as illustrative examples interspersed in this Handbook.



CHAPTER 2:

Special Considerations for Cycle 14

In this chapter. . .

- | |
|---|
| 2.1 STIS Unlikely to be Available During Cycle 14 / 13 |
| 2.2 HST Two-Gyro Science Mode / 14 |
| 2.3 New versions of STIS Exposure Time Calculators / 15 |
| 2.4 Use of Available-but-unsupported Capabilities / 17 |
| 2.5 Scheduling Efficiency and Visit Orbit Limits / 18 |
| 2.6 MAMA Scheduling Policies / 19 |
| 2.7 Prime and Parallel Observing: MAMA Bright Object Constraints / 19 |
| 2.8 STIS Snapshot Policies / 20 |

2.1 STIS Unlikely to be Available During Cycle 14

On Tuesday, August 3, 2004, STIS suffered a failure of a 5-Volt power supply in its Side-2 electronics. This unit powers all the mechanisms in STIS, including the slit and grating wheels, the CCD shutter, etc. The STIS was idle at the time the failure occurred, so the light path was blocked to prevent potential exposure of the MAMA detectors to excessive light. Without the 5-volt power supply, these mechanisms cannot be moved. The Side-1 electronics suffered a short circuit in May 2001 and are currently not functioning. Since the two redundant sides are currently not working, STIS is unusable for the time being. While it is not impossible that further investigation will point out a way to restore STIS to a useful state, it is currently believed unlikely that STIS can be revived without physical

servicing. All other science instruments and the observatory itself continue to function normally.

Shortly before this Handbook was finalized, the HST Project at Goddard Space Flight Center assembled a Failure Review Board (FRB) to determine the cause of the STIS failure and to recommend further testing and potential recovery options. We expect this process to continue until after this Handbook will be issued. The HST user community will be kept informed of the status of STIS via the STIS web site, <http://www.stsci.edu/hst/stis>.

2.2 HST Two-Gyro Science Mode

HST normally uses three gyros out of the six installed onboard the spacecraft to provide accurate pointing information. All information about STIS performance in this Handbook has been written under the assumption that three gyros are being used during observations. However, over time these gyros eventually fail, leaving the spacecraft with less redundancy, and eventually with fewer than the number required for normal pointing. The HST Project at GSFC and STScI are developing a Two-Gyro Science (TGS) mode for use when fewer than three gyros are available. The TGS mode will use only two gyros to provide slew capability and spacecraft attitude control (guiding) of sufficient accuracy to continue obtaining high-quality science data.

There is a finite probability that HST will have to switch to TGS mode during Cycle 14. At the time this Handbook is being finalized, a (rough) estimate of the time when there is a 50% probability that HST will be down to two gyros is March 2006 (i.e., during the second half of Cycle 14).

The potential impacts of the Two-Gyro Science mode to STIS observations (e.g., exposure time calculations), along with all other relevant information regarding this mode, are provided in a separate Handbook.



See the Two-Gyro Handbook for detailed information.

Up-to-date information on the TGS mode can be found at the following URL: http://www.stsci.edu/hst/HST_overview/TwoGyroMode

2.3 New versions of STIS Exposure Time Calculators

As part of the Astronomer's Proposal Tool (APT) project, new Java-based versions of the exposure time calculators (ETCs) have been developed for all HST instruments. The switch to the APT ETCs was made in order to standardize the calculators for all the instruments, both to simplify development and support, and to provide a more consistent interface. Users will find that the new ETCs provide more realistic calculations and improved cross-instrument consistency.

The new STIS APT ETCs are available from our website at:

<http://www.stsci.edu/hst/stis/software/etc>

Differences and improvements with respect to CGI ETCs

Most results obtained from the latest versions of the APT ETCs should be close to those calculated by the older Common Gateway Interface (CGI) ETCs. There are, however, some notable differences and enhancements.

- The new sky background model of Giavalisco, Sahu, & Bohlin (2002), discussed in [WFC3 ISR 2002-12](#), has been implemented for all HST instruments.
- More realistic curves of encircled energy as a function of wavelength have been adopted. This is especially important for the CCD at IR wavelengths, where in-chip scattering puts a large fraction of the detected light in an extended halo.
- Calculations for extended and emission-line sources are significantly more accurate, and relax a number of approximations made in older versions.
- The full complement of supported apertures for each configuration is now included.
- Imaging pickup calculations for point-sources are now included in the Target Acquisition ETC.
- Bruzual synthetic spectra are offered in addition to Kurucz models as stellar templates.
- A selectable extraction radius for imaging of point-sources has been implemented.
- Rectangular (in addition to square) CCD binning is now available.
- Additional background specification options are offered.

- Total counts are now given for resolution elements rather than lambda-pixels.
- The extended source lambda-pixel is now 2 pixels high.
- Many additional parameters, particularly for backgrounds and noise, are listed in the APT output page. The time to saturation for CCD images is now also included.

Significant changes since the Phase I version of the APT Spectroscopic ETC

A preliminary version of the new Java-based APT ETCs was available for GO use during the Phase I of Cycle 13. However, a warning was also given indicating that this version had not been exhaustively tested. Indeed, subsequent testing did turn up a few issues with the Spectroscopic ETC which have since been corrected.

- ETC calculations for extended sources are now correct. Results with the earlier APT version may have underestimated extended source count rates by as much as a factor of three when observations are done using narrow slits.
- An error in the reported count rates for G230LB and G230MB modes has been fixed. Note that this error did not affect the reported S/N ratio.
- The results for the full output table are now given per resolution element, rather than per lambda-pixel.
- The extraction box heights used for calculating dark and sky counts for point-sources have been changed back to the smaller values (3 or 5 pixels) that they had in the old CGI ETC. The earlier APT release had changed the extraction box sizes to the larger values used in the **calstis** pipeline. However, when reducing observational data where the S/N is limited by the dark or sky counts, the user can easily exclude this extra background by recalibrating the data with a smaller-than-default extraction box. Adopting the smaller box sizes gives a more realistic estimate of the exposure time required to achieve a given S/N ratio in these cases. In the near future we plan to implement an option to allow the user to specify the extraction box size in the ETC.

2.4 Use of Available-but-unsupported Capabilities

We have established a set of core scientific capabilities of STIS which will be supported for Cycle 14 and are described in this Handbook. They provide an enormous range of scientific applications.

STIS has capabilities that are not described in this Handbook, and which are not supported for Cycle 14. They include additional slits and data-taking formats. These capabilities are “available-but-unsupported” upon consultation with a STIS Instrument Scientist. If you find that your science *cannot* be performed with the parameters described in this Handbook, you may wish to consider use of an unsupported capability. A full list of STIS’s available-but-unsupported capabilities are described in Appendix A.

Use of unsupported modes comes at a price, and they should be used only if the technical requirement and scientific justification are particularly compelling. Proposers should be aware of the following caveats regarding unsupported modes:

- Calibrations for unsupported capabilities will not be provided by STScI. Either users must determine that they can create calibration files from data in the HST Archive or they must obtain calibrations as part of their observations. The STScI pipeline will not calibrate data taken in unsupported modes but will deliver uncalibrated FITS files (or in some cases partially calibrated FITS files) to the observer and the HST Archive.
- STScI adopts a policy of shared risk with the observer for the use of unsupported capabilities. Requests to repeat failed observations taken with unsupported capabilities will not be honored if the failure is related to the use of the unsupported capability.
- User support from STScI for observation planning, as well as data reduction and analysis, with unsupported capabilities will be limited and provided at a low priority. Users taking data with unsupported capabilities should be prepared to shoulder the increased burden of the planning, calibration, reduction and analysis.

Cycle 14 Phase I proposals that include use of unsupported STIS capabilities must include the following:

1. Justification of why the science cannot be done with a supported configuration;
2. A request for any observing time needed to perform calibrations;
3. Justification for the added risk of using an unsupported mode in terms of the scientific payback;

4. Demonstration that the observers are able to bear the increased burden of calibration, reduction and analysis of their data.

During the Phase II proposal submission process, the Spectrographs Branch lead must also formally approve your use of an available-but-unsupported mode. This allows the Spectrographs Branch to evaluate your request and ensures that no problems associated with your request have come to light since the submission of your Phase I proposal. We require that you summarize the above four points in a brief email message requesting approval for use of an available-but-unsupported mode.

The increased burden of calibrating data taken using available-but-unsupported modes also makes the use of such data for archival research significantly more difficult. As a result, requests for use of available modes which do not adequately address the above four points, or which will result in only marginal improvements in the quality of the data obtained, may be denied by the Spectrographs Branch, even if the request was properly included in your Phase I proposal.

2.5 Scheduling Efficiency and Visit Orbit Limits

The availability of calendar time for scheduling and execution of long visits has become severely oversubscribed. To assure a greater degree of scheduling efficiency and avoid such heavy oversubscription, a 5-contiguous-orbit limit has been imposed for Cycle 8 and beyond for both CCD and MAMA visits. Observers with many (>5) orbits-per-target programs should take note of the following advice when splitting their observations into multiple visits:

1. Target acquisition sequences will need to be repeated at the start of each visit when using small entrance apertures with STIS (imaging and slitless spectroscopy do not normally require a target acquisition), and
2. there exists the potential for some image rotation between visits unless the SAME ORIENT AS <first visits #> special requirement is used. When SAME ORIENT AS is used, the accuracy is a few milliarcseconds.

HST pointing is generally very stable within a visit (~5 milliarcseconds rms). Small inaccuracies (~20 milliarcseconds rms) can occur between different visits, due to the way guide star acquisitions are handled at the start of a new visit. Although these offsets cannot be avoided, there are many situations where they are unimportant, or where their impact can be greatly reduced. For example, if the visit makes observations of several different targets by moving the telescope, and if there is no need for exact

offsets (few milliarcsecond accuracy) between the different targets, then the visit could simply be split into separate visits with one target per visit. In cases where a target acquisition is performed for slit spectroscopy, one should follow the same sequence for the target acquisition in the second visit as in the first.

Visits can be scheduled close in time by specifying the GROUP WITHIN visit requirement. Timing constraints of this type, however, should be used only if required by the science, since overconstraining visits affects the ability to schedule efficiently.

2.6 MAMA Scheduling Policies

Since the MAMA (see Section 3.2.1) control electronics were found in orbit to be subject to resets due to cosmic-ray impacts, the MAMAs are operated only during the contiguous orbits of each day which are free of the South Atlantic Anomaly (SAA). We therefore limit the duration of any single MAMA visit (i.e., a single continuous observation series) to five orbits. Additionally, to facilitate scheduling and maximize the orbits available for MAMA observations, we require observers to split their CCD and MAMA exposures into separate visits. Specifically, for STIS programs containing both CCD and MAMA scientific (not target-acquisition) exposures, in which there are more than 30 minutes of observing time using the CCD in a single visit (inclusive of overheads), and for which that visit requires more than a single orbit, you *must* split the exposures into visits that separate the CCD from the MAMA exposures. Hence, this policy allows multi-orbit mixed visits with 30 minutes or less of total CCD scientific time, or single-orbit mixed visits regardless of the CCD/MAMA ratio. For programs which *require* CCD and MAMA scientific exposures in the same visit (e.g., variability monitoring programs), exceptions can be made if you provide a well-justified explanation in the Special Requirements section of your Phase I proposal.

2.7 Prime and Parallel Observing: MAMA Bright Object Constraints

The STIS ultraviolet MAMA detectors are subject to damage at high illumination rates, as explained in greater detail in Section 7.6. To protect the instrument, we have established limits on the maximum count rate at which the detectors may be illuminated. These count-rate limits translate into a set of configuration dependent bright-object screening magnitudes.

The spectroscopic bright-object screening magnitudes are summarized in Table 13.44, and the imaging counterparts in Table 14.39.

STScI will perform screening of all MAMA exposures prior to scheduling. Targets not established as safe for the configuration in which they are being observed will not be scheduled. Observations that pass screening but are lost in orbit due to a bright-object violation will not be rescheduled. Observers are responsible for assuring that their observations do not violate the MAMA count-rate limits. A detailed description of the MAMA bright-object limits and the observers' responsibility is presented in Section 7.6. and in [STIS ISR 2000-01](#).

To assure that STScI can adequately screen observations, special constraints are imposed on parallel observing with the MAMAs:

- No pure parallels are allowed using the MAMA detectors.
- Coordinated parallels are allowed with the MAMA detectors only if an exact spacecraft orientation (ORIENT) is requested and the RA and Dec of the parallel field determined. Note that the specification of an exact orient usually limits the scheduling of observations to a ~4–8 week period each year. The observer is responsible for assuring that observations do not violate the MAMA count rate limits both for coordinated parallel MAMA observations and for primes.

Targets that are one magnitude or more fainter than the magnitude limits in the screening tables generally automatically pass screening. For a target that is within one magnitude of the screening limits after correction for extinction and slit losses, observers must provide a spectrum of the source at the intended observing wavelength. If such a spectrum is not available, the prospective General Observer (GO) must request an orbit in Phase I for a pre-qualification exposure, during which the target spectrum must be determined by observation in an allowed configuration (see Section 7.6 for more details).

Normal MAMA bright object limits apply to all objects that may be within 5 arc-seconds of the entrance aperture. In addition, there are special limits that apply to any extremely bright object that may be within 13.5 arc-seconds of the aperture. Full details are given in Section 7.6.4.

Please also note that if you are proposing MAMA target-of-opportunity observations, we ask you to provide an explanation in your Phase I proposal of how you will ensure that your target can be safely observed.

2.8 STIS Snapshot Policies

Both imaging and spectroscopic STIS/MAMA snapshots are allowed, but the combined total of STIS/MAMA snapshot targets accepted in Cycle 14 will not exceed 300, with imaging targets limited to a total of 100, due

to the target and field bright-object checking requirements. Moving targets are not permitted for STIS/MAMA snapshot visits. Variable STIS/MAMA snapshot targets must have well defined maximum UV fluxes, which will be used for the bright-object checking. There are no restrictions on the numbers or variability of proposed STIS/CCD snapshot targets, as they do not require bright-object checking and have a significantly higher expected completion rate. Thus, use of the STIS/CCD G230LB or G230MB gratings is encouraged as an alternative to the NUV MAMA.

In addition, STIS/MAMA snapshot proposals should be limited to one or a few straightforward configurations. Specifically, use of the F25NDQ filters will not be allowed in MAMA snapshot proposals. Use of the 0.2X0.2 echelle aperture is recommended for first-order programs without a scientific need for a long-slit in order to expedite the field bright object screening process; these configurations will be supported as of Cycle 14. Because of the limited resources available for bright-object checking combined with the relatively low expected completion rate, excessively complex STIS/MAMA snapshot targets, fields, or instrumental configurations may not be implemented in Phase II. If you are in doubt on this issue, you may consult with a member of the Spectrographs Group via the [Help Desk](#).

Introduction to STIS

In this chapter. . .

3.1 Instrument Capabilities / 23
3.2 Instrument Design / 24
3.3 Basic Instrument Operations / 28
3.4 Designing STIS Observations / 31

In this chapter we provide an overview of the capabilities and scientific applications of STIS. We describe the opto-mechanical layout and basic operation of the instrument, with a flow chart and discussion to help you design a technically feasible, scientifically optimized STIS observing proposal.

3.1 Instrument Capabilities

STIS uses two-dimensional detectors operating from the ultraviolet to the near-infrared. First-order gratings cover the full spectral range and are designed for spatially resolved spectroscopy using a long slit. The echelle gratings, available only in the ultraviolet are designed to maximize the spectral coverage in single observations of point sources. The STIS Flight Software supports onboard target acquisitions and peakups to place targets on slits and coronagraphic bars. The STIS optics and detectors have been designed to exploit HST's high spatial resolution.

STIS can be used to obtain:

- Spatially resolved, long-slit (or slitless) spectroscopy from the ultraviolet to the near infrared (1150–10,300 Å) at low to medium spectral resolution ($R \sim 500\text{--}17,000$) in first order.

- Echelle spectroscopy at medium to high spectral resolution ($R \sim 30,000\text{--}110,000$), covering a broad simultaneous spectral range ($\Delta\lambda \sim 800$ or 200 \AA , respectively) in the ultraviolet ($1150\text{--}3100 \text{ \AA}$).

In addition to these two prime capabilities, STIS also provides:

- Imaging capability using the solar-blind far-ultraviolet MAMA detector ($1150\text{--}1700 \text{ \AA}$), the solar-insensitive near-ultraviolet MAMA detector ($1150\text{--}3100 \text{ \AA}$), and the optical CCD ($2000\text{--}10,300 \text{ \AA}$), through a small complement of narrow-band and broad-band filters.
- Objective-prism spectroscopy ($R \sim 500\text{--}10$) in the ultraviolet ($1150\text{--}3100 \text{ \AA}$).
- High-time-resolution ($\Delta\tau = 125$ microseconds) imaging and spectroscopy in the ultraviolet ($1150\text{--}3100 \text{ \AA}$) and moderate-time-resolution ($\Delta\tau \sim 20$ seconds) CCD imaging and spectroscopy in the near-UV, optical, and near-IR ($2000\text{--}10,300 \text{ \AA}$).
- Coronagraphic imaging in the near-UV, optical, and near IR ($2000\text{--}10,300 \text{ \AA}$) and bar-occulted spectroscopy over the entire spectral range ($1150\text{--}10,300 \text{ \AA}$).

Table 4.1 and Table 5.1 provide a full list of gratings for spectroscopy and filters for imaging.

STIS is a versatile instrument that can be applied to a broad range of scientific programs. For instance, the combination of high spectral resolution covering a large simultaneous wavelength range and low per-pixel background improves the efficiency of programs such as quasi-stellar object (QSO) and interstellar absorption-line studies. STIS's wavelength coverage in a single exposure is 15 to 35 times that of its predecessor GHRS for such applications. Studies of the dynamics of galactic nuclei and the kinematics of active galaxies and diffuse galactic nebulae benefit from the ability to obtain spatially resolved spectroscopy over a 50-arcsecond long slit and from the high quantum efficiency in the optical provided by the CCD. The wide wavelength coverage of STIS facilitates line-ratio studies; for instance, the low-resolution first-order gratings span the range $1150\text{--}10,300 \text{ \AA}$ in just four exposures. Slitless spectroscopy provides emission-line images of astronomical objects, and coronagraphic imaging and spectroscopy can reveal the nature of extended gaseous regions surrounding bright continuum sources.

3.2 Instrument Design

In this section, we provide a high-level summary of the basic design and operation of STIS, concentrating on the information most relevant to your

HST observing proposal. Subsequent chapters provide more detailed information.

3.2.1 Detectors

STIS uses three large-format (1024 x 1024 pixel) detectors (see Chapter 7 for more details), as follows:

- A Scientific Image Technologies (SITE) CCD, called the STIS/CCD, with ~ 0.05 arcsecond square pixels, covering a nominal 52 x 52 arc-second square field of view (FOV), operating from ~ 2000 to $10,300 \text{ \AA}$.
- A Cs_2Te Multi-Anode Microchannel Array (MAMA) detector, called the STIS/NUV-MAMA, with ~ 0.024 arcsecond square pixels, and a nominal 25 x 25 arcsecond square field of view (FOV), operating in the near ultraviolet from 1600 to 3100 \AA .
- A solar-blind CsI MAMA, the STIS/FUV-MAMA, with ~ 0.024 arc-sec pixels, and a nominal 25 x 25 arc-second square FOV, operating in the far ultraviolet from 1150 to 1700 \AA .

The CCD

The CCD provides high quantum efficiency and good dynamic range in the near ultraviolet through near infrared. The CCD produces a time-integrated image in the ACCUM data-taking mode. As with all CCDs, there is noise (*read noise*) and time (*read time*) associated with reading out the detector. Time-resolved work with this detector is done by taking a series of multiple short exposures. The minimum exposure time is 0.1 sec, and the minimum time between successive identical exposures is 45 sec for full-frame, but can be reduced to 20 sec for subarray readouts. CCD detectors are capable of high-dynamic-range observations. The dynamic range for a single exposure ultimately is limited by the depth of the CCD full well ($144,000 e^-$), which determines the total amount of charge (or counts) that can accumulate in any one pixel during any one exposure without causing saturation. For GAIN=1, it is further limited (to $33,000 e^-$) by saturation in the gain amplifier. Cosmic rays will affect all CCD exposures. CCD observations should be broken into multiple exposures (called CR-SPLITS) of no more than 1000 sec each, whenever possible, to allow removal of cosmic rays in post-observation data processing; During Phase II you can specify the CR-SPLIT optional parameter to do this (see Chapter 11).

The MAMAs

The two MAMAs are *photon-counting* detectors which provide a two-dimensional ultraviolet capability. They can be operated either in ACCUM mode, to produce a time-integrated image, or in TIME-TAG mode

to produce an event stream with high (125 μs) time resolution. Doppler correction for the spacecraft motion is applied automatically onboard for data taken in ACCUM high-spectral-resolution modes.

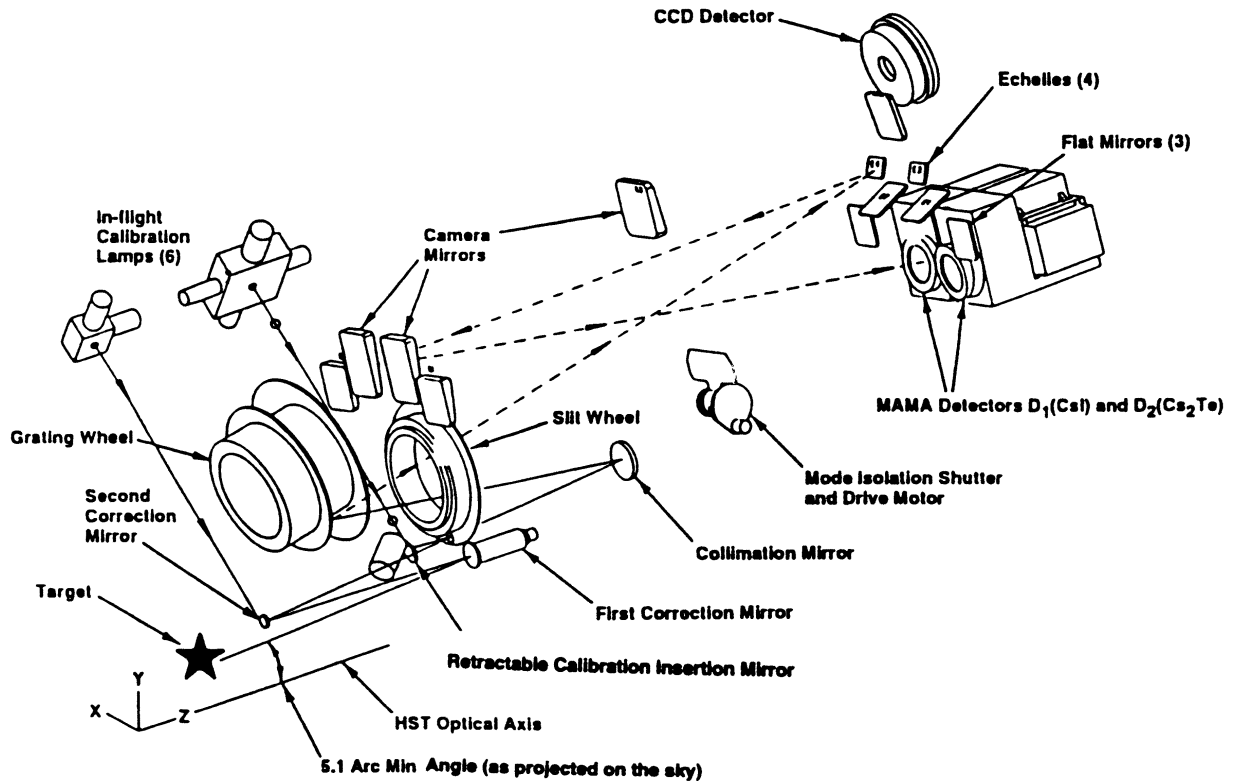
The STIS MAMA detectors are subject to both *scientific* and *absolute* brightness limits. At high local (≥ 50 counts sec^{-1} pixel^{-1}) and global ($> 285,000$ counts sec^{-1}) illumination rates, counting becomes nonlinear in a way that is not correctable. At only slightly higher illumination rates, the MAMA detectors are subject to damage. We have therefore defined absolute local and global count-rate limits, which translate to a set of configuration dependent bright-object screening limits. Sources which violate the absolute count-rate limits in a given configuration *cannot be observed in that configuration*, as discussed in Section 7.6.

Early concerns about the signal-to-noise attainable with the MAMAs have been alleviated by experience in orbit. Values of 50:1 per spectral resolution element in extracted spectra are routinely obtained for point sources with sufficient counting statistics when integrated over the extraction aperture. Higher signal-to-noise values of 100–300 can be obtained by stepping the target along the slit in the first-order modes, or by use of special multiple slits with the echelles (see Chapter 12). Current information indicates that the flat fields are stable to $\pm 1\text{--}2\%$, but the UV flat-field lamps have been used sparingly due to their limited lifetimes, so the long-term stability of the UV flats is not yet certain. See also Section 16.1.

3.2.2 STIS Physical Configuration

The STIS optical design includes corrective optics to compensate for HST's spherical aberration, a telescope focal-plane slit-wheel assembly, collimating optics, a grating-selection mechanism, fixed optics, and camera focal-plane detectors. An independent calibration-lamp assembly can illuminate the focal plane with a range of continuum and emission-line lamps. A simplified schematic showing major mechanisms and detectors, and a medium-resolution echelle mode light path is shown in Figure 3.1.

Figure 3.1: Simplified STIS Optical Design



Slit and Grating Wheels

The *slit wheel* contains apertures and slits for spectroscopic use and the clear, filtered and coronagraphic apertures for imaging. The slit-wheel positioning is repeatable to very high precision: ± 7.5 and 2.5 milli-arcseconds in the spatial and spectral directions, respectively.

The *grating wheel*, or so-called Mode-Selection Mechanism (MSM), contains the first-order gratings, the cross-disperser gratings used with the echelles, the prism, and the mirrors used for imaging. The MSM is a nutating wheel which can orient optical elements in three dimensions. It permits the selection of one of its 21 optical elements as well as adjustment of the tip and tilt angles of the selected grating or mirror. As described in “Routine Wavecals” below, the grating wheel exhibits non-repeatability which is corrected for in post-observation data processing using contemporaneously obtained comparison-lamp exposures.

For some gratings, only a portion of the spectral range of the grating falls on the detector in any one exposure. These gratings can be scanned (tilted by the MSM) so that different segments of the spectral format are moved onto the detector for different exposures. For these gratings a set of

pre-specified central wavelengths, corresponding to specific MSM positions, i.e., grating tilts, has been defined (see Chapter 4).

Calibration-Lamp Systems

STIS has two independent calibration subsystems, the so-called HITM (Hole in the Mirror) system and the IM (Insert Mechanism) system. The HITM system contains two Pt-Cr/Ne line lamps used to obtain wavelength comparison exposures and to illuminate the slit during target acquisitions. Light from the HITM lamps is projected through a hole in the second correction mirror (CM2). Thus, when the HITM lamps are used, light from the external sky still falls on the detector unless the STIS external shutter (not shown in Figure 3.1) is closed. The IM system contains flat-fielding lamps (a tungsten lamp for CCD flats, a deuterium lamp for NUV-MAMA flats, and a krypton lamp for FUV-MAMA flats) and a single Pt-Cr/Ne line comparison lamp. When the IM lamps are used, the Calibration Insert Mechanism (CIM) is inserted into the light path and all external light is blocked. Observers will be relieved to know that the ground system will *automatically* choose the right subsystem (see Section 3.3) and provide the necessary wavelength calibration exposures.

3.3 Basic Instrument Operations

Target Acquisitions and Peakups

Once the telescope acquires its guide stars, your target will normally be within $\sim 1\text{--}2$ arcseconds of the aperture center. For science observations taken through slits which are smaller than 3 arcseconds in either dimension, and for use of the coronagraphic bars, you will need to specify a target-acquisition exposure to center the target in the science aperture. The nominal accuracy of STIS point source ($V < 21$) target acquisitions is 0.01 arcsecond. If either dimension of the aperture is less than or equal to 0.1 arcsecond, the acquisition exposure should be followed by one or more peakup exposures to refine the centering of point or point-like sources. Peakup accuracy is 5% of the slit width used. Acquisition exposures always use the CCD, one of the filtered or unfiltered apertures for CCD imaging, and a mirror as the optical element in the grating wheel. Peakup exposures use a science slit or coronagraphic aperture and also use the CCD, with either a mirror or a spectroscopic element in the grating wheel. Target acquisitions and acquisition peakups are described in detail in Chapter 8.

Routine Wavecal

Each time the MSM is moved to select a new optical element or to tilt a grating, the resulting spectrum is projected onto the detector with a positional error (lack of repeatability) of $\leq \pm 3$ low-resolution (MAMA)

pixels. Additionally, thermal effects can cause small drifts over multi-orbit observations. An internal calibration-lamp observation (WAVECAL) will automatically be taken following each use of a new grating element or new tilt position and after ~ 1 orbit in any one setting in order to allow calibration of the zero point of the wavelength (dispersion) and spatial (perpendicular to dispersion) axes in the spectroscopic science data during post-observation data processing. These routine, automatically occurring, wavecal observations are expected to provide sufficient wavelength zero point accuracy for the vast majority of GO science. Only if your science requires particularly accurate tracking of the wavelength zeropoints do you need to insert additional wavecal observations in your exposure sequence (see also Chapter 11).

Data Storage and Transfer

At the conclusion of each ACCUM exposure, the science data are read out from the detector in use and placed in STIS's internal memory buffer, where they are stored until they can be transferred to the HST data recorder (and thereafter to the ground). This design makes for more efficient use of the instrument, as up to eight CCD or 1024 x 1024 MAMA, or two 2048 x 2048 MAMA (see "Highres" on page 228) full-frame images can be stored in the internal buffer at any time. A frame can be transferred out of the internal buffer to the data recorder during subsequent exposures, as long as those exposures are longer than 3 minutes in duration.

STIS's internal buffer stores the data in a 16 bit per pixel format. This structure imposes a maximum of 65,536 data numbers per pixel. For the MAMA detectors this maximum is equivalent to a limit on the total number of *photons* per pixel which can be accumulated in a single exposure. For the CCD, the full well (and not the 16 bit buffer format) limits the photons per pixel which can be accumulated without saturating in a single exposure. See Chapter 7 and Chapter 11 for a detailed description of detectors and data taking with STIS.

Parallel Operations

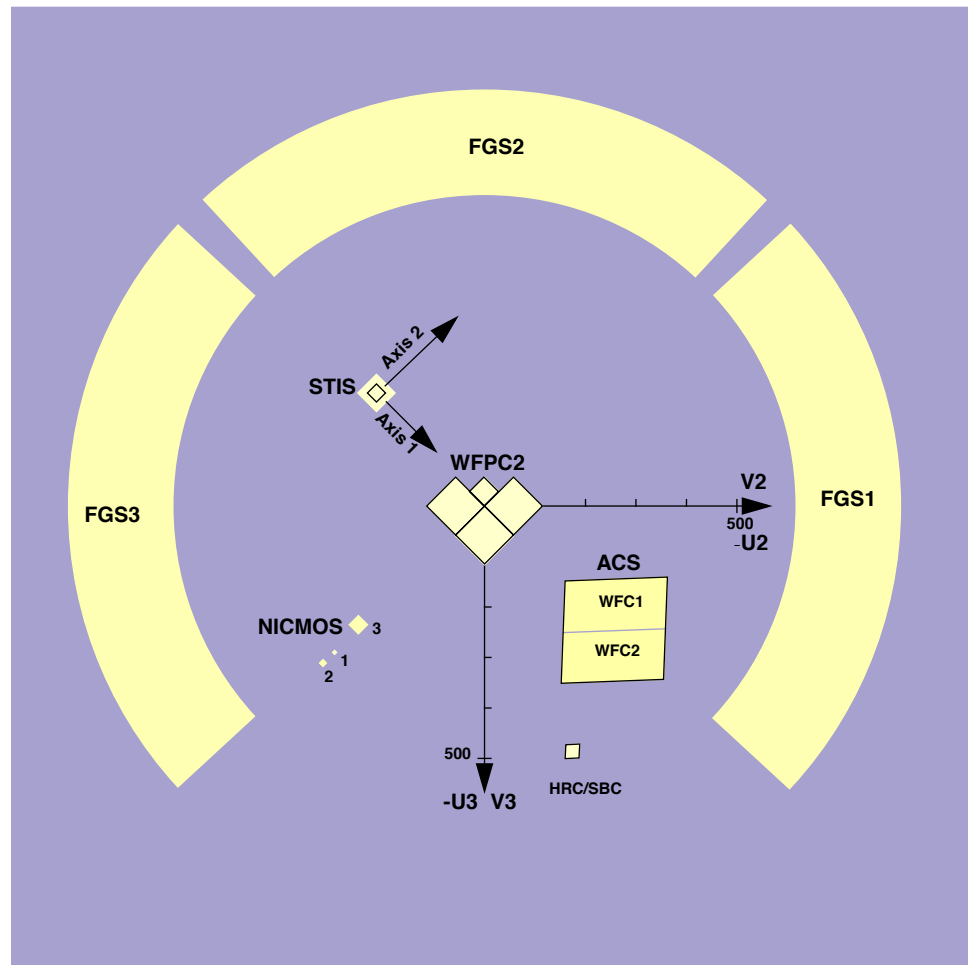
STIS's three detectors do *not* operate in parallel with one another—only one detector can be used at any one time. Exposures with different STIS detectors can, however, be freely interleaved in an observing sequence, and there is no extra setup time or overhead in moving from one detector to another. The three detectors, sharing the bulk of their optical paths, also share a common field of view of the sky.

STIS *can* be used in parallel with any of the other science instruments on HST. Figure 3.2 shows the HST field of view with ACS installed. Dimensions in this figure are approximate; accurate aperture positions can be found on STScI's Observatory web page under "Pointing".¹ The STIS dispersion is along AXIS1 and the slits are parallel to AXIS2. The policy

1. Pointing web page: <http://www.stsci.edu/hst/observatory/pointing>

for applying for parallel observing is described in the Call for Proposals. We provide suggestions for designing parallel observations with STIS in Section 12.8. While the STIS CCD can always be used in parallel with another instrument, there are some restrictions on the use of the MAMA detectors in parallel, as described in Section 2.7.

Figure 3.2: HST Field of View



3.3.1 Typical STIS Observing Sequence

In the optical, STIS is often used to observe extremely faint objects, so long observations are common. The combination of high spatial resolution, spectral resolution, and low read noise from the CCD will encourage the taking of multiple (~15 minute) exposures to allow cosmic ray rejection. Observations with the MAMA detectors do not suffer from cosmic rays or read noise, but long integration times will often be needed to obtain sufficient signal-to-noise in the photon-starved ultraviolet.

A typical STIS observing sequence is expected to consist of an initial target acquisition and possibly an acquisition peakup to center the target in a slit, followed by a series of long (~10–40 minute) exposures with a single optical element at a given wavelength setting. It may also include a series of multiple long exposures taken with different gratings or with a single grating at a number of tilts. Observers will generally not take their own wavecal exposures; routine automatic wavecal will allow wavelength and spatial zero points to be determined in post-observation data processing, requiring no input from the user. Observations at ≥ 7000 Å should be accompanied by fringe-flat exposures as discussed in Chapter 11.

3.4 Designing STIS Observations

In this section, we describe the sequence of steps you will need to take when designing your STIS observing proposal. The process is an iterative one, as you trade off between maximum spatial and spectral resolution, signal-to-noise, and the limitations of the instrument itself. The basic sequence of steps in defining a STIS observation (see Figure 3.3 below) is:

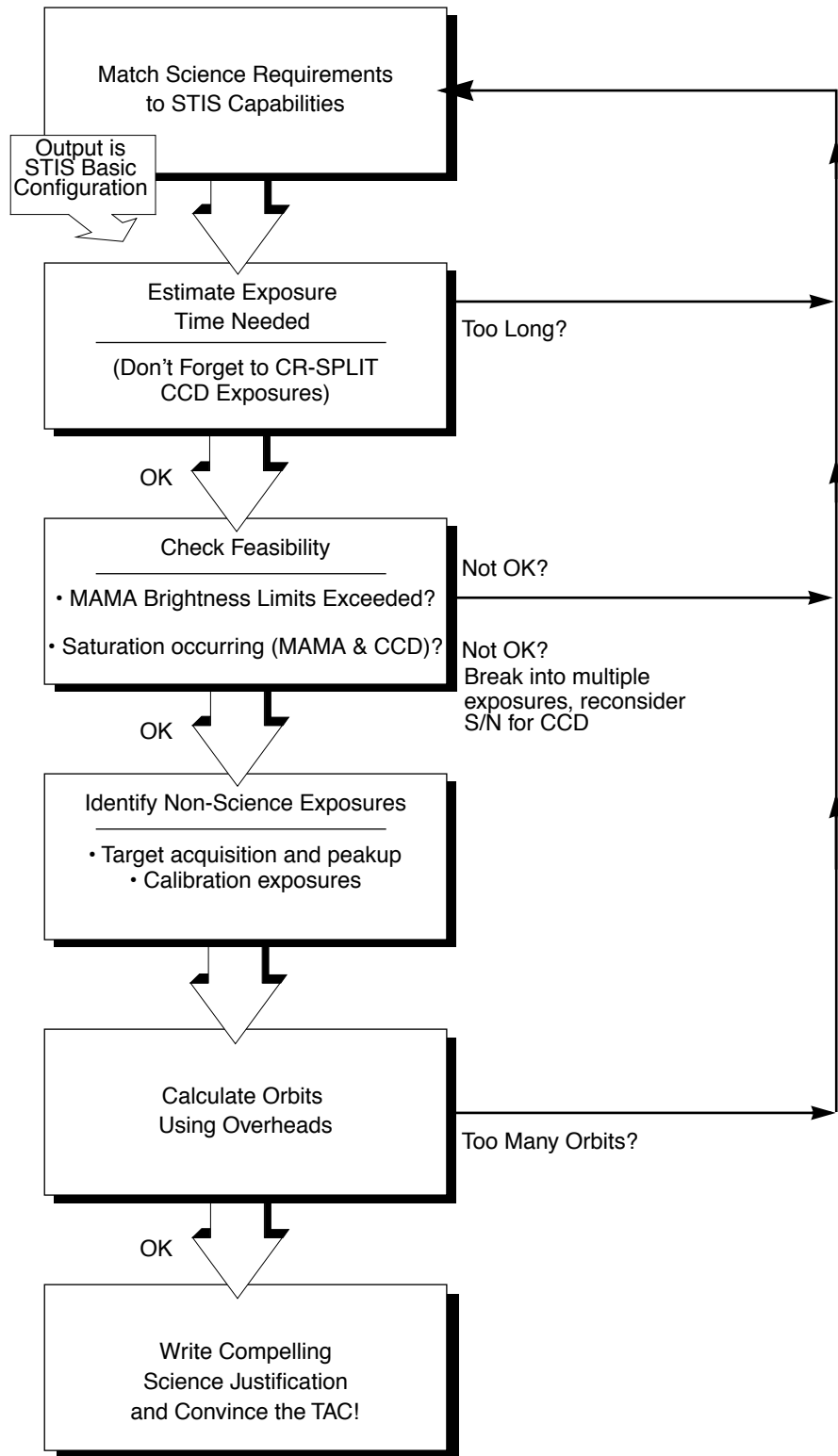
- Identify science requirements and select basic STIS configuration to support those requirements.
- Estimate exposure time to achieve required signal-to-noise ratio and check feasibility, including saturation and bright-object limits.
- Identify any additional non-science (target-acquisition, peakup and calibration) exposures needed.
- Calculate total number of orbits required, taking into account the overhead.

3.4.1 Identify Science Requirements and Define STIS Configuration

First and foremost, of course, you must identify the science you wish to achieve with STIS. Basic decisions you will need to make are:

- Spectroscopy or imaging?
- Wavelength region(s) of interest?
- Spectral resolution and spectral coverage required?

Figure 3.3: Defining a STIS Observation



- Nature of target—extended source (long slit or full aperture) or point source?

In addition you will need to establish whether you require:

- High signal-to-noise ratio
- Time resolution
- Coronagraphy
- High photometric accuracy

As you choose your science requirements and work to match them to the instrument’s capabilities, keep in mind that those capabilities differ greatly depending on whether you are observing in the optical with the CCD, or in the ultraviolet using the MAMA detectors. Tradeoffs are described in Table 3.1.

Table 3.1: Science Decision Guide

Decision	Affects	Tradeoffs
Wavelength regime	Detector and gratings	2000–10,300 Å — CCD; 1600–3100 Å — NUV–MAMA; 1150–1700 Å — FUV–MAMA
Spectral resolution	Gratings and detector	R < 20,000 (first order) with CCD, NUV or FUV–MAMA, or R ≥ 30,000 (echelle) with NUV or FUV–MAMA only.
Spectral range	Gratings	Spectral range covered in a single exposure differs radically for different gratings.
Extended or point source	Gratings	First-order gratings designed for spatially resolved and point-source observations. Echelle gratings designed for point-source observations (long-slit echelle spectroscopy will suffer order overlap for extended sources, but can be done for sources with weak continua).
Time resolution	Detector	If time resolution <20 seconds required, must use NUV or FUV–MAMA.
Coronagraphy	Detector and aperture	<i>Bright-object</i> ¹ coronagraphy available with CCD only. Coronagraphic imaging available with CCD only. Barred coronagraphic spectroscopy available with all detectors.

1. The bright-object limits for MAMA observations apply to coronagraphic observations as well, i.e., coronagraphic observations of targets which are too bright for the MAMA detectors are not allowed.

Spectroscopy

For spectroscopic observations, the base configuration you need is: detector (configuration), operating mode (mode=ACCUM or TIME–TAG), slit (aperture), grating (spectral element) and central wavelength (cenwave). In Chapter 4 we provide detailed information about each of the spectroscopic grating modes of STIS.

Imaging

For imaging observations, the base configuration is detector (configuration), operating mode (mode=ACCUM or TIME–TAG), and filter

(aperture).² Chapter 5 presents detailed information about each of STIS's imaging modes.

Special Uses

We refer you to Chapter 12 if you are interested in any of the following special uses of STIS: slitless spectroscopy or extended-source echelle observations, time-resolved work, bright-object or high signal-to-noise observations, planetary studies, parallel observations and coronagraphy.

3.4.2 Determine Exposure Time and Check Feasibility

Once you have selected your basic STIS configuration, the next steps are:

- Estimate the exposure time needed to achieve your required signal-to-noise ratio, given your source brightness. (You can use the STIS Exposure Time Calculator for this: see Chapter 6 and the plots in Chapter 13 and Chapter 14.)
- For observations using the MAMA detectors, assure that your observations do not exceed brightness (count-rate) limits. (You can use the STIS Exposure Time Calculator for this.)
- For observations using the MAMA detectors, assure that for pixels of interest your observations do not exceed the limit of 65,536 accumulated counts per pixel per exposure imposed by the STIS 16 bit buffer.
- For observations using the CCD detector, assure that for pixels of interest, you do not exceed the per pixel saturation count limit of the CCD. (You can use the STIS Exposure Time Calculator for this.)
- For MAMA TIME-TAG exposures check that your observations are feasible and do not violate any TIME-TAG specific count rate or data volume constraints (see Chapter 11).

To determine your exposure-time requirements consult Chapter 6 where an explanation of how to calculate signal-to-noise and a description of the sky backgrounds are provided. To assess whether you are close to the brightness, signal-to-noise, and dynamic-range limitations of the detectors, refer to Chapter 7. For a consideration of data-taking strategies and calibration exposures, consult Chapter 11.

If you find that the exposure time needed to meet your signal-to-noise requirements is too great, or that you are constrained by the detector's brightness or dynamic-range limitations, you will need to adjust your base STIS configuration. Table 3.2 summarizes the options available to you and

2. The mirror will be used as the spectral element for imaging observations.

steps you may wish to take as you iterate to select a STIS configuration which is both suited to your science and technically feasible.

Table 3.2: Feasibility Guide

Action	Outcome	Recourse
Estimate exposure time	If too long -> re-evaluate instrument configuration.	Reduce resolving power, or use wider slit, or change detectors and wavelength regime, or use larger binning.
Check saturation limit for CCD observations	If you wish to avoid saturation-> reduce time per exposure.	Divide total exposure time into multiple, short exposures. ^{1,2}
Check bright-object limits for MAMA observations	If source is too bright -> re-evaluate instrument configuration.	Increase spectral resolution, or choose narrower slit, or use neutral-density filter, or change detectors and wavelength regime.
Check 65,536 counts per pixel limit for MAMA observations	If limit exceeded -> reduce time per exposure.	Divide total exposure time into multiple, short exposures. ^{1,2}

1. Splitting CCD exposures affects the exposure time needed to achieve a given signal-to-noise ratio because of the read noise. Splitting MAMA exposures has no effect since there is no read noise with the MAMAs.
2. Splitting an exposure into multiple exposures increases the overheads, slightly reducing on-source time.

3.4.3 Identify Need for Non-Science Exposures and Constraints

Having identified your desired sequence of *science* exposures, you need to determine what *non-science* exposures you may require to achieve your scientific goals. Specifically, you need to:

- Determine which (if any) target acquisition and acquisition peakup exposures will be needed to center your target in your aperture to the accuracy required for your scientific aims (e.g., you may wish to center the nucleus of a galaxy in the 52 X 0.1 arcsecond slit and orient the long axis of the slit along the major axis of the galaxy to some accuracy). To assess your acquisition needs, refer to Chapter 8. To determine a specific orientation for the STIS long slit, refer to Chapter 11.
- If you require more accurate wavelength zeropoints than the routine calibrations provide, you can insert additional comparison lamp exposures (`TARGET_NAME=WAVE`) at shorter intervals or of longer duration than the routine, automatic `WAVECAL` observations. To determine your wavelength calibration exposure needs, refer to Chapter 11.

- CCD observations longward of 7000 Å are subject to severe fringing, which can be well corrected only by flat-field exposures obtained contemporaneously with the science exposures. Hence, you should include such flat-field exposures if observing near 7000 Å or longward. Fringing is discussed in Chapter 7 and the specification of corrective flat fields (CCDFLATs) is discussed in Chapter 11.

3.4.4 Determine Total Orbit Request

In this, the final step, you place all your exposures (science and non-science, alike) into orbits, including tabulated overheads, and determine the total number of orbits you require. Refer to Chapter 9 when performing this step. If you are observing a point source and find your total time request is significantly affected by data-transfer overheads (which will be the case *only* if you are taking many separate exposures under 3 minutes), you can consider the use of CCD subarrays to lessen the data volume. Subarrays are described in “CCD Subarrays” on page 224.

There are some special constraints on the duration and structure of MAMA visits, due to the sensitivity of certain STIS electronic components to charged particles which preclude operating the MAMAs at all during orbits which cross the South Atlantic Anomaly (SAA). Since there are a limited number of SAA-free orbits per day, MAMA visits are limited to a maximum of five orbits. Longer programs must be broken into shorter visits. Moreover, in order to conserve orbits available for MAMA observations, programs which combine CCD and MAMA observations must be divided into separate visits for each detector type, unless the CCD portion consumes less than 30 minutes including overheads or the visit is only one orbit long (see Chapter 2).

At this point, if you are happy with the total number of orbits required, you’re done! If you are unhappy with the total number of orbits required, you can, of course, iterate, adjusting your instrument configuration, lessening your acquisition requirements, changing your signal-to-noise or wavelength requirements, until you find a scenario which allows you to achieve (and convince the Telescope Allocation Committee (TAC) of the merits of) your science goals with STIS.



PART II:

User's Guide

The chapters in this part describe the basics of observing with STIS. Included are a description of the instrumental layout and basic operations, the spectroscopic and imaging capabilities of STIS, the performance and limitations of its detectors, exposure-time calculations, target acquisitions, and overhead and orbit-request determinations.

This part of the Handbook is all you need to read to plan your Phase I STIS Proposal.

Spectroscopy

In this chapter. . .

4.1 Overview / 39
4.2 First-Order Long-Slit Spectroscopy / 49
4.3 Echelle Spectroscopy in the Ultraviolet / 56
4.4 Objective-Prism Spectroscopy / 58

In this chapter, we provide information to help you choose the most appropriate spectroscopic configuration for your scientific program. We briefly describe the properties of each grating mode and its associated slits, and provide an overview of their scientific uses. Curves of sensitivity, the central wavelengths and wavelength ranges for the grating settings, detailed aperture throughputs and line-spread functions referenced in this chapter are all presented in Chapter 13.

For MAMA spectroscopy there are bright-object limits. We mention these limits here, and describe them in detail in Chapter 7. Tables of the MAMA spectroscopic bright-object screening magnitudes by spectral type and mode are presented in Chapter 13.

4.1 Overview

There are 15 spectroscopic modes which are summarized in Table 4.1 below. They comprise low and intermediate-resolution first-order modes designed to be used with a complement of long slits over the entire wavelength range, and intermediate and high-resolution echelle modes which have been optimized for point-source observations through short echelle slits and are available only in the ultraviolet (see Figure 4.2).

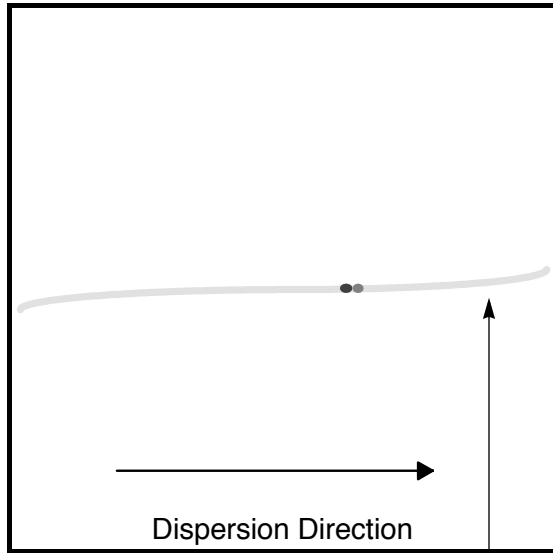
Table 4.1: STIS Spectroscopic Capabilities

Grating	Spectral Range (Å)		Spectral Resolution			Detector	Reference material page	Recommended Slits (apertures) ^{2,3,4,5,6,7,8,9}	
	Complete	Per Tilt	Scale $\Delta\lambda$ (Å per pixel)	Resolving Power ($\lambda/2\Delta\lambda$)	No. Prime Tilts ¹				
<i>MAMA First-Order Spectroscopy</i>									
G140L	1150–1730	610	0.60	960–1440	1	FUV-MAMA	316	<div style="display: flex; align-items: center;"> <div style="border-left: 1px solid black; border-right: 1px solid black; padding: 0 5px;"> 52X0.05D1 52X0.1D1 52X0.2D1 52X0.5D1 52X2D1 25MAMAD1 F25SRF2D1 F25QTZD1 </div> <div style="margin-left: 20px;"> 52X0.05 52X0.1 52X0.2 52X0.5 52X2 52X0.2F1 0.2X0.2 </div> </div>	
G140M	1140–1740	55	0.05	11,400–17,400	12	FUV-MAMA	319		
G230L	1570–3180	1610	1.58	500–1010	1	NUV-MAMA	310		
G230M	1640–3100	90	0.09	9110–17,220	18	NUV-MAMA	313		
<i>CCD First-Order Spectroscopy</i>									
G230LB	1680–3060	1380	1.35	620–1130	1	CCD	302		
G230MB	1640–3190	155	0.15	5470–10,630	11	CCD	306		
G430L	2900–5700	2800	2.73	530–1040	1	CCD	296		
G430M	3020–5610	286	0.28	5390–10,020	10	CCD	299		
G750L	5240–10,270	5030	4.92	530–1040	1	CCD	290		
G750M	5450–10,140	570	0.56	4870–9050	9	CCD	293		
<i>MAMA Echelle Spectroscopy</i>									
E140M	1150–1710	620	$\lambda/91,700$	45,800	1	FUV-MAMA	328	0.2X0.2, 0.2X0.06	
E140H	1150–1700	210	$\lambda/228,000$	114,000	3	FUV-MAMA	331	0.2X0.2, 0.2X0.09	
E230M	1570–3110	800	$\lambda/60,000$	30,000	2	NUV-MAMA	322	0.2X0.2, 0.2X0.06	
E230H	1620–3150	267	$\lambda/228,000$	114,000	6	NUV-MAMA	325	0.2X0.2, 0.2X0.09	
<i>MAMA Prism Spectroscopy</i>									
PRISM	1150–3620	2470	0.2 - 72	10-2500	1	NUV-MAMA	334	25MAMA, 52X0.05, 52x0.1, 52X0.2, 52X0.5, 52X2	

1. Number of exposures at distinct tilts needed to cover spectral range of grating with 10% wavelength overlap between adjacent settings.
2. For a complete list of supported and available-but-unsupported apertures for each grating, see Table A.1 on page 490.
3. Naming convention gives dimensions of slit in arcseconds. E.g., 52X0.1 indicates the slit is 52 arcsec long perpendicular to the dispersion direction and 0.1 arcsec wide in the dispersion direction. The F (e.g., in 52X0.2F1) indicates a fiducial bar to be used for coronagraphic spectroscopy.
4. For MAMA first-order modes, only ~ 25 arcsec of a long slit's length projects on the detector. (See also Section 4.2.2.).
5. Full-aperture clear (50CCD or 25MAMA), longpass-filtered (F25QTZ or F25SRF2 in UV), and neutral-density-filtered slitless spectroscopy are also supported with the appropriate first-order and echelle gratings, as well as the PRISM.
6. The following slits are also supported for all echelle gratings. The 6X0.2 and 52X0.05 long slits are intended for use with extended emission line objects; order overlap must be considered when using these slits. Also the high S/N multi-slits 0.2X0.2FP (A-E) and 0.2X0.06FP (A-E) (see Chapter 12), the very narrow 0.1X0.03 slit for maximum spectral resolution, and the 0.2X0.05ND and 0.3X0.05ND neutral density slits.
7. The 0.1X0.09 and 0.1X0.2 slits are supported with E230H only. F25MGII is supported with all NUV-MAMA gratings and the PRISM.
8. The 0.2X0.2 aperture is also supported with all first-order gratings. It is available-but-unsupported with the PRISM.
9. The F25SRF2 aperture can be used with the prism to filter out (geocoronal) Lyman- α emission.

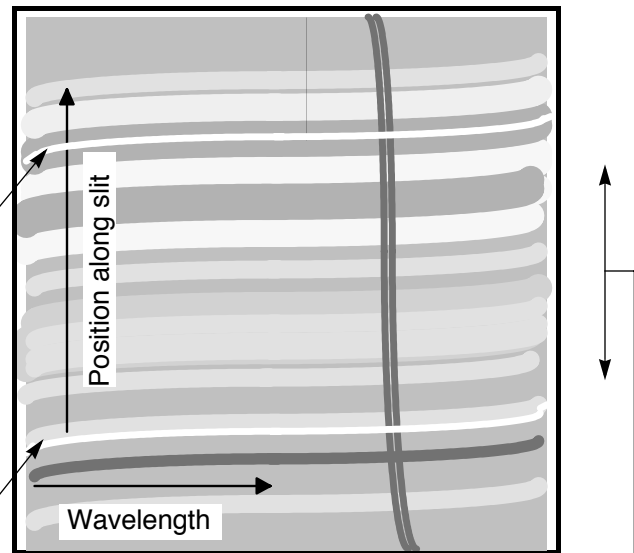
Table 4.2: Sample Uncalibrated Spectral Images (distortion is exaggerated)

a.) Uncalibrated Long-Slit Spectrum of Point Source



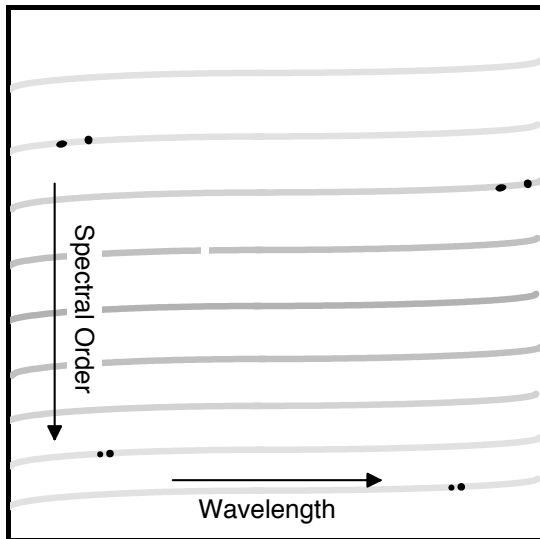
Point source showing continuum and two strong emission lines

b.) Uncalibrated Long-Slit Spectrum of Diffuse Source



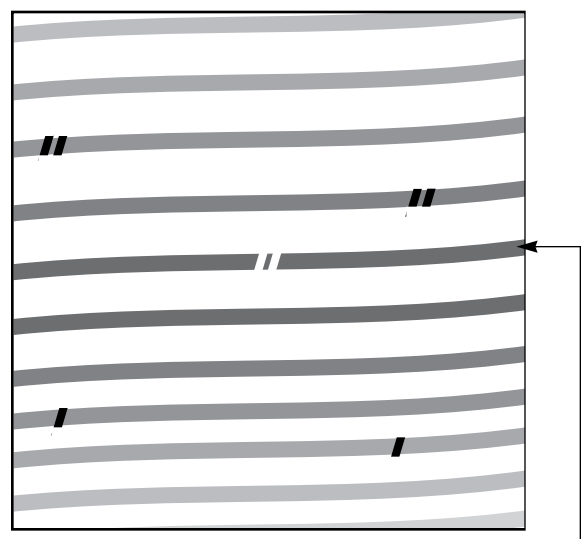
Strong doublet emission line
Bars on long slit
Spatially varying continuum

c.) Echelle Spectrum of Point Source Showing Multiple Orders on One Image



Two strong emission lines. Adjacent orders have ~10% overlap in wavelength so lines appearing at the start of one order will also appear at the end of the next.

d.) Echelle Spectrum of Diffuse Source



Absorption lines at wavelength near center of order. Continuum from extended object fills short slit.

4.1.1 Throughputs

To illustrate the broad wavelength coverage provided by STIS, and the relative throughputs achievable across STIS's wavelength regime, we show in Figure 4.1 the system throughput of the four low-resolution, first-order modes on a single plot (where the throughput is defined as the end-to-end effective area divided by the geometric area of a filled, unobstructed, 2.4 meter aperture). To allow you to judge the relative throughputs of different spectroscopic configurations, we plot in Figure 4.2 the efficiency of all grating modes for each of the four primary wavelength regimes on a common plot. These plots allow you to gauge the relative efficiencies of STIS in different configurations. Note, however, that these curves give the throughput at the time that STIS was initially calibrated (approximately 1997.7). Throughput changes in the first-order modes, determined from monitoring observations since STIS was installed, are discussed in Chapter 13. The throughput curves shown for the echelle modes trace the peak of the echelle blaze function for each order; throughputs near the ends of each order are lower by ~ 20 to 40%.

Figure 4.1: System Throughput of STIS's Low-Resolution, First-Order Grating Modes

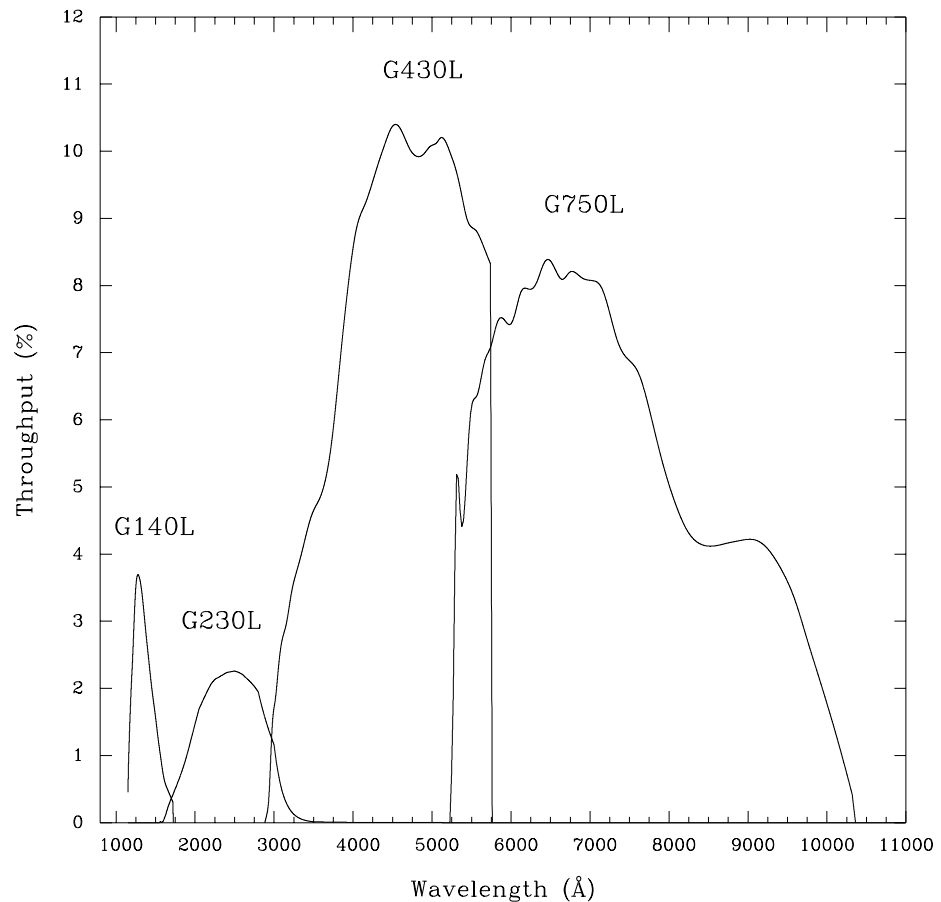
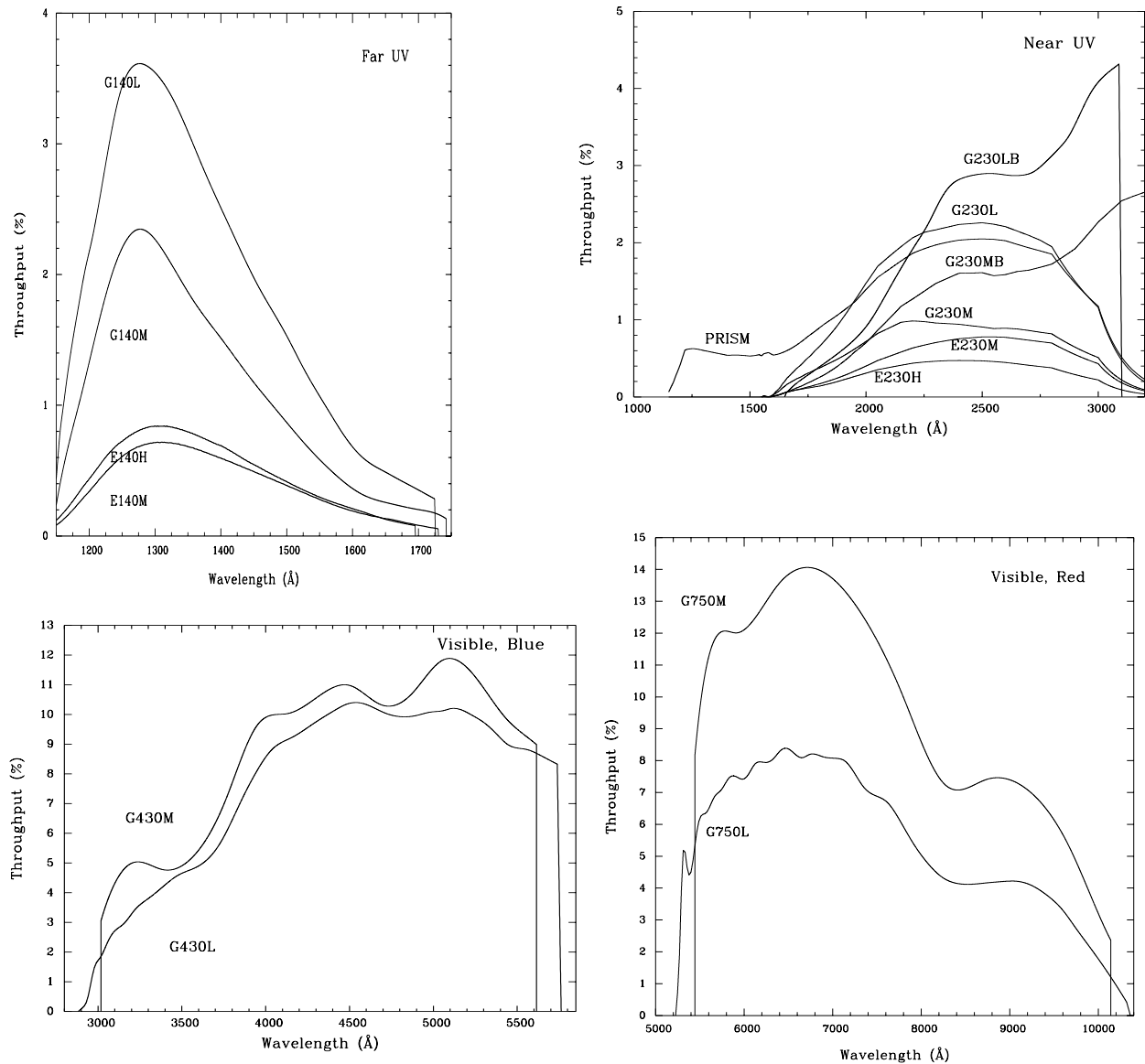


Figure 4.2: System Throughput of STIS's Grating Modes



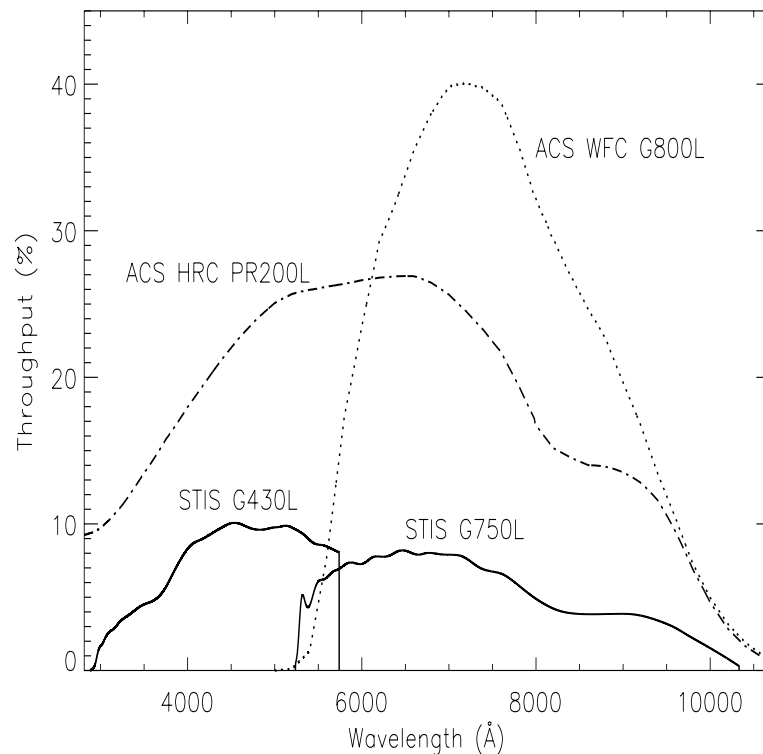
4.1.2 STIS vs. ACS Spectroscopy

Optical wavelengths

Although ACS is primarily an imaging instrument, it has a few prisms and a grism which can be used for very low-resolution slitless spectroscopy. In the optical wavelength region of 5500 to 11,000 Å, ACS offers the G800L grism which can be used with either the WFC or the HRC. The resolving powers of the STIS gratings and the ACS grism are however very different: the resolving power of ACS G800L grism is 100 to 200, whereas the resolving power of the STIS gratings are 500 to 10,000.

Their spectral coverage also differs. The entire wavelength range of 5500 to 11,000 Å is generally covered in a single exposure with the ACS G800L grism. With STIS, the spectral coverage depends on the grating used: with G750L it is possible to cover the entire wavelength range of 5240 to 10,200 Å in a single exposure, while a smaller spectral range at much higher dispersion can be obtained with the medium resolution M-gratings. Figure 4.3 shows a comparison of the transmissions of the ACS G800L grism and the STIS G750L grating. The ACS can be used only in slitless mode, so the spectral purity will be lower, and both source confusion and background contributions may be higher. These background differences must be correctly taken into account in any signal-to-noise estimates.

Figure 4.3: The total system throughputs of the STIS CCD G430L and G750L configurations (solid lines) are compared with the throughputs of the ACS WFC G800L and HRC PR200L modes (broken lines).

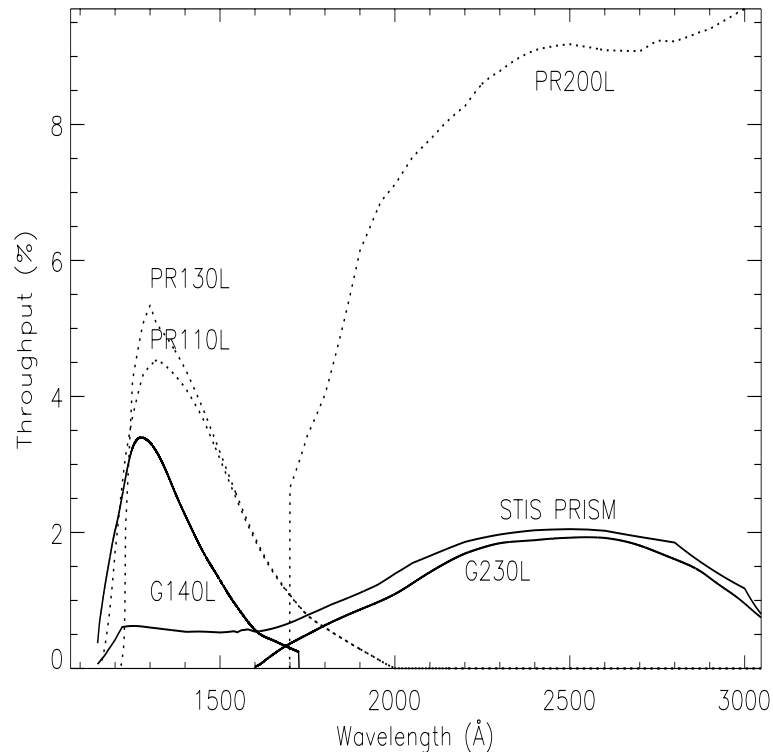


UV-wavelengths

In the ultraviolet, the ACS offers 3 prisms: PR200L with the HRC, and PR110L and PR130L with the SBC. Figure 4.4 shows a comparison of the transmissions of the ACS prisms and the STIS prism and low-resolution gratings. Note that the STIS prism uses the NUV-detector for the entire wavelength range; as a result the ACS prism has much higher sensitivities at FUV wavelengths. On the other hand, the STIS prism allows the entire wavelength range of 1150 to 3600 Å to be covered in a single exposure. Also, an appropriate slit can be used with the STIS prism whereas the ACS prism can be used only in slitless mode. While the ACS PR200L has a

much higher throughput and wider spectral range than any of the STIS spectroscopic configurations, this comes at the price of a much lower dispersion, especially at the long wavelength end. Observers should carefully consult the [ACS Instrument Handbook](#) before choosing between STIS and ACS slitless spectroscopy.

Figure 4.4: The total system throughputs for the STIS G140L, G230L and NUV-PRISM modes (solid lines) are compared with the ACS SBC PR110L and PR130L and the ACS HRC PR200L prisms (dotted lines).



4.1.3 Limiting Magnitudes

In Table 4.3 below, we give the V magnitude for an A0V star that gives a signal-to-noise ratio of 10 in the continuum (per spectral resolution element around the peak of the grating response), in a 1 hour exposure, where we have integrated over the PSF in the direction perpendicular to the dispersion, and assumed the 52×0.2 slit for the first-order gratings and the 0.2×0.2 slit for the echelles.

Table 4.3: Limiting A0 V Star V Magnitudes

Grating	Wavelength (Å)	Magnitude
G750L	7000	20.9
G750M	7000	19.1
G430L	5500	20.9
G430M	5500	18.5
G230LB	3000	18.4
G230MB	3000	15.4
G230L	2600	18.4
G230M	2600	14.5
G140L	1350	16.7
G140M	1350	13.8
E230M	2700	13.5
E230H	2600	11.4
E140M	1400	11.4
E140H	1350	10.5
PRISM		20.1 @ $\lambda = 2300$ (slitless)

4.1.4 Saturation

Both CCD and MAMA observations are subject to saturation at high total accumulated counts per pixel. The CCD can be saturated due to the saturation of the detector itself or of the gain amplifier for $\text{CCDGAIN}=1$. MAMA saturation can occur due to the 16-bit format of its memory buffer. The nature of the saturation for CCD and MAMA spectroscopic observations is described in Section 7.2.1 and Section 7.4.1, respectively.

4.1.5 MAMA Bright-Object Limits

The MAMA detectors are subject to absolute bright-object limits, above which targets cannot be observed.

We direct MAMA observers to the discussion presented in Section 7.6. For summary tables of bright-object screening magnitudes for all spectroscopic modes, see Section 13.8. It is the observer's responsibility to be sure that proposed observations do not exceed the MAMA bright-object limits.

4.1.6 Scanned Gratings: Prime and Secondary (Tilt) Positions

For the intermediate-resolution gratings and echelles (except E140M), only a portion of the full spectral range of the grating falls on the detector in any one exposure, and the gratings must be scanned (tilted) with a separate exposure taken at each tilt position, in order to cover the full spectral range (see Figure 4.5 and Figure 4.6 below). Accordingly, for these scanned gratings, the user may select a single exposure at a given wavelength, or a series of exposures at different wavelengths to cover a larger wavelength range. The user must choose either prime or secondary settings. The prime settings cover the full spectral range with 10% wavelength overlap between observations taken at adjacent settings. The secondary settings cover selected absorption or emission lines and may be more convenient to use in some applications. We expect the photometric and wavelength calibration accuracies to be higher for the prime settings than for most of the secondary settings, as calibrations for the latter will be inferred from those taken at prime settings. A few frequently used secondary settings are being calibrated directly as noted in Chapter 13. The central wavelengths, and corresponding minimum and maximum wavelengths, are presented in the individual grating sections in Chapter 13.

Figure 4.5: Scanned First-Order Gratings

First-Order Format: The solid box shows a single grating setting. Dashed boxes show sequential prime wavelength settings with 10% wavelength overlap between adjacent settings.

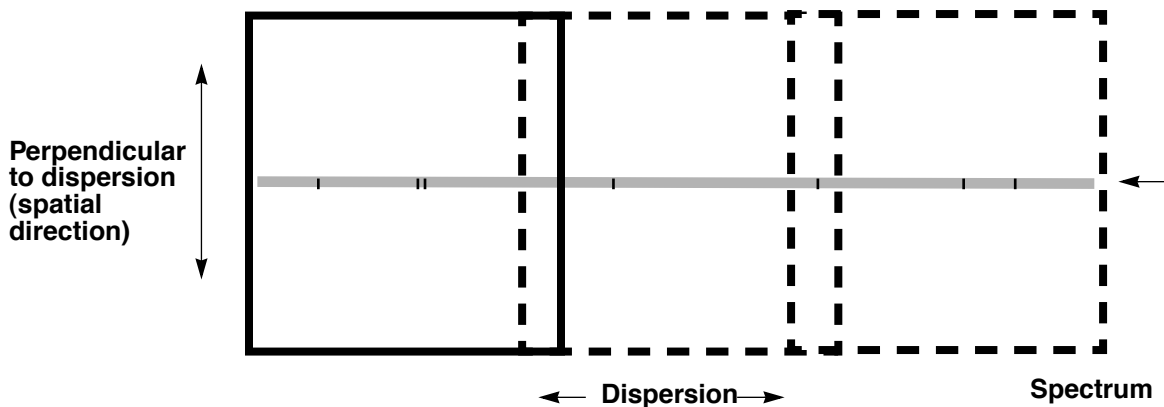
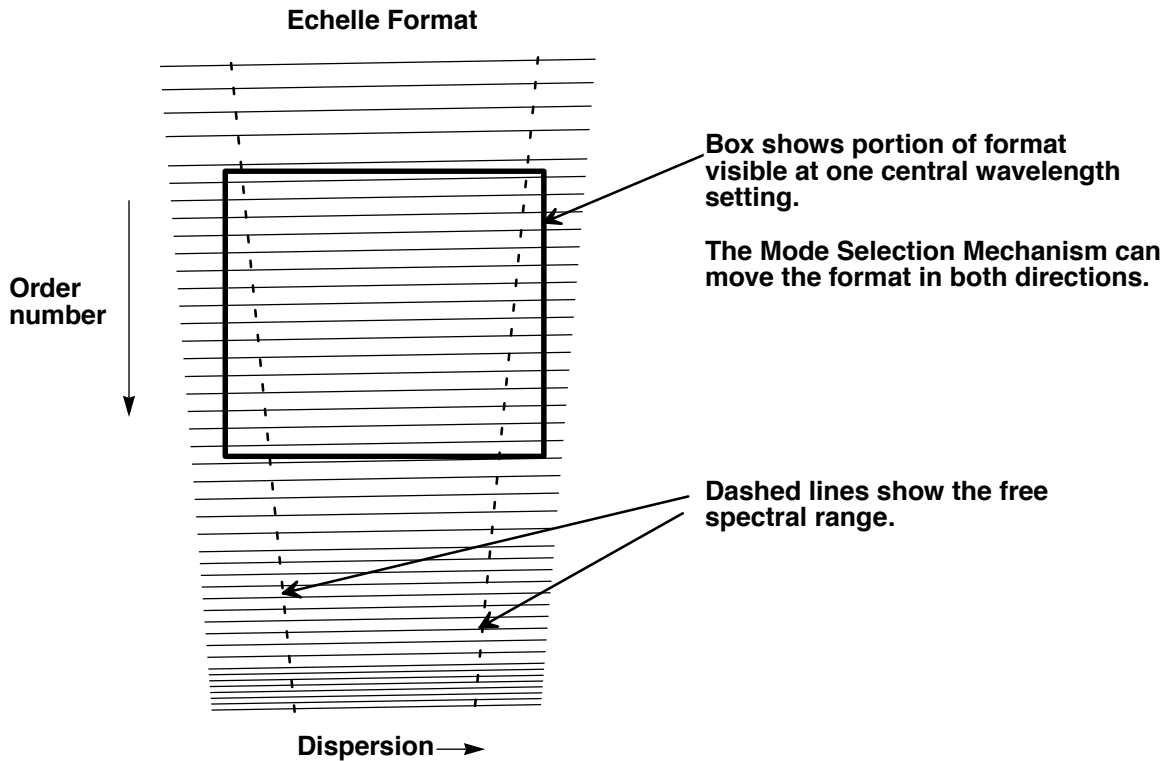


Figure 4.6: Scanned Echelle Gratings



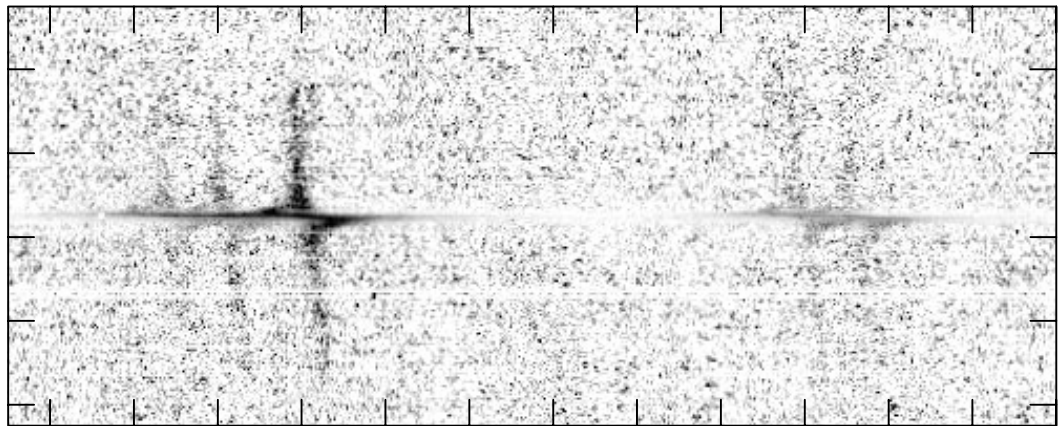
4.1.7 Cross-Over Regions

In the near UV, where the CCD has comparable sensitivity to the NUV-MAMA, you may want to consider using the G230LB or G230MB gratings with the CCD instead of the G230L and G230M gratings with the MAMA. You will get improved throughput down to at least 2500 Å, a larger slit length, and use of the CCD rather than the MAMA (see Figure 4.2 and Chapter 13). On the other hand, the CCD has read noise, cosmic-ray sensitivity, hot pixels, and charge transfer efficiency losses. Also, for *red* objects, scattered light can be more of a problem with the red-sensitive CCD than with the solar-insensitive NUV MAMA. For a solar-type spectrum, CCD data at wavelengths shorter than 2100 Å are dominated by scattered light.

4.2 First-Order Long-Slit Spectroscopy

STIS first-order mode long-slit spectroscopy has a wide observing range from the near IR through the optical and into the ultraviolet. Figure 4.7 shows an early STIS result measuring the black hole mass in the nucleus of a nearby galaxy.

Figure 4.7: Greyscale Representation of STIS G750M 52X0.2 Long-Slit Spectrum of the nuclear region of M84, showing the velocity structure of the $H\alpha$, [NII], and [SII] emission lines in the inner gaseous disk. The continuum has been subtracted from the data and they have been renormalized. (Figure courtesy of Gary Bower and Richard Green, see also Bower et al. 1998, ApJ, 492, L111).

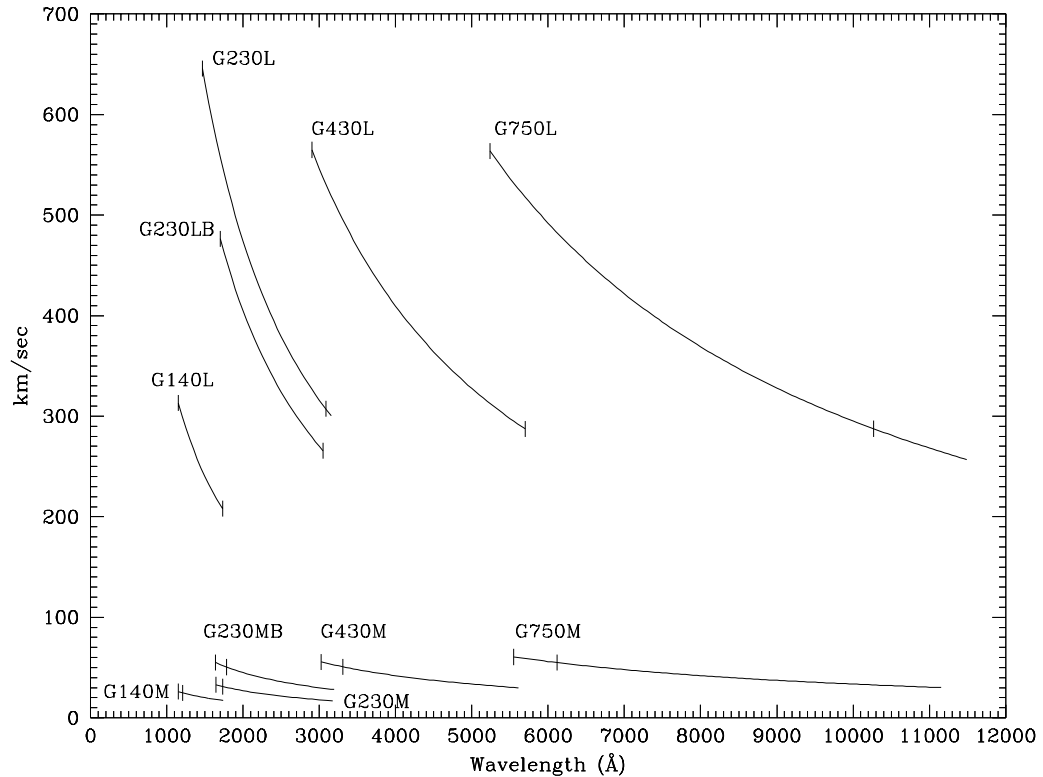


4.2.1 Gratings for First-Order Spectroscopy

There are 10 first-order gratings available for long-slit spectroscopy, providing resolving powers of ~ 500 – $17,000$ from the UV at 1150 \AA through the near IR at $\sim 10,000 \text{ \AA}$. The wavelength coverage and kinematic resolution of the first-order gratings are summarized in Figure 4.8. Briefly:

- For resolutions of $\sim 500 \text{ km sec}^{-1}$ use:
 - G140L at 1150 – 1700 \AA .
 - G230L (MAMA) or G230LB (CCD) at 1600 – 3100 \AA .
 - G430L at 2900 – 5700 \AA .
 - G750L at 5250 – $10,300 \text{ \AA}$.
- For resolutions of $\sim 50 \text{ km sec}^{-1}$ use:
 - G140M at 1150 – 1700 \AA .
 - G230M (MAMA) or G230MB (CCD) at 1650 – 3100 \AA .
 - G430M at 3050 – 5600 \AA .
 - G750M at 5450 – $10,100 \text{ \AA}$.

Figure 4.8: Wavelength Coverage Versus Kinematic Resolution of First-Order Modes. The hatches indicate the wavelength coverage at a single scan setting.



4.2.2 Slits for First-Order Spectroscopy

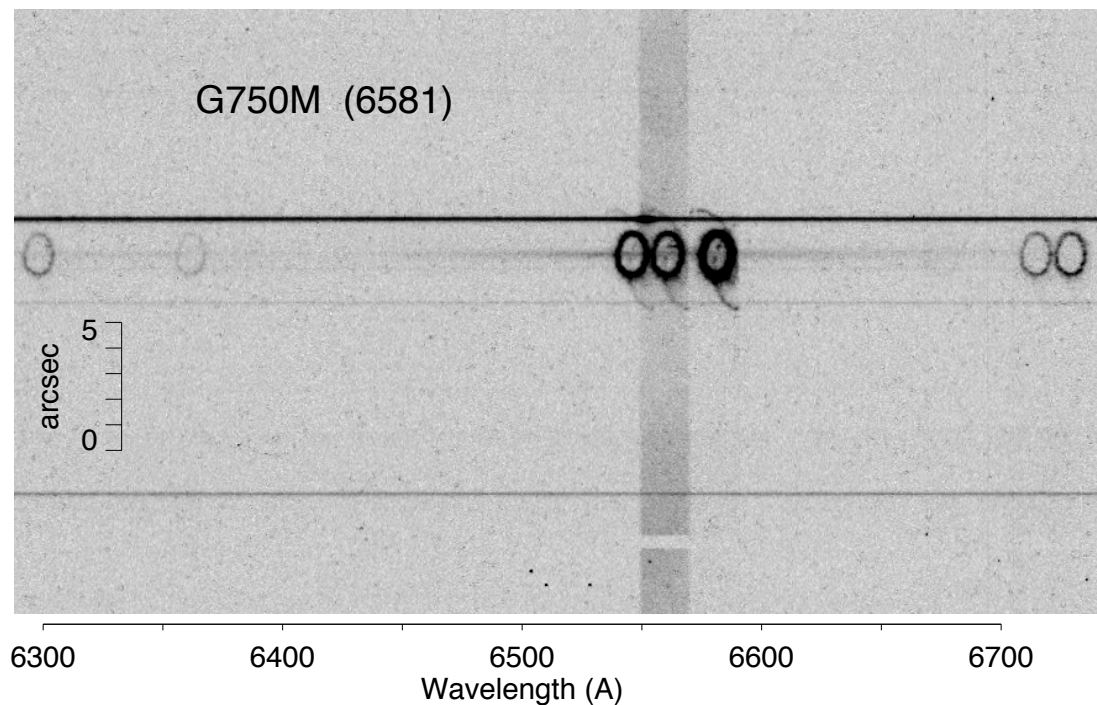
Supported for use with the first-order gratings are long slits of widths 0.05, 0.1, 0.2, 0.5 and 2.0 arcseconds (in the dispersion direction), and lengths of 52 arcseconds (as projected on the CCD detector) or 25 arcseconds (as projected on the MAMA detectors) for the MAMA low-resolution, first-order gratings (G230L and G140L) and 28 arcseconds for the MAMA intermediate-resolution, first-order gratings (G230M and G140M).¹ Note that the 0.1 arcsecond width matches the 2 pixel resolution of the CCD, while the 0.05 arcsecond width does so for the MAMAs, providing maximum spectral resolution. The 0.2 arcsecond-wide slit is the general utility slit used most often; it provides a good compromise between resolution and throughput. Programs requiring accurate absorption-line measurements in continuum sources should always use slits of widths ≤ 0.2 arcsecond, since for larger apertures the spectral purity is significantly degraded by the telescope plus instrumental Point-Spread Function (PSF); see Section 13.7. Finally, we expect the wider 0.5 and 2.0 arcsecond slits to be used predominantly in

1. The MAMA first-order modes have varying spatial plate scales; see Chapter 13.

photon-starved ultraviolet observations of extended sources, but provide them for use in the optical as well to assure that line-ratio studies with coverage from the ultraviolet to the optical can sample the same physical region on the sky. Additionally, they are the most photometric slits as their throughput is least affected by centering and telescope breathing. Of course, observations of *extended* sources with wide slits will have correspondingly degraded spectral resolutions.

The first-order gratings can also be used “slitless” to obtain two-dimensional spectra of targets, or pseudo “images.” Slitless spectroscopic data will not be fully calibrated by the STScI pipeline, and it will require directed post-observation data processing by the user, as ambiguous overlap of wavelengths from different parts of sources can occur in the image (see Section 12.1). Figure 4.9 shows an example of the use of the 52X2 slit with the G750M grating to obtain such a series of emission line images of SN1987A.

Figure 4.9: STIS G750M 6581 Å 52X2 Spectral Image of SN1987A. This shows the images of the inner circumstellar ring in [OI], H α , [NII], and [SII]. Diffuse H α emission from the LMC fills the 52X2 slit, and broad H α emission from the SN is also visible. The continua of stars produce the horizontal bands. The image shown is a 950 x 450 subsection of the 1024 x 1024 image. (Figure courtesy of Jason Pun and George Sonneborn, see also Sonneborn et al. 1998, ApJ, 492, L139).



Note that for the FUV-MAMA first-order modes, the projection of the spectrum on the detector has deliberately been shifted 120 low-resolution pixels or 3 arcseconds below center (3 arcseconds above center prior to March 15, 1999) to avoid having the spectrum fall on the shadow of the

repeller wire (see also Section 7.5 and Section 11.1.2). This shift applies to all data taken with the G140L and G140M gratings, regardless of the aperture used.

Note also that the monthly offsetting of MAMA first-order spectral modes can additionally shift the projection of the spectrum on the detector by up to $\sim \pm 40$ low-resolution AXIS2 pixels (about 1 arcsecond). See Section 7.5 for further discussion.

The 0.2X0.2 aperture is now supported for use with all first-order gratings. This is intended to be used for observations where a long slit might allow light from another target into the aperture, thereby creating either contamination problems or bright object concerns. Note, however, that the use of such a short slit will make background subtraction more difficult, especially at wavelengths where airglow lines are important.

4.2.3 STIS Pseudo-aperture Positions

A number of "pseudo-aperture" positions have been defined for STIS spectroscopy which allow a target to be placed at positions other than the geometrical center of the aperture without the need to specify a POS TARG. These include the E1 and E2 positions which place the target closer to the CCD readout to minimize losses due to charge transfer inefficiency (CTI), and the D1 aperture positions, which can be used to place a faint target near the bottom of the FUV MAMA detector, where the dark current is significantly reduced. Note that the E1 positions may be used with any first-order STIS CCD grating. The E2 positions may only be used with G750M and G750L. The D1 positions may only be used with the G140L and G140M gratings.

Here we describe these pseudo-aperture locations and their intended purposes. Note that all of these pseudo-apertures define new positions within existing apertures. As a result, the APERTURE keyword in the headers of the archived data will contain the name of the parent aperture, while the PROPAPER keyword will contain the aperture name specified in the Phase II proposal. For example, if the Phase II proposal requests the 52X0.1D1 position, the APERTURE keyword will be set to 52X0.1, while the PROPAPER keyword will be 52X0.1D1.

E1 Aperture Positions to decrease CTE Loss

As the STIS CCD detector has accumulated radiation damage over time, the Charge Transfer Efficiency (CTE) has decreased (see Section 7.2.6). For faint sources observed near the center of the CCD detector, this can result in loss of 18% or more of the detected signal during the readout. Since the amount of these CTE losses depends on both the observed signal and background counts, there is no simple way to correct for these losses, and they can significantly affect the shape of a measured spectrum. Noticeable effects can be seen even in well exposed spectra. In addition to

its effects on the counts from the observed astronomical source, CTE effects re-distribute some of the electrons in hot pixels and cosmic rays into “tails” that lag behind during the readout. These tails add significant background noise to long exposures that is not taken into account by the STIS Exposure Time Calculator (ETC), and which can be difficult to remove.

All of these effects can be significantly ameliorated by moving the location of the source image on the detector closer to the amplifier, thereby reducing the number of parallel transfers that occur during the readout. To this end, new aperture positions (52X0.05E1, 52X0.1E1, 52X0.2E1, 52X0.5E1, and 52X2E1) have been defined near row 900 on the STIS CCD detector for use with the STIS first-order gratings. The use of these new aperture positions is strongly recommended for the observation of faint sources. For high signal-to-noise observations of bright targets we recommend continuing to use the regular aperture positions near the center of the detector. Extensive calibration observations were planned during cycles 11 and 12 to ensure that the calibration at the E1 aperture positions is of the same quality as it is for sources observed at the usual location on the STIS CCD. Further information regarding the use of these new aperture positions can be found in Section 7.2.7.

E2 Aperture Positions for Better Fringe Flats

In 1999, the E1 aperture positions were introduced to allow first-order CCD spectra to be positioned at row 900 near the CCD readout amplifier, thereby reducing the effects of Charge Transfer Inefficiency (CTI). This works well, however, for G750L and G750M spectra taken near row 900, the fringe flats have to be done using the 52X0.1 aperture rather than the 0.3X0.09 aperture, which is usually used for fringe flats near the center of the detector (see Section 11.2.3 for a more detailed discussion of IR fringe flats). Unfortunately, the 52X0.1 slit is shifted by about one pixel in the dispersion direction from the centers of the wider long slits. This misalignment reduces the accuracy of fringe subtraction.

To address this, we have defined three new aperture locations: 52X0.2E2, 52X0.5E2, and 52X2E2. When these apertures are specified, the target is placed off-center in the slit, at a position coincident with the 52X0.1E1 aperture. This improves the match between the fringes in the target and lamp spectra. Be aware, however, that the 52X0.2E2 aperture position is offset sufficiently from the physical center of the aperture that there will be noticeable changes in the aperture throughput.

These E2 aperture positions should only be used for ACCUM exposures with the G750L or G750M gratings when fringe flats with the 52X0.1 aperture are also being done. If a peakup is desired before using the E2 apertures, the peakup should be done using the 52X0.1E1 aperture.

D1 Aperture Positions for Low FUV Dark Current

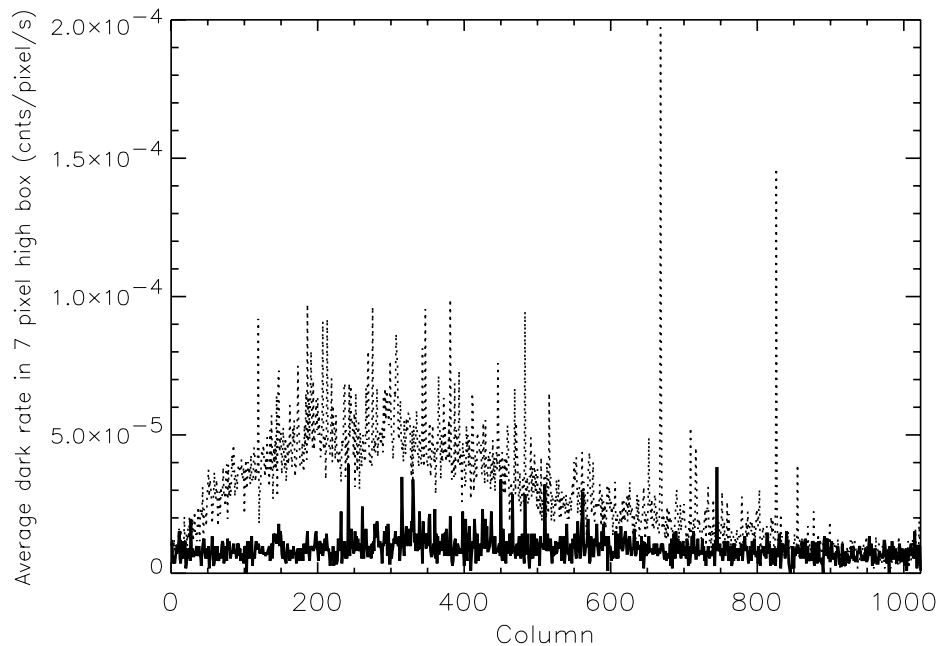
The FUV MAMA suffers from an irregular dark glow that varies unpredictably in intensity. When this glow is absent, the typical dark rate of the FUV MAMA detector is about 6×10^{-6} cts/pixel/s. When the glow is strong, it can enhance the dark current to as much as 1×10^{-4} cts/pixel/s over a large fraction of the detector. For first-order spectra, the best way to minimize this extra dark current is to put the target at a location on the detector where the extra dark current is small.

For first-order spectra of faint sources less than about 1" in angular extent, we recommend that this be done by placing the target about 2" above the bottom edge of the FUV MAMA detector. Since for the G140L and G140M the regular aperture positions are projected about 3" below the center (in order to avoid the shadow of the FUV MAMA repeller wire), an additional displacement of about -6.8" is required in the cross-dispersion, or y, direction. This can reduce the extra dark current by up to a factor of 6 (see Figure 4.10). For G140L observations, the default D1 position will place the spectrum about 2 arcseconds above the bottom edge of the detector. The monthly offsetting of the spectral location (see Figure 7.5) will shift this by as much as ± 1 arcsecond. Because of the larger cross dispersion plate scale of the G140M, variations of the default spectral position for different G140M CENWAVE values, and the monthly spectral offsetting, G140M spectra taken at the D1 aperture positions will be located 3 to 5 arcseconds above the bottom edge of the FUV MAMA detector.

Note that the background subtraction might be more difficult due to the proximity to the edge of the detector, depending on the extent of the target. Therefore, use of this position is recommended only for objects sufficiently faint that the FUV MAMA dark current is the major limitation on the achievable accuracy.

The D1 apertures listed in the Table 4.4 will be supported for first-order spectroscopic ACCUM or TIME-TAG observations with the G140L and G140M. The 52X0.1D1 and 52X0.05D1 are also supported for CCD ACQ/PEAK observations. Note that the 25MAMAD1, F25QTZD1, and F25SRF2D1 aperture locations are intended only for first-order FUV MAMA slitless spectroscopy. Users who wish to offset faint imaging targets to avoid the worst of the FUV dark current should look at Figure 7.18 or consult with a STIS Instrument Scientist via help@stsci.edu.

Figure 4.10: The FUV MAMA mean dark current as a function of the detector column number (in a seven pixel high extraction box near the standard extraction position located 3" below the detector center)-(dotted line)- is compared with that in a box near the proposed pseudo-aperture position 6.8" further down (solid line). The data used are an average of 116 dark monitor exposures, each of 1380 seconds, taken between July 2001 and September 2002. This illustrates the typical reduction in the dark current affecting first-order spectra that will result from putting the target 2" above the bottom of the detector.



Sensitivity Differences at the Pseudo-aperture Positions

The throughput of the E1 and D1 apertures as a function of wavelength is similar to that of the corresponding regular positions. However, there is some vignetting of the gratings that changes the overall system throughput slightly with varying position along the slit. At the E1 positions, the overall low dispersion throughputs are decreased by 2 to 3%, while at the D1 position the G140L throughput is increased by 2 to 7%. Throughput changes for the medium resolution gratings are not well characterized, but should be similar. Since these throughput changes do not depend simply on the wavelength, but also on the grating and the position on the detector, they are handled in the pipeline calibration by the use of low-order flat fields (lfl files) rather than by a change in aperture throughput curve.

The throughput of the 52X2E2 and 52X0.5E2 positions are similar to that of the corresponding E1 positions. For the 52X0.2E2 aperture, the throughput is about 20% lower than for the 52X0.2E1 position.

Table 4.4: Gratings supported with STIS pseudo-aperture positions.

Pseudo-aperture	Science Gratings	Supported Peak-up Elements
52X0.05E1	CCD first-order	CCD first-order, CCD Mirror
52X0.1E1	CCD first-order	CCD first-order, CCD Mirror
52X0.2E1	CCD first-order	none
52X0.5E1	CCD first-order	none
52X2E1	CCD first-order	none
52X0.2E2	G750L, G750M	none (52X0.1E1 recommended)
52X0.5E2	G750L, G750M	none
52X2E2	G750L, G750M	none
52X0.05D1	G140L, G140M	CCD first-order, CCD Mirror
52X0.1D1	G140L, G140M	CCD first-order, CCD Mirror
52X0.2D1	G140L, G140M	none
52X0.5D1	G140L, G140M	none
52X2D1	G140L, G140M	none
25MAMAD1	G140L, G140M	none
F25SRF2D1	G140L, G140M	none
F25QTZD1	G140L, G140M	none

4.2.4 Detailed First-Order Spectroscopic Information

The properties of each of the first-order gratings are described in detail, grating by grating, in Chapter 13; see the second-to-last column of Table 4.1 for easy reference to the appropriate page for each grating.

The detailed properties of the long slits (e.g., throughputs and line spread as functions of wavelength), plate scales, and encircled energies for the first-order gratings are presented under Section 13.4, Section 13.5, and Section 13.6.

4.3 Echelle Spectroscopy in the Ultraviolet

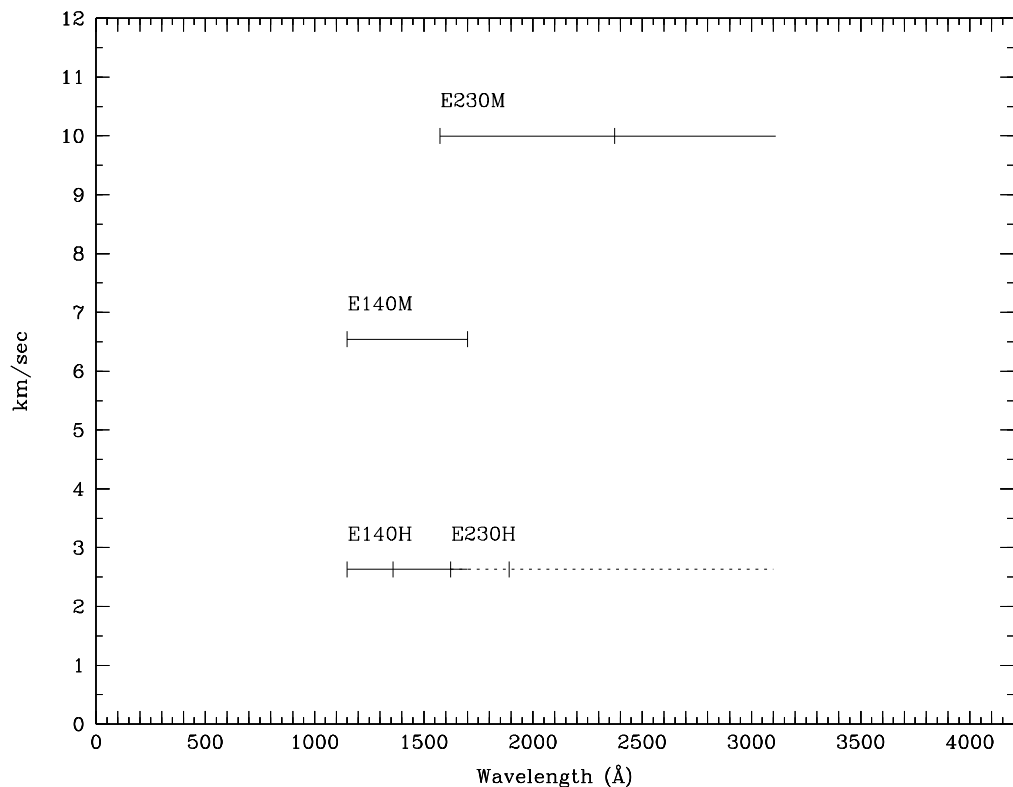
An example of STIS E230H echelle spectroscopy (both the echelle spectrum and a few sample extracted orders) of star CPD-59D2603 showing the interstellar absorption from the Carina Nebula is given in Figure 15.3. (See also Walborn et al. 1998, ApJ, 492, L169.)

4.3.1 Echelle Gratings

There are four echelle grating modes which provide spectroscopic coverage from 1150 Å to 3100 Å at resolving powers from $R \sim 30,000$ to $R \sim 110,000$. Through simultaneous observation of multiple orders, they are designed to maximize the spectral coverage achieved in a single exposure of a point source. Figure 4.11 below summarizes the wavelength coverage and kinematic resolutions of the echelle gratings. In short:

- For $\sim 10 \text{ km sec}^{-1}$ resolution use:
 - E140M at 1150–1700 Å.
 - E230M at 1600–3100 Å.
- For $\sim 2.5 \text{ km sec}^{-1}$ resolution use:
 - E140H at 1150–1700 Å.
 - E230H at 1600–3100 Å.

Figure 4.11: Echelle Wavelength Coverage vs. Kinematic Resolution. Hatches indicate wavelength coverage at a single scan setting. The dashed line shows the E230H coverage. See Table 4.1 and Chapter 13 for more details.



4.3.2 Slits for Echelle Spectroscopy

Short echelle slits, which ensure order separation, are available for use with the echelle gratings. For each mode a short slit of width 0.2 arcsecond is provided, along with a slit whose width matches a two pixel projection in the dispersion direction; either 0.09 arcsecond for the H modes, or 0.06 arcsecond for the M modes. In addition, an ultra-narrow slit of width 0.025 arcsecond (0.1X0.03 in the Proposal Instructions) is supported with all of the echelles, for the highest spectral resolution of bright objects. Also, two multi-slits with different widths (called the FP-SPLIT slits) are supported for use with the echelles to provide optimally placed multiple exposures which maximize S/N. Their use is discussed in Chapter 12.

Although we do not recommend routine use, the echelle gratings can be used with a long slit (the 6X0.2 slit) to obtain echelle spectroscopy of extended objects with weak continua. Long-slit echelle data, however, will not be calibrated by the STScI pipeline, and they will require more extensive post-observation processing by the user since ambiguous overlap of wavelengths from different parts of sources will occur in the image (see Section 12.2 if you are considering such observations). In addition to the spectral purity considerations in the dispersion direction mentioned above for the first-order gratings, echelle observations are subject to contamination in the cross-dispersion direction by scattered light. This effect is aggravated toward shorter wavelengths as the orders become more crowded. Continuum sources should never be observed with slit lengths greater than 0.2 arcsecond, and even then special data analysis may be required to optimize the accuracy of the results. See Section 13.7.

4.3.3 Detailed Echelle Information

The properties of each of the echelle gratings are described in detail, grating by grating, in Chapter 13; see the second-to-last column of Table 4.1 for easy reference to the appropriate page for each grating.

The detailed properties of the echelle slits (e.g., throughputs and line spreads as functions of wavelength), the plate scales, and the encircled energies for the echelle modes are presented under Section 13.4, Section 13.5, and Section 13.6.

4.4 Objective-Prism Spectroscopy

The STIS PRISM is used with the STIS/NUV-MAMA and provides spectra from 1150 to 3620 Å at resolving powers of up to ~2500 in the far-ultraviolet declining to ~10 at optical wavelengths. In Figure 4.12 we compare a direct NUV MAMA image of the star cluster NGC 604 with a

PRISM exposure of the same field. This example illustrates the power of the prism mode to simultaneously provide spectra covering a wide wavelength range of many objects in a single field of view. Note that the ACS also has the capability of performing slitless UV spectroscopy. See Section 4.1.2 for a comparison of these capabilities.

As can be seen in Figure 4.12, an NUV objective-prism spectrum does not cover the full range of the detector in the dispersion direction. In many cases, there will be a significant number of counts only over an extent of ~ 200 pixels due to the large dispersion and low sensitivity at short wavelengths. This characteristic can be an advantage over a grating such as the G230L in crowded fields, since it reduces the possibility of overlap between different sources.

The PRISM can be used at two wavelength settings, 1200 and 2125 Å. These are approximately the wavelengths that will lie at the center of AXIS1 on the detector for the two settings. The relationship between wavelength and pixel number along the central spectral trace is shown in Figure 4.13 for each setting. The dispersion as a function of wavelength is shown in Figure 4.14 for each setting.

Figure 4.12: NUV-MAMA image (left) and objective-prism exposure (right) of NGC 604, a Scaled OB Association, obtained under GO program 9096. The dispersion direction is nearly parallel to the x-axis.

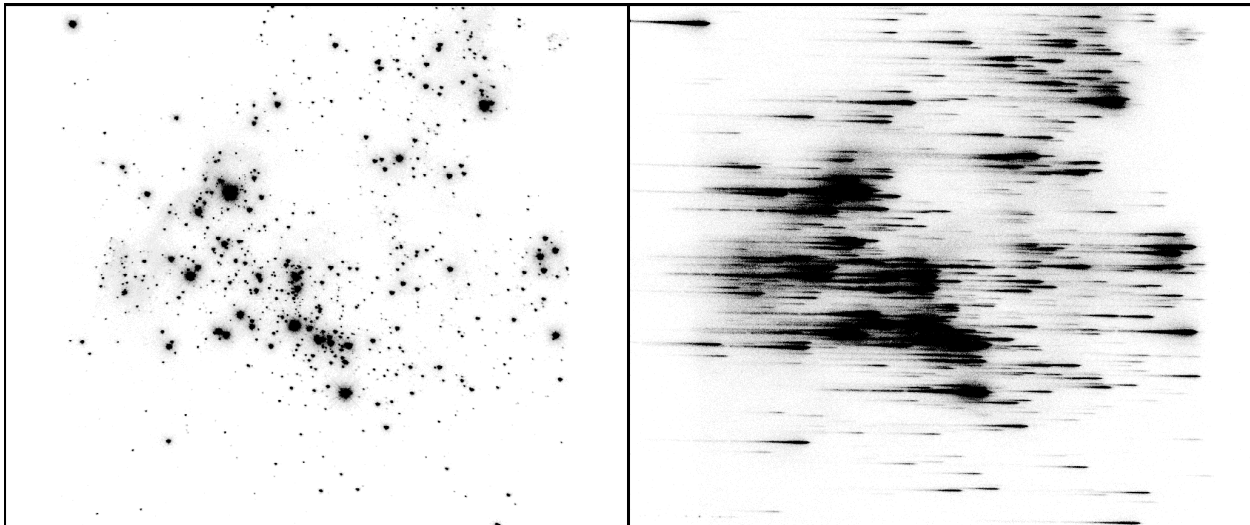


Figure 4.13: Wavelength vs. Pixel Number along the Central Spectral Trace for the PRISM at wavelength settings 1200 and 2125 Å.

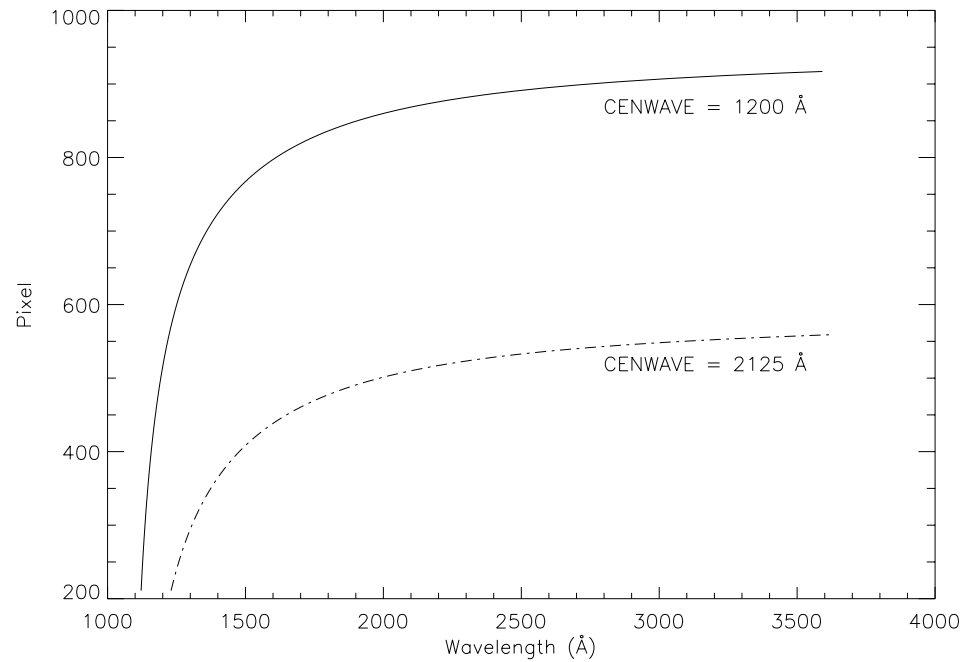
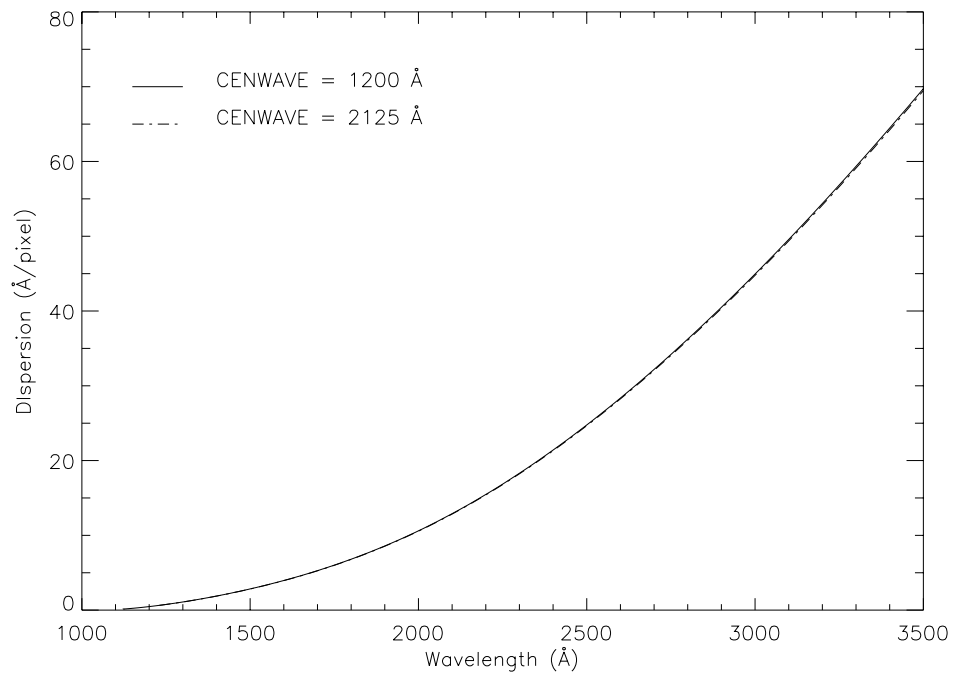


Figure 4.14: Dispersion as a function of wavelength for the PRISM at wavelength settings 1200 Å (solid) and 2125 Å (dot-dash). The lines for the two settings nearly overlap.



The PRISM can be used with the clear MAMA aperture (25MAMA) or with either longpass ultraviolet filtered aperture (F25SRF2 or F25QTZ) to

provide a 25x25 arcsecond field of view (see also “F25SRF2—NUV-MAMA, Longpass” on page 421 and “F25ND5—NUV-MAMA” on page 414). The longpass filter F25SRF2 blocks geocoronal Lyman- α 1216 Å and the F25QTZ longpass filter blocks both geocoronal Lyman- α and geocoronal O I 1302 + 1306 Å, significantly reducing the background from these lines (which is otherwise spread throughout the image) at the price of losing the short-wavelength range of the spectrum. In addition, the neutral-density filters (Table 5.1) are supported for PRISM spectroscopy, as are the 52X0.05, 52X0.1, 52X0.2, 52X0.5, and 52X2 long slits.

Observers will generally want to also obtain a *direct image* of the field when taking an objective prism spectrum, so they can later determine the centering of the objects in their prism data. Because the PRISM and the mirrors used for imaging are both in the Mode Selection Mechanism, zero-point shifts will occur between the PRISM and imaging data (see “Slit and Grating Wheels” on page 27). For a discussion of the observations needed to measure these shifts, see Section 12.1.

Note that slitless PRISM spectroscopy produces images in which, a priori, the wavelength at a given pixel is not known, and source-dependent overlap of spectra can occur. For these reasons, slitless PRISM spectroscopic data will not be calibrated automatically by the STScI pipeline. Instead, users will have to reduce and analyze their data off-line. The Spectrographs Branch at STScI is currently working on a self-extraction tool for objective-prism data.

CHAPTER 5: Imaging

In this chapter. . .

5.1 Imaging Overview / 63
5.2 Optical CCD Imaging / 74
5.3 Ultraviolet Imaging with the MAMA Detectors / 78
5.4 Neutral-Density Filters / 86

In this chapter we describe the imaging capabilities of STIS. Each imaging mode is described and plots of throughput and comparisons to the capabilities of WFPC2 and ACS are provided. (Signal-to-noise comparisons to WFPC2 assume the use of the WF chips.) Curves of sensitivity and exposure time as a function of source brightness to achieve a given signal-to-noise ratio are referenced in this chapter, but presented in Chapter 14. We note the existence of bright-object observing limits for MAMA imaging modes which are described in detail in Chapter 7, and tables of the MAMA imaging bright-object screening magnitudes as a function of mode and spectral type which are presented in Chapter 14.

5.1 Imaging Overview

STIS can be used to obtain images in undispersed light in the optical and ultraviolet. When STIS is used in imaging mode, the appropriate clear or filtered aperture on the slit wheel is rotated into position, and a mirror on the Mode-Selection Mechanism is moved into position (see Figure 3.1).

Table 5.1 provides a complete summary of the clear and filtered apertures available for imaging with each detector. In Figure 5.6 through Figure 5.9 we show the integrated system throughputs.

Table 5.1: STIS Imaging Capabilities

Aperture Name	Filter	Pivot ¹ Wavelength (λ_c in Å)	FWHM ¹ ($\Delta\lambda$ in Å)	Field of View (arcsec ²)	Detector	ref. page
<i>Visible - plate scale ~ 0.0507 arcseconds per pixel²</i>						
50CCD	Clear	5852	4410	52 x 52	STIS/CCD	395
F28X50LP	Optical longpass	7229	2722	28 x 52 ³	STIS/CCD	398
F28X50OIII	[O III]	5006	6	28 x 52 ³	STIS/CCD	401
F28X50OII	[O II]	3737	62	28 x 52 ³	STIS/CCD	404
50CORON	Clear + coronagraphic fingers	5852	4410	52 x 52	STIS/CCD	407
<i>Ultraviolet - plate scale ~0.0246 arcseconds per pixel²</i>						
25MAMA	Clear	2250 1374	1202 324	25 x 25	STIS/NUV-MAMA STIS/FUV-MAMA	409 436
F25QTZ	UV near longpass	2365 1595	995 228	25 x 25	STIS/NUV-MAMA STIS/FUV-MAMA	418 446
F25SRF2	UV far longpass	2299 1457	1128 284	25 x 25	STIS/NUV-MAMA STIS/FUV-MAMA	421 450
F25MGII	Mg II	2802	45	25 x 25	STIS/NUV-MAMA	423
F25CN270	Continuum near 2700 Å	2709	155	25 x 25	STIS/NUV-MAMA	426
F25CIII	C III]	1989	173	25 x 25	STIS/NUV-MAMA	429
F25CN182	Continuum near 1800 Å	1981	514	25 x 25	STIS/NUV-MAMA	432
F25LYA	Lyman- α	1221	72	25 x 25	STIS/FUV-MAMA	454
<i>Neutral-Density-Filtered Imaging</i>						
F25NDQ1 ⁴	ND=10 ⁻¹	1150–10,300 Å		13.4 x 9.7	STIS/NUV-MAMA STIS/FUV-MAMA STIS/CCD ⁵	416
F25NDQ2	ND=10 ⁻²			13.8 x 15.1		444
F25NDQ3	ND=10 ⁻³			11.4 x 15.3		
F25NDQ4	ND=10 ⁻⁴			11.8 x 9.5		
F25ND3	ND=10 ⁻³	1150–10,300 Å		25 x 25	STIS/NUV-MAMA STIS/FUV-MAMA STIS/CCD ⁵	412 440
F25ND5	ND=10 ⁻⁵	1150–10,300 Å		25 x 25	STIS/NUV-MAMA STIS/FUV-MAMA STIS/CCD ⁵	414 442

1. See Section 14.2.1 for definition of pivot wavelength and FWHM.

2. The CCD and MAMA plate scales differ by about 1% in the AXIS1 and AXIS2 directions, a factor that must be taken into account when trying to add together rotated images. Also, the FUV-MAMA uses a different mirror in the filtered and unfiltered modes. In the unfiltered mode, the plate scale is 0.3% larger (more arcsec/pixel). Information on geometric distortions can be found in Section 14.6.

3. The dimensions are 28 arcsec on AXIS2=Y and 52 arcsec on AXIS=X. See Figure 3.2 and Figure 11.1.

4. Information on the F25NDQ aperture can be found on page 360.

5. The neutral density filters can only be used as available-but-unsupported apertures with the CCD detector.

5.1.1 STIS versus ACS Imaging

The Advanced Camera for Surveys (ACS) was installed on HST during servicing mission SM3B in March of 2002, and has been performing very well since that time. Compared with STIS, ACS offers detectors with a much larger field of view, significantly higher throughputs at most wavelengths, a wider selection of filters, better suppression of point spread function (PSF) wings, and newer CCD detectors with far less accumulated radiation damage. Observers will therefore find that, especially at optical wavelengths, most imaging programs are better and more efficiently done with ACS than with STIS. There will, however, still be some cases where imaging with STIS is a better choice. The following points should be considered when choosing between STIS with ACS imaging:

- STIS does have a few filters that offer capabilities not duplicated by ACS. These include the narrow band STIS CCD F28X50OII filter, and the STIS NUV-MAMA F25MGII and F25CIII filters. The NUV-MAMA intermediate band F25CN182 and F25CN270 filters may also prove useful for some programs.
- For very deep optical imaging, ACS WFC imaging with F606W or F814W will usually be a better choice than the STIS 50CCD or F28X50LP configurations (see Figure 5.1).
- For many programs the ACS HRC with the F220W or F250W filter should be considered as an alternative to broadband imaging with the STIS NUV-MAMA (see Figure 5.2 and Figure 5.3). The NUV MAMA has no read noise, a very low red sensitivity (so that filter redleaks have very little impact), and a lower dark current (the MAMA's dark current advantage over the HRC should increase as the HRC CCD ages), while the HRC has a higher peak sensitivity and, unlike the NUV-MAMA detector, is not subject to bright object constraints. The NUV-MAMA does have a slightly smaller pixel size than the HRC, but the much cleaner PSF of the HRC will often offset this advantage when attempting to detect faint sources near bright objects. Furthermore, there is a significant focus change with position across the STIS NUV-MAMA (see Section 5.1.3). The final choice between the NUV-MAMA and the ACS HRC will depend on the details of each program's science requirements.
- The choice between the STIS FUV-MAMA and ACS SBC for far-ultraviolet imaging also largely depends on the details of the science requirements. ACS offers a larger variety of filters and better throughput at most wavelengths (see Figure 5.4 and Figure 5.5). On the other hand, the STIS FUV-MAMA has better sampling of the PSF, thus providing higher spatial resolution. The STIS FUV-MAMA generally has a lower dark current (see Section 7.4.2).

Figure 5.2: The throughput of the NUV-MAMA with the 25MAMA, F25QTZ, and F25SRF2 apertures is compared with that of the ACS HRC F220W and F250W.

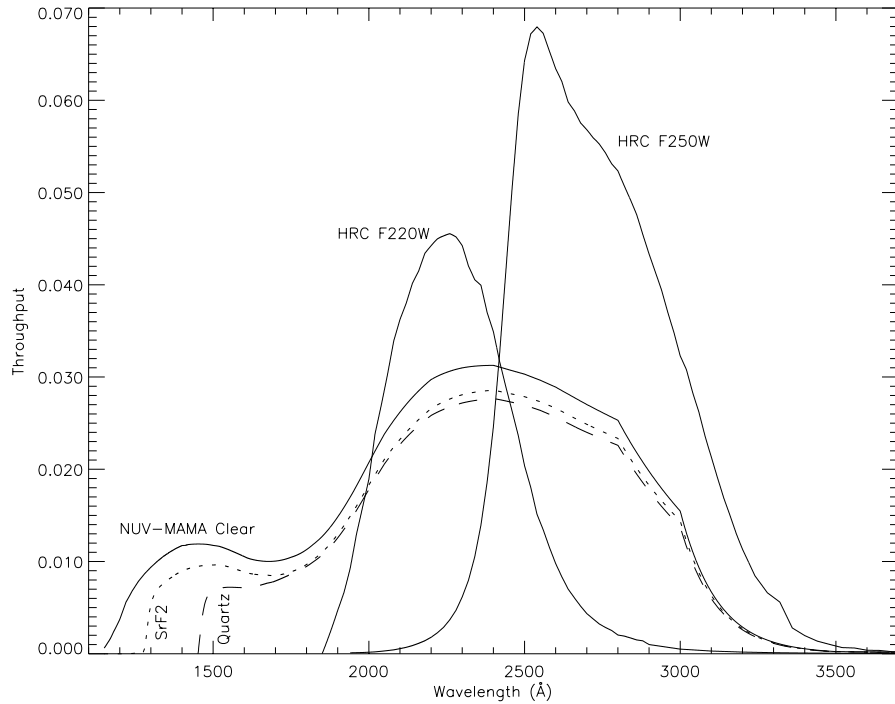


Figure 5.3: Exposure time required to reach S/N=10 versus the target V magnitude, for various STIS NUV-MAMA and ACS HRC filtered configurations, assuming a B1 V target spectrum. The relative sensitivities of the various configurations will depend strongly on the shape of the target object's spectrum.

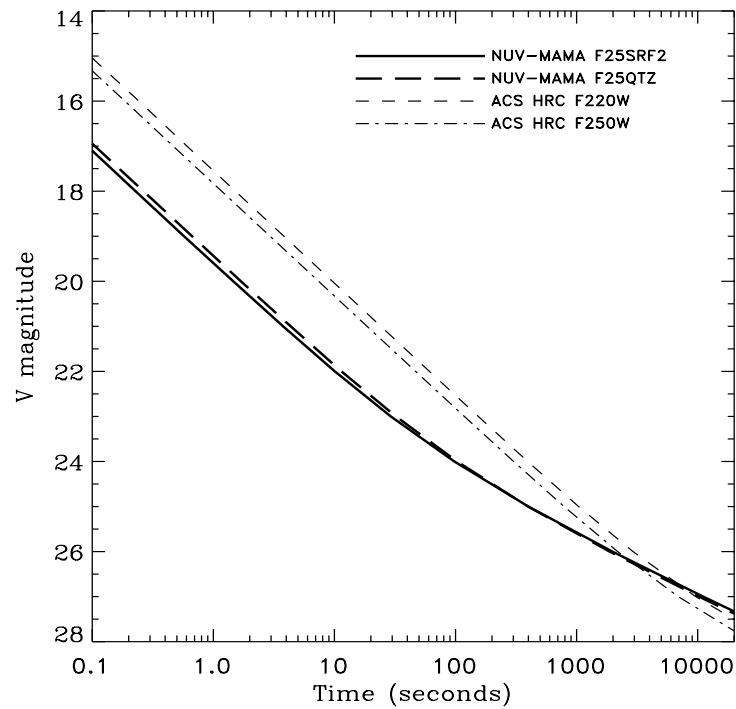


Figure 5.4: The throughputs of STIS FUV-MAMA configurations (solid lines) are compared with the filtered ACS SBC detector throughputs (dotted lines).

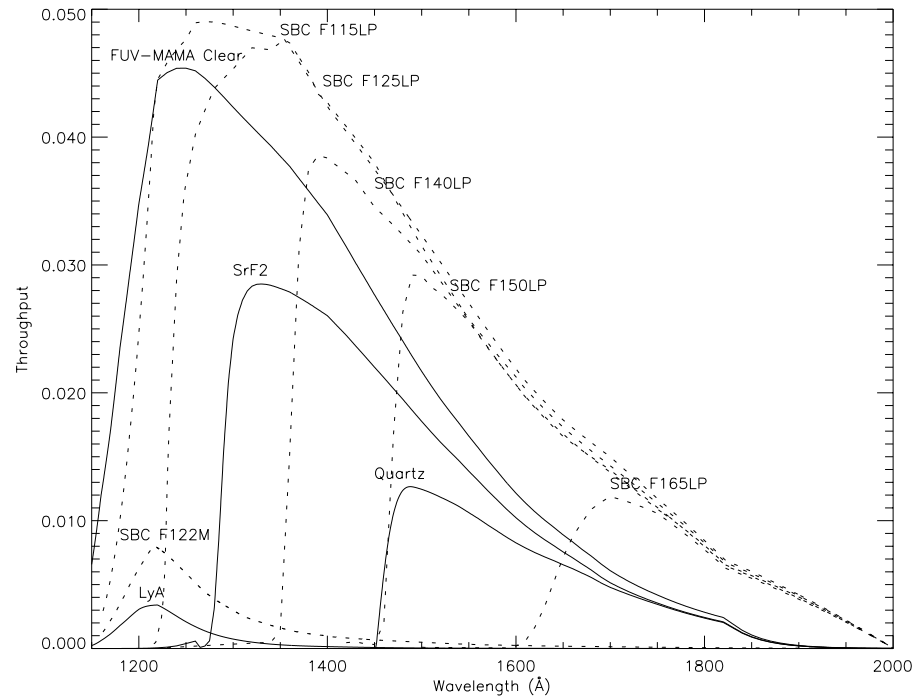
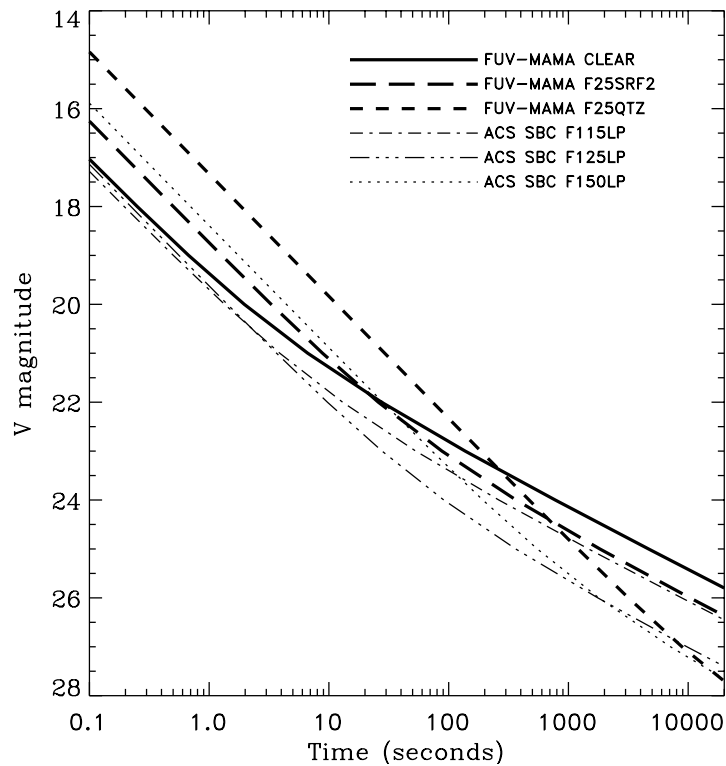


Figure 5.5: Exposure time required to reach S/N=10 versus the target's V magnitude, for various STIS FUV-MAMA and ACS SBC filtered configurations, assuming a B1 V target spectrum. The relative sensitivities of the various configurations will depend very strongly on the shape of the target object's spectrum.

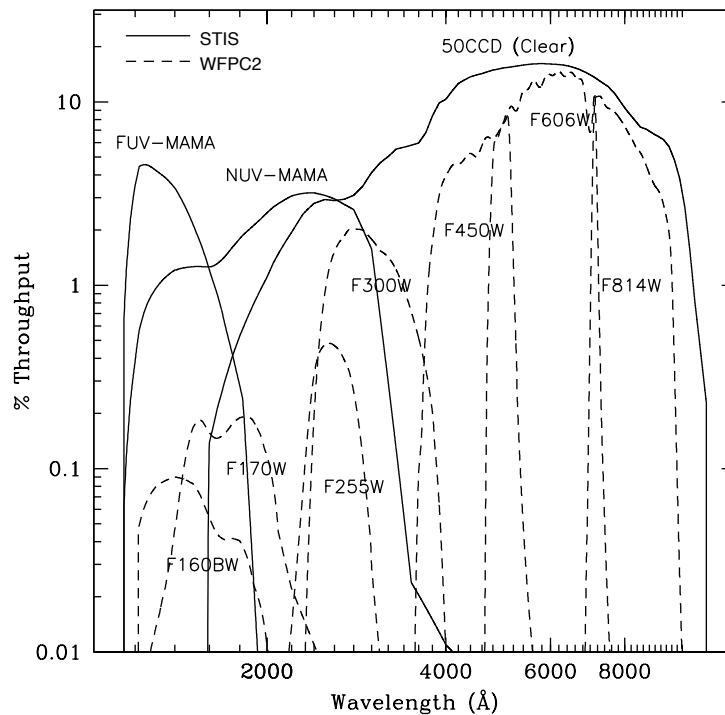


5.1.2 STIS vs. WFPC2 Imaging

While ACS has clear advantages over either STIS or WFPC2 for most prime GO imaging science, the great success of ACS also means that there will be ample opportunities for parallel observing with the other HST instruments. It is therefore still useful to compare the imaging capabilities of STIS and WFPC2.

- The STIS CCD detector, although it covers a much smaller field of view (52×52 arcsec) than WFPC2, has higher throughput over a much wider range of the spectrum (2000–11,000 Å). The STIS CCD also has a low read noise and dark current; thus STIS CCD observations with the clear 50CCD aperture have significantly higher sensitivity to faint sources than WFPC2 (see Figure 5.6). The CCD long-pass imaging filter, F28X50LP, has similar sensitivity longward of 5500 Å. The STIS CCD also has a low read noise and dark current; thus STIS CCD observations with the clear or long-pass apertures are extremely sensitive to faint sources (see Figure 5.6). The STIS CCD clear imaging mode is especially useful when no color information is needed, for example, for finding faint variable sources, or imaging the faintest possible sources in a given integration time.
- The wings of the point-spread function in the STIS CCD imaging modes are suppressed by an internal Lyot stop. This feature provides a significant advantage for detecting faint sources near much brighter sources.
- The STIS FUV-MAMA detector enables true solar-blind imaging with high throughput from 1150 to 1700 Å with a considerably higher throughput than WFPC2. The NUV-MAMA is also relatively insensitive to red light and has also high relative throughput. Both provide near-critical sampling of the PSF (0.024 arcsecond per pixel).
- Remember that, because of the need to screen all MAMA observations for the presence of bright objects, the STIS MAMA detectors cannot be used for pure parallel observing, and can only be used for coordinated parallels when an exact orientation is specified.
- Charge Transfer Inefficiency (CTI) is larger for WFPC2 ($\geq 4\%$) compared to the STIS CCD (1%).

Figure 5.6: STIS's Clear Imaging Throughputs Versus WFPC2



5.1.3 Caveats for STIS Imaging

There are several important points about imaging with STIS which should be kept in mind:

- The filters are housed in the slit wheel, and while they are displaced from the focal plane, they are not far out of focus. This location means that imperfections (e.g., scratches, pinholes, etc.) in the filters cause artifacts in the images. These features do not directly flat-field out because the projection of the focal plane on the detector shifts from image to image due to the nonrepeatability of the Mode Selection Mechanism's (MSM) placement of the mirror (careful post-processing may be able to account for registration errors).
- The quality of the low-order flat fields for the MAMA imaging modes limits the photometric accuracy obtained over the full field of view (see Section 16.1).
- The focus varies across the field of view for imaging modes, with the optical performance degrading by $\sim 40\%$ at the edges of the field of view for MAMA and by $\sim 30\%$ for the CCD (see Section 14.7).
- STIS CCD imaging slightly undersamples the intrinsic PSF. The use of dithering (See Section 11.3) to fully sample the intrinsic spatial resolution and to cope with flat-field variations and other detector nonuniformities may be useful for many programs.
- Two of the STIS narrow-band filters (F28X50OIII and F25MGII) have substantial red leaks (see Figure 5.11 and Figure 5.16, respectively).

- The STIS CCD will have far more “hot” pixels and a much higher dark current than the newer ACS CCDs. Relative to WFPC2, a STIS CCD image will have a slightly larger proportion of the pixels affected by cosmic rays and “hot” dark current.
- Programs requiring high photometric precision at low count levels with the CCD should use `GAIN=1`; programs at high count levels should use `GAIN=4`. At `GAIN=4` the CCD exhibits a modest read-noise pattern that is correlated on scales of tens of pixels. (See Section 7.1.8.)
- At wavelengths longward of $\sim 9000 \text{ \AA}$, internal scattering in the STIS CCD produces an extended PSF halo (see Section 7.3.4). Note that the ACS WFC CCDs have a front-side metallization that prevents a similar problem in that camera.
- The dark current in the MAMA detectors varies with time due to temperature fluctuations, and in the FUV-MAMA, it also varies strongly with position, although it is far lower overall than in the NUV-MAMA (see the discussion of Section 7.4.2).
- The repeller wire in the FUV-MAMA detector (see Section 7.3) leaves a 5-pixel-wide shadow that runs from approximately pixel 0,543 to 1024,563 in a slightly curved line. The exact position of the wire varies with the optical element used.
- The Charge Transfer Efficiency (CTE) of the STIS CCD is decreasing with time. The effects of the CTE decline are most serious for the lower rows of the detector and for faint sources with low background levels. For further details see Section 7.2.6.

These caveats are not intended to discourage observers from using STIS for imaging; indeed, for many imaging projects, particularly those not requiring a large field of view or the range of filters provided by WFPC2 and ACS, STIS may be the best choice.

5.1.4 Throughputs and Limiting Magnitudes

In Figure 5.6 above, we show the throughput (where the throughput is defined as the end-to-end effective area divided by the geometric area of a filled, unobstructed, 2.4 meter aperture) of the three STIS clear imaging modes, with the CCD, the NUV-MAMA, and the FUV-MAMA. Superposed on this plot, we show the broadband WFPC2 throughputs. In Figure 5.7, Figure 5.8, and Figure 5.9, we show the throughputs of the full set of available filters for the CCD, the NUV-MAMA, and the FUV-MAMA, respectively.

Figure 5.7: STIS CCD Clear and Filtered Imaging Mode Throughputs

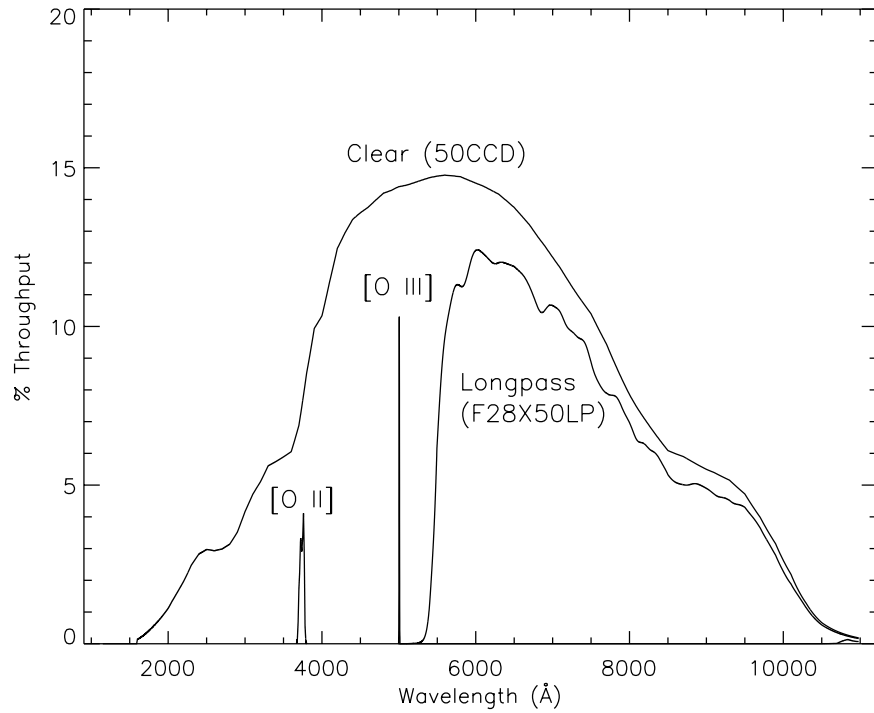


Figure 5.8: STIS NUV-MAMA Clear and Filtered Imaging Mode Throughputs

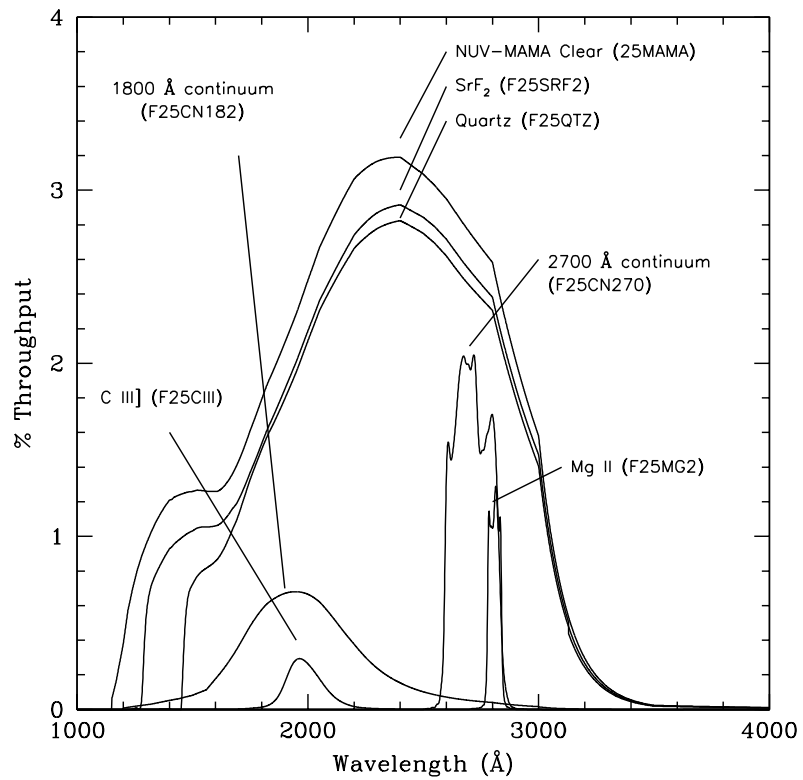
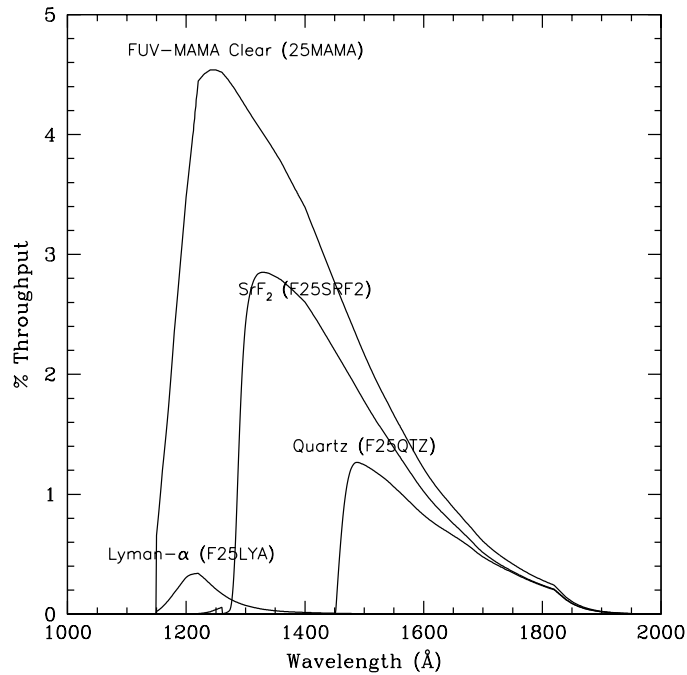


Figure 5.9: STIS FUV-MAMA Clear and Filtered Imaging Mode Throughputs



Limiting Magnitudes

In Table 5.2 below, we give the A0 V star V magnitude reached during a one-hour integration which produces a signal-to-noise ratio of 10 integrated over the number of pixels needed to encircle 80% of the PSF flux. The observations are assumed to take place under average zodiacal background and low earth shine conditions. These examples are for illustrative purposes only and the reader should be aware that for dim objects, the exposure times can be highly dependent on the specific background conditions. For instance, if a 26.9 magnitude A star were observed under high zodiacal light and high earth shine, the exposure time required to reach signal-to-noise of 10 with CCD clear would be twice as long as the one stated in Table 5.2.

Table 5.2: Limiting A Star V Magnitudes*

Detector	Filter	Magnitude	Filter	Magnitude
CCD	Clear	26.9	[O II]	21.5
CCD	Longpass	26.0	[O III] ¹	20.7
NUV-MAMA	Clear	24.1		
NUV-MAMA	Longpass quartz	24.1	Longpass SrF ₂	24.1
NUV-MAMA	C III]	19.4	1800 Å continuum	21.4
NUV-MAMA	Mg II ¹	20.4	2700 Å continuum ¹	22.1
FUV-MAMA	Clear	20.9	Lyman-α	16.0
FUV-MAMA	Longpass quartz	21.7	Longpass SrF ₂	22.4

1. These filters have substantial red leaks (see “[O III]—F28X50OIII” on page 76, “Mg II—F25MGII” on page 83, and “2700 Å Continuum—F25CN270” on page 84).

5.1.5 Signal-To-Noise Ratios

In Chapter 14 we present, for each imaging mode, plots of exposure time versus magnitude to achieve a desired signal-to-noise ratio. These plots, which are referenced in the individual imaging-mode sections below, are useful for getting an idea of the exposure time you need to accomplish your scientific objectives. More detailed estimates can be made either by using the sensitivities given in Chapter 14 or by using the [STIS Imaging Exposure Time Calculator](#). The exposure time calculator is also available as part of the [APT](#) package.

5.1.6 Saturation

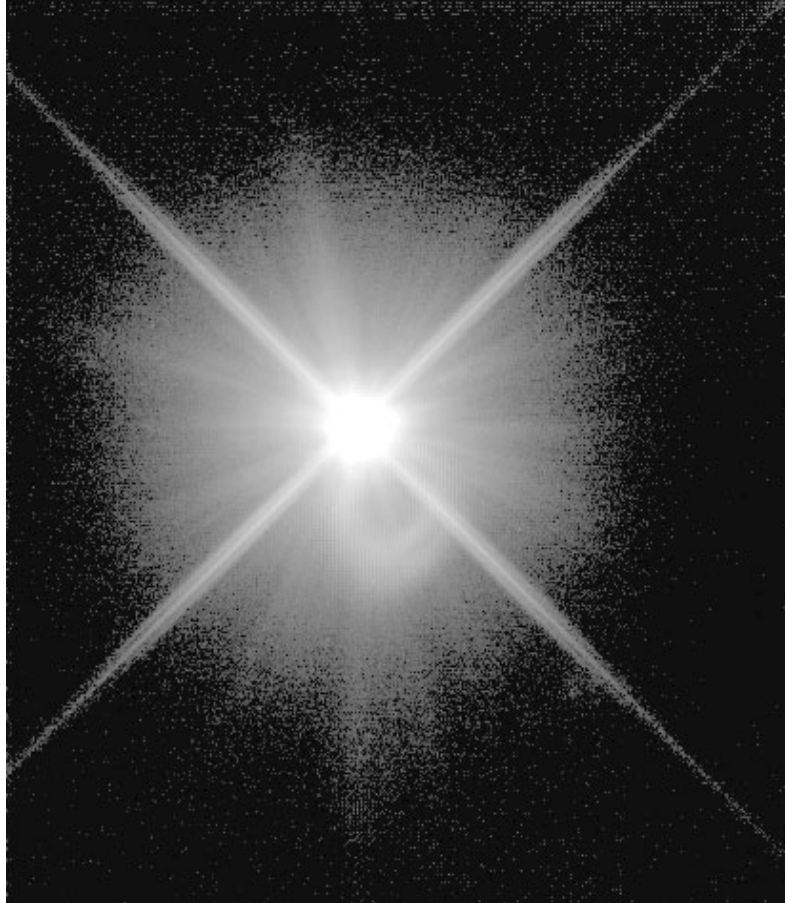
Both CCD and MAMA imaging observations are subject to saturation at high total accumulated counts per pixel: the CCD due to the depth of the full well and the saturation limit of the gain amplifier for $\text{CCDGAIN} = 1$; and the MAMA due to the 16-bit format of the buffer memory (see Section 7.2.1 and Section 7.4.1). In Chapter 14, saturation levels as functions of source magnitude and exposure time are presented in the S/N plots for each imaging mode.

5.2 Optical CCD Imaging

The CCD imaging capability of STIS was designed primarily for target acquisitions, and therefore, only a small number of filters are available. Nevertheless, STIS CCD imaging has scientific utility of its own, due to the high throughput and relatively low read noise of the CCD detector. STIS CCD imaging can be obtained as prime pointings or in parallel with other instruments.

The optical performance of the CCD in imaging mode is good, and the plate scale of the CCD is 0.0507 arcsecond per pixel, providing a good compromise between sampling of the PSF and field of view. There is some degradation of the image quality towards the edge of the field. Observers can assume that 15 to 20% of the light from a point source falls in a single STIS CCD pixel and that ~80% of the light from a point source is contained within a 5 x 5 pixel region. An image of a typical point source is shown in Figure 5.10. See Chapter 14 for encircled energies at the field center for the different imaging modes and information on the field dependence of the PSF. For a discussion of the coronagraphic mask, see Section 12.10.

Figure 5.10: A co-added image of SAO 255271 taken using 50CCD shows the structure in the STIS PSF. This figure is plotted with a logarithmic intensity scale and is about 10" across. The ring seen below the center of the PSF is a ghost image. The position angle of this ghost varies as a function of location on the CCD (see Section 7.1.7 and Figure 7.6).



The throughputs used for the CCD imaging modes are for the most part based on measurements of on-orbit calibration data and are accurate to within 5%.

5.2.1 Effect of the optical baffles on STIS CCD imaging

Calibration observations were taken to investigate whether the baffle structures around the CCD detector scatter light from the stars outside the CCD detector into its field of view, and if so, by how much. Images were taken with a bright star placed at 12 different positions, 10 and 37 arcsec away from the edge of the detector. The analysis of the images showed that there is no measurable scattering components by the baffle structures around the detector. Placing the bright star beyond the edge of the detector thus acts as an effective coronagraph for the STIS CCD detector (see Proffitt et al. 2004, ApJ (in press), astro-ph/0405319) for more details).

5.2.2 Unfiltered (Clear) CCD Imaging—50CCD

The 50CCD aperture is a clear, unvignetted aperture which provides maximum sensitivity over the full 52x52 arcsecond field of view. The shape of the bandpass is governed by the detector, which has sensitivity from ~2000 to 10,300 Å. Figure 5.6 shows the throughput as a function of wavelength for this imaging mode (see also Chapter 14 for sensitivities, and signal-to-noise and saturation plots). If color information and a wide field of view are not required, then there is a clear advantage of this imaging mode over the WFPC2.

Figure 12.5 shows an example of a deep CCD image of a random field taken as part of the Archival Pure Parallel Program.

5.2.3 Optical Longpass—F28X50LP

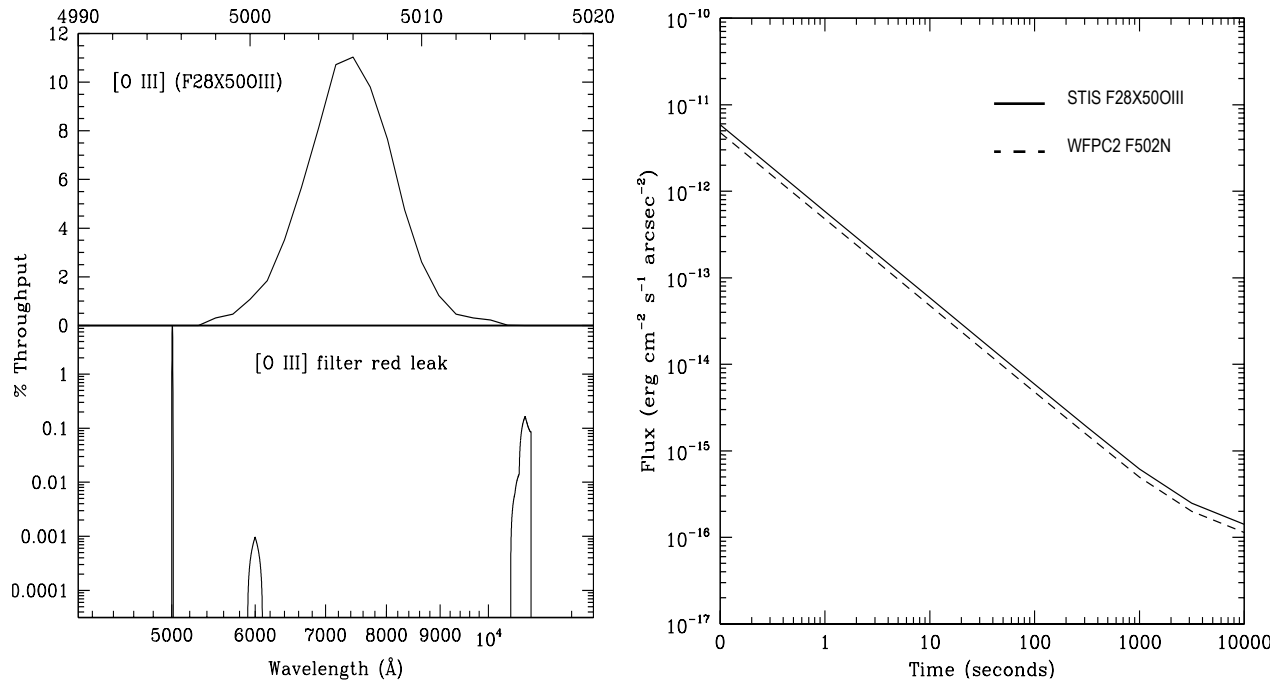
STIS's longpass filter cuts off at $\lambda < 5500$ Å. It images a 28 x 52 arcsecond field of view. The F28X50LP filter is the principal target-acquisition aperture (see "Selecting the Imaging Aperture" on page 176). The integrated system throughput for this filter is given in Figure 5.7 (see also page 398 for sensitivities, and signal-to-noise and saturation plots).

The combination of 50CCD and F28X50LP can provide deep imaging with sufficient color information for some types of color-magnitude diagrams.

5.2.4 [O III]—F28X50OIII

This filter images a 28 x 50 arcsecond field of view and can be used in target acquisitions or for direct imaging in the light of [O III]. The [O III] filter integrated system throughput and a signal-to-noise comparison with the WFPC2 [O III] filter are shown in Figure 5.11 (see also "F28X50OIII—CCD" on page 401 for sensitivities, and signal-to-noise and saturation plots). The STIS [O III] filter is very narrow: only 5 Å wide, compared to the WFPC2 [O III] filter which is roughly 30 Å wide. The STIS [O III] filter has a substantial red leak that begins at 10,600 Å and continues to at least 12,000 Å. In the case of a very red star (K0 spectral type), the red leak will contribute approximately one third of the detected counts. The red leak for this filter is included in the passbands used by the [STIS Exposure Time Calculator](#) (ETC) and **synphot**. Observers are encouraged to use these tools to predict source and background count rates carefully.

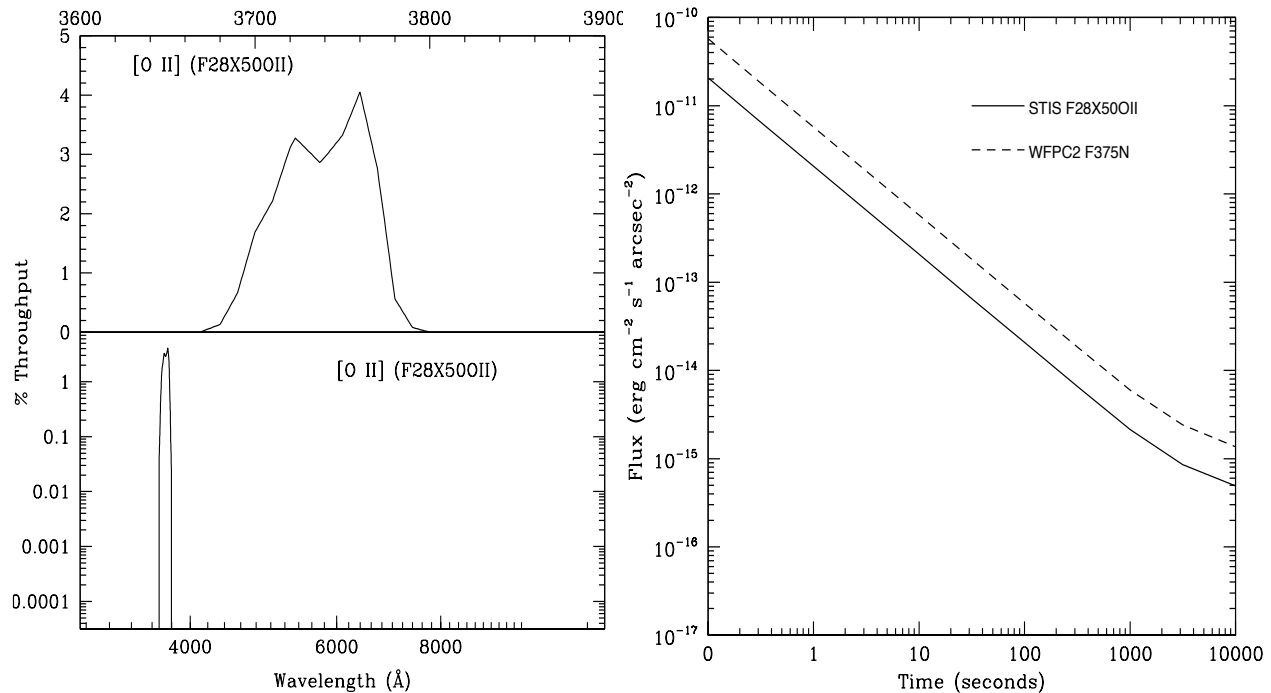
Figure 5.11: F28X50OIII: (a) Integrated System Throughput and (b) Flux vs. Exposure Time to achieve a signal-to-noise=5 compared to WFPC2 for a FWHM=1 Å line, integrated over an area of one square arcsecond.



5.2.5 [O II]—F28X50OII

The [O II] filter images a 28 x 52 arcsecond field of view and can be used in target acquisitions or for direct imaging in the light of [O II]. The [O II] filter integrated system throughput and a signal-to-noise ratio comparison with WFPC2's [O II] filter are shown in Figure 5.12. See page 404 for sensitivities, signal-to-noise and saturation plots.

Figure 5.12: F28X500II: (a) Integrated System Throughput and (b) Flux vs. Exposure Time to achieve a signal-to-noise=5 compared to WFPC2 for a FWHM=1 Å line, integrated over an area of one square arcsecond. There is no substantial red leak in this filter.



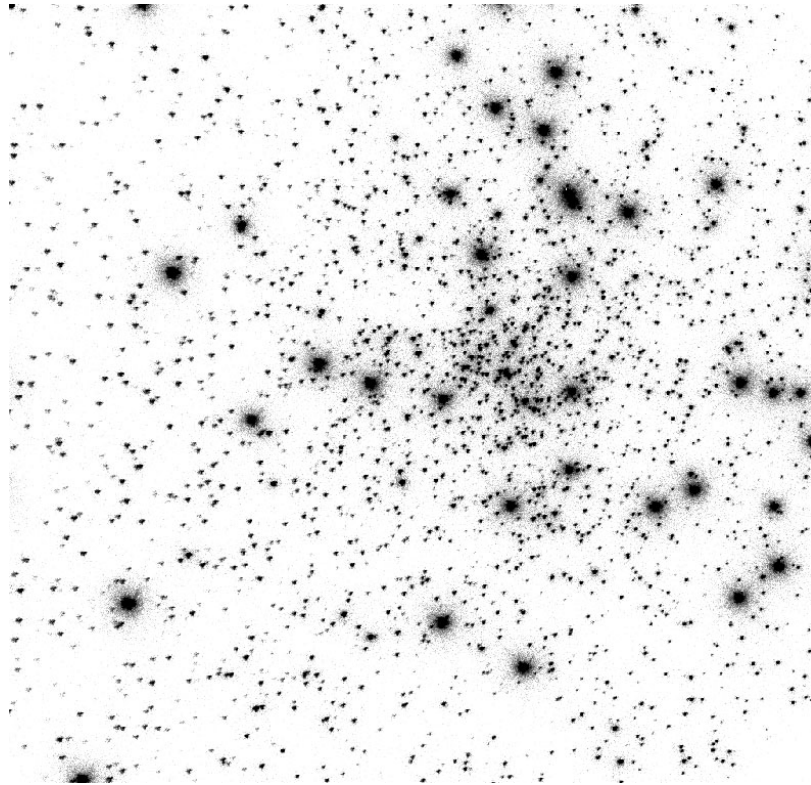
5.3 Ultraviolet Imaging with the MAMA Detectors

The filtered and clear apertures available for ultraviolet imaging are summarized in Table 5.1. Although there are only a small number of filters available, the solar-blind and solar-insensitive properties of the FUV-MAMA and NUV-MAMA detectors, respectively, coupled with their 25 x 25 arcsecond field of view, good spatial sampling, and ability to detect rapid variability, give STIS ultraviolet imaging capabilities that are complementary to those of ACS.

The throughputs of the STIS MAMA imaging modes in this Handbook are mostly based on on-orbit calibration observations. These throughputs are good to within 5% in the FUV and the NUV. The throughputs in the ETC, the calibration reference files, and in the STSDAS **synphot** package will continue to be updated as further analysis of calibration data continues.

Figure 5.13 shows an example of MAMA imaging data of a globular cluster taken as part of the Cycle 7 calibration of STIS using the quartz filter and the NUV-MAMA.

Figure 5.13: 320 Second NUV-MAMA Image of NGC6681 taken with the F25QTZ filter as part of the Cycle 7 Calibration Monitoring Program 7720. All the points are stars.



5.3.1 Bright-Object Limits

The MAMA detectors are subject to absolute bright-object limits, above which targets cannot be observed. They are particularly stringent for the MAMA imaging modes (being as faint as $V=20.3$ for the clear modes), and apply to all sources illuminating the field of view.

We direct MAMA observers to Section 7.6. For summary tables of absolute bright-object screening magnitudes for the imaging modes, see Section 14.8.

It is the observers' responsibility to ensure that their observations do not exceed the MAMA bright-object limits.

5.3.2 Optical Performance

The MAMA plate scale is ~ 0.0246 arcsecond pixel^{-1} in imaging mode, providing a good compromise between sampling of the PSF in the ultraviolet and field of view. Chapter 14 shows encircled energies as a function of wavelength for MAMA imaging, and provides information on the geometric distortions of the images. The MAMA detector PSFs exhibit

broad wings, which are substantially higher in the NUV-MAMA than the FUV-MAMA. Figure 7.14 shows sample detector PSFs for the MAMAs.

5.3.3 Unfiltered (Clear) MAMA Imaging—25MAMA

Each MAMA can be used with the 25MAMA clear aperture to image a 25x25 arcsecond field of view of the sky, providing the maximum throughput and wavelength coverage in the NUV and FUV as shown in Figure 5.6. The FUV-MAMA quantum efficiency drops dramatically longward of $\sim 2000 \text{ \AA}$ making it effectively solar blind, while the NUV-MAMA also has a reduced response toward the red, longward of $\sim 3500 \text{ \AA}$ (see Figure 5.14). Table 5.3 and Table 5.4 give the percentages of detected photons arising in the UV versus optical for observations of different stellar types with the clear MAMA imaging modes. The red rejection of the MAMA detectors makes them well suited to UV imaging of red objects.

However, NUV-MAMA clear direct images will be slightly out of focus, because the corresponding mirror on the MSM optimally focuses for use of a filter. It is recommended that the F25SRF2 longpass filter (see next section) be used instead of 25MAMA (clear) for direct imaging with the NUV-MAMA. The same does not apply to the FUV-MAMA, which has separate MSM mirrors for clear and filtered imaging.

The sky background can be significant for unfiltered FUV-MAMA observations. The strongest contributor is the geocoronal Lyman- α line. Global count rates of several 10^4 counts per second over the whole detector are not unusual during daytime observations. The same applies to slitless far-UV spectroscopy. For observations of large, UV-faint targets, where background subtraction becomes critical, unfiltered imaging may introduce significant noise. In addition, the background may be variable during long exposures. Longpass filtered imaging may be profitable in this case.

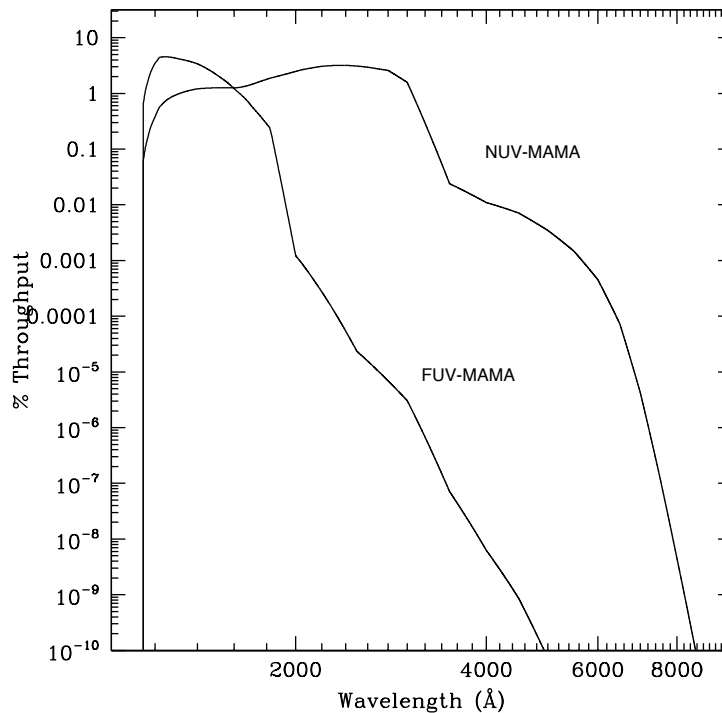
Table 5.3: Visible-Light Rejection of the FUV-MAMA Clear Imaging Mode

Stellar Type	Percentage of all Detected Photons which have $\lambda < 1800 \text{ \AA}$	Percentage of all Detected Photons which have $\lambda < 3000 \text{ \AA}$
O5	99.5	100
B1 V	99.4	100
A0 V	98.1	100
G0 V	72.7	99.8
K0 V	35.1	94.4

Table 5.4: Visible-Light Rejection of the NUV-MAMA Clear Imaging Mode

Stellar Type	Percentage of all Detected Photons which have $\lambda < 3000 \text{ \AA}$	Percentage of all Detected Photons which have $\lambda < 5000 \text{ \AA}$
O5	98.1	100
B1 V	97.6	100
A0 V	94.3	99.9
G0 V	68.1	99.0
K0 V	56.4	97.6

Figure 5.14: Out-of-Band Spectral Responses of FUV- and NUV-MAMA Clear Imaging Modes.

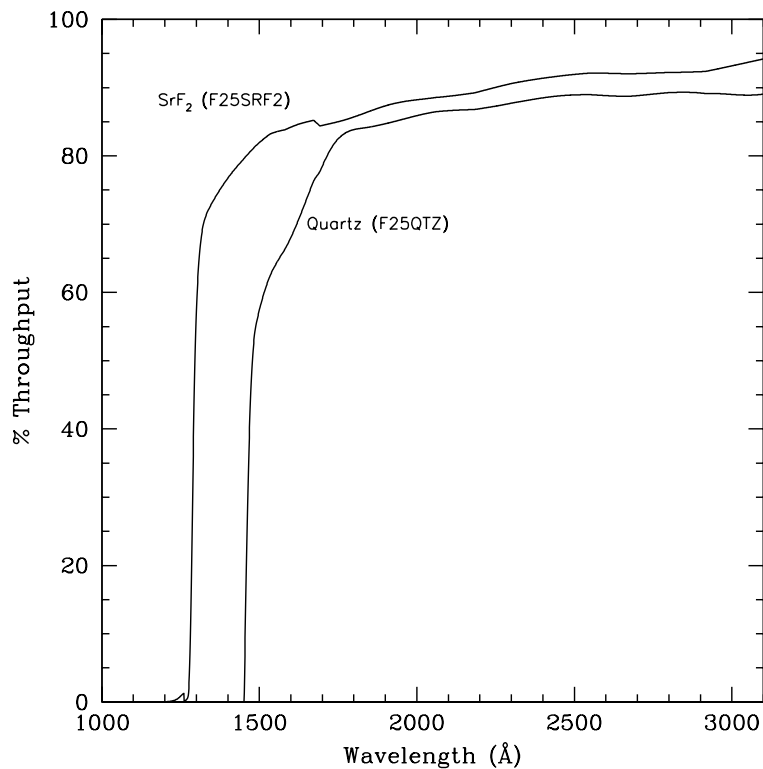


5.3.4 Longpass-Filtered MAMA Imaging—F25SRF2 and F25QTZ

The integrated system throughputs of the two UV longpass filters when used with the NUV-MAMA and FUV-MAMA are shown in Figure 5.8 and Figure 5.9 (for sensitivities, and signal-to-noise and saturation plots see pages 421 and 450 for F25SRF2, 418 and 446 for F25QTZ). The filter (only) throughputs of these two filters are shown in Figure 5.15. These filters image a 25×25 arcsecond field of view. The cutoff wavelengths of

F25SRF2 and F25QTZ were chosen to exclude a) geocoronal Lyman- α 1216 Å and b) [O I] 1302+1306 and O I] 1356 Å, respectively; use of these filters significantly reduces the total sky background in the ultraviolet. These filters can be used by themselves in imaging mode, or with the prism or any first-order UV grating in slitless spectroscopic observations, to reduce the background due to geocoronal emission (see Section 4.4 and Section 12.1). F25SRF2 images, combined with images taken in series with the FUV-MAMA/25MAMA clear, can also be used to obtain Lyman- α images (see “Lyman Alpha—F25LYA and Clear-minus-SRF2” on page 85).

Figure 5.15: F25SRF2 and F25QTZ Filter-Only Transmissions



5.3.5 MAMA Narrow-band-Filtered Imaging

The filters for MAMA imaging include:

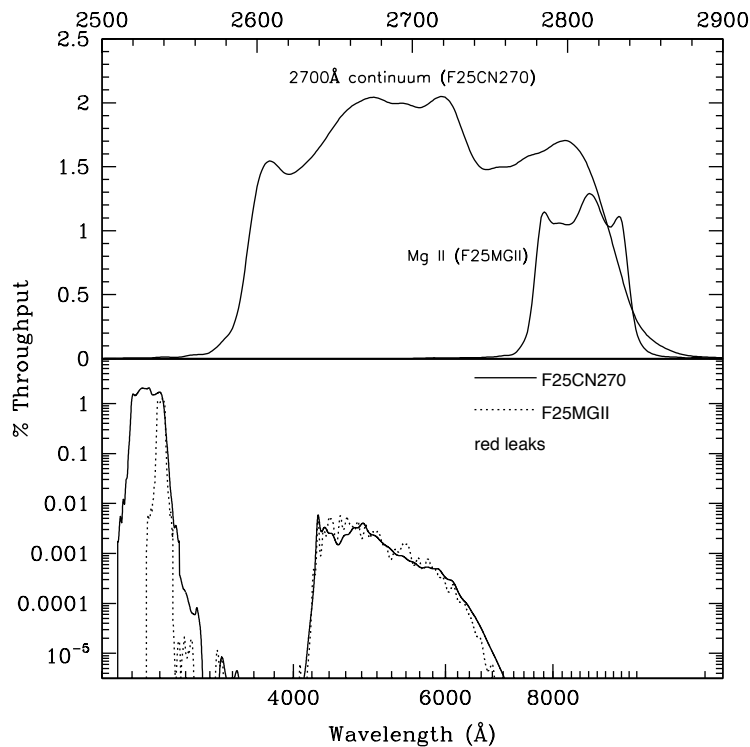
- A narrow-band filter (F25MGII) which images the magnesium doublet at 2796–2803 Å, and a matched medium-band continuum filter (F25CN270) centered at 2700 Å.
- A narrow-band filter (F25CIII) which images the semi-forbidden CIII] lines at 1907–1909 Å, among the strongest nebular (low-density) lines in the UV, and a matched medium-band continuum filter (F25CN182) centered at 1800 Å.

- A narrow-band filter which images Lyman- α ; this filter has an unusually poor throughput, and we recommend that you consider, instead, obtaining two FUV-MAMA images, one through the 25MAMA unfiltered aperture and a second with the SrF2 longpass filter. The difference of these two images will isolate Lyman- α with much higher throughput than the F25LYA filter. Alternatively, the ACS SBC can be used with the F122M filter.

Mg II—F25MGII

The F25MGII filter images a 25 x 25 arcsecond field of view in the light of the doublet lines of Mg II (2796 and 2803 Å). Figure 5.16 shows the integrated system throughput (see also page 423 for sensitivities, and signal-to-noise and saturation plots). There is a substantial red leak in this filter starting at approximately 4200 Å and extending to at least 13,000 Å. For stellar spectral types O and B, less than 2% of the detected counts will be due to red leak. This percentage rises to 7% for an A0 star. For a K0 star, 75% of the counts will be due to red leak. The red leak for this filter is included in the passbands used by the [STIS Exposure Time Calculator](#) and [synphot](#). Observers are encouraged to use these tools to predict source and background count rates carefully.

Figure 5.16: F25MGII and F25CN270 Integrated System Throughputs



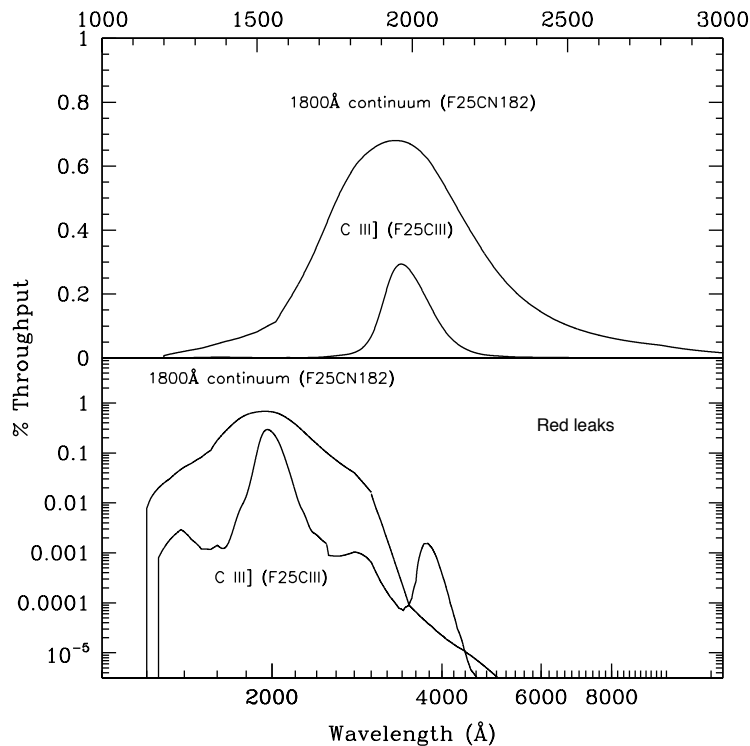
2700 Å Continuum—F25CN270

The 2700 Å continuum filter images a 25x25 arcsecond field of view and can be used to measure the continuum for Mg II emission-line images. The F25CN270 filter integrated system throughput is shown in Figure 5.16 above (see also page 426 for sensitivities, and signal-to-noise and saturation plots). There is a substantial red leak in this filter starting at approximately 4200 Å and extending to at least 12,000 Å. For a K0 star, roughly 40% of the detected counts will be due to red leak. The red leak for this filter is included in the passbands used by the [STIS Exposure Time Calculator](#) and [synphot](#). Observers are encouraged to use these tools to predict source and background count rates carefully.

C III]—F25CIII

The F25CIII filter images a 25x25 arcsecond field of view in the light of C III] at 1907–1909 Å. The F25CIII integrated system throughput is shown in Figure 5.17 (see also page 429 for sensitivities, and signal-to-noise and saturation plots). The out-of-band suppression for this filter is fairly good.

Figure 5.17: F25CIII and F25CN182 Integrated System Throughputs



1800 Å Continuum—F25CN182

The 1800 Å continuum filter images a 25 x 25 arcsecond field of view, and can be used to measure the continuum for C III] emission-line images.

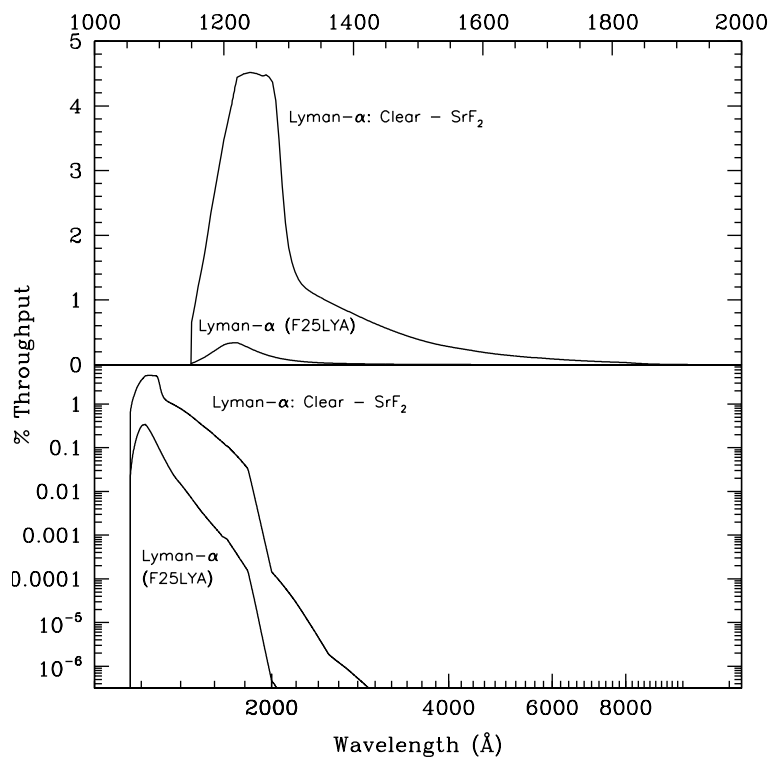
The F25CN182 filter integrated system throughput is shown in Figure 5.17 above (see also page 432 for sensitivities, and signal-to-noise and saturation plots).

Lyman Alpha—F25LYA and Clear-minus-SRF2

The F25LYA filter images a 25 x 25 arcsecond field of view and can be used to obtain emission-line images in the light of Lyman- α . The F25LYA filter integrated system throughput is shown in Figure 5.18 (see also page 454 for sensitivities, and signal-to-noise and saturation plots).

At the price of a slightly wider bandpass, and the need to take two exposures, Lyman- α can be isolated by taking one image with the clear (25MAMA) aperture and a second with the longpass (F25SRF2) filter and differencing the two. The integrated system throughput for this imaging sequence is appreciably higher than for the narrowband F25LYA filter, as shown Figure 5.18.

Figure 5.18: Lyman- α Imaging Integrated System Throughputs



5.4 Neutral-Density Filters

STIS has a complement of neutral-density (ND) filters, which can be used with the CCD, the NUV-MAMA, and the FUV-MAMA spanning from ND1 (attenuation of 10^{-1}) to ND5. The ND5 filter appears to have a UV throughput of at most 10^{-6} , substantially smaller than prelaunch estimates.

F25NDQ1, F25NDQ2, F25NDQ3, and F25NDQ4 are physically four separate quadrants of a single 25 x 25 arcsecond filter occupying a single position on the slit wheel. The target is put into the appropriate quadrant when one of these apertures is requested. However, it should be noted that all four quadrants project onto the detector, and each quadrant plus a 5" surrounding perimeter must be considered for bright-object limits. Thus, although one may request placement of a bright object centered in F25NDQ4, no other objects in the surrounding region may violate the bright-object limits for the other quadrants. This includes a 5" restrictive border around the interior of the selected quadrant, effectively reducing its size. In practice, for safety reasons any object that would produce a global count rate exceeding 1.5×10^6 counts s^{-1} or a local count rate above 500 counts sec^{-1} $pixel^{-1}$ in F25NDQ1, may not be observed using any of the other quadrants, since pointing problems could cause this bright source to end up in F25NDQ1 anyway. To ensure accurate placement of a bright object in the selected quadrant, a CCD target acquisition must also be specified. Also note that the boundaries between the four quadrants are not well centered, and as a result the sizes of the quadrants vary. Figure 13.82 shows a lamp image of this aperture, and Table 13.33 gives the approximate dimensions of each quadrant and the default locations where targets are placed.

F25ND3 and F25ND5 are each individual 25 x 25 arcsecond filtered apertures, occupying unique locations on the slit wheel. Detailed information for F25ND3 and F25ND5 are given in "F25ND3—NUV-MAMA" on page 412, "F25ND3—FUV-MAMA" on page 440, "F25ND5—NUV-MAMA" on page 414, and "F25ND5—FUV-MAMA" on page 442.

Exposure Time Calculations

In this chapter. . .

6.1 Overview / 87
6.2 Determining Count Rates from Sensitivities / 88
6.3 Throughput and Sensitivity / 93
6.4 Computing Exposure Times / 94
6.5 Detector and Sky Backgrounds / 96
6.6 Tabular Sky Backgrounds / 103
6.7 Extinction Correction / 105
6.8 Exposure Time Examples / 106

6.1 Overview

In this chapter we explain how to use the sensitivities and throughputs provided in Chapter 13 and Chapter 14 to determine the expected count rate from your source and how to calculate exposure times to achieve a given signal-to-noise ratio for your STIS observations taking various background contributions into account. At the end of the chapter, in Section 6.8, you will find examples to guide you through specific cases.

6.1.1 The STIS Exposure Time Calculators

Three [STIS Exposure-Time Calculators](#) (ETCs) are available to help you with your proposal preparation. The three ETCs—available via the [STIS web pages](#)—are the [Imaging ETC](#), the [Spectroscopic ETC](#), and the [Target Acquisition ETC](#). These calculators provide count rates for given source and background parameters and calculate signal-to-noise ratio for a given exposure time, or exposure time for a given signal-to-noise ratio. If

you have a calibrated spectrum of your source, you can pass it as input via FTP to the Exposure Time Calculator. The ETC also determines peak per-pixel count rates and total (integrated over the detector) count rates to aid you in your feasibility assessment. The ETC also warns you if your observations exceed the local or global brightness limits for MAMA observations (see Chapter 7). Lastly, in the case of the spectroscopic ETC, the task produces a simulated one-dimensional spectrum for a given STIS configuration and source. A graphical interface allows WWW browsers to plot the output spectra or write them out as ASCII text files to your local disk. The input and output parameters in the target acquisition ETC are specifically designed to facilitate exposure-time estimates for target acquisition purposes (see Chapter 8 for more details on acquisitions). The ETCs have extensive online help which explains how to use them and gives the details of the performed calculations.

The original ETCs have been replaced with improved Java versions that are part of the APT ([Astronomers' Proposal Tool](#)).

6.2 Determining Count Rates from Sensitivities

In the simplest terms, the instrumental sensitivity (S) times the flux from your object of interest gives the counts sec^{-1} (C) expected from your source times the gain (G) (i.e., it gives counts for the MAMA and electrons for the CCD):

$$C \times G = S \times Flux$$

Later in this chapter we provide specific formulae appropriate for imaging and spectroscopic modes, which can be used to calculate the expected count rates from your source and the signal-to-noise ratio. The formulae are given in terms of sensitivities, but we also provide transformation equations between the throughput (T) and sensitivity (S) for imaging and spectroscopic modes.

Sensitivities and throughputs are presented in graphical and tabular form as a function of wavelength for the spectroscopic modes in Chapter 13, and for the imaging modes in Chapter 14. Given the source characteristics and the sensitivity of the STIS configuration, calculating the expected count rate over a given number of pixels is straightforward. The additional information you will need for spectroscopic observations is the aperture transmission (T_A), the encircled energy fraction (ϵ_f) in the direction perpendicular to the dispersion, the number of pixels per spectral resolution element (or line-spread function $FWHM$) and the plate scale, which are provided in Chapter 13. For imaging observations you need only the

encircled energies and plate scales. Below, we describe how to determine two quantities:

1. The counts sec^{-1} (C) from your source over some selected area of N_{pix} pixels.
2. The peak per-pixel count rate (P_{cr}) from your source—useful for avoiding saturated exposures and for assuring that MAMA observations do not exceed the bright-object limits.

We consider the cases of point sources and diffuse sources separately.

6.2.1 Spectroscopy

Sensitivity Units and Conversions

The spectroscopic *point-source sensitivity*, S_{λ}^p , has the units
 for CCD: electrons $\text{sec}^{-1} \text{pix}_{\lambda}^{-1}$ per incident $\text{erg cm}^{-2} \text{sec}^{-1} \text{\AA}^{-1}$
 for MAMA: counts $\text{sec}^{-1} \text{pix}_{\lambda}^{-1}$ per incident $\text{erg cm}^{-2} \text{sec}^{-1} \text{\AA}^{-1}$.

Where:

- pix_{λ} = a pixel in the dispersion direction
- counts and electrons refer to the total received from the point source integrated over the PSF in the direction perpendicular to the dispersion (along the slit)

The spectroscopic *diffuse source sensitivity*, S_{λ}^d , has the units
 for CCD: electrons $\text{sec}^{-1} \text{pix}_{\lambda}^{-1} \text{pix}_s^{-1}$ per incident $\text{erg sec}^{-1} \text{cm}^{-2} \text{\AA}^{-1} \text{arcsec}^{-2}$
 for MAMA: counts $\text{sec}^{-1} \text{pix}_{\lambda}^{-1} \text{pix}_s^{-1}$ per incident $\text{erg sec}^{-1} \text{cm}^{-2} \text{\AA}^{-1} \text{arcsec}^{-2}$.

Where:

- pix_{λ} = a pixel in the dispersion direction
- pix_s = a pixel in the spatial direction

S_{λ}^p and S_{λ}^d are related through the relation:

$$S_{\lambda}^d \cong (S_{\lambda}^p \times m_s \times W)$$

Where:

- m_s is the plate scale in arcsec per pixel in the spatial direction (i.e. in the direction perpendicular to the dispersion)
- W is the slit width in arcseconds

In general, we have assumed that the diffuse source has a uniform brightness over the area of interest and that the spectrum can be approximated as a continuum source (i.e., any emission or absorption lines

are broader than the resolution after taking the effect of the slit into account).

Point Source

For a point source, the count rate, C , from the source integrated over an area of $N_{pix} = N_{\lambda pix} \times N_{spix}$ pixels can be expressed as:

$$C = \frac{F_{\lambda} \times S_{\lambda}^p \times T_A \times \varepsilon_f \times N_{\lambda pix}}{G}$$

Where:

- G is the gain (always 1 for the MAMA, and 1 or 4 depending on the choice of CCDGAIN for the CCD)
- F_{λ} = the continuum flux from the astronomical source, in $\text{erg sec}^{-1} \text{cm}^{-2} \text{\AA}^{-1}$
- T_A = the aperture transmission (a fractional number less than 1)
- ε_f = the fraction of the point-source energy contained within N_{spix} pixels in the spatial direction
- $N_{\lambda pix}$ = the number of wavelength pixels integrated over. For an unresolved emission line, $N_{\lambda pix}$ is just the number of pixels per spectral resolution element and F_{λ} is simply the total flux in the line in $\text{erg sec}^{-1} \text{cm}^{-2}$ divided by the product of the dispersion in \AA per pixel and $N_{\lambda pix}$ (i.e., divided by the $FWHM$ of a resolution element in \AA).
- N_{spix} = the number of pixels integrated over in the spatial direction.

The peak counts $\text{sec}^{-1} \text{pixel}^{-1}$ from the point source is given by:

$$P_{cr} = \frac{\varepsilon_f(1) \times F_{\lambda} \times S_{\lambda}^p \times T_A}{G}$$

Where:

- $\varepsilon_f(1)$ is the fraction of energy contained within the peak pixel.
- F_{λ} , S_{λ}^p , and T_A are as above.

Diffuse Source

For a diffuse continuum source over $N_{pix} = N_{\lambda pix} \times N_{spix}$, the count rate C can be expressed as:

$$C = \frac{I_{\lambda} \times S_{\lambda}^d \times N_{\lambda pix} \times N_{spix}}{G}$$

Where:

- I_λ = the surface brightness of the astronomical source, in $\text{erg sec}^{-1} \text{cm}^{-2} \text{\AA}^{-1} \text{arcsec}^{-2}$.
- $N_{\lambda pix}$ = the number of wavelength pixels integrated over in the dispersion direction. For an unresolved emission line, $N_{\lambda pix}$ is just the number of pixels per spectral resolution element, and I_λ is simply the total flux in the line in $\text{ergs sec}^{-1} \text{cm}^{-2} \text{arcsec}^{-2}$ divided by the product of the dispersion in \AA per pixel and $N_{\lambda pix}$, (i.e., divided by the $FWHM$ of the resolution element in \AA).
- N_{spix} = the number of pixels integrated over in the spatial direction.

For a diffuse continuum source the peak counts $\text{sec}^{-1} \text{pixel}^{-1}$, P_{cr} , is given by:

$$P_{cr} = \frac{I_\lambda \times S_\lambda^d}{G}$$

For a diffuse, *spectrally unresolved emission line source* the peak counts $\text{sec}^{-1} \text{pixel}^{-1}$, P_{cr} , is essentially independent of slit size and is given by:

$$P_{cr} = \frac{I_{line} \times S_\lambda^d \times w}{G \cdot W \cdot FWHM}$$

Where:

- I_{line} is the intensity in $\text{erg sec}^{-1} \text{cm}^{-2} \text{arcsec}^{-2}$ in the line.
- $FWHM$ is the full width half max of the instrumental profile in \AA , which for STIS is nearly always 2 pixels $\times d$, where d is the dispersion in \AA pixel^{-1} .
- w is the slit width in arcseconds which projects to n pixels in the detector plane, where n is the width of the resolution element in pixels. Note that w is numerically equal or close to twice the plate scale in the dispersion direction for all modes.
- W is the actual slit width in arcseconds.

Thus, for STIS in particular, this expression reduces to:

$$P_{cr} \sim \frac{I_{line} \times S_\lambda^d \times m_\lambda}{W \cdot d \cdot G}$$

Where:

- d is the dispersion in \AA pixel^{-1} .
- m_λ is the plate scale in the dispersion direction. All else is as above.

The counts from the emission line will be spread over $N_{\lambda pix}$ pixels where $N_{\lambda pix}$ is the slit width per plate scale in the dispersion direction ($N_{\lambda pix} = W / m_\lambda$).

6.2.2 Imaging

Sensitivity Units and Conversions

The *imaging point-source sensitivity*, S_{λ}^p , has the units
 for CCD: electrons $\text{sec}^{-1} \text{ \AA}^{-1}$ per incident $\text{erg sec}^{-1} \text{ cm}^{-2} \text{ \AA}^{-1}$
 for MAMA: counts $\text{sec}^{-1} \text{ \AA}^{-1}$ per incident $\text{erg sec}^{-1} \text{ cm}^{-2} \text{ \AA}^{-1}$.

Where:

- counts and electrons refer to the total number received from the point source integrated over the PSF.

The *imaging diffuse-source sensitivity*, S_{λ}^d , has the units
 for CCD: electrons $\text{sec}^{-1} \text{ \AA}^{-1} \text{ pixel}^{-1}$ per incident $\text{erg sec}^{-1} \text{ cm}^{-2} \text{ \AA}^{-1} \text{ arcsec}^{-2}$.
 for MAMA: counts $\text{sec}^{-1} \text{ \AA}^{-1} \text{ pixel}^{-1}$ per incident $\text{erg sec}^{-1} \text{ cm}^{-2} \text{ \AA}^{-1} \text{ arcsec}^{-2}$.

Thus S_{λ}^p and S_{λ}^d are related through the relation:

$$S_{\lambda}^d \equiv (S_{\lambda}^p \times m_s^2)$$

where m_s is the plate scale in arcsec per pixel.

Point Source

For a point source, the count rate, C , over an area of N_{pix} pixels can be expressed as:

$$C = \frac{\int F_{\lambda} \times S_{\lambda}^p \times \varepsilon_f d\lambda}{G}$$

Where:

- F_{λ} = the flux from the astronomical source, in $\text{ergs sec}^{-1} \text{ cm}^{-2} \text{ \AA}^{-1}$.
- ε_f = the fraction of the point source energy encircled within N_{pix} pixels.
- the integral is over the bandpass.

The peak counts $\text{sec}^{-1} \text{ pixel}^{-1}$ from the point source are given by:

$$P_{cr} = \frac{\int F_{\lambda} \times S_{\lambda}^p \times \varepsilon_f(1) d\lambda}{G}$$

Where:

- $\varepsilon_f(1)$ is the fraction of energy encircled within the peak pixel.
- F_{λ} , and S_{λ}^p are as above.
- the integral is over the bandpass.

If the flux from your source can be approximated by a flat continuum, then:

$$C = \frac{F_{\lambda} \epsilon_f \int S_{\lambda}^p d\lambda}{G}$$

We can now define an equivalent bandpass of the filter (B_{λ}) such that:

$$\int S_{\lambda}^p d\lambda = S_{peak}^p B_{\lambda}$$

Where:

- S_{peak}^p is the peak sensitivity.
- B_{λ} is the effective bandpass of the filter.

The count rate from the source can now be written as:

$$C = \frac{F_{\lambda} \epsilon_f S_{peak}^p B_{\lambda}}{G}$$

In Chapter 14, we give the value of B_{λ} and S_{peak}^p for various filters.

Diffuse Source

For a diffuse source, the count rate, C , can be expressed as:

$$C = \frac{\int I_{\lambda} \times S_{\lambda}^d \times N_{pix} d\lambda}{G} = \frac{\int I_{\lambda} \times S_{\lambda}^p \times m_s^2 \times N_{pix} d\lambda}{G}$$

Where:

- I_{λ} = the surface brightness of the astronomical source, in $\text{erg sec}^{-1} \text{cm}^{-2} \text{\AA}^{-1} \text{arcsec}^{-2}$.
- N_{pix} = the number of pixels integrated over.
- the integral is over the bandpass.

For a diffuse source the peak counts $\text{sec}^{-1} \text{pixel}^{-1}$, P_{cr} , is given trivially by:

$$P_{cr} = \frac{\int I_{\lambda} \times S_{\lambda}^d d\lambda}{G}$$

where we have assumed the source to be uniformly bright.

6.3 Throughput and Sensitivity

So far, we have given the formulae for count rates in terms of the sensitivity (S). If you would like to use the throughput (T) rather than the sensitivity, you can use the following conversion equations.

For *imaging modes*, the transformation between T and S is given by:

$$S_{\lambda} = \frac{T_{\lambda} A \lambda}{hc} = \frac{A_{eff} \lambda}{hc}$$

Where:

- S_{λ} is the sensitivity at wavelength λ .
- T_{λ} is the system throughput at λ .
- A is the area of an unobstructed 2.4 meter telescope (i.e., 45,239 cm²).
- h is Planck's constant.
- c is the velocity of light.
- The effective area A_{eff} is given by $A_{eff} = T_{\lambda} A$

For *spectroscopic modes*, the transformation equation can be written as:

$$S_{\lambda} = \frac{T_{\lambda} A \lambda d}{hc} = \frac{A_{eff} \lambda d}{hc}$$

Where d is the dispersion in Å per pixel.

In the first two examples given at the end of this chapter, we specifically show how the calculations can be done both in terms of the sensitivity and the throughput.

6.4 Computing Exposure Times

To derive the exposure time to achieve a given signal-to-noise ratio, or to derive the signal-to-noise ratio you will achieve in a given exposure time for your source, there are four principal ingredients:

- Expected count rate from your source over some area (C).
- The area (in pixels) over which those counts are received (N_{pix}).
- Sky background (B_{sky}) in counts pixel⁻¹ sec⁻¹.
- The detector background, or dark current, (B_{det}) in counts sec⁻¹ pixel⁻¹, and the read noise (RN) in counts, if using the CCD.

Section 6.5 provides the information you need to determine the sky-plus-detector background for your observation.

6.4.1 Calculating Exposure Times for a Given Signal-to-Noise

The signal-to-noise ratio, $StoN$ is given by:

$$StoN = \frac{CtG}{\sqrt{CtG + N_{pix}(B_{sky} + B_{det})Gt + (N_{pix}/N_{bin})(N_{read}RN^2)}}$$

Where:

- C = the signal from the astronomical source in counts sec^{-1}
- t = the integration time in seconds
- G = the gain (always 1 for the MAMAs and 1 or 4 for the CCD, depending on your choice of CCDGAIN)
- N_{pix} = the total number of detector pixels integrated over to achieve C
- B_{sky} = the sky background in counts $\text{sec}^{-1} \text{pixel}^{-1}$
- B_{det} = the detector dark current in counts $\text{sec}^{-1} \text{pixel}^{-1}$
- N_{bin} = the total number of on-chip binned pixels for the CCD ($N_{bin} = \text{BINAXIS1} \times \text{BINAXIS2}$ (see “Binning” on page 223))
- N_{read} = the number of CCD readouts
- RN = the read noise in electrons; = 0 for MAMA observations

Observers using the CCD normally take sufficiently long integrations so that the CCD read noise is not important. This condition is met when:

$$CGt + N_{pix}(B_{sky} + B_{det})Gt \gg 2(N_{pix}/N_{bin})N_{read}RN^2$$

For all MAMA observations, and for CCD observations in the regime where read noise is not important, the integration time to reach a signal-to-noise ratio $StoN$, is given by:

$$t = \frac{(StoN)^2 (CG + N_{pix}G[B_{sky} + B_{det}])}{C^2 G^2}$$

If your source count rate is much higher than the sky plus detector backgrounds, then this expression reduces further to:

$$t = \frac{(StoN)^2}{CG}$$

More generally, the required integration time to reach a signal to noise ratio $StoN$, is given by:

$t =$

$$\frac{(StoN)^2(CG + N_{pix}G[B_{sky} + B_{det}]) + \sqrt{(StoN)^4(CG + N_{pix}G[B_{sky} + B_{det}])^2 + 4(StoN)^2C^2G^2((N_{pix}/N_{bin})N_{read}RN^2)}}{2C^2G^2}$$

Special Case—Spectroscopic CCD Observations at $\lambda < 2500 \text{ \AA}$

In the optical, each photon generates a single electron (i.e., counts \times the gain correspond to the total number of electrons). However, in the near UV, shortward of $\sim 3200 \text{ \AA}$, there is a finite probability of creating more than one electron per UV photon (see Christensen, O., 1976, *J. App. Phys.*, **47**, 689). Theoretically, the quantum yield (Q , or the mean number of electrons generated per photon) is given by the energy of the photon divided by 3.65 eV, and ranges from $Q=1.06$ electrons for every UV photon at 3200 \AA , to $Q=1.89$ electrons for every photon at 1800 \AA . The actual electron yield of the STIS CCD has not been measured in the near UV.

The sensitivity plots correctly predict the number of electrons generated per UV photon. However, since multiple electrons are generated from a single photon, the signal-to-noise achieved in a given integration time is affected. The explicit expression is given by:

$$StoN = \frac{Q^{-1}CtG}{\sqrt{Q^{-1}(C + N_{pix}B_{sky})Gt + N_{pix}B_{det}Gt + (N_{pix}/N_{bin})N_{read}RN^2}}$$

For observations which are not in the read-noise or dark-current limited regime, the effective signal-to-noise you should expect to achieve is then $\sim 1/\sqrt{Q}$ times the signal-to-noise ratio calculated directly from the sensitivities given in Chapter 13 ignoring this effect. This effect is negligible at 3000 \AA but amounts to 40% at 1800 \AA .

6.5 Detector and Sky Backgrounds

When calculating expected signal-to-noise ratios or exposure times, the background from the sky and the background from the detector must be taken into account.

6.5.1 Detector Backgrounds

Table 6.1 shows the read-noise and dark-current characteristics of the detectors, taken from Chapter 7.

Table 6.1: Detector Backgrounds

Detector	CCD	NUV-MAMA	FUV-MAMA
Read noise (electrons pix ⁻¹)	5.4 (for CCDGAIN=1) 7.7 (for CCDGAIN=4) ¹	0	0
Dark current (electrons sec ⁻¹ pix ⁻¹)	~4.5 x 10 ⁻³	~1.2 x 10 ⁻³	0.07 - 1.50 x 10 ⁻⁴

1. To convert to counts sec⁻¹ pix⁻¹ for CCDGAIN=4, divide by 4.039.

6.5.2 Sky Background

The sources of sky background which will affect STIS observations include:

- Earthshine (ES)
- Zodiacal light (ZL)
- Geocoronal emission (GC)

The continuum background in counts sec⁻¹ pixel⁻¹ for *spectroscopic observations* can be computed as:

$$B_{sky}^{\lambda} = \frac{I_{\lambda} \times S_{\lambda}^d}{G}$$

Where:

- I_{λ} is the surface brightness of the sky background, in erg sec⁻¹ cm⁻² Å⁻¹ arcsec⁻².
- S_{λ}^d is the diffuse-source sensitivity for the grating mode.

The background in counts sec⁻¹ pixel⁻¹ for *imaging observations* can be computed as:

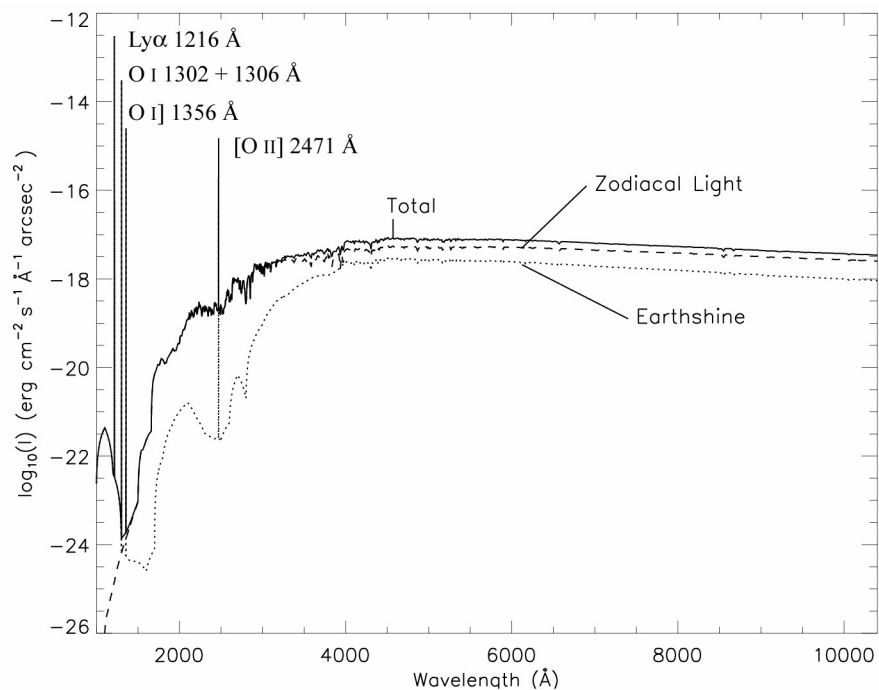
$$B_{sky} = \frac{\int I_{\lambda} \times S_{\lambda}^d d\lambda}{G}$$

Where:

- I_{λ} is the surface brightness of the sky background, in erg sec⁻¹ cm⁻² Å⁻¹ arcsec⁻².
- S_{λ}^d is the diffuse-source sensitivity for the imaging mode.
- The integral is over the bandpass.

In Figure 6.1 we plot the “high” sky background intensity as a function of wavelength, identifying the separate components which contribute to the background. The information in this figure is presented in tabular form in Table 6.4. In the Exposure Time Calculators (ETCs) and in this Handbook, the choices for Earthshine of “shadow”, “average”, and “extremely high” correspond to 0, 50% of, and twice the “high” values in Table 6.4. For the zodiacal sky background, the values in Table 6.4 correspond to a high value of $m_V = 22.1 \text{ arcsec}^{-2}$ from Table 6.2, while the low and average zodiacal light are scaled to $m_V = 23.3 \text{ arcsec}^{-2}$ and 22.7 arcsec^{-2} , respectively. The strength of the geocoronal (airglow) line emissions are as shown in Table 6.5.

Figure 6.1: High Sky Background Intensity as a Function of Wavelength. The zodiacal contribution corresponds to $m_V = 22.7 \text{ arcsec}^{-2}$. The Earthshine is for a target which is 38 degrees from the limb of the sunlit Earth. The upper limit to the [O I] 2471 Å intensity is shown. Use Figure 6.2 to estimate background contributions at other angles. The geocoronal airglow line intensities are in $\text{erg cm}^{-2} \text{ s}^{-1} \text{ arcsec}^{-2}$.



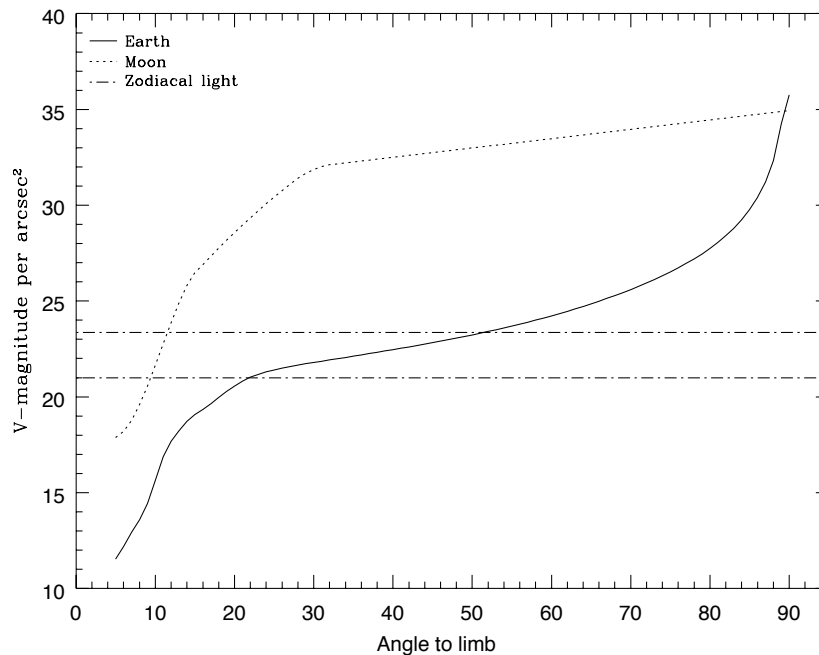
Background Variations and LOW-SKY

In the ultraviolet, the background contains important contributions from airglow lines. These vary from day to night and as a function of HST orbital position. The airglow lines are an important consideration for imaging-mode observations and can be for spectroscopic observations as well. Away from the airglow lines, at wavelengths shortward of $\sim 3000 \text{ Å}$, the background is dominated by zodiacal light and is generally much lower than the intrinsic detector background. The contribution of zodiacal light does not vary dramatically with time and varies by only a factor of about three throughout most of the sky. Table 6.2 gives the variation of the zodiacal background as a function of helio ecliptic latitude and longitude.

For a target near ecliptic coordinates of (50,0) or (-50,0), the zodiacal light is relatively bright at $m_v = 20.9 \text{ arcsec}^{-2}$, i.e. about 9 times the polar value of $m_v = 23.3 \text{ arcsec}^{-2}$.

Earthshine, on the other hand, varies strongly depending on the angle between the target and the bright Earth limb. The variation of the Earthshine as a function of limb angle from the sunlit Earth is shown in Figure 6.2. The figure also shows the contribution of the Moon which is typically much smaller, and the full range of the zodiacal contribution. For reference, the limb angle is approximately 24° when the HST is aligned toward its orbit pole (i.e., the center of the CVZ).

Figure 6.2: Background Contributions in V Magnitude arcsec^{-2} from the Moon and the Sunlit Earth as a Function of Angle Between the Target and the Limb of the Earth or Moon.



For observations longward of 3500 \AA , the Earthshine always dominates the background at small ($<22^\circ$) limb angles. In fact, the background increases exponentially for limb angles $<22^\circ$. The background near the bright Earth limb can also vary by a factor of ~ 2 on time scales as short as two minutes, which suggests that the background from Earthshine also depends upon the reflectivity of the terrain over which HST passes during the course of an exposure. The total background at limb angles greater than the bright-Earth avoidance angle of 20° appears to show no significant dependence on position within the small HST fields of view. Details of the

sky background as it affects STIS are discussed by Shaw et al. (STIS ISR 1998-21) and Giavalisco et al. (WFC3 ISR 2002-12).

Table 6.2: Approximate Zodiacal Sky Background as a Function of Helio ecliptic Latitude and Helio ecliptic Longitude (in V magnitude arcsec⁻²). A value of “SA” denotes positions in the solar avoidance zone.

Helio ecliptic Longitude (deg)	Helio ecliptic Latitude (deg)						
	0°	15°	30°	45°	60°	75°	90°
180°	22.1	22.4	22.7	23.0	23.2	23.4	23.3
165°	22.3	22.5	22.8	23.0	23.2	23.4	23.3
150°	22.4	22.6	22.9	23.1	23.3	23.4	23.3
135°	22.4	22.6	22.9	23.2	23.3	23.4	23.3
120°	22.4	22.6	22.9	23.2	23.3	23.3	23.3
105°	22.2	22.5	22.9	23.1	23.3	23.3	23.3
90°	22.0	22.3	22.7	23.0	23.2	23.3	23.3
75°	21.7	22.2	22.6	22.9	23.1	23.2	23.3
60°	21.3	21.9	22.4	22.7	23.0	23.2	23.3
45°	SA	SA	22.1	22.5	22.9	23.1	23.3
30°	SA	SA	SA	22.3	22.7	23.1	23.3
15°	SA	SA	SA	SA	22.6	23.0	23.3
0°	SA	SA	SA	SA	22.6	23.0	23.3

Table 6.3 contains the expected count rates from different sky backgrounds in various STIS modes, which you can use to determine whether your observations would be background limited.

Table 6.3: Count Rates by Sky Background and STIS Mode

Mode	counts sec ⁻¹ pix ⁻¹				
	Zodiacal ¹	Earthshine + Geocoronal Lines			
		Extremely High ²	High ³	Average ⁴	Dark (shadow) ⁵
CCD Clear	1.0 x 10 ⁻¹	1.0 x 10 ⁻¹	5.0 x 10 ⁻²	2.5 x 10 ⁻²	0
CCD Longpass	6.0 x 10 ⁻²	6.0 x 10 ⁻²	3.0 x 10 ⁻²	1.5 x 10 ⁻²	0
NUV-MAMA Clear	6.3 x 10 ⁻⁵	9.9 x 10 ⁻³	4.9 x 10 ⁻³	2.5 x 10 ⁻³	4.4 x 10 ⁻³
NUV-MAMA SrF ₂	5.9 x 10 ⁻⁵	1.9 x 10 ⁻³	9.4 x 10 ⁻⁴	4.7 x 10 ⁻⁴	5.6 x 10 ⁻⁶
NUV-MAMA Qtz	5.6 x 10 ⁻⁵	3.9 x 10 ⁻⁴	1.9 x 10 ⁻⁴	9.5 x 10 ⁻⁵	1.5 x 10 ⁻⁶
FUV-MAMA Clear	1.6 x 10 ⁻⁸	9.0 x 10 ⁻²	4.5 x 10 ⁻²	2.2 x 10 ⁻²	4.0 x 10 ⁻³
FUV-MAMA SrF ₂	1.4 x 10 ⁻⁸	6.5 x 10 ⁻³	3.2 x 10 ⁻³	1.6 x 10 ⁻³	2.4 x 10 ⁻⁵
FUV-MAMA Qtz	1.3 x 10 ⁻⁸	5.7 x 10 ⁻⁹	2.8 x 10 ⁻⁹	1.4 x 10 ⁻⁹	1.4 x 10 ⁻¹¹
FUV-MAMA Lyman- α	1.3 x 10 ⁻¹¹	6.5 x 10 ⁻³	3.2 x 10 ⁻³	1.6 x 10 ⁻³	2.5 x 10 ⁻⁴

1. Zodiacal contribution is the same as in Figure 6.1 and Table 6.4 ($m_V=22.1$ arcsec⁻²).

2. Corresponds to HST pointing 24° from the limb of the sunlit Earth.

3. Corresponds to HST pointing around 38° from the limb of the sunlit Earth, where the Earthshine is 50% of the “extremely high” value.

4. Corresponds to HST pointing around 50° from the limb of the sunlit Earth, where the Earthshine is 25% of the “extremely high” value.

5. Earthshine for shadow is 0 in the continuum, while the UV geocoronal emission lines are reduced from the high to the low values in Table 6.5.

Observations of the faintest objects may need the special requirement LOW-SKY in the Phase II observing program. LOW-SKY observations are scheduled during the part of the year when the zodiacal background light is no more than 30% greater than the minimum possible zodiacal light for the given sky position. LOW-SKY in the Phase II scheduling also invokes the restriction that exposures will be taken only at angles greater than 40° from the bright Earth limb to minimize Earthshine and the UV airglow lines. The LOW-SKY special requirement limits the times at which targets within 60 degrees of the ecliptic plane will schedule and limits visibility to about 48 minutes per orbit.

The ETC provides the user with the flexibility to separately adjust both the zodiacal (low, average, high) and Earthshine (shadow, average, high, extremely high) sky background components in order to determine if LOW-SKY is advisable for a given program. However, the absolute sky levels that can be specified in the ETC may not be achievable for a given target; e.g., as shown in Table 6.2 the zodiacal background minimum for an ecliptic target is $m_V = 22.4$, which is still brighter than both the low and average options with the ETC. By contrast, a target near the ecliptic pole

would always have a zodiacal=low background in the ETC. The user is cautioned to carefully consider sky levels as the backgrounds obtained in HST observations can cover significant ranges.

Geocoronal Emission and Shadow

Background due to geocoronal emission originates mainly from hydrogen and oxygen atoms in the exosphere of the Earth. The emission is concentrated in a very few lines. The brightest line is Lyman- α at 1216 Å. The strength of the Lyman- α line varies between about 2 and 30 kilo-Rayleighs (i.e., between 6.1×10^{-14} and 9.2×10^{-13} erg sec $^{-1}$ cm $^{-2}$ arcsec $^{-2}$ where 1 Rayleigh = 10^6 photons sec $^{-1}$ cm $^{-2}$ per 4π steradians) depending on the time of the observation and the position of the target relative to the Sun. The next strongest contribution is the from the doublet [O I] 1302 + 1306 Å, which rarely exceeds 10% of Lyman- α . The typical strength of the [O I] 1302 + 1306 Å doublet is about 2 kilo-Rayleighs (which corresponds to about 5.7×10^{-14} erg sec $^{-1}$ cm $^{-2}$ sec $^{-1}$ arcsec $^{-2}$) at the daylight side and about 150 times fainter on the night side of the HST orbit. O I] 1356 Å and [O II] 2471 Å lines may appear in observations on the daylight side of the orbit, but these lines are at least 10 times weaker than the [O I] 1302 + 1306 Å line. The widths of the lines also vary. The line widths given in Table 6.4 are representative values assuming a temperature of 2000 K.

The geocoronal emission lines are unresolved at the first-order resolutions of STIS but the emission fills the slit in the spatial dimension. A wider slit or slitless observing does not increase the background counts per pixel from geocoronal emission but does increase the area (range of wavelengths or pixels in the dispersion direction) over which that background is received. Observations with a slit which is n pixels wide in dispersion will be affected by geocoronal emission in a roughly n pixel region centered on the relevant geocoronal emission-line wavelength. For slitless spectroscopy in the UV, the effects of geocoronal emission must be taken into account at all pixels, unless a longpass filter is employed to block off the short wavelength emission (see also Section 5.3.4 and Section 12.1).

It is possible to request that exposures be taken when HST is in the umbral shadow of the earth to minimize geocoronal emission (e.g., if you are observing weak lines at ~ 1216 or ~ 1304 Å) using the special requirement SHADOW. Exposures using this special requirement are limited to roughly 25 minutes per orbit, exclusive of the guide-star acquisition (or reacquisition) and can be scheduled only during a small percentage of the year. SHADOW reduces the contribution from the geocoronal emission lines by roughly a factor of ten, while the continuum earthshine is set to 0. If you require SHADOW, you should request it in your Phase I proposal (see the Call for Proposals).

An alternate strategy for reducing the effects of geocoronal emissions is to use time resolved observations, so that any data badly affected by geocoronal emission can simply be excluded from the final coaddition. This can be done either by doing the observations in TIME-TAG mode or

by just taking a series of short (~ 5 min) ACCUM mode exposures over the course of each orbit.

6.6 Tabular Sky Backgrounds

We provide a table of the “high” sky background numbers as plotted in Figure 6.1, for easy reference. See the text and the caption in Figure 6.1 for more details. The high sky values are defined as the earthshine at 38° from the limb and by the high zodiacal light of $m_V = 22.1$ arcsec $^{-2}$. The contributions of the geocoronal emission lines are tabulated separately in Table 6.5.

Table 6.4: High Sky Background (excluding geocoronal emission lines)

Wavelength \AA	Earthshine $\text{erg sec}^{-1} \text{cm}^{-2}$ $\text{\AA}^{-1} \text{arcsec}^{-2}$	Zodiacal Light $\text{erg sec}^{-1} \text{cm}^{-2}$ $\text{\AA}^{-1} \text{arcsec}^{-2}$	Total Background $\text{erg sec}^{-1} \text{cm}^{-2}$ $\text{\AA}^{-1} \text{arcsec}^{-2}$
1000	1.32E-22	2.56E-28	1.32E-22
1100	3.38E-22	1.37E-26	3.38E-22
1200	8.25E-23	1.27E-25	8.26E-23
1300	5.41E-24	6.88E-25	6.10E-24
1400	4.65E-25	2.68E-24	3.14E-24
1500	3.97E-25	4.60E-23	4.64E-23
1600	3.42E-25	2.32E-22	2.33E-22
1700	1.24E-23	6.49E-21	6.50E-21
1800	1.26E-22	1.35E-20	1.37E-20
1900	4.69E-22	2.13E-20	2.18E-20
2000	1.02E-21	4.22E-20	4.32E-20
2100	1.42E-21	1.21E-19	1.22E-19
2200	8.02E-22	2.00E-19	2.01E-19
2300	3.73E-22	1.97E-19	1.97E-19
2400	2.59E-22	2.14E-19	2.14E-19
2500	2.80E-22	2.05E-19	2.06E-19
2600	1.29E-21	4.73E-19	4.75E-19
2700	5.42E-21	8.26E-19	8.31E-19
2800	7.72E-21	7.48E-19	7.56E-19
2900	4.43E-20	1.52E-18	1.56E-18
3000	1.01E-19	1.72E-18	1.82E-18
3100	2.12E-19	1.92E-18	2.14E-18

Table 6.4: High Sky Background (excluding geocoronal emission lines)

Wavelength Å	Earthshine $\text{erg sec}^{-1} \text{cm}^{-2}$ $\text{Å}^{-1} \text{arcsec}^{-2}$	Zodiacal Light $\text{erg sec}^{-1} \text{cm}^{-2}$ $\text{Å}^{-1} \text{arcsec}^{-2}$	Total Background $\text{erg sec}^{-1} \text{cm}^{-2}$ $\text{Å}^{-1} \text{arcsec}^{-2}$
3200	3.50E-19	2.24E-18	2.59E-18
3300	4.45E-19	2.72E-18	3.17E-18
3400	6.36E-19	2.65E-18	3.28E-18
3500	8.28E-19	2.67E-18	3.50E-18
3600	1.05E-18	2.53E-18	3.58E-18
3700	1.20E-18	3.03E-18	4.23E-18
3800	1.26E-18	2.87E-18	4.13E-18
3900	1.59E-18	2.83E-18	4.42E-18
4000	2.33E-18	4.22E-18	6.55E-18
4250	2.31E-18	4.42E-18	6.73E-18
4500	2.70E-18	5.16E-18	7.86E-18
4750	2.75E-18	5.23E-18	7.98E-18
5000	2.65E-18	5.10E-18	7.75E-18
5250	2.56E-18	5.02E-18	7.58E-18
5500	2.55E-18	5.16E-18	7.71E-18
5750	2.53E-18	5.25E-18	7.78E-18
6000	2.43E-18	5.14E-18	7.57E-18
6250	2.31E-18	5.00E-18	7.31E-18
6500	2.18E-18	4.80E-18	6.98E-18
6750	2.08E-18	4.69E-18	6.77E-18
7000	1.94E-18	4.48E-18	6.42E-18
7250	1.83E-18	4.30E-18	6.13E-18
7500	1.74E-18	4.13E-18	5.87E-18
7750	1.64E-18	3.97E-18	5.62E-18
8000	1.56E-18	3.83E-18	5.39E-18
8250	1.48E-18	3.68E-18	5.15E-18
8500	1.38E-18	3.47E-18	4.84E-18
8750	1.30E-18	3.31E-18	4.61E-18
9000	1.22E-18	3.17E-18	4.40E-18
9250	1.15E-18	3.03E-18	4.18E-18
9500	1.10E-18	2.92E-18	4.02E-18

Table 6.4: High Sky Background (excluding geocoronal emission lines)

Wavelength Å	Earthshine $\text{erg sec}^{-1} \text{cm}^{-2}$ $\text{Å}^{-1} \text{arcsec}^{-2}$	Zodiacal Light $\text{erg sec}^{-1} \text{cm}^{-2}$ $\text{Å}^{-1} \text{arcsec}^{-2}$	Total Background $\text{erg sec}^{-1} \text{cm}^{-2}$ $\text{Å}^{-1} \text{arcsec}^{-2}$
9750	1.05E-18	2.81E-18	3.86E-18
10000	9.99E-19	2.70E-18	3.70E-18
10250	9.48E-19	2.60E-18	3.55E-18
10500	8.99E-19	2.49E-18	3.39E-18
10750	8.42E-19	2.36E-18	3.20E-18
11000	8.02E-19	2.24E-18	3.04E-18

Table 6.5: Geocoronal (Airglow) Emission Lines

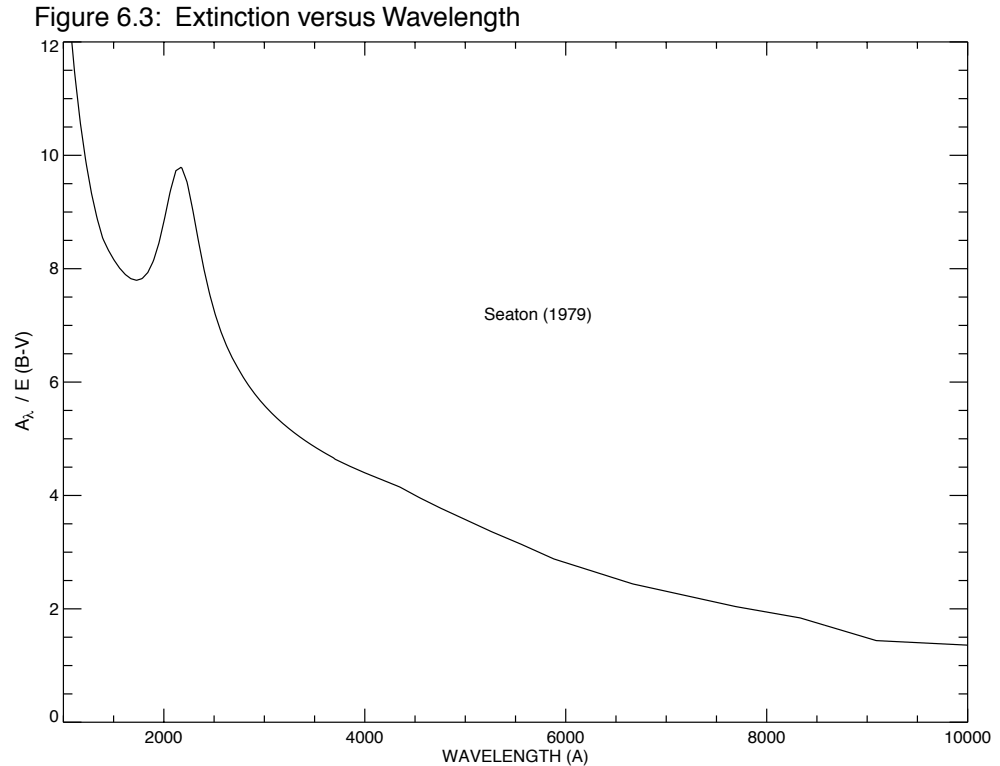
Wavelength (Å)	ID	Line Width (Å)	Intensity					
			High		Average		Low	
			kilo- Rayleighs	$\text{erg s}^{-1} \text{cm}^{-2}$ arcsec^{-2}	kilo- Rayleighs	$\text{erg s}^{-1} \text{cm}^{-2}$ arcsec^{-2}	kilo- Rayleighs	$\text{erg s}^{-1} \text{cm}^{-2}$ arcsec^{-2}
1216	Ly α	0.04	~20	6.1×10^{-13}	~10	3.05×10^{-13}	2	6.1×10^{-14}
1302 + 1306	O I	0.013	~2	5.7×10^{-14}	~1	2.85×10^{-14}	0.013	3.8×10^{-16}
1356	O I]	0.013	~0.2	5×10^{-15}	~0.1	2.50×10^{-15}	~0.001	3×10^{-17}
2471	[O II]	0.023	< 0.2	3×10^{-15}	< 0.1	1.50×10^{-15}	< 0.001	1.5×10^{-17}

6.7 Extinction Correction

Extinction can dramatically alter the counts expected from your source, particularly in the ultraviolet. Figure 6.3 shows $A_\lambda/E(B-V)$ values applicable to the Galaxy, taken from Seaton (*MNRAS*, **187**, 73p, 1979).

Extinction curves, however, have a strong metallicity and environment dependence, particularly at the UV wavelengths. Sample extinction curves can be seen in Koornneef and Code, *ApJ*, **247**, 860, 1981 (LMC); Bouchet et al., *A&A*, **149**, 330, 1985 (SMC); and Calzetti, Kinney, and Storchi-Bergmann, *ApJ*, **429**, 582, 1994, and references therein. At lower metallicities, the 2200 Å bump, which is so prominent in the galactic extinction curve, disappears and $A_\lambda/E(B-V)$ increases at UV wavelengths.

The easiest way to understand how to determine the extinction correction for your source is to work through an example; see Section 6.8.4. A choice of extinction laws is offered in the ETCs.



6.8 Exposure Time Examples

Here are a few simple examples to illustrate how an integration time may be computed for point sources and diffuse sources. The flux values given here are for illustrative purposes only; you need to check the flux values if you are planning your own observations of one of these targets.

6.8.1 Spectroscopy of Diffuse Source (M86)

We want to observe M86, an elliptical galaxy in Virgo, using the G750M grating at a central wavelength setting of $\lambda_c = 6768 \text{ \AA}$, the CCD detector and the $52 \times 0.2 \text{ arcsec}$ slit. Our aim is to calculate the $H\alpha$ count rate in the central region of M86 and the expected signal-to-noise ratio per resolution element in an exposure time of 1 hour. M86 has an inhomogeneous surface brightness distribution in $H\alpha$ and the line is well resolved with this grating. Let us consider a region with an $H\alpha$ surface brightness of $I_\lambda = 1.16 \times 10^{-15} \text{ erg sec}^{-1} \text{ cm}^{-2} \text{ \AA}^{-1} \text{ arcsec}^{-2}$ (note the unit - it is not the entire $H\alpha$ flux but the flux per unit wavelength interval) and a continuum surface brightness $I_\lambda = 2.32 \times 10^{-16} \text{ erg sec}^{-1} \text{ cm}^{-2} \text{ \AA}^{-1} \text{ arcsec}^{-2}$. To derive the $H\alpha$ and continuum count rates from the source we use the formula from Chapter 13:

- $S_{\lambda}^d = 1.14 \times 10^{13}$ counts sec^{-1} $\text{pix}_{\lambda}^{-1}$ pix_s^{-1} per incident erg sec^{-1} cm^{-2} \AA^{-1} arcsec^{-2} .
- $N_{\lambda\text{pix}} = 4$ and $N_{\text{spix}} = 2$ (1 resolution element).

Using the equation given in the second section (Spectroscopy, Diffuse Source), we get the count rate $C = 0.106$ counts sec^{-1} in $\text{H}\alpha$ and $C=0.021$ counts sec^{-1} in the continuum. Since we are interested in the properties of the $\text{H}\alpha$ line, the $\text{H}\alpha$ counts constitute the signal, while both the $\text{H}\alpha$ counts and the continuum counts contribute to the noise.

The sky background is negligible in comparison to the source, but the dark current (4.5×10^{-3} count sec^{-1} $\text{pixel}^{-1} \times 8$ pixels = 0.020 count sec^{-1}) and the read noise squared (29 electrons $\text{pixel}^{-1} \times 8$ pixels $\times 3$ reads = 465 counts, for $\text{CR-SPLIT}=3$) are important here. Substituting the numbers into the equation for signal-to-noise, we get:

$$S\text{to}N = 10.7 = \frac{0.106 \times 3600}{\sqrt{(0.127 \times 3600) + (8 \times 0.0045 \times 3600) + (8 \times 3 \times 29)}}$$

To increase our signal-to-noise or decrease our exposure time, we can consider using on-chip binning. Let us bin 2 pixels in the spatial direction so that $N_{\text{bin}} = 2$. To allow adequate sampling of our new binned pixels, we leave $N_{\lambda\text{pix}} = 4$, but set $N_{\text{spix}} = 4$, so $N_{\text{pix}} = 16$ and then $C = 0.212$ for $\text{H}\alpha$ and $C=0.254$ for the sum of $\text{H}\alpha$ and continuum. To compute the time to achieve a signal-to-noise of 12 using this configuration, we use the full expression for the exposure time given on page 95, generalized to treat the line counts (for signal) and total counts (for noise) separately, and determine that roughly 35 minutes are needed in this configuration:

$$t = 2104 =$$

$$\frac{144 \times (0.254 + 16 \times 0.0045) + \sqrt{20736 \times (0.254 + 16 \times 0.0045)^2 + 4 \times 144 \times 0.212^2 \times 8 \times 3 \times 29}}{2 \times 0.212^2}$$

6.8.2 Spectroscopy of Solar-Analog Star P041-C

We wish to study the shape of the continuum spectrum of the solar-analog star P041-C from the near IR to the near UV. We wish to obtain spectroscopy with the CCD detector covering the entire useful spectral range from 2000 \AA to 10,300 \AA with gratings G230LB, G430L, and G750L. Since we require accurate photometry, we use the wide 52X0.5 slit. The goal is to reach a signal-to-noise ratio of 25 in the near UV (at 2300 \AA), 100 in the blue, and 280 in the red. P041-C has $V = 12.0$.

The fluxes of P041-C at the desired wavelengths obtained from a spectrum of the Sun scaled from $V = -26.75$ to $V = 12.0$, are available via the web at:

<http://www.stsci.edu/ftp/cdbs/cdbs2/calspec>

G230LB

We illustrate the calculation of the exposure time for the G230LB grating. P041-C is found to have a flux of 1.7×10^{-15} erg sec $^{-1}$ cm $^{-2}$ Å $^{-1}$ at 2300 Å.

We get the following values for G230LB from Chapter 13:

- $S_{2300}^p = 1.7 \times 10^{14}$ counts sec $^{-1}$ pix $_{\lambda}^{-1}$ per incident erg sec $^{-1}$ cm $^{-2}$ Å $^{-1}$.
- $T_A = 0.86$ for the aperture throughput, taken from Chapter 13
- $\epsilon_F = \sim 0.8$.
- $N_{spix} = 3$, since $\sim 80\%$ of the point-source light is encircled with 3 pixels.
- $N_{\lambda pix} = 2$, since two pixels resolve the LSF.

Using the equation on page 90, we calculate a point-source count rate of $C = 0.34$ counts sec $^{-1}$ over $N_{pix} = 6$ pixels for GAIN=1.

The source count rates can be compared with the background and detector dark current rates. Both background and detector rates are negligibly small for this setting; therefore we can neglect their contributions. Since we are aiming for a signal-to-noise ratio of 25, we can estimate that we must obtain 625 counts minimum. The read noise squared (~ 192 over 6 pixels for 2 readouts) must therefore be taken into account. Finally, since we are observing with the CCD in the near-UV, we must correct for the effect of the multiple-electron process (see page 96). This will cause the exposure time to be scaled approximately by Q , where Q is ~ 1.5 at 2300 Å. Using the [STIS Exposure Time Calculator](#), we estimate the required time for S/N=25 is ~ 3560 seconds. To check that we indeed get S/N=25, we use the formula on page 95 as follows.

$$S/N \approx 25 = \frac{(0.34/1.5) \times 3560}{\sqrt{(0.34/1.5) \times 3560 + 192 + 40}}$$

G750L and G430L

Exposure times for the two remaining wavelength settings can be calculated directly as $time = signal-to-noise^2 / C$ since the read noise, detector background, and sky background are negligible. As above, 3 pixels are taken to contain 80% of the flux. The results are summarized in Table 6.6.

Table 6.6: Low Resolution Spectroscopy of Solar Analog Star

Grating	G230LB	G430L	G750L $\lambda_c=7751$
Wavelength (Angstroms)	2300	5000	7800
Flux (ergs sec ⁻¹ cm ⁻² Å ⁻¹)	1.7x10 ⁻¹⁵	5.9x10 ⁻¹⁴	3.5x10 ⁻¹⁴
Point Source Sensitivity (counts sec ⁻¹ pix _λ ⁻¹ per ergs sec ⁻¹ cm ⁻² Å ⁻¹)	1.7x10 ¹⁴	3.1x10 ¹⁵	5.0x10 ¹⁵
Aperture throughput (T _λ)	86%	90%	89%
N _{λpix}	2	2	2
N _{pix} to encircle 80% of PSF	3	3	3
C (counts sec ⁻¹ from source over N _{pix} =6)	0.34	240	240
Signal-to-noise ratio desired	25	100	280
Total exposure time	3560 seconds	41 seconds	330 seconds

6.8.3 Extended Source with Flux in cgs units (NGC 6543): Imaging and Spectroscopy

Let us consider NGC 6543, the Cat's Eye planetary nebula, where the aim is to use the CCD to image using the [O II] filter, and to do spectroscopy both in the visible and in the UV.

Imaging

The aim is to get a signal-to-noise ratio of 30 using the [O II] filter. We know that NGC 6543 is about 6 times fainter in [O II] than in Hβ, and its total flux at [O II] 3727 Å is $\sim 4.4 \times 10^{-11}$ erg sec⁻¹ cm⁻² contained within 1 Å. Since the radius of the object is about 10 arcsec, the average [O II] surface brightness is about 1.4×10^{-13} erg sec⁻¹ cm⁻² arcsec⁻² Å⁻¹.

We take:

- $S_{\lambda}^d = 6.7 \times 10^{11}$ counts sec⁻¹ pix⁻¹ Å⁻¹ per incident erg sec⁻¹ cm⁻² Å⁻¹ arcsec⁻² as given in Chapter 14.
- We take $N_{pix} = 4 \times 4 = 16$, since a resolution element has radius of two pixels (see Chapter 14).

To calculate the count rate we use the equation on page 93 for diffuse sources and determine a per-pixel count rate of 0.094 counts sec⁻¹ pixel⁻¹ or a count rate $C = 1.5$ counts sec⁻¹ over 16 pixels. The background and the dark current can be neglected. To get a signal-to-noise of 30 we need $\sim 10^3$ counts, so the read noise can also be neglected and we can use the simplified expression to calculate exposure time (see page 95). We obtain 10^3 counts in ~ 667 seconds. To allow post-observation removal of cosmic

rays we use CR-SPLIT=2. We note that in each ~330 second exposure we predict a mean of ~31 counts pixel⁻¹, and thus we are safely within the limits of the CCD full well.

Diffuse-Source Spectroscopy in the Visible and UV Regions

In the visible, the aim is to get a signal-to-noise of about 100 at $\lambda = 4861 \text{ \AA}$, with the G430M grating at a central wavelength setting of $\lambda_c = 4961 \text{ \AA}$, the CCD detector, and the 52X0.1 arcsec slit. In the UV, the aim is to get a signal-to-noise ratio of about 20 at the C IV ~1550 \AA line with the G140M grating at a central wavelength setting of $\lambda_c = 1550$ and the FUV-MAMA detector. To increase our signal-to-noise ratio in the UV, we use the 52X0.2 arcsec slit for the G140M spectroscopic observations.

Visible Region

NGC 6543 has an average H β surface brightness of $S(\text{H}\beta) \sim 8.37 \times 10^{-13} \text{ erg sec}^{-1} \text{ cm}^{-2} \text{ \AA}^{-1} \text{ arcsec}^{-2}$ at 4861 \AA and has a radius of about 10 arcsec.

We take from Chapter 13.

- $S_{\lambda}^d = 1.62 \times 10^{12} \text{ counts sec}^{-1} \text{ pix}_{\lambda}^{-1} \text{ pix}_s^{-1}$ per incident $\text{erg sec}^{-1} \text{ cm}^{-2} \text{ \AA}^{-1} \text{ arcsec}^{-2}$ for G430M.
- $N_{\lambda \text{pix}} = N_{\text{spix}} = 2$ since 2 pixels resolves the LSF and PSF.

Using the equation for diffuse sources on page 90, we derive a per-pixel count rate of 1.4 counts sec⁻¹ pixel⁻¹ and a count rate integrated over the four pixels of $C = 5.4 \text{ counts sec}^{-1}$ at 4861 \AA from the astronomical source. The sky background and the detector background are much lower. To allow cosmic-ray removal in post-observation data processing, we use CR-SPLIT=3. To achieve a signal-to-noise of 100, we require a total of roughly 10,000 counts, so read noise should be negligible, even over 4 pixels and with NREAD = 3. We calculate the time required to achieve signal-to-noise of 100, using the simplified equation on page 95, and determine that we require roughly 30 minutes.

$$t = 1850 = \frac{10000}{5.4}$$

At a count rate of ~1 count sec⁻¹ pixel⁻¹ for 600 seconds per CR-SPLIT exposure, we are in no danger of hitting the CCD full-well limit.

UV Region

The C IV flux of NGC 6543 is $\sim 2.5 \times 10^{-12} \text{ erg sec}^{-1} \text{ cm}^{-2} \text{ arcsec}^{-2}$ spread over ~1 \AA . The line, with a FWHM ~0.4 \AA , will be well resolved in the G140M configuration using the 52X0.2 slit.

We take from Chapter 13:

- $S_{\lambda}^d = 5.15 \times 10^9 \text{ counts sec}^{-1} \text{ pix}_{\lambda}^{-1} \text{ pix}_s^{-1}$ per incident $\text{erg sec}^{-1} \text{ cm}^{-2} \text{ \AA}^{-1} \text{ arcsec}^{-2}$ for G140M at $\lambda=1550\text{\AA}$ using the 0.2 arcsecond wide slit.

- We take $N_{\lambda pix} = N_{spix} = 8$, since the line emission is spread over the ~ 8 pixels of the slit width in dispersion, and we are willing to integrate flux along the slit to improve the signal-to-noise ratio.

Using the equation for diffuse sources on page 90, we determine a per-pixel peak count rate of ~ 0.013 counts sec^{-1} pixel^{-1} and a count-rate over the 64 pixels of $C = 0.82$ counts sec^{-1} at 1550 \AA from the astronomical source. The sky and detector backgrounds are still negligible, and the read noise is zero for the MAMA detector so we can use the simplified equation for exposure time on page 95 directly. We determine that we require ~ 7 minutes.

$$t = 490 = \frac{400}{0.82}$$

We are well below the MAMA local linearity limit of 50 counts sec^{-1} pixel^{-1} . Even assuming the nebula evenly illuminates the full 28 arcseconds of the long slit, we are well below the global absolute and linearity limits, since the flux from the nebula is concentrated in the C IV emission line. Then the global count rate, if the source fully fills the slit in the spatial direction, is given roughly by $(0.015 \times 8 \times 1024) \ll 200,000$ counts sec^{-1} . Finally, we are well below the MAMA 16 bit buffer limit of a maximum of $65,536$ counts pixel^{-1} integrated over the exposure duration.

6.8.4 Echelle Spectroscopy of a Bright Star with Large Extinction (Sk $-69^\circ 215$)

The aim here is to do high-resolution echelle spectroscopy of an O5 star in the LMC (such as Sk $-69^\circ 215$) at 2500 \AA , using the E230H grating at a central wavelength of $\lambda_c = 2513 \text{ \AA}$ and using the 0.2×0.09 arcsec slit. The aim is to get a signal-to-noise ratio of about 50 from photon statistics. We will assume that the exact UV flux of the star is unknown and we need to estimate it from the optical data. This calculation of the stellar flux at 2500 \AA involves 2 steps:

1. Calculation of the dereddened flux at 5500 \AA .
2. Calculation of predicted flux at 2500 \AA taking reddening with standard extinction and stellar models into account.

Dereddened Magnitude and Prediction of 2500 \AA Flux

We assume that it is an O5 V star with $V = 11.6$ (its exact spectral type is slightly uncertain). The expected $B - V$ value from such a star is -0.35 , whereas the observed $B - V$ is -0.09 ; we thus get $E(B - V) = 0.26$ mag.

We assume all the extinction to be due to the LMC, and use the appropriate extinction law (Koornneef and Code, *ApJ*, **247**, 860, 1981). The total visual extinction is then $R \times E(B - V) = 3.1 \times 0.26 = 0.82$, leading to an unreddened magnitude of $V_0 = 10.78$. The corresponding flux at 5500 \AA (using the standard zero point where $V = 0$ corresponds to $F(5500 \text{ \AA}) =$

$3.55 \times 10^{-9} \text{ erg sec}^{-1} \text{ cm}^{-2} \text{ \AA}^{-1}$) is $F(5500 \text{ \AA}) = 1.73 \times 10^{-13} \text{ erg sec}^{-1} \text{ cm}^{-2} \text{ \AA}^{-1}$.

The model atmosphere of Kurucz predicts $F(2500 \text{ \AA}) / F(5500 \text{ \AA}) = 17.2$ for an O5 star, which leads to a flux of $F_{2500 \text{ \AA}} = 2.98 \times 10^{-12} \text{ erg sec}^{-1} \text{ cm}^{-2} \text{ \AA}^{-1}$ at 2500 \AA for the unreddened star. Reddening will diminish this flux by a factor of $10^{-0.4 \times A(2500 \text{ \AA})}$, where the absorption at 2500 \AA can be determined from the extinction curve; the result in this case is $A(2500 \text{ \AA}) = 1.3$. Thus the predicted flux of this star at 2500 \AA is $9.0 \times 10^{-13} \text{ erg sec}^{-1} \text{ cm}^{-2} \text{ \AA}^{-1}$.

Exposure-Time Calculation

We take from Chapter 13:

- $S_{2500}^p = 2.9 \times 10^{11} \text{ counts sec}^{-1} \text{ pix}_{\lambda}^{-1}$ per incident $\text{erg sec}^{-1} \text{ cm}^{-2} \text{ \AA}^{-1}$ for E230H.
- $T_A = 0.659$ for the aperture throughput.
- $\varepsilon_f = 0.8$ for the encircled energy.
- $N_{\lambda \text{ pix}} = 2$, since two pixels resolve the LSF.
- $N_{\text{spix}} = 3$, since 80% of the point source light is encircled by 3 pixels.

Using the equation for point sources on page 90, we determine a total count rate from the star of $C = 0.3 \text{ counts sec}^{-1}$ over 6 pixels. From Chapter 13 we see that ~ 22 percent of the point-source flux will be contained within the peak pixel. Thus the peak per pixel count rate will be approximately $0.3 \times 0.22 / (0.8 \times 2) = 0.045 \text{ counts sec}^{-1} \text{ pixel}^{-1}$ and well within the local linear counting regime. We can use the information that we register $\sim 0.3 \text{ counts sec}^{-1}$ for every two pixels in the dispersion direction to estimate the global count rate (over the entire detector) as follows. Each order contains ~ 1024 pixels, and the E230H grating at the central wavelength setting of 2513 \AA covers 33 orders (see Chapter 13). A rough estimate of the global count rate is thus $\sim 33 \times 512 \times 0.3 / 0.8 \sim 6400 \text{ count sec}^{-1}$ and we are well within the linear range.

To calculate the integration time, we can ignore both the sky background and the detector dark current which are several orders of magnitude fainter than the source. To achieve a signal-to-noise ratio of 50 we then require ~ 2500 counts which would take a total of ~ 2.3 hours. Fortunately, this is a CVZ target!

6.8.5 Imaging a Faint Stellar Source

Consider a case where the aim is to image a faint ($V = 28$), A-type star with the clear filter and the CCD detector. We want to calculate the integration time required to achieve a signal-to-noise ratio of 5. The count rate from the source is $0.113 \text{ counts sec}^{-1}$ distributed over about 25 pixels

using the information in Chapter 14. If we assume the background to be “typical high” (Table 6.3), the count rate due to the background integrated over the bandpass is ~ 0.15 counts sec^{-1} pixel^{-1} or 3.8 counts sec^{-1} in 25 pixels (and the detector dark rate is 35 times lower). We will need to be able to robustly distinguish cosmic rays if we are looking for faint sources, so we will use $\text{CR-SPLIT}=4$. We use the STIS Exposure Time Calculator to estimate the required exposure time to be 8548 seconds. To reproduce the numbers given by the ETC, we use the equation on page 95:

$$S/N=5 = \frac{0.113 \cdot 8548}{\sqrt{0.113 \cdot 8548 + 0.15 \times 25 \times 8548 + 0.0045 \times 25 \times 8548 + 25 \times 29 \times 4}}$$

Alternately, we could have requested LOW-SKY (see Section 6.5.2), since these observations are sky-background limited. In that case the sky background integrated over the bandpass produces ~ 0.035 counts sec^{-1} pixel^{-1} to which we add the detector dark current to get a total background of 0.039 counts sec^{-1} pixel^{-1} . Using the full equation for exposure time again, we then determine that we require only ~ 60 minutes. This option is preferable to perform this experiment. To check the S/N , we use the equation on page 95:

$$S/N=5 = \frac{0.113 \times 3645}{\sqrt{(0.113 \times 3645) + (0.035 \times 25 \times 3645) + (0.0045 \times 25 \times 3645) + (25 \times 29 \times 4)}}$$

6.8.6 Time-Tag Observations of a Flare Star (AU Mic)

Suppose the aim is to do TIME-TAG observations of a flare star such as AU Mic, in the hydrogen Lyman- α 1216 Å line (see Section 11.1.3). We wish to observe it with the G140M grating, the MAMA detector and a 0.2 arcsec slit. AU Mic has $V = 8.75$, the intensity of its the Ly- α line is about $6 (\pm 3) \times 10^{-12}$ erg sec^{-1} cm^{-2} Å $^{-1}$, and the width (FWHM) of the line is about $0.7 (\pm 0.2)$ Å. We will assume that during bursts, the flux might vary by a factor of 10, so that the line flux may be up to 60×10^{-12} erg cm^{-2} sec^{-1} Å $^{-1}$. AU Mic is an M star and its ultraviolet continuum is weak and can be neglected.

We use from Chapter 13:

- $S_{\lambda}^p = 2.30 \times 10^{12}$ counts sec^{-1} $\text{pix}_{\lambda}^{-1}$ per incident erg sec^{-1} cm^{-2} Å $^{-1}$.
- Aperture throughput $T_A = 0.6$.
- Encircled energy $\varepsilon_f = 0.8$.
- $N_{\text{spix}} = 10$.
- Derive $N_{\lambda\text{pix}} = 14$ since the line FWHM is ~ 0.7 Å and the dispersive plate scale for G140M is 0.05 Å pixel^{-1} .

Plugging these values into the point-source equation on page 90, we get $C = 927 \text{ counts sec}^{-1}$ over 10×14 pixels, or $\sim 1160 \text{ counts sec}^{-1}$ from the source during a burst (taking $\epsilon_f = 1.0$). This is well below the MAMA TIME-TAG global linearity limit of $30,000 \text{ count sec}^{-1}$ and the continuous observing limit of $26,000 \text{ count sec}^{-1}$. The line is spread over 14 pixels in dispersion and roughly only 10% of the flux in the dispersion direction falls in the peak pixel; thus the peak per-pixel count rate, P_{cr} , is roughly $927 / (14 \times 10) = 7 \text{ counts sec}^{-1} \text{ pixel}^{-1}$, and we are not near the MAMA local linearity limit.

For a TIME-TAG exposure, we need to determine our maximum allowed total observation time, which is given by $6.0 \times 10^7 / C$ seconds or roughly 1079 minutes = 18 hours. For Phase II only, we will also need to compute the value of the BUFFER-TIME parameter, which is the time in seconds to reach 2×10^6 counts, in this case 2157 seconds ($= 2 \times 10^6 / 927$).

Feasibility and Detector Performance

In this chapter. . .

7.1 The CCD / 115
7.2 CCD Operation and Feasibility Considerations / 129
7.3 The MAMA Detectors / 140
7.4 MAMA Operation and Feasibility Considerations / 147
7.5 MAMA Spectral Offsetting / 153
7.6 MAMA Bright-Object Limits / 154

STIS employs two fundamentally different types of detectors: a UV-optimized CCD for use from the near-UV to the near-IR, and Multi-Anode Microchannel Array detectors, known as MAMAs, for use in the ultraviolet. The CCD and the MAMA detectors are used in different ways and impose their own unique limitations on the feasibility of observations performed with them. In this chapter we present the properties of the STIS detectors, describe how to use them to optimize scientific programs, and list the steps you should take to ensure the feasibility of your observations.

7.1 The CCD

7.1.1 Detector Properties

The STIS/CCD is a low-noise device capable of high sensitivity in the visible and the near-UV. It is a thinned, backside-illuminated device

manufactured by Scientific Imaging Technologies (SITE). In order to provide near-UV imaging performance, the CCD was backside-treated and coated with a wide-band anti-reflectance coating. The process produces acceptable near-UV quantum efficiency (QE) without compromising the high QE of the visible bandpass. The CCD camera design incorporates a warm dewar window, designed to prevent buildup of contaminants on the window, which were found to cause a loss of UV throughput for the WFPC2 CCDs. A summary of the STIS CCD performance is given in Table 7.1. The performance values on read noise and dark current are those valid as of February 2002.

Table 7.1: CCD Detector Performance Characteristics

Characteristic	CCD Performance
Architecture	Thinned, backside illuminated
Wavelength range	2000–11,000 Å
Pixel format	1024 x 1024 illuminated pixels
Field of view	52 x 52 arcseconds
Pixel size	21 x 21 μm^2
Pixel plate scale	0.0507 arcseconds
Quantum efficiency	~ 20% @ 3000 Å ~ 67% @ 6000 Å ~ 29% @ 9000 Å
Dark count at -83°C	0.004 $\text{e}^- \text{sec}^{-1} \text{pix}^{-1}$ (but varies with detector T)
Read noise (effective values)	5.4 e^- rms at GAIN=1 (1 e^- of which is pattern noise) 7.6 e^- rms at GAIN=4 (0.2 e^- of which is pattern noise)
Full well	144,000 e^- over the inner portion of the detector 120,000 e^- over the outer portion of the detector
Saturation limit	33,000 e^- at GAIN=1 144,000 e^- at GAIN=4

7.1.2 Effects of the Change to STIS Side-2 Electronics on CCD Performance

In May 2001, the primary Side-1 electronics on STIS failed. Operations were subsequently resumed using the backup Side-2 electronics. CCD observations have been affected in two ways.

First, the Side-2 electronics do not have a working CCD temperature controller, and the detector can no longer be held at a fixed temperature. As a result, the CCD dark current now fluctuates with the detector temperature. Fortunately, the dark current variation correlates well with the CCD housing temperature, with the dark current varying by $\sim 7\%/^\circ\text{C}$.

Further details are given in [STIS ISR 2001-03](#). All reference file dark images prepared for use with STIS/CCD data taken during Side-2 operations are now scaled to a standard housing temperature of 18°C before being delivered. Before subtraction of the appropriate dark file from Side-2 CCD data, the **calstis** package rescales the dark using the CCD housing temperature value in the OCCDHTAV keyword which is found in the extension header of each sub-exposure.

The second change is an increase in the read noise by about $1e^-/s$ when CCDGAIN=1 and by $0.2 e^-/s$ when CCDGAIN=4. This extra read noise appears in the form of coherent pattern noise, and under some circumstances it may be possible to ameliorate this noise by using Fourier filtering techniques. See [STIS ISR 2001-05](#) for additional discussion.

7.1.3 CCD Spectral Response

The spectral response of the unfiltered CCD is shown in Figure 5.6 (labeled as 50CCD). This figure illustrates the extremely wide bandpass over which this CCD can operate. The wide wavelength coverage is an advantage for deep optical imaging (although the new Advanced Camera for Surveys is better suited to most optical imaging programs). The near-UV sensitivity of the CCD makes it a good alternative to the NUV-MAMA for low- and intermediate-resolution spectroscopy from ~ 2500 to 3100 \AA using the G230LB and G230MB grating modes (Table 4.1).

Based on data to date, the STIS CCD does not suffer from Quantum Efficiency Hysteresis (QEH)—that is, the CCD responds in the same way to light levels over its whole dynamic range, irrespective of the previous illumination level.

7.1.4 CCD Sensitivity

Sensitivity variations in CCD spectroscopic configurations have been determined to be due primarily to increasing charge transfer efficiency (CTE) losses (see Section 7.2.6), temperature fluctuations since the switch to the Side-2 electronics (see Section 7.1.2), and actual time-dependent changes in sensitivity. For a more detailed analysis of the STIS Sensitivity Monitor observations from 1997 through March 2004 please refer to [STIS ISR 2004-?](#).

Since the switch to Side-2 operations, a linear trend of the sensitivity with temperature has been found for the first-order modes G230LB and G430L, and is of the order of $+0.42$ and $+0.20 \text{ \%}/^\circ\text{C}$, respectively. In contrast, the G750L sensitivity does not show any significant dependence on temperature.

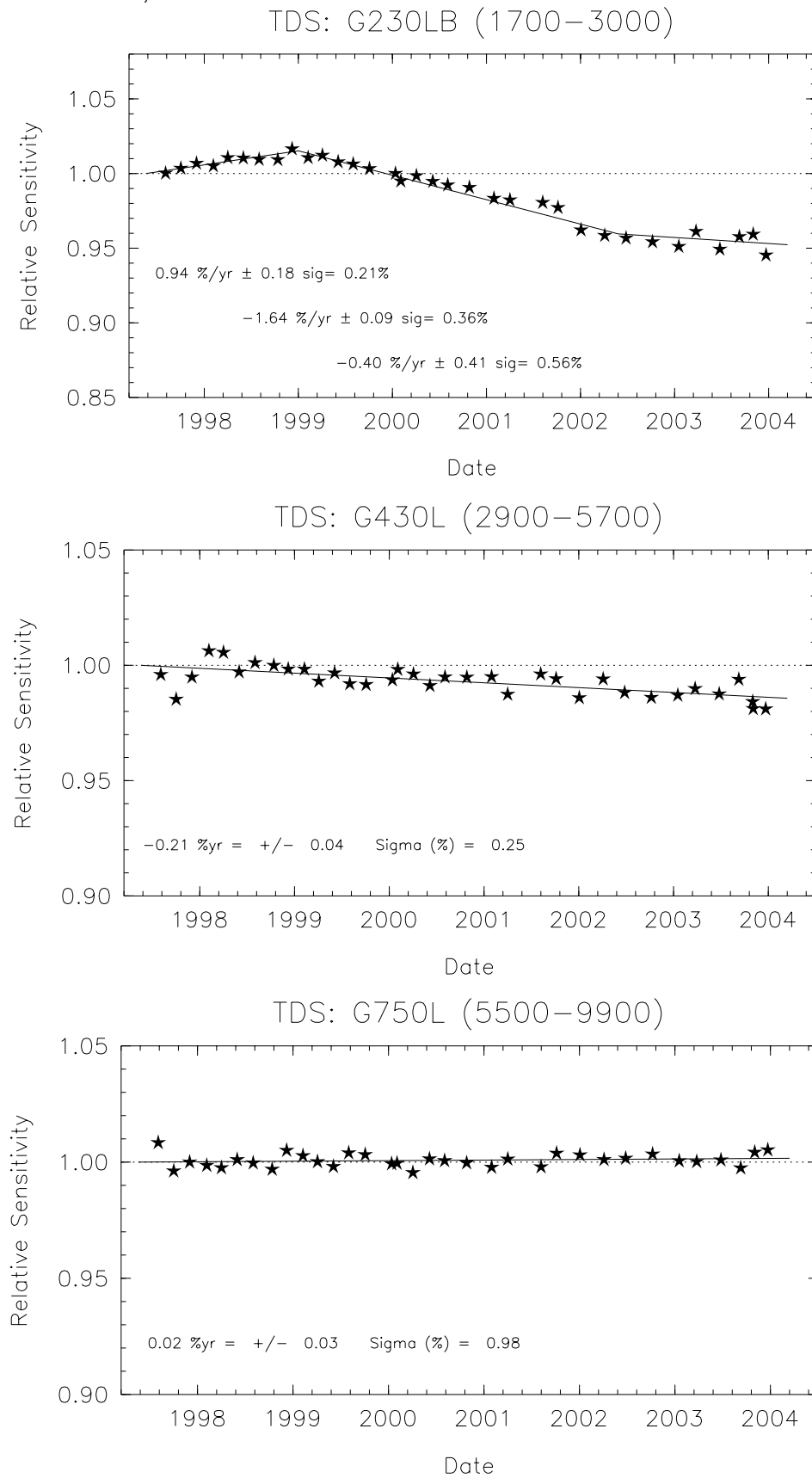
After temperature and CTE effects are taken into account, the sensitivity of the G230LB and G430L modes is seen to vary with time at a

rate that has significantly slowed down in the most recent epoch of observations (beginning in early 2002), and ranges, on average, from 0.40%/yr (G230LB) to 0.21%/yr (G430L). The G750L mode does not show significant time-dependence. Trends for time-dependent sensitivity (TDS) for the CCD low-resolution (L) modes are shown in Figure 7.1. Selected wavelength settings of the medium-resolution (M) gratings G230MB, G430M, and G750M have also been monitored. Sensitivity trends measured for the limited M-mode wavelength coverage are similar to those observed in the L-modes at corresponding wavelengths. The G230LB and G230MB CCD configurations exhibit the same behavior found for the NUV MAMA G230L mode (see Section 7.3.3), featuring an increase in sensitivity during the first 1.5 years of STIS operations, followed by decreasing sensitivity, and a slow-down in the decline in the last two years (see Figure 7.13).

TDS corrections for all first-order CCD modes have been implemented into the STIS pipeline as new TDSTAB reference files (see Section 15.1) and will correct fluxes of extracted spectra for sensitivity changes to a typical accuracy of 1% or better. CTE corrections have also been implemented (see Section 7.2.6), however no correction for temperature dependence of the sensitivity is yet performed in the STIS pipeline. These new TDS trends have also been incorporated into reference files used by SYNPHOT and the STIS ETCs. This enables count rate predictions to take the sensitivity changes into account. The default TDS throughputs for SYNPHOT and STIS ETC calculations will assume a date of 2004-Jul-01 (beginning of Cycle 13).

TDS corrections for CCD imaging modes are currently being tested and will be implemented in the pipeline in the near future. On the other hand, the CTE effects for imaging modes will be addressed by means of tailored post-pipeline IRAF tasks, in view of the inability of the pipeline to identify all targets on the image for which CTE effects are to be corrected. These IRAF tasks are planned to become available during Cycle 13.

Figure 7.1: Relative sensitivity vs. time for first-order CCD L-modes G230LB, G430L, and G750L.



7.1.5 CCD Long-Wavelength Fringing

Like most CCDs, the STIS CCD exhibits fringing in the red, longward of ~ 7500 Å. This fringing limits the signal-to-noise routinely achievable in the red and near-IR unless contemporaneous fringe flats are obtained (see below). In principle, fringing can also affect imaging observations if the source's emission over the 50CCD or F28X50LP bandpass is dominated by emission lines redward of 7500 Å. However, if the bulk of the emission comes from blueward of 7500 Å, then emission from multiple wavelengths will smooth over the fringe pattern so that imaging will not be affected by fringing.

The amplitude of the fringes is a strong function of wavelength and spectral resolution. Table 7.2 lists the observed percentile peak-to-peak and rms amplitudes of the fringes as a function of central wavelength for the G750M and G750L gratings. The listed "peak-to-peak" amplitudes are the best measure of the impact of the fringing on your data. The rms values at wavelengths < 7000 Å give a good indication of the counting statistics in the flat-field images used for this analysis.

Table 7.2: Fringing Amplitude in Percent as a Function of Wavelength

Wavelength (Å)	G750M peak-to-peak	G750M rms	G750L peak-to-peak	G750L rms
6100		1.21		
6250		1.23		
6600		1.23		
6750		1.29		
7250	4.62	1.52	3.18	2.13
7750	9.61	3.10	8.58	3.08
8250	10.53	3.26	6.76	2.80
8750	14.83	3.85	10.81	3.98
9250	27.16	9.00	23.42	7.92
9750	32.09	10.78	25.35	8.96
10250	18.23	6.04	17.30	5.89

The fringe pattern can be corrected by rectification with an appropriate flat field. The fringe pattern is a convolution of the contours of constant distance between the front and back surfaces of the CCD and the wavelength of the light on a particular part of the CCD. The fringe pattern has been shown to be very stable, as long as the wavelength of light on a particular part of the CCD stays constant. However, due to the grating wheel positioning uncertainty ("Slit and Grating Wheels" on page 27) and the effect of temperature drifts in orbit, the wavelength on a particular part

of the CCD will vary from observation to observation. Thus, the best de-fringing results are obtained by using a contemporaneous flat (“fringe flat”), i.e., a tungsten lamp flat taken at the same grating wheel setting and during the same orbit as your scientific exposures.

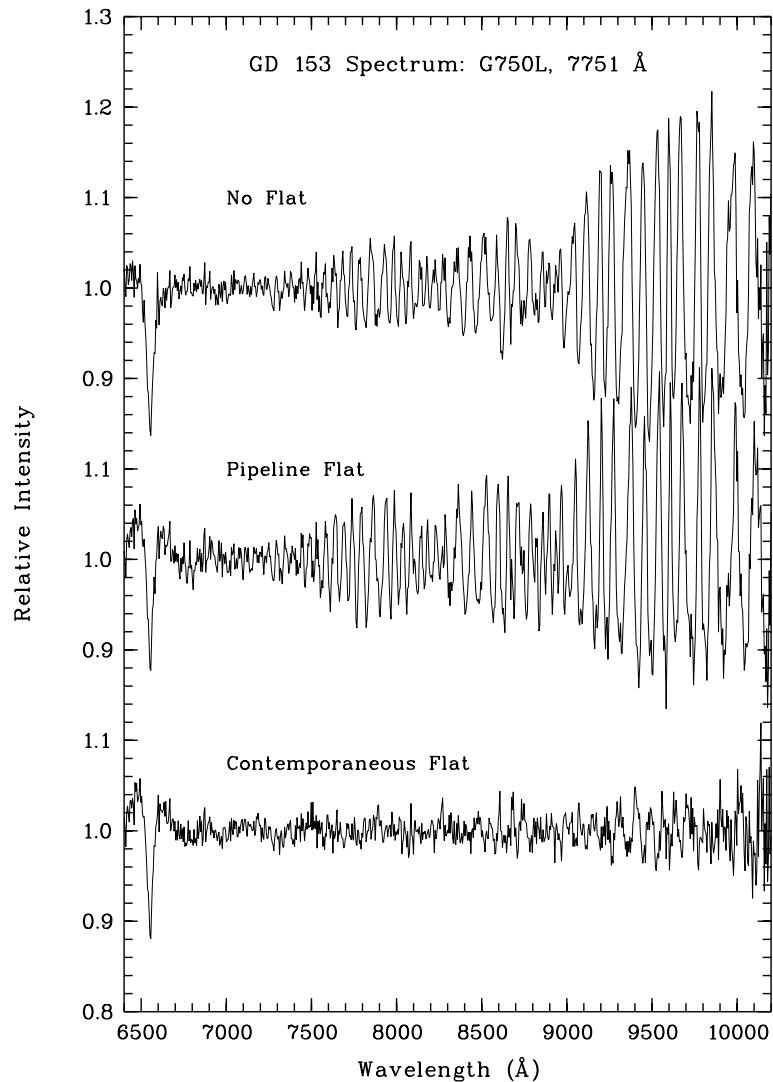
Table 7.3 compares the estimated peak-to-peak fringe amplitudes *after* flat-fielding by the library flat and by those after flat fielding with an appropriately processed contemporaneous flat. These estimates are based upon actual measurements of spectra of both point sources and extended sources made during Cycle 7 (the results for point sources and extended sources were essentially the same). Figure 7.2 shows such a comparison for a G750L spectrum of a white dwarf; in this figure, the top panel shows white dwarf GD153 (central wavelength 7751 Å) with no flat field correction, the second spectrum shows the result of de-fringing with the standard pipeline flat field, and the third spectrum shows the result of de-fringing with a contemporaneous flat (all spectra were divided by a smooth spline fit to the stellar continuum). It is clear that a contemporaneous flat provides a great improvement over the use of a library flat. Therefore, if you are observing in the far red (> 7500 Å) and using grating G750L or G750M, you should take a contemporaneous flat field along with your scientific observations. More detailed information and analysis on fringe correction for STIS long-wavelength spectra can be found in STIS ISRs [1998-19](#), [1998-29](#), and the references therein.

Table 7.3: Residual fringe amplitude (rms, in percent) after flat-fielding with library pipeline flat and a contemporaneous flat

Wavelength (Å)	G750M, library flat: residual	G750M, contemp. flat: residual ¹	G750L, library flat: residual	G750L, contemp. flat: residual
7500	3.0	1.2	4.0	0.9
7750	2.5	1.3	5.3	0.8
8000	4.2	1.3	7.5	1.0
8250	4	1.0	5.3	0.9
8500	5	0.9	8.3	1.0
8750	6	0.9	6.5	0.9
9000	8	—	8.3	1.0
9250	10	—	17.5	1.4
9500	11	—	18.7	2.0
9750	12	—	19.7	2.4
10000	10	—	11.7	2.4

1. Measurements of the fringe amplitude have not been made yet for G750M wavelength settings redward of 8561 Å. However, from our experience with fringe corrections we expect the residual fringe amplitudes to be of order 1% when contemporaneous fringe flats are used.

Figure 7.2: Comparison of De-fringing Capabilities of Pipeline Flats and Those of Contemporaneous Flats

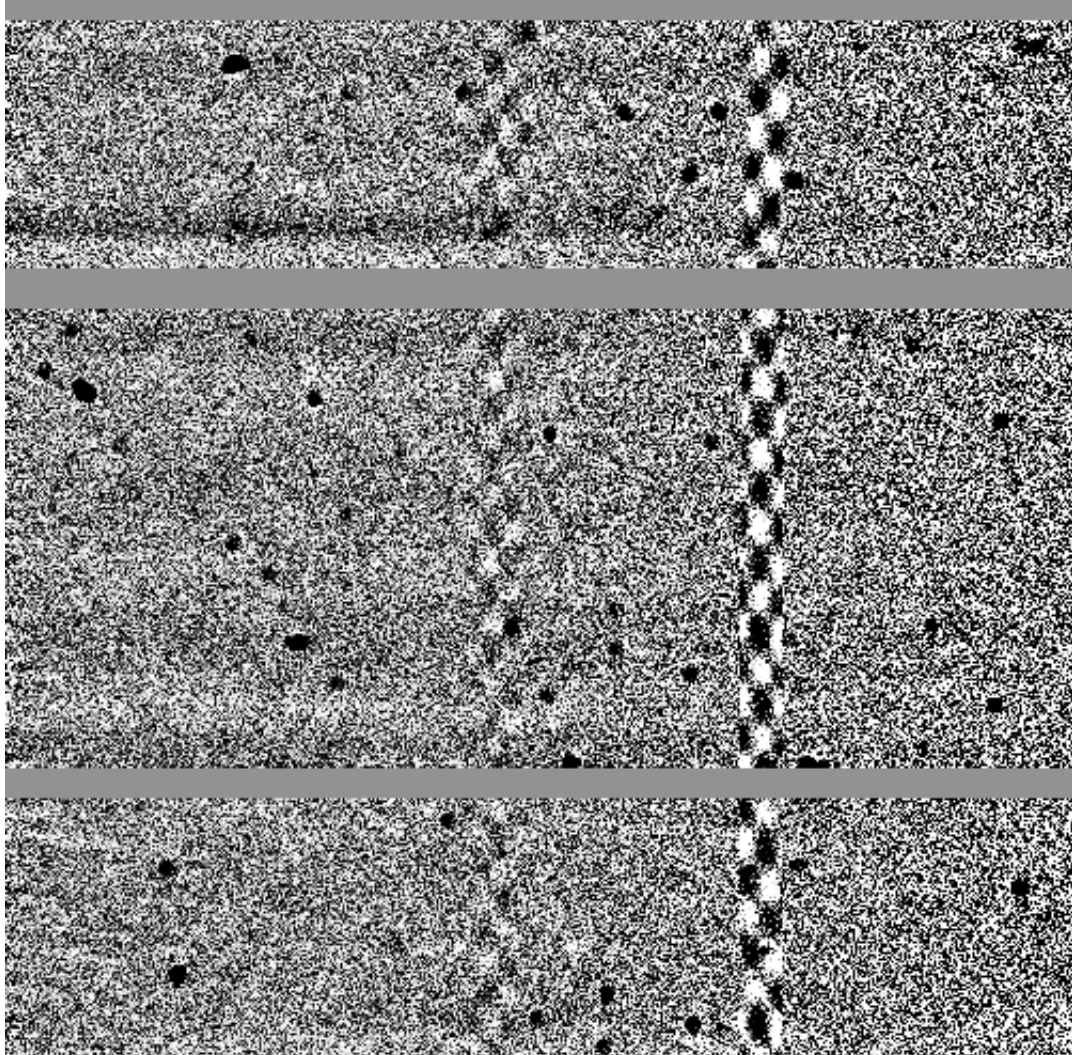


7.1.6 Fringing due to the Order Sorter Filters

Examination of long slit observations in the CCD spectroscopic modes has revealed periodic variations of intensity along the slit when highly monochromatic, calibration lamp sources are used. An example of such 'chevron-pattern' variations is shown in Figure 7.3 and Figure 7.4. These variations are thought to be the result of transmission variations through the highly parallel faces of the order sorting filters that are situated next to the gratings in the optical path. In the cross dispersion direction, the modulation amplitude depends on the line width with a maximum of 13% for a monochromatic source in G430L and G430M modes, and 4.5% in G750L and G750M modes. Periods range from 40 - 80 pixels/cycle. In the dispersion direction, there is a small, residual, high frequency modulation

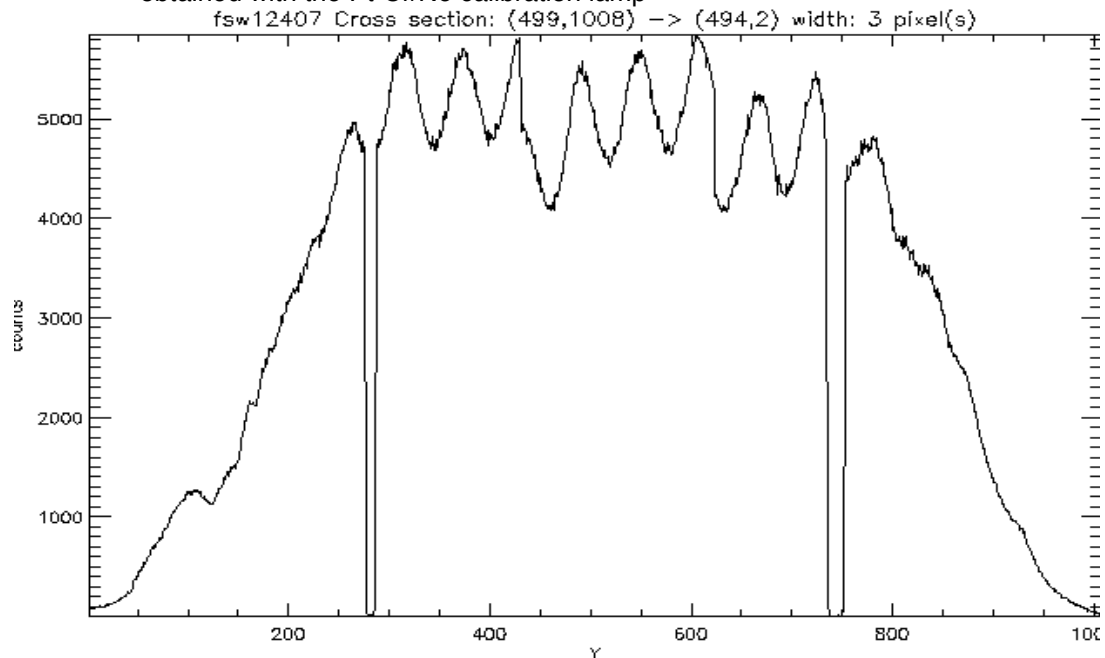
with a peak amplitude of about 1.5% in G430M at the 5471Å setting and with smaller amplitudes in all other modes and settings. No such modulation has been observed in any of the MAMA modes. Some modulation is also apparent in the CCD G230LB and G230MB modes, however the amplitudes of these modulations are much smaller and analysis of these modes is ongoing.

Figure 7.3: CCD image of a calibration lamp exposure which shows the chevron-pattern variations. The image is taken with G430L grating and a 2 arcsec slit. The chevron patterns are seen at the position of the emission lines.



It should be noted that this effect is pronounced only for monochromatic sources; the modulation is negligible for continuum sources. So far, such modulation has not been observed in any astronomical observations. A calibration program would be necessary to investigate this effect further.

Figure 7.4: A plot of the 52x0.2 slit illumination near 4269Å in mode G430L obtained with the Pt-Cr/Ne calibration lamp



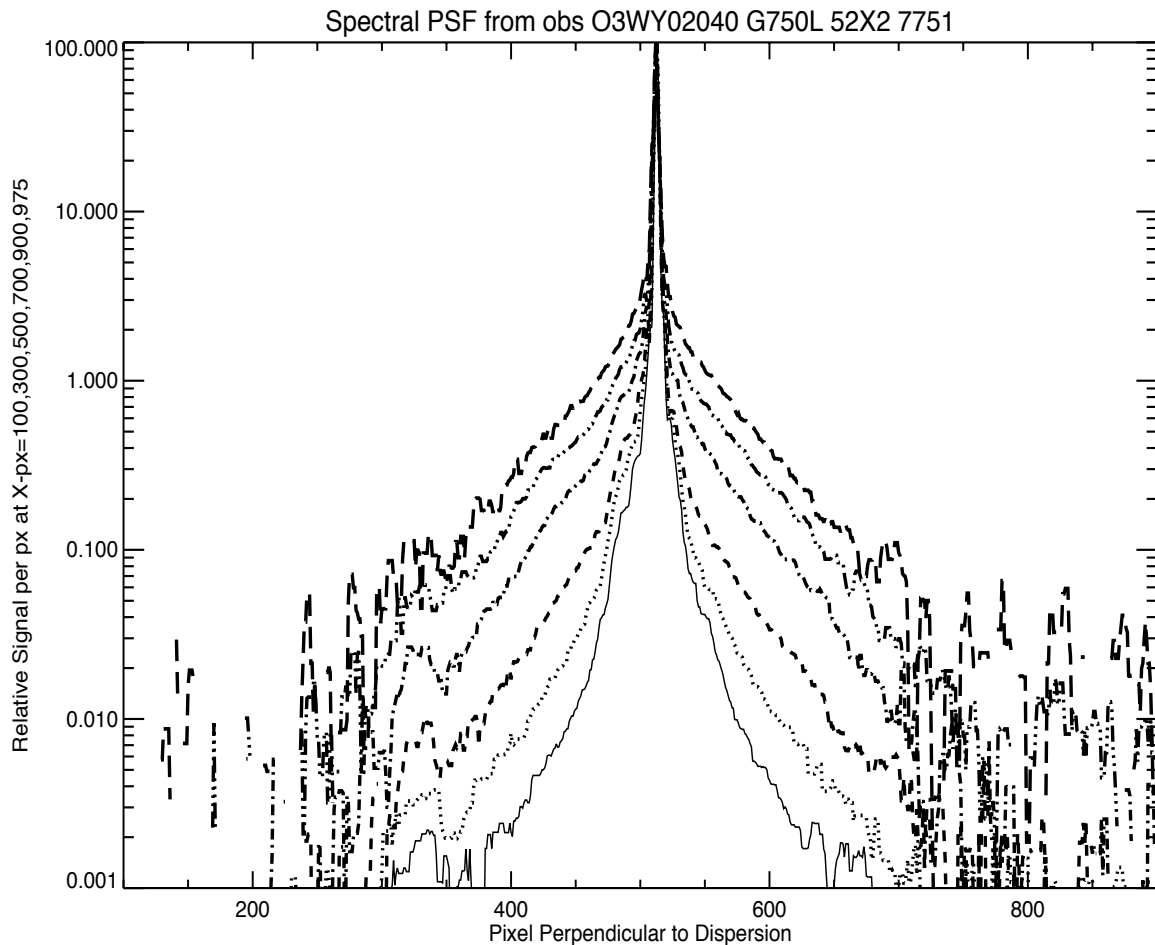
7.1.7 Optical Performance

Verification testing has shown that STIS meets its image-quality specifications. While the optics provide fine images at the focal plane, the detected point-spread functions (PSFs) are degraded somewhat more than expected by the CCD at wavelengths longward of about 7500 Å, where a broad halo appears, surrounding the PSF core. This halo is believed to be due to scatter within the CCD mounting substrate, which becomes more pronounced as the silicon transparency increases at long wavelengths. The effects of the red halo (see Figure 7.5), which extend to radii greater than 100 pixels (5 arcsec), are not included in the encircled energies as a function of observing wavelength that are described for the CCD spectroscopic and imaging modes in Chapters 13 and 14, respectively. However, estimates of the encircled energy vs. radius that include the halo are shown in Table 7.4. The integrated energy in the halo amounts to approximately 20% of the total at 8050 Å and 30% at 9050 Å (see also [STIS ISR 1997-13](#) for the implication for long-slit spectroscopic observations at long wavelengths). Note that the ACS WFC CCDs have a front-side metallization that eliminates the large angle long wavelength halo problem in those detectors.

The CCD plate scale is 0.0507 arcseconds per pixel for imaging observations (see [STIS ISR 2001-02](#)), and in the spatial (across the dispersion) direction for spectroscopic observations. Due to the effect of anamorphic magnification, for spectroscopic observations the plate scale in

the dispersion direction is slightly different and it depends on the grating used and its tilt. The plate scale in the dispersion direction ranges from 0.0512 to 0.0581 arcseconds per pixel (see [STIS ISR 1998-23](#)).

Figure 7.5: Cross-sections of the signal distribution perpendicular to the dispersion direction for G750L, at six wavelengths from 5752 Å to 10020 Å. Each PSF is normalized to a peak value of 100. The strong wavelength dependence of the PSF provides a clean separation of the curves.



The CCD detector produces a relatively faint, out-of-focus, ring-shaped “ghost” image, due to specular reflection from the CCD surface and window. The ring contains about 1% of the total energy in the image and is very stable. Additional rings of similar size can be seen at other locations in the field in grossly saturated images, but these contain only of order 10^{-5} of the total energy and are thus not likely to be detected in normal scientific images. Lines drawn from stars in images through their respective ghosts are found to converge at a “radiant point” located to the lower right of the image center. This effect is illustrated in Figure 7.6 where the line segments are drawn from pixel coordinates 528,342 (in 1024 x 1024 user coordinates) through the centroids of the brightest stars in the image. Note that these line segments intercept the centers of the ring-like ghosts very

well. Observers who wish to avoid placing very faint objects within the range of the ghosts may want to take this geometry into account when writing Phase II submissions.

Figure 7.6: Ring-Shaped Ghost Images Near Bright Point Sources (50CCD Image)

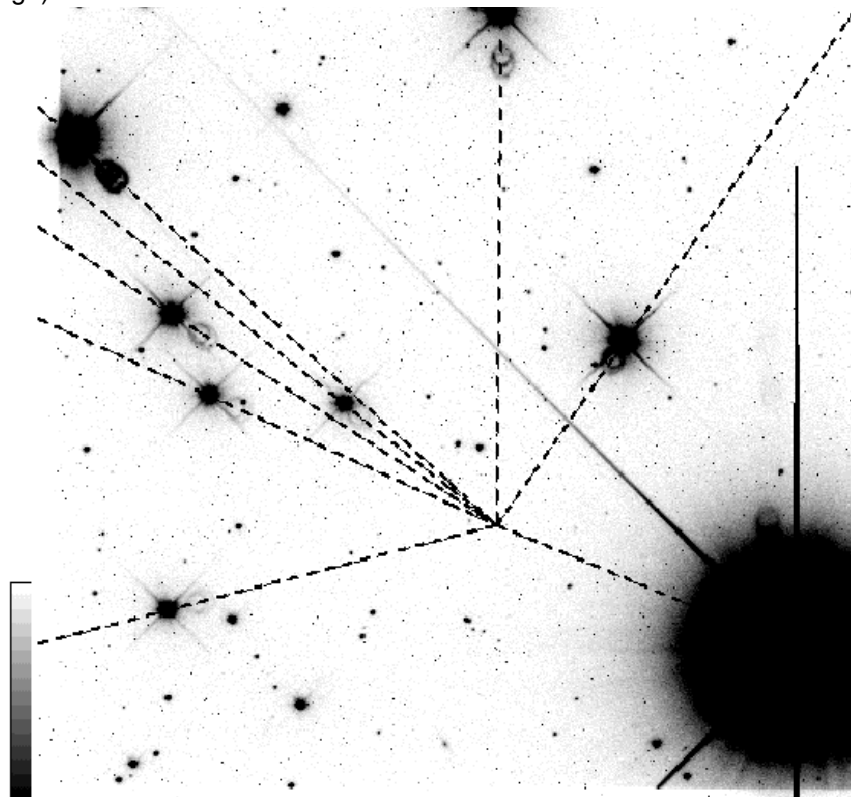


Table 7.4: Model of encircled energy fraction as a function of wavelength for STIS/CCD imaging.

λ (Å)	Fraction in central pixel	Aperture Radius in pixels							
		2	5	10	15	19.7	39.4	59	118
1750	0.246	0.667	0.873	0.949	0.979	0.990	0.998	1.000	1.000
3740	0.283	0.704	0.857	0.920	0.945	0.960	0.994	0.999	1.000
5007	0.253	0.679	0.857	0.916	0.934	0.948	0.985	0.997	1.000
6500	0.214	0.597	0.865	0.902	0.927	0.942	0.966	0.975	0.992
7500	0.178	0.536	0.825	0.866	0.892	0.909	0.942	0.957	0.986
8500	0.141	0.463	0.748	0.799	0.827	0.848	0.897	0.924	0.973
9500	0.100	0.342	0.607	0.672	0.705	0.733	0.809	0.857	0.946
10000	0.080	0.275	0.518	0.589	0.624	0.655	0.748	0.810	0.926
10500	0.064	0.238	0.447	0.517	0.553	0.585	0.690	0.764	0.907

7.1.8 Readout Format

A full detector readout is 1062 x 1044 pixels including physical and virtual overscans. Scientific data are obtained on 1024 x 1024 pixels, each projecting to $\sim 0.05 \times 0.05$ arcseconds on the sky. For spectroscopic observations, the dispersion axis runs along **AXIS1** (image X or along a row of the CCD), and the spatial axis of the slits runs along **AXIS2** (image Y or along a column of the CCD). The CCD supports the use of subarrays to read out only a portion of the detector, and on-chip binning. For more details see Section 11.1.1.

7.1.9 Analog-to-Digital Conversion: Selecting the CCDGAIN

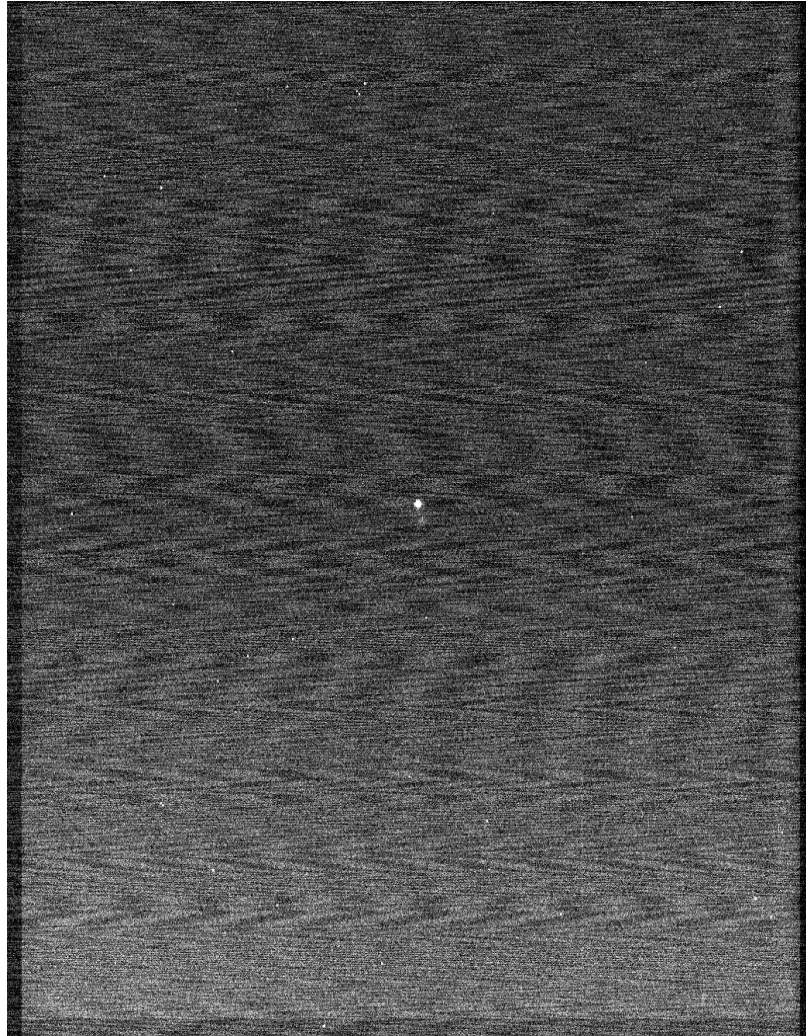
Electrons that accumulate in the CCD wells are read out and converted to data numbers (DN, the format of the output image) by the analog-to-digital converter at a default **CCDGAIN** of $1 \text{ e}^-/\text{DN}$ (i.e., every electron registers 1 DN). The CCD is also capable of operating at a gain of $4 \text{ e}^-/\text{DN}$. The analog-to-digital converter operates at 16 bits, producing a maximum of $65,536 \text{ DN pixel}^{-1}$. This is not a limitation at either gain setting, because other factors set the maximum observable DN to lower levels in each case (Section 7.2 below).

The **CCDGAIN=1** setting has the lower read noise (Table 7.1) and digitization noise. Although the read noise has increased since the switch to the Side 2 electronics in July 2001 (see Section 7.1.2), **CCDGAIN=1** is still the most appropriate setting for observations of faint sources. However, saturation occurs at about $33,000 \text{ e}^-$ at the **CCDGAIN=1** setting (as described in Section 7.2 below).

The **CCDGAIN=4** setting allows use of the entire CCD full well of $144,000 \text{ e}^-$, and use of the **CCDGAIN=4** setting is therefore recommended for imaging photometry of objects whenever more than $33,000 \text{ e}^-$ might be obtained in a single pixel of an individual sub-exposure. However, short exposures taken in **CCDGAIN=4** show a large-scale pattern noise (“ripple”) that is not removed by the standard bias images. This pattern noise is in addition to the usual coherent noise visible since STIS switched to using the backup Side-2 electronics. Figure 7.7 (a 0.2 second exposure of a lamp-illuminated small slit) shows an example of the **CCDGAIN=4** ripple. The peak-to-peak intensities of these ripples vary from near zero to about 1 DN, and there is a large amount of coherence in the noise pattern. This coherence makes background determination difficult and limits the precision of photometry of faint objects in shallow exposures taken using **CCDGAIN=4**.

The CCD response when using **CCDGAIN=4** remains linear even beyond the $144,000 \text{ e}^-$ full well limit if one integrates over the pixels bled into (Section 7.2.1), and for specialized observations needing extremely high S/N, this property may be useful.

Figure 7.7: Ripple Effect in Short Exposures with CCDGAIN=4



7.2 CCD Operation and Feasibility Considerations

7.2.1 CCD Saturation

There are no hard bright-object limits to worry about for CCD observations, because the CCD cannot be damaged by observations of bright sources. However, the CCD pixels do saturate at high accumulated count levels, due to the finite depth of the CCD full well. The CCD saturates at $\sim 144,000$ electrons pixel^{-1} in most of the effective area of the chip; however, over the outer-most (serial= x) portion the CCD saturates at $120,000$ electrons pixel^{-1} . The variation of the CCD full well over the chip occurs because of nonuniformity in the process of boron implantation, which creates the potential wells in this type of CCD. Accumulations up to

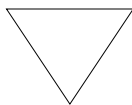
the full well limit can be observed only in the CCDGAIN=4 setting, as the gain amplifier already saturates at $\sim 33,000$ electrons pixel^{-1} in the CCDGAIN=1 setting (see Section 7.1.9).

Saturation imposes a limit on the product of the count rate and the integration time. Keep the total counts *in the pixels of interest* below the saturation level, either by keeping the exposure time short enough that the limit is not violated in any single integration or by choosing a more appropriate configuration. You can allow saturation to occur in regions of the image over which you do not wish to extract information (e.g., you can allow a star or single emission line to saturate if you are interested in other features). Remember, however, that once the CCD well is over full, charge will bleed along the columns of the CCD so that neighboring pixels (along the slit for spectroscopic observations) will also be affected. Saturation *cannot* be corrected in post-observation data processing.

An interesting exception to this is described in Gilliland, Goudfrooij & Kimble, 1999, *PASP*, 111, 1009. For CCDGAIN=4 the response remains linear up to, and even far beyond saturation if one integrates over the pixels receiving the charge bleed. Because the bleeding is perpendicular to the dispersion direction, for point sources such saturation does not compromise spectral purity. Signal to noise values of $\sim 10,000$ have been demonstrated for saturated data (see [STIS ISR 1999-05](#) for a time series application and Bohlin & Gilliland, 2004, *AJ* 127, 3508 for a measurement of Vega's absolute flux).

In Section 6.2, we explained how to determine the peak counts $\text{sec}^{-1} \text{pixel}^{-1}$ expected for your observation. In Chapter 13 for each spectroscopic mode and in Chapter 14 for each imaging mode, we provide plots of exposure time to fill the CCD well versus source flux for each STIS configuration. Lastly, [exposure time calculators](#) are available on the STScI STIS web site. Use one of these sources to ensure that your observations will not saturate sources of interest.

The minimum CCD exposure time is 0.1 seconds, providing a true limit to the brightest source that can be observed *without saturating*.



For standard applications keep the accumulated electrons pixel^{-1} per exposure below 120,000 at CCDGAIN=4 (determined by the CCD full well), and below 30,000 at CCDGAIN=1 (determined by gain amplifier saturation).

7.2.2 CCD Shutter Effects

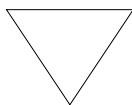
The STIS CCD camera features a high-speed shutter that eliminates the need for a shutter illumination correction, even at the shortest commandable exposure time of 0.1 seconds. The only two minor drawbacks of using this shortest exposure time are the following: (i) a non-reproducible large-scale variation in intensity of a very low amplitude ($\sim 0.2\%$) which is due to a slight non-uniformity of the shutter speed, and (ii) a mean count rate which is $\sim 3\%$ lower than those of longer exposures, which is due to an inaccuracy of the shutter timing at this setting. These minor effects occur *only* for the shortest exposure times, and disappear completely for exposure times of 0.3 seconds and longer.

7.2.3 Cosmic Rays

All CCD exposures are affected by cosmic rays. The rate of cosmic ray hits in orbit is very high compared to ground-based observations. The current rate at which pixels are affected by cosmic-ray hits is $30.0 (\pm 3.7)$ pixels per second for the STIS CCD. To allow removal of cosmic rays in post-observation data processing we recommend that whenever possible, given signal-to-noise constraints, you take two or more exposures in any given CCD configuration (see also Section 11.2.2). The greater the number of independent exposures, the more robust is the removal of cosmic rays and for very long integrations it is convenient to split the exposure into more than two separate images to avoid coincident cosmic-ray hits. As an example, for two 1200 sec exposures, about 1250 CCD pixels will be hit in both images and will therefore be unrecoverable. Moreover, since cosmic ray hits typically affect ~ 5 pixels per event, these pixels will not be independently placed, but rather will frequently be adjacent to other unrecoverable pixels. In general, we recommend that individual exposures should not exceed ~ 1000 sec duration to avoid excessive amounts of uncorrectable cosmic rays in the images. However, observers must balance the benefit of removing cosmic rays against the loss in signal-to-noise that results from the splitting of exposures when in the read-noise-limited regime.

In observations of faint sources, particularly for dispersed light exposures, the intrinsic count rates can be very low. The exposure time needed to reach a break-even between the read-out noise and the Poisson noise per pixel associated with the minimal sky background is ~ 15 minutes for imaging in 50CCD mode, and ~ 36 minutes for slitless spectroscopy with G750L. With a dark current of $\sim 0.004 \text{ e}^- \text{ sec}^{-1}$ it takes ~ 80 minutes of integration for the Poisson statistics on the detector background to equal the read noise. Therefore, repeated short exposures of faint sources can significantly increase the total noise from added readouts. Selecting the correct number and length of repeated integrations requires a consideration

of the trade-off between increased read noise and more robust cosmic-ray elimination. The [STIS Exposure Time Calculators](#), or the S/N plots in Chapter 13 and Chapter 14, can help you determine whether your observations are in the read-noise dominated regime.



Be sure to take at least two identical CCD exposures in each configuration to allow removal of cosmic rays in post-observation data processing.

7.2.4 Hot Pixels

Hot pixels, caused by radiation damage, occur in the STIS CCD. Dark frames are currently obtained twice a day in order to maintain a master list of hot pixels and to update the pipeline superdark reference files on a weekly basis. On a monthly time scale, the CCD is raised to ambient temperature, from its normal operating temperature of $\sim -83^{\circ}\text{C}$, in order to permit annealing of hot pixels.

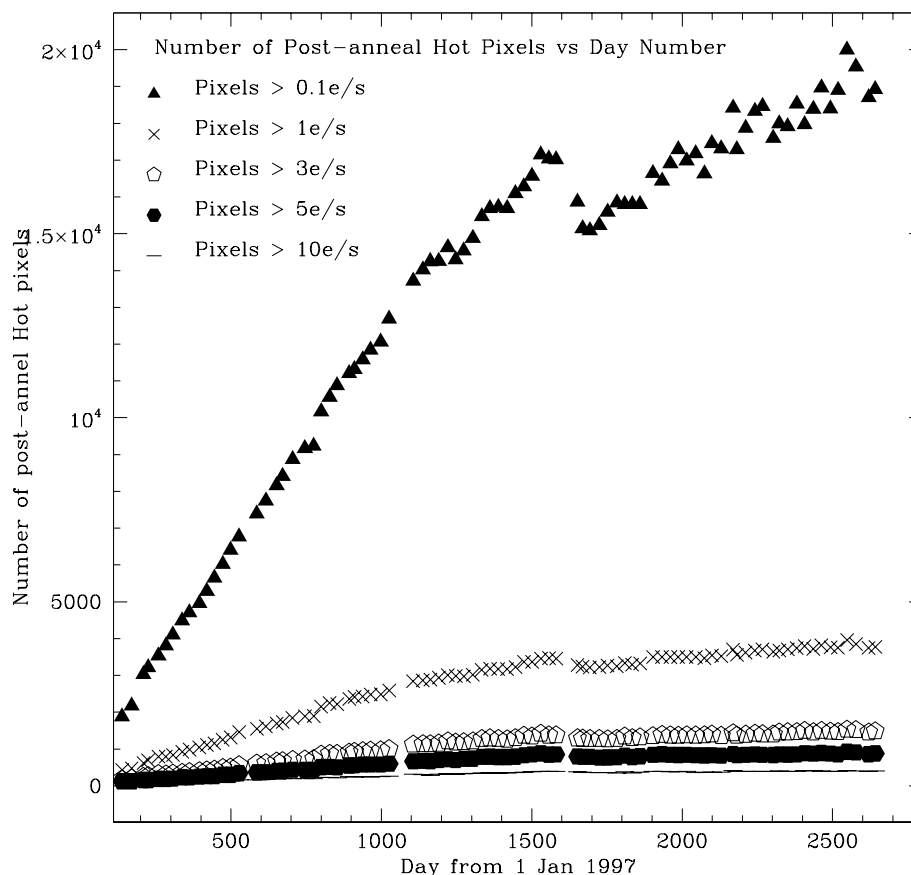
Analysis of on-orbit data has shown that the annealing process is successful in that at least $\sim 80\%$ of transient hot pixels (hotter than $0.1 \text{ electron sec}^{-1} \text{ pix}^{-1}$) are currently annealed away each month. Apart from the transient hot pixels, there is a substantial number of hot pixels that stay persistently hot after anneals. At present, $\sim 1.8\%$ of the pixels of the STIS CCD are persistently hot. The total number of hot ($>0.1 \text{ electron sec}^{-1} \text{ pix}^{-1}$) pixels is $\sim 20,000$ after an anneal, as of April 2004 (see Figure 7.8). The different points in Figure 7.8 represent pixels with dark current above each listed threshold. Note the increase in hot pixels with time. The break in the trend near day 1600 reflects the switch to the STIS Side-2 electronics. Side-2 darks are scaled to a housing temperature of 18°C , which corresponds to a detector temperature lower than the -83°C setpoint that was used when the Side-1 electronics were functional. A detailed description of the variation in hot pixel numbers since launch can be found in [STIS ISR 1998-06](#).

Note that both binned and spectral data will increasingly suffer from the effects of hot pixels as the percentage of non-annealed pixels increases. Just prior to an anneal, up to 2% of all CCD pixels are hot, i.e., both persistent and “annealable” hot pixels. In the case of spectral data, with a normal extraction box height of 7 pixels, this means that 14% of the extracted pixels will be affected by a hot pixel. For imaging data involving rectification, the rectification process interpolates unremoved hot pixels into the four adjacent pixels. For the case of $M \times N$ binning, therefore, $4 \times M \times N$ pixels will be affected by a combination of the binning and rectification process.

While post-pipeline calibration using appropriate STIS reference superdarks allows one to subtract most hot pixels correctly (to within the accuracy set by Poisson statistics), the best way to eliminate all hot pixels is by *dithering* (making pixel-scale positional offsets between individual exposures). Dithering as a method of data taking is described in detail in Chapters 11. An HST handbook on dither strategies and advantages, together with example data is available on-line at:

http://www.stsci.edu/instruments/wfpc2/Wfpc2_driz/dither_handbook.html.

Figure 7.8: Hot Pixels Remaining after each Anneal



7.2.5 CCD Bias Subtraction and Amplifier Non-Linearity

Analysis of CCD images taken during ground calibration and in Cycle 7 has revealed low-level changes in the bias pattern (at the tenths of a DN level) and a low-level amplifier non-linearity. This non-linearity (“amplifier ringing”) was uncovered during the analysis of the overscan region on flat-field images (reported in [STIS ISR 1997-09](#)). The bias value of a given row in the serial overscan region of flat-field images is *depressed* with respect to the nominal bias value by an amount proportional to the mean signal in that row. However, the small proportionality factors and low DN levels at which the non-linearity occurs render the problem negligible for

most STIS scientific applications. Instances of data that may be slightly affected by this problem (at the <1% level) are aperture photometry of faint sources (in imaging mode), especially in the case of a crowded region with nearby bright sources that would cause a local depression of the bias value, and photometry of diffuse extended objects that cover a large number of pixels. The brightest hot pixels (see Section 7.2.4) also cause a measurable local depression in the bias value, but their effect is corrected by using the appropriate superdark reference file (or daily dark file) during CCD calibration.

Observers taking full-frame CCD images obtain both physical overscan (i.e., actual CCD pixels; columns 1-19 and 1016-1062 on the raw image) and virtual overscan (i.e., added electronically to the image; rows 1-20 on the raw image) on their frames; the virtual overscan is not subject to the amplifier nonlinearity problem and can be used to estimate the importance of this effect in the images. Observers using subarrays (e.g., to reduce the time interval between reads and limit the data volume when performing variability observations in the optical; see also Chapter 11) will obtain only the physical overscan.

7.2.6 Charge Transfer Efficiency

Radiation damage at the altitude of the HST orbit causes the charge transfer efficiency (CTE) of the STIS CCD to degrade with time. The effect of imperfect CTE is the loss of signal when charge is transferred through the CCD chip during the readout process. As the nominal read-out amplifier (Amp D) is situated at the top right corner of the STIS CCD, the CTE problem has two possible observational consequences: (1) making objects at lower row numbers (more pixel-to-pixel charge transfers) appear fainter than they would if they were at high row numbers (since this loss is suffered along the *parallel* clocking direction, it is referred to as *parallel CTE loss*); and (2) making objects on the left side of the chip appear fainter than on the right side (referred to as *serial CTE loss*). In the case of the STIS CCD, the *serial CTE loss* has been found to be negligible for practical purposes. Hence we will only address *parallel CTE loss* for the STIS CCD in this Handbook.

The current lack of a comprehensive theoretical understanding of CTE effects introduces an uncertainty for STIS photometry. The CTE problems are caused by electron traps in the CCD that are filled as charge passes through the pixels. However, not all traps are accessible to all electrons passing through. Some traps are only accessible if there is significant charge involved. This model suggests that there will not be significant CTE losses in the presence of background, particularly for faint stars, because background electrons fill the traps before the charge associated with such stars passes through. There will still be some loss for brighter stars with background, because their charge may access traps that are unaffected by

the background that previously clocked through. Faint stars in areas with little background may suffer from larger losses.

In general, the amount of (parallel) CTE loss depends on the elapsed time on orbit, the distance (i.e., the number of CCD rows) from the source location on the CCD chip to the readout amplifier, the source signal, and the background level.

It should be noted at the outset that the effect of CTE loss has not, as yet, been incorporated into the [STIS Exposure Time Calculators \(ETCs\)](#). Thus, should you believe the CTE losses described herein may impact your spectroscopic or imaging observing program, you will need to provide longer exposure times in your Cycle 14 Phase II proposal to compensate for the anticipated losses¹. In particular, Cycle 14 observers using the STIS CCD to observe faint targets (especially in spectroscopic mode) producing less than a few hundred electrons above a low background, are advised to adjust their exposure times appropriately (within the restrictions of their allocated number of HST orbits).

Recent analysis of a comprehensive calibration program has allowed us to derive a formula to correct spectroscopic observations of point sources for the parallel-register Charge Transfer Inefficiency (CTI = 1-CTE). This correction has already been implemented in the standard calibration pipeline. For spectra at the standard reference position at the CCD center, CTE losses as big as 20% are corrected to within 1% at high signal levels, and to within ~1.5% at low signal levels of ~100 electrons. Further information on CTE loss in spectroscopic mode, including the CTI correction formula, can be found in [STIS ISR 2003-03](#). For the CCD imaging mode no correction is available at present in the pipeline, and we refer the reader to Goudfrooij and Kimble's [2002 HST Calibration Workshop article](#) for the parametrization of the CTE loss.

Figure 7.9 depicts the amount of CTE loss suffered as a function of source signal and background level, for spectra taken at epoch 2004.5. Note that the CTE loss can be significant. A typical spectrum with a signal of about 150 electrons per pixel along the dispersion direction (extracted over the spatial extent of the PSF) and a background level of 5 electrons per pixel (appropriate for a 1000 sec exposure in G430L mode) will experience a CTE loss of ~15% (at epoch 2004.5) when located in the center of the CCD. For a background of 1 electron per pixel (e.g., a 200 sec exposure), a spectrum with the same intrinsic signal would suffer a CTE loss of ~21%. This emphasizes the need to take CTE losses into account when estimating exposure times needed to accomplish your science goals.

For the observer, a few strategies for minimizing the effect of CTE loss should be noted. First of all, one should maximize the exposure time whenever possible in order to increase the object counts and the sky

1. To help observers evaluate the impact of CTE loss on their intended spectroscopic exposures, we have created an IRAF CL script, `cte1oss`, which is described and available from the STIS website at <http://www.stsci.edu/hst/stis/software/scripts/>.

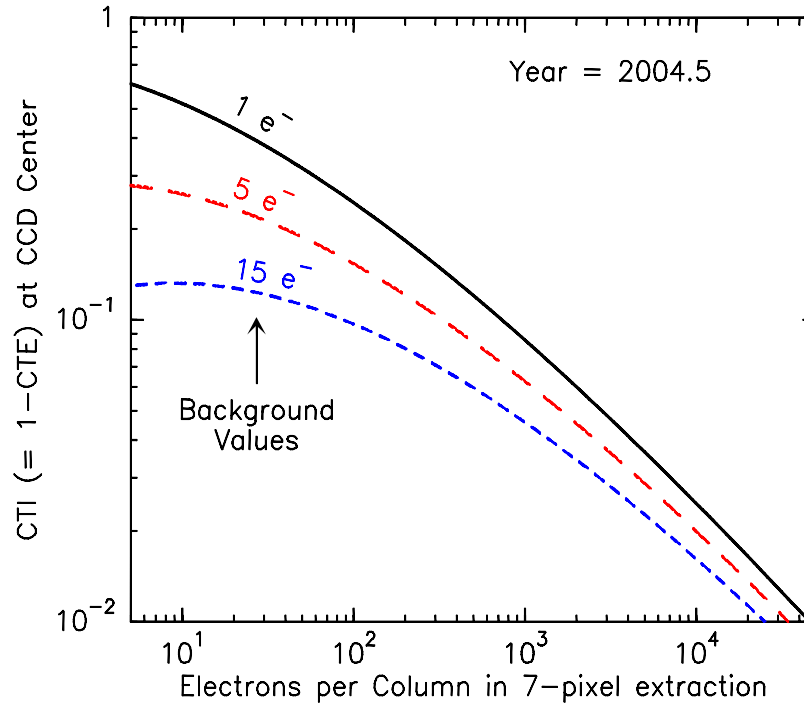
background per exposure, both of which reduce CTE loss. Users who are thinking about dithering and shortening their exposure times (e.g., to allow for more dither positions) may want to take this into account. Furthermore, observers using the CCD for long-slit spectroscopy of sources having a spatial extent of less than about 3" are urged to use the pseudo-apertures located near row 900 of the CCD (the 52X*E1 apertures; see Section 7.2.7).

Further analyses of CTE effects on imaging and spectroscopic observations of *extended* objects (e.g., galaxies) are in progress and will be published as STIS Instrument Science Reports. For now, we recommend observers of extended objects to use the CTI correction formula mentioned in [STIS ISR 2003-03](#) (which was derived using observations of point sources), and follow the strategies mentioned above just as well.

7.2.7 Mitigation of CTE Loss for Long-slit Spectroscopy

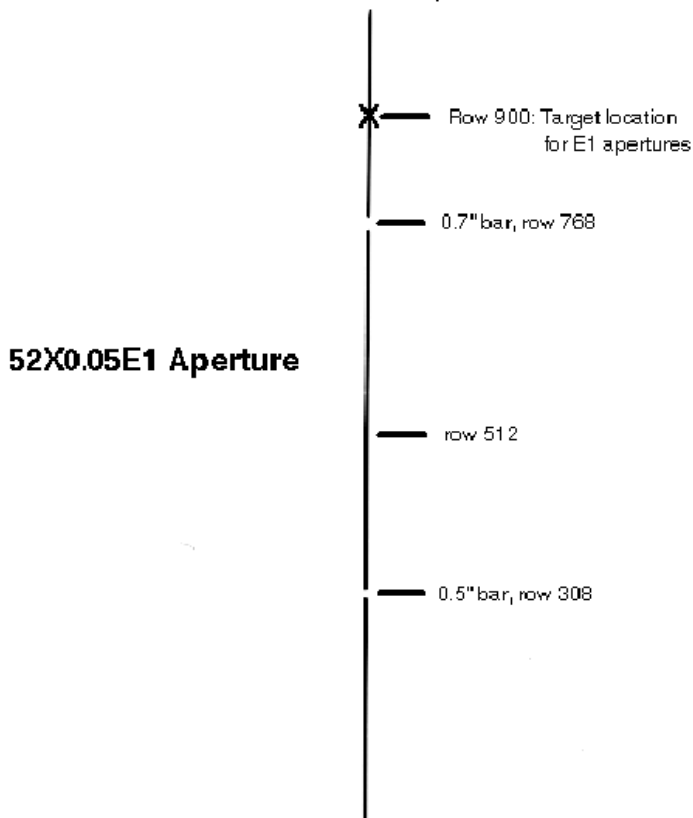
Decreasing charge transfer efficiency in the STIS CCD has a detrimental effect on faint spectra acquired at the default location at the center of the chip. For sources with fluxes less than $\sim 1 \times 10^{-16}$ erg cm⁻² s⁻¹ Å⁻¹, less than ~ 100 electrons are accumulated per pixel in exposure times of 1000 s or less. (This is the longest integration time we recommend due to the deleterious impact of multiple cosmic rays in a CR-SPLIT at longer integration times.) At signal levels of 50 - 100 e⁻, 15% or more of the charge can be lost during readout due to charge-transfer inefficiencies. Many STIS science programs have fluxes in this range. For spectra of point sources and compact objects such as galactic nuclei, the full length of the slit is not needed. A target location closer to the read-out amplifier near the end of the slit can decrease the charge lost during parallel transfers by a factor of ~ 5 . One could achieve this offset through the use of offset targets or appropriate POS-TARG entries on the Phase II proposal, but these methods are a bit cumbersome and can be prone to error.

Figure 7.9: Estimated Charge Transfer Inefficiency (CTI = 1-CTE) as a function of signal level (per column) for spectroscopy of a point source observed in calendar year 2004.5. The solid line depicts the CTI for a background of 1 electron per pixel, the long-dashed line does so for a background of 5 electrons per pixel, and the short-dashed line does so for a background of 15 electrons per pixel. The CTI is expressed as the fraction of charge lost outside the default signal extraction box of 7 pixels perpendicular to the dispersion. Note the CTI-decreasing effect of added background, which argues for an observing strategy involving long exposure times.



Therefore, for first-order spectra we have defined a set of pseudo-apertures that use the same physical long slits available for STIS CCD observations, but have their default target placement near row 900, ~5 arcseconds from the top of the STIS CCD. This is schematically illustrated in Figure 7.10. Observers can use these aperture names to place their targets at this location in a rather transparent fashion.

Figure 7.10: Location of the New Pseudo Apertures.



The E1 aperture names and the approximate Y location of the resulting spectra are given in Table 7.5. Use of the new aperture name eliminates the need to specify an offset for the ACQ/PEAK and a POS-TARG. The new apertures are also recognized by the calibration pipeline software, so spectra are extracted from the correct location using appropriate wavelength solutions, spectral traces, and background regions. For optimum throughput when using these apertures, we recommend using an ACQ/PEAK exposure to center the target in the aperture when using aperture 52X0.1E1 and 52X0.05E1. While use of these apertures will ameliorate CTE losses, we caution observers to carefully assess the potential impact on their science programs due to the decreased spatial coverage and the relative locations of the bars on the slit.

Table 7.5: New Aperture Names and Approximate Y Location of the Resulting Spectra

Aperture	Y Location	ACQ/PEAK
52X2E1	894	no
52X0.5E1	893	no
52X0.2E1	893	no
52X0.1E1	898	yes
52X0.05E1	898	yes

7.2.8 UV Light and the STIS CCD

In the optical, each photon generates a single electron. However, in the near UV, shortward of $\sim 3200 \text{ \AA}$ there is a finite probability of creating more than one electron per UV photon (see Christensen, O., *J. App. Phys.* **47**, 689, 1976). Users will need to take this into account when calculating signal-to-noise ratios and exposure times for the G230LB and G230MB gratings, as described in “Special Case—Spectroscopic CCD Observations at $\lambda < 2500 \text{ \AA}$ ” on page 96.

Initial laboratory testing of STIS CCDs showed that excessive illumination by UV light can cause an elevation in residual dark current, due to a surface chemistry effect. However, the actual STIS flight CCD was tested for this effect during ground calibration by the STIS IDT and the effect was found to be much less than previously suspected; this effect is now a concern *only* for clear (50CCD) imaging of *extremely UV-bright targets*. Observations of fields with UV-bright objects should be dithered (i.e., positional offsets applied between readouts) to ensure that the UV tail from bright sources does not cause a residual elevation of the dark current for subsequent science observations. It is also recommended to use the longpass-filtered aperture, F28X50LP, rather than the 50CCD clear aperture, during target acquisitions (see also Section 8.2.3) when possible. The specific results of the ground testing on the effect of UV overillumination are summarized in Table 7.6.

Table 7.6: Effect of CCD UV Overillumination on Elevation of Dark Current

Overillumination Rate ($e^- \text{ pixel}^{-1}$)	Initial Dark Current Elevation (%)	Time to Return to Nominal
500,000	500	30 min
5,000,000	1500	40 min

7.3 The MAMA Detectors

7.3.1 MAMA Properties

There are two MAMA detectors: the STIS/FUV-MAMA provides coverage from 1150 to 1700 Å and the STIS/NUV-MAMA provides coverage from 1600 to 3100 Å (with lower response below 1600 Å). The STIS MAMA detectors are photon-counting devices that process events serially. They can be used to take data in either an accumulate (ACCUM) mode in which a time-integrated image is produced, or in a time series (TIME-TAG) mode in which the detector location and time of arrival of each photon are recorded as an event stream (see Section 11.1.2 and Section 11.1.3, respectively). The primary benefits afforded by the STIS MAMAs, in comparison with previous HST UV spectroscopic detectors such as those of the GHRs and FOS, are high spatial resolution, two-dimensional imaging over a relatively large field of view, and low background for point sources. The MAMA detector was developed by J. Timothy and R. Bybee for X-ray and UV imaging applications. The properties of the STIS MAMA detectors are summarized in Table 7.7.

Table 7.7: STIS MAMA Detector Performance Characteristics

Characteristic	FUV-MAMA Performance	NUV-MAMA Performance
Photocathode	CsI	Cs ₂ Te
Wavelength range	1150–1700 Å	1600–3100 Å
Pixel format	1024 x 1024	1024 x 1024
Pixel size	25 x 25 μm ²	25 x 25 μm ²
Image mode pixel plate scale	0.0245 x 0.0247 arcseconds (clear) 0.0246 x 0.0247 arcseconds (filtered)	0.0245 x 0.0248 arcseconds
Field of view	25.1 x 25.3 arcseconds (clear) 25.2 x 25.3 arcseconds (filtered)	25.1 x 25.4 arcseconds
Quantum efficiency	25% @ 1216 Å	10% @ 2537 Å
Dark count	5 x 10 ⁻⁶ to 1 x 10 ⁻⁴ counts sec ⁻¹ pix ⁻¹	8 x 10 ⁻⁴ to 1.7 x 10 ⁻³ counts sec ⁻¹ pix ⁻¹
Global count-rate linearity limit ¹	285,000 counts sec ⁻¹	285,000 counts sec ⁻¹
Local count-rate linearity limit ¹	~220 counts sec ⁻¹ pix ⁻¹	~340 counts sec ⁻¹ pix ⁻¹

1. Rate at which counting shows 10% deviation from linearity. These count rates are well above the bright-object screening limits.

Figure 7.11 and Figure 7.12 illustrate the design of the FUV- and NUV-MAMA, respectively. A photocathode material is deposited on the front surface. The FUV-MAMA has an opaque CsI photocathode deposited

directly on the face of the curved microchannel plate (MCP); the NUV-MAMA has a semi-transparent Cs_2Te photocathode deposited on the back side of the detector's entrance window.

Target photons strike the photocathode, liberating single photoelectrons which pass into the microchannel plate (MCP). There they are multiplied to a pulse of $\sim 4 \times 10^5$ electrons. The pulse is recorded by an anode array behind the photocathode and detected by the MAMA electronics which process it, rejecting false pulses and determining the origin of the photon event on the detector.

The FUV-MAMA has a field electrode (*repeller wire*) which is used to repel electrons emitted away from the microchannel plate back into the channels. This provides an increase in quantum efficiency of the detector at the price of a small increase in the detector PSF halo. The repeller wire is normally on for FUV-MAMA observations (but see Section 7.3.4).

Figure 7.11: Design of the FUV-MAMA

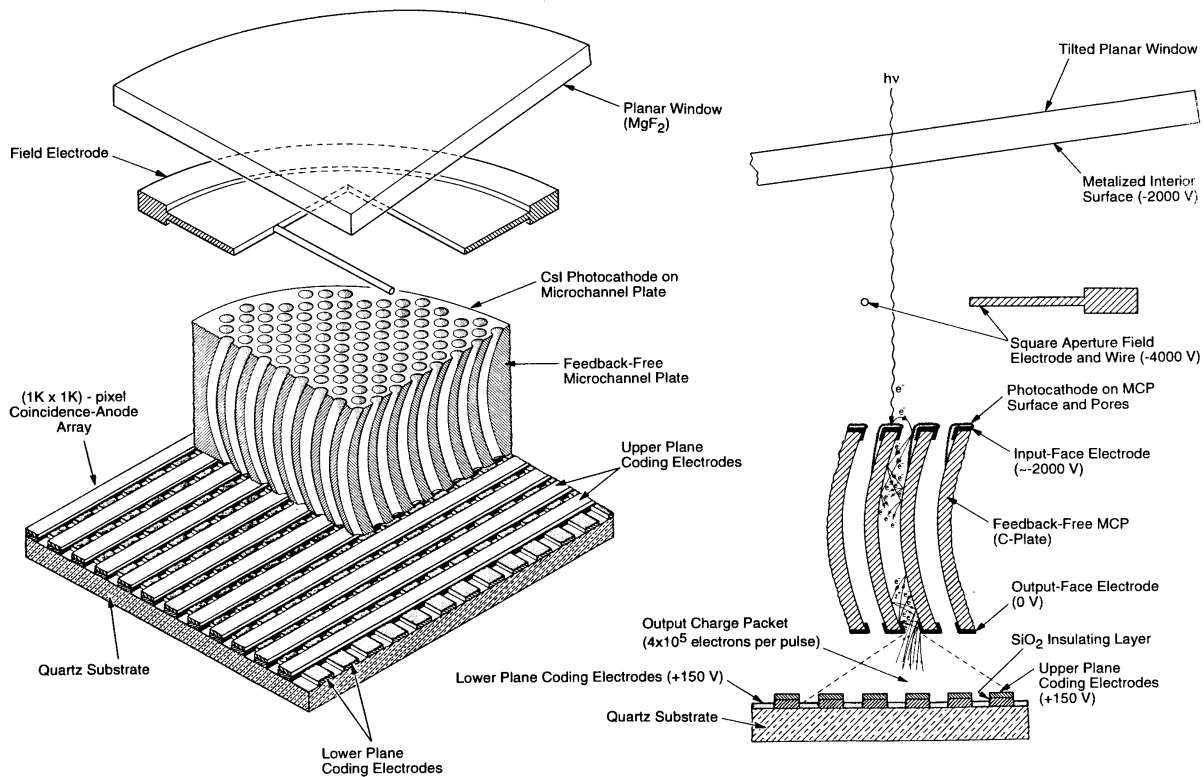
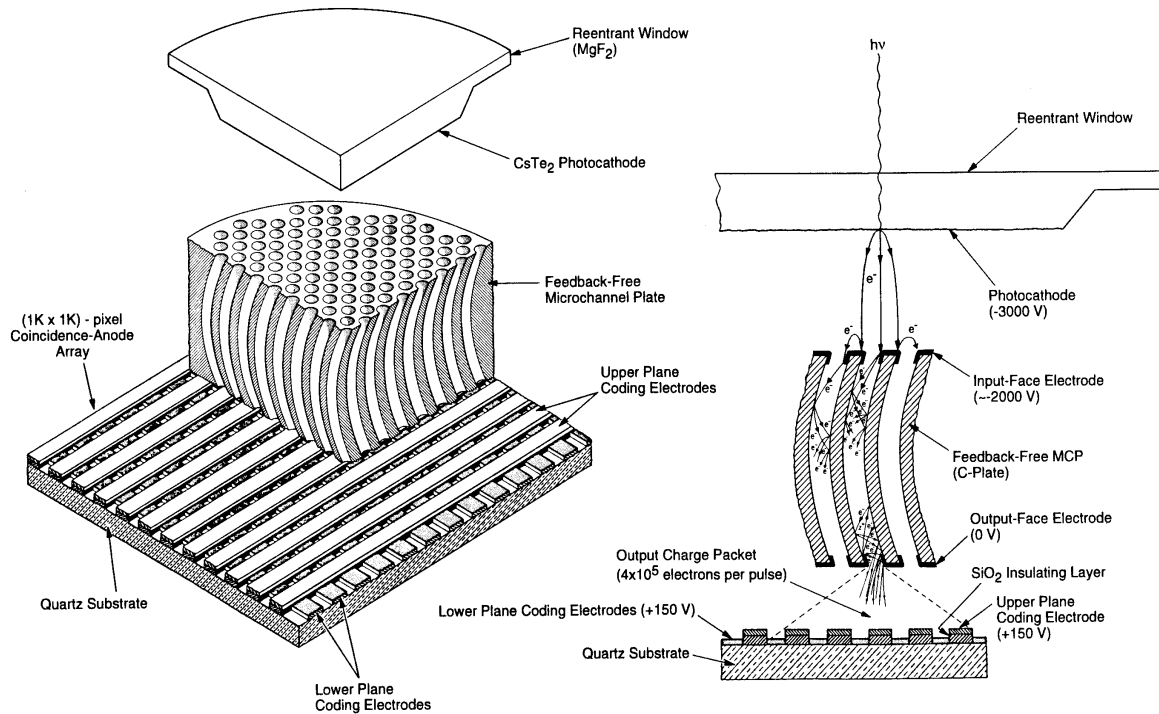


Figure 7.12: Design of the NUV-MAMA



7.3.2 MAMA Spectral Response

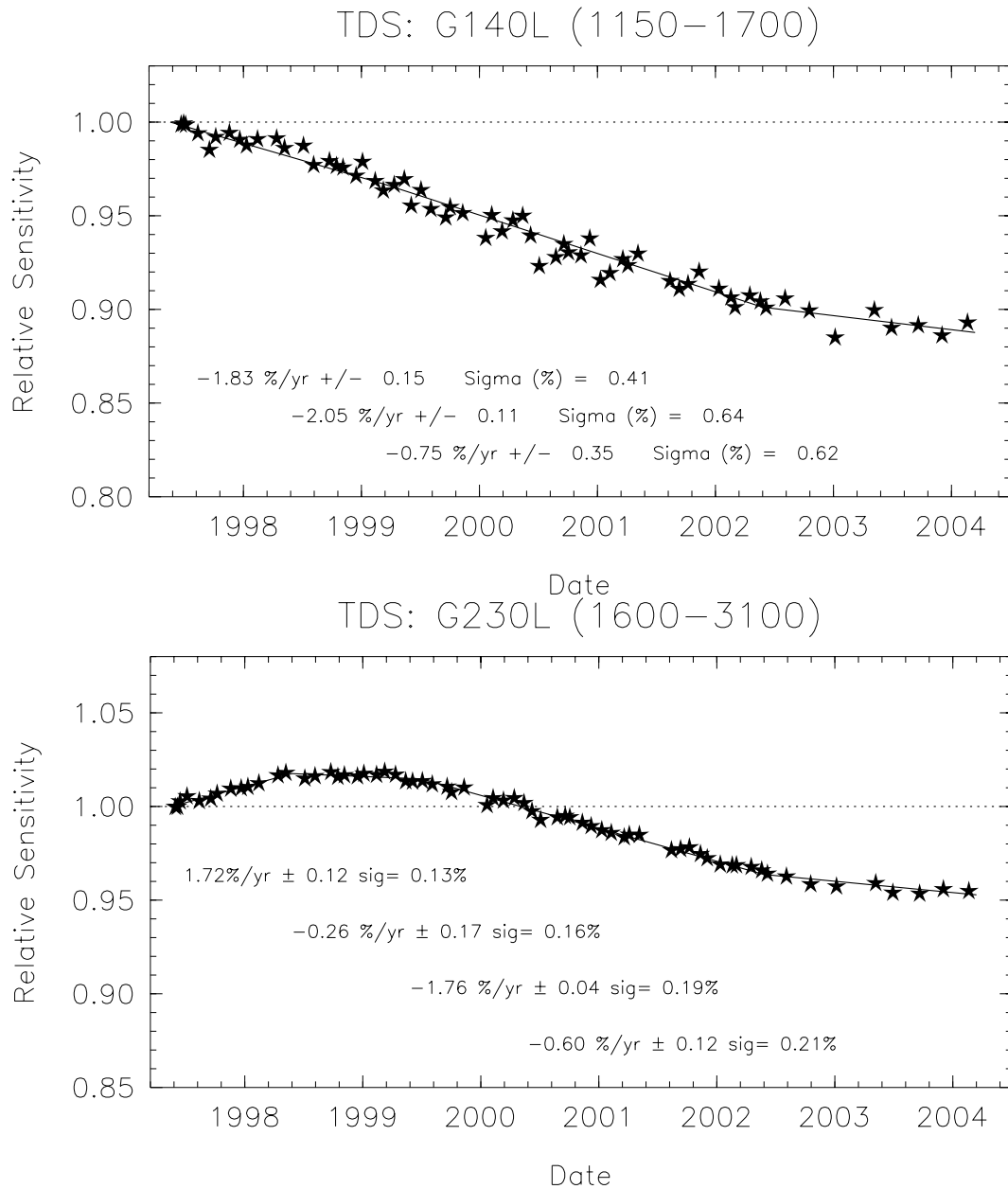
The spectral responses of the unfiltered FUV- and NUV-MAMAs are illustrated in Figure 5.14. The peak photocathode response of the FUV-MAMA occurs at Lyman- α . Its spectral response is defined by the cutoff of the MgF_2 window at 1150 \AA at short wavelengths, and by the relatively steep decline of the CsI photocathode at long wavelengths. Out-of-band QE at longer wavelengths ($>2000 \text{ \AA}$) is $<10^{-6}$ yielding excellent solar-blind performance. The NUV-MAMA spectral response has a relatively flat maximum ($\sim 10\%$) that encompasses $1800\text{--}2600 \text{ \AA}$. The photocathode QE declines to $\sim 4\%$ at 3150 \AA , while at longer wavelengths the out-of-band QE is $\sim 10^{-4}$. (See also Section 5.3.3.)

7.3.3 MAMA Sensitivity

The MAMA detectors, similarly to the CCD, suffer from changes in sensitivity which depend on both temperature and time. A similar STIS Sensitivity Monitoring program aimed at characterizing the CCD behavior has been used to characterize the MAMAs (see Section 7.1). The well-known sensitivity of the FUV MAMA to temperature for the first-order mode G140L has been confirmed to be $-0.30\%/^{\circ}\text{C}$. No significant change with temperature for the NUV-MAMA first-order

G230L mode has been registered. Following a correction for the temperature dependence, the sensitivities of the FUV first-order modes decrease linearly with time (see Figure 7.13) by wavelength-dependent amounts ranging up to a few percent per year. For the NUV first-order configurations, the sensitivities increased during the 1.5 years of STIS operations and then began to drop, by wavelength-dependent amounts comparable to those in the FUV (see Figure 7.13). There has been a significant slow-down in the decline of the time-dependent sensitivity (TDS) of all STIS observational modes in the last two years. Currently, MAMA sensitivity losses range on average from $-0.75\%/yr$ (G140L) to $-0.60\%/yr$ (G230L). Full details of the changes in the sensitivity over time for all STIS first-order L and M spectroscopic configurations can be found in STIS ISR 2004-?. TDS corrections for all first-order MAMA spectra have already been implemented in the data-reduction pipeline (see Section 15.1). All OTFR retrievals of such data will have corrected fluxes regardless of their acquisition epoch with an accuracy of 1% or better. SYNPHOT and the ETC have also been updated to apply TDS corrections to MAMAs. Sensitivity-monitor data for the echelle and MAMA imaging configurations are currently under investigation; they appear to show analogous effects, but no pipeline corrections are yet available. TDS corrections for these modes will be added during Cycle 13.

Figure 7.13: Relative sensitivity of STIS MAMA first-order low-resolution modes G140L and G230L as a function of time..



7.3.4 Optical Performance

Both MAMAs exhibit low-level extended wings in their detector point-spread functions (PSFs), with the NUV-MAMA PSF being considerably worse. Sample MAMA detector PSFs are shown in Figure 7.14. For those wishing to model their effect on absorption- or emission-line equivalent-width measurements or coronagraphic

observations, the LSFs and detector PSFs are maintained on the STScI [STIS World Wide Web site](http://www.stsci.edu/hst/stis/performance/spectral_resolution/). Data for spectral modes can be found at:

http://www.stsci.edu/hst/stis/performance/spectral_resolution/

and for imaging modes at:

http://www.stsci.edu/hst/stis/performance/image_quality/.

The FUV-MAMA includes a repeller wire that establishes a field above the microchannel plate and reflects forward-ejected photoelectrons back into the microchannel pores. The repeller wire is normally on for FUV-MAMA observations, but an improvement to the FUV-MAMA PSF (at the expense of a 35% decrease in sensitivity) can be made by disabling the high voltage to this wire. This procedure is only recommended for observations that use the E140H, and perhaps also the E140M, gratings when used with the 0.1X0.03 aperture (sometimes called the “Jenkins slit”) for observations shortward of 1400 Å. In pre-launch testing, resolutions as high as $R \sim 220,000$ were obtained in observations of a mono-isotopic emission line lamp in highres mode (see “Highres” on page 228), and $R \sim 200,000$ has been achieved on-orbit (Jenkins 2000, BAAS 32, 731). Figure 7.15 shows the effect of disabling the repeller voltage for the case of an observation of a linelamp with the E140H CENWAVE = 1234 Å setting. Note that the main difference is not the FWHM of the central core, but a decrease in the intensity of the line wings.

Only a small number of proposals per cycle (of the order of one to two) requesting the repeller off mode will be accepted. Note that repeller off observations will require special treatment, so a scientific case will need to be made for why these observations are necessary.

Also note that, due to the large PSF of HST in imaging mode (currently 3.5 low-resolution pixels), there is no advantage in performing FUV-MAMA imaging observations with the repeller wire voltage turned off.

Figure 7.14: MAMA Detector PSFs

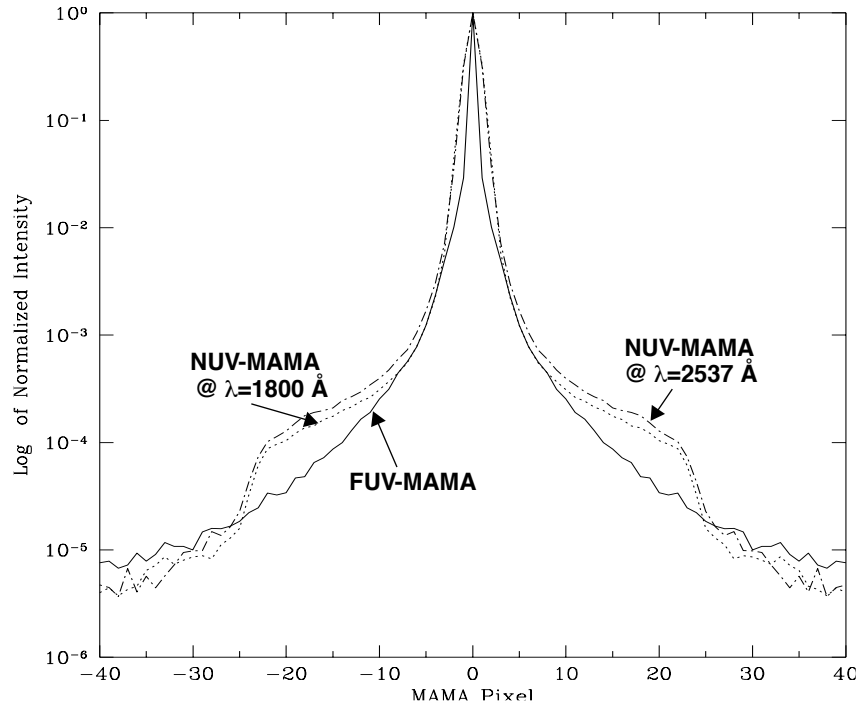
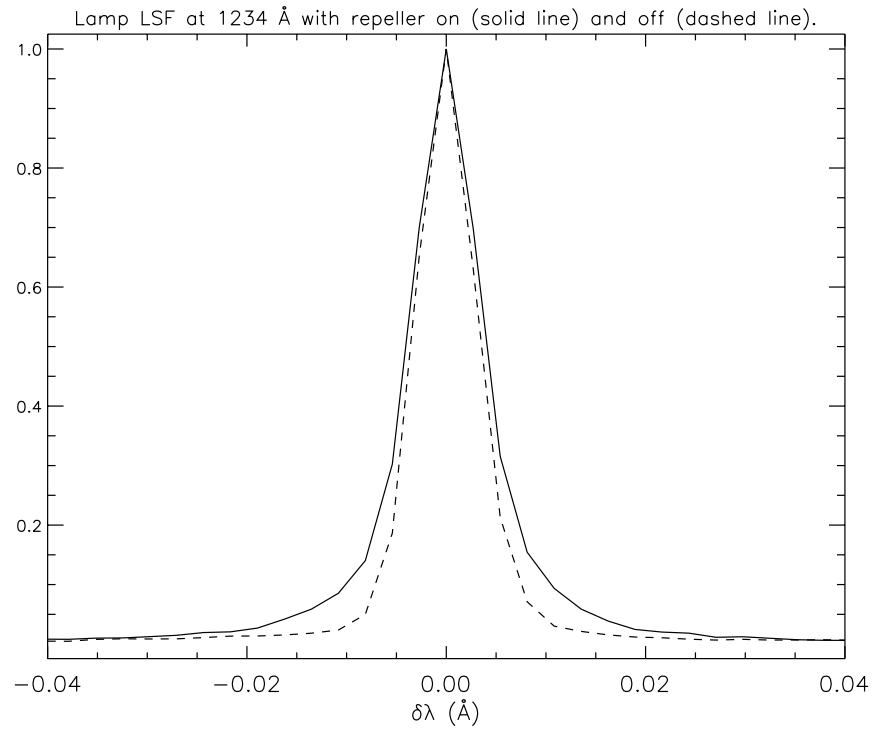


Figure 7.15: Average Profile of Calibration Lamp Line at 1234 \AA with the Repeller Wire On and Off

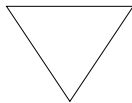


7.4 MAMA Operation and Feasibility Considerations

7.4.1 MAMA Saturation—Overflowing the 16 Bit Buffer

The MAMAs are photon-counting detectors: as each photon is recorded, it is placed into buffer memory. The STIS buffer memory stores values as 16-bit integers; hence the maximum number it can accommodate is 65,536 counts per pixel in a given ACCUM mode observation. When accumulated counts per pixel exceed this number, the values will wrap. As an example, if you are counting at $25 \text{ counts sec}^{-1} \text{ pixel}^{-1}$, you will reach the MAMA saturation limit in ~ 44 minutes.

Keep accumulated counts per pixel^{-1} below this value, by breaking individual exposures into multiple identical exposures (see also Section 11.2.4), each of which is short enough that fewer than 65,536 counts are accumulated per pixel. There is no read noise for MAMA observations, so no penalty is paid in lost signal-to-noise ratio when exposures are split. There is only a small overhead for each MAMA exposure (Chapter 9).



Keep the accumulated counts per pixel below 65,536, by breaking single exposures into multiple exposures, as needed.

7.4.2 MAMA Darks

The STIS MAMA detectors have intrinsically very low dark currents. Dark currents measured during ground testing were less than 10 counts/sec for the FUV-MAMA and less than 30 counts/sec for the NUV-MAMA over the whole detector. For the FUV-MAMA, this exceptionally low dark current was initially achieved on orbit. For the NUV-MAMA, charged particle impacts on the MgF_2 faceplate cause a higher background that results in a dark current of 800–2000 counts per second, varying both with temperature and the past thermal history of the detector. This particular phenomenon is not present for the FUV-MAMA, but the dark current nevertheless varies with time, temperature and position on the detector. The different dark-current behaviors of the detectors are discussed in more detail below, and up-to-date information can be found on the “[Monitoring](#)” page of the STIS web site.

NUV-MAMA Dark Current

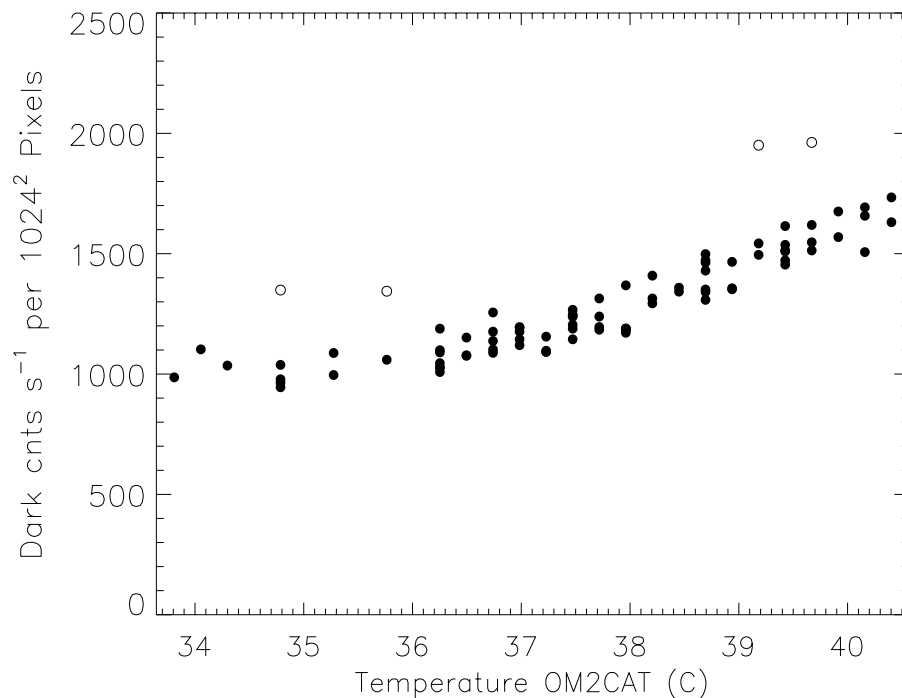
Most of the dark-current in the NUV-MAMA comes from phosphorescence of impurities in the MgF_2 detector faceplate. A simple model of the phenomenon has been developed by Jenkins and Kimble that

envisioned a population of impurity sites each having three levels: (1) a ground state, (2) an excited energy level which can decay immediately to the ground state, and (3) a metastable level that is at an energy slightly below the one that can emit radiation. The metastable state can be thermally excited to the upper level, and this excitation rate is proportional to $e^{-\Delta E/kT}$, where ΔE is the energy difference between the levels. The behavior of the count rate vs. temperature leads to an estimate of 1.1 eV for ΔE . At a fixed detector temperature of 30° C, the time-constant for the dark current to reach an equilibrium value is about 8 days. In practice because the MAMA high-voltage power supplies have to be shut down during SAA impacted orbits, the detector temperature varies from about 27° C to 40° C, and the dark current never reaches equilibrium.

MAMA temperatures cycle on a roughly daily time scale, being lowest just after the high-voltage is turned on after a SAA passage. The dark current can be predicted with about 5 to 10% accuracy using the contemporaneous temperature of the NUV-MAMA charge amplifier recorded in the OM2CAT parameter in the raw file (_raw) that is part of the standard data products. Originally the NUV MAMA dark current was fit with the curve $darkrate = 9.012 \times 10^{20} * \exp(-12710 / T)$. This worked well for the first two years of STIS operations, but as the mean time-averaged temperature of the detector has increased, this formula has begun to predict too large a dark current. Recently, a new more flexible fitting formula has been implemented in the **calstis** package and the calibration pipeline. The prediction for the dark current now uses the formula $darkrate = norm * 1.805 \times 10^{20} * \exp(-12211.8 / \max(T, T_{min}))$, where both *norm* and T_{min} are slowly varying functions of time that are empirically adjusted to give a good match to the observed dark rate, and which are tabulated in the temperature dependent dark correction table (tdc) reference file.

The NUV-MAMA dark current measurements during the first four months of 2002 are shown in Figure 7.16. The four open symbols in this figure represent measurements done immediately after SM3B, when the population of metastable states was far from equilibrium. Except for this interval, the NUV-MAMA dark rate early in 2002 varied between 9×10^{-4} and 1.7×10^{-3} counts/low-res-pixel/sec, with a mean rate of $\sim 1.2 \times 10^{-3}$ counts/low-res-pixel/sec. The mean OM2CAT during these observations was $\sim 37.6^\circ$ C. Updates will be provided to the user community should there be any significant changes in the behavior of the NUV-MAMA dark current.

Figure 7.16: NUV Dark Current vs. OM2CAT temperature between Jan. 1 and May 2, 2002.



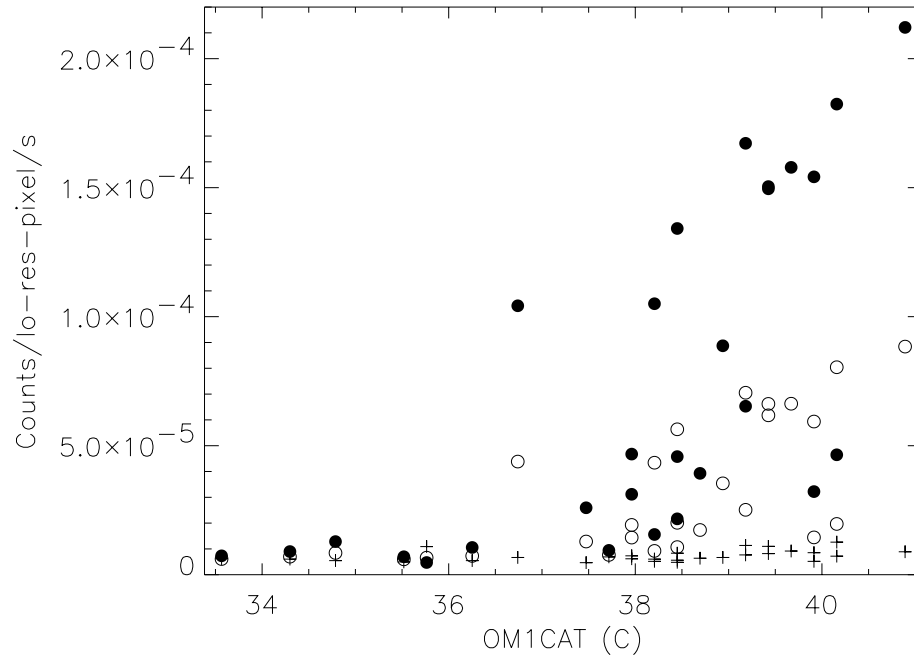
Because 99% of the NUV-MAMA dark current is due to photons hitting the detector, it is appropriate to apply the flat-field prior to subtracting the dark current. The dark current varies slowly across the face of the detector, being about 1.25 times higher near the lower left corner (AXIS1, AXIS2 < 300) than at the center. This shape varies with time and temperature enough that subtraction of the scaled dark reference may leave a residual, spatially varying dark current. This is easiest to remove by fitting a low-order two-dimensional function to the background vs. pixel position.

FUV-MAMA Dark Current

The FUV-MAMA dark current is substantially lower than that of the NUV-MAMA. Initially values as low as 7 counts/sec across the face of the detector (7×10^{-6} counts s^{-1} pix $^{-1}$) could be routinely expected. However, there is also an intermittent temperature dependent glow that covers a large fraction of the detector (see Figure 7.18). The source of the dark current is not phosphorescence but is intrinsic to the micro-channel plate array (it was seen in ground testing). This glow can substantially increase this current over a large fraction of the detector, and this leads to count rates of up to 100 counts/s integrated across the face of the detector. During the first two years of STIS operations, this glow was only present intermittently, but since mid-1999 it has been present more often than not (see Figure 7.17). The FUV-MAMA glow as a function of temperature is much less predictable than the NUV-MAMA dark current, and in the future it may be higher due to the increased instrument temperature. We currently expect

count rates in the glow region to have a typical value of $\sim 1.5 \times 10^{-4}$ cts/low-res-pixel/s during Cycle 14. During Cycle 12, the D1 apertures were implemented in order to minimize the glow effect. See Section 4.2.3 for further details on their use.

Figure 7.17: FUV Dark Current vs. OM1CAT temperature between Jan. 1 and May 2, 2002. Filled symbols show the measured dark rate in the glow region (pixels [200:400,600:800]), open symbols show the average rate over the entire detector, and the + symbols show the dark rate in the lower right corner of the detector, where the glow is faintest.

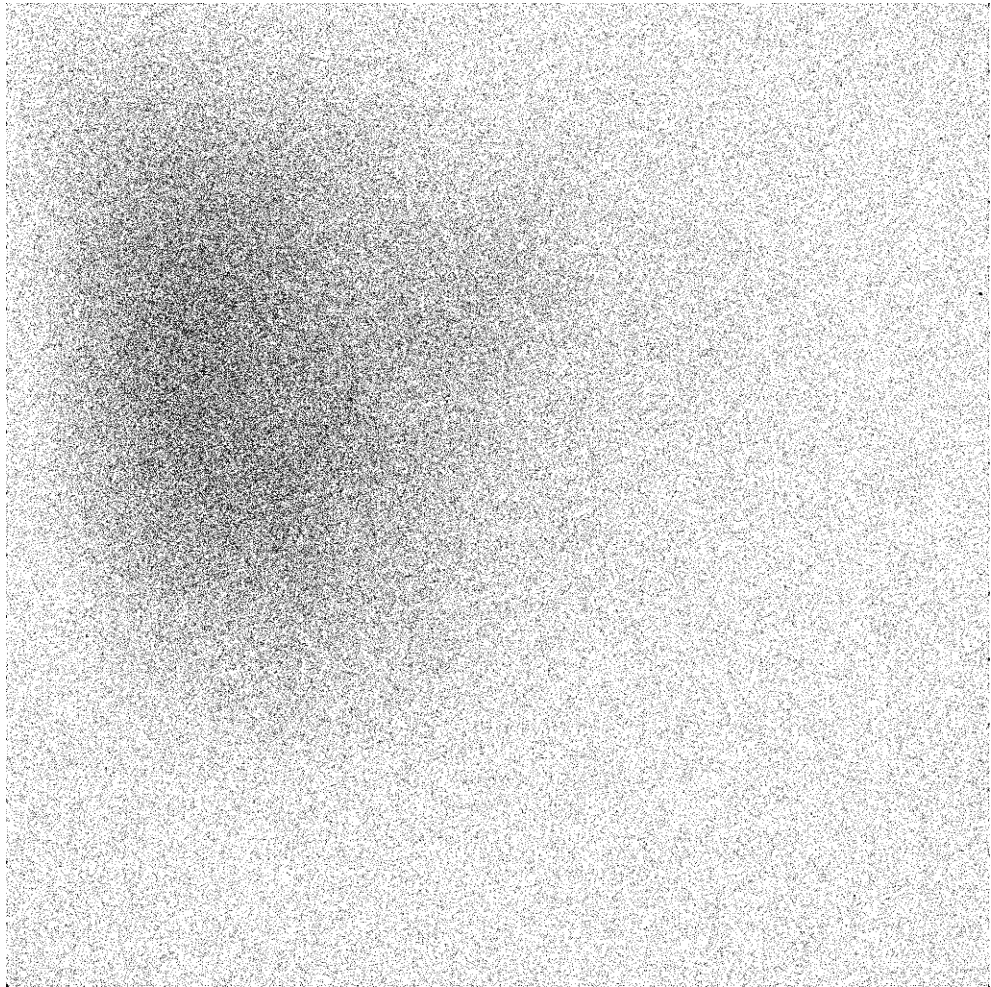


An example of the dark current variation across the detector can be seen in Figure 7.18, which is the sum of a number of 1380-second dark frames taken during periods of high dark current. The dark current in the lower right quadrant (pixels [900:1000,10:110] in IRAF notation) appears to be stable to within 10% over time. The dark current in the upper left quadrant (pixels [200:400,600:800]) varies with time and temperature. The total dark current can be approximated by the sum of a constant dark current plus a “glow” image, scaled to the net rate in the upper left quadrant. Dark current for the FUV-MAMA is not currently subtracted by the pipeline. However, the “glow” image is available from the [STIS web site](http://www.stsci.edu/hst/stis/performance/background/), at

<http://www.stsci.edu/hst/stis/performance/background/>

and can be used for off-line reduction. Revised information on the FUV-MAMA glow, suitable for off-line reduction, will be posted on the STIS web site as it becomes available.

Figure 7.18: Dark Current Variation Across Detector. The region in the upper left quadrant has the higher dark current.



Because the dark current is so low in the MAMA detectors, a typical STIS FUV-MAMA observation will have less than one count per pixel from the dark. It is good to keep this in mind when reducing the data, as various standard measures of background (the median for example) are not good estimates when the data are quantized into just a few values. The best way to estimate the background is to identify hot pixels using the standard reference files, then use an unclipped mean for the remaining pixels in a source-free region of the image.

7.4.3 MAMA Signal-to-Noise Ratio Limitations

MAMA detectors are capable of delivering signal-to-noise ratios of the order of 100:1 per spectral resolution element or even higher. Tests in orbit have demonstrated that such high S/N is possible with STIS (Kaiser et al., 1998, Proc. SPIE, 3356, 415; Gilliland, [STIS ISR 1998-16.](#))

High S/N observations of several standard stars were obtained during STIS commissioning, and they were reduced with flats obtained during preflight testing of the detectors. Signal-to-noise ratios of 125 and 150 per spectral resolution element (for an 11 pixel extraction height in the cross dispersion direction) were achieved for the FUV- and NUV-MAMA observations, respectively; see Chapter 12 for a more detailed discussion.

For targets observed at a fixed position on the detector, the signal-to-noise ratio is limited by systematic uncertainties in the small-scale spatial and spectral response of the detector. The MAMA flats show a fixed pattern that is a combination of several effects including beating between the MCP array and the anode pixel array, variations in the charge-cloud structure at the anode, and low-level capacitive cross-coupling between the fine anode elements. Intrinsic pixel-to-pixel variations are 3.9% and 2.8% rms for the FUV- and NUV-MAMA, respectively, in 1024 x 1024 pixel format. In the highres 2048 x 2048 format (see Chapter 11) the intrinsic variations are much larger. This fixed pattern appears to be stable at the 1–2% level. The structure of the flat may vary slightly for different modes due to different incidence angles of the incoming photons on the microchannel-plate pores.

Observing strategies for achieving spectral S/N higher than ~50:1 are discussed in Chapter 12. For echelle-mode spectra, observers may want to consider the use of the FP-SPLIT slits; for first-order mode observations, they may wish to dither the target along the slit.

Since MAMA observations can be binned in post-observation data processing with no additional signal-to-noise price, the option to obtain MAMA observations with unequal binning (e.g. BINAXIS1=1, BINAXIS2=2) were disabled starting in Cycle 8.

7.4.4 MAMA Non-linearity

Global

The MAMA detectors begin to experience non-linearity (photon impact rate not equal to photon count rate) at global (across the entire detector) count rates of 200,000 counts sec^{-1} . The non-linearity reaches 10% at 300,000 counts sec^{-1} and can be approximately corrected in post-observation data processing. Additionally, the MAMA detectors plus processing software are not able to count reliably at rates exceeding 285,000 count sec^{-1} . For this reason and to protect the detectors, observations beyond this rate are not allowed (see Section 7.6, below).

Local

The MAMA detectors remain linear to better than 1% in their counting up to ~22 counts sec^{-1} pixel^{-1} for the FUV-MAMA and 34 counts sec^{-1} pixel^{-1} for the NUV-MAMA. At higher rates, they experience local (at a given pixel) non-linearity. The non-linearity effect is image

dependent—that is, the non-linearity observed at a given pixel depends on the photon rate affecting neighboring pixels. This property makes it impossible to correct reliably for the local non-linearity in post-observation data processing. In addition, the MAMA detectors are subject to damage at high local count rates (see Section 7.6).

7.5 MAMA Spectral Offsetting

For the FUV-MAMA, the repeller wire produces a small shadow on the detector (with a depth of $\sim 10\%$) which is apparent on FUV-MAMA flat field images (see Section 7.3.1). To avoid first-order mode spectra falling on the repeller wire shadow, all data taken with the G140L and G140M gratings are projected to fall 3 arcseconds or ~ 120 low-resolution pixels below the repeller wire (to $AXIS2 = 392$) from the detector center (see also Section 11.1.2). This offsetting is done using the Mode Select Mechanism to tilt the grating. For these modes the projected field of view is therefore asymmetric with respect to the specified target coordinates. Note that in Cycle 7, prior to March 15, 1999, the offset from the detector center was done in the opposite direction (to $AXIS2 = 632$). However, as this caused G140L and G140M point source spectra to fall onto the region of the FUV-MAMA with the highest dark current, this was changed to the current setting. Observers who wish to match the field of views of Cycle 7 observations will need to take this difference into account.

Beginning in January 1998 the projection of the spectra on the detector for *all* NUV- and FUV- MAMA spectroscopic modes were shifted slightly each month. This procedure was instituted in order to minimize uneven charge depletion in the microchannel plates that would increase the non-uniformity of the flat fields. These monthly charge-offsetting shifts can shift the spectrum ± 15 low-resolution pixels in $AXIS1$ (dispersion) and ± 40 low-resolution pixels in $AXIS2$ (cross-dispersion). Hence observers are advised to select settings that keep wavelength ranges and targets of interest away from the extreme ends of the long slits. *Starting in August 2002 this monthly offsetting was disabled for the MAMA echelle modes*, although it continues to be done for 1st order MAMA spectroscopic modes, as it was realized that moving the echelle spectrum in the $AXIS1$ direction shifts the echelle blaze function by a different amount than it shifts the wavelength scale. This misalignment of the blaze function with the wavelength scale makes proper flux calibration of the extracted spectrum significantly more difficult.

7.6 MAMA Bright-Object Limits

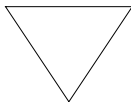


STScI has responsibility to ensure that the MAMA detectors are not damaged through over-illumination. Consequently, we have developed procedures and rules to protect the MAMAs. We ask all potential users to share in this responsibility by reading and taking note of the information in this section and designing observing programs that operate in the safe regime for these detectors.

7.6.1 Overview

The MAMA detectors are subject to catastrophic damage at high global and local count rates and cannot be used to observe sources that exceed the defined safety limits. Specifically, charge is extracted from the microchannel plate during UV observations, and overillumination can cause a decrease of quantum efficiency in the overexposed region, or even catastrophic failure if excess gas generation from the microchannel plates causes arcing in the sealed tube.

To safeguard the detectors, checks of the global (over the whole detector) and local (per pixel) illumination rates are automatically performed in flight for all MAMA exposures. The *global illumination rate* is monitored continuously; if the global rate approaches the level where the detector can be damaged, the high voltage on the detector is automatically turned off. This event can result in the loss of all observations scheduled to be taken with that detector for the remainder of the calendar (~1 week). The *peak local illumination rate* is measured over the MAMA field at the start of each new exposure; if the local rate approaches the damage level, STIS will shutter, and the exposure will be lost.



Sources that would over-illuminate the MAMA detectors cannot be observed. It is the responsibility of the observer to avoid specifying observations that exceed the limits described below.

7.6.2 Observational Limits

To ensure the safety of the MAMA detectors and the robustness of the observing timeline, we have established observational limits on the incident count rates. Observations that exceed the allowed limits will not be scheduled.

The definitive guidelines for bright object limits are given in [STIS ISR 2000-01](#), but the following brief discussion is included here for convenience. The allowed limits are given in Table 7.8, which includes separate limits for non-variable and irregularly-variable sources. The global limits for irregularly variable sources are a factor 2.5 more conservative than for sources with predictable fluxes. Predictable variables are treated as non-variable for this purpose. Examples of sources whose variability is predictable are Cepheids or eclipsing binaries. Irregularly variable sources are, for instance, cataclysmic variables or AGN. Here and in general, “pixel” refers to the 1024x1024 format (low-res pixels).

Table 7.8: Absolute MAMA Count-Rate Limits for Non-variable and Variable Objects

Target	Limit Type	Mode	Channel	Screening Limit
Non-variable	Global	All modes other than 1st-order spectroscopy	FUV and NUV	200,000 c/s ¹
Non-variable	Global	1st-order spectroscopy	FUV and NUV	30,000 c/s
Non-variable	Local	Imaging	FUV and NUV	100 c/s/p ²
Non-variable	Local	Spectroscopy	FUV and NUV	75 c/s/p
Irregularly Variable	Global	All modes other than 1st-order spectroscopy	FUV and NUV	80,000 c/s ³
Irregularly Variable	Global	1st-order spectroscopy	FUV and NUV	12,000 c/s ³
Irregularly Variable	Local	Imaging	FUV and NUV	100 c/s/p ³
Irregularly Variable	Local	Spectroscopy	FUV and NUV	75 c/s/p ³

1. c/s is counts sec⁻¹.

2. c/s/p is counts sec⁻¹ pix⁻¹.

3. Applies to the phase when the target is brightest.

7.6.3 How Do You Determine if You Violate a Bright Object Limit?

As a first step, you can check your source V magnitude and peak flux against the bright-object screening magnitudes in Table 13.44 or Table 14.39 for your chosen observing configuration. In many cases, your source properties will be much fainter than these limits, and you need not worry further.

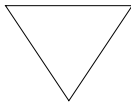
However, if you are near these limits (within 1 magnitude or a factor of 2.5 of the flux limits), then you need to carefully consider whether your source will be observable in that configuration. Remember the limits in these tables assume zero extinction and for spectroscopic observations do

not include slit losses. Thus you will want to correct the limits appropriately for your source's reddening and the aperture throughput.

You can use the information presented in Section 6.2 to calculate your peak and global count rates. Perhaps better, you can use the [STIS Exposure Time Calculators](#) available through the [STIS World Wide Web site](#) to calculate the expected count rate from your source. They have available to them a host of template stellar spectra. If you have a spectrum of your source (e.g., from IUE, FOS, or GHRS) you can also input it directly to the calculators. The calculators will evaluate the global and per pixel count rates and will warn you if your exposure exceeds the absolute bright-object limits. We recommend that you use the STIS ETCs if you are in *any doubt* that your exposure may exceed the bright-object MAMA limits.

You should also be aware that when a short (~300 ms) exposure is taken, in order for the local rate monitor to check whether the bright object limit is violated, the actual check does not involve a real measurement of the maximum flux per pixel. Instead, the obtained short-exposure image is binned into “superpixels,” each one with a size of 8x8 (imaging) or 4x8 (spectroscopy) regular (low-res) pixels, and the resulting measured flux for each superpixel is transformed into a peak flux per pixel, assuming that a single isolated point source contributes to the flux in that bin. Therefore, you should be extra careful when observing a crowded field or a slightly resolved source in imaging mode, since it is possible for the exposure to be aborted even when no single source violates the local rate limit (e.g., two or more stars fall inside the same bin or a source with a non-point-source radial profile is present in the field). See [STIS ISR 1996-31](#) for more details.

7.6.4 Policy and Observers' Responsibility in Phase I and Phase II



It is the observers' responsibility to ensure that their observations do not exceed the bright-object count limits stated in Table 7.8.

It is *your responsibility* to ensure that you have checked your planned observations against the brightness limits prior to proposing for Phase I. If your proposal is accepted and we, or you, subsequently determine (in Phase II), that your source violates the absolute limits, then you will either have to: a) choose a different configuration, if possible, b) change the target, if allowed, or c) lose the granted observing time. We encourage you to include a justification in your Phase I proposal if your target is within 1 magnitude of the bright-object limits for your observing configuration. For

MAMA target-of-opportunity proposals, please provide an explanation of how you will ensure that your target can be safely observed in your Phase I proposal.

STScI will screen all STIS observations that use the MAMA detectors to ensure that they do not exceed the bright-object limits. In Phase II, you will be required to provide sufficient information to allow screening to be performed.

Here we describe the required information you must provide.

Spectroscopy

To allow screening of your target in Phase II for spectroscopic MAMA observations you must provide the following for your target (i.e., for all sources which will illuminate the detector during your observations):

- V magnitude
- Expected source flux at observing wavelength
- Spectral type (one of the types in the screening tables)
- E_{B-V}
- B-V color

If you wish to observe a target that comes within one magnitude (or a factor of 2.5 in flux) of the limits in the spectroscopic bright-object screening table (Table 13.44) for your configuration, after correction for aperture throughput and reddening, but which you believe will not exceed the absolute limits in Table 7.8 and so should be observable, you must provide auxiliary information to justify your request. Specifically:

- You must provide an existing UV spectrum (e.g., obtained with IUE, HUT, FOS, GHRS, or STIS) of the object that proves that neither the global nor the local absolute limits will be exceeded.
- If you do not have such data, then you must obtain them, by taking a “pre-exposure” in a MAMA-safe configuration (e.g., with a ND filter in place or in a higher resolution mode) before we will schedule your observations. *Be sure to include the time (1 orbit in a separate visit) for such an observation in your Phase I Orbit Time Request, as needed.*

Imaging

The MAMA imaging bright-object screening magnitudes (see Table 14.39) are very stringent, ranging from $V = 15.3$ to $V = 20.3$ for the different imaging apertures, and apply to all sources imaged onto the MAMA detector (i.e., not just the intended target of interest). Table 14.39 can be used to determine if the target of interest is above the bright-object limit. Since the start of Cycle 9, STScI has been using the second-generation Guide-Star Catalog (GSC II) to perform imaging

screening for objects in the field of view other than the target itself. The GSC II contains measurements from photometrically calibrated photographic plates with color information for magnitudes down to at least $V = 22$ mag. This information will be used to support bright-object checking for fixed and for moving targets (major planets). STScI will make a best effort to perform the imaging screening using GSC II. However, observers should be prepared for the possibility that under exceptional circumstances GSC II may be insufficient. For instance, fields close to the Galactic plane may be too crowded to obtain reliable photometry. If for any reason the screening cannot be done with GSC II, the observer is responsible for providing the required photometry. In the case of moving targets, STScI will identify “safe” fields, and the observations will be scheduled accordingly. Observers will then be updated on the status of their observations. We anticipate that bright-object considerations will not have a significant effect on the scheduling of such observations.

Pointings Close To Objects Violating Safety Limits

Pointings close to objects violating safety limits must be screened since (i) the possibility of HST pointing errors exists, and (ii) the light of a bright point source may pose a safety threat even if observed at a distance of several arcsec.

The typical HST pointing accuracy is about 0.5 arcsec, but cases have been observed when HST was pointing 1-2 arcsecs off its expected position. This results from some guide stars having less accurate coordinates or because they are not single. STScI will perform a screening of not only the targets in the field of view themselves (spectroscopy and imaging modes), but also of targets within 5 arcsec of the boundaries of the used apertures (full field of view of the MAMA detector for imaging and slitless spectroscopy, field covered by slit for spectroscopy). If objects are found that would exceed the Bright Object Protection limit for the particular instrument configuration, the observations will not be executed.

Targets or field objects falling in an annular region extending from 5 to 13.5 arcsec from the edge of the aperture used in a MAMA observation also have additional restrictions. Any object in this zone producing either a real global count rate in excess of 1.5×10^6 counts s^{-1} or a local count rate greater than 500 counts sec^{-1} pixel $^{-1}$ is not permitted. See [STIS ISR 2000-01](#) for a discussion of the new screening procedures.

7.6.5 Policy on Observations That Fail Because they Exceed Bright-Object Limits

If your source passes screening, but causes the automatic flight checking to shutter your exposures or shut down the detector voltage causing the loss of your observing time, *then that lost time will not be returned to you*; it is

the observer's responsibility to ensure that observations do not exceed the bright-object limits.

7.6.6 What To Do If Your Source is Too Bright for Your Chosen Configuration?

If your source is too bright for one configuration, it may be observable in another configuration (e.g., in a higher-dispersion configuration). The options open to you if your source count rate is too high in a given configuration include:

- Select a narrower slit that passes only a fraction of the source flux, for spectroscopic observations.
- Select a higher dispersion grating.
- For near-UV low-resolution and medium-resolution spectroscopy, consider using the CCD G230LB and G230MB modes (see Section 4.1.7).
- Employ a neutral-density filter.
- Change configurations totally to observe a different portion of the spectrum of your target (e.g., switching to the CCD).

For further advice, see Section 12.4.

7.6.7 Bright-Object Protection for Solar System Observations

Observations of planets with STIS require particularly careful planning due to the very stringent overlight limits of the MAMAs. In principle Table 13.44 and Table 14.39 can be used to determine if a particular observation of a solar-system target exceeds the safety limit. In practice the simplest and most straightforward method of checking the bright object limits for a particular observation is to use the [STIS Exposure Time Calculator](#). With a user-supplied input spectrum, or assumptions about the spectral energy distribution of the target, the ETC will determine whether a specified observation violates any bright object limits.

Generally speaking, for small ($< \sim 0.5$ – 1 arcsec) solar-system objects the local count rate limit is the more restrictive constraint, while for large objects ($> \sim 1$ – 2 arcsec) the global limit is much more restrictive.

As a first approximation, small solar system targets can be regarded as point sources with a solar (G2 V) spectrum, and if the V magnitude is known, Table 13.44 and Table 14.39 can be used to estimate whether an observation with a particular STIS grating or filter is near the bright-object limits. V magnitudes for the most common solar-system targets (all planets

and satellites, and the principal minor planets) can be found in the *Astronomical Almanac*. This approximation should provide a conservative estimate, particularly for the local limit, because it is equivalent to assuming that all the flux from the target falls on a single pixel, which is an overestimate, and because the albedos of solar-system objects are almost always < 1 (meaning that the flux of the object will be less than that of the assumed solar spectrum at UV wavelengths where the bright-object limits apply). A very conservative estimate of the global count rate can be obtained by estimating the peak (local) count rate assuming all the flux falls on one pixel, and then multiplying by the number of pixels subtended by the target. If these simple estimates produce numbers near the bright-object limits, more sophisticated estimates may be required to provide assurance that the object is not too bright to observe in a particular configuration.

For large solar-system targets, checking of the bright-object limits is most conveniently done by converting the integrated V magnitude (V_0 , which can be found in the *Astronomical Almanac*) to V magnitude/arcsec² as follows:

$$V / \text{arcsec}^2 = V_0 - 2.5 \log(1/\text{area})$$

where *area* is the area of the target in arcsec². This V / arcsec^2 and the diameter of the target in arcsec can then be input into the ETC (choose the Kurucz model G2 V spectrum for the spectral energy distribution) to test whether the bright-object limits can be satisfied.

Alternatively, an observed spectrum obtained with a known slit size can be used as input to the ETC. Most calibration techniques produce units of flux (e.g., ergs sec⁻¹ cm⁻² Å⁻¹), even for extended targets. Such a calibration implicitly assumes a flux per solid angle (i.e., the angle subtended by the observing slit or object, whichever is smaller), and it is more appropriate to convert to units of surface brightness (ergs sec⁻¹ cm⁻² Å⁻¹ arcsec⁻²) by dividing the calibrated flux by the appropriate area (slit size or object size, whichever is *smaller*). If such a spectrum is available, it can be immediately examined and compared with the local limit in units of surface brightness given in Table 13.44 and Table 14.39, or passed to the ETC as a user-supplied spectrum. It can also be easily converted to counts sec⁻¹ pix⁻¹ by using the diffuse-source sensitivities for the appropriate grating or filter provided in this Handbook. Note that the sensitivities in this Handbook assume a specific slit *width*, so they need to be scaled by the desired slit width. The ETC provides another check of the local limit: if the peak count rate per pixel exceeds the local limit of 75 (for spectroscopic observations) or 100 (for imaging observations) counts sec⁻¹ pix⁻¹, such an observation would not be allowed. The global limit can be checked by summing the count rate per pixel over wavelength, and multiplying by the desired slit length (in arcsec) divided by the pixel size (0.0247 arcsec) to

produce total counts per second for the observation. If this number is larger than the appropriate global limit, the observation should not be performed because it will cause the instrument to enter safe mode. For such cases, a smaller slit size or higher-resolution grating could then be considered.

7.6.8 Jupiter and Saturn

To further aid the observer, we provide results of test simulations with Jupiter and Saturn; the input spectra are observed surface fluxes of Jupiter and Saturn from 1200 Å to 7000 Å. Jupiter and Saturn have corresponding visual magnitudes of $V = 4.9$ and 6.5 mag arcsec⁻², respectively. No variation of the surface brightness over the disk is taken into account. We assume that both planets have diameters >25 arcsec, i.e., exceeding the field size of the MAMA detectors. This assumption is appropriate for Jupiter and conservative for Saturn.

MAMA Spectroscopy

We adopt slit lengths of 6 and 25 arcsec for echelle and first-order grating observations, respectively. Slit widths are 1 arcsec in both cases. The slits are centered on the planets so that the planets overfill the apertures. The results for the local limits are in Table 7.9. The table gives the observed V magnitudes arcsec⁻² of the two planets and the limiting magnitudes for all echelle and first-order gratings. If the planet were as bright as the limiting magnitude, it would reach the limiting local count rates (75 counts sec⁻¹ pix⁻¹ for the FUV and NUV). No safety margin was added to the magnitudes listed in this and the subsequent tables. Table 7.9 suggests that only Jupiter observed with G230L would come close to the local brightness limit.

Table 7.9: Local Brightness Limits (V mag arcsec⁻²) for Spectroscopy

	Observed	G140L	G140M	E140M	E140H	G230L	G230M	E230M	E230H
Jupiter	4.9	-5.2	-8.7	-10.2	-11.7	4.6	0.5	-0.5	-2.9
Saturn	6.5	-5.8	-9.2	-11.8	-12.8	4.4	0.3	-0.7	-3.1

Next we discuss the global limits. The global limits for echelle spectroscopy are in Table 7.10. As for point sources, they are determined by the screening limit count rate of 200,000 counts sec⁻¹. Both Jupiter and Saturn are fainter than the limit for the FUV echelles and brighter for the NUV echelles. Recall that a slit length of 6 arcsec was adopted, with the planets filling the aperture. This assumption makes the brightness limits 1.9 mag ($2.5 \times \log 6$) more stringent than for a point source having the same spectrum.

Table 7.10: Global Brightness Limits (V mag arcsec⁻²) for Echelle Spectroscopy

	Observed	E140M	E140H	E230M	E230H
Jupiter	4.9	-0.6	-1.2	10.1	8.9
Saturn	6.5	-1.8	-2.7	9.9	8.7

The results for first-order spectroscopy are in Table 7.11. Because we assumed that both Jupiter and Saturn completely fill the 25 arcsec long slit, the limiting magnitude is determined by the global screening limit value of 200,000 counts/sec. This situation differs from that of point-source observations where the limiting magnitude is usually determined by the count rate per pixel or by the total number of counts along the dispersion direction. For extended objects, the total number of counts accumulated over the whole detector sets the limit. Note that the limits for the two planets are always set by the global, and not by the local rates. As was the case for echelle spectroscopy, both Jupiter and Saturn are fainter than the limit for the FUV and brighter for the NUV gratings.

Table 7.11: Global Brightness Limits (V mag arcsec⁻²) for First-Order Spectroscopy

	Observed	G140L	G140M	G230L	G230M
Jupiter	4.9	1.4	0.0	12.9	10.1
Saturn	6.5	1.3	-1.0	12.8	9.9

The examples demonstrate that careful choices of slit sizes and neutral-density filters are required to prevent instrument damage.

MAMA Imaging

As is the case with spectroscopy, the global limit is much more restrictive than the local limit, and careful simulations are required to determine which filters can be safely used for imaging.

Target Acquisition

In this chapter. . .

8.1 Introduction / 163
8.2 STIS Onboard CCD Target Acquisitions (ACQ) / 169
8.3 Onboard Target Acquisition Peakups (ACQ/PEAK) / 183
8.4 Determining the PLATE-ID of HST Observations / 189
8.5 Acquisition Examples / 190
8.6 STIS Post-Observation Target Acquisition Analysis / 200

8.1 Introduction

All STIS spectroscopy using apertures less than 3 arcseconds in size and all coronagraphic observations will require an onboard STIS target acquisition (ACQ) and possibly an acquisition/peakup (ACQ/PEAK) exposure to center the target in the scientific aperture. In this Chapter, we provide the basic information you need to choose an acquisition strategy for your program.

STIS target acquisitions employ the CCD camera to image the target's field directly and onboard flight software processes the image to locate the position of the target. STIS acquisitions are very reliable, accurate (typically ± 0.01 arcsecond for $V < 21$ point sources), and quick (~ 6 minutes). For the narrow slits (≤ 0.1 arcsecond), an ACQ/PEAK is required, which is accurate to $\sim 5\%$ of the slit width used in the peakup, and takes typically ~ 6 minutes. For particularly faint targets ($V > 21$) or complex diffuse sources, overheads will be somewhat more and accuracies somewhat reduced (see details below).

For Phase I proposals, you do not need to determine the details of your acquisition, but need only to determine if an ACQ, and possibly an ACQ/PEAK, is required, include the necessary orbital time (which is normally dominated by the associated overheads), and assure yourself that your program can be accomplished.

For Phase II, you will need to work out the details of your acquisition procedure, and we provide two tools to assist in this task, as well as examples of different TA scenarios (see Section 8.5). To determine the correct exposure time, we provide (via the STIS web page) a [Target Acquisition Exposure Time Calculator](#) (TA ETC). The input and output parameters in the TA ETC (as compared with the Imaging ETC) are specifically designed to facilitate exposure-time estimates for target acquisition purposes. For example, the TA ETC input and output parameters take into account the following:

- The target acquisition can be done only with the CCD detector.
- The CHECKBOX (see below) size is always 3 x 3 pixels for a point source, and $n \times n$, where n is an odd number between 3 and 105, for diffuse sources.
- The CCDGAIN is always 4.
- The default S/N is 40 for the calculation of exposure time.

To determine the correct CHECKBOX size for DIFFUSE targets, we provide a [Target Acquisition Simulator](#) (TAS), which implements the same algorithms as the flight software, and so should give results in good agreement with what will happen in orbit. The TAS takes as input an image, extracts a subarray centered on the coordinates provided, and searches for the brightest location by passing a CHECKBOX over the subarray.

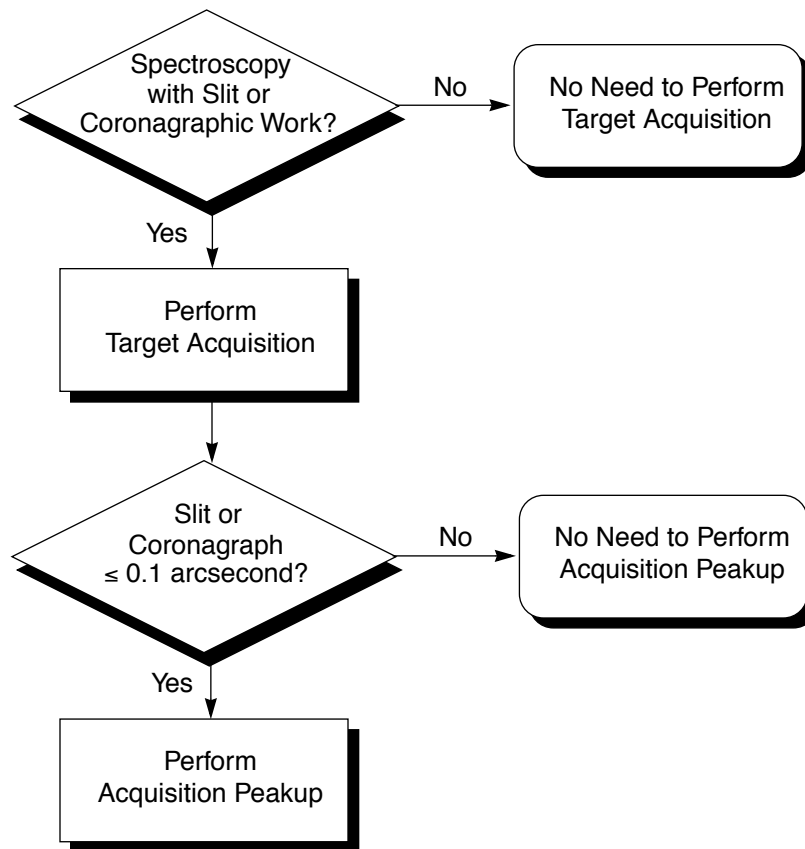
Below we describe acquisition and pickup exposures for spectroscopy. More details on centering of targets behind the coronagraphic bars and wedges are described in Section 12.9, but examples are provided at the end of this chapter.

8.1.1 Initial Pointing

Following the initial guide-star acquisition for your visit, the target location in the aperture plane will be known to an accuracy of ~1–2 arcseconds. For scientific observations taken through spectroscopic slits which are less than 3 arcseconds in either dimension, and for imaging observations with one of the coronagraphic apertures, you will need to use an onboard STIS target acquisition and possibly an acquisition pickup exposure to center your target.

Figure 8.1 shows a decision flow for determining whether you require an acquisition or both an acquisition and a pickup to center your target.

Figure 8.1: Determining Acquisition Requirements



8.1.2 Acquisitions

STIS target acquisition exposures (MODE=ACQ) always use the CCD, one of the filtered or unfiltered apertures for CCD imaging, and a mirror as the optical element in the grating wheel. Acquisition exposures center your target in the slit or behind a coronagraphic bar to an accuracy (2σ) of ~ 0.01 arcsecond for a point source, and 0.01 to 0.1 arcsecond for a diffuse object (larger targets have larger errors). A typical STIS point source target acquisition takes ~ 6 minutes.

8.1.3 Peakups

An acquisition peakup exposure (MODE=ACQ/PEAKUP) must be taken following the target acquisition exposure to refine the centering of point or point-like sources in slits less than or equal to 0.1 arcsecond wide (or tall).

Peakup exposures use a slit or coronagraphic aperture and are taken with the CCD as the detector and with either a mirror or a spectroscopic element in position on the grating wheel. Typical target acquisition centering accuracies following a peakup sequence are 0.05 times the dimension of the slit or bar. Typical STIS imaging point source peakups take ~5–10 minutes; see Table 8.5 for the formulae needed to determine the duration of a peakup acquisition.

Figure 8.2 shows the complete decision tree for STIS target acquisitions.

8.1.4 Drift Rates

For most exposures, two guide stars will be used to support the observation, enabling correction of drift. In some cases, however, it may not be possible to find a guide star pair to support the observation, or the observation may drop to single guide star mode because one of the guide stars cannot be acquired. In that case, the roll of the telescope is under GYRO control, which will allow a slow drift of the target on a circular arc centered on the single guide star. If you are informed that only single guide stars can be found for your observation, you can try to get a guide star pair by relaxing the scheduling requirements (e.g. expand the ORIENT range). If you must use a single guide star for a multiple-orbit visit, or if your observation is especially time-critical and would be significantly degraded by failure to single guide star mode, you should consider including a re-centering ACQ/PEAK during the visit.

Table 8.1 gives what is generally the worst case object motion of the target on the detector for a single guide star observation. For example, if a science observation in an 0.2 arcsecond slit is 3 orbits in duration, then the target would move to the edge of the aperture; a 2 orbit visit would leave the target halfway toward the edge. Thus, only single orbit visits should be done on a single guide star. However, for science in a 2 arcsecond slit, the motion over 4 orbits only takes the target 13% of the way to the edge of the slit. Thus, if high photometric accuracy is not required, a single guide star should be sufficient for the larger slits.

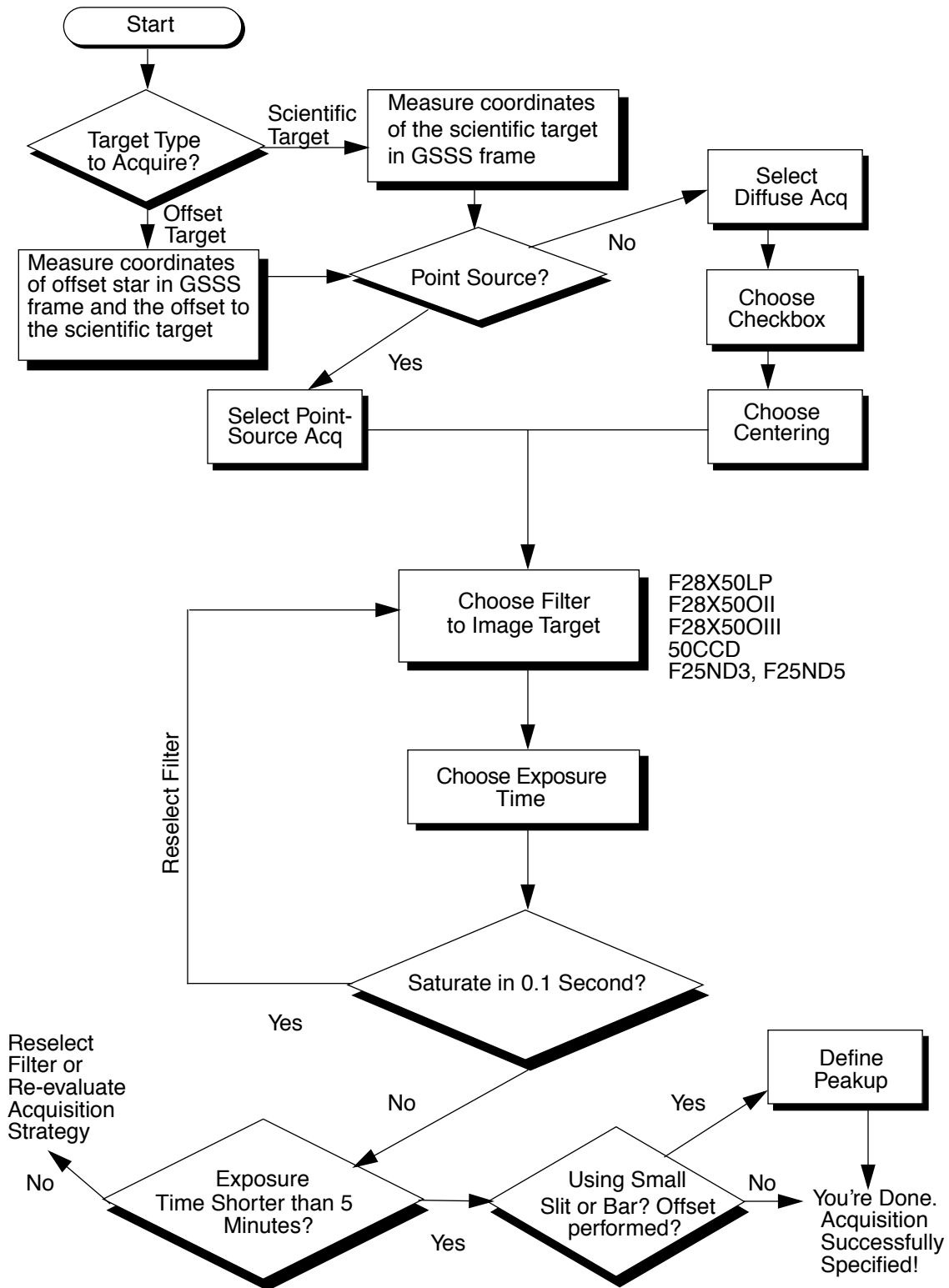
Table 8.1: Single Guide Star Target Position Shift in Arcseconds vs. Time and Orbits.

	Seconds (x1000)						Orbits			
	1	2	5	10	15	20	1	2	3	4
Drift (arcsec)	0.005	0.01	0.03	0.06	0.08	0.10	0.03	0.06	0.10	0.13

For a completed observation, you can use information in the headers of the archived files to make a better estimate of the drift of the target for a single guide star observation. The rate of the drift of the radiant of the

circle traced by the target about the guide star is unknown for any particular observation, but typically is expected to be in the range of 1.0 to 1.5 milliarcsec/sec. To calculate the approximate magnitude of the drift of the target on the detector, you will need to find the distance of the target from the acquired guidestar. The header of the observation log file `jif.fits` identifies the acquired guidestar (`GSD_ID`) and gives its right ascension (`GSD_RA`) and declination (`GSD_DEC`) in degrees. For example, for a target 10 arcmin from the guidestar, a drift of the guidestar-to-target radiant of 1 milliarcsec/sec during a 1000 second exposure would cause the target to move 0.0029 arcsec on the detector. The direction of the motion on the detector can be deduced from header keywords in the science data describing the position angle of the detector (e.g., `PA_APER`), in combination with the direction perpendicular to the radiant.

Figure 8.2: Process of Defining a Target Acquisition Scheme



8.2 STIS Onboard CCD Target Acquisitions (ACQ)

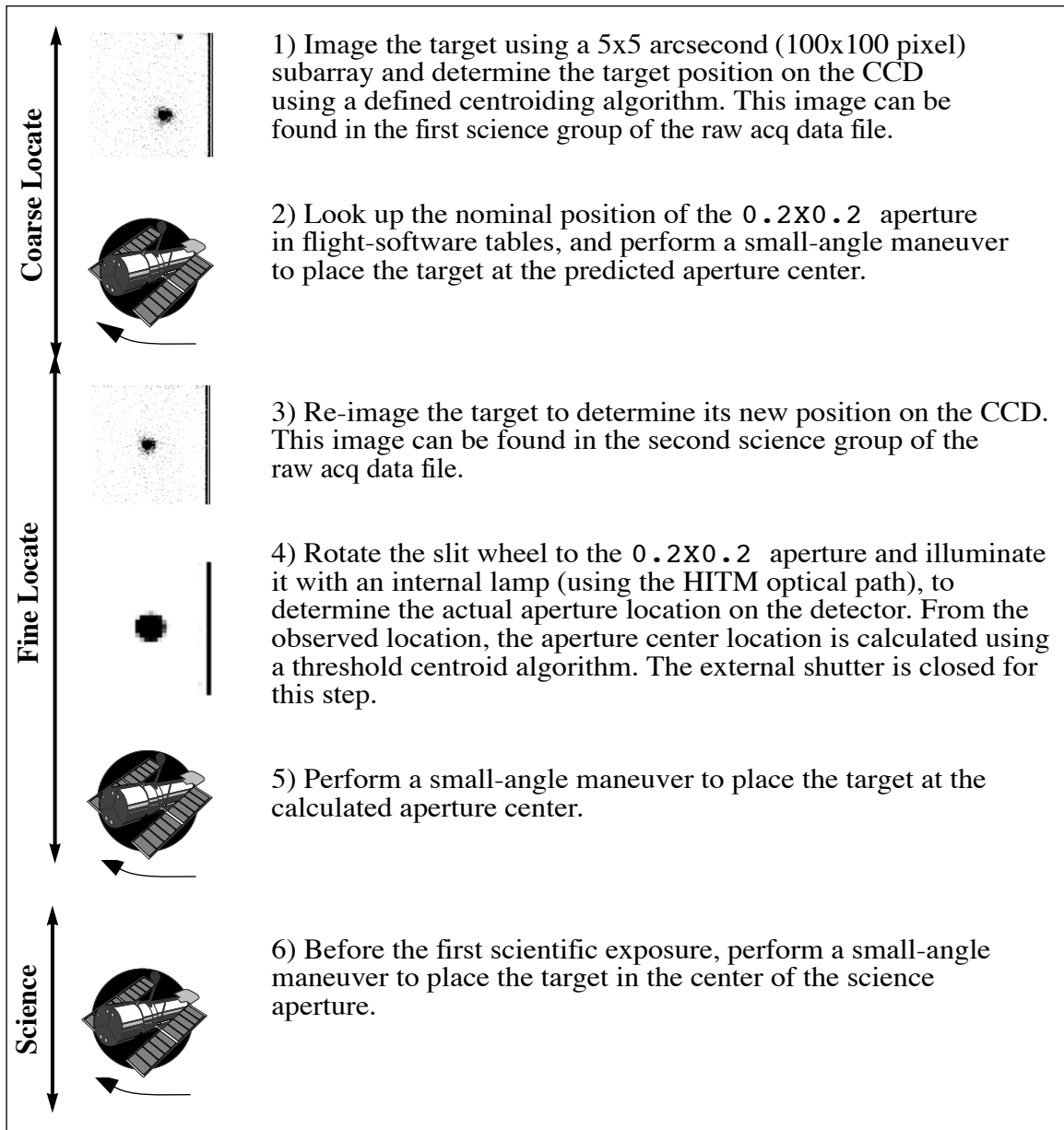
8.2.1 How it Works

Acquisition exposures are controlled by the Flight Software (FSW). Figure 8.3 highlights the basic steps in the acquisition process. The sequence comprises two discrete stages: the coarse-locate phase (steps 1–2) and the fine-locate phase (steps 3–5); a sixth step centers the target in the science aperture. The coarse-locate phase is performed to place the target as close as possible to the aperture center prior to the final telescope move. This step ensures that the final slew needed to move the target into the aperture is a small one, and it minimizes uncertainties in the calculation of the required slew caused by detector or optical distortions.

1. The target is located. A pair of 5 x 5 arcsecond (100 x 100 pixel) CCD images is taken of the sky using a user-selected filtered or unfiltered imaging aperture; for diffuse acquisitions, the field will be larger (see Section 8.2.2). The images are offset by 3 pixels in both X and Y to allow for removal of hot pixels via dithering. The flight software processes the images as needed (to realign the images, remove the bias level, flag bad pixels, and remove cosmic rays)¹ and applies one of two possible finding algorithms to determine the coordinates of the target. The “bright” column at the edge of the acquisition field is an artifact of the subarray readout and is ignored by the flight software.
2. The spacecraft is then moved to place the target at the nominal center of the 0.2X0.2 slit.
3. The target is re-imaged and the target coordinates are redetermined. This second target location is performed to minimize the final slew in step 5, and to reduce the error associated with that slew.
4. The location of the 0.2X0.2 slit is determined relative to the target. The external shutter is closed (to prevent a possible overlight condition), the 0.2X0.2 slit is rotated into position by the slit wheel, and an image is obtained with the slit illuminated by a HITM line lamp (see “Calibration-Lamp Systems” on page 28 for a description of the HITM optical path). The slit image is processed and a finding algorithm is then used to determine the coordinates of the center of the slit.

1. The processing done by the FSW is rudimentary: a single, pre-determined, bias number is subtracted, bad pixels are set to the average of the 4 adjacent pixels, negative-valued pixels are set to zero, and each pixel is assigned the minimum from the two images (as a form of cosmic-ray and hot pixel rejection). Hence, ACQ exposures are *not* suited for accurate photometry.

Figure 8.3: Target Acquisition Schematic



5. The flight software calculates the offset between the target location and the 0.2X0.2 slit, and performs a small-angle maneuver of HST to place the target in the center of the aperture.
6. The object is placed in the science aperture (by a small-angle maneuver) just prior to the execution of the scientific exposure. If another science exposure is made with a different aperture, the pointing is automatically adjusted to account for any difference in the locations of the science apertures.

An acquisition exposure produces scientific data, which include the images of the target produced in steps 1 and 3, and the image of the 0.2X0.2 slit produced in step 4. These data will be returned to you with your scientific data as part of the pipeline products, and they can be analyzed with the **tastis** tool in STSDAS.

8.2.2 Target-Location Algorithms

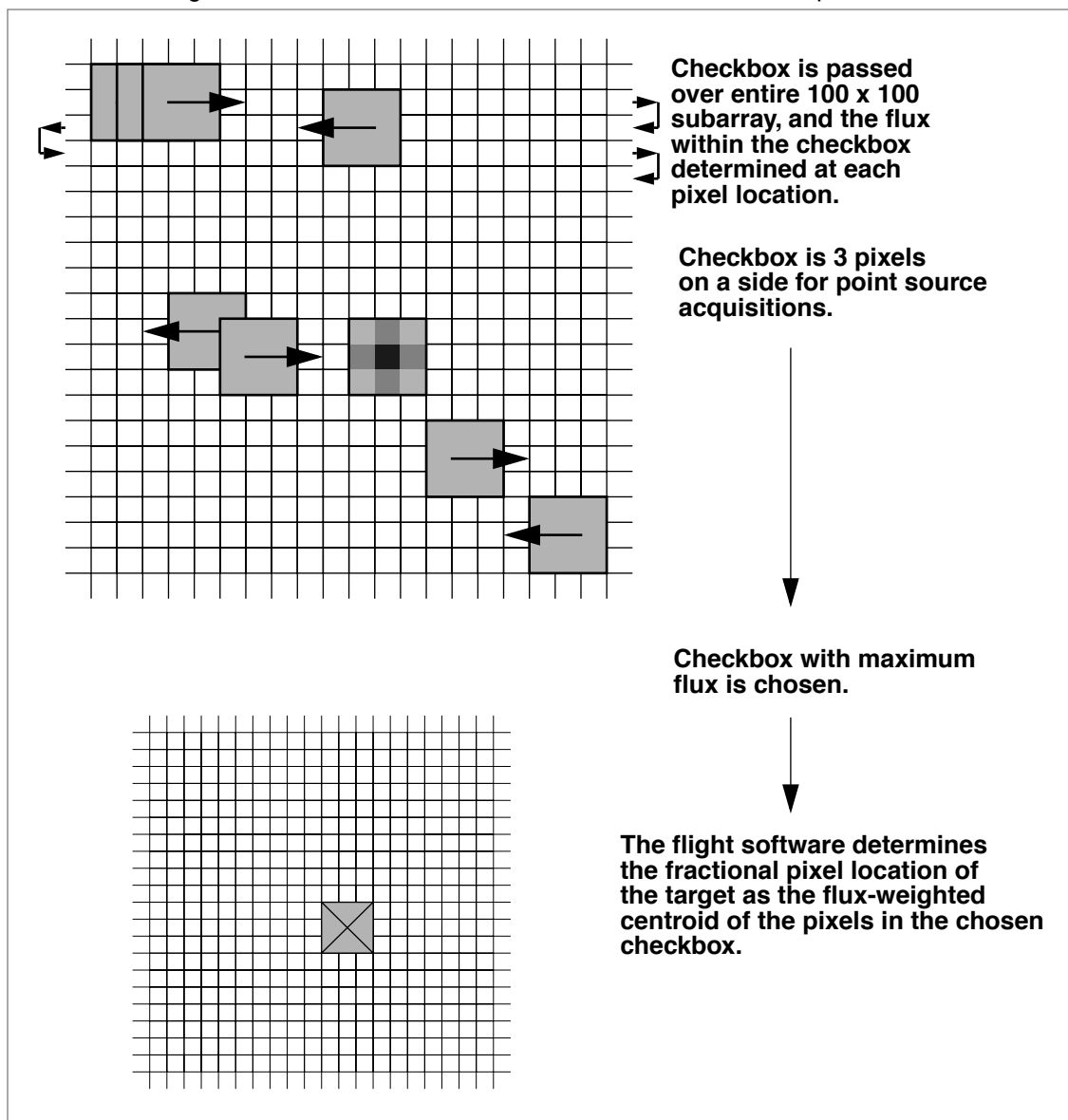
STIS supports two basic types of acquisitions: point source acquisitions (**ACQTYPE=POINT**) and diffuse-source acquisitions (**ACQTYPE=DIFFUSE**). Diffuse-source acquisitions are appropriate for sources that exhibit smooth or peaked surface brightness *on some size scale*, such as centers of galaxies, some planets and planetary satellites (see Section 8.2.5), or nebulae.

To locate the target, the flight software first passes a square *checkbox* over the image and determines the flux contained within the checkbox at each pixel in the subarray. The flight software then selects the checkbox with the maximum flux and determines the target center within that checkbox according to the type of acquisition specified.

Point source Acquisition

For point source acquisitions (**ACQTYPE=POINT**), the checkbox size is fixed at 3x3 pixels (0.15x0.15 arcsecond) and the flight software determines the target location by finding the flux-weighted centroid of the pixels in the brightest checkbox (see Figure 8.4).

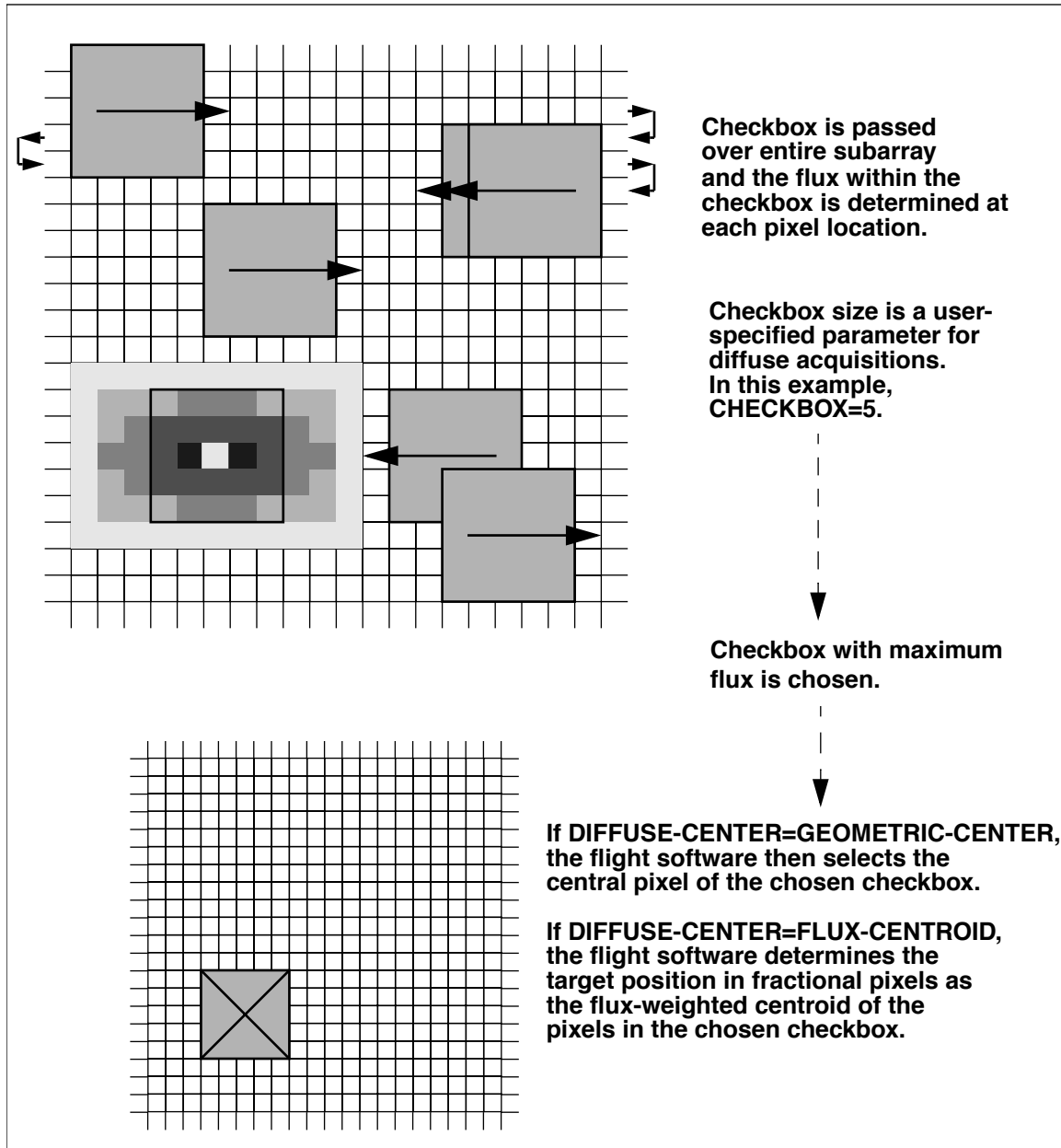
Figure 8.4: How the Checkbox Works for Point source Acquisitions



Diffuse Acquisition

For diffuse acquisitions (ACQTYPE=DIFFUSE), the flight software determines the target location either by finding the flux-weighted centroid of the pixels in the brightest checkbox or by determining the geometric center of the brightest checkbox (see Figure 8.5).

Figure 8.5: How the Checkbox Works for Diffuse Acquisitions

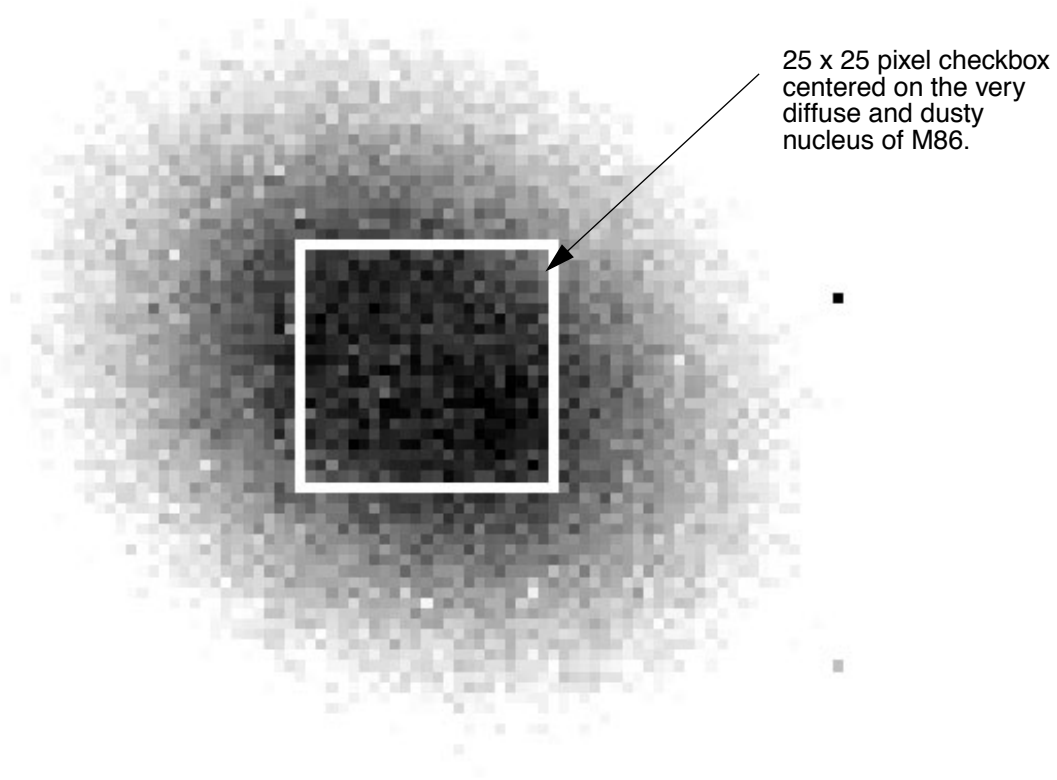


For DIFFUSE acquisitions, the user must specify both the target acquisition centering method (DIFFUSE-CENTER=GEOMETRIC-CENTER or FLUX-CENTROID) and the checkbox size. The user sets CHECKBOX= n , where n must be an odd number between 3 and 105: the checkbox will then have dimension $n \times n$ pixels. CHECKBOX should be set to the minimum size which ensures that the brightest checkbox will be the one centered on the region of interest (i.e., if your object is peaked within a region of 1 arcsecond, set CHECKBOX=21 ($= 1 + (1 \text{ arcsecond}/0.05 \text{ arcsecond pixel}^{-1})$)). The maximum checkbox is 105 pixels on a side, or $\sim 5 \times 5$ arcseconds. The subarray used for a diffuse-source acquisition target

image is CHECKBOX+101 pixels on a side. The [STIS Target Acquisition Simulator](#) can be used to determine the optimal CHECKBOX size.

Figure 8.6 shows a simulated example of a diffuse source, the nucleus of the galaxy M86, acquired using a diffuse-source acquisition.

Figure 8.6: Simulated Diffuse Acquisition of Elliptical Galaxy M86. Created by running the flight-software algorithm on a STIS image. CHECKBOX=25 produced good centering. Smaller values caused checkbox to center on local brightness enhancements offset from galaxy center.



8.2.3 Selecting Target Acquisition Parameters

To plan your acquisition, you must select:

- The target you are going to acquire (scientific target or offset object).
- The type of acquisition, point or diffuse, and if you are performing a diffuse acquisition, the target acquisition centering algorithm and checkbox size.
- The filtered APERTURE to be used for target imaging during the acquisition.

- The exposure time for the image used to determine the location of the target.
- The program aperture, which determines if you need a pickup acquisition.

Figure 8.2 shows the flow of specifying a target acquisition scheme.

Selecting the Acquisition Object

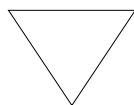
The first step is to determine what object you are going to use for your target acquisition. Note that the STIS software will always acquire the brightest object in the 5x5 arcsecond search area. If your target is isolated, or if there are no brighter objects *in the STIS bandpass* you have selected (see below) within 5 arcseconds of your target, then you can acquire your target directly. If there are brighter targets nearby, then you will need to acquire an offset target (generally the brightest nearby star), and then perform a slew to the scientific target. The offset technique is also recommended for precise pointing to specific surface or atmospheric features for large (>~4 arcseconds) planetary targets such as Mars, Jupiter, and Saturn, with the offset target being a planetary satellite (see Section 8.2.5 for further details). Note that HST performs small-angle maneuvers (SAM) quite accurately, with a 3 arcsecond maneuver having an error of 0.003 arcsecond, while a 2 arcminute maneuver (the maximum to ensure that a single set of guide stars can be used for both targets) yields a 0.02 arcsecond error. The offset should not significantly affect target acquisition centering accuracy even in the smallest echelle slits, and your target acquisition centering uncertainty will generally be dominated by your knowledge of the absolute offset between the acquisition star and your target. If you are uncertain whether a nearby object is brighter than your target in the STIS bandpass, it is safest to select an isolated object and perform your acquisition on it.

If you are observing a diffuse source, you should first check to see if there is a suitable star which you can use as an acquisition target; an offset can then be used to move to the desired position, as needed. If you wish to acquire a diffuse object directly, then it is important to know your source structure as seen at ~0.1 arcsecond resolution to properly plan your acquisition strategy if you need accurate (a few tenths of an arcsecond) centering. We recommend that you first check the HST archive to determine if your target has been observed by HST with WF/PC-1, WFPC2, FOC, STIS or ACS. If it has, that exposure can be used to determine the optimal acquisition strategy using the [Target Acquisition Simulator](#). If it has not yet been observed with HST, we suggest you take an early acquisition image, either with the STIS or with WFPC2, which you can use to determine your optimal acquisition strategy. This is particularly important if your program requires placement of a narrow slit accurately on a diffuse object.

Once you have selected your acquisition object, you need to measure its coordinates (when possible, i.e. not for moving targets) in the Guide Star reference frame; information on measuring coordinates can be found on the following web page:

<http://www-gsss.stsci.edu/support/phase2.html>

You will need to include the PLATE-ID along with your coordinates so that we can be certain to select the guide stars for your observation from the same plate on which your measurement was based. If you are deriving coordinates from WFPC2 data (i.e., from the **metric** task) or other HST data (i.e., from the **xy2rd** task), you still need to provide a PLATE-ID; see Section 8.4 for instructions on determining the PLATE-ID from HST data.



Note that the initial acquisition subarray is 5" on a side; your target coordinates must be supplied accurately in the GSSS frame during Phase II to assure your target will be in the initial ACQ image, given that the initial guide star pointing accuracy is ~1–2".

Selecting the Acquisition Type

If you are acquiring a point-like object, you should select the point source acquisition (ACQTYPE=POINT). This selection will find the flux-weighted centroid of the object using a 3 x 3 checkbox. If you are acquiring a diffuse object, you should select the diffuse source acquisition (ACQTYPE=DIFFUSE). A diffuse acquisition will also require selecting the target acquisition centering algorithm (DIFFUSE-CENTER=FLUX-CENTROID or GEOMETRIC-CENTER) and a checkbox size (CHECKBOX=3–105). Note that selecting a DIFFUSE acquisition with CHECKBOX=3 and DIFFUSE-CENTER=FLUX-CENTROID is equivalent to selecting the POINT source algorithm. A [Target Acquisition Simulator](#) is available to assist you in selecting the best checkbox size if you have an image at a similar resolution to that of STIS and in a similar bandpass.

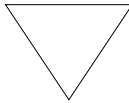
Selecting the Imaging Aperture

The apertures available for target acquisitions are the same set that can be used for CCD imaging and are listed in Table 8.2 below. They include the visible longpass filter, the clear unfiltered aperture, the [O III] narrowband filter, the [O II] narrowband filter, and the neutral-density filters which provide attenuations for bright sources of 10^{-3} and 10^{-5} . F28X50LP is the preferred target acquisition aperture. The longpass filter is preferred (compared to the clear 50CCD aperture) because it blocks the ultraviolet photons, which can otherwise elevate the detector dark count in the subsequent scientific exposures (see Section 7.2.8). For bright sources

which saturate the CCD in 0.1 second with the longpass filter (see Table 8.3), you can use either the narrowband [O III] (F28X50OIII) or [O II] (F28X50OII) filters as the acquisition aperture, or one of the neutral density filters. The [O II] and [O III] filters can also be used to locate the target in the light of an emission line. Note that the [O III] filter has a large red leak at $\lambda > 10,000 \text{ \AA}$ (see Chapter 14), so it should be used with caution; the [O II] filter has no measurable red leak.

Table 8.2: Apertures for Target Acquisitions

Aperture Name	Filter Type	Comment
F28X50LP	Optical longpass	Preferred target acquisition aperture
F28X50OII	[O II]	Use for bright sources or to center on emission-line structure
F28X50OIII	[O III] (has severe red leak)	Use for bright sources or to center on emission-line structure
F25ND3	Neutral density, ND= 10^{-3}	Use only for targets too bright for other filters
F25ND5	Neutral density, ND= 10^{-5}	Use only for targets too bright for other filters
50CCD	Clear	Use for acquisitions of faintest sources only



We recommend the longpass F28X50LP filter for all target acquisitions of sources with V magnitudes between 10 and 23.

Determining Exposure Time for the ACQ Exposure

To achieve robust target location:

- A *minimum* signal-to-noise ratio of at least 40 (over the checkbox) or 1700 electrons (425 DN) must be obtained on each target image obtained during the ACQ exposure. Higher signal-to-noise ratios should be considered if practical (see below).
- For DIFFUSE acquisitions with large checkbox sizes (i.e., CHECKBOX > 9), a contrast relative to surrounding regions of *at least* 40 electrons pixel^{-1} (or equivalently 10 DN pixel^{-1}) must be obtained for the region of the source being “found”.
- The target image cannot be allowed to saturate the CCD full well (144,000 electrons).

- The exposure time must be less than 5 minutes for point source acquisitions and less than the maximum allowed (see below) for diffuse acquisitions.
- A CCDGAIN of 4 is used for all acquisition images.

It should be considered that the count rates recommended above are the *minimum* count rates needed for the acquisition to have a high chance of success. However, obtaining ACQ images with significantly higher signal-to-noise ratios than these minima do provide an additional degree of protection against failures caused by a poor estimate of the source count rate or by a bad initial pointing that puts the target just outside the acquisition subarray (in the latter case, the diffraction spikes or the wings of the PSF may well be detected in the initial image and moved to the detector center, allowing the ACQ to succeed during the fine-locate phase). Such deeper exposures are therefore recommended if the additional overheads are small compared to the overhead time for ACQ exposures (typically 6 minutes), and if there is no chance of saturating the CCD. For a point source, the full well limit of 144,000 electrons in the central pixel corresponds to an ETC S/N estimate of about 400:1.

The maximum possible exposure time for a point source acquisition (ACQTYPE=POINT) exposure is 5 minutes; this limit restricts acquisitions to sources brighter than 24.5 mag in *V*. This limit is imposed because, for longer exposure times, the target acquisitions become compromised by coincident cosmic-ray impacts, which will lead to acquisition failures. The maximum possible exposure time for a diffuse acquisition (ACQTYPE=DIFFUSE) depends on the checkbox and is given by:

$$t_{max} = 5 \times 100 / (101 + CHECKBOX) \quad \text{minutes}$$

The minimum exposure time allowed for an acquisition is 0.1 second. Table 8.3 gives the limiting magnitudes at which the CCD will saturate in a 0.1 second exposure; sources brighter than these limits cannot be acquired with the CCD using these filters. Remember that the ND filters can also be used to acquire targets; these filters provide attenuations of 10^{-3} (7.5 magnitudes) and 10^{-5} (12.5 magnitudes) relative to the clear (50CCD) filter. Note that the ND filters are contained in the slit wheel with other slits and apertures, and so cannot be used in conjunction with other filters. The table illustrates that it is possible to image any star using a filter from the suite, including the neutral-density filters, available for STIS.

Table 8.3: V Magnitude Limits for saturation of a 0.1 Second CCD Exposure Time as a Function of Aperture

Spectral Type	Limiting Magnitude				
	50CCD	F28X50LP	F28X50OII	F28X50OIII	F25ND3/5
O5 V	10.3	8.4	4.8	2.7	3.3/-1.8
B1 V	10.2	8.4	4.6	2.7	3.2/-2.0
B5 V	10.0	8.5	4.2	2.7	3.1/-2.3
B8 V	9.9	8.5	3.8	2.7	3.1/-2.4
A1 V	9.8	8.6	3.3	2.7	3.0/-2.4
A3 V	9.8	8.6	3.2	2.7	3.0/-2.4
A5 V	9.8	8.7	3.2	2.6	3.0/-2.4
F0 V	9.8	8.8	3.2	2.6	3.1/-2.3
F5 V	9.8	9.0	3.1	2.6	3.2/-2.2
G2 V	9.9	9.1	2.8	2.6	3.2/-2.1
G5 V	9.9	9.1	2.7	2.6	3.2/-2.1
K0 V	9.9	9.2	2.2	2.6	3.3/-2.0
K4 V	10.0	9.4	1.4	2.6	3.5/-1.8
K7 V	10.2	9.7	0.9	2.8	3.7/-1.6
M2 V	10.4	10.0	0.7	3.3	4.0/-1.2
M6 V	10.4	10.0	0.6	3.3	4.0/-1.2
Power Law	10.4	9.8	2.9	3.4	3.4/-1.9

Figure 8.7 and Figure 8.8 can help you estimate exposure times—they plot exposure time versus V magnitude to achieve a signal-to-noise ratio of 40 for stars having a range of spectral types, for the clear, longpass, [O III], and [O II] filters. To determine the exact exposure time for your target, you should use the [STIS Target Acquisition Exposure Time Calculator](#) (see Section 8.5). Note that the overheads in target acquisitions are substantially longer than most exposure times, so as long as you do not approach saturation (i.e., come within 30% of the full well) you should increase your exposure time by a factor of at least a few above the minimum required (e.g., if the exposure time to obtain a S/N of 40 is 0.3 second, then you should lengthen it to 1 second if no saturation occurs). Also consider whether a shorter exposure in a higher throughput filter might give better S/N (see Table 8.3 for the brightest magnitude as a function of filter and target spectral type which can be observed without saturating the acquisition exposure). The exposure time entered into your Phase II

template is the time for each of the two exposures in the ACQ sequence, unlike the case of CR-SPLIT observations where it is the total time.

Figure 8.7: Time to Achieve a Signal-to-Noise ratio of 40 for CCD Acquisitions

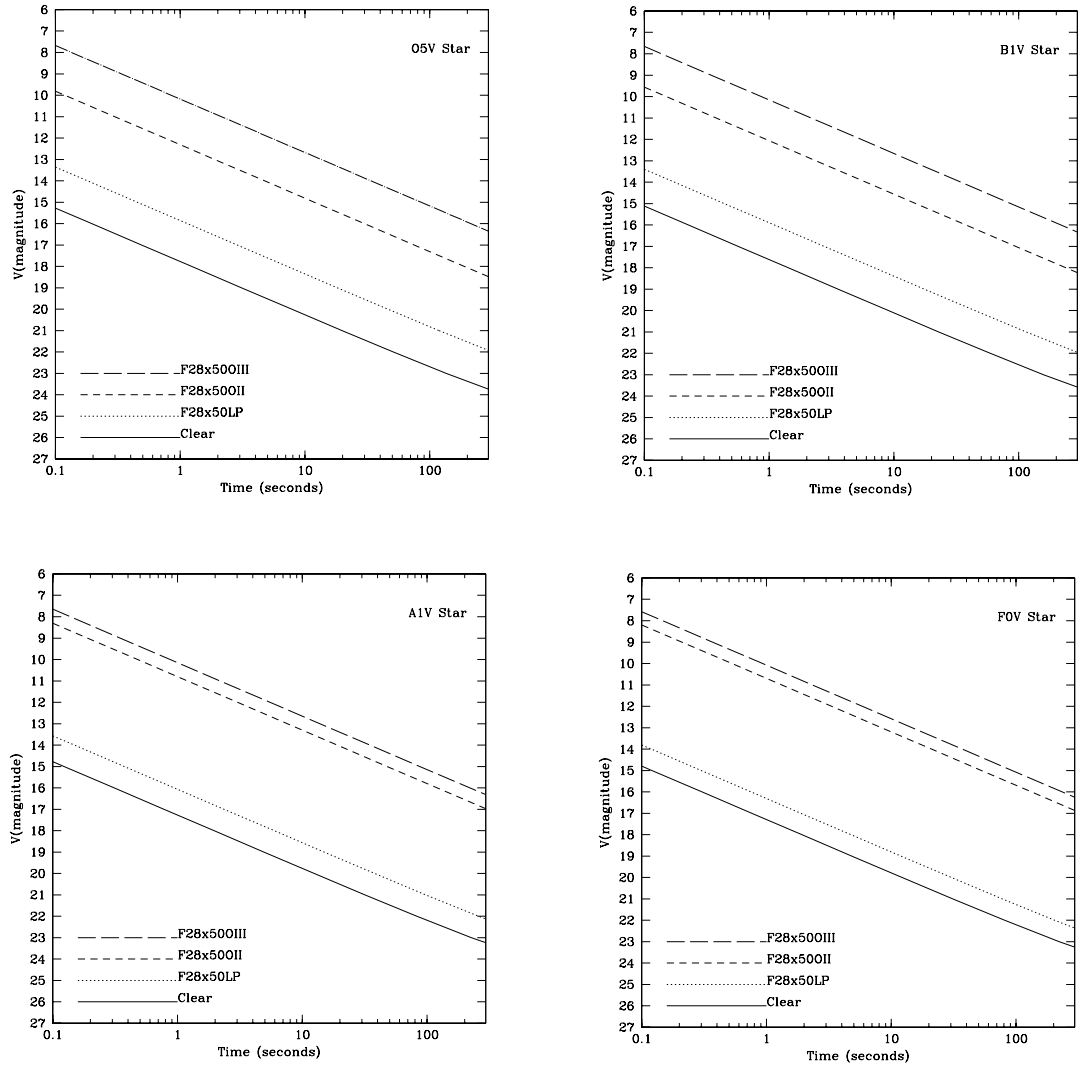
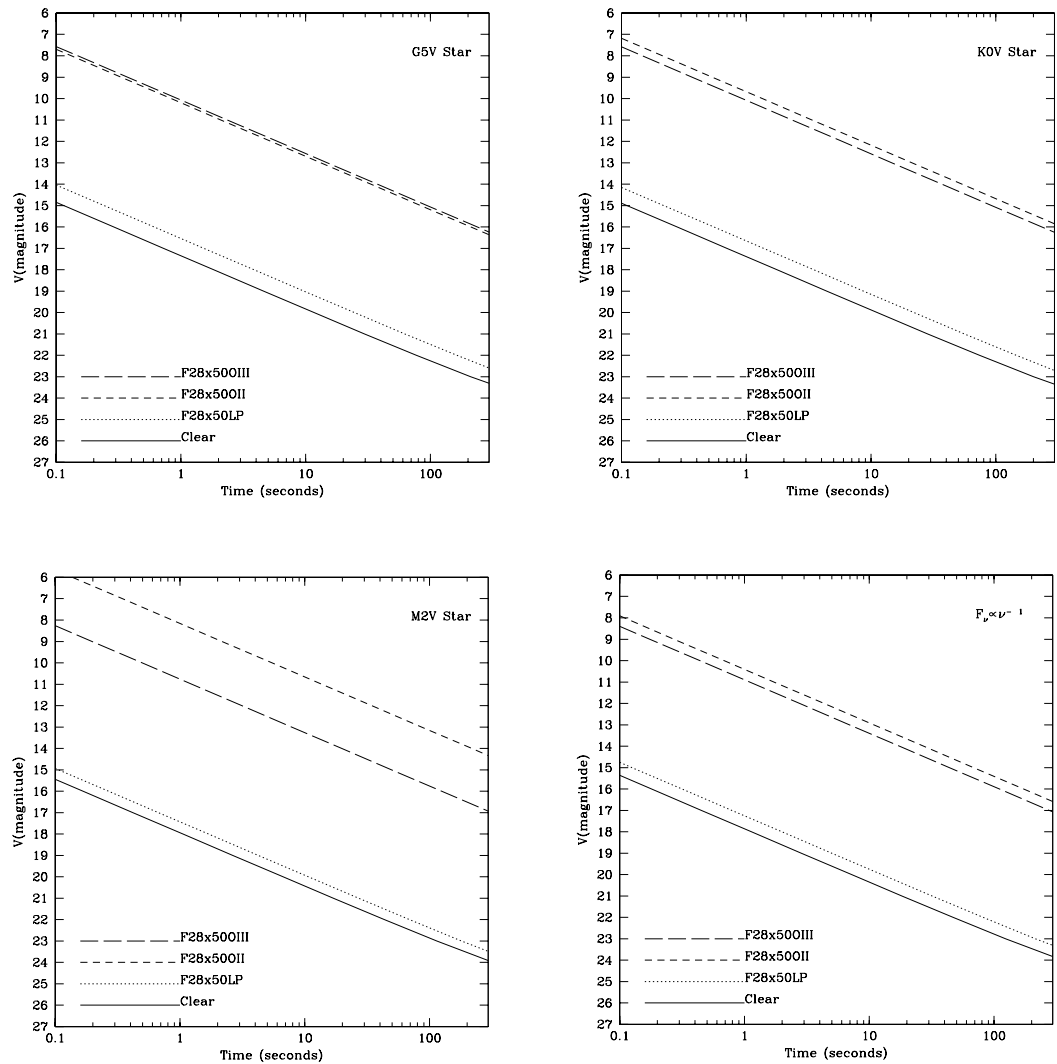


Figure 8.8: Time to Achieve a Signal-to-Noise ratio of 40 for CCD Acquisitions



8.2.4 Specifying Acquisitions in Phase II

Acquisition exposures must be specified during Phase II before the scientific exposures for which they are intended. The user requests a target acquisition exposure by specifying `MODE=ACQ` on the APT Phase II exposure parameters page and setting the optional parameter `ACQTYPE=POINT` or `ACQTYPE=DIFFUSE`. If `ACQTYPE=DIFFUSE` is selected, the observer must also specify `DIFFUSE-CENTER` and `CHECKBOX`.

Exposure-Time Calculator and Phase II examples are provided in Section 8.5.

8.2.5 Solar-System Acquisitions

The ACQ procedure can be used for solar system targets as well as fixed targets. The difference is in the specification of the target position, which is outlined in chapter 4 of the HST Phase II Proposal Instructions. For satellites less than 0.1 arcsec in diameter, a point source ACQ is sufficient. For satellites of greater diameter, ACQTYPE=DIFFUSE with DIFFUSE-CENTER=GEOMETRIC and a CHECKBOX size chosen to match the satellite diameter are recommended. To acquire a planetary feature or a satellite transiting the planet, another satellite in the system can generally be used as an offset target. If precise pointing to a specific feature is not required, then blind pointing (which is generally accurate to ~1-2") can be used for larger targets such as Mars, Jupiter, and Saturn. The types of acquisitions recommended for the most common solar system targets is summarized in Table 8.4.

The coordinates of the planets and their satellites are derived from ephemerides obtained by STScI from JPL. The accuracies of the ephemerides are maintained by JPL at the following web site:

http://ssd.jpl.nasa.gov/sat_eph.html.

Contact help@stsci.edu to find out which sets of ephemerides are currently being used. Your Program Coordinator can provide information on tracking for a specific visit.

Special care must be taken when tracking satellites with rapidly changing direction or velocity. Observers should be aware that moving targets are tracked by HST with the assumption that the object is moving on a linear track with constant velocity. Depending on the visit structure, the same linear track may continue through several exposures. The scheduling software sets a generally appropriate limit on the duration of a linear track which depends on the target being tracked, but not on details of the target motion at the time. In some situations (for example, near the inflection point of an orbit), the approximation could result in inadequate tracking when using a narrow slit. If this may be a problem, the observer can consult the Program Coordinator of his/her proposal to find out how long the same track will be used for a series of exposures, and whether it is possible to break the visit into shorter tracks. Alternatively, one can plan to observe during a more linear part of the orbit.

Acquisition exposure times can be accurately estimated using the **STIS Target Acquisition ETC**: use the Kurucz model G2 V (solar spectrum), and normalize it using the V magnitude for point-like (≤ 0.1 arcsec) objects or the V magnitude per arcsec² and the appropriate target size in arcseconds for more extended targets.

For convenience, we summarize the types of acquisitions recommended for the most common solar-system targets in Table 8.4 below. If precise pointing to a specific feature is not required, then blind pointing (which is

accurate to $\sim 1\text{--}2''$) can be used for the larger targets such as Mars, Jupiter, and Saturn.

Table 8.4: Solar-System Acquisitions

Target	Type of Acquisition	Offset Target
Venus	Offset target	Star
Mars	Offset target	Deimos
Jupiter	Offset target	Galilean satellite
Saturn	Offset target	Satellite
Uranus	Diffuse source	
Neptune	Diffuse source	
Satellite or asteroid $< \sim 0.1$ arcsec	Point source	
Satellite or asteroid $> \sim 0.1$ arcsec	Diffuse source	
Transiting satellite	Offset target	Another satellite
Comet	Diffuse source	

8.3 Onboard Target Acquisition Peakups (ACQ/PEAK)

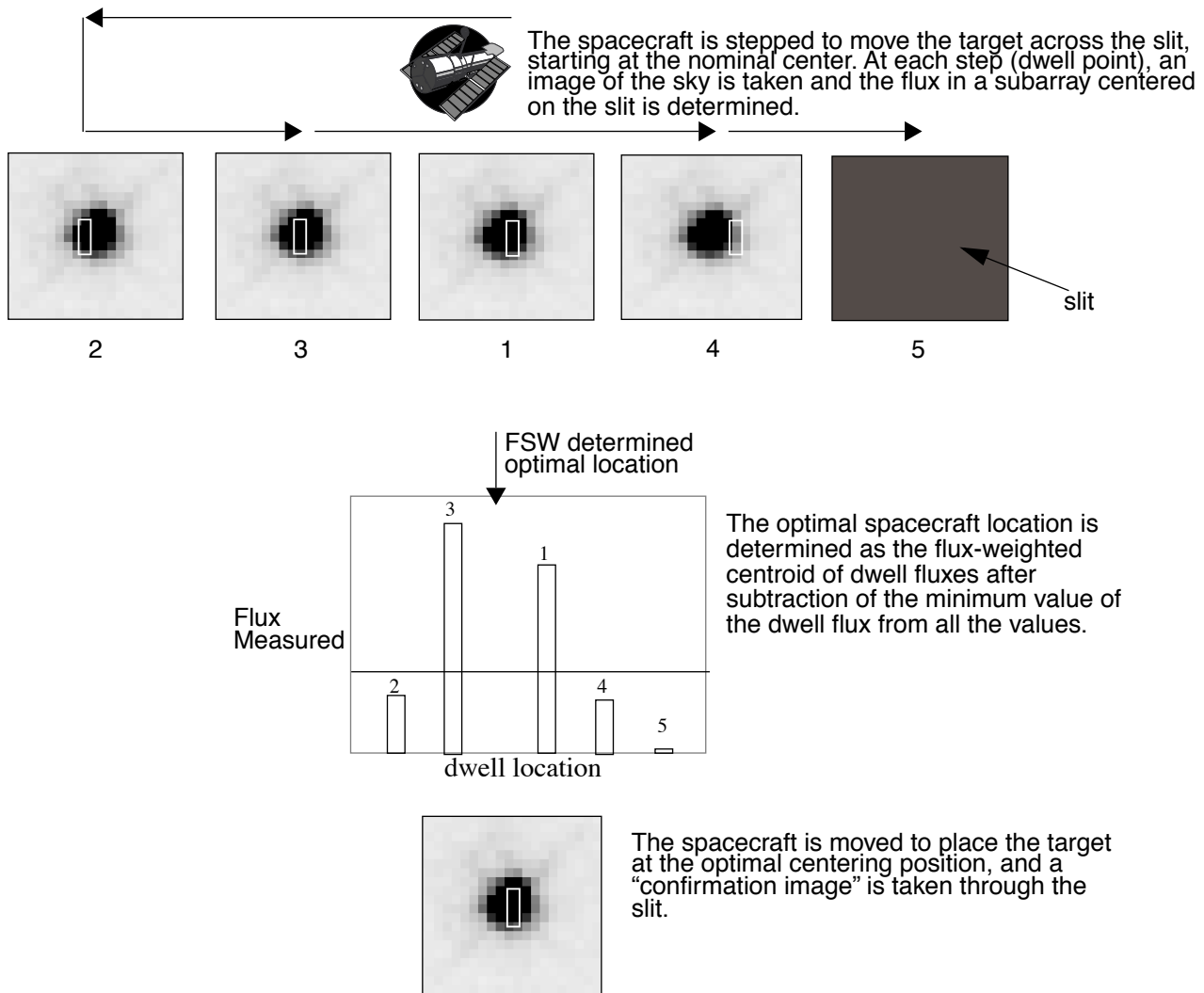
When slits less than or equal to 0.1 arcsecond wide or the narrow coronagraphic bars are used, an acquisition-peakup exposure should be performed following the acquisition exposure to center the target in the slit or coronagraphic bar. You should also consider performing a peakup if you have acquired an offset star, rather than your target, to compensate for any additional uncertainties in your knowledge of the offsets. We recommend that for a long series of exposures taken through slits which are less than or equal to 0.1 arcsecond in either dimension, a peakup be performed at least every 4–5 orbits. This will ensure that drifts (see Section 8.1.4) do not cause the target to move out of the slit. Programs with more stringent requirements on position or wavelength stability will need more frequent peakups.

Figure 8.9 illustrates the basic peakup sequence. When a peakup exposure is performed, the telescope is moved to step the target across the slit or bar. At each step (or dwell point), an image² of the sky is taken and the total flux in a specified subarray is determined. To allow for a more

2. For CCD ACQ/PEAKs the same type of processing is applied as in acquisitions by the FSW to remove the bias and cosmic rays, with the only difference being that there is no offset performed between the two images taken at each pointing, for obvious reasons.

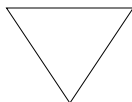
accurate calculation, the minimum flux value in the peakup (the PEDESTAL) is subtracted from each step. The flight software (FSW) then selects the position of maximum flux, using a flux-weighted centroiding technique to determine the optimum position to a fraction of a dwell step. At the conclusion of the ACQ/PEAK exposure, the FSW moves the telescope to position the target at the derived optimal position within the aperture. A “confirmation image” is then taken through the aperture on the subarray and is included in the ACQ/PEAK data set.

Figure 8.9: Schematic of Peakup Sequence



Peakup exposures can be taken with either a mirror (to peak up in undispersed white light) or a grating (to peak up in dispersed light), and with the CCD detector only. Subarrays can be specified to limit the region of the detector (sky) over which the flux is determined at each dwell point.

The default subarray sizes, 32 by 32 for white-light (mirror) peakups and 32 (perpendicular to the dispersion) by 1022 (in the dispersion direction) for dispersed-light peakups, are appropriate for peakups on point sources. They should be changed only if you are performing diffuse-source peakups or if you wish to isolate a single line in dispersed-light peakups, and only upon consultation with an Instrument Scientist.



We recommend performing all CCD peakups using the mirror unless your target is too bright.

You do not specify the parameters of the stepping sequence employed during the peakup; it is predetermined, based on the aperture you have chosen. Table 8.5 below shows the scan sequence employed for all of the long and echelle slits. The scan sequence for a peakup may include a linear scan in the dispersion direction (SEARCH=LINEARAXIS1), a linear scan perpendicular to the dispersion axis (SEARCH=LINEARAXIS2), or a spiral search pattern (SEARCH=SPIRAL). Additional parameters are the number of steps (NUMSTEPS) and the step intervals between each dwell point (STEP SIZE). Note that all ACQ/PEAKs are single-stage peakups, except for the smallest slit (0.1X0.03), which requires a 2-stage peakup.

Table 8.5: Peakup Scan Sequences and Parameters for Supported Spectroscopic Slits

Slit (APERTURE)	AXIS2 spatial (arcsec)	AXIS1 dispersion (arcsec)	AXIS2 stepsize (arcsec)	AXIS1 stepsize (arcsec)	Scan Type	NSTEPS AXIS2	NSTEPS AXIS1	Total NSTEPS	CCD Duration (seconds)
Long Slits									
52X0.05, 52X0.05E1, 52X0.05D1	52	0.05		0.036	LINEARAXIS1		7	7	$300+16*t_{exp}$
52X0.1, 52X0.1E1, 52X0.1D1	52	0.1		0.075	LINEARAXIS1		5	5	$220+12*t_{exp}$
52X0.2F1-R	52	0.2		0.150	LINEARAXIS1		3	3	$150+8*t_{exp}$
Echelle Slits for E230M and E140M									
0.2X0.06	0.2	0.063	0.150	0.048	1) LINEARAXIS1 2) LINEARAXIS2	3	5	8	$360+24*t_{exp}$
Echelle Slits for E230H and E140H									
0.2X0.09	0.2	0.09	0.150	0.069	1) LINEARAXIS2 2) LINEARAXIS1	3	5	8	$360+20*t_{exp}$
Specialty Slits									
0.2X0.05ND	0.2	0.05	0.150	0.039	1) LINEARAXIS1 2) LINEARAXIS2	3	7	10	$460+24*t_{exp}$
0.3X0.05ND	0.3	0.05	0.250	0.039	1) LINEARAXIS1 2) LINEARAXIS2	3	7	10	$450+24*t_{exp}$
0.2X0.06FP (A-E)	0.2	0.06	0.150	0.048	1) LINEARAXIS1 2) LINEARAXIS2	3	7	10	$360+24*t_{exp}$
0.1X0.03	0.2	0.09	0.150	0.069	1) LINEARAXIS2 2) LINEARAXIS1	3	5	8	$720+40*t_{exp}$
(peakup in 0.2x0.09 ¹ followed by spiral in 0.1X0.03)	0.1	0.025	0.018	0.018	3) SPIRAL	3	3	9	

1. The 0.2X0.05ND or the 0.3X0.05ND slits can be used in place of the 0.2X0.09 slit.

8.3.1 Selecting Peakup Parameters

To plan your acquisition peakup, you must specify:

- The optical element.
- The APERTURE (program slit) upon which to peak up.
- The exposure time for the peakup image.

Selecting the Optical Element

Peakups can be performed by using the STIS CCD either with a dispersive element in a spectroscopic configuration with any of the allowed grating combinations, or in undispersed white light in an imaging configuration. Most peakup exposures should be performed in imaging mode (white light).

If your target is otherwise too bright to perform a peakup with the CCD camera mirror in place, you can use the echelle slits 0.2X0.05ND (which has an ND filter with a factor of 100 attenuation) or the 0.3X0.05ND (with attenuation by a factor of 1000), or use a dispersed-light peakup. Also note that if you wish to peak up in a particular line for which there is no imaging filter, a dispersed light peakup using a grating should be used. Observers should generally perform dispersed light peakups with the same gratings and apertures they intend to use for their scientific observations.

If extremely high target acquisition centering accuracy is required, observers should consider peaking up in a smaller slit than the program slit; the slit-to-slit positioning accuracy is 0.005 arcsecond.

Selecting the Aperture

A peakup can be done using any of the long or echelle slits in Table 8.5 as the APERTURE. You will (typically) want to specify the peakup aperture as the aperture used for the subsequent scientific observations, although it is possible to specify a smaller aperture than your program aperture if you require higher target acquisition centering accuracy. Instances in which you may wish to utilize a smaller aperture for the acquisition are coronagraphic observations, observations requiring accurate photometry (where the source should be properly centered in a wide slit), and bright-source acquisitions. Note that peakups using the NX0.2 apertures (those with widths of 0.2 arcseconds in the dispersion direction) are no longer recommended as they provide no refinement in pointing over that routinely achieved in a normal ACQ. If an ACQ/PEAK is needed for an NX0.2 science exposure (e.g., after an ACQ on an offset target or to re-center after a few orbits), better positioning accuracy can be achieved with a narrower aperture, such as NX0.1.

For acquisitions under the narrow occulting fiducial (52X0.2F1), a peakup acquisition using a small slit should be used. The bar and wedge positions on the 50CORON aperture (imaging) are all large enough that a peakup is not required. However, if you require accurate target acquisition

centering (for example, to place a calibration star at the same position under the bar or wedge to measure the scattered-light profile), then a peakup is required. Note that a peakdown acquisition is no longer recommended (see Section 12.9).

Determining the Peakup Exposure Time

The *minimum* required exposure time for CCD imaging (mirror) peakups is the time to obtain a minimum of 5000 electrons (1250 DN) from a point source, or equivalently, 5000 electrons from the peak of a diffuse source which is contained in a 4 x 4 pixel region. For CCD dispersive (grating) peakups, the *minimum* exposure time is the time to obtain a minimum of 80,000 electrons (20,000 DN) integrated across the spectrum from a point source, or equivalently, 80,000 electrons from the peak of a diffuse source integrated over 4 pixels perpendicular to the dispersion axis. For CCD dispersive peakups on a single emission line, the exposure time is the time to obtain a minimum of 5000 electrons in the chosen line; a small subarray is selected to isolate the line.

To determine the exact exposure time, you should use the [STIS Target Acquisition ETC](#) (for acquisitions and imaging peakups) or the [Spectroscopic ETC](#) (for dispersive peakups). Be sure to include the effect of your chosen slit throughput (see Chapter 13) in your calculation (e.g., for imaging peakups, if the ETC does not account for slit loss). For acquisitions and peakups *you must be sure not to saturate* the CCD during your exposure. Table 8.3 lists, for a range of spectral types, the brightest magnitude at which a CCD peakup exposure can be performed in white light, assuming zero slit losses. Note that the overheads in target acquisition are substantially longer than most exposure times, so as long as you do not approach saturation (within 30% of the full well) your target, you should increase your exposure time by a factor of 2–5 above the minimum required (e.g., if the exposure time to obtain the requisite number of electrons is 0.3 second, then you can lengthen it to 1 second if no saturation occurs). This is specially important for peakups, where low signal-to-noise is the leading cause of poor centering.

There is a limit on the maximum exposure time allowed for CCD peakups, which is imposed to ensure that multiple coincident cosmic rays do not affect the target acquisition centering accuracy. Table 8.6 lists the maximum CCD exposure time for point source white-light and dispersed-light peakups for each aperture.³

3. More generally, the maximum allowed exposure time for CCD ACQ/PEAKs is:

$$t_{max} = 17 \times 1 / \sqrt{\text{numsteps} \times \text{SIZEAXIS1} \times \text{SIZEAXIS2} / (32 \times 32)} \text{ minutes.}$$

Table 8.6: Maximum Allowed Exposure Times for CCD Peakups

Slit (APERTURE)	Imaging Maximum Exposure Time for Dwell (minutes)	Spectroscopic Maximum Exposure time for Dwell (minutes)
52X0.1, 52X0.1E1, 52X0.1D1	7.6	1.3
52X0.2F1-R	9.8	1.7
0.2X0.06	7.6	1.3
0.2X0.09	7.6	1.3
0.2X0.05ND	6.4	1.1
0.3X0.05ND	6.4	1.1

8.3.2 Specifying Acquisition Peakups in Phase II

The user requests a peakup acquisition exposure during Phase II by specifying `MODE=ACQ/PEAK` on the APT Phase II exposure parameters page. The default settings for the scan (`SEARCH`, `NUMSTEPS`, `STEPSIZE`) for your chosen `APERTURE` are then automatically selected from the lookup table.

8.4 Determining the PLATE-ID of HST Observations

All HST data have at least one guide-star ID in the Standard Header Packet (SHP). Data from the SHP will be recorded in the `shh` (WFPC2) or the `spt` (STIS) file that accompanies all HST observations. The guide stars that were used in any pointing will be recorded in the SHP as character strings associated with specific keywords in the header.

The *primary* or *dominant* guide star is associated with the keyword `DGESTAR` and the *secondary* or *subdominant* guide star is associated with the keyword `SGESTAR`. The guide-star ID is a concatenation of the region number from the Guide Star Catalogue, the star number, and the FGS used in the pointing, e.g., “0123406789F2”, as a quoted character string. The actual guide star in this example is 01234 06789 and FGS2 was used.

To find the PLATE-ID that was used for the coordinates, use the WWW Guide Star Catalogue interface:

http://www-gsss.stsci.edu/support/rgscid_form.html

The form will prompt you for the guide-star ID (in two fields)—you should use the primary guide star only. This web page will provide the coordinates, estimated magnitude, associated errors, flags internal to the

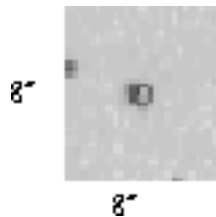
catalogue's structure, and the PLATE-ID. Note that for most guide stars there will be multiple entries (corresponding to multiple PLATE-IDs), as the plates taken for the Guide Star Catalogue overlap. The first line from your output will be for the primary plate—the preferred plate for the guide star in question, and, if two guide stars were used, the PLATE-ID you should specify in your Phase II program. If the observation used a single guide star, it is possible that a secondary plate was used. Please consult the help desk (help@stsci.edu) or an Instrument Scientist if this is the case.

8.5 Acquisition Examples

The following are examples of how to determine the acquisition scenario, and how to derive the correct exposure times. Each example shows an image of the target, the input parameters for the Exposure Time Calculators, and the parameters that you will need to provide in your Phase II proposal. *Note that the APT preview format used throughout this section may not be the one in use at the time you are crafting your proposal.*

8.5.1 Point source Acquisition of an Isolated Object

In this first example an isolated $V = 19$ mag QSO ($z = 1.5$) is to be acquired, with the scientific exposures to be obtained in the 52X0.5 slit.



The target is isolated, so it will be acquired with a point source acquisition. The object is faint, so we can use the preferred F28X50LP filter. The TA ETC is then used to determine an exposure time of 11.4 seconds. Note that the GAIN=4 and CR-SPLIT=1 *must be used* for the ETC to ensure that you have a S/N of at least 40 in each of the two images obtained during the ACQ process. The object does not saturate the CCD, and the exposure time is less than 5 minutes, so we have devised a valid target acquisition. Given that the exposure time is so short, we can lengthen the time to 15.0 seconds (which yields a peak value of 1600 electrons, well below saturation) to make certain we have enough signal for a good acquisition. Since the data are being obtained in a wide slit, we do not need to perform an ACQ/PEAKUP, and our acquisition is complete.

Target Acquisition ETC Parameters - ACQ

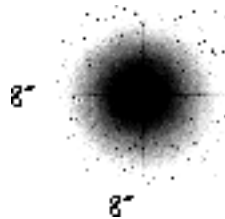
- Detector = ccd
- Filter = LongPass
- Gain = 4 e⁻/ADU
- Check Box = 3x3
- Target was a point source
- Spectrum: QSO with z = 1.5
- Source Flux: v = 19
- Average Galactic Extinction of E(B-V) = 0.0
- The Zodiacal Light is average
- The Earthshine is average

Phase II Parameters for ACQ Exposure

Exp	Label	Target Name	Config	OpMode	Aperture	SpElement	Wavlen	Iter	Exp Time (secs)
1		QSO	STIS/CCD	ACQ	F28X50LP	MIRROR		1	15.0
Special Requirements: Comments: Optional Parameters: ACQTYPE=POINT,									
		Sub-exposures:	Copy	Split	Orbit Num	Actual Time			

8.5.2 Point Source Acquisition of Bright, Isolated Object with CCD Dispersed Light Peakup

In this example—point source acquisition of a bright, isolated object with a CCD dispersed light peakup—an isolated V = 3.5 mag M2 I star is to be acquired, with the scientific exposures to be obtained in the 0.2X0.06 echelle slit.



The scientific target will be acquired with a point source acquisition, but because the object is so bright, we cannot use the preferred F28X50LP filter. Instead, we will use the F28X50OII filter, and the [Target Acquisition ETC](#) yields an exposure time of 0.06 second, which is less than the minimum allowed time of 0.1 second. Note that the GAIN=4 and CR-SPLIT=1 *must be used* for the ETC to assure that you have a S/N of at least 40 in each of the two images obtained during the ACQ process. We

will therefore increase the exposure time to 1.0 second. The object does not saturate the CCD, and the exposure time is less than 5 minutes, so we have devised a valid target acquisition.

The data are being obtained in a narrow slit, so we need to perform an ACQ/PEAK acquisition. The target is far too bright to perform the peakup with the MIRROR, so we will do a dispersed light peakup. Since we cannot perform a CCD peakup with an echelle grating, we will use the G430M grating with the CCD and the program slit (0.2X0.06); note that for an ACQ/PEAK, this combination is legal. The best approximation of this slit available in the Spectroscopic ETC is 52X0.05 (the correction to a shorter slit). For a 1 second exposure with 1x1 binning, the ETC gives a peak count of 1880 electrons (well below saturation) and a total count of 2.5×10^6 electrons (30 times the recommended minimum).

Target Acquisition ETC Parameters - ACQ

- Detector = ccd
- Filter = OII
- Gain = 4 e⁻/ADU
- Check Box = 3x3
- Target was a point source
- Spectrum: M2I (Model Spectrum)
- Source Flux: $v = 3.5$
- Average Galactic Extinction of $E(B-V) = 0.0$
- The Zodiacal Light is average
- The Earthshine is average

Spectroscopic ETC Parameters - ACQ/PEAK

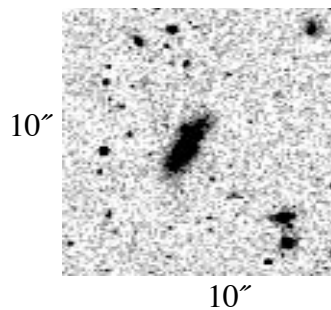
- Grating = g430m
- Grating Setting = c4194
- Slit = 52x0.05
- Specified Wavelength = 4194.1 Å
- Gain = 4 e⁻/ADU
- CR-split (Total number of images) = 1
- Target was a point source
- Spectrum: M2I (Model Spectrum)
- Source Flux: $v = 3.5$
- Average Galactic Extinction of $E(B-V) = 0.0$
- The Zodiacal Light is average
- The Earthshine is average

Phase II parameters for ACQ and ACQ/PEAK exposures

Exp	Label	Target Name	Config	OpMode	Aperture	SpElement	Wavlen	Iter	Exp Time (secs)
1		BRIGHT-STAR	STIS/CCD	ACQ	F28X50OII	MIRROR		1	1.0
Special Requirements: Comments: Optional Parameters: ACQTYPE=POINT,									
Sub-exposures:		Copy	Split	Orbit Num	Actual Time				
2		BRIGHT-STAR	STIS/CCD	ACQ/PEAK	0.2X0.06	G430M	4194	1	1.0
Special Requirements: Comments: Optional Parameters:									
Sub-exposures:		Copy	Split	Orbit Num	Actual Time				

8.5.3 Diffuse-Source Acquisition of a Spiral Galaxy

In this example an isolated galaxy with a flux of 1.5×10^{-14} erg cm⁻² s⁻¹ Å⁻¹ arcsec⁻² at 8000 Å is to be acquired, with the scientific exposures to be obtained in the 52X0.2 slit.



The target is isolated, so it will be acquired using a diffuse-source acquisition. After trying various checkbox sizes in the **TAS** (the image is from WFPC2), we determine that the appropriate **CHECKBOX** size is 9, and that we will use the **FLUX-CENTROID** algorithm. The object is faint, so we can use the preferred **F28X50LP** filter. The **TA ETC** is then used to determine an exposure time of 0.21 second. Note that the **GAIN=4** and **CR-SPLIT=1** *must be used* for the ETC to ensure that you have a S/N of at least 40 in each of the two images obtained during the ACQ process. The object does not saturate the CCD, and the exposure time is less than 5 minutes, so we have devised a valid target acquisition. Given that the exposure time is so short, we can lengthen it to 2.0 seconds to make certain we have enough signal for a good acquisition. Since the data are being obtained in a wide slit, we do not need to perform an ACQ/PEAKUP, and our acquisition is complete.

Target Acquisition ETC Parameters - ACQ

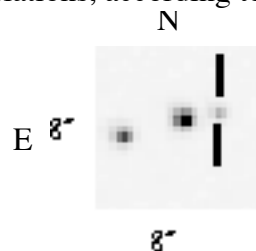
- Detector = ccd
- Filter = LongPass
- Gain = $4 \text{ e}^-/\text{ADU}$
- Check Box = 9x9
- Target was an extended source with a diameter of 3 arcseconds.
- Spectrum: Spiral Spectrum
- Source Flux: $1.5\text{e-}14 \text{ erg cm}^{-2} \text{ s}^{-1} \text{ \AA}^{-1}$ at 8000 \AA
- Average Galactic Extinction of $E(B-V) = 0.0$
- The Zodiacal Light is average
- The Earthshine is average

Phase II parameters for ACQ exposure

Exp	Label	Target Name	Config	OpMode	Aperture	SpElement	Wavlen	Iter	Exp Time (secs)
1		GALAXY	STIS/CCD	ACQ	F28X50LP	MIRROR		1	2.0
Special Requirements: Comments: Optional Parameters: ACQTYPE=DIFFUSE, DIFFUSE-CENTER=FLUX-CENTROID, CHECKBOX=9,									
Sub-exposures:		Copy	Split	Orbit Num	Actual Time				

8.5.4 Point Source Acquisition in a Crowded Field

In this example a $V = 19$ mag nova in a field with a brighter companion is to be acquired, with the scientific exposures to be obtained in the 52×0.1 slit. We have a spectrum of the nova that we will use to perform the exposure time calculations, according to the ETC instructions.



The target is in a crowded field and the on-board acquisition procedure will acquire the brightest object in the field, not our target. If a ground-based image were the only image of this field available and the spectral types of the neighboring stars were unknown, then an isolated offset star outside of the immediate field of the nova would need to be acquired. However, the above image was obtained with WFPC2 and the F555W filter, which has a similar bandpass to the STIS F28X50LP filter.

We therefore know that the object to the southeast of the nova is clearly the brightest object in the field ($V = 16.5$), and it will be our acquisition object. The object is faint enough that we can use the preferred F28X50LP filter. Since we do not know the spectral type of the acquisition star, we will make a worst-case (i.e., fewest counts) assumption that the star is of spectral type O5 and unreddened. The [Target Acquisition ETC](#) is then used to determine an exposure time of 2.0 seconds. Note that the `GAIN=4` and `CR-SPLIT=1` *must be used* for the ETC to ensure that you have a S/N of at least 40 in each of the two images obtained during the ACQ process. The object does not saturate the CCD, and the exposure time is less than 5 minutes, so we have devised a valid target acquisition. Note that since we do not know the spectral type of the object, we need to confirm that if the star had a spectral type of M6 V (which gives the most counts in the F28X50LP bandpass), it would still not saturate. Given that the exposure time is so short, we can lengthen it to 3.0 seconds to make certain we have enough signal for a good acquisition.

After acquiring the offset star, we need to slew the telescope to the nova, and since the data will be taken with a narrow slit, we need to perform an ACQ/PEAK acquisition. The peakup will be performed in the program slit (52X0.1), and we will use the CCD and the MIRROR. A 1 second exposure with 1x1 binning yields 655 electrons in the central 25 pixels of the target, so an exposure time of 8 seconds yields 5240 electrons, which meets the minimum requirement of 5000 electrons. We need to lengthen the exposure time by a factor of 1.5 to account for the slit throughput (see Chapter 13), for a time of 12.0 seconds, and then lengthen this time to 20 seconds to ensure getting more than the minimum required. The object does not saturate the CCD, and the exposure time is less than 7.6 minutes (the maximum time for a peakup with the 52X0.1 slit), so we have devised a valid peakup target acquisition.

Target Acquisition ETC Parameters - ACQ

- Detector = ccd
- Filter = LongPass
- Gain = 4 e⁻/ADU
- Check Box = 3x3
- Target was a point source
- Spectrum: O5V (Model Spectrum)
- Source Flux: $v = 16.5$
- Average Galactic Extinction of $E(B-V) = 0.0$
- The Zodiacal Light is average
- The Earthshine is average

Imaging ETC Parameters - ACQ/PEAK

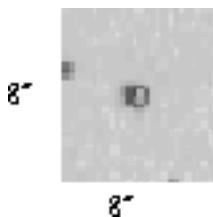
- Detector = ccd
- Filter = Clear
- Gain = $4 e^-/ADU$
- CR-split (Total number of images) = 1
- Target was a point source
- Spectrum: nova.dat (User's)
- Source Flux: $v = 19$
- Average Galactic Extinction of $E(B-V) = 0.0$
- The Zodiacal Light is average
- The Earthshine is average

Phase II Parameters for ACQ and ACQ/PEAK exposures

Exp	Label	Target Name	Config	OpMode	Aperture	SpElement	Wavlen	Iter	Exp Time (secs)
1		OFFSET-STAR	STIS/CCD	ACQ	F28X50LP	MIRROR		1	3.0
Special Requirements: Comments: Optional Parameters: ACQTYPE=POINT,									
	Sub-exposures:		Copy	Split	Orbit Num	Actual Time			
2		NOVA	STIS/CCD	ACQ/PEAK	52X0.1	MIRROR		1	20.0
Special Requirements: Comments: Optional Parameters:									
	Sub-exposures:		Copy	Split	Orbit Num	Actual Time			

8.5.5 Point Source Acquisition of a QSO with Fuzz Behind the Fiducial Bar

In this example an isolated $V = 16.5$ mag QSO ($z = 0.2$) is to be acquired, with the scientific exposures to be obtained with the QSO behind the 52X0.2F1 fiducial bar.



The target is isolated, so it will be acquired using a point source acquisition. The object is faint, so we can use the preferred F28X50LP filter. The [Target Acquisition ETC](#) is then used to determine an exposure time of 2.2 seconds. Note that the GAIN=4 and CR-SPLIT=1 *must be*

used for the ETC to ensure that you have a S/N of at least 40 in each of the two images obtained during the ACQ process. The object does not saturate the CCD, and the exposure time is less than 5 minutes, so we have devised a valid target acquisition. Given that the exposure time is so short, we can lengthen it to 3.0 seconds to make certain we have enough signal for a good acquisition.

The QSO is to be placed behind a fiducial bar, so to ensure an accurate centering we will perform an ACQ/PEAK acquisition. The peakup will be performed in the 52X0.2F1-R slit. This peaks up the target at the offset reference position (see “Barred Spectroscopy” on page 270). Peakdown acquisitions are not recommended. We will use the CCD and the MIRROR. A one-second exposure yields 5130 electrons in the central 25 pixels of the target, and correcting for the aperture throughput (80%) yields 4100 electrons; note that the [Imaging ETC](#) must be used for this calculation. We thus require slightly longer than 1 second to obtain the minimum requirement of 5000 electrons in the target, so we can expand our final exposure time to 5.0 seconds. The object does not saturate the CCD, and the exposure time is less than 9.8 minutes (the maximum time for a peakup with the 52X0.2 slit), so we have devised a valid peakup target acquisition.

Target Acquisition ETC Parameters - ACQ

- Detector = ccd
- Filter = LongPass
- Gain = 4 e⁻/ADU
- Check Box = 3x3
- Target was a point source
- Spectrum: QSO with z = 0.2
- Source Flux: $\nu = 16.5$
- Average Galactic Extinction of E(B-V) = 0.0
- The Zodiacal Light is average
- The Earthshine is average

Imaging ETC Parameters - ACQ/PEAK

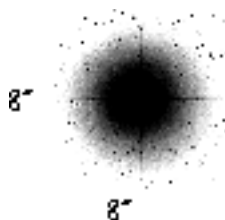
- Detector = ccd
- Filter = Clear
- Gain = 4 e⁻/ADU
- CR-split (Total number of images) = 1
- Target was a point source
- Spectrum: QSO with z = 0.2
- Source Flux: $\nu = 16.5$
- Average Galactic Extinction of E(B-V) = 0.0
- The Zodiacal Light is average
- The Earthshine is average

Phase II Parameters for ACQ and ACQ/PEAK exposures

Exp	Label	Target Name	Config	OpMode	Aperture	SpElement	Wavlen	Iter	Exp Time (secs)
1		G-STAR	STIS/CCD	ACQ	F25ND3	MIRROR		1	0.5
Special Requirements: Comments: Optional Parameters: ACQTYPE=POINT,									
		Sub-exposures:	Copy	Split	Orbit Num	Actual Time			
2		G-STAR	STIS/CCD	ACQ/PEAK	0.3X0.05ND	MIRROR		1	1.0
Special Requirements: Comments: Optional Parameters:									
		Sub-exposures:	Copy	Split	Orbit Num	Actual Time			

8.5.6 Point Source Acquisition of a Bright, Isolated Star Into the Wedge

In this example an isolated $V = 6.0$ mag G2 V star is to be acquired, with the scientific exposures to be obtained with the star behind the WEDGEA1.8 mask.



The target will be acquired with a point source acquisition, but because the object is so bright, we cannot use the preferred F28X50LP filter. Instead, we will use the F25ND3 neutral-density filter, and the [Target Acquisition ETC](#) yields an exposure time of 0.02 second, which is less than the minimum allowed time of 0.1 second. Note that the $GAIN=4$ and $CR-SPLIT=1$ *must be used* for the ETC to assure that you have a S/N of at least 40 in each of the two images obtained during the ACQ process. We will therefore increase the exposure time to 0.5 second. The object does not saturate the CCD, and the exposure time is less than 5 minutes, so we have devised a valid target acquisition.

The star is to be accurately placed behind the WEDGE which is 1.8" in size, so we need to perform an ACQ/PEAK acquisition. The peakup will be performed in the 0.3X0.05ND slit (peakdown acquisitions are not recommended), and we will use the CCD and the MIRROR. A 1 second exposure yields 47,000 electrons in the target *after* you correct it for the

8.6 STIS Post-Observation Target Acquisition Analysis

Unlike with earlier HST spectrographs, it is now possible to determine what the instrument acquired during an observation. The methods described below can be used to make either a coarse (eyeball estimate) or a fine (exact pixel) determination.

8.6.1 Paper Products—Coarse Centering

Once you have your data, you may produce a set of paper products providing a high-level overview of your observations; note that you need all the files from the observation (not just the calibrated files) to generate a complete set of paper products. Included in the output will be a summary page for the CCD acquisition, which contains an image of the initial HST pointing, as well as an image following the initial target acquisition centering (step 3 in the acquisition sequence). The object in the center of this image is the target acquired by STIS; the remaining steps in the acquisition sequence just center that target in the aperture. This level of accuracy is sufficient to check your acquisition of point sources. If you also performed an ACQ/PEAK, the output will also include a grid of the counts at each point in the peakup pattern and a confirmation image of the target after the final centering.

8.6.2 TAS—Fine Centering

Once you have your data, you can use the [Target Acquisition Simulator](#) to determine the exact position of the source that was acquired. The TAS will take the STIS image of the initial pointing and, using the same algorithm as the flight software, tell you the location of the target, in pixel coordinates. This level of accuracy will be needed to check your acquisition on a diffuse source.

8.6.3 Did the Acquisition Succeed?

[Section 5.7.4](#) of the *HST Data Handbook* describes in detail how to determine if your acquisition succeeded. To determine the accuracy of your acquisition, you must either have obtained a confirmation image immediately after your ACQ, or have performed a follow-on ACQ/PEAK (the amount of the ACQ/PEAK slew tells you the error in the ACQ). We recommend you use the **tastis** tool in STSDAS to determine how your acquisition worked.

Overheads and Orbit-Time Determination

In this chapter. . .

9.1 Overview / 201
9.2 STIS Exposure Overheads / 202
9.3 Orbit Use Determination Examples / 205

This chapter describes the overheads associated with STIS observations and provides examples showing how to determine the number of orbits that your program will require.

9.1 Overview

After you establish the set of scientific exposures and any additional target-acquisition or calibration exposures that you require for your program, you are ready to determine the total number of orbits to request. Generally, this is a straightforward exercise involving compilation of the overheads on the individual exposures, packing the exposure plus overhead time into individual orbits, and tallying up the results to determine your total orbit request. In some cases, it may be an iterative process as you refine your exposure requests to more fully exploit the orbits.

The Call for Proposals and the HST Primer provide information on the Observatory policies and practices with respect to orbit-time requests.

Below, we provide a summary of the STIS-specific overheads and give several examples that illustrate how to calculate your orbit requirements for Phase I Proposals. Note that the HST Primer provides a more limited summary of overheads that are intended to be conservative. In the unlikely case that an overhead calculation using the HST Primer requires less time than one calculated using the information in this chapter, you should use the result from this chapter to ensure that you do not end up with a time allocation that is insufficient to carry out your program in Phase II.

Alternatively, you could also use the APT to create a simple program (the APT takes all appropriate overheads into account).

9.2 STIS Exposure Overheads

Our current estimates of the overheads on STIS exposures are summarized in Table 9.1 and Table 9.2. All numbers given are approximate and rounded up to the nearest half minute; they do not differentiate in detail the overheads for different STIS modes and configurations. These overhead times are to be used (in conjunction with the actual exposure times and the HST Primer) to estimate the total number of orbits for your proposal. After your HST proposal is accepted, you will be asked to submit a Phase II proposal to support scheduling of your approved observations. At that time you will be presented with actual, up-to-date overheads by the scheduling software. *Allowing sufficient time for overheads in your Phase I proposal is important; additional time to cover unplanned overheads will not be granted later.*

The following list presents important points for each type of overhead:

- ***Generic (Observatory Level) Overheads:***

- The first time you acquire an object you must include the overhead for the guide-star acquisition (6 minutes).
- In subsequent contiguous orbits you must include the overhead for the guide-star reacquisition (5 minutes). If you are observing in the Continuous Viewing Zone (see the HST Primer), no guide-star *reacquisitions* are required.
- Time needs to be allowed for each deliberate movement of the telescope; e.g., if you are performing a target-acquisition exposure on a nearby star and then offsetting to your target, or if you are taking a series of exposures in which you move the target relative to the slit, you must allow time for the moves (20 seconds to 60 seconds depending on length of slew, see Table 9.1 and Table 9.2).
- Remember the policy with regard to MAMA and CCD observations in the same visit (see Chapter 2).

- ***STIS Onboard Target-Acquisition Overheads:***

- All STIS spectroscopic exposures that use a slit (long slit or echelle slit) will need to include a target-acquisition exposure to place the target in the slit (see Section 8.2). As discussed in Section 8.3, for the narrower slits you may also need to perform a peakup exposure to center the target in the slit.
- An onboard target acquisition needs to be done only once in a series of continuous orbits (i.e., once per visit).
- The drift rate induced by the Observatory is less than 10 milliarcseconds per hour. Thermal drifts internal to STIS at the slit plane are less still. We recommend that for long series of exposures taken through slits which are less than or equal to 0.1 arcsecond in either dimension, a peakup be performed every 4-5 orbits. This procedure will ensure that drifts do not cause the target to move out of the slit. (See also Section 11.2 and Section 8.1.4.)

- ***Scientific Exposures:***

- The overhead times are dominated by the time to move the grating wheel (MSM), which is ~3.0 minutes per move, worst case, and the readout time (CCD). Again, we stress that in Phase II the overheads will frequently be less, but it is important to plan Phase I using the conservative overheads given in Table 9.2 to ensure that you will have adequate time for your scientific goals.

- ***CCD and MAMA Spectroscopic Exposures and Wavecal:***

- The quoted overheads on the first spectroscopic exposure in a visit, or a spectroscopic exposure within a visit containing a change of grating or grating tilt, allow for the taking of a single automatic wavecal exposure to permit post-observation determination of the zero point of the wavelength (and spatial) scales. If you plan a series of exposures at a given grating setting which extends over 40 minutes in exposure time, then you need to include time for an additional automatic wavecal for each 40-minute period.

- ***Moving Targets:***

- Additional overheads will be incurred for observations of solar-system targets. The moving-target overheads (~1 minute in duration) are dependent upon current slew rates and are updated as necessary.

Table 9.1: Scientific Exposure Overheads: General, Acquisition, and Peakup

Action	Overhead	
	<i>Generic (Observatory Level)</i>	
Guide-Star acquisition	Initial acquisition overhead = 6 minutes. Reacquisitions on subsequent orbits = 5 minutes per orbit.	
Spacecraft POS-TARG moves	For offsets less than 1 arcminute and more than 10 arcseconds = 1 minute. For offsets between 10 arcseconds and 1 arcsecond = 0.5 minute. For offsets less than 1 arcsecond in size = 10 seconds.	
<i>Acquisitions and Peakups</i>		
Target acquisition (to place target in STIS aperture); see also Chapter 8.	For $V \leq 21$ point sources, 6 minutes. For diffuse acqs, add $0.2 \times \text{checkbox}^2$ seconds to the nominal 6 minutes.	
Acquisition peakups; see also Chapter 8.	For $V \leq 21$, 6 minutes for one peakup; note that a second peakup is required for the 0.1×0.03 aperture. More generally, see Table 8.5.	
<i>End of CVZ Visit</i>		
End of CVZ visit	Final STIS buffer dump = 3 minutes. Return mechanisms to normal = 4.5 minutes. For non-CVZ observations, these activities occur during the final occultation period, with no impact on target visibility.	

Table 9.2: STIS Scientific Exposure Overheads: Imaging and Spectroscopy

Action	Overhead			
	Imaging		Spectroscopy	
	CCD (minutes)	MAMA (minutes)	CCD (minutes)	MAMA (minutes)
First scientific exposure	4.5	5.0	5.0 ¹	8.0 ¹
Identical exposure in series (within an orbit)	1.0 ²	0.5	1.0	0.5
Exposure in series with grating move only	3.0	3.0	5.0 ¹	8.0 ¹
Move of aperture wheel (change of slit or aperture) (change of filter)	1.0	1.0	1.0	1.0
Additional automatic wavecal for series of identical exposures extending more than ~40 minutes	n/a	n/a	1.5	4.0

Table 9.2: STIS Scientific Exposure Overheads: Imaging and Spectroscopy

Action	Overhead			
	Imaging		Spectroscopy	
	CCD (minutes)	MAMA (minutes)	CCD (minutes)	MAMA (minutes)
Overhead for data management for exposures > 3 minutes in duration	0	0	0	0
Overhead for data management, for a series of full-frame exposures, each SHORTER than 3 minutes in duration (see “CCD Subarrays” on page 224 for subarray rules)	3 minutes every 7 exposures	2 minutes every exposure	3 minutes every 7 exposures	2 minutes every exposure
<i>Additional Calibration Exposures: Extra GO Wavecals³ and Fringe Flats</i>				
MAMA wavecal exposure	4.0 minutes			
CCD wavecal exposure	1.5 minutes			
CCD fringe flat exposure	2 minutes			
Slitless Spectroscopy (image of field, image of slit, wavecal)	9 minutes			

1. Includes auto wavecal. At Phase II, wavecals occurring at the beginning or end of an orbit will be pushed into occultation, providing increased time for scientific observing.
2. For $CR-SPLIT=n$, each exposure has a 1 minute overhead, so there will be $(n - 1)$ minutes of *extra* overhead. If small CCD subarrays are used, the overhead per exposure decreases to 20 seconds.
3. Use these only for additional wavecal exposures beyond those taken automatically.

9.3 Orbit Use Determination Examples

The easiest way to learn to compute total orbit time requests is to work through a few examples. Below we provide five different examples:

- Example 1 is a pattern-stepped series of long-slit CCD spectroscopic exposures mapping out the $H\alpha$ nebula in the center of the galaxy M86.
- Example 2 is a series of spectroscopic observations of the solar-analog, CVZ star P041-C, using all of the first-order, low-resolution CCD gratings.
- Example 3 is an imaging and spectroscopic program observing NGC 6543, the Cat’s Eye Nebula.

- Example 4 is a set of long MAMA spectroscopic exposures of Sk -69° 215 using the E230H grating through a narrow echelle slit, taken in the CVZ.
- Example 5 is a faint CCD imaging program.

These examples represent fairly typical uses of STIS. The target acquisitions used in each example differ slightly as well:

- Example 1 uses a diffuse-source acquisition and no peakup.
- Example 2 uses a point-source acquisition and peakup on the target.
- Example 3 uses a point-source acquisition.
- Example 4 uses a point-source acquisition and peakup on the target, and includes re-peakups during the course of the long observations.
- Example 5 uses no acquisition.

9.3.1 Sample Orbit Calculation 1: Long-Slit Spectroscopy of the Galaxy M86

This example is for an observation of the H α nebula in the center of the Virgo elliptical M86, using the CCD, the 52X0.2 slit and the G750M grating. A series of exposures is taken, each stepped relative to the next by 0.2 arcsecond, in the direction perpendicular to the slit, in order to cover the inner 0.6 arcseconds of the galaxy completely. Based on the signal-to-noise ratio calculation presented in Section 6.8.1, we require an integration time of ~ 30 minutes per position to obtain a signal-to-noise ratio of ~ 10 . The scientific exposures for this proposal, therefore, comprise *all* of the following:

- A CR-SPLIT=2, ~ 30 minute spectroscopic exposure¹ with G750M at a central wavelength of $\lambda=6768$ Å at location 1.
- A CR-SPLIT=2, ~ 30 minute spectroscopic exposure with G750M at a central wavelength of $\lambda=6768$ Å at location 2.
- A CR-SPLIT=2, ~ 30 minute spectroscopic exposure with G750M at a central wavelength of $\lambda=6768$ Å at location 3.

We need to include time for the guide-star acquisition at the start of the first orbit, followed by an acquisition exposure. No peakup will be done, since we are covering the nebula by stepping the slit and the slit is wider than 0."1. In this example, we assume a diffuse source acquisition, with a

1. Here and below, a 'CR-SPLIT= n , m minute' exposure implies there will be n exposures with a total of m minutes across the exposures. In this example there will be 2 exposures each of 15 minutes for a total of 30 minutes.

checkbox size of 25 pixels (roughly 1.25 arcseconds). The checkbox needs to be large as this galaxy has a very flat and dusty profile; see Figure 8.5.

The mean surface brightness of the galaxy within this region is $\sim 2 \times 10^{-15}$ ergs sec⁻¹ cm⁻² Å⁻¹ arcsec⁻², based on WFPC2 V-band images in the HST archive. Using the information in Section 6.4 or the [STIS Target Acquisition Exposure Time Calculator](#) we determine that, using the CCD longpass filter, F28X50LP, for $t_{\text{exp}} = 1$ second, we achieve more than the required signal-to-noise ratio needed over the checkbox for the target acquisition. We use the formula in Table 9.1, plug in CHECKBOX=25 and exptime=1.0, and determine that the acquisition will take roughly 8 minutes.

This is not a CVZ observation, so because more than 1 orbit is required we need to include time for the guide-star reacquisition at the beginning of each orbit. The individual exposures in this example are long enough that we do not need to include extra overhead for data management. We are satisfied with the automatic wavecal exposures which are taken for each spectroscopic observation at a new MSM position. We do not require fringe flats as we are observing at wavelengths shortward of 7500 Å.

We assume a visibility period of 52 minutes per orbit, appropriate for a target at M86's declination (see the Call for Proposals). Based on the reasoning presented in Table 9.3, below, we conclude that the observations can be squeezed into ~ 2 orbits with some loss of sensitivity. Alternately, one could choose to increase the signal-to-noise, and ask for 3 orbits.

Table 9.3: Orbit Calculation for Example 1

Action	Time (minutes)	Explanation
<i>Orbit 1</i>		
Initial Guide-Star acquisition	6.0	Needed at start of observation of new target
Target acquisition	8.0	Diffuse acquisition with checkbox=25, $t_{\text{exp}}=1.0$ sec
Offset target 0.2" to initial position	0.33	Position target to position 1 in pattern
Scientific exposure, G750M, $\lambda_c = 6768 \text{ \AA}$, position 1	36.0	30.0 minutes exposure time 5.0 minutes for first CCD spect. exposure in orbit 1.0 minutes for exposure overhead for CR-SPLIT
<i>Orbit 2</i>		
Guide-Star Reacquisition	5.0	Start of new orbit
Offset target 0.2" to position 2	0.33	Move target to position 2 in pattern
Additional wavecal	1.5	New orbit
Scientific exposure, G750M, $\lambda_c = 6768 \text{ \AA}$, position 2	22.0	21.0 minutes exposure time 1.0 minutes for exposure overhead for CR-SPLIT
Step target 0.2" perp. to slit	0.33	Move to position 3 in pattern
Scientific exposure, G750M, $\lambda_c = 6768 \text{ \AA}$, position 3	22.0	21.0 minutes exposure time 1.0 minutes for exposure overhead for CR-SPLIT

9.3.2 Sample Orbit Calculation 2: Low-Dispersion Spectroscopy of Solar-Analog Star P041-C

In this example the scientific objective is to observe the solar-analog CVZ star P041-C from the near IR to the near UV with STIS's low-resolution, first-order gratings and the 52X0.5 arcsecond slit. The series includes:

- CR-SPLIT=2, ~5 minute spectroscopic exposure with G750L at a central wavelength of $\lambda = 7751 \text{ \AA}$.
- CR-SPLIT=2, ~7 minute spectroscopic exposure with G430L at the central wavelength of $\lambda = 4300 \text{ \AA}$.
- CR-SPLIT=3, ~43 minute spectroscopic exposure with G230LB at the central wavelength of $\lambda = 2375 \text{ \AA}$.

We need to include time for the guide-star acquisition at the start of the first orbit, followed by an acquisition exposure. This target is a bright point source. We will use the longpass filter F28X50LP for the target acquisition and the default overhead of 6.0 minutes from Table 9.1. No pickup is needed as we are using the 0.5 arcsecond wide slit. This is a CVZ observation so each orbit is ~96 minutes. We need to include time for the CCD long-wavelength fringe flats, and since this is a CVZ observation the

fringe flat will not move into the occultation. As shown in Table 9.4, we can easily perform this observation in a single orbit.

Table 9.4: Orbit Calculation for Example 2

Action	Time (minutes)	Explanation
<i>Orbit 1</i>		
Initial Guide-Star acquisition	6.0	Needed at start of observation of new target
Target acquisition	6.0	Point source acquisition on target
Scientific exposure, G430L, $\lambda = 4300 \text{ \AA}$	13.0	7.0 minutes exposure time 5.0 minutes - CCD spect. exp with grating-wheel move overhead 1.0 minutes for CR-SPLIT=2 exposure overhead
Scientific exposure, G230LB, $\lambda = 2375 \text{ \AA}$	50.5	43.5 minutes exposure time 5.0 minutes - CCD spect. exp with grating-wheel move overhead 2.0 minutes for CR-SPLIT=3 exposure overhead
Autowavecal	1.5	1.5 minutes for autowavecal after 40 minutes
Scientific exposure, G750L, $\lambda = 7751 \text{ \AA}$	11.0	5.0 minutes exposure time 5.0 minutes - CCD spect. exp with grating-wheel move overhead 1.0 minutes for CR-SPLIT=2 exposure overhead
CCD fringe flat G750L	2.0	Fringe flat overhead

9.3.3 Sample Orbit Calculation 3: Imaging and Spectroscopy of the Cat's Eye Planetary Nebula, NGC 6543

In this example the scientific objectives are to obtain [O II] images of planetary nebula NGC 6543, as well as an optical spectrum at H β and an ultraviolet spectrum at C IV. The exposure-time calculations for these observations are presented in Section 6.8.3. The specific exposures in this series include:

- A CR-SPLIT=2, ~5 minute exposure with the F28X50OII filter.
- A CR-SPLIT=2, ~30 minute exposure with G430M at a central wavelength of $\lambda_c = 4961 \text{ \AA}$ using the 52X0.1 long slit.
- A ~30 minute exposure with G140L at C IV and the 52X0.1 long slit.

We need to include time for the guide-star acquisition at the start of the first orbit, followed by an acquisition exposure. The central star of the Cat's Eye Nebula is used as the acquisition target. It has a V magnitude ~11.5. Checking Table 8.2, we conclude that the star is faint enough to not saturate

the CCD in imaging mode with the longpass aperture F28X50LP, and we therefore use it for the target acquisition. We use the overhead information in Table 9.1 and Table 9.2 to conclude that the target acquisition will take 6 minutes. We wish to perform a pickup exposure as well, to center the star in the 0.1 arcsecond wide slit. We consult Table 8.2 and conclude that the source is not bright enough to saturate the CCD if we perform an undispersed (white-light) pickup with the mirror. Again using the information in Table 9.1 and Table 9.2, we conclude the pickup will take 6 minutes.

This is not a CVZ observation, so because more than 1 orbit is required we need to include time for the guide-star reacquisition at the beginning of each orbit. The individual exposures in this example are long enough that we do not need to include extra overhead for data management. We are satisfied with the automatic wavecal exposures which are taken for each spectroscopic observation at a new MSM position.

We assume a visibility period of 57 minutes per orbit, appropriate for a target at our source's declination of 66 degrees (see the Call for Proposals). Based on the reasoning presented in Table 9.5 below, we conclude that a total of 2 orbits is required to perform these observations. Note that the MAMA and CCD observations have been split into separate visits in accordance with the required policy.

Table 9.5: Orbit Calculation for Example 3

Action	Time (minutes)	Explanation
<i>Orbit 1</i>		
Initial Guide-Star acquisition	6.0	Needed at start of observation of new target
Target acquisition	6.0	Performed on central star
Pickup acquisition	6.0	White light pickup performed on central star
G140L scientific exposure	39.0	31 minutes total scientific exposures time 8.0 minutes—first spectroscopic MAMA exposure overhead
<i>Orbit 2 (A whole new visit to keep MAMA and CCD exposures separate)</i>		
Initial Guide-Star acquisition	6.0	Needed at start of observation of new target
Target acquisition	6.0	Performed on central star
Pickup acquisition	6.0	White light pickup performed on central star
CR-SPLIT=2 scientific exposure with G430M at $\lambda_c = 4961 \text{ \AA}$	28.0	22.0 minutes total scientific exposure time 5.0 minutes first CCD spectroscopic exposure in visit 1.0 minutes for exposure overhead for CR-SPLIT
CR-SPLIT=2 [O II] imaging using F28X50OII	11.5	6.0 minutes total scientific exposure time 4.5 minutes overhead, imaging exposure 1.0 minutes for exposure overhead for CR-SPLIT

9.3.4 Sample Orbit Calculation 4: MAMA Echelle Spectroscopic Exposures in the CVZ

In this example we wish to obtain a long total integration (420 minutes) in the CVZ using E230H and the 0.2X0.09 slit. The exposure-time calculations for this example are presented in Section 6.8.4.

We choose to break the observation up into roughly identical 60 minute exposures (though the actual scientific exposure time per orbit will be reduced to accommodate the required overheads and still remain within the MAMA 5 orbit limit). We acquire the target using a CCD point-source acquisition and then peakup in dispersed light using the CCD and the same slit as intended for the scientific observations. The star is Sk -69° 215, an O5 star with a V magnitude of 11.6. Checking Table 8.2, we conclude that the source will not saturate the CCD if observed for 0.1 seconds in the longpass filter F28X50LP, and we choose to perform the acquisition then on Sk -69° 215 with this filter as the aperture. We take the acquisition time as 6 minutes, from the overheads in Table 9.1.

We then perform a dispersed-light peakup using the G230LB grating with the CCD detector. We can estimate the exposure time required by determining with the spectroscopic ETC the total counts over the detector in 1 second for the clear filter and scaling by 65% for the slit throughput for 0.2X0.09 (“0.2X0.09 Aperture” on page 351). Since we must attain 80,000 counts over the detector, we require roughly 9 seconds per dwell point of the peakup. The peakup overhead for this slit is $360 + 20 \times t_{\text{exp}}$. We thus conclude that the peakup will require $360 + 20 \times 9 = 540$ seconds or ~ 9 minutes.

Since this is a CVZ observation, we do not need to include time for reacquisitions. However, since it is a long observation and a narrow slit, we decide we will re-perform a peakup midway through the observation.

Additionally, since this is a long observation taken at a given grating position, we need to include time for the automatic wavecalcs which will be taken every 40 minutes of elapsed pointed time.

For CVZ time, an orbit is 96 minutes. We conclude we require a total of 5 orbits to perform this program, as summarized in Table 9.6.

Table 9.6: Orbit Calculation for Example 4

Action	Time (minutes)	Explanation
<i>CVZ Observations: Total Time = 486 minutes or 486 / 96 = 5 orbits</i>		
Initial Guide-Star acquisition	6.0	Needed at start of observation of new target
Target acquisition	6.0	Point-source acquisition on target
Peakup exposure in 0.2X0.09 slit	9.0	Echelle slit dispersed-light peakup
First scientific exposure E230H	48.0	40.0 minutes exposure time 8.0 minutes for first MAMA spect. exposure in visit
Automatic wavecal after 40 minutes	4.0	4.0 minutes
Second scientific exposure E230H	41.0	40.0 minutes exposure time ~1 minute overhead on identical exposure
Automatic wavecal after 40 minutes	4.0	4.0 minutes
Third scientific exposure	41.0	40.0 minutes exposure time ~1 minute overhead on identical exposure
Automatic wavecal after 40 minutes	4.0	4.0 minutes
Fourth scientific exposure	41.0	40.0 minutes exposure time ~1 minute overhead on identical exposures
Automatic wavecal after 40 minutes	4.0	4.0 minutes
Fifth scientific exposure	41.0	40.0 minutes exposure time ~1 minute overhead on identical exposure
Automatic wavecal after 40 minutes	4.0	4.0 minutes
Peakup to recenter target	9.0	Echelle slit peakup
Sixth scientific exposure	41.0	40.0 minutes exposure time ~1 minute overhead on identical exposure
Automatic wavecal after 40 minutes	4.0	4.0 minutes
Seventh scientific exposure	41.0	40.0 minutes exposure time ~1 minute overhead on identical exposure
Automatic wavecal after 40 minutes	4.0	4.0 minutes
Eighth scientific exposure	41.0	40.0 minutes exposure time ~1 minute overhead on identical exposure
Automatic wavecal after 40 minutes	4.0	4.0 minutes
Ninth scientific exposure	41.0	40.0 minutes exposure time ~1 minute overhead on identical exposure
Automatic wavecal after 40 minutes	4.0	4.0 minutes
Tenth scientific exposure	41.0	40.0 minutes exposure time ~1 minute overhead on identical exposure
Automatic wavecal after 40 minutes	4.0	4.0 minutes

9.3.5 Sample Orbit Calculation 5: Faint CCD Imaging

In this program we wish to take deep images of a field to look for faint point sources, as described in Section 6.8.5. We request LOW-SKY as this observation is background limited. At our declination, we find from the CP/HST Primer that there are 45 minutes of visibility per orbit. The observations consist of:

- A single CR-SPLIT=4, ~28 minute exposure using the 50CCD clear aperture with the CCD.

We determine that we can execute this program in 1 orbit, as summarized in Table 9.7.

Table 9.7: Orbit Calculation for Example 5

Action	Time (minutes)	Explanation
<i>Orbit 1</i>		
Initial Guide-Star acquisition	6.0	Needed at start of observation of new target
CR-SPLIT=4 exposure, using 50CCD in imaging mode.	36.0	28.0 minutes exposure time 5.0 minutes for first imaging exposure in orbit 3.0 minute overhead for CR-SPLIT exposures

Summary and Checklist

In this chapter. . .

10.1 Phase I Proposing / 215 10.2 Phase II—Scheduling Approved Observations / 217
--

In this chapter we provide a summary and a checklist to help ensure that you have correctly planned your Phase I (proposing for HST time) and Phase II (scheduling your approved observations) submissions.

10.1 Phase I Proposing

At this point you should have assembled all the information you need to submit your Phase I HST observing proposal. During the course of this process you should review the items listed below.

For All Proposals:

- Check the catalog of previously executed and accepted programs to search for any duplications, and if present, provide a justification for duplicate observations.
- Justify any special requirements (e.g., SHADOW, interactive acquisition, CVZ, target-of-opportunity, time-critical scheduling, or the re-use target capability).

- Consider any special calibrations (e.g., unusually accurate wavelength determination requiring additional (non-automatic) wavecal exposures, fringe flats, or slitless spectroscopy), and account for their time in your request.
- Check your exposure times and configurations to ensure they are sufficient to provide the desired signal-to-noise ratios and accuracies, without saturation.
- Check that no visit is longer than 5 orbits.
- Allocate time for a target acquisition with appropriate centering accuracy. If a pre-acquisition image is needed, include the necessary extra orbit in the total orbit-time request.
- Consider the need for, and benefit of, obtaining coordinated parallel exposures with other instruments. Take into account any applicable data-volume restrictions.
- Include all applicable overheads so that in Phase II you will have enough orbits available to successfully implement your observations.
- Make sure that all configurations used in your proposal are included in the summary table.
- If applicable, justify the use of any available-but-unsupported modes, and explain how you plan to deal with calibration issues.

For CCD Observations:

- Check that you are not exceeding the CCD full-well counts pixel^{-1} limit for pixels (emission lines or objects) of interest.
- Allow time for CR-SPLIT observations and dithering, as needed.

For MAMA Observations:

- Check that your source does not exceed the absolute bright-object count-rate limits for MAMA exposures. For target-of-opportunity programs, explain how you plan to show that the target does not exceed the bright-object limits.
- Check that you are not exceeding the MAMA 65,536 counts pixel^{-1} buffer-imposed limit over pixels (emission lines or objects) of interest.
- Check that your proposal does not violate the policy that restricts the mixing of CCD and MAMA observations in the same visit, (see Section 2.6). Be sure that you are requesting sufficient orbits to allow the MAMA and CCD observations to be done in separate visits. Provide a justification if the scientific needs of your program require violating this policy.

- If early acquisition images in support of MAMA bright-object checking are necessary, they must be included in the Phase I orbit request.
- Remember that MAMA pure parallels are not allowed (see Section 2.7).
- Be aware of the limits on the number of targets for MAMA snapshot programs (see Section 2.8).

10.1.1 Phase I Orbit-Allocation Examples

Phase I orbit-allocation examples are presented in the HST Primer. Additional examples of Phase I orbit estimations are worked through in this Handbook (see Section 1.1.2, Section 6.8, and Section 9.3).

10.2 Phase II—Scheduling Approved Observations

Below, we provide a checklist for observers filling out Phase II proposals. You should do the following prior to submitting your program.

For All Proposals:

- Update the text in the Phase II template (“Observing Description” and “Special Requirements”—they were copied from your Phase I proposal and may need modification based on TAC comments and definition of the observation details).
- Specify your coordinates (especially for spectroscopic observations) in the “Guide Star Reference” frame. Be sure to specify the coordinate source used, and, if applicable, include the GSC PLATE-ID in your Phase II proposal file. If your target has significant proper motion, be sure to also include this information in the appropriate fields in the Phase II proposal file. Check that the units of the proper motion are correct, and that the epoch specified is consistent with the coordinates supplied.
- Specify accurate V magnitude, fluxes, spectral type, and colors for your target. This is required for MAMA targets to allow for bright-object screening.
- Properly specify your exposures.
- Include target acquisitions and pickups as needed.
- Specify any needed orientation and/or timing requirements. To facilitate scheduling, please provide the broadest possible ranges for these requirements that are consistent with your scientific needs. If multiple ORIENTs are possible, please include the alternatives.

- Specify any allocated coordinated parallel exposures.
- Include any additional wavecal exposures if needed.
- Verify the correct usage (i.e., direction) of your PATTERN optional requirement or POS-TARGs (if used).
- For slitless spectroscopy or prism observations, remember to take an image and the proper calibration sequence if needed.
- Check the [Phase II](#) web page for any updates. You can also find there instructions for requesting changes to your program and observing policies.

For CCD Observations:

- CR-SPLIT CCD exposures, as appropriate. Keep individual exposure times < 1000 s if possible to avoid excessive cosmic ray events.
- Add fringe-flat exposures for G750L and G750M observations at $\lambda > 7500 \text{ \AA}$.
- Consider the use of dithering for imaging observations, or stepping along the slit for spectroscopic observations.
- Consider whether moving the target closer to the CCD readout by using the E1 pseudo-aperture positions to reduce charge transfer efficiency (CTE) effects would benefit your program. If observing in the far red, consider the E2 pseudo-apertures to improve fringe removal.

For MAMA Observations:


- Re-verify that your target falls below the bright-object limits.
- For TIME-TAG observations, verify the value for BUFFER-TIME.
- Consider the use of dithering for imaging observations.
- Consider the use of stepping along the slit for first-order modes or the use of FP-SPLIT slits for echelle modes, when high signal-to-noise is required.
- For faint objects, consider using the D1 pseudo-apertures to mitigate the FUV-MAMA dark current.



PART III:

Supporting Material

The chapters in this Part present more detailed material in support of the User's Guide. Included are a description of the data-taking modes of STIS, special uses of the instrument, and spectroscopic and imaging reference material.



“Space is big, really big.”

Douglas Adams, Hitchhiker's Guide to the Galaxy.

Data Taking

In this chapter. . .

11.1 Basic Operating Modes / 221
11.2 Exposure Sequences and Contemporaneous Calibrations / 232
11.3 Patterns and Dithering / 239
11.4 Fixing Orientation on the Sky / 248

In this chapter we describe the basic ways in which data can be taken with STIS. Included are descriptions of the operating modes of the STIS CCD and MAMAs, the use of subarrays, taking of time-resolved data, associated exposures in a series, automatic and extra wavecalcs, fringe flats, the use of patterns and dithering, and fixing the slit orientation on the sky.

11.1 Basic Operating Modes

STIS currently supports four basic operating modes:

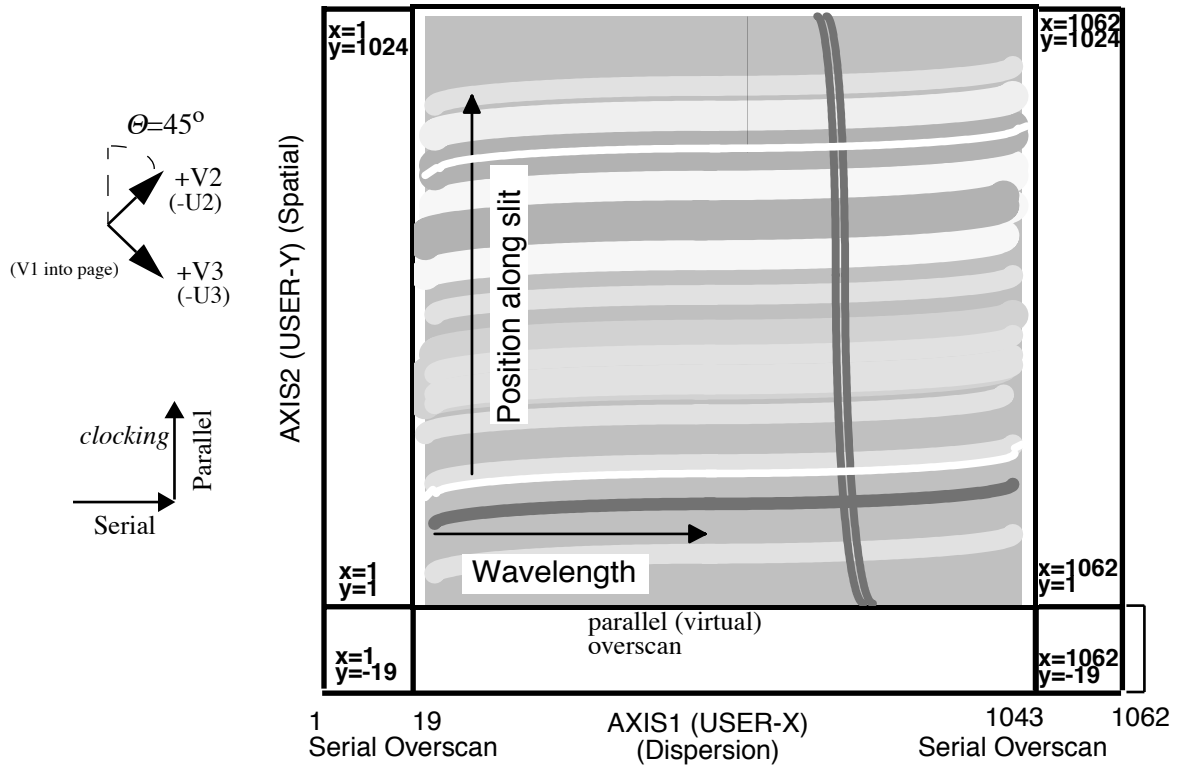
- **ACCUM** operating modes for the CCD and MAMAs, which produce a time- integrated accumulated image. These are the most commonly used modes.
- **TIME-TAG** operating mode for the MAMA detectors, which outputs an event stream of high-time-resolution observations in the UV.
- **ACQ** (acquisition) and **ACQ/PEAKUP** operating modes for the CCD and MAMAs used to acquire targets in the spectroscopic slits and behind coronagraphic bars and masks. Target acquisitions are described further in Chapter 8.

11.1.1 CCD ACCUM Mode

The STIS CCD has only the single operating mode, ACCUM, for science data. The CCD pixels accumulate charge during the exposure in response to photons. The charge is read out at the end of the exposure at a selectable gain (number of electrons per DN) and converted to 16 bit data numbers (DN) by the A-to-D converter. The DN are stored as 16 bit words (with a range 0 to 65,535) in the STIS data-buffer memory array. At the default CCDGAIN=1, the gain amplifier saturation level (33,000 e⁻), and not the 16-bit format, limits the total counts that can be sustained in a single exposure without saturating (see also Section 7.1.9 and Section 7.2.1). At the other supported gain, CCDGAIN=4, the CCD full well (144,000 e⁻ or 36,000 DN, except in the outermost regions of the CCD where the full well is 120,000 e⁻, see Chapter 7 for details) still determines the saturation limit.

A full detector readout is actually 1062 x 1044 pixels with physical and virtual overscans. Scientific data are obtained on 1024 x 1024 pixels, each projecting to ~0.05 x 0.05 arcsecond on the sky. The dispersion axis runs along AXIS1 (image x or along a row of the CCD), and the spatial dimension of the slit runs along AXIS2 (image y or along a column of the CCD). Figure 11.1 illustrates the full CCD format and its orientation with respect to the spacecraft (U2 and U3 or V2 and V3) axes. Arrows indicate the orientation of the parallel and serial clocking. The readout directions depend on the amplifier used. For the default amplifier D, the readout is at the upper right corner. It includes 19 columns of leading and 19 columns of trailing physical overscan in AXIS1, and 20 trailing rows of virtual overscan in AXIS2. The trailing serial overscan as well as the parallel overscan pixels are used to determine the bias level in post-observation data processing. The parallel overscan can also be used in the diagnosis of charge-transfer problems.

Figure 11.1: CCD ACCUM Mode Format for a Long-Slit Spectrum



The minimum CCD exposure time is 0.1 second and the maximum possible exposure time is 4.7 hours (though we cannot imagine wanting a single exposure longer than 60 minutes). The minimum time between *identical* exposures for CCD full-frame (1062x1044) images is ~45 seconds.¹ This time is dominated by the time it takes to read out the CCD (29 seconds for the full frame) and can be reduced to ~19 seconds if you use a subarray (see "CCD Subarrays" on page 224).

Binning

The CCD supports on-chip binning. When on-chip binning is used the specified number of pixels in the serial and parallel directions is read out as a single pixel. The advantage of CCD binning is that the read noise per binned pixel is comparable to the read noise per unbinned pixel. Thus if your signal-to-noise per pixel is dominated by read noise when no binning is used, you can increase the signal-to-noise by binning. The *disadvantages* of using on-chip binning are (a) that it reduces the resolution of your spectrogram or image, (b) that the relative number of pixels affected by cosmic rays increases, and (c) that the relative number of 'hot' pixels

1. This constraint implies there will be 45 seconds of overhead per full-frame CR-SPLIT, i.e., if CR-SPLIT=3, there will be 3 x 45 seconds of overhead on the set of 3 exposures due to CCD setup and readout.

(which is $\sim 2\%$ of all CCD pixels for unbinned data by the time this handbook is issued, see Chapter 7), increases by a factor proportional to the binning factor. On-chip binning of 1, 2, or 4 pixels in both the **AXIS1** and **AXIS2** directions is supported. Note that on-chip binning is not allowed when subarrays are used.

The number of hot pixels has been increasing steadily with time due to accumulated radiation damage on the STIS CCD (see the discussion on hot pixels in Chapter 7). Thus the impact of hot pixels on binned data has become significantly larger. Also note that when spectral data are spatially rectified, a single pixel in the original data will be interpolated into four pixels in the rectified image. For data binned $N \times M$ on board the spacecraft, a single bad pixel will, after rectification, affect the equivalent of $4 \times N \times M$ pixels in an unbinned image.

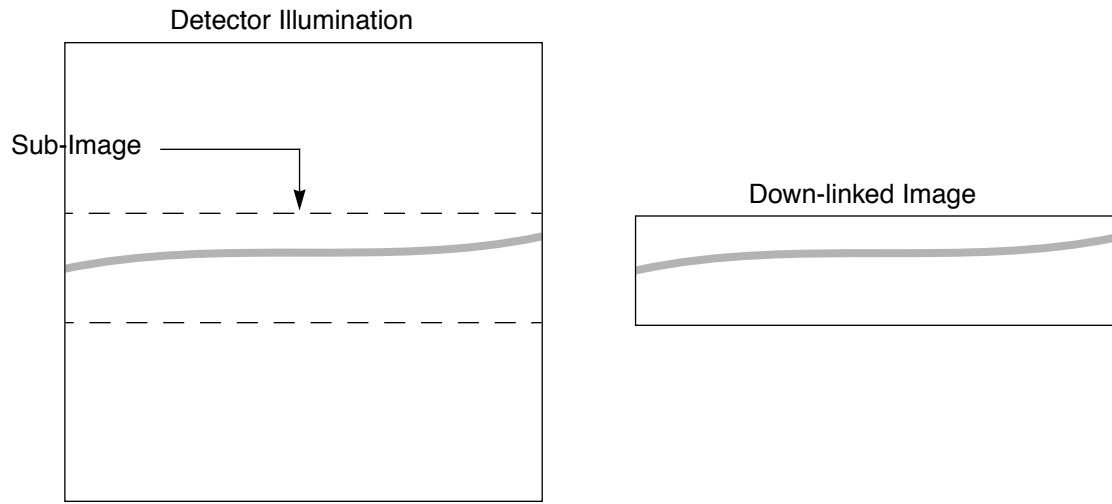
When using the ETC to estimate the effects of on-board binning on the S/N of CCD observations, be aware that increasing the binning in the dispersion direction may cause the ETC to use a larger resolution element for its S/N calculation. Be sure to understand how much of any increase in the S/N number output by the ETC is due to an actual decrease in the read noise and how much is simply due to a change in the size of the resolution element assumed for the calculation.

During Phase II, you specify the binning for your CCD observations using the **BINAXIS1** and **BINAXIS2** optional parameters. The default values are 1.

CCD Subarrays

Subarrays can be used when the CCD detector is read out. Generally, there is no need to use a subarray for STIS data. The main scientific use of CCD subarrays is for time-resolved optical spectroscopy, where subarrays can be used to reduce the CCD read time and keep the data volume at a manageable level. CCD subarrays can also be specified for CCD **ACQ/PEAK** observations to limit the region in a diffuse object (e.g., a galaxy) over which the flux is summed for the pickup. When a subarray is used, only the portion of the detector which is within the specified subarray is read out and transmitted to the ground (see Figure 11.2—note that the spectrogram curvature is exaggerated in this figure).

Figure 11.2: Using Subarrays



As described in Section 11.1.1, full-frame CCD readouts are composed of 1062 x 1044 pixels: 1024 x 1024 data pixels, 19 leading and 19 trailing serial-overscan pixels, and 20 trailing parallel-overscan pixels. Dispersion runs along `AXIS1` and the long dimension of the slit runs along `AXIS2`. Subarrays are required to span the full width of the CCD detector in the serial (dispersion) direction in order to ensure they contain the serial overscan needed to determine the bias level; however, you can control the height of the subarray in the parallel direction (i.e., along the slit for long-slit spectroscopic observations). Note that no parallel overscan is returned for subarrays (see also Section 7.2.5). Subarray size is specified in Phase II by the parameter:

- `SIZEAXIS2` – size in pixels of the subarray in the `AXIS2` direction.

The minimum allowed value of `SIZEAXIS2` for `ACCUM` mode observations is 30 pixels (corresponding to 1.5 arcsec), and `SIZEAXIS2` must be an even number of pixels. By default the target is placed within a few pixels of the center of the subarray. For a few central wavelength settings, however, the target may be systematically offset by up to 30 pixels in the spatial direction. Observers should consult with help@stsci.edu prior to using `SIZEAXIS2` with a value of less than 64 pixels.

Use of Subarrays to Reduce the CCD Read Time

The minimum time between identical CCD exposures is the readtime + 16 seconds. The time to read out a CCD subarray is:

$$\text{readtime} = 2.0 + \text{SIZEAXIS2} \times 0.026 \quad \text{seconds}$$

Thus, using the smallest available subarray, which is 30 pixels high, you can reduce the minimum time between identical exposures to ~19 seconds (16 seconds overhead plus 3 seconds read time). The minimum time between full-frame CCD exposures is $16 + 29 = 45$ seconds.

Use of Subarrays to Reduce Data Volume

The format of the data you receive when you use a CCD subarray will have dimensions $1062 \times \text{SIZEAXIS2}$, will cover the full range in the dispersion direction, and will include the serial overscan. The STIS buffer can hold eight full-frame CCD exposures at one time, or $8 \times (1024 / \text{SIZEAXIS2})$ exposures at any one time. Full-frame CCD data acquired in one exposure can be transferred to the HST data recorder during the subsequent exposure(s) so long as the integration time of the subsequent exposure is longer than 3.0 minutes. If you are taking a series of exposures which are shorter than that, the buffer cannot be emptied during exposure, and once the STIS buffer fills up, there will be a pause in the exposures sequence of roughly 3 minutes as the buffer is emptied. This problem can sometimes be avoided with the judicious use of subarrays.

11.1.2 MAMA ACCUM Mode

In MAMA ACCUM mode exposures, photons are accumulated into a 2048×2048 , 16-bit-per-element oversampled array in the STIS data buffer memory as they are received. At the end of the exposure, the data can be left in the over-sampled (or highres) format, which is the default for scientific exposures, or they can be binned along **AXIS1** and **AXIS2** to produce a 1024×1024 native-format image. ACCUM is the mode of choice for all observations that do not require time resolution on minute or less scales. Dispersion runs along **AXIS1** and the spatial dimension of the slit run along **AXIS2**. Figure 11.3 and Figure 11.4 illustrate the format and coordinate system for MAMA images, showing how first-order and echelle ACCUM mode spectrograms appear. PRISM images have dispersion along **AXIS1**. Note that for FUV-MAMA G140L and G140M the target is placed near $\text{AXIS2}=392$ to ensure that they will not fall on the shadow of the repeller wire (see Section 7.5). Thus there will be ~3 arcseconds less spatial sky coverage to decreasing **AXIS2** and ~3 arcseconds more spatial sky coverage to increasing **AXIS2** along the slit. Said another way, slit center will project ~3 arcseconds below the detector center along **AXIS2** for G140L and G140M observations. Note also the effects of the monthly offsetting which applies to all MAMA modes (see Section 7.5). (Data taken prior to March 15, 1999 have the slit center offset above the detector center.)

Figure 11.3: MAMA Mode Format for First-Order, Long-Slit Spectroscopy

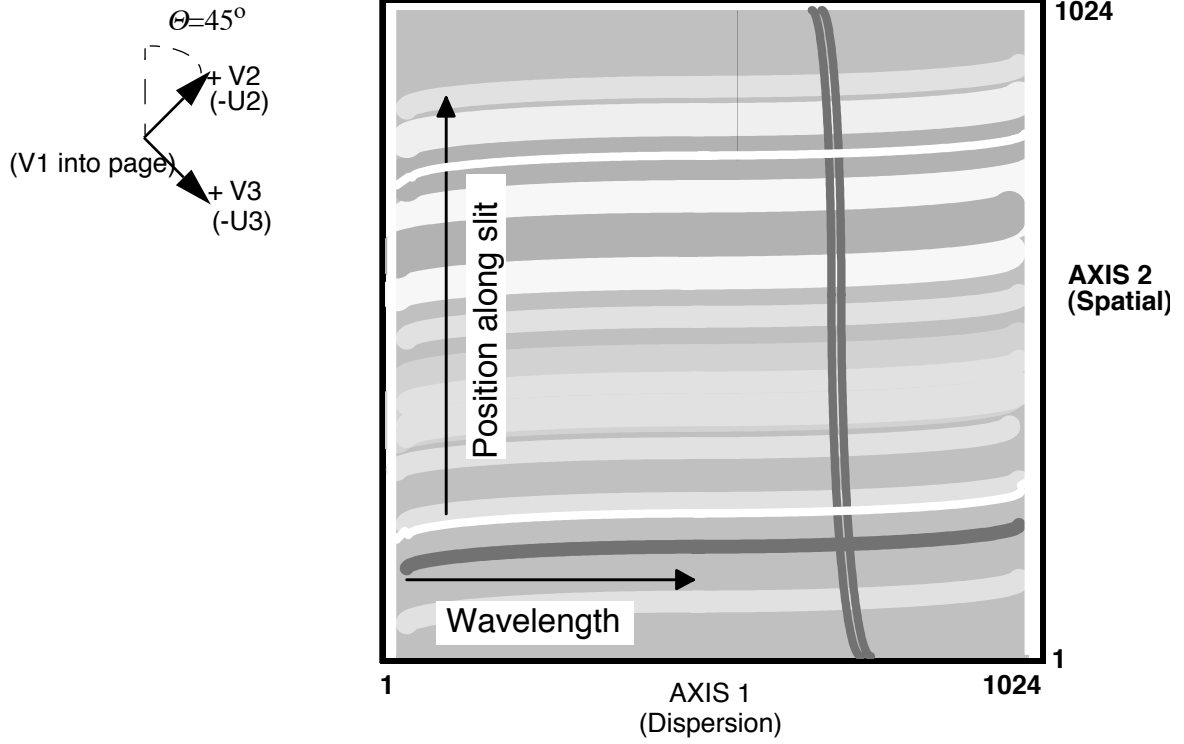
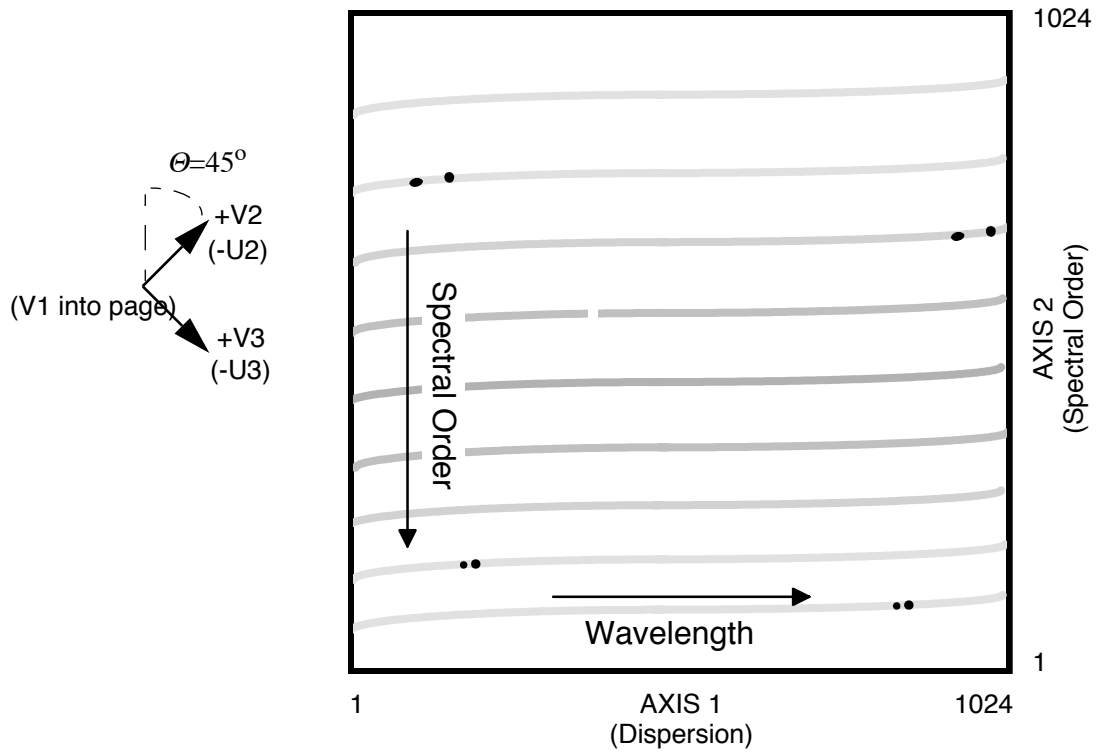


Figure 11.4: MAMA Mode Format for Echelle Spectroscopy



The minimum MAMA ACCUM mode exposure time is 0.1 second and the maximum exposure time is 1.8 hours. The minimum time between *identical* MAMA ACCUM exposures is ~ 30 seconds, for exposures which are longer than 3 minutes, and it is 2.5 minutes for exposures which are shorter than 3 minutes. This difference arises because in the former case the buffer can be dumped to the HST recorder during the subsequent exposure (i.e., in parallel), but in the latter case there is insufficient time to dump the buffer during the subsequent exposure and the buffer must be dumped serially (i.e., using observing time).

For the MAMA medium-resolution, first-order modes and medium and high-resolution echelle modes (i.e., gratings G140M, G230M, E230M, E230H, E140M, and E140H), a correction for Doppler shifting of the photon energies due to HST spacecraft motion is applied as the photons are counted, prior to their addressing in STIS data-buffer memory. The leading and trailing pixels in the dispersion direction (AXIS1) for Doppler-corrected exposures therefore receive less effective integration time, since source photons at the corresponding wavelengths have been Doppler-shifted off the edge of the detector for some fraction of the total exposure time. This effect is strongest in the high-resolution echelle modes, where for a maximum HST spacecraft velocity of 7.5 km sec^{-1} , the leading and trailing ~ 20 AXIS1 pixels will have reduced effective exposure times.

Highres

The MAMA detectors record scientific data in the so-called *highres* mode, producing 2048×2048 images of super resolution - one half the 1024×1024 “native”-format pixel size defined by the anode readout itself. All scientific data are taken in this format by default. Below we explain in more detail the nature of highres data.

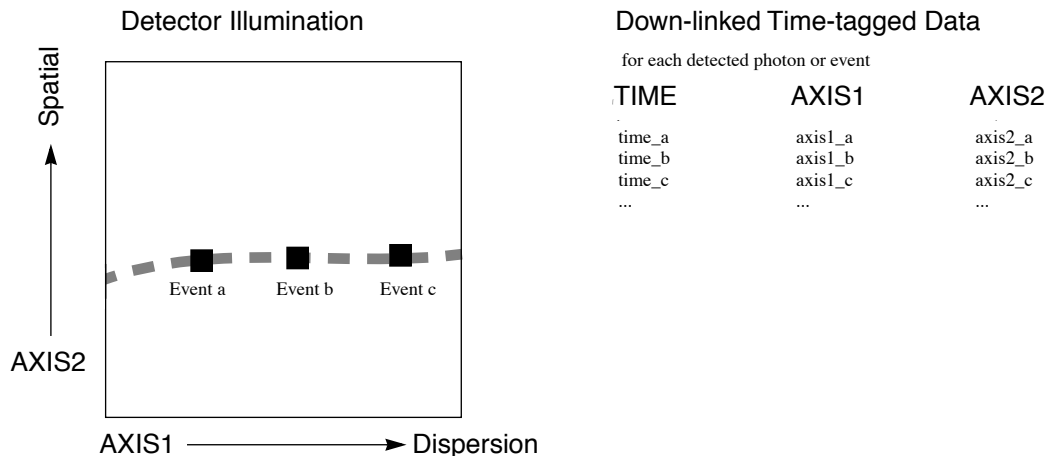
The MAMA detectors have 1024×1024 physical or so-called native-format pixels. However, each count is detected by multiple electrodes, so the charge distribution among the electrodes can be used to centroid the incident charge cloud to subpixel resolution. The gain of the highres 2048×2048 mode is a $\sim 10\text{--}30\%$ increase in resolution at the price of the increased fixed-pattern noise due to poorly characterized charge partition among the electrodes. The highres flat fields have much more structure than the 1024×1024 flats, with adjacent columns and rows differing by $\sim 30\%$ in an off/on pattern whose variability is appreciably higher than for 1024×1024 format images. This effect and the inherently lower signal-to-noise ratio in the full-resolution flat-field images (nominally ~ 20 to 1 per highres pixel) suggest that it may be difficult to routinely realize the benefit in resolution. However, we note that data taken in highres mode can always be binned to 1024×1024 on the ground in post-observation data processing, and since the extra overheads in highres mode are typically quite small, highres is the default data-taking mode for the MAMA. The pipeline bins the data to 1024×1024 format during calibration so that the pipeline-output calibrated images are native format (see the *HST Data Handbook* for more details).

11.1.3 MAMA TIME-TAG Mode

TIME-TAG mode is used for high-time-resolution spectroscopy and imaging in the ultraviolet. When used in TIME-TAG mode, the MAMA produces an event stream of AXIS1, AXIS2, and TIME data points, with a time resolution of 125 microseconds. The volume of data produced in TIME-TAG mode can be very large and the data therefore must be continuously transferred from the STIS internal buffer to the data recorders to sustain TIME-TAG exposures of any significant duration.

The axis orientation in TIME-TAG is the same as in ACCUM mode (see Figure 11.3). The spacecraft time (absolute zero point of the time) is routinely known to 10 millisecond accuracy. No Doppler correction is applied by the flight software for TIME-TAG mode, but the correction can be applied during the post-processing of the data. The recorded times are the spacecraft times, which can be converted to heliocentric times using the ephemeris of the Earth and the spacecraft. TIME-TAG mode is illustrated in Figure 11.5. Processing of TIME-TAG data by the STScI pipeline is described in Section 15.1.

Figure 11.5: TIME-TAG Mode



Event Processing in TIME-TAG Mode

In TIME-TAG mode, events detected on the anode wires are queued in a 4096-event FIFO prior to time assignment and subsequent storage in a STIS memory buffer. When the FIFO is less than half full, 4 events can be processed during each 125 microsecond tick of the STIS clock, corresponding to a maximum stable count rate of 32,000 counts/sec. Times are assigned shortly after detection, when the event is extracted from the FIFO. This is the desired operating state in TIME-TAG mode. Higher count rate situations (described below) should be avoided because they result in less accurate times, lost events, and buffer management problems.

For global count rates up to 50,000 counts/sec, the FIFO will gradually fill until more than 2048 events are queued. At this point 2048 events are processed in a tight loop requiring only 41 milliseconds, instead of the usual 64 milliseconds. Processing then reverts to the slower rate until the FIFO is again more than half full. In this mode, the times associated with each event have 125 microsecond resolution, but suffer from significantly larger systematic delays. Also, the observing sequence will be frequently interrupted to handle STIS buffer dumps (described below).

For count rates above 50,000 counts/sec, the FIFO will fill faster than events can be processed, even in fast mode. When the FIFO fills, all events in the FIFO are discarded and the empty FIFO begins filling with new events. In this mode event times are essentially uniform, providing essentially no information about source variability.

Buffer Management in TIME-TAG Mode

For TIME-TAG observations, STIS memory is divided into two 8 megabyte buffers, each of which can hold up to 2×10^6 events. If the cadence between scheduled buffer dumps is at least 99 seconds, then one buffer can be actively recording new events, while previously recorded events in the other buffer are being dumped to an HST data recorder. Thus, events can be dumped to STIS memory without gaps only if the global count rate is below 20,000 counts/sec.

During Phase II proposal preparation, observers must specify in advance the time between dumps using the BUFFER-TIME parameter. The following constraints should be considered when selecting a BUFFER-TIME:

To prevent loss of data, BUFFER-TIME should be short enough that fewer than 2×10^6 events are expected in the interval between dumps. If R is the expected count rate (predicted by the STIS Exposure Time Calculator, for example), then BUFFER-TIME should be smaller than $2 \times 10^6/R$. A bit of margin protects against source variability or inaccurate count rate predictions. Be sure to include sky and detector backgrounds when estimating count rates.

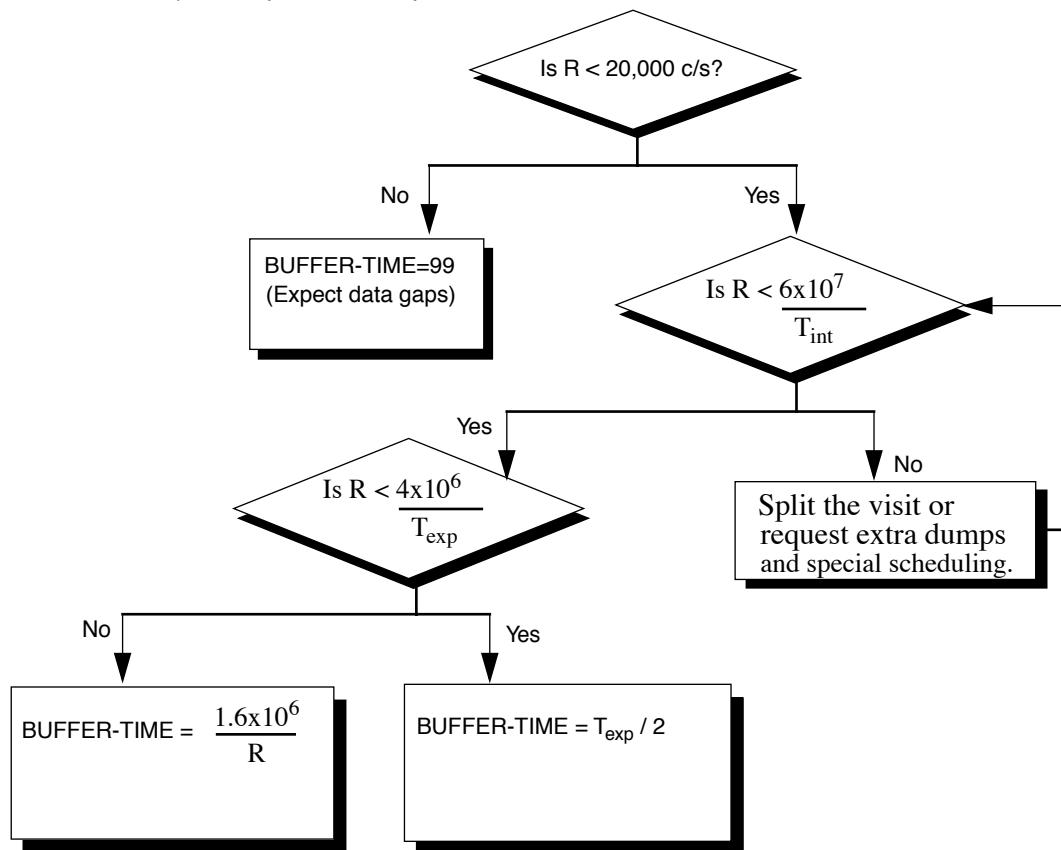
On the other hand, the nominal STIS allocation on the HST data recorders allows at most 30 total buffer dumps in any one visit, and fewer is desirable. For the minimum continuously sustainable BUFFER-TIME of 99 seconds, this limit on dumps corresponds to a total exposure time of only 50 minutes. It is sometimes possible to schedule downlinks from the HST data recorders to the ground during a specific TIME-TAG visit. Thus, with a strong scientific justification, it may be possible to accommodate visits that require more than 30 dumps. Such requests should be justified quantitatively in the Phase I proposal.

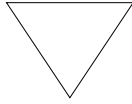
Finally, BUFFER-TIME should be at least 99 seconds when more than 2 dumps are expected. Otherwise, the observing sequence will be interrupted whenever both buffers are in the process of being dumped. In such cases it is probably better to choose a BUFFER-TIME of 99 seconds. This

guarantees that photons will be recorded whenever the active buffer has remaining space. If the active buffer fills in less than the selected BUFFER-TIME, additional photons will be discarded until the next dump begins. Reliable flux calibration is not possible in such cases.

In summary, BUFFER-TIME should be less than $2 \times 10^6/R$, but longer than $1/30$ the total exposure time and longer than 99 seconds. In some cases it will not be possible to satisfy all of these criteria, in which case multiple short ACCUM exposures should be considered as an alternative.

Figure 11.6: Estimation of BUFFER-TIME. T_{int} refers to the total integration time (in sec) of all the exposures in the visit, and T_{exp} refers to the integration time (in sec) of the particular exposure under consideration.





Remember to include contributions from all the sources expected to fall on the detector, the sky, geocoronal line emissions and detector backgrounds along with your source counts when computing R . It is important that you include a safety margin of at least 20% in your estimation of R . Specifying too small a `BUFFER-TIME` can lead to loss of data after the first dump of 2 million events.

11.2 Exposure Sequences and Contemporaneous Calibrations

There are several instances when a series of associated STIS exposures (rather than a single exposure) will be taken. The data from these exposure sequences are generally processed as a single unit through the STScI calibration pipeline, with the scientific data from the multiple *associated* exposures appearing in a single file (for a high-level overview of the STIS calibration pipeline and the data-product format see Chapter 15). While you do not have to specify that you plan a series of associated exposures in your Phase I proposal, it is helpful to know about these sequences when planning your proposal. In Phase II, once your proposal has been accepted and you are working on scheduling your observations, you will be able to see and use these sequences. All are generated from a single exposure logsheet line in your Phase II proposal.

We discuss several types of associated exposures below:

- *Automatic* wavecal exposures taken with scientific data to allow calibration of the spectroscopic and spatial zeropoints.
- `CCD CR-SPLIT` exposures taken to allow removal of cosmic rays in the scientific data during post-observation data processing.
- Multiple identical *repeat* exposures, which can be taken to provide time resolutions of tens of seconds (CCD) or minutes (MAMA).
- *Pattern* sequences, in which the target is stepped, for example along the slit to mitigate the impact of hot pixels or perpendicular to the slit (to map a two-dimensional region) for spectroscopic observations, or in a dither pattern for imaging observations.

In addition there are two types of contemporaneous calibration observations that observers may take with their scientific observations in special circumstances:

- *GO wavecal*s, taken if exceptional wavelength accuracy is required, or for slitless spectroscopy.
- *CCD fringe flats* (CCDFLAT) which need to be taken for near-IR ($\lambda > 7500 \text{ \AA}$) observations in the grating modes if high signal-to-noise is required.

11.2.1 Auto-Wavecal

The STIS optical path from source to detector passes through the aperture (slit) wheel (where the filters for imaging also are housed) and then reflects from one of the elements mounted on the Mode Selection Mechanism (MSM) which houses the first-order gratings, the prism, the cross-dispersers for use with the echelles, and the mirrors for imaging work (see Figure 3.1). Lack of repeatability in the MSM causes the center of the spectrogram (as defined by the aperture and wavelength centers) to fall on a slightly different detector location each time there is a movement of the MSM (the MSM-induced offsets in dispersion and the spatial direction have been measured to be ± 3 pixels or less). In addition, for MAMA first order spectrographic observations, the aperture location on the detector is deliberately shifted each month to ensure equalization of extracted charge across the detector.

To allow calibration of the zero point of the aperture location and the zero point of the wavelength scale for spectroscopic observations, a line-lamp observation (so called wavecal) is taken *automatically* each time the MSM is moved. In addition, if a series of exposures or a single long exposure is taken at a single MSM setting, then an additional wavecal will automatically be taken when there is a pause in data taking *if* 40 minutes of exposure time has passed since the previous wavecal. Here, 40 minutes is the time constant for thermal changes which might affect the wavelength accuracy. Testing in orbit has shown that in extreme conditions (when there is a swing from hot to cold), worst-case thermal shifts of roughly 0.3 pixels/hour can be seen; however, monitoring shows that under typical observing conditions thermal drifts are of the order of 0.1 pixels/hour (see also the [Monitoring page](#) on the STIS web site).

To summarize, each set of spectroscopic scientific exposures taken at a given grating tilt (i.e., MSM position) will be accompanied by at least one automatically taken wavecal exposure, and if the exposures extend over a period of 40 minutes or more, multiple wavecal exposures will be taken. These wavecal exposures will be processed along with the scientific data, and they will be used by the pipeline to automatically correct the zero-point offsets in the wavelength and spatial scales (see Chapter 15).

The automatic wavecals are designed to be of sufficient duration to produce spectrograms which contain at least 3 emission lines with 3 counts per pixel and 50 counts summed over the line. In those regions of the spectrum where 3 lines are not obtainable, there will be at least 1 emission line with 18 counts per pixel and 300 counts summed over the line. For the CCD where integration times are short, the automatic wavecals will typically be taken to ensure roughly 8 times this signal.

The combination of thermal changes between the wavecal and scientific exposures, coupled with the ability to measure the zero points in the wavecal exposures, limits the accuracy of the absolute zero points to ≤ 0.2 pixel (see Section 16.1). In addition to the automatic wavecals, observers can also take their own wavecal exposures, using the WAVE target option (see “GO Wavecals”, below) if they desire more accurate wavelengths than will automatically be provided, or they are particularly concerned about the time variation of the zero point.

GO Wavecals

Only if you require particularly accurate wavelengths do you need to consider using the TARGET=WAVE option to insert additional wavecal exposures into your observing sequence.

The wavecals taken with TARGET=WAVE are identical to those taken automatically (i.e., the auto-wavecals) with two important exceptions. First, you can explicitly specify which aperture (slit) you wish to use for the TARGET=WAVE exposure (whereas for automatic wavecals the program slit or a pre-defined alternative for each grating is used). Second, you can take longer exposures, increasing the signal-to-noise of the lamp exposures or possibly saturating some lines to bring out weaker lines near astronomical lines of interest.

TARGET=WAVE exposures *cannot be taken with all slit-grating combinations* as the line lamps can be too bright for the MAMA detectors when used with wide slits. Therefore only certain aperture-grating combinations can be used for MAMA TARGET=WAVE observations (all are available for the CCD). Tables of lines and observed count rates from the line lamp for each grating mode for several different apertures and the complete list of allowed combinations are provided in the “Phase II” area on the STIS web page. Although the slit-wheel repeatability is very high (see “Slit and Grating Wheels” on page 27), observers wishing particularly accurate wavelength calibrations are best off using a slit for their scientific exposures for which there is an allowed slit-grating wavecal; otherwise, the slit wheel will be moved each time they take a wavecal exposure, producing an additional uncertainty.

TARGET=WAVE exposures are processed through the STScI pipeline as individual (unassociated) exposures and are not used to calibrate the scientific data in the pipeline itself. For this reason, the x1dcorr and x2dcorr steps will not be performed by the pipeline when this setting is used.

11.2.2 CR-SPLIT

In order to allow rejection of cosmic rays in post-observation data processing, observers using the STIS CCD should always try (as much as possible given signal-to-noise ratio constraints when in the read-noise-limited regime) to obtain at least two—preferably three or more—identical CCD exposures (see Section 7.2.3). In Phase II, the CR-SPLIT optional parameter (default value 2) allows easy scheduling of such multiple associated exposures. You specify the total exposure time and set CR-SPLIT= n , where n is the number of exposures to break the total observing time into. For example, if the total exposure time is 12 minutes, and CR-SPLIT=3, then three 4 minute exposures will be taken. Those three exposures will be associated with one another, passed through the STScI calibration pipeline as a unit, and a cosmic-ray free image will be produced during pipeline processing (see the “STIS Calibration” Chapter of the HST Data Handbook). Allowed values of CR-SPLIT are integers from 1 to 8. Note that overheads are incurred for each CR-SPLIT subexposure.

11.2.3 Fringe Flat Fields

The STIS CCD exhibits fringing in the far red, limiting the signal-to-noise achievable at wavelengths longward of ~ 7500 Å in the G750L and G750M spectral modes. As discussed in Section 7.2, the best way of eliminating the fringes in the far red is by obtaining contemporaneous flat fields along with the scientific observations. These “fringe flats” must be taken at the same position of the Mode Selection Mechanism as the scientific data. STIS users can insert such contemporaneous fringe flat fields into the same visits as their scientific data, as described below.

Designing your Fringe-Flat-Field Observations

Observers of extended sources will typically want to take their fringe flat fields using the same slits as they use for their scientific targets, since the flat-field lamp will then illuminate the detector in the most similar way to the targets. However, observers of point sources will typically fare better if they use small slits (e.g., those which are otherwise used for echelle observations) for their fringe flat fields. The main reason for this difference is that the PSF of the STIS CCD features a substantial halo in the far red containing up to 20% of the total source flux, which causes the fringes in lamp flat fields to behave differently from those of external sources, especially in the case of point sources (see also Section 7.1.7). Fringe flat fields taken with short slits simulate the spatial structure of point sources significantly better than those taken with long slits.

The slits supported for scientific observations with the G750L and G750M gratings and the associated slits to use for fringe flat fields in the cases of

both extended- and point-source observations in the far red are in Table 11.1.

Table 11.1: Slits for Extended-Source and Point-Source Fringe Flat Fields

Supported Scientific Slit	Fringe Flat Slit for Extended Source Observations	Fringe Flat Slit ¹ for Point Source Observations
52X2	52X2	0.3X0.09
52X2E1	52X2	52X0.1
52X2E2	N/A	52X0.1
52X0.5	52X0.5	0.3X0.09
52X0.5E1	52X0.5	52X0.1
52X0.5E2	N/A	52X0.1
52X0.2	52X0.2	0.3X0.09
52X0.2E1	52X0.2	52X0.1
52X0.2E2	N/A	52X0.1
52X0.2F1	52X0.2F1	52X0.2F1 <i>and</i> 0.3X0.09 (optional)
52X0.1	52X0.1	0.2X0.06
52X0.1E1	52X0.1	52X0.1
52X0.05	52X0.05	0.2X0.06
52X0.05E1	52X0.05	52X0.05

1. Short slits are chosen so as to be concentric with matched long slit. E2 positions are chosen to be concentric with 52X0.1 aperture at row 900.

A few notes are of importance on the use of short slits for obtaining fringe flat fields:

- Fringe removal for sources that are offset from the center of the (long) slit will not be possible with a short-slit fringe flat field; one has to use long-slit fringe flat fields for those cases. A special case in this respect is that of point source spectra with the 52X0.2F1 slit, as the 0.3X0.09 slit (which is in principle the appropriate one to use for fringe flats in that case, cf. Table 11.1) is only a few CCD pixels larger than the occulting bar of the 52X0.2F1 slit. However, a short-slit fringe flat does give a somewhat better fringe correction for the area covered by both the short slit and the 52X0.2F1 slit, so if that area is of particular scientific interest, we recommend taking a short-slit fringe flat as well.

- The limited length of the short slits used for obtaining contemporaneous flat fields of point sources (0.2–0.3 arcsec) does not allow one to sample the full PSF, so that absolute spectrophotometry cannot be performed with the short-slit fringe flat fields alone. However, a comparison with the pipeline-reduced point-source spectrograms will enable a proper flux calibration.
- At wavelengths longward of ~ 7500 , fringing is the dominant calibration concern at high S/N, whereas imperfect charge transfer efficiency (CTE) is the dominant concern at low S/N ratios. We therefore recommend using the “E1” or “E2” pseudo-apertures for faint sources and the normal aperture positions in the long slits for high S/N observations.
- The “E2” aperture positions are, like the “E1” aperture positions, located near row 900 of the detector, and are intended to be used to mitigate CTE effects. However, in order to better align with the 52×0.1 aperture, which is used for fringe flats near row 900, the targeted position is offset about 1 pixel in the dispersion direction from the physical center of each aperture. Fringe flat alignment will be slightly better than when using the “E1” positions, although for the 52×0.2 E2 aperture, the throughput will be slightly reduced. The “E2” positions should only be used for point source observations where fringe flats are needed and CTE is a concern. If a peakup is desired before using the “E2” aperture positions, it should be done using the 52×0.1 E1 aperture.
- The limited length of the short slits used for obtaining contemporaneous flat fields of point sources (0.2–0.3 arcsec) imposes a minimum requirement on the accuracy of the acquisition of target point sources in the slit. The final accuracy should be of the order of 1 pixel (i.e., ~ 0.05 arcsec). In case the observer has to use offset acquisition targets, it is therefore recommended that an ACQ/PEAK exposure in a short slit be performed to ensure centering in both directions (see Chapter 8).

Inserting Fringe Flat Field Exposures in Phase II

You specify a fringe flat field exposure in your Phase II proposal input as follows.

- Specify `Target_Name = CCDFLAT` to indicate the exposure as a fringe flat field. The flat-field exposure will automatically be taken at `CCDGAIN=4`.
- Specify `Number_Of_Iterations = 2` (to allow cosmic-ray rejection and to obtain adequate signal-to-noise)
- Specify `Config`, `Opmode`, `Aperture`, `Sp_Element`, and `Wavelength`.

- Config must be STIS/CCD
- Opmode must be ACCUM
- Aperture must be one of 52X2, 52X0.5, 52X0.2, 52X0.2F1, 52X0.1, 52X0.05, 0.3X0.09, or 0.2X0.06.
- Sp_Element and Wavelength must be one of the following combinations:
 - Sp_Element: G750L and Wavelength: 7751
 - Sp_Element: G750M and Wavelength: one of 6768, 7283, 7795, 8311, 8561, 8825, 9286, 9336, 9806, or 9851.
- Specify Time_Per_Exposure as DEF (Default). The default exposure time is determined from in-flight calibration data and ensures a signal-to-noise of 100 to 1 per pixel for all settings mentioned above and Number_Of_Iterations = 2.
- If the scientific data are taken in binned mode, specify Optional Parameters BINAXIS1 and BINAXIS2 in the same way as for scientific observations. Supported binning factors are 1, 2, and 4.

Two very important issues for fringe flat fields:

- Fringe-flat-field exposures are moved into the occulted period by whenever they occur as the first or last exposure in an orbit. Thus you can fill the unocculted portion of your orbit with scientific observations and take the fringe flat during the occultation by placing it at the beginning or end of the orbit.
- Fringe flat fields are effective *only* if taken *without* a move of the Mode Selection Mechanism between the scientific exposure and the fringe flat field. *Observers must ensure that if the spectral element or wavelength setting is changed during an orbit in which they wish to obtain a fringe flat, then they place the fringe-flat-field exposure immediately before or after the scientific exposure(s) they wish to de-fringe.* In some cases (e.g., for a long series of exposures) the observer may choose to bracket the scientific exposures with fringe-flat-field exposures to be able to account for any thermal drifts.

Please refer to the [Instrument Science Reports 1997-15](#) for more details about near-IR fringe flats; [1997-16](#) which deals with fringing in spectrograms of extended sources; [1998-19](#) (Revision A) which deals with fringing in spectrograms of point sources as well as more general fringing analysis and details related to the 52X0.2F1 aperture; and [1998-29](#) which is a tutorial on the use of IRAF tasks in the `stsdas.hst_calib.stis` package to remove fringes.

11.2.4 Repeat Exposures

A series of multiple repeated identical exposures can be taken most easily using the `Number_Of_Iterations` optional parameter in Phase II. In this way, time-resolved observations at minimum time intervals of roughly 20 seconds for the CCD (if subarrays are used) and 30 seconds for the MAMA can be taken in ACCUM operating mode. The output of this mode is a series of identical exposures. If your exposure time is 60 seconds, and you set `Number_Of_Iterations=20`, you will obtain twenty 60 second exposures. These twenty exposures will be associated with one another and processed through the pipeline as a unit—the individual exposures will be fully calibrated and a summed image will also be produced for MAMA data and a cosmic-ray-rejected image for CCD data (see also Chapter 15).

11.3 Patterns and Dithering

A *pattern* refers to a series of exposures of a single target taken at slightly different telescope pointings, with the same set of guide stars. For STIS, patterns are commonly used to:

- *Dither* to decrease the effects of small-scale detector nonuniformity, eliminate hot pixels, and/or increase the spatial resolution (the latter requires subpixel stepping) by offsetting the target along a long slit in the spatial direction for spectroscopic observations, or performing a small stepping pattern for imaging or slitless spectroscopic observations (see Section 11.3.5).
- Spectroscopically map out a two-dimensional region of the sky, by stepping the slit across the object of interest.
- Spectroscopically subsample the line-spread function by stepping a fraction of a pixel along the dispersion direction—see Section 12.6.

Predefined patterns were available in Cycles 7 and 8 for STIS, as the RPS2 Optional Parameter `PATTERN`, and for WFPC2, as the Optional Parameter `DITHER-TYPE`. In Cycles 9 through 11, patterns were defined and then added to exposures as special requirements. In the APT Orbit Planner, this approach was replaced by the use of Pattern containers. The observer selects a pattern (or constructs a composite pattern) from a list of generic and instrument-specific patterns, and then defines one or more pattern containers which use this selected pattern. The exposures to be dithered are then put into these containers.

The predefined STIS patterns have a number of adjustable parameters. All patterns allow the `Point_Spacing`, which is given in units of arc-seconds, as well as the `Pattern_Orient`, given in units of degrees,

to be adjusted by the observer. Specifying `Center_Pattern = YES`, will cause the pattern as a whole to be centered at the specified coordinates; otherwise, the given coordinates will apply to the first point in the pattern.

A full description of all patterns, including illustrations and a list of all adjustable parameters and default values for each pattern type, are given in the [HST Phase II Proposal Instructions](#). Additional examples and advice are given in the Dither Handbook at:

http://www.stsci.edu/instruments/wfpc2/Wfpc2_driz/dither_handbook.html.

11.3.1 STIS Imaging Patterns

`STIS-SPIRAL-DITH` can be used to make a mosaic of images. It performs a spiral dither pattern, starting at the center and moving outward counterclockwise. For this pattern, both the `Number_of_Points` and the `Point_Spacing` (in arc-seconds) must be specified by the observer.

`STIS-CCD-BOX` and `STIS-MAMA-BOX` are parallelograms based on the `BOX` patterns used with WFPC2 and STIS in Cycle 8 to dither images. The default parameters for these two patterns give offsets in integer numbers of pixels along the X-axis and Y-axis, which can be used, for example, to dither hot pixels. By dividing the default point spacing by 2, one can achieve half-pixel shifts in each coordinate to improve spatial sampling.

11.3.2 STIS Spectroscopic Patterns

`STIS-ALONG-SLIT`, which steps the target along the slit, can be used to dither hot pixels (integer pixel steps) or to improve spatial sampling (fractional pixel steps) in spectroscopic images (see Figure 11.7).

`STIS-PERP-TO-SLIT` can be used to step the slit across an extended source to map the spectral characteristics of the source (see Figure 11.8). It can also be used to subsample the line-spread function by moving a target by fractions of a pixel.

For both of these patterns, the `Point_Spacing` (in arc-seconds) and the `Number_of_Points` must be specified by the observer.

11.3.3 Generic Patterns

Generic patterns, available for all instruments, have been added for flexibility in pattern design. The generic `LINE` pattern allows for movement along a line at an arbitrary angle. The generic `SPIRAL` pattern is essentially the same as the `STIS-SPIRAL-DITH`.

11.3.4 Combining Patterns

A feature that was introduced during Cycle 9 is the ability to combine two patterns. After selecting a pattern and defining the parameters, you can choose to add a secondary pattern. In this case, the secondary pattern is executed at each point in the primary pattern. It can either be centered on the primary points, or can use the primary points as its initial points. For example, instead of just stepping a slit across an extended target at five points with `STIS-PERP-TO-SLIT`, you can add `STIS-ALONG-SLIT` with two points to make a 5x2 grid of observations. If `CENTER_PATTERN=YES` for both patterns, the grid will be centered on the target position. To check that you have specified a pattern correctly, you can display it using the `APT`.

Figure 11.7: Stepping Target Along Long Slit to dither hot pixels or improve spatial sampling. This example shows the pattern *STIS-ALONG-SLIT*, with *NUMBER_OF_POINTS* = 5 and *POINT_SPACING* = 0.15 (arcsec).

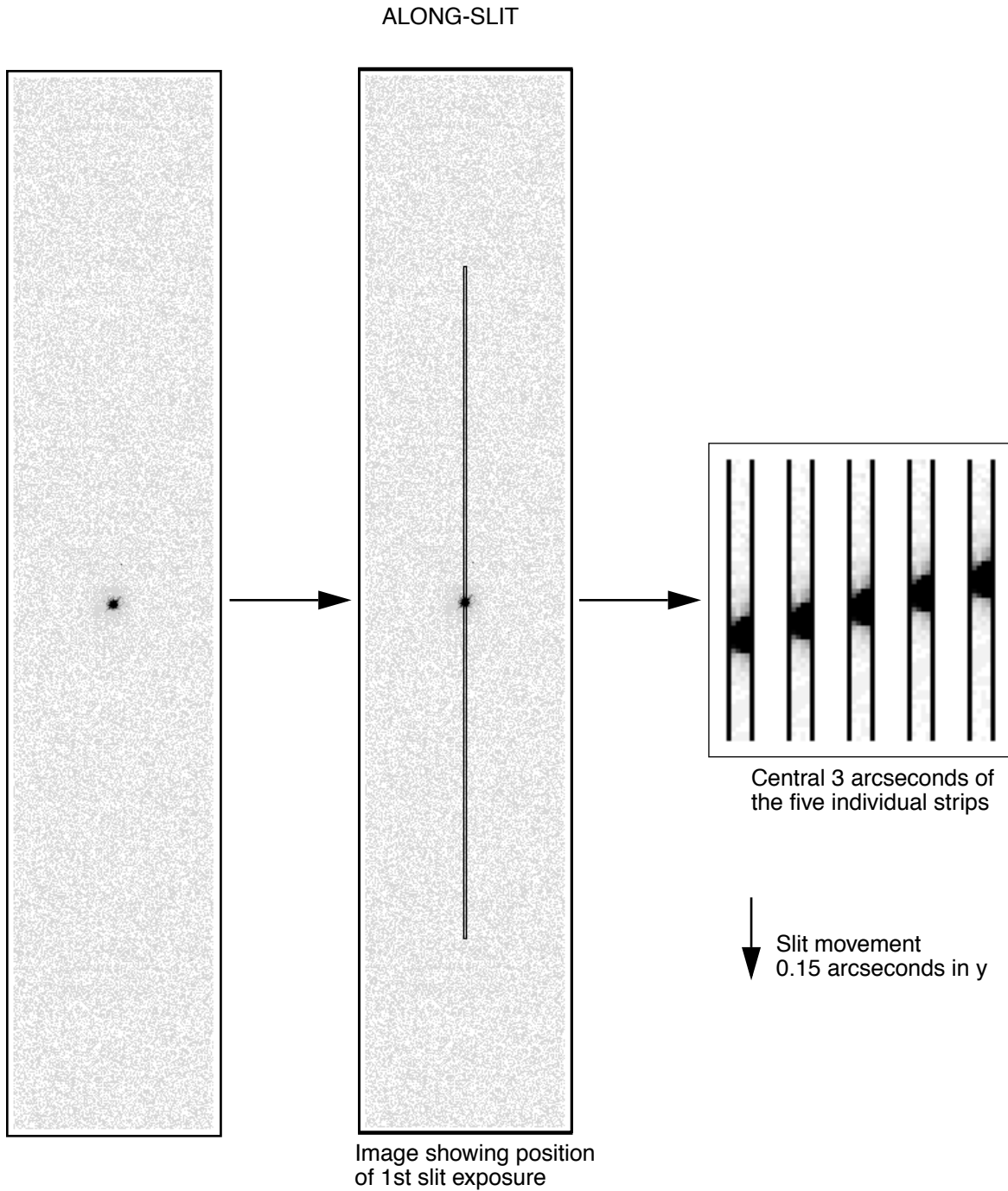
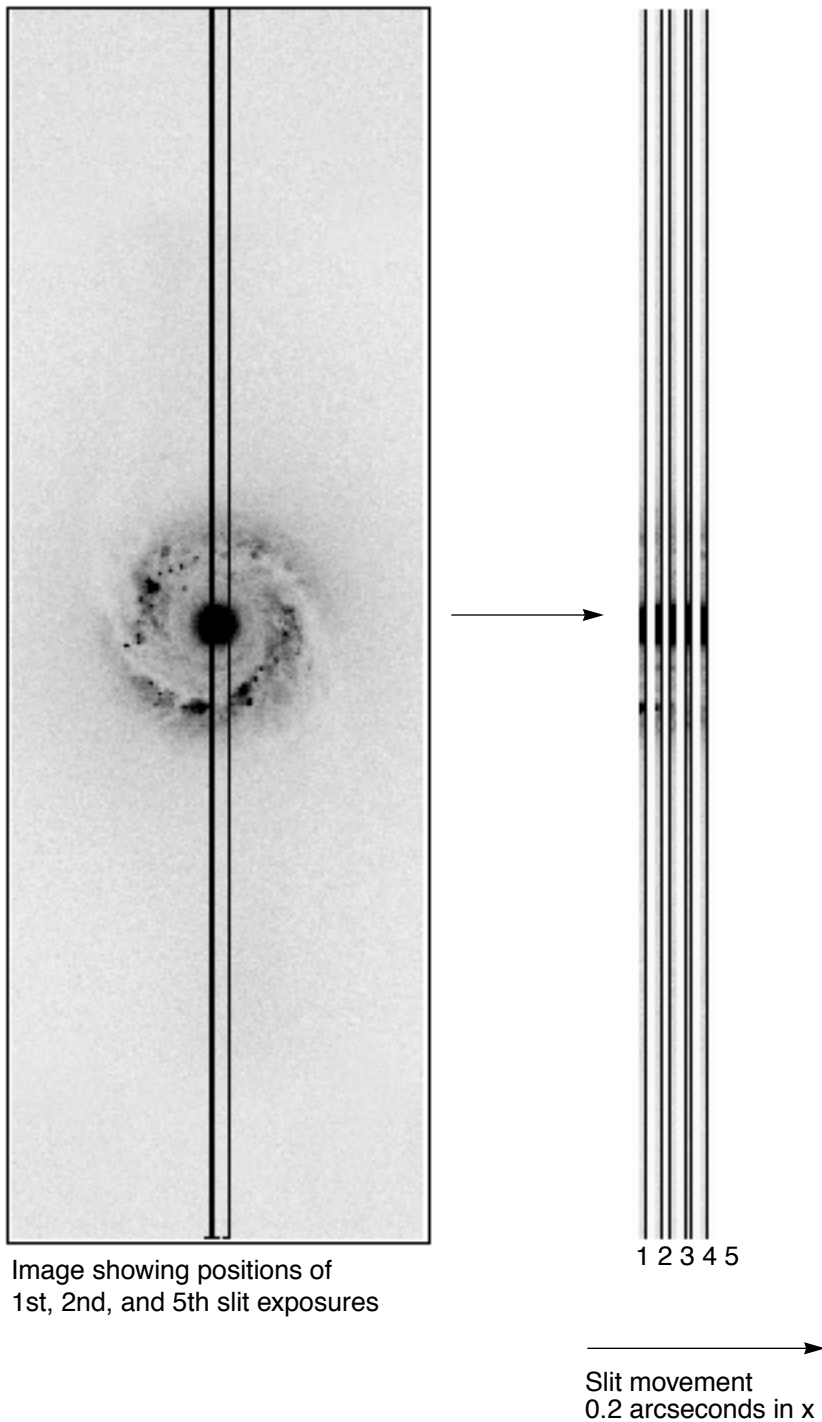


Figure 11.8: Stepping Target Perpendicular to Slit to Map 2-D Region of Sky. This example shows the pattern STIS-PERP-TO-SLIT, with NUMBER_OF_POINTS = 5 and POINT_SPACING = 0.2 (arcsec).



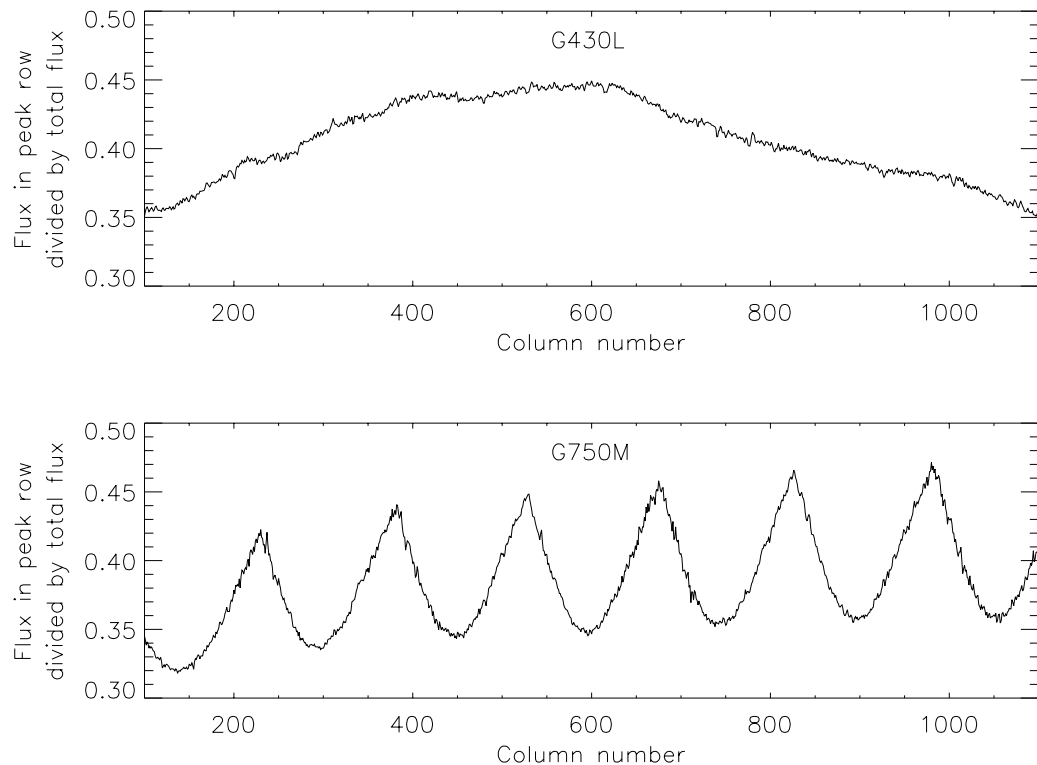
11.3.5 Dither Strategies

There is no single observing strategy that is entirely satisfactory in all circumstances for STIS. One must consider cosmic rays, hot pixels (pixels with high, time-variable dark current), and spatial undersampling of the image. One strategy that can be used to minimize the effects of undersampling and to reduce the effects of hot pixels is to *dither*, that is, to offset the telescope between exposures by either integer or subpixel steps. The best choice for the number and size of the dithers depends on the amount of time available and the goals of the project. In the following we will address a few issues related to dithering:

- ***Undersampling of images:*** Individual images taken with subpixel offsets can be combined to form an image with higher spatial resolution than that of the original images. A single dither from the original pixel position—call it (0,0)—to one offset by half a pixel in both x and y —(0.5,0.5)—will produce a gain in spatial information. On the other hand, very little extra information is gained from obtaining more than four positions. Therefore the recommended number of subpixel dither positions is between 2 and 4. Note that the STIS CCD only marginally undersamples the HST PSF at optical wavelengths, so that the overall gain will not be as substantial as in, e.g., the case of the WF CCDs of WFPC2.
- ***Undersampling of spectral images:*** The spatial undersampling of compact sources in spectral images becomes apparent after the images are rectified. Interpolation during the rectification process spreads flux from the local peak row of the spectrum into adjacent rows. The result is undulation of the flux level in the individual spectral rows of the rectified image. If the spectrum is nearly horizontal on the detector (which is the case for gratings G140L, G230LB, G230MB, G430L, and G750L), the resulting undulation pattern is broad and irregular. On the other hand, if the spectrum has an appreciable tilt across the detector (as for gratings G140M, G230M, G230L, G430M, and G750M; see e.g., STIS Instrument Science Report 1998-19), the undulation is quasi-periodic. Two representative cases are shown in Figure 11.9, which displays the flux in the peak row in the rectified image normalized by the total flux for stellar observations taken with G430L and G750M. Note that this effect is inconsequential in most cases: if the source is unresolved, several rows of the spectrum will be extracted to make a single spectrum, eliminating the effect; if the source is sufficiently extended to be well sampled, the undulations will not occur. A problematic situation is encountered when row-by-row spectral analyses are needed of an extended component which is affected by the undulations produced by a compact component (e.g., near the center of a galaxy containing an active nucleus). For example, kinematic measurements of spatially

extended emission or absorption lines can be affected in cases where a compact continuum component produces a baseline that fluctuates rapidly across the spectral lines of interest. The remedy is to perform spatial dithering by a non-integer number of pixels along the slit, (e.g., $N+0.5$ pixels; see below under “Dithering Spectroscopic Observations”), then combine the dithered images before rectification.

Figure 11.9: Undulations in the flux level of individual rows in rectified spectra of point sources, caused by rectification of spatially undersampled spectral images



- **Hot Pixels:** There are three ways to deal with hot pixels: (1) correct using “superdarks” constructed from darks taken on the day of the observation (these can be created using STSDAS task `daydark`); (2) use a task such as `warmpix` in STSDAS to filter out the known hot pixels. Hot pixels are flagged in the data quality array during dark subtraction and propagate through to the output images; (3) dither by an integer number of pixels. Note that the integer dither strategy would ideally consist of six images, i.e., two `CR-SPLIT` images at each of three different dither positions. The reason is that in addition to hot pixels, low or *cold* pixels can be present and simple strategies

selecting the minimum of two pixel values can fail. However, even four images (two each at two dither positions) will greatly aid in eliminating hot-pixel artifacts.

- The MAMA detectors show few hot pixels and they appear to evolve slowly. Thus they are usually not an issue. Nevertheless, dithering is an easy way to avoid them, and there is no read noise or cosmic-ray removal penalty for doing so.
- ***Cosmic Rays:*** Although dithering naturally provides many images (or spectra) of the same field it is better to take several exposures at each individual pointing in order to remove cosmic rays. In principle, it should be possible to remove cosmic rays using dithered data with only one exposure per position. Indeed, publicly released software is available for this task (the **dither** package within IRAF/STSDAS, see below). However, this software is *only applicable to imaging mode observations*, and one should realize that calibrating dithered data with only one exposure per position will require significantly more work (and CPU cycles) than processing data with two or more exposures per position. Hence we generally recommend obtaining two or more exposures (i.e., CR-SPLIT) at each position in the dithered sequence, especially for spectroscopy mode observations (see also Section 7.2.3).
- ***Dithering Spectroscopic Observations:*** In case of spectroscopic observations, extra care should be taken in choosing the optimum dither strategy, which depends on the spatial extent of the extractions and the nature of the science target. However, beware that dithering spectroscopic observations will only be useful if your exposure times are long enough, otherwise your spectra will become severely read-noise limited (see page Section 7.2.3).
 - ***Spectra of Point Sources:*** 1-D first-order spectra of point sources are usually extracted over 7 spatial pixels for CCD, 11 spatial pixels for MAMA (e.g., during STIS pipeline processing). Hence, the effect of hot pixels is exacerbated compared to the case of imaging observations. If sufficient time is available to perform dithers, the best practice is to dither the target by an offset large enough to avoid having the same hot pixels fall in the individual extracted spectrograms. This means that you should move the spectrum by more than 0.55 arcsec (for an 11 pixel extraction) along the slit between dither positions. Unfortunately, that will make cosmic ray removal more difficult unless you get two or more spectra at each individual pointing (using CR-SPLIT). Ideally, taking CR-SPLIT=3 observations at multiple dither positions allows the most robust cosmic ray rejection *and* hot pixel removal in post-observation data processing for spectra.

- ***Spectra of Extended Sources:*** For extended sources, one should consider the spatial size of the extractions to be made during post-observation analysis before deciding on a dither strategy. To enable a proper rejection of hot pixels within the extractions, the telescope move between dithers should be larger than the spatial size of the extractions made. In case the region of interest is at or near a sharp peak in the surface brightness distribution, one should consider dithering by a non-integer number of pixels to deal with the undulation issue due to undersampling (cf. above).
- ***Accuracy of Dithering:*** During the Hubble Deep Field campaign, nearly all dithers were placed to within 10 milliarcsec (mas) (during ± 1.3 arcsec offsets and returns separated by multiple days), although in a few cases the dither was off by more than 25 mas, and on one occasion (out of 107 reacquisitions) the telescope locked on a secondary FGS peak causing the pointing to be off by approximately 1 arcsec, as well as a field rotation of about 4 arcminutes. The software which was developed for the Hubble Deep Field is able to reconstruct images even for these nonoptimal dithers, still gaining in resolution over nondithered data. This software is presently available in STS-DAS (the **dither** package) and is based on the variable-pixel linear-reconstruction technique developed by Fruchter and Hook (known as drizzling). It has been used successfully on STIS imaging data.
- ***Flat-Field Accuracy:*** For the MAMAs, the accuracy of flat fielding has not been extensively tested, especially for the imaging modes. Dithering on scales of several pixels can help to smooth out pixel-to-pixel variations in detector sensitivity. For this purpose it is best to use dither steps that are not integral multiples of half a pixel (the intrinsic high-resolution format of the MAMAs); integral pixel steps should be used instead.

The simplest way to schedule dithers with STIS is to use the patterns STIS-CCD-BOX or STIS-MAMA-BOX (four-point parallelogram dithers, centering on fractional pixels to gain spatial resolution) or, for spectroscopic observations that use a long slit, the pattern STIS-ALONG-SLIT (for linear dithers in the AXIS2 direction, with user-specified offsets). An alternate approach is to use POS TARG.

Note that large dithers will incur small errors due to the camera geometric distortion which increases toward the CCD corners and alters the image scale by about 1% at the corners. For instance, a 20 pixel offset at the field center will suffer a 0.2 pixel error at the CCD corners. Large dithers may also occasionally require a different set of guide stars for each pointing, thus greatly reducing the expected pointing accuracy (accuracy of only ~ 1 arcsec due to limits to the accuracy of the Guide Star Catalogue).

For related articles on dither strategies, see the following papers (all available through the STScI web pages): “A Package for the Reduction of Dithered Undersampled Images,” by Fruchter et al., in the *1997 HST Calibration Workshop Proceedings*, the *WFPC2 Instrument Science Report 98-04*, and “A Method for the Linear Reconstruction of Undersampled Images” by Fruchter & Hook (2002, *PASP*, 114, 144), and the Dither Handbook of Koekemoer et al., which can be found at:

http://www.stsci.edu/instruments/wfpc2/Wfpc2_driz/dither_handbook.html.

11.4 Fixing Orientation on the Sky

STIS users, particularly those using the long slit to observe extended sources, will commonly wish to specify the orientation of the slit on the sky. Observers planning coordinated parallel observations may also wish to specify the orientation of the HST focal plane, so as to place the appropriate instrument to cover a given patch of sky. When you set the orientation of the telescope, you effectively constrain the times when your observation can be scheduled, since HST must maintain a spacecraft orientation (sometimes called *roll angle*) which keeps its solar panels roughly perpendicular to the incoming sunlight.

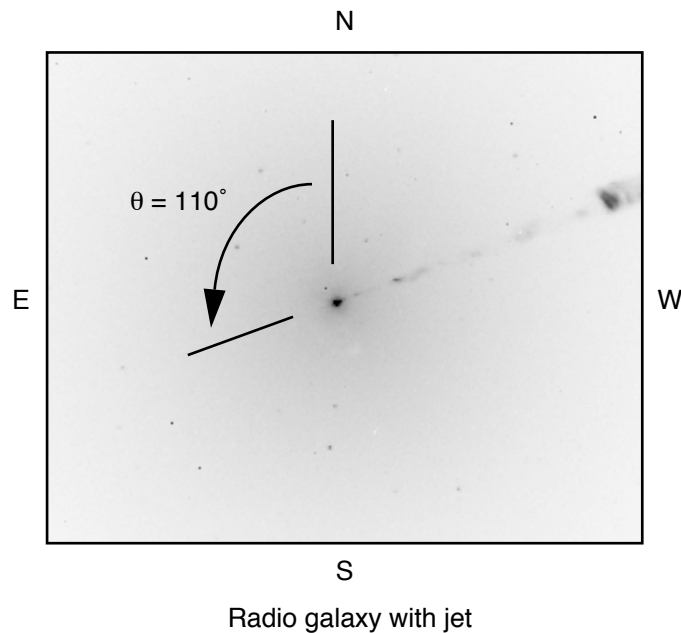
The orientation of the spacecraft (and therefore of the STIS long slits which are fixed in relation to the HST focal plane) is controlled by the ORIENT special requirement, which is entered during Phase II. The Phase II Proposal Instructions will contain a detailed description of orientations and how to specify them. A specific orientation can be set, or a range of allowed orientations (e.g., 90–110 degrees) can be given. The tighter the constraints, the more difficult it will be to schedule the observation.

The ORIENT parameter gives the orientation of the HST focal plane projected onto the sky and is defined by the U2 and U3 axes. Figure 3.2 shows the HST focal plane containing all the HST instruments, with the U2 and U3 axes defined. Figure 11.1 shows the relationship between these axes and the PA of the long slit on the sky. Note that the long slit is approximately aligned with the detector’s AXIS2, i.e., it is directly perpendicular to the dispersion axis (AXIS1). The important point to note is that if you fix the orientation of the long slit on the sky to be PA X , where X is measured in degrees east of north, then the ORIENT parameter (which determines where the other HST instruments lie for parallel observations) is given as $X+45$ or $X+225$ degrees. Likewise, for PRISM mode observations, if you wish to fix the orientation of the spatial direction (i.e., perpendicular to the dispersion) to be X , then the ORIENT parameter should be set to $X+45$ or $X+225$ degrees. It is possible during Phase II to specify more than one permissible ORIENT range.

Users who wish to determine their orientation requirements using existing HST images should consult the HST Observatory Support Group's instructions at <http://www.stsci.edu/instruments/observatory/faq.html>. It is especially important to be careful when using HST data taken before 15 Sept. 1997, as for such data there may be errors of $\sim 0.5^\circ$ in the ORIENT and PA_V3 header keywords.

We show two examples below. Figure 11.10 illustrates how to set the ORIENT parameter to place the long slit along the M87 jet. Figure 11.11 illustrates how to set the ORIENT parameter to fix the dispersion axis for PRISM observations to be perpendicular to a double star system.

Figure 11.10: Placing the STIS Long Slit Along the Jet of M87



$\theta = \text{Angle of jet on sky} = 110^\circ$

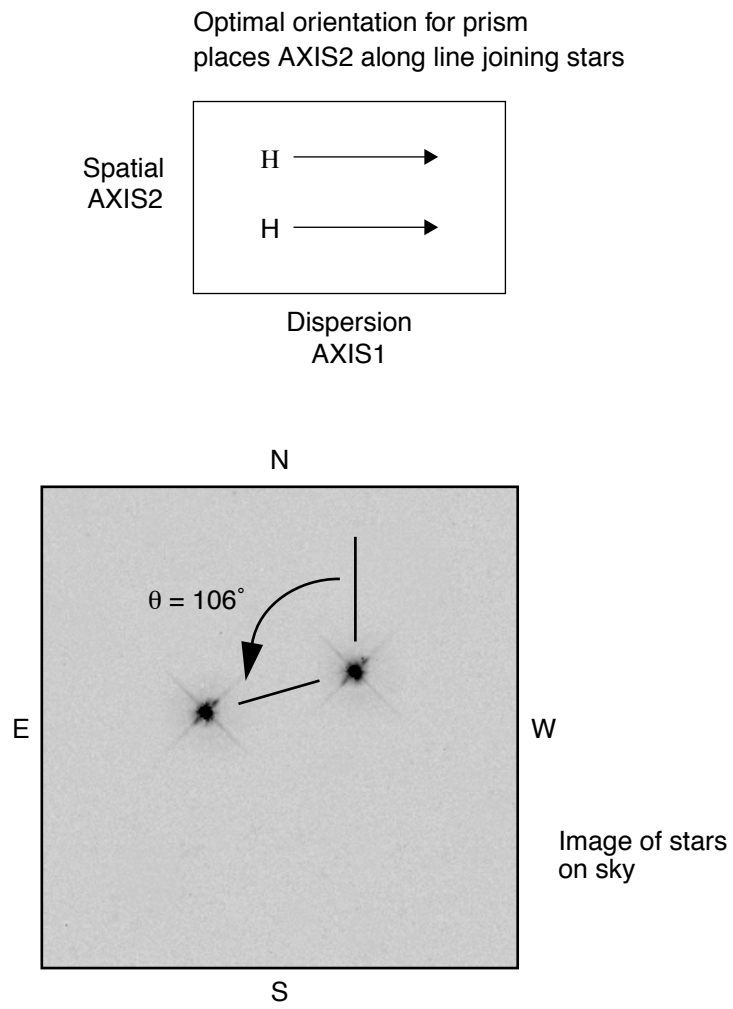
To place long slit axis (AXIS2 on the CCD) on jet:

Orient = $\theta + 45^\circ$ or $\theta + 225^\circ$

Orient = $110^\circ + 45^\circ$ or $110^\circ + 225^\circ$

Orient = 155° or 335°

Figure 11.11: Placing Dispersion Direction Perpendicular to a Binary Star System



$\theta = \text{Angle of line joining stars on sky} = 106^\circ$

To place AXIS2 along θ :

Orient = $\theta + 45^\circ$ or $\theta + 225^\circ$

Orient = $106^\circ + 45^\circ$ or $106^\circ + 225^\circ$

Orient = 151° or 331°

This relation between ORIENT and position angle will satisfy most needs. Observers with extremely stringent orientation requirements should be aware that each STIS aperture has a specific U3 offset angle which is close to, *but not equal to*, 45°. In Table 11.2 below we list the offset angles for all supported spectroscopic slits. If ultimate precision is required, observers may wish to use the offset angles given in this table instead of the standard 45°. Observers should also note that the position angles for the 52'' long slits have recently been revised by up to 0.33°.

Table 11.2: Offset angles between supported STIS slits and the spacecraft orientation reference vector U3.

STIS Aperture	Offset Angle (degrees)
0.2X0.06	44.94
0.2X0.09	44.94
0.2X0.2	44.94
6X0.2	45.31
0.1X0.03	44.94
52X0.05	45.35
52X0.1	45.35
52X0.2	45.35
52X0.5	45.35
52X2	45.35
0.2X0.06FPA	44.94
0.2X0.06FPB	44.94
0.2X0.06FPC	44.94
0.2X0.06FPD	44.94
0.2X0.06FPE	44.94
0.2X0.2FPA	44.94
0.2X0.2FPB	44.94
0.2X0.2FPC	44.94
0.2X0.2FPD	44.94
0.2X0.2FPE	44.94
52X0.2F1	46.30
0.3X0.05ND	44.95
0.2X0.05ND	44.94

Special Uses of STIS

In this chapter. . .

12.1 Slitless First-Order Spectroscopy / 253
12.2 Long-Slit Echelle Spectroscopy / 256
12.3 Time-Resolved Observations / 257
12.4 Observing Too-Bright Objects with STIS / 259
12.5 High Signal-to-Noise Ratio Observations / 261
12.6 Improving the Sampling of the Line-Spread Function / 265
12.7 Considerations for Observing Planetary Targets / 266
12.8 Parallel Observing with STIS / 267
12.9 Coronagraphic Spectroscopy / 270
12.10 Coronagraphic Imaging—50CORON / 273

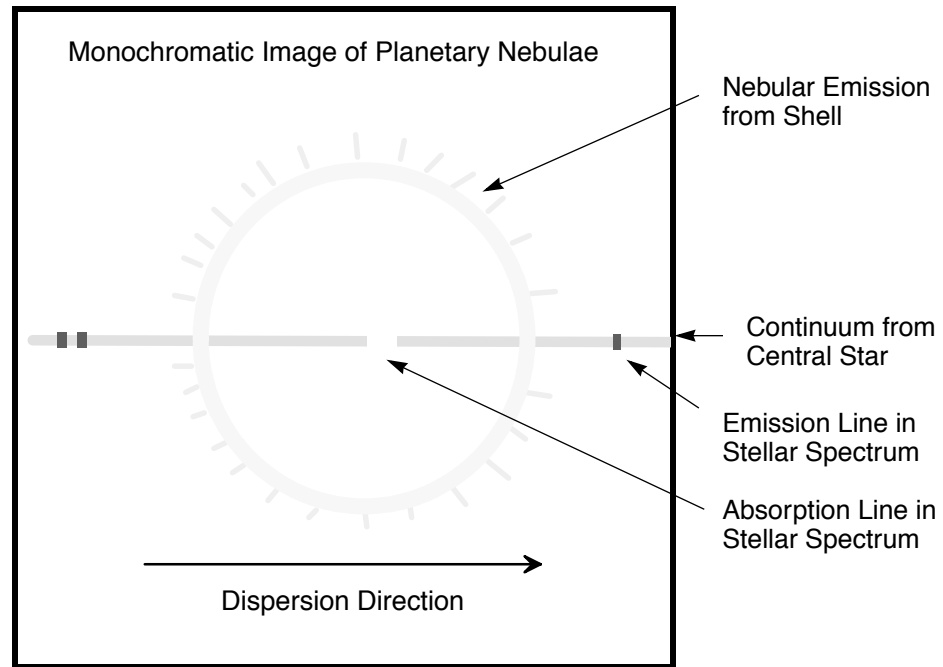
In this chapter we describe some of the nonstandard uses of STIS and provide guidance in the use of the standard capabilities for specific scientific purposes.

12.1 Slitless First-Order Spectroscopy

The vast majority of STIS first-order grating mode observations use a long slit. The use of a long slit ensures a clean separation of emission lines arising from different spatial features. However, all of STIS's first-order gratings as well as the NUV-PRISM (see Table 4.1) can also be used slitless or with a wide slit to obtain emission-line images. Figure 12.1 below shows a schematic example of a slitless spectrogram. Figure 4.9 shows an image of SN1987A observed using the 52X2 aperture, and as the source is smaller than the slit, this is effectively a slitless image.

The Advanced Camera for Surveys (ACS) also can be used for slitless spectroscopy. A comparison of STIS and ACS spectroscopy can be found in Section 4.1.2.

Figure 12.1: Schematic Slitless Spectrogram of Planetary Nebula



When STIS is used slitless (or with a wide slit), the image obtained will be the sum of a series of shifted monochromatic images of the field of view. The range of wavelengths covered in the series of monochromatic images is dictated by the spectral range of the grating. The result is that there is *not* a one-to-one mapping of pixel location to wavelength in your image or of pixel location to spatial location on the sky. Depending on the structure of your source and the grating you use, it may be easy to deconvolve the spatial and spectral information, or it may be very difficult.

Slitless spectroscopy can be employed either for prime or parallel STIS observing, (although MAMA pure parallels are not allowed). If you are designing a slitless spectroscopic observation there are a few important points to keep in mind:

- The more complex the emission-line, velocity, and spatial structure of your target field, the more difficult it will be to deconvolve the spatial and spectral information. It is important to match the grating you choose to the structure of your source. Gratings which produce images of multiple, kinematically resolved emission lines will be the most challenging to deconvolve. At the other extreme, a grating which covers only a single strong emission line at a resolution where the lines are kinematically unresolved will produce a clean image of

the source in the single emission line (see Figure 12.1, above). You may also wish to specify the orientation for slitless spectroscopic observations to ensure that the most complex source structure is oriented perpendicular to the dispersion axis (see Section 11.4).

- Since each point in the sky emits geocoronal light, the background due to the geocoronal emission lines (Lyman- α λ 1216, [O I] $\lambda\lambda$ 1302,1306, and occasionally on the day side O I] λ 1356 and [O II] λ 2471; see “Geocoronal Emission and Shadow” on page 102) will be observed at all pixels in the image when a slitless spectrum is obtained which covers these wavelengths. This background must be taken into account in your signal-to-noise calculations. For this reason, you may wish to consider using one of the two longpass ultraviolet blocking filters (see Section 5.3.4), instead of a clear aperture when performing ultraviolet slitless spectroscopy. Note that when a spectroscopic exposure is obtained with a slit, these sky emission lines are localized in the resulting image to the pixels at the corresponding wavelengths.
- Slitless spectroscopic data will not be fully calibrated by the STScI STIS pipeline. Slitless spectroscopic data will be passed through the first phase of calibration and a flat-fielded calibrated image will be produced; however, the pipeline will not attempt to spectroscopically calibrate the data. This process must be interactively done by the observer since, as described above, ambiguous overlap of spatial and spectral information will occur. The **slitless** task in the **stsdas.contrib** package (originally contributed by ST-ECF) is available to aid in performing this post-pipeline processing. The Spectrographs Branch at STScI is currently working on a self-extraction tool for objective-prism data.

In order to properly calibrate slitless data it is necessary to know the position of each source along the dispersion direction. To do this it is usually necessary to take in the same visit a STIS image of the field for which you are obtaining slitless spectroscopy. Variations in the positioning of the Mode Select Mechanism (MSM), which contains the mirrors and gratings, can result in an uncertainty of the position of an image or spectrum on the detector by as much as five pixels, and an additional special calibration may be needed in order to fix the absolute offset between the images and the spectrograms. The standard STIS ACQ procedure automatically measures the offset between the location of a star and a reference aperture on the CCD detector and uses this to place the target accurately in the desired slit. So if the ACQ target appears in the field of view, there is no need for an additional image to calibrate the MSM offset, although a separate full field image may still be needed to measure the relative positions of other sources with respect to the ACQ target. In cases where no STIS ACQ exposure is done, an image of the field should be

taken either immediately following or immediately preceding a lamp image taken through a narrow slit. For the CCD, a 1 second tungsten lamp exposure with the 52X0.1 slit will do nicely. This will allow the MSM offset for that image to be determined. It is important that no MSM motion (mirror or grating change) occur between the sky image and the lamp image of the slit. The MSM offset for the spectrographic exposure itself can usually be measured from the standard wavecal exposure. If extremely precise alignment between the spectrum and the field image in the cross dispersion direction is also required for source identification, this procedure may require some modifications, and observers should consult their contact scientist or the STScI help desk at help@stsci.edu.

Finally, we note that to achieve an accurate wavelength calibration for targets observed in slitless mode, when those targets are well displaced from the nominal AXIS1 center, the dispersion coefficients at the off-nominal centerings must be well known. Currently, the incidence-angle offset corrections are based on ground calibration data and are somewhat less accurate than the on-axis dispersion solutions. We recommend that observers consult help@stsci.edu if they are concerned about the calibration of observations taken of targets which are expected to be off-center by more than 1 arcsecond in the dispersion direction.

12.2 Long-Slit Echelle Spectroscopy

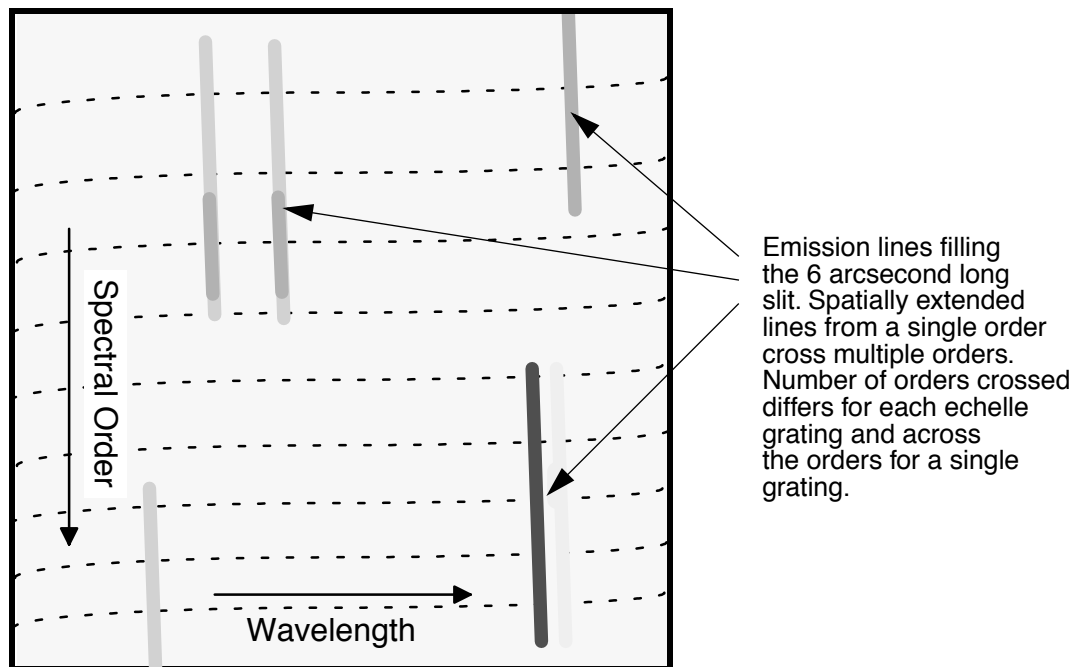
The STIS echelle gratings (see Section 4.3.1) were designed to maximize the spectral range covered in a single echellogram. The orders are therefore closely spaced and to avoid overlap between orders, short echelle slits must be used. Indeed, the majority of STIS echelle observations are of point sources and use these customized echelle slits (see Section 4.3.2). Nevertheless, at the price of confusion due to order overlap, the echelle gratings can be used with a long slit to obtain high-resolution spectroscopy of extended objects, or they can be used slitless with a full clear, filtered, or ND aperture. An example of a scientific application that would benefit from long-slit echelle spectroscopy might be observations designed to map the kinematics of planetary nebulae and stellar outflows around young stars. Observers contemplating such observations should be aware that the problems of order overlap, scattered light, and the broad wings of the PSF from the Optical Telescope Assembly will make accurate calibration and line-profile work extremely complex for extended sources with a continuum (see Section 13.7).

The 6X0.2 slit (6 arcseconds in the spatial direction and 0.2 arcseconds wide in the dispersion direction) is supported for use with all four of the echelle gratings. However, observers should be aware of the ambiguous

overlap in the resulting echellogram that makes the reduction of long-slit echelle data an inherently source-dependent and interactive process.

Observers should also note that, for long-slit echelle spectra, images of monochromatic lines on the detector are rotated by an angle that differs significantly from the physical angle of the slit, and which varies from one echelle grating to another. When using the 6X0.2 aperture with an echelle grating, the same aperture is also used for the auto-wavecal, and this wavecal image can be used to measure the change of the wavelength scale as a function of position along the slit. However, long-slit wavecal lines will overlap multiple orders, causing **calstis** to calculate incorrect wavelength and spatial offsets. Users may wish to consider adding an additional GO wavecal exposure using a smaller aperture (e.g., 0.2X0.2) to more easily derive an accurate wavelength scale for their science image. When using any other long-slit aperture with the echelle gratings, the auto-wavecal will be done by default with a small aperture. In such cases, the user may wish to add an additional GO wavecal with the 6X0.2 aperture in order to measure the change in the projected slit angle.

Figure 12.2: Echelle Long-Slit Spectrogram of Extended Emission-Line Source filling the Long Slit (partial image)



12.3 Time-Resolved Observations

There are two ways to obtain time-resolved spectroscopic and imaging observations with STIS:

- Use the MAMA `TIME-TAG` operating mode (described in Section 11.1.3) in the ultraviolet.
- Take a series of multiple, short, identical repeated observations (described in Section 11.2.4) of your target in `ACCUM` operating mode with either the CCD or the MAMAs.

Both the data products received (an event stream in the case of `TIME-TAG` and a series of individual images from each `ACCUM`-mode exposure in a repeated sequence) and the basic parameters of the time-resolved observations (e.g., sample time, interval between samples, total number of samples or equivalently duration) differ dramatically in these modes. In Table 12.1 we summarize and contrast the ranges of parameter space covered by the different methods of obtaining time-resolved observations.

The information presented in Table 12.1 can be summarized into the following set of guidelines for performing time-resolved observations with STIS:

- If you wish to observe variability on second or less timescales, observe in the ultraviolet using `TIME-TAG` mode. Figure 12.3 shows an example of a time profile of the Crab Pulsar obtained with STIS G140L in `TIME-TAG` mode overlaid on prior HSP observations.
- In the optical, variability can be observed on tens-of-seconds timescales using subarrays and multiple exposures with the CCD.
- In the ultraviolet, variability on the several-minute or more timescale can be observed by multiple `ACCUM`-mode exposures with the MAMAs or using `TIME-TAG` (subject to count rate limitations).
- Remember that a series of identical exposures that are each less than three minutes in length incurs additional data management overheads when compared to longer exposures (see Table 9.2).
- Remember that single MAMA visits are limited to five orbits (see Chapter 2, so continuous variability can be tracked for only that duration with the MAMAs.

Table 12.1: Summary of Time-Resolved Imaging and Spectroscopy

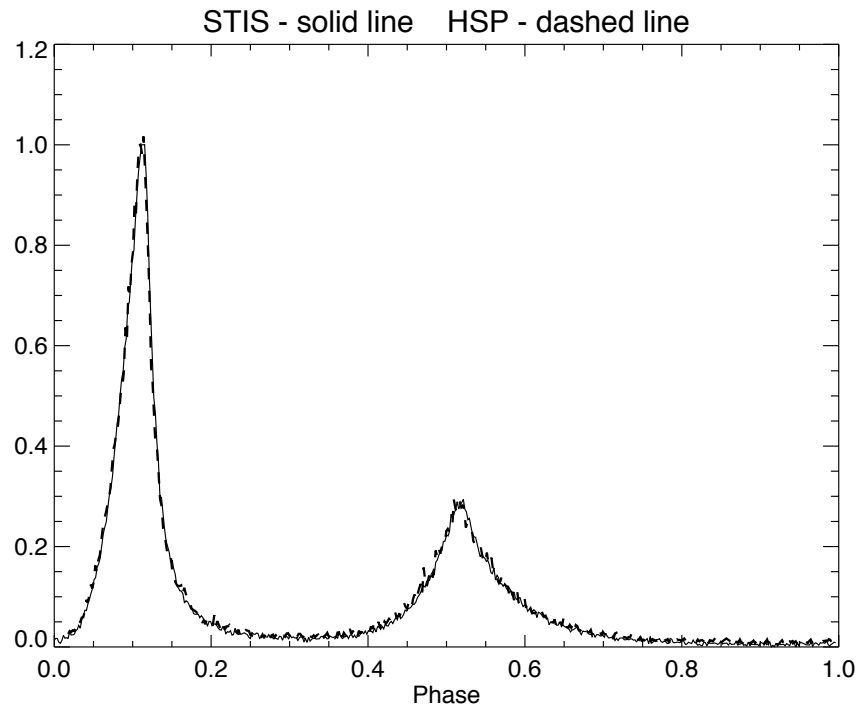
Observation Type	Detector	Spectral Range (Å)	Minimum Sample Time (τ)	Interval Between Samples ($\Delta\tau$)	Total Duration of Uninterrupted Time Series ¹
Repeat ACCUM	CCD	2000– 10,300	0.1 sec	45 sec—full frame 20 sec—1060 x 32 subarray	For $\tau > 3$ min, no limit For $\tau < 3$ min: dur= $(\tau + \Delta\tau) \times 7$, full frame (1062 x 1044) dur= $(\tau + \Delta\tau) \times 256$, 1060 x 32 subarray
Repeat ACCUM	MAMAs	1150– 3100	0.1 sec	30 sec for $\tau > 3$ min 2 min for $\tau < 3$ min	No limit ² No limit
TIME-TAG ³	MAMAs	1150– 3100	125 μ sec	0	$6.0 \times 10^7 / R$ seconds if $R < 21,000$ counts/sec or $4.0 \times 10^6 / R$ seconds if $R > 21,000$ counts/sec where R is rate in counts/sec,

1. τ = duration of an individual exposure.

2. Note, with BINAXIS1=BINAXIS2=2, 7 images separated by 1 minute and each of duration $\tau < 3$ minutes can be obtained.

3. Above 30,000 counts/sec timing accuracy suffers.

Figure 12.3: Crab Pulsar Observed Using the STIS FUV-MAMA with G140L in TIME-TAG Mode. The resulting integrated time profile is shown superimposed on the early results from the HSP. The full period of the Crab pulsar is 33 milliseconds. (Figure courtesy of Don Lindler and Ted Gull, see also Gull et al. 1998, ApJ, 495, L51).



12.4 Observing Too-Bright Objects with STIS

As described in Section 7.6, the STIS MAMA detectors would suffer damage at high local and global count rates. The MAMA detectors also suffer uncorrectable non-linearity at similar count rates (see Section 7.4.4). There are therefore configuration-specific count-rate limits for all observations that use the MAMA detectors; sources brighter than allowed by the limits *cannot be observed* in that configuration.

The STIS CCDs are not subject to the same bright-object constraints, as the CCD cannot be damaged by observations of bright sources. At high *accumulated* count/pixel levels, however, the CCD saturates and charge bleeds along the columns. When `CCDGAIN=4`, the saturated counts can be recovered by summing over the pixels bled into, and this spatially integrated count rate remain linear with exposure level (STIS ISR 1999-05). This is not true for `CCDGAIN=1`. As described previously (see Section 7.2.1), CCD saturation can be avoided by keeping exposure times short when observing bright targets. The minimum exposure time for CCD observations (0.1 sec) dictates the maximum source brightness which can be observed without saturating.

The only way to use STIS to observe a source that is too bright is to use a configuration which reduces the flux from the target, bringing it into the observable regime. The options available to achieve this reduction are:

- Use a smaller slit to reduce the transmitted light for spectroscopic observations (see Section 13.4—you will find there the percent flux transmitted through each slit as a function of wavelength).
- Select a more appropriate grating or filter configuration. The solution may be a configuration with higher resolving power if it is the local limit which is being violated, or a configuration that covers a smaller spectral range if the global limit is being violated. In more extreme cases, you may be forced to choose a grating (filter) that covers an entirely different region of the spectrum. Note that if you are observing in first order in the near-UV, you can consider using the CCD near-UV first-order spectroscopic modes `G230LB` and `G230MB` (see Section 4.1.7).
- Use a neutral-density-filtered full aperture. The neutral-density filters are described in the section Section 5.4; they produce attenuations ranging by factors from 10^{-1} to 10^{-6} . Note, however, that the ND filters are located in the slit wheel. Thus, all supported ND full-filtered exposures will be slitless; i.e., you cannot use a slit and an ND full filter together. Similarly, you cannot use a ND full filter and another filter in imaging mode. Also note that the `NDQ1`, `NDQ2`, `NDQ3`, and `NDQ4` filters are four distinct quadrants of a single filter, all of which

are simultaneously imaged. Note that NDQ4 is of little use, as any target that requires this filter is too close to the NDQ1 quadrant to pass bright object screening.

- Use one of the echelle or long calibration slits which contain neutral-density filters. Supported neutral-density slits for the echelles are $0.2 \times 0.05 \text{ND}$ (with $\text{ND}=2.0$) and $0.3 \times 0.05 \text{ND}$ (with $\text{ND}=3.0$), where if $\text{ND}=x$, the flux is attenuated by approximately 10^{-x} . Available-but-unsupported long neutral-density slits that can be used for first order, echelle, or PRISM observations are $31 \times 0.05 \text{NDA}$ (with $\text{ND}=0.4$), $31 \times 0.05 \text{NDB}$ (with $\text{ND}=0.8$), and $31 \times 0.05 \text{NDC}$ (with $\text{ND}=1.2$). Use of these long slits with an echelle grating will cause order overlap problems (see Section 12.2), but for point sources the order separation may be adequate for many science programs.

12.5 High Signal-to-Noise Ratio Observations

The maximum achievable signal-to-noise (S/N) ratio of STIS observations for well exposed targets is, in general, limited by the S/N ratio and stability of the flatfields. CCD reference flats are obtained monthly. Ultimately, CCD flats in the pipeline should have an effective illumination of up to 10^6 electrons/pixel. Thus, it should be possible to achieve a S/N ratio of a several 100 over larger spatial scales given sufficient source counts. The limitation is the temporal stability of the CCD reference flats, which show variations of a few tenths of a percent. Dithering techniques can and should be considered for high S/N CCD observations (see Section 11.3). The realizable S/N ratio for spectroscopy will be less in the far red due to fringing, unless appropriate fringe flats are applied (see the caveats on long-wavelength spectroscopy in the red in Section 7.1.3).

The S/N ratio of MAMA flatfields is limited by the long integration times needed to acquire them and the limited lamp lifetimes. (see Section 16.1). S/N ratios of $\sim 100:1$ should routinely be achievable for spectroscopic observations of bright sources with the MAMAs if supported by counting statistics. If your program requires high S/N ratios, we recommend using some form of dithering (described below) and co-adding the spectrograms to ameliorate the structure in the flatfields.

Kaiser et al. (1998, *PASP*, 110, 978) and Gilliland ([STIS ISR 1998-16](#)) reported quite high S/N ratios for spectrograms of bright standard stars obtained during a STIS commissioning program. The realizable S/N ratio depends on the technique used to correct for the flat-field variations, as shown in Table 12.2. The S/N ratios quoted are for wavelength bins from an extraction box of 2 x 11 lowres pixels (2 in *AXIS1* or dispersion, 11 in *AXIS2* or across the dispersion). In the table, the Poisson limit is just the S/N ratio that would be expected on the basis of counting statistics alone;

“No Flat” means the realized S/N ratio without applying any flatfield at all to the data; “Reference Flat” means the realized S/N ratio after applying the best available reference flat, and the “Full FP-SPLIT Solution” is discussed under Section 12.5.2 below. Clearly, S/N ratios in excess of 100:1 per resolution element are well within the capabilities of the MAMAs for spectroscopy.

Table 12.2: Results of S/N Ratio Tests with STIS MAMAs in Orbit

Grating	Poisson Limit	No Flat	Reference Flat	Full FP-Split Solution ¹
E140M	470	200	360 ²	390
G140L	295	90	180	N/A
E230M	400	250	320 ²	380
G230M	200	100	150	N/A

1. Results obtainable in echelle modes using the FP-SPLIT slits and an iterative solution for the spectrogram and flatfield.
2. Results obtained using the FP-SPLIT slits and simply shifting, and co-adding the spectrograms after flat-fielding.

12.5.1 Dithering

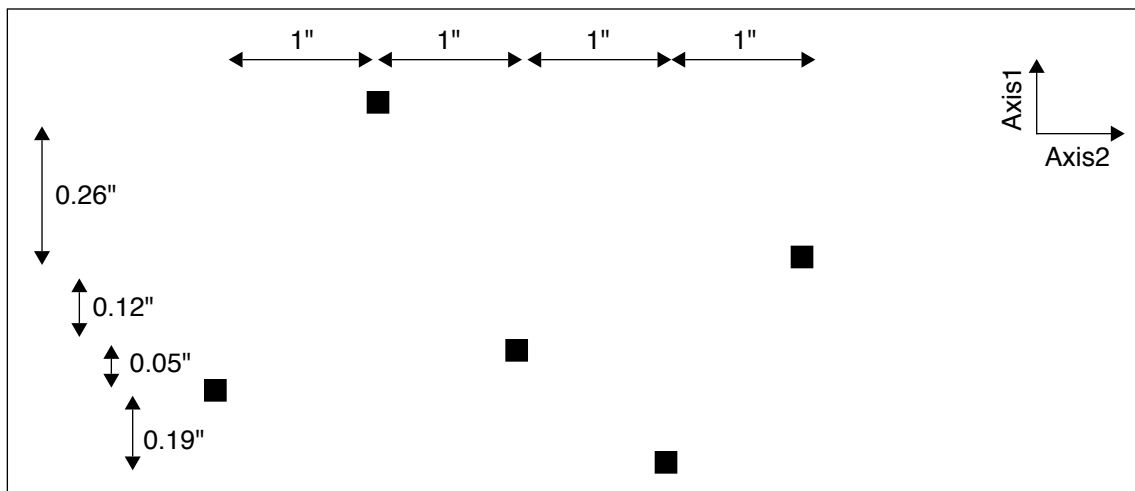
In first-order spectroscopic modes, improved S/N ratios can be achieved by stepping the target along the slit, taking separate exposures at each location, which are subsequently shifted and added in post-observation data processing (PATTERN=STIS-ALONG-SLIT, see Section 11.3). This stepping, or dithering, in the spatial direction effectively smooths the detector response over the number of steps, achieving a reduction of pixel-to-pixel nonuniformity by the square root of the number of steps, assuming the pixel-to-pixel deviations are uncorrelated on the scale of the steps. In imaging modes, the same dithering can be done in two dimensions, i.e., the steps need not be along a straight line (see Section 11.3.5). For echelle modes, stepping along the slit is possible only with the long echelle slit (6X0.2), but see Section 12.2, above, and note the ameliorating effects of Doppler smearing as noted below. In practice, using the FP-SPLIT slits (see Section 12.5.2) provides a better means of dithering echelle observations.

In a slitless or wide-slit mode, stepping along the dispersion direction provides another method to achieve high S/N ratio data. Data so obtained permit, at least in principle, an independent solution for spectrogram and flat field, but at a cost of lower spectral resolution and line-profile confusion due to the wings of the LSFs transmitted through a wide slit (see Section 13.7). Such an approach for STIS data has not been attempted as of this writing.

12.5.2 FP-SPLIT Slits for Echelle Observations

A special kind of dithering in the spectral direction is possible for echelle-mode observations with one of two sets of fixed-pattern (or FP-SPLIT) slits. These slit sets are each comprised of a mask with five apertures that are all either 0.2×0.2 or 0.2×0.06 in size. A schematic of the configuration is shown in Figure 12.4. During a visit, the target is moved from one aperture to another, and the slit wheel is repositioned, so that the spectrogram is shifted (relative to the detector pixels) along the dispersion direction only. The slits are spaced to place the spectrogram at different detector locations, so that flat-field variations can be ameliorated by co-adding many such spectrograms. The FP-SPLIT slits can be a good choice for obtaining high S/N ratio echelle data, since it is usually not possible to dither in the spatial direction. However, since $S/N=100$ is routinely achieved using the normal echelle apertures, the FP-SPLIT slits are rarely used.

Figure 12.4: Schematic of the STIS Fixed-Pattern Slit Configuration. AXIS1 corresponds to the dispersion direction, and AXIS2 to the spatial direction. Dimensions are not to scale.



With echelle modes, Doppler-induced spectral shifts move the spectrogram on the detector. The STIS flight software automatically applies an onboard compensation for Doppler motion for echelle and MAMA medium-resolution, first-order data taken in ACCUM mode (see Chapter 11). The MAMA control electronics correct (to the nearest highest pixel) the location of each event for the Doppler shift induced by the spacecraft motion prior to updating the counter in the image being collected. Thus, the flat-field correction for any image pixel would be an appropriately weighted average over a small range of nearby pixels and the effect of spacecraft-induced Doppler shifts is therefore to naturally provide some smoothing over the flat fields in the echelle modes.

The source of the Doppler-induced spectral shifts during an exposure is the variation of the projected HST spacecraft velocity along the line of sight to the target. Column 2 of Table 12.3 gives the maximum shift in highres pixels that would apply, based upon an HST orbital velocity of ~ 7.5 km/s during an orbit. The actual shift will of course depend upon the cosine of the target latitude, i , above or below the HST orbital plane, and upon the sine of the orbital phase at which the exposure is obtained. (Note that in general the observer can predict neither the latitude nor the orbit phase of the exposures in advance with any precision.) Column 3 gives, for a target lying in the HST orbit plane, the maximum duration of an exposure for which the Doppler shift will be one highres pixel or less; the actual duration will scale as $\sec(i)$, so that targets near the CVZ are scarcely affected by Doppler motion. This information on T_{max} is relevant only if you are trying to derive the flatfield response simultaneously with the source spectrogram (see below) and not for the straightforward flat-field and shift-and-add methodology described above.

Table 12.3: Effect of Doppler Shift on Exposure Times

Grating	Maximum Doppler Shift (hi-res pixels)	T_{max}^1 (minutes)
E140H	11.41	2.7
E140M	4.59	7.0
E230H	11.41	2.7
E230M	3.00	11.3

1. For inclination $i = 0$; actual duration will scale as $\sec(i)$. See text for details.

Obtaining the Highest S/N Ratio with the FP-SPLIT Slits

As described above, the FP-SPLIT slits have been used with the echelles to provide signal-to-noise as high as ~ 350 with the direct *shift-and-add* method. Additionally, data obtained with the FP-SPLIT slits make it possible to solve independently for the fixed-pattern (i.e., the flat-field variation) and the source spectrogram. An iterative technique for combining FP-SPLIT data was applied successfully to data obtained with GHRS (see Lambert et al., *ApJ*, **420**, 756, 1994), based on a method described by Bagnuolo and Gies (*ApJ*, **376**, 266, 1991). This same technique was applied by Gilliland (STIS ISR 1998-16) to STIS observations of a standard star. The S/N ratio that was achieved with these slits is summarized in the last column of Table 12.2, which shows that the FP-SPLIT slits can offer some advantage when one is attempting to achieve the highest possible S/N ratio. In general, though, it may be difficult to improve upon the S/N ratio that can be achieved by simply calibrating with the standard flatfield and co-adding the spectrograms.

There are a number of caveats to use of the FP-SPLIT slits to solve independently for the spectrogram and flatfield. The most notable is that the targets must be relatively bright point sources. The restriction to bright targets results both from the need to limit the duration of individual exposures to keep the Doppler-induced spectral shifts to less than one hires pixel, and from the need to have appreciable counts in the individual exposures—at least in the orders of interest. Very high counts in the sum of all exposures are essential for a good (and stable) solution to both the spectrogram and the underlying flatfield.

If you are using the FP-SPLIT slits to distinguish the signature of the flatfield from the target spectrogram, then Doppler smearing (and the discrete compensation) will defeat that solution. In this case, the exposures must be kept as short as if there were no Doppler compensation at all, if the goal is to solve for the pixel-to-pixel variation at a precision higher than that of the available flat-field reference files.

The utility of FP-SPLIT observations is also limited by the modest range of slit offsets in wavelength space, and by the distribution and character of the features in the target spectrum itself. That is, if the spectrum in the order(s) of interest is dominated by absorption over a width comparable to or larger than the largest offset range, the solution may not be stable or unique. A corollary is that some of the spectral orders must contain moderately prominent spectral features with good signal in order to distinguish the spectrum from flat-field variations. Table 12.4 gives the FP-SPLIT offsets for each grating, including offsets in Ångstroms for typical central-wavelength settings.

Table 12.4: Magnitude of Spectrogram Offset for the FP-SPLIT Slits

Grating	Minimum Offset (hires pix)	Maximum Offset (hires pix)	CENWAVE (Å)	Max. Offset @CENWAVE (Å)
E140H	2.128	26.383	1416	0.164
E140M	2.778	34.444	1425	0.535
E230H	2.128	26.383	2390	0.277
E230M	2.857	35.429	2340	1.382

12.6 Improving the Sampling of the Line-Spread Function

In most configurations the point-source spectral-line FWHM is slightly less than two detector pixels (see Section 13.6). Most observations should not be affected, but if you are observing lines which are near to being unresolved in the grating of interest and require accurate line profiles, you can consider the following technique:

- Stepping of the target in the dispersion direction in a wide slit or slitless aperture to subsample the line-spread function by displacing the spectrogram. This technique can also be used to increase the signal-to-noise (see above). Note that in employing this strategy one will have to trade off the benefits of the sampling with the negative impact of increased wings in the line-spread function with a wide slit, particularly for MAMA observations (see Section 13.7).
- For MAMA observations, *highres* pixels may provide twice the sampling; however, flat-field variability may make it difficult to realize the benefit in resolution (see “Highres” on page 228). Note that all STIS data are taken by default in *highres* format, and then binned in calibration on the ground so all you need to do is recalibrate your data, changing the switch settings (see “[STIS Calibration](#)” chapter in the [HST Data Handbook](#)) to fully exploit the *highres* data.
- Use of a higher resolution grating mode in which the intrinsic line width of the source is well sampled.

12.7 Considerations for Observing Planetary Targets

STIS’s FUV solar-blind and NUV solar-insensitive MAMA detectors make it particularly well suited to slitted spectroscopic and imaging planetary observations. In addition, the 52X2 long slit (2 arcseconds wide in the dispersion direction) is particularly well suited to the “slitless” ultraviolet spectroscopic study of small planetary bodies (using a slit limits the background continuum contribution; see Section 6.5.2). STIS has been used successfully to perform long-slit and echelle spectroscopy and UV imaging of several solar-system objects including comets, planetary satellites, and planets.

Planetary observers may wish to use the sequence `PATTERN=STIS-PERP-TO-SLIT` (see Section 11.3) to map out the surface of a planet by taking a series of long-slit observations, each one stepped by the slit width perpendicular to the slit’s long dimension, relative to the last. Advice on performing target acquisition for solar-system targets is provided in Chapter 8.

12.7.1 Long-Slit Spectroscopy

Planetary observers requiring specific long-slit orientations will want to be aware of the tight scheduling constraints of specific orientations for observations of targets in the ecliptic plane (see discussion of “Orient from Nominal” in the Phase II instructions).

For example, say an observer wanted to orient the STIS long (52 arcsecond) slit in the north-south direction on Jupiter. For a Jupiter north-pole position angle of $\sim 20^\circ$ from celestial north, this would require an ORIENT constraint of $\sim 20\text{--}25^\circ$ or $\sim 200\text{--}205^\circ$ would be required. The nominal roll angle (orientation) for Jupiter varies from $\sim 250^\circ$ before opposition to $\sim 70^\circ$ after opposition, and it goes through the intervening 180° range during a four-day period centered on opposition. Deviations from nominal roll are allowed as follows:

- 5° when the sun-target angle is $50\text{--}90^\circ$.
- 30° when the sun-target angle is $90\text{--}178^\circ$.
- Unlimited when the sun-target angle is $178\text{--}180^\circ$.

Thus orientation of the long slit in a north-south direction on Jupiter is possible only during a single four-day period near Jovian opposition, since no allowable deviation from nominal roll is large enough at any other time to permit a north-south orientation of the slit on the planet. Although the situation for Saturn is not nearly as extreme, observers should be aware of the tight scheduling constraints on observations requiring specific slit orientations.

12.8 Parallel Observing with STIS

The second servicing mission installed solid-state data recorders on HST. The volume capacity of these recorders is roughly ten times that of the mechanical tape recorders in use for Cycles 1 through 6. Coupled with changes to the ground system and the flight software of the second-generation instruments designed to fully exploit this capability, this translates into a greatly increased capability for parallel observing.

STIS can be used to observe simultaneously with WFPC2, FGS, and ACS. Figure 3.2 shows the HST field of view following ACS installation. The three infrared cameras of NICMOS (which themselves could be operated in parallel), STIS, WFPC2, and ACS are all shown, with their fields of view drawn to scale, in their relative focal-plane positions. The three STIS cameras share a common field of view, and only one can be used at a time.

The policy for proposing for parallel observations and technical advice on parallel observing are provided in the Call for Proposals/Phase II

Proposal Instructions. We remind you that there are two types of parallel observations:

- Coordinated parallels, in which you explicitly link the taking of exposures in parallel to your own prime scientific exposures.
- Pure parallels, in which exposures are taken in parallel with other observers' prime exposures.

Both coordinated and pure parallels must be explicitly proposed in Phase I. Implementing parallels requires significant resources; only those recommended by the TAC process will be implemented. If you are considering coordinated parallels, you may wish to consider constraining the orientation of HST, to place an object of interest in the parallel instrument's field of view. `ORIENT` constraints do affect observation scheduling, however, and should not be entered lightly (see Chapter 11).

12.8.1 Using STIS in Parallel with Other Instruments

Observations for which STIS is the parallel instrument are likely to be most useful when the full STIS field of view is used. If you wish to use a small slit, the STIS should be used as prime, and the other imaging instruments used in parallel with it.

If STIS is used as the secondary instrument in coordinated parallel observations, the STIS exposures cannot contain both external and internal exposures. Assuming the first exposure is external, *all* STIS exposures will be declared external. Therefore no internal exposures are allowed. This includes any user specified internals, such as fringe flat fields, as well as automatic internals, such as autowavevals. If STIS is used as the prime instrument, this restriction does not apply.

The MAMA detectors cannot be used for *pure* parallel observing. The MAMA detectors can be used in coordinated parallel observing if an explicit `ORIENT` is specified and precise RA and Dec coordinates for the parallel field are given (see Section 2.7).

Four types of STIS exposures which have particular scientific utility with STIS as the parallel instrument are:

- Optical imaging taking advantage of the ability to go deep very fast with the 50CCD wide-open mode.
- Optical slitless spectroscopy.
- Ultraviolet slitless spectroscopy (available only for coordinated parallels with exact `ORIENT` specification).
- Prism and ultraviolet imaging observations (available only for coordinated parallels with exact `ORIENT` specification).

12.8.2 The STIS Archival Pure Parallel Program

Following on the recommendations of the Cycle 7 HST Time Allocation Committee, and following the advice of the Parallels Working Group, an HST Archival Pure Parallel Program was begun at the start of Cycle 7. This program was designed to maximize the scientific return from HST to the community by taking parallel data with instruments that are not being used as the prime instrument. The data immediately become nonproprietary and are available through the HST Archive. This program continues today.

The STIS Archival Pure Parallel observing program consists of:

- G750L slitless spectroscopy to search for star-forming galaxies and AGN out of the plane, and brown dwarfs in the plane.
- 50CCD and F50X28LP imaging in the outskirts of nearby galaxies and globular clusters for stellar-population studies.
- Short (≤ 1 orbit) 50CCD images of extragalactic fields to study cosmic shear.
- Narrowband [O II] and [O III] CCD images of the outskirts of nebulae in the Galactic Plane.
- Deep CCD imaging of extragalactic fields.

Figure 12.5 shows an example of a deep 50CCD STIS Archival Pure Parallel image and Figure 12.6 shows an example of slitless spectroscopy from the Archival Pure Parallel Program. An overview of the HST Pure Parallels for all HST instruments can be found at

<http://www.stsci.edu/instruments/parallels/>.

Figure 12.5: Deep 50CCD STIS Pure Parallel Image from the Archival Pure Parallel Program, with 3.72 hours of Integration Time. (Figure courtesy of Ed Smith.)

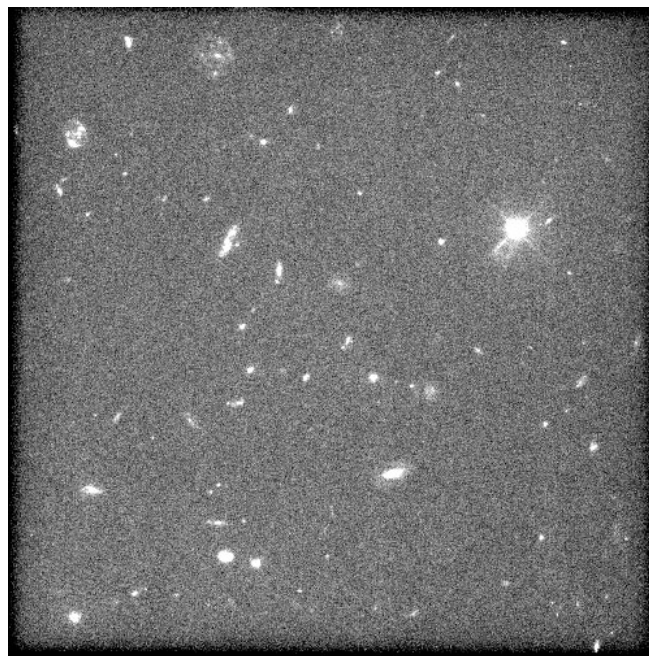
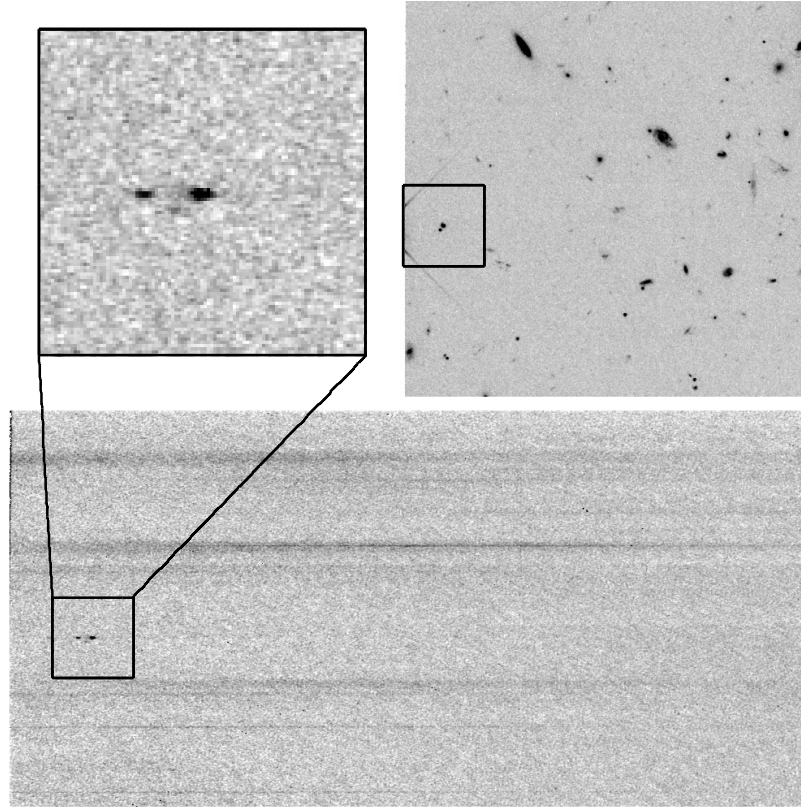


Figure 12.6: G750L Slitless Spectroscopy from the Archival Pure Parallel Program Showing the Detection of a High Redshift Emission Line in a Galaxy. (Figure courtesy of Jon Gardner, see also Gardner et al. 1997, in the [1997 HST Calibration Workshop Proceedings](#).) Left and below are the G750L slitless spectra. Top right is the image of the field.



12.9 Coronagraphic Spectroscopy

STIS offers the capability to perform spectroscopic observations with occulting bars located in the long slits, and imaging observations with occulting bars in the coronagraphic mask 50CORON. Coronagraphic imaging is described in detail in Chapter 5.

Barred Spectroscopy

The 52X0.2F1 aperture is the same physical slit as 52X0.2 with the target centered on the smaller of the two occulting bars (i.e., 0.5 arcseconds), instead of at the center of the 52X0.2 long slit. When this aperture is specified the slit wheel is rotated slightly to bring the bar into the center of the detector's field of view. This results in a tilt of 1.30° with respect to AXIS2 (i.e., the spatial axis perpendicular to the dispersion). Also, the full 52 arcseconds length of the long-slit field of view is decreased by about 20% for CCD spectroscopy.

This occulting bar is well suited to scientific programs conducting spectroscopy of faint extended material around a bright central source. Typical examples of such a program include QSO host galaxies, dynamics of jets in young stellar objects, and spectroscopy of resolved binaries. Observers performing barred spectroscopy should be sure to consult the section Section 13.7.3. Spectroscopic observations with the 0.5 arcsecond occulting bar are limited to first-order spectroscopic modes.

To simplify the use of the occulting bar, an aperture name, 52X0.2F1, has been assigned for the occulting bar itself, as well as an aperture name for a reference position located just off the bar. The reference aperture is used if the observer wishes to pickup the source in the slit, prior to offsetting to place the target behind the occulting bar. (Note that peakdowns behind the occulting bar, while possible in principle, are not recommended in practice).

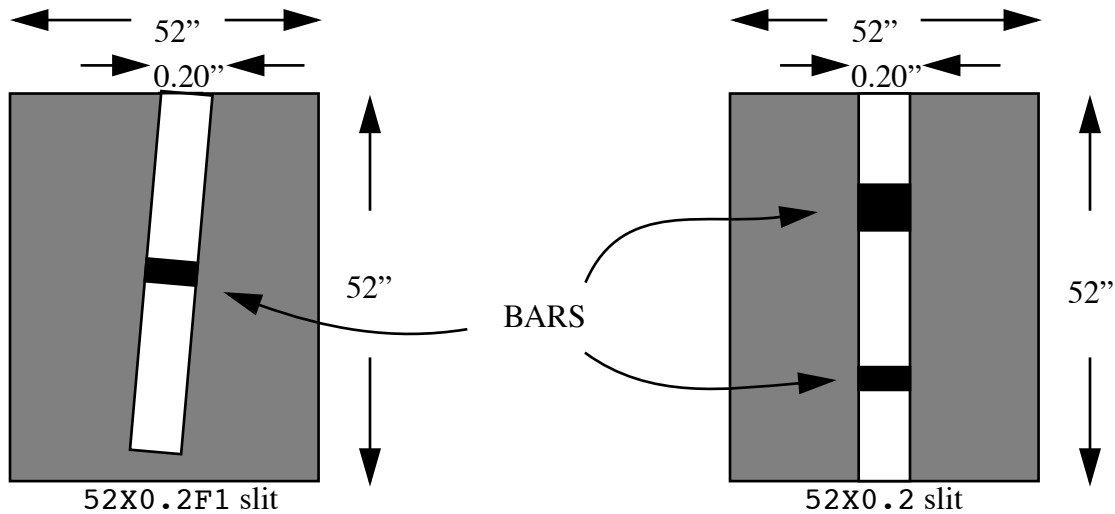
The table below shows the complete set of aperture names and their application for the 0.5 arcsecond fiducial on the 52X0.2 slit. An example of an acquisition into the 52X0.2F1 aperture is provided in Chapter 8.

Table 12.5: Aperture Names and Applications on 52X0.2 Slit

Aperture Name	Description	Destination	Application
52X0.2	Slit (width=0."2, length=52")	Target centered in slit	Long-slit spectroscopy
52X0.2F1-R	Slit (width=0."2, length=52"). Fiducial=0."5 Reference point off-fiducial	Target centered in slit at reference position, offset from fiducial bar.	Locates target at reference position ready for pickup in slit.
52X0.2F1	Slit (width=0."2, length=52"). Fiducial=0."5	Target centered in slit and located under fiducial bar	Locates target under bar ready for occulted observation

There are two important ramifications you should be aware of when using the 52X0.2F1 aperture: (1) ORIENT specification and (2) fringing correction.

Figure 12.7: A cartoon illustrating the 1.30° tilt of the 52X0.2F1 aperture



Specifying ORIENT with the 52X0.2F1 Aperture

The ORIENT special requirement parameter is a specified position angle of the orientation reference vector U3, which is offset by 45° from the STIS detector spatial axis (AXIS2), in the direction North through East. Given a position angle on the sky of θ and taking into account the additional 1.30° offset for the 52X0.2F1 aperture:

$$\text{ORIENT} = \theta + 46.30^\circ \text{ or } \theta + 226.30^\circ$$

For example, if we want to place the STIS 52X0.2F1 aperture along the jet of M87 (the example in Figure 11.10 for a standard slit), we would do the following. Given a position angle of 110° on the sky:

$$\text{ORIENT} = 110^\circ + 46.30^\circ = 156.3^\circ$$

or

$$\text{ORIENT} = 110^\circ + 226.30^\circ = 336.3^\circ$$

Correcting Fringing for the 52X0.2F1 Aperture

The STIS CCD shows fringing for wavelengths longward of 7000 angstroms with the G750L and G750M gratings, limiting the signal-to-noise that can be obtained in these modes. The fringing is caused by interference of multiple reflections between the two surfaces of the CCD. (See Chapter 7 for details.) The recommended way to correct for fringing is by using contemporaneous fringe flats in conjunction with your science observations. A contemporaneous flat field exposure may be included in the Phase II template by using CCDFLAT as the target name. It is the observers' responsibility to include contemporaneous flat fields in their Phase II proposals.

In case of point-source spectra, contemporaneous fringe flats are normally taken using a short slit which is concentric with the long slit used for the science exposures. In the special case of the 52X0.2F1 aperture, however, we recommend obtaining long slit fringe flats to fully sample the PSF, since the spatial coverage of the short slit is only a few CCD pixels larger than that of the occulting bar of the 52X0.2F1 slit. A short slit fringe flat does give a somewhat better fringe correction for point sources than a long slit fringe flat so if you are additionally taking an unocculted image of your star with 52X0.2, we still recommend obtaining a short slit flat as well as a long slit flat to rectify that image.

Please refer to the Instrument Science Reports [1997-15](#) (Revision A) for more details about near-IR fringe flats; [1997-16](#) that deals with fringing in spectrograms of extended sources; [1998-19](#) (Revision A) that deals with fringing in spectrograms of point sources and current fringing analysis, as well as details related to the 52X0.2F1 aperture; and [1998-29](#) that is a tutorial on the use of IRAF tasks in the *stsdas.hst_calib.stis* package to remove fringing.

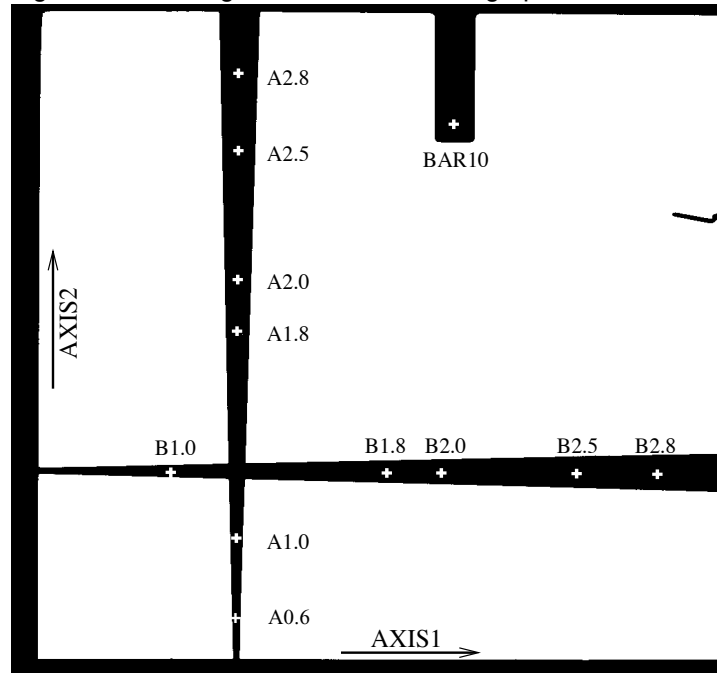
12.10 Coronagraphic Imaging—50CORON

STIS has a single coronagraphic mask aperture for direct imaging. The aperture (50CORON) contains one occulting bar and two intersecting wedges and is shown in Figure 12.8. This illustration of the coronagraphic aperture is derived from an on-orbit lamp flat. The approximate positions of the predefined aperture locations are marked. The wedges vary in width from 0.5 to 3.0 arcsec over their 50 arcsec length, while the rectangular bar measures 10 by 3 arcsec. The small occulting finger on the right was damaged during the assembly of STIS and is not used. The entire coronagraphic aperture measures 50x50 arcsec, slightly smaller than the size of the unobstructed CCD aperture. The parallel readout of the CCD is along the *AXIS2* direction, and heavily saturated images will bleed in this direction (vertically in this figure).

The aperture cannot be combined with a filter and so, when used with the CCD, yields a bandpass of $\sim 2000\text{--}10,300 \text{ \AA}$. See Section 5.2.2 for the spectral properties of the images obtained. A number of locations on the occulting masks have been specified, to correspond to widths of 2.75, 2.5, 2.0, 1.75, 1.0, and 0.6¹ arcseconds on each wedge. The mask is not available for use with the MAMA detectors due to concerns about bright-object protection of the MAMAs.

1. The 0.6 arcsecond location is on wedge A only and was added in Cycle 12.

Figure 12.8: Design of the STIS Coronagraphic Mask



In combination with the option of a coronagraphic mask, there is a limited amount of apodization via a Lyot stop which masks the outer perimeter of the re-imaged exit pupil. Consequently, diffraction from the secondary mirror assembly and the telescope spider is not apodized. The STIS coronagraphic imaging facility is well suited to imaging problems involving faint material surrounding a relatively bright source. Typical examples include circumstellar disks, such as β Pictoris, and the host galaxies of bright QSOs.

In Figure 12.9 we provide a comparison of the PSF suppression provided by STIS coronagraphic imaging relative to WFPC2 imaging and the Optical Telescope Assembly scatter. It had been hoped that the optical performance of the STIS CCD clear aperture without the coronagraph would be comparable to that with the coronagraph, although, without the coronagraph, the CCD long wavelength halo from the central source and the window reflection ghosts are present. In practice the coronagraph does provide substantial additional suppression of the PSF wings, especially at wavelengths $>8000 \text{ \AA}$, where the halo of light scattered within the CCD itself dominates the far wings of the PSF.

Due to the very broad bandpass of the unfiltered STIS CCD, the STIS coronagraphic PSF shape is very strongly dependent on the target's spectral energy distribution. When using the coronagraph to look for a point source or a localized structure that is strongly asymmetric (such as an edge-on disk), the best approach is to observe the target star at least two and preferably three different roll angles, and then compare the images to separate the stellar PSF from the real circumstellar structure. When looking for more diffuse or symmetric material, it will be necessary to use a

separate comparison star. Here it is important to match the colors of the target and comparison star as closely as possible. We suggest that all the broadband UVBRI color differences be less than 0.08 magnitudes. In either case, it is also essential to compare stars at the same location on the coronagraphic mask.

Breathing and focus differences will also significantly affect the quality of such a subtraction, but the observer has only limited control over these parameters. The best alignment of STIS PSF images tends to occur when comparing images taken in the same part of adjacent orbits. When observing the same star at multiple roll angles, it is therefore often useful to do a sequence of adjacent one-orbit visits, each at a different roll angle. As large departures from the nominal roll angle can also affect the PSF shape, it may be helpful to keep the roll changes as small as is consistent with the structure to be imaged. When observing a separate comparison star, it is best if possible to observe a star in the same part of the sky, during an adjacent orbit, and at the same angle relative to the nominal spacecraft roll, as the observations of the prime target, but remember that picking a comparison star with a good color match must be the first priority.

An alternative strategy would be to take observations separated by a several days, but constrained so that each observation is done at the nominal spacecraft roll. When very large roll changes or several orbit long visits are required, this might give better results than doing the observations in adjacent orbits, but there is very little operational experience using this approach.

Attempting to observe in a single orbit multiple coronagraphic targets or the same target at different roll angles is not recommended. The overheads required to do separate visits in a single orbit are very large, and the PSF alignment between different parts of the same orbit are usually inferior to that obtained between the same part of adjacent orbits.

Coronagraphic images of stars of various colors have been obtained as parts of calibration programs 7151, 7088, 8419, 8842, and 8844 and are available from the archive. These images may be useful in providing comparison objects or in estimating exposure times. However, for the best PSF subtraction, we still recommend that each coronagraphic program include its own tailored PSF observations. A searchable STIS PSF Library containing both direct and coronagraphic images is available that allows the user to easily find and retrieve PSF images for particular detector, filter, and stellar color combinations.

In planning any observing program with the 50CORON aperture, observers should carefully consider the required orientation of the target. The telescope's V2 and V3 axes are at 45° to the STIS AXIS1/AXIS2 coordinate system (see Figure 11.1) and so diffraction spikes further reduce the unocculted field of view.

A series of apertures has been defined for the coronagraphic mask so that targets can be placed on the 3" wide bar and 5 locations on each of the

two wedges. These apertures are summarized in Table 12.6 below. We defined a special coronagraphic acquisition technique for placing stars at these predefined locations. This involves performing a bright-target acquisition with a filtered aperture, followed by a slew to the chosen location on the coronagraphic mask. An example of an acquisition into one of the bars on the 50CORON aperture is provided in Section 8.5.6).

Figure 12.9: Comparison of PSF Suppression: STIS Coronagraph, WFPC2, and the Diffraction of the OTA

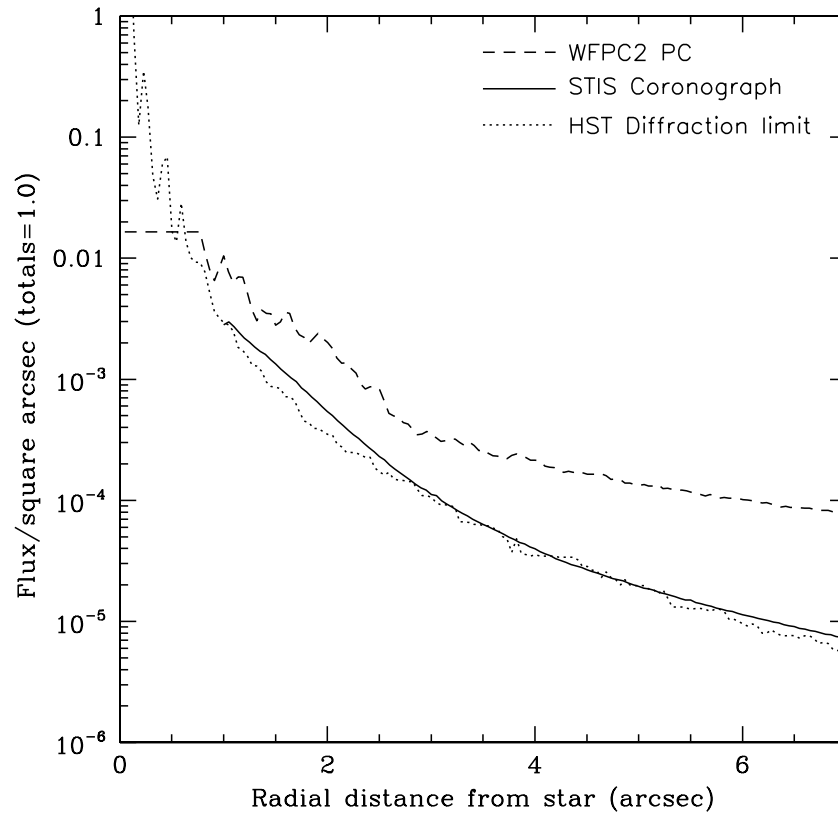


Table 12.6: Apertures for Coronagraphic Mask

Proposal Instructions Aperture Name	Description
50CORON	Coronagraphic mask—clear aperture in center of the field of view
BAR10	Coronagraphic bar of width 3."0
WEDGEA2.8	Coronagraphic Wedge A (vertical in AXIS1) Posn. 1: bar width = 2."75
WEDGEA2.5	Coronagraphic Wedge A (vertical in AXIS1) Posn. 2: bar width = 2."5
WEDGEA2.0	Coronagraphic Wedge A (vertical in AXIS1) Posn. 3: bar width = 2."0
WEDGEA1.8	Coronagraphic Wedge A (vertical in AXIS1) Posn. 4: bar width = 1."75
WEDGEA1.0	Coronagraphic Wedge A (vertical in AXIS1) Posn. 5: bar width = 1."0
WEDGEA0.6	Coronagraphic Wedge A (vertical in AXIS1) Posn. 6: bar width = 0."6
WEDGEB2.8	Coronagraphic Wedge B (vertical in AXIS2) Posn. 1: bar width = 2."75
WEDGEB2.5	Coronagraphic Wedge B (vertical in AXIS2) Posn. 2: bar width = 2."5
WEDGEB2.0	Coronagraphic Wedge B (vertical in AXIS2) Posn. 3: bar width = 2."0
WEDGEB1.8	Coronagraphic Wedge B (vertical in AXIS2) Posn. 4: bar width = 1."75
WEDGEB1.0	Coronagraphic Wedge B (vertical in AXIS2) Posn. 5: bar width = 1."0

Spectroscopic Reference Material

In this chapter. . .

13.1 Introduction / 279
13.2 Using the Information in this Chapter / 280
13.3 Gratings / 289
13.4 Apertures / 337
13.5 Spatial Profiles / 362
13.6 Line-Spread Functions / 368
13.7 Spectral Purity, Order Confusion, and Peculiarities / 373
13.8 MAMA Spectroscopic Bright-Object Limits / 383

In this chapter, we provide spectroscopic reference material, in support of the information presented in Chapter 4.

13.1 Introduction

The information in this chapter will help you select your grating configuration and observing slit and determine your observing plan (e.g., total required exposure time, and number of exposures). This chapter is basically organized by *grating and slit* (corresponding to Spectral Element and Aperture in the [Phase II Proposal Instructions](#).)

For each grating mode the following are provided:

- A brief description of the grating mode's specifications, including recommended uses and special considerations.

- The central-wavelength settings and range of wavelength covered at each setting, together with the dispersions and plate scales.
- Plots and tables of sensitivities and throughputs as a function of wavelength.
- Plots of signal-to-noise as a function of $V+STMAG_{\lambda}$ (the color-dependent correction from V magnitude to STMAG at wavelength λ), F_{λ} , and exposure time.

For each slit the following are provided:

- A brief description of the slit's specifications, including recommended uses and special considerations.
- Plots and tables of relative throughputs as a function of wavelength.

For representative grating-slit combinations we provide:

- Tables of encircled energy for the flux in the default pipeline extraction aperture, and the percent flux contained in the peak pixel.
- Plots of representative spatial (perpendicular to the dispersion) profiles at selected wavelengths.
- Line-spread functions and FWHM as a function of wavelength.

In addition,

- Section 13.8 provides a summary of the screening brightness limits for the MAMA spectroscopic modes.

The next section explains the plots and tables found in the grating sections in this chapter.

13.2 Using the Information in this Chapter

13.2.1 Wavelength Ranges

The complete wavelength range for each grating, as well as the wavelength coverage per tilt for the scanned grating modes, is shown in a table and graphically. The exact wavelengths at the ends of the ranges for the MAMA detectors will depend on the MAMA monthly offsetting. This procedure shifts the spectrogram so that it falls on slightly different parts of the MAMA detectors from month to month in order to minimize charge depletion in the microchannel plates and can cause the loss of ± 30 pixels from either end of the spectrogram in dispersion (AXIS1) and ± 80 pixels in cross-dispersion (AXIS2). [Spectral format plots](#) of the STIS grating and central wavelength settings are available from the STIS web page under

“Gratings.” For the echelles, the monthly offsetting will project the extreme orders of formats off of the detector in some months. The wavelength ranges for the echelles given in the chapter therefore include only the orders which are guaranteed to project onto the detector. Whenever possible, choose a central wavelength that keeps your features of interest away from the extremes of the wavelength ranges.

Wavelengths in this handbook and in STIS data products are always measured in vacuum conditions.

13.2.2 Grating Sensitivities and Throughputs

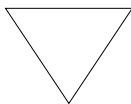
This chapter contains plots and tables of sensitivities and throughputs for each grating mode. Section 6.2 in the Exposure-Time Calculation chapter explains how to use these sensitivities to calculate expected count rates from your source.

The total system¹ *spectroscopic point-source sensitivity*, S_{λ}^p , has the unit:

counts $\text{sec}^{-1} \text{pix}_{\lambda}^{-1}$ per incident $\text{erg cm}^{-2} \text{sec}^{-1} \text{\AA}^{-1}$ for the MAMA and electrons $\text{sec}^{-1} \text{pix}_{\lambda}^{-1}$ per incident $\text{erg cm}^{-2} \text{sec}^{-1} \text{\AA}^{-1}$ for the CCD,

where:

- pix_{λ} = a pixel in the dispersion direction.
- counts refer to the total counts from the point source integrated over the PSF in the direction perpendicular to the dispersion (along the slit).



Note that the spectroscopic point-source sensitivity does not include slit losses.

The *spectroscopic diffuse source sensitivity*, S_{λ}^d , has the units counts $\text{sec}^{-1} \text{pix}_{\lambda}^{-1} \text{pix}_s^{-1}$ per incident $\text{erg sec}^{-1} \text{cm}^{-2} \text{\AA}^{-1} \text{arcsec}^{-2}$ for the MAMA and electrons $\text{sec}^{-1} \text{pix}_{\lambda}^{-1} \text{pix}_s^{-1}$ per incident $\text{erg sec}^{-1} \text{cm}^{-2} \text{\AA}^{-1} \text{arcsec}^{-2}$ for the CCD,

where:

- pix_{λ} = a pixel in the dispersion direction.
- pix_s = a pixel in the spatial direction.

1. STIS plus HST Optical Telescope Assembly (OTA).

S_{λ}^p and S_{λ}^d are related through the relation:

$$S_{\lambda}^d \equiv S_{\lambda}^p \times m_s \times W$$

where:

- m_s is the platescale in arcsec per pixel in the direction perpendicular to the dispersion.
- W is the width of the slit used in arcsec.

Here, we have assumed that the diffuse source has a uniform brightness over the area of interest and that the spectrum can be approximated as a continuum source. The throughput is defined as the end-to-end effective area divided by the geometric area of a filled, unobstructed 2.4 meter aperture (see Chapter 6).

Tables of sensitivities and throughputs are given for a point source placed in the center of the largest clear aperture for each detector. (Sensitivities and throughputs for a point source placed high on the CCD detector in the long-slit “E1” pseudo-apertures will be measured from calibration data taken in Cycles 10 and 11; see Section 7.2.7). The sensitivity plots give values for point and diffuse sources. In the plots in this chapter we show the diffuse source sensitivity for a 0.1 arcsec wide slit. For an extended continuum source, S_{λ}^d scales directly with slit width, as above.

For the echelles, the sensitivities given were derived from fits of a smooth curve as a function of wavelength to the measured sensitivities at the central wavelength of each order (i.e., they do not include the effect of the echelle ripple). The [Spectroscopic Exposure Time Calculator](#) (see Chapter 6) will properly take the echelle ripple into account and should be used for more detailed S/N analysis.

Small but significant changes in the STIS sensitivity have been revealed by continuous observations of the same standard stars in the 52X2 slit. These changes are discussed in detail in the sections entitled Section 7.1.4, and Section 7.3.3, and the mean variations in sensitivity with time for some first order MAMA configurations are illustrated in Figure 7.13.

The sensitivities and throughputs listed in this chapter have *not* been corrected for the time dependent changes discussed above, but rather are the values as originally measured in 1997-1998. In many cases they are therefore higher than the current sensitivities by a few to several percent. The STIS ETC takes these changes into account, and will correct the sensitivity to that appropriate for July 1, 2005.

13.2.3 Signal-To-Noise Plots

For each grating mode, a plot is provided to help you estimate the signal-to-noise (S/N) for a class of sources and a range of exposure times,

corresponding to a fiducial taken at wavelengths near the peak of the responses. The fiducial wavelength is indicated in the ordinate label of each plot. To estimate signal-to-noise at alternate wavelengths, you can scale your source flux or magnitude by the relative sensitivities (or throughputs) at the wavelength of interest and at the fiducial. The point source plots show S/N as a function of F_λ and of $V+STMAG(\lambda)$ for a range of exposure times; the diffuse source plots show I_λ and $V+STMAG(\lambda)$ per arcsec² for a range of exposure times. Using STMAG units is natural in this plot given that a particular STMAG value corresponds to a flux distribution with a constant value of F_λ . In producing these plots we assumed an average sky background (as described in Chapter 6) and the appropriate values for read noise and dark current for each detector. Note the following:

- The point-source S/N has been calculated per two dispersion pixels, and has been integrated over the PSF to contain 80% of the flux in the spatial direction.
- The point-source S/N calculations assume the use of the 52X0.2 slit for the first-order modes and the use of the 0.2X0.2 slit for the echelle modes.
- The diffuse-source S/N is calculated with the 0.2 arcsecond wide slit and the assumption that the slit is fully filled by a diffuse continuum source. The S/N is given per 2 spatial pixels and 4 spectral pixels for the CCD and is given per 2 spatial pixels and 6 spectral pixels for the MAMA (these are the equivalent spectral resolution elements for these observations).
- For the CCD, the plots assume CR-SPLIT=2 and CCDGAIN=1.
- The different symbols in the S/N figures delineate regions where different sources of noise dominate. A particular source of noise (read-noise for example) is presumed to dominate if it contributes more than half the total noise in the observations. Saturation is likewise indicated.
- The vertical dashed line indicates the MAMA bright-object *observing* limits; if F_λ (or I_λ) exceeds the indicated value, the observation would exceed the observing limits (recall that the observing limits are at slightly higher count rates than the *screening* limits given in Table 13.44). For diffuse sources we indicate only the local rate limit, since the global limit is dependent on the source extent. If no line is seen on the plot, it indicates the limit is higher than the range of fluxes plotted.

In situations requiring more detailed calculations (non-stellar spectra, extended sources, other sky background levels, etc.), the STIS ETC, available from the STIS web site under “[Software Tools](#),” should be used instead.

Follow these steps to use the S/N plots:

1. Look up in Table 13.1 the spectral type and wavelength region of interest of your target observation (e.g., G0 V @ 4300 Å). Interpolate in the table to get $STMAG_{\lambda}$.
2. Add the V magnitude of the target to the interpolated value of $STMAG_{\lambda}$ derived from the table.
3. Find the appropriate plot for the desired grating, and locate $V+STMAG_{\lambda}$ on the horizontal axis. Read off the S/N for the desired exposure time, or vice-versa. Alternatively use F_{λ} directly on the horizontal axis.
4. To get accurate values for repeated or CR-SPLIT exposures, one should use the sub-exposure time when consulting the plot, and then multiply the resulting S/N by \sqrt{N} , where N is the number of sub-exposures to be averaged. Recall that these plots assume CR-SPLIT=2 for CCD observations.

We now give a sample S/N calculation using these plots. Consider a $V=18$ star of spectral class B0 V, for which we want to derive the S/N for a 100 sec CR-SPLIT exposure in G430L with the CCD. We look up the B0 V spectral class and interpolate in the table between 4000 Å ($STMAG_{\lambda} = -1.20$) and 4500 Å ($STMAG_{\lambda} = -0.78$) to obtain $STMAG_{\lambda} \sim -1$ at 4300 Å. We thus have $V+STMAG_{\lambda} = 17$. We look at Figure 13.12 and find this value on the horizontal axis. We locate exposure time 100 and find $S/N \sim 10$. This exposure is well below the saturation lines in the plot, so saturation is not a concern.

13.2.4 Plate Scales

In the grating information section, the plate scale (units: arcseconds/pixel) is given in the table for each grating. The values used have been obtained from imaging observations and have been approximated at 0.05 arcseconds/pixel for the CCD modes, and 0.025 arcseconds/pixel for the G140L and G230L MAMA modes (see Section 14.6). The other MAMA spectroscopy modes operate at a lower magnification, yielding a cross-dispersion plate scale of 0.029 arcseconds/pixel. Anamorphic magnification by the gratings further modifies the plate scales in the dispersion direction, particularly for the echelle modes. The relevant scales in both directions have been used in the generation of each grating's diffuse source sensitivity and signal-to-noise plots.

The exact level of anamorphic magnification is a function of grating and central wavelength. More detailed information on the CCD modes can be found in [ISR 1998-23](#) "Plate Scales, Anamorphic Magnification & Dispersion: CCD Modes" by C. Bowers and S. Baum.

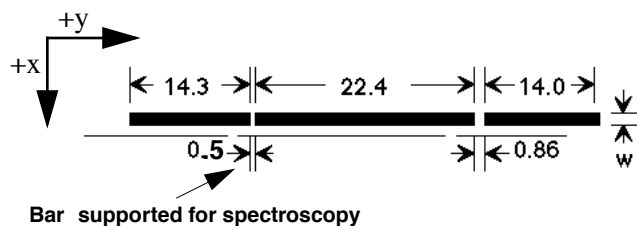
13.2.5 Apertures

For each supported slit (aperture) we provide a table giving the name of the slit, length (in the spatial direction) and width (in the dispersion direction) of the slit as well as a table and plot of the relative throughput of the slit (with respect to a large clear aperture) as a function of wavelength. Recall, that the point source sensitivities that we have derived assume zero slit losses. Your calculations of exposure times must account for light losses for the desired slit. Aperture throughputs measured in orbit are given in Instrument Science Reports 1998-20 and 1998-25. These measurements were used to revise pre-launch models of the aperture throughputs as a function of wavelength, and these revised models were then used to calculate the aperture throughput information given in this chapter and in the aperture throughputs (apt) reference file. Currently, aperture throughputs at the CTE E1 positions (see Section 7.2.7) in the 52" long slits are assumed to be the same as the throughputs at the standard positions in the same aperture. Calibration data taken in Cycles 10 and 11 will be used to directly measure the aperture throughputs at the E1 positions, and resulting revisions will be made available in a STIS Instrument Science Report and on the “STIS Apertures” web page.

13.2.6 Fiducials on Bars

Each STIS long slit has two fiducial bars, located 11.2 arcseconds above and below the slit center, 0.86 and 0.5 arcseconds long, respectively (see Figure 13.1 below). They have several purposes. First, the bars provide structural integrity for the long slits. Second, the image of the bars obtained in wavecal (and target acquisition) images is used by the calibration software to locate the projection of the aperture on the detector in post-observation data processing. Lastly, the bars can be used to occult a source thereby providing a coronagraphic spectroscopic capability for STIS. Use of the 0.5 arcsecond bar is supported only on the 52X0.2 slit (the 52X0.2F1 aperture) for coronagraphic observations. We refer you to Section 12.9 for more information about performing coronagraphic spectroscopy, and Section 13.7.3 for some caveats.

Figure 13.1: 52" Long Slits and Location of Fiducial Bars.



13.2.7 Spatial Profiles

For each grating mode information about the cross dispersion (spatial) profiles is provided as follows:

- Plots of model fits to on-orbit data of the spectral profile in the cross dispersion (spatial) direction for a series of central wavelengths and gratings.
- A table of “encircled energies” containing two values: the percent of the total flux contained in the default calibration pipeline 1-D spectrum extraction aperture and the percent of the total flux contained in the central pixel.

13.2.8 Line-Spread Functions (Instrumental Profiles)

We show plots of predicted line-spread functions (LSFs) for CCD and MAMA spectroscopic modes (Section 13.6), as a function of wavelength and slit width. These plots are based on models of the PSFs at the aperture plane and detector PSFs that have been updated and verified using on-orbit data.

Table 13.1: $STMAG_{\lambda}$ as a Function of Wavelength for Stellar Objects. $STMAG_{\lambda}$ is defined as the color-dependent correction from V magnitude to $STMAG$ at wavelength λ .

Temp (K)	Wavelength (\AA)												
	1500	2000	2500	3000	3500	4000	4500	5000	6000	7000	8000	9000	10000
50000	-4.87	-3.95	-3.09	-2.35	-1.76	-1.30	-0.79	-0.32	0.41	0.97	1.64	2.17	2.62
30000	-4.36	-3.53	-2.73	-2.08	-1.54	-1.25	-0.77	-0.30	0.41	0.95	1.61	2.16	2.56
20000	-3.44	-2.77	-2.14	-1.61	-1.16	-1.14	-0.73	-0.29	0.38	0.89	1.52	2.05	2.41
15000	-2.68	-2.13	-1.55	-1.17	-0.81	-1.06	-0.69	-0.28	0.36	0.85	1.46	1.97	2.29
10000	-0.78	-0.74	-0.30	-0.21	-0.05	-0.82	-0.62	-0.25	0.32	0.76	1.34	1.85	2.09
9000	1.21	-0.28	0.07	0.00	0.09	-0.69	-0.58	-0.22	0.29	0.67	1.22	1.69	1.92
8000	6.07	0.66	0.60	0.18	0.14	-0.49	-0.45	-0.17	0.25	0.56	1.05	1.48	1.72
7000	8.90	1.77	1.30	0.37	0.17	-0.28	-0.31	-0.08	0.18	0.45	0.89	1.26	1.52
6000	13.33	5.15	2.90	0.95	0.40	-0.01	-0.16	0.01	0.10	0.28	0.65	0.93	1.17
5000	19.41	9.70	6.29	3.07	1.32	0.51	0.03	0.17	-0.03	0.07	0.36	0.58	0.75
4000	22.27	14.10	9.24	5.41	2.65	1.17	0.40	0.64	-0.26	-0.43	-0.38	-0.32	-0.16
3000	34.85	24.46	14.38	8.06	3.82	1.18	0.74	1.50	-0.15	-0.76	-1.81	-2.36	-2.37

Table 13.2: $STMAG_{\lambda}$ as a Function of Wavelength for Non-Stellar Objects. $STMAG_{\lambda}$ is defined as the color-dependent correction from V magnitude to $STMAG$ at wavelength λ .

Spectrum	Wavelength (\AA)												
	1500	2000	2500	3000	3500	4000	4500	5000	6000	7000	8000	9000	10000
Elliptical	3.35	3.19	4.17	2.92	1.60	0.70	0.17	0.15	-0.04	-0.08	-0.07	-0.13	n/a
S0	4.63	3.95	3.27	2.23	1.61	0.71	0.18	0.13	-0.03	-0.13	-0.02	-0.08	n/a
Sa	2.64	2.27	2.39	1.78	1.31	0.36	0.12	0.07	-0.06	-0.05	-0.00	0.02	n/a
Sb	1.70	2.59	2.04	1.32	1.12	0.43	0.17	0.10	0.02	-0.05	-0.01	-0.04	n/a
Sc	-0.18	0.44	-0.17	-0.68	-0.67	-0.51	-0.44	-1.25	0.18	0.40	n/a	n/a	n/a
Starburst, $E(B-V)<0.1$	-1.71	-1.15	-0.68	-0.43	-0.13	-0.42	-0.23	-1.24	0.21	0.40	0.70	0.85	n/a
Starburst, $0.25<E(B-V)<0.35$	-0.95	-0.87	-0.33	-0.10	0.08	-0.19	-0.19	-0.28	0.15	0.44	0.41	0.47	n/a
Starburst, $0.51<E(B-V)<0.60$	-0.40	-0.18	0.01	0.23	0.03	-0.14	-0.12	-0.36	0.07	0.07	0.18	0.29	n/a
Starburst, $0.61<E(B-V)<0.70$	0.05	0.31	0.31	0.15	0.27	-0.17	-0.13	-0.11	0.06	0.17	0.26	0.24	n/a

How to Use The $STMAG_{\lambda}$ Tables

1. Interpolate in the table to get $STMAG_{\lambda}$ for the spectral type and wavelength region of your target observation (e.g. 6000K star @ 4300 \AA).
2. Add the target V magnitude to the $STMAG_{\lambda}$ derived from Step 1.
3. Find the S/N plot for the grating you want to use.
4. Locate $V+STMAG_{\lambda}$ on the horizontal axis and read off the S/N for the desired exposure time (or read off the exposure time for the desired S/N).

13.3 Gratings

Below, for each grating mode of STIS, we provide the basic properties of the mode, wavelength ranges covered in each central wavelength setting, sensitivities and throughputs, dispersions and plate scales. Advice on use is provided where appropriate and comparisons of the G230L, G230M MAMA modes with their G230LB, G230MB CCD counterparts are shown.

Wavelengths in this handbook and in STIS data products are always measured in vacuum conditions.

- “First-Order Grating G750L,” page 290.
- “First-Order Grating G750M,” page 293.
- “First-Order Grating G430L,” page 296.
- “First-Order Grating G430M,” page 299.
- “First-Order Grating G230LB,” page 302.
- “First-Order Grating G230MB,” page 306.
- “First-Order Grating G230L,” page 310.
- “First-Order Grating G230M,” page 313.
- “First-Order Grating G140L,” page 316.
- “First-Order Grating G140M,” page 319.
- “Echelle Grating E230M,” page 322.
- “Echelle Grating E230H,” page 325.
- “Echelle Grating E140M,” page 328.
- “Echelle Grating E140H,” page 331.
- “PRISM,” page 334.

First-Order Grating G750L

Description

The G750L grating is used with the CCD. It has high throughput but low resolving power (~500), and is designed for efficient, full spectral coverage. The grating has one prime tilt setting.

Recommended Uses

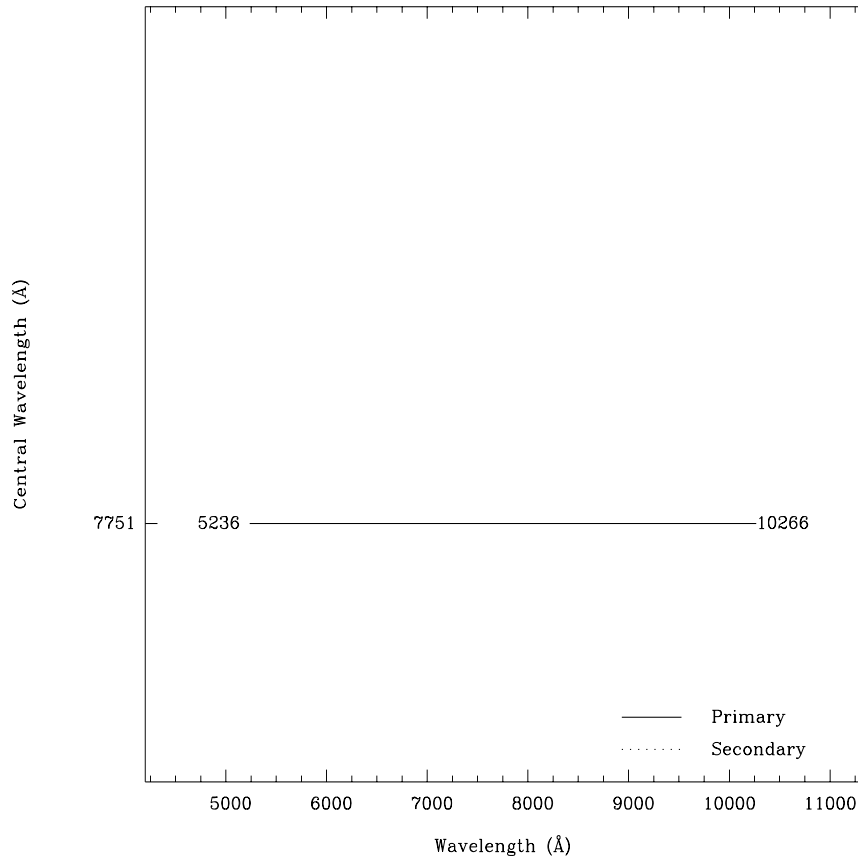
This grating is recommended for observations where high spectral resolution is not required, but efficient coverage in the red portion of the optical is desired.

Special Considerations

Fringing in the CCD compromises the realizable signal-to-noise longward of 7500 Å if contemporaneous fringe flats are not obtained (see Section 7.2).

Grating	Spectral Range		Average Dispersion (Å / Pixel)	Plate Scale (arcsec / pixel)	Tilts	Central Wavelengths
	Complete	Per Tilt				
G750L	5240–10270	5030	4.92	0.05	Prime	7751

Figure 13.2: Wavelength Range for the G750L Grating Setting

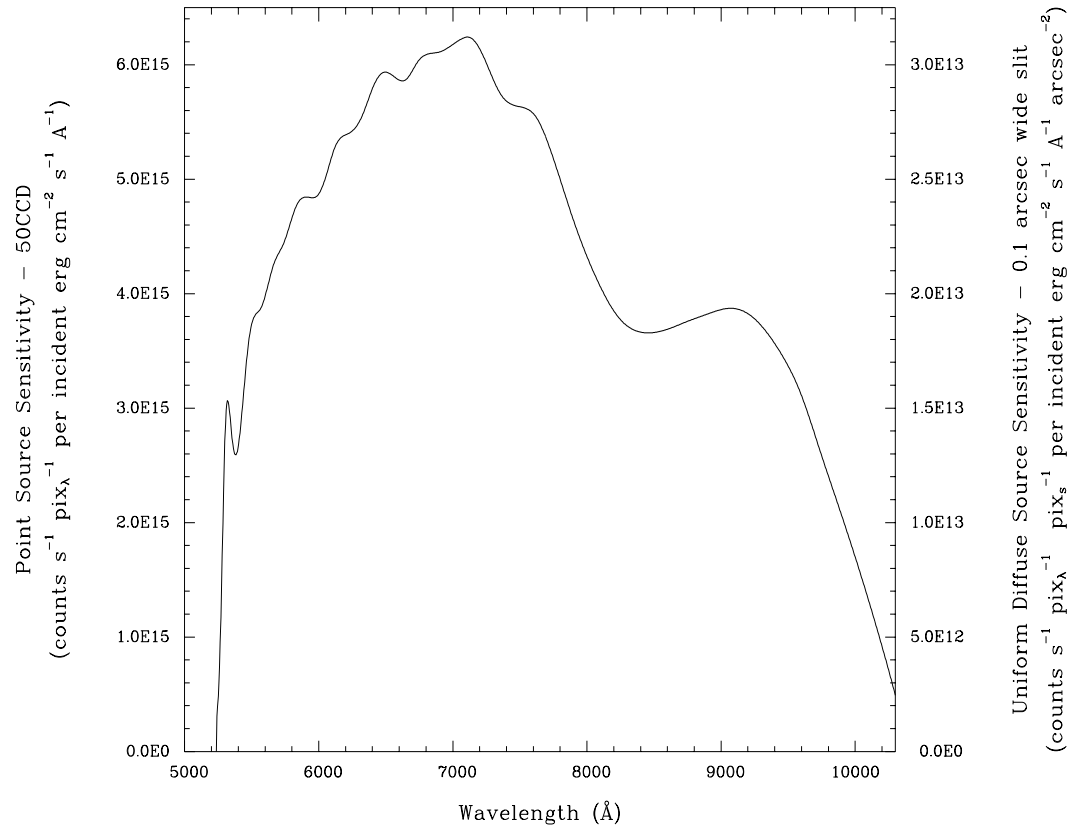


G750L Sensitivities

Table 13.3: G750L Sensitivities & Throughputs for a Point Source

λ	Sensitivity	% Throughput
5500	3.4E15	5.5
6000	5.0E15	7.5
6500	5.8E15	8.0
7000	6.1E15	7.9
7500	5.6E15	6.7
8000	4.4E15	4.9
8500	3.7E15	3.9
9000	3.8E15	3.8
9500	3.3E15	3.1
10000	1.1E15	1.5

Figure 13.3: G750L Point Source (left axis), and Diffuse Source (right axis) Sensitivities



Note

Point source sensitivity assumes full transmission (zero slit losses). Diffuse source sensitivity assumes a 0.1" wide slit. To convert point source sensitivities to diffuse source sensitivities multiply the point source values by the grating spatial (cross dispersion) plate scale in units of arcseconds per pixel and by the width of the desired slit in units of arcseconds.

G750L Signal-to-Noise

Note:

The top axis displays constant F_λ values corresponding to the STMAG units ($V+STMAG_\lambda$) on the bottom axis. Recall that $STMAG=0$ is equivalent to $F_\lambda = 3.63E-9 \text{ erg cm}^{-2} \text{ s}^{-1} \text{ \AA}^{-1}$. The curves are labeled with exposure times in seconds

Figure 13.4: Diffuse Source Signal-to-Noise as a Function of STMAG for G750L. λ Fiducial = 7500 \AA .

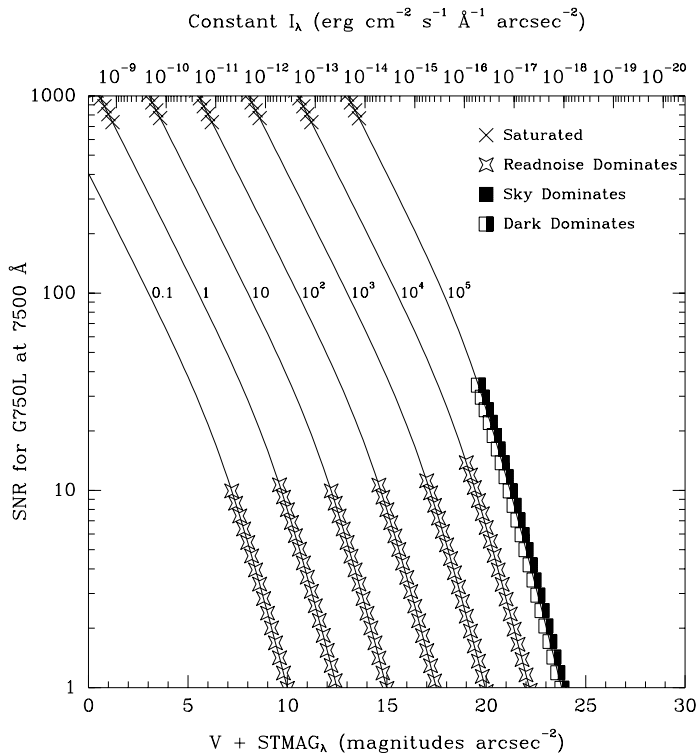
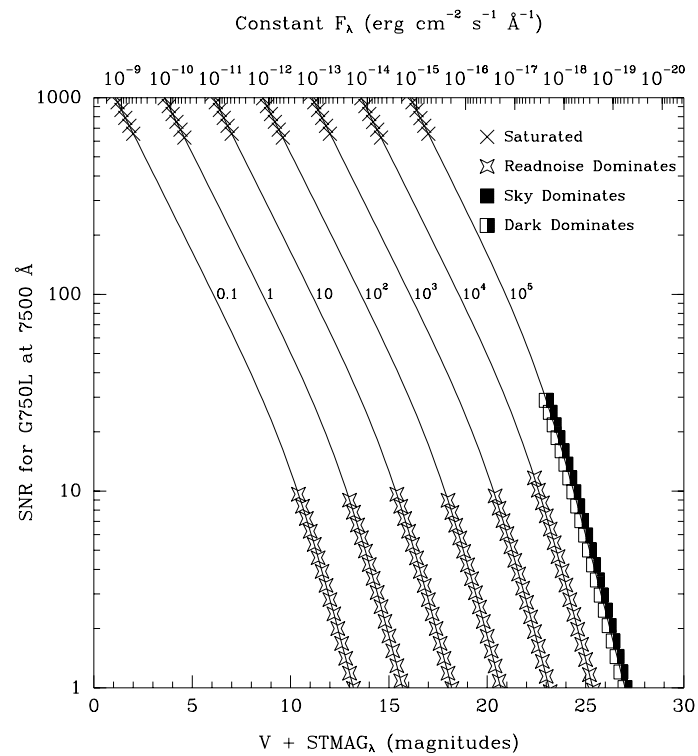


Figure 13.5: Point Source Signal-to-Noise as a Function of STMAG for G750L



First-Order Grating G750M

Description

Like G750L, the G750M grating is used with the CCD and has a spectral range from 5500–10,000 Å. With a resolving power $R \sim 5000$, a single exposure with this grating covers only 570 Å, and the grating must be scanned, with a series of exposures taken at 9 distinct settings to cover the full range of the grating.

Recommended Uses

This grating is designed for relatively high spectral resolution work centered on selected wavelength regions of the optical to near-IR.

Special Considerations

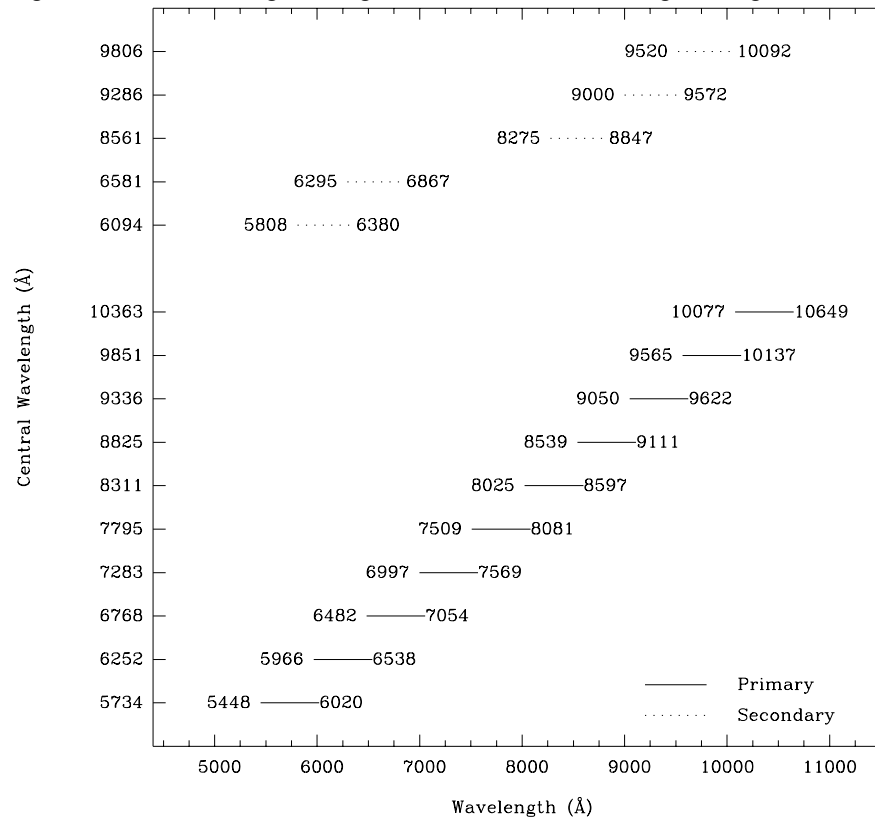
There is a partial ghost spectrum present in the $\lambda_c = 5734$ setting which is $\sim 1.2\%$ of, is inverted with respect to, is offset by ~ 70 pixels from, the prime spectrum, arising from back reflections between the CCD and the order sorter.

Fringing in the CCD compromises the realizable signal-to-noise longward of 7500 Å if contemporaneous fringe flats are not obtained (see Section 7.2).

The secondary central wavelengths at 6581 & 8561 Å have had direct sensitivity and wavelength calibrations performed during Cycle 7 to support the large number of observations using these positions.

Grating	Spectral Range		Average Dispersion (Å per Pixel)	Plate Scale (arcsec / pixel)	Tilts	Central Wavelengths
	Complete	Per Tilt				
G750M	5450-10140	570	0.56	0.05	Prime	5734, 6252, 6768, 7283, 7795, 8311, 8825, 9336, 9851
					Secondary	6094, 6581, 8561, 9286, 9806

Figure 13.6: Wavelength Ranges for the G750M Grating Settings

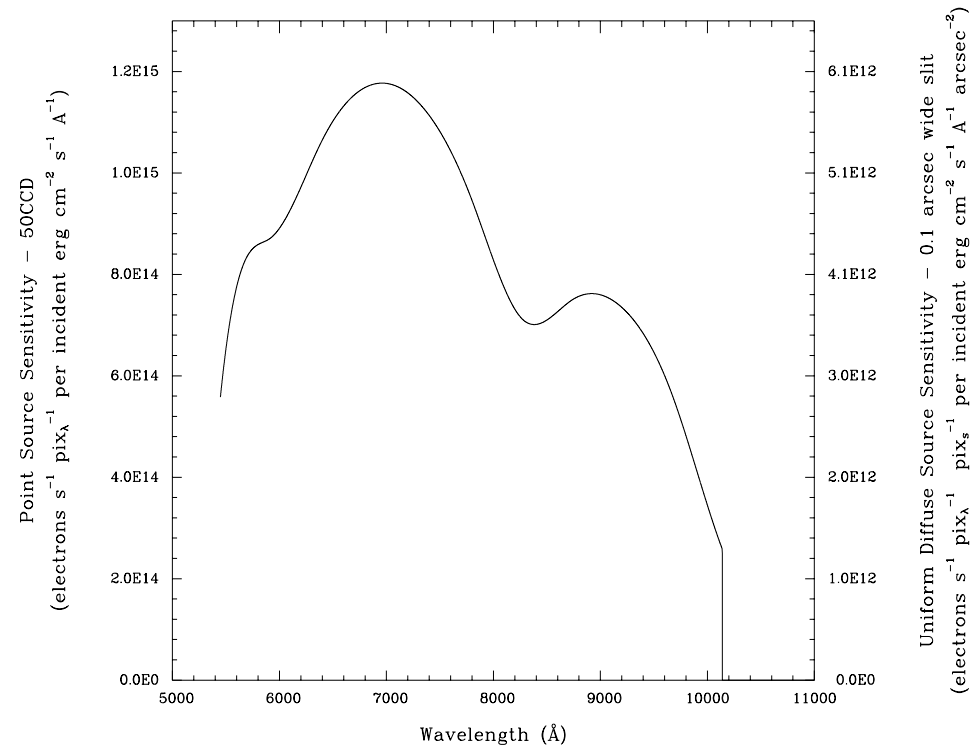


G750M Sensitivities

Table 13.4: G750M Sensitivities & Throughputs for a Point Source

λ	Sensitivity	% Throughput
5500	6.6E14	9.6
6000	9.0E14	12.0
6500	1.1E15	13.4
7000	1.2E15	13.3
7500	1.1E15	11.5
8000	8.3E14	8.3
8500	7.2E14	6.7
9000	7.5E14	6.7
9500	6.4E14	5.4
10000	3.0E14	2.8
10500	0.0E0	0.0

Figure 13.7: G750M Point Source (left axis), and Diffuse Source (right axis) Sensitivities.



Note

Point source sensitivity assumes full transmission (zero slit losses). Diffuse source sensitivity assumes a 0.1" wide slit. To convert point source sensitivities to diffuse source sensitivities multiply the point source values by the grating spatial (cross dispersion) plate scale in units of arcseconds per pixel and by the width of the desired slit in units of arcseconds.

G750M Signal-to-Noise

Note:

The top axis displays constant F_λ values corresponding to the STMAG units ($V+STMAG_\lambda$) on the bottom axis. Recall that $STMAG=0$ is equivalent to $F_\lambda = 3.63E-9 \text{ erg cm}^{-2} \text{ s}^{-1} \text{ \AA}^{-1}$. The curves are labeled with exposure times in seconds

Figure 13.8: Diffuse Source Signal-to-Noise as a Function of STMAG for G750M

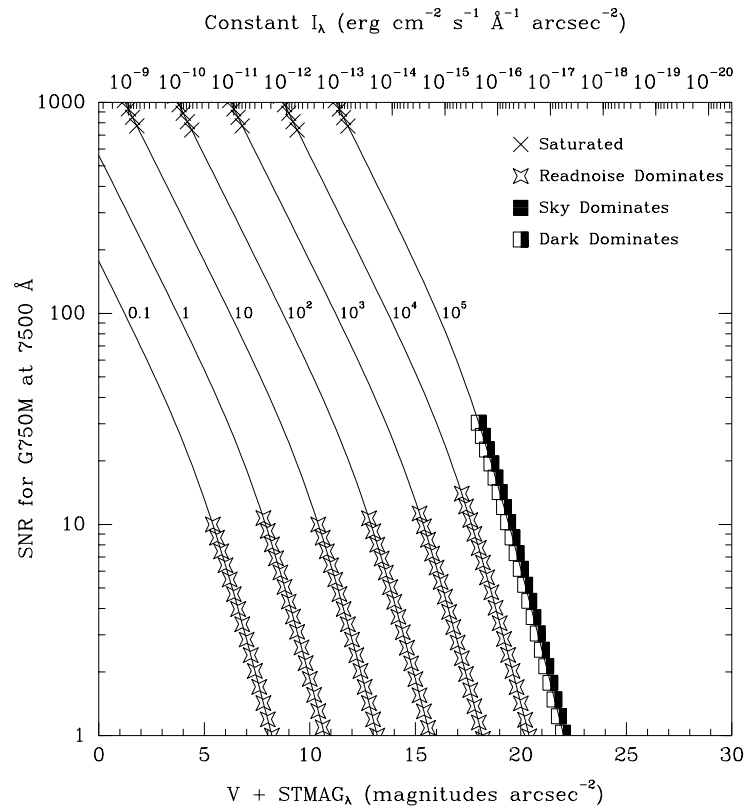
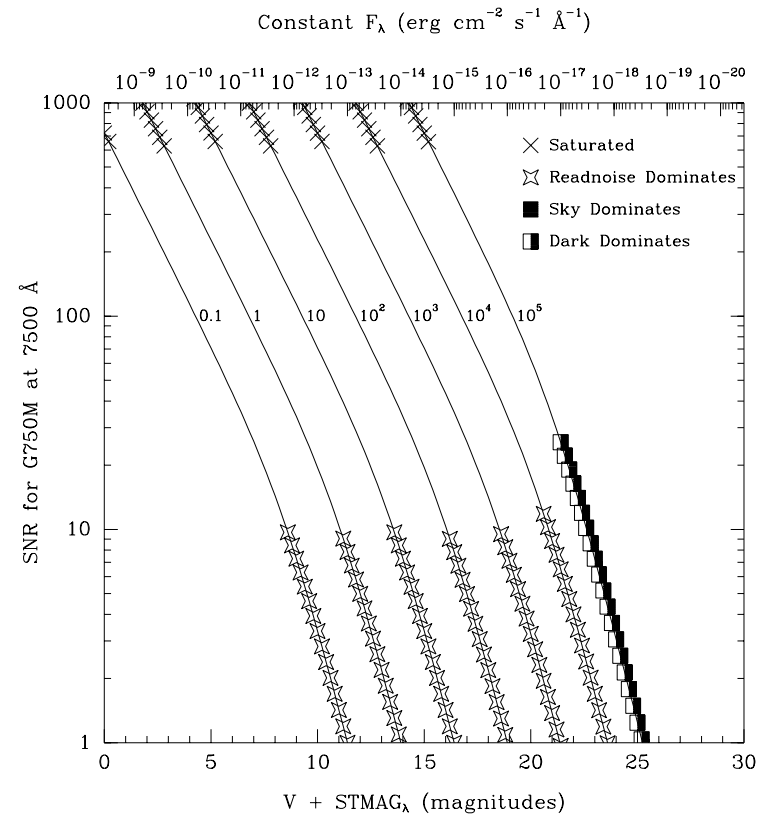


Figure 13.9: Point Source Signal-to-Noise as a Function of STMAG for G750M



First-Order Grating G430L

Description

G430L, used with the CCD, is a low resolution grating ($R \sim 500$) with a relatively high throughput. The grating has only a single setting.

Recommended Uses

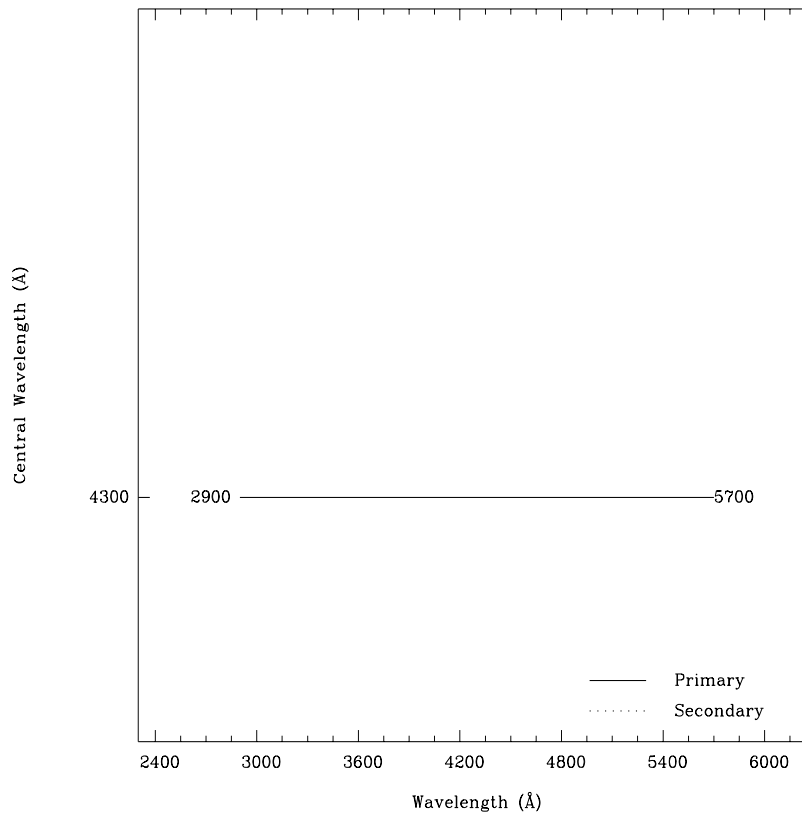
This grating is designed for observations where high spectral resolution is not required, but efficient spectral coverage in the blue portion of the optical is desired.

Special Considerations

Notice, that by taking two observations, one with G750L and one with G430L, the full spectral region, from the near-IR at 10000 \AA through the optical at 3000 \AA can be efficiently observed at an $R \sim 500$.

Grating	Spectral Range		Average Dispersion (\AA per Pixel)	Plate Scale (arcsec / pixel)	Tilts	Central Wavelengths
	Complete	Per Tilt				
G430L	2900-5700	2800	2.73	0.05	Prime	4300

Figure 13.10: Wavelength Ranges for the G430L Grating Settings

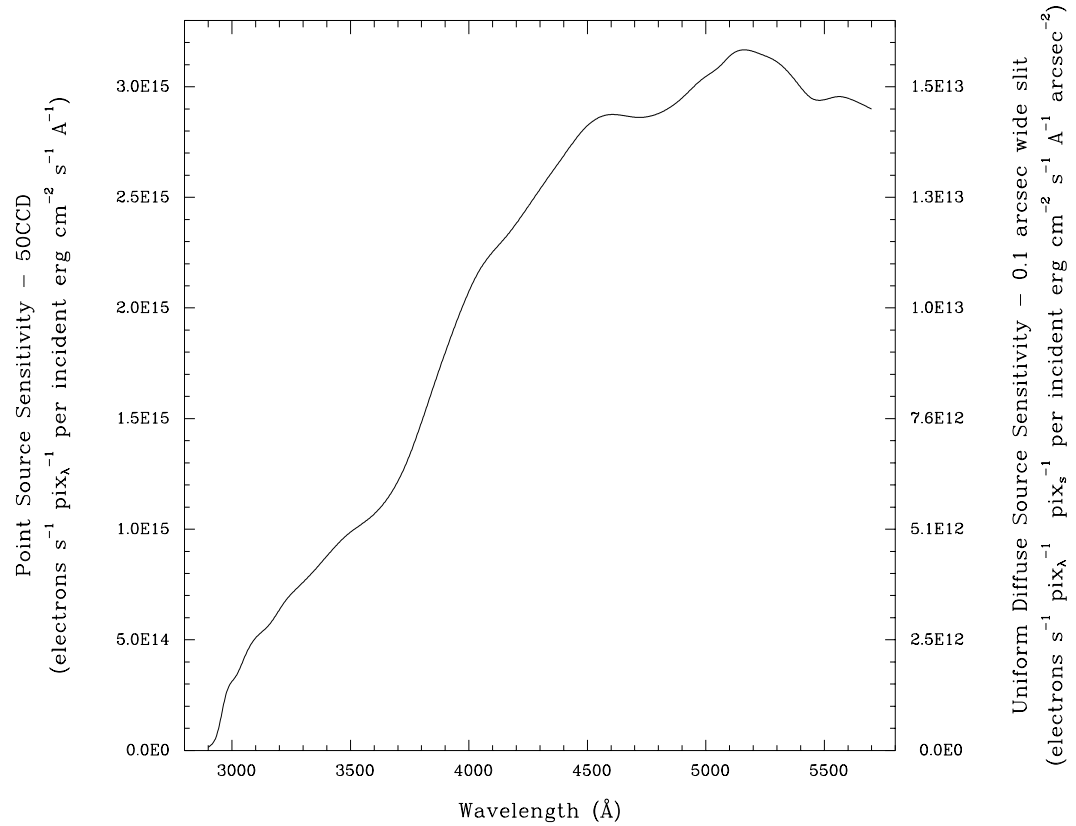


G430L Sensitivities

Table 13.5: G430L Sensitivities & Throughputs for a Point Source

λ	Sensitivity	% Throughput
3000	2.7E14	1.5
3250	7.0E14	3.5
3500	9.8E14	4.5
3750	1.4E15	5.9
4000	2.0E15	8.3
4250	2.5E15	9.4
4500	2.8E15	10.1
4750	2.9E15	9.9
5000	3.0E15	9.9
5250	3.1E15	9.7
5500	3.0E15	8.7

Figure 13.11: G430L Point Source (left axis), and Diffuse Source (right axis) Sensitivities.



Note

Point source sensitivity assumes full transmission (zero slit losses). Diffuse source sensitivity assumes a 0.1" wide slit. To convert point source sensitivities to diffuse source sensitivities multiply the point source values by the grating spatial (cross dispersion) plate scale in units of arcseconds per pixel and by the width of the desired slit in units of arcseconds.

G430L Signal-to-Noise

Note:

The top axis displays constant F_λ values corresponding to the STMAG units ($V+STMAG_\lambda$) on the bottom axis. Recall that $STMAG=0$ is equivalent to $F_\lambda = 3.63E-9 \text{ erg cm}^{-2} \text{ s}^{-1} \text{ \AA}^{-1}$. The curves are labeled with exposure times in seconds

Figure 13.12: Diffuse Source Signal-to-Noise as a Function of STMAG for G430L

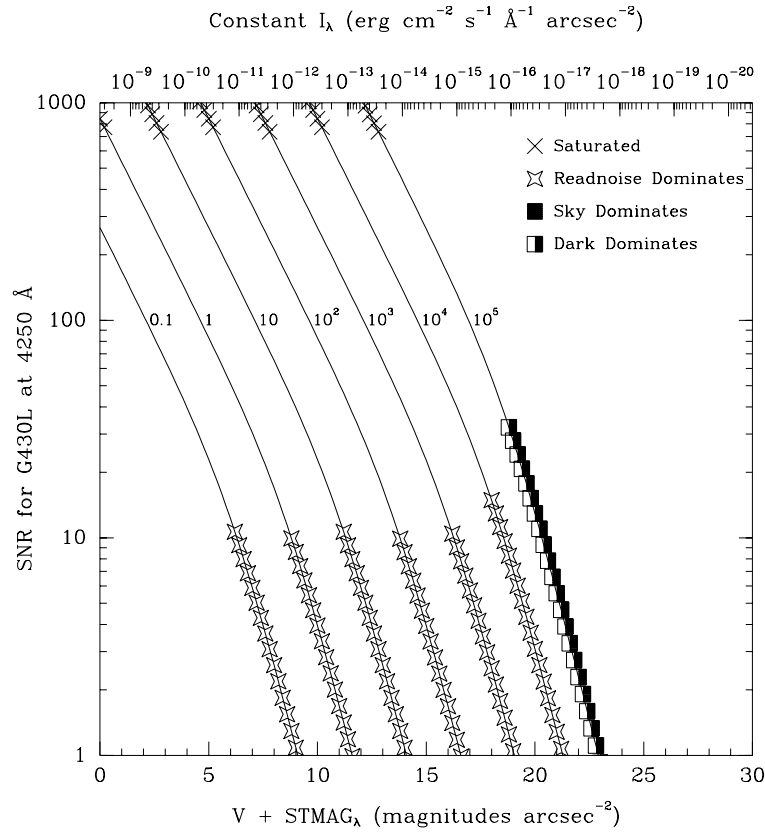
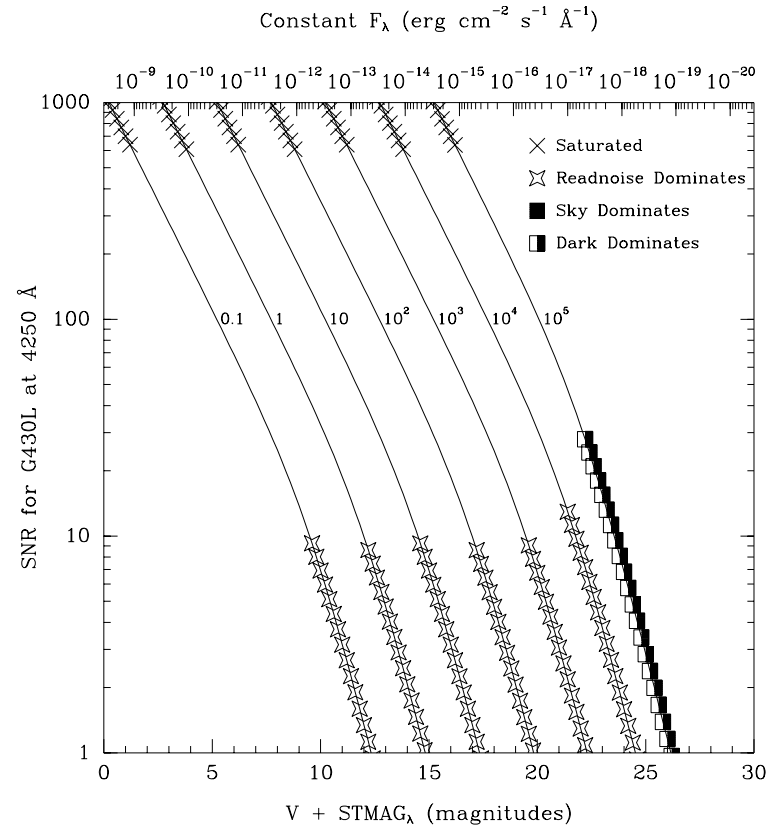


Figure 13.13: Point Source Signal-to-Noise as a Function of STMAG for G430L



First-Order Grating G430M

Description

Like the G430L grating, the G430M grating is used with the CCD and has a spectral range from 3020–5600 Å.

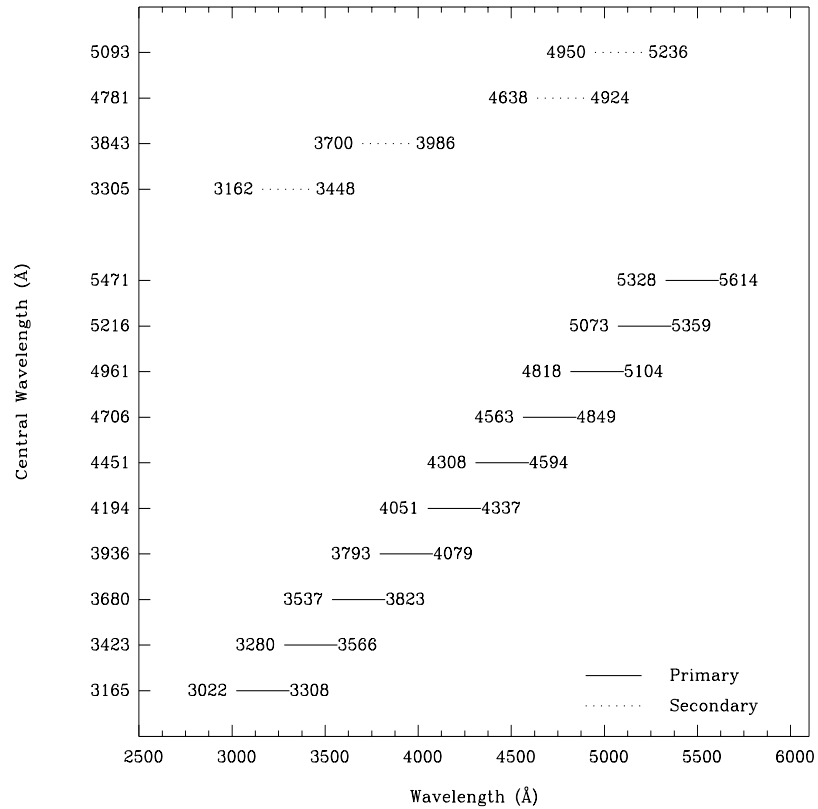
Since a single exposure taken with this grating covers only 286 Å the grating must be scanned, with a series of exposures taken at 10 distinct settings, to cover the full spectral range of the grating.

Recommended Uses

The G430M grating mode is designed for observations where spatially resolved, long slit spectroscopy is desired at relatively high spectral resolution ($R \sim 6000$) over a limited region of the near-ultraviolet or optical spectrum.

Grating	Spectral Range		Average Dispersion (Å per Pixel)	Plate Scale (arcsec / pixel)	Tilts	Central Wavelengths
	Complete	Per Tilt				
G430M	3020-5610	286	0.28	0.05	Prime	3165, 3423, 3680, 3936, 4194, 4451, 4706, 4961, 5216, 5471
					Secondary	3305, 3843, 4781, 5093

Figure 13.14: Wavelength Ranges for the G430M Grating Settings

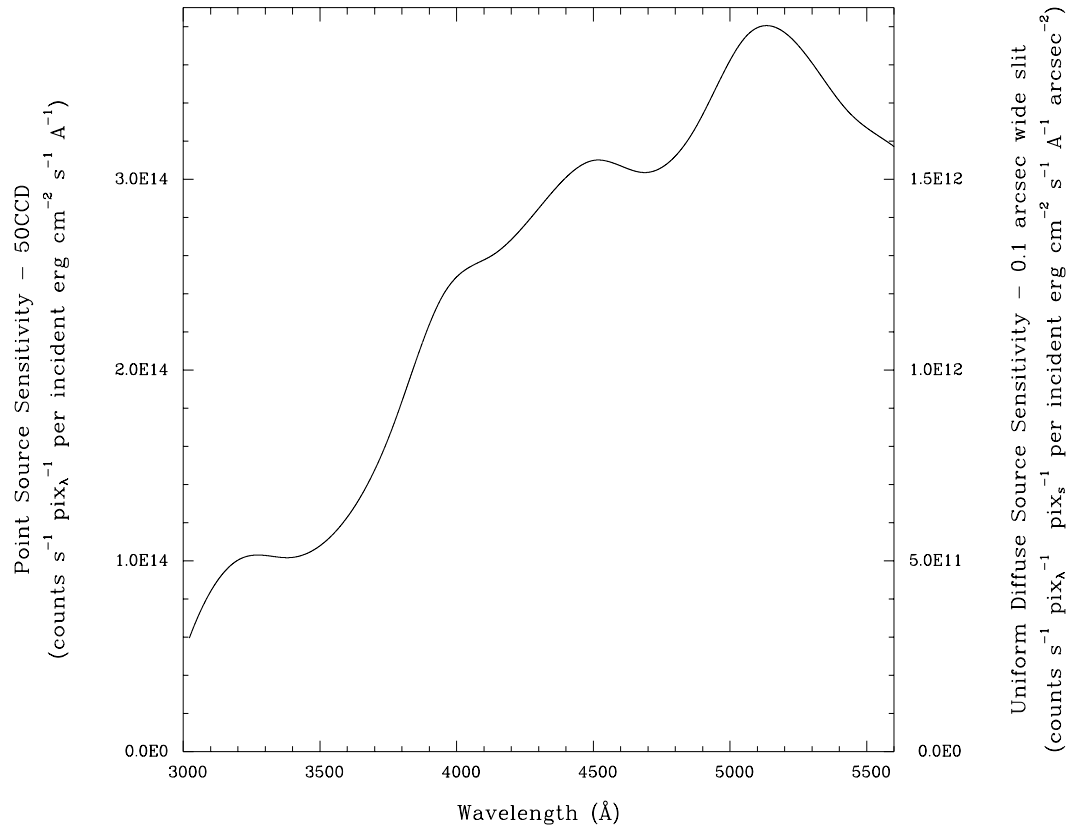


G430M Sensitivities

Table 13.6: G430M Sensitivities & Throughputs for a Point Source

λ	Sensitivity	% Throughput
3100	8.3E13	4.2
3300	1.0E14	4.9
3500	1.1E14	4.8
3700	1.5E14	6.3
3900	2.2E14	9.0
4100	2.6E14	9.9
4300	2.8E14	10.4
4500	3.1E14	10.8
4700	3.0E14	10.1
4900	3.3E14	10.7
5100	3.8E14	11.6
5300	3.6E14	10.7
5500	3.3E14	9.3

Figure 13.15: G430M Point Source (left axis), and Diffuse Source (right axis) Sensitivities.



Note

Point source sensitivity assumes full transmission (zero slit losses). Diffuse source sensitivity assumes a 0.1" wide slit. To convert point source sensitivities to diffuse source sensitivities multiply the point source values by the grating spatial (cross dispersion) plate scale in units of arcseconds per pixel and by the width of the desired slit in units of arcseconds.

G430M Signal-to-Noise

Note:

The top axis displays constant F_λ values corresponding to the STMAG units ($V+STMAG_\lambda$) on the bottom axis. Recall that $STMAG=0$ is equivalent to $F_\lambda = 3.63E-9 \text{ erg cm}^{-2} \text{ s}^{-1} \text{ \AA}^{-1}$. The curves are labeled with exposure times in seconds.

Figure 13.16: Diffuse Source Signal-to-Noise as a Function of STMAG for G430M

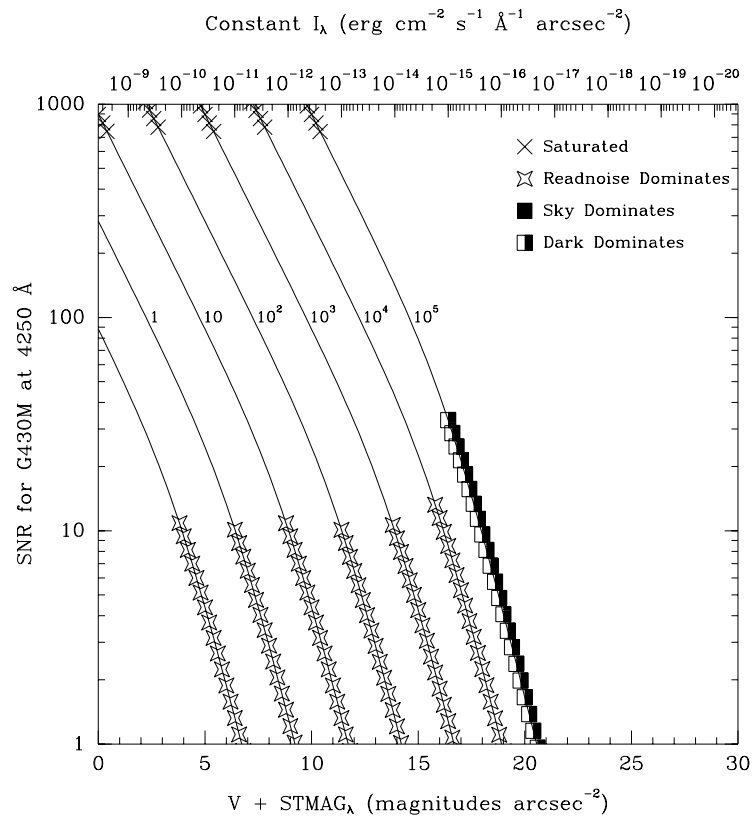
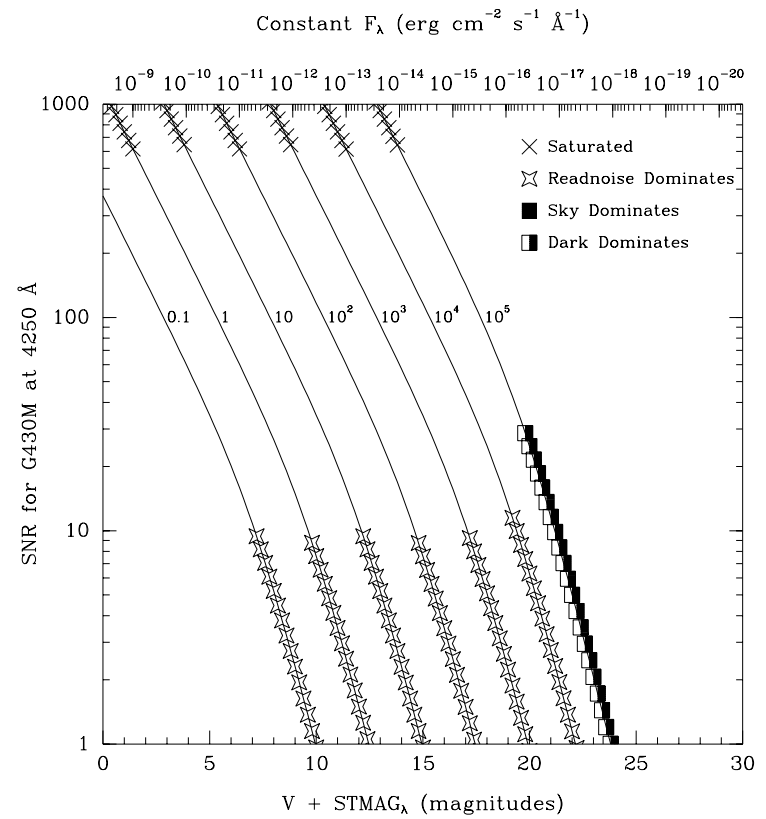


Figure 13.17: Point Source Signal-to-Noise as a Function of STMAG for G430M



First-Order Grating G230LB

Description

The G230LB grating mode uses a low resolution grating originally designed for use with the STIS/NUV-MAMA which has been re-directed for use with the STIS/CCD to enable R~700 spectroscopy in the near-UV which takes advantage of the CCD's higher throughput and dynamic range longward of $\lambda=2500 \text{ \AA}$.

Recommended Uses

The G230LB grating mode is designed for programs needing the highest available sensitivity in the near-UV from ~2500 to 3100 \AA or more generally to allow observation of sources too bright for the MAMA in the near UV.

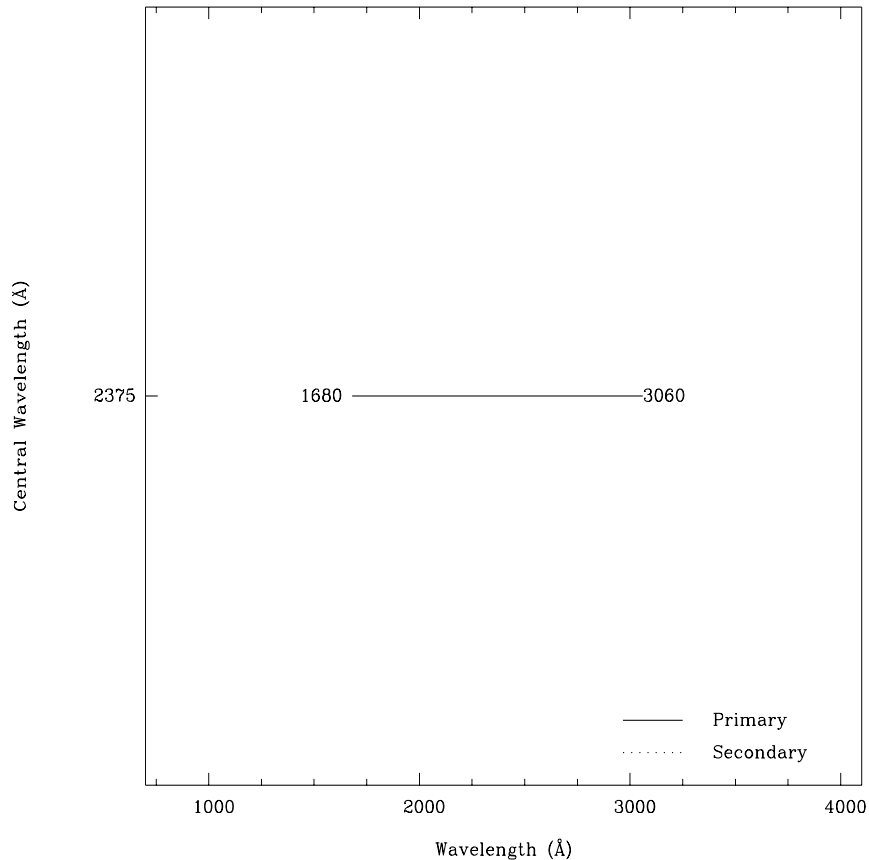
Special Considerations

In making the plots for the G230LB grating mode, we assumed that the CCD is subject to a change in the effective quantum yield resulting in the creation of multiple electron-hole pairs per photon for $\lambda < 3400 \text{ \AA}$.

Also be aware that because of the high sensitivity of the CCD to red light, observations of red stars with G230LB are more likely to be affected by scatter than observations of red stars using the MAMA G230L mode.

Grating	Spectral Range		Average Dispersion (\AA per Pixel)	Plate Scale (arcsec / pixel)	Tilts	Central Wavelengths
	Complete	Per Tilt				
G230LB	1680-3060	1380	1.35	0.05	Prime	2375

Figure 13.18: Wavelength Range for the G230LB Grating Setting

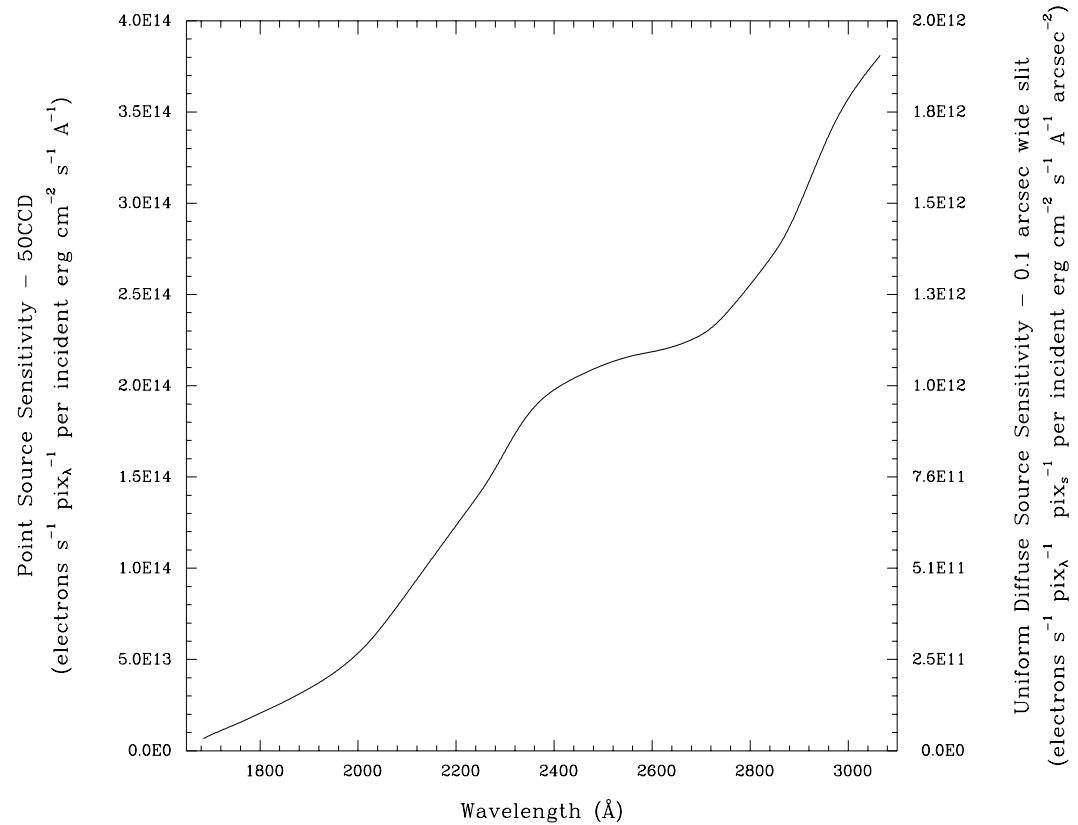


G230LB Sensitivities

Table 13.7: G230LB Sensitivities & Throughputs for a Point Source

λ	Sensitivity	% Throughput
1750	1.5E13	0.3
1850	2.7E13	0.5
1950	4.3E13	0.7
2050	6.9E13	1.1
2150	1.1E14	1.6
2250	1.4E14	2.1
2350	1.8E14	2.6
2450	2.1E14	2.8
2550	2.2E14	2.9
2650	2.2E14	2.8
2750	2.4E14	2.9
2850	2.7E14	3.3
2950	3.3E14	3.8
3050	3.8E14	4.2

Figure 13.19: G230LB Point Source (left axis), and Diffuse Source (right axis) Sensitivities.



Note

Point source sensitivity assumes full transmission (zero slit losses). Diffuse source sensitivity assumes a 0.1" wide slit. To convert point source sensitivities to diffuse source sensitivities multiply the point source values by the grating spatial (cross dispersion) plate scale in units of arcseconds per pixel and by the width of the desired slit in units of arcseconds.

G230LB Signal-to-Noise

Note:

The top axis displays constant F_λ values corresponding to the STMAG units ($V+STMAG_\lambda$) on the bottom axis. Recall that $STMAG=0$ is equivalent to $F_\lambda = 3.63E-9 \text{ erg cm}^{-2} \text{ s}^{-1} \text{ \AA}^{-1}$. The curves are labeled with exposure times in seconds.

Figure 13.20: Diffuse Source Signal-to-Noise as a Function of STMAG for G230LB

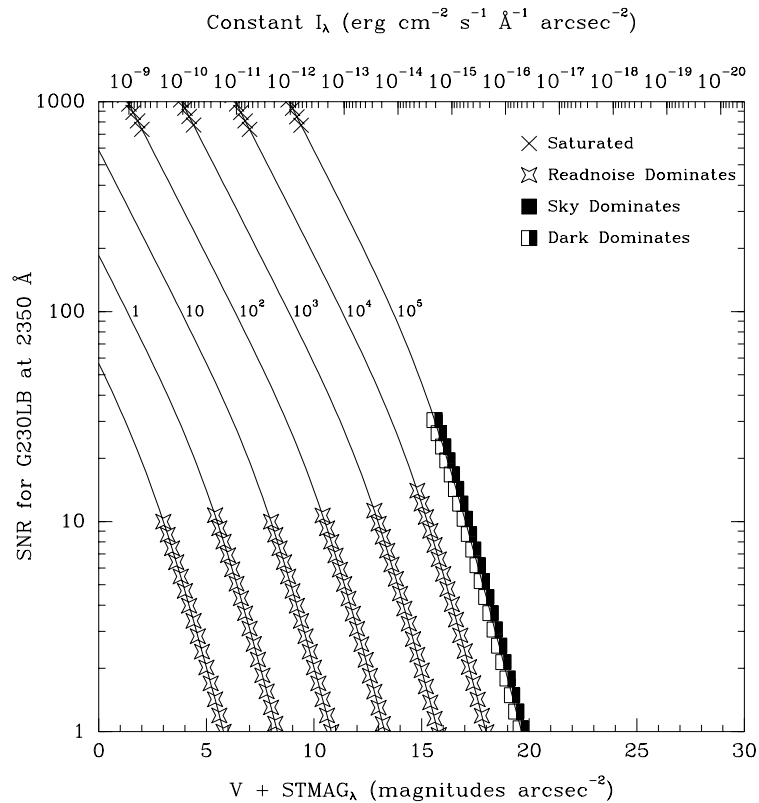
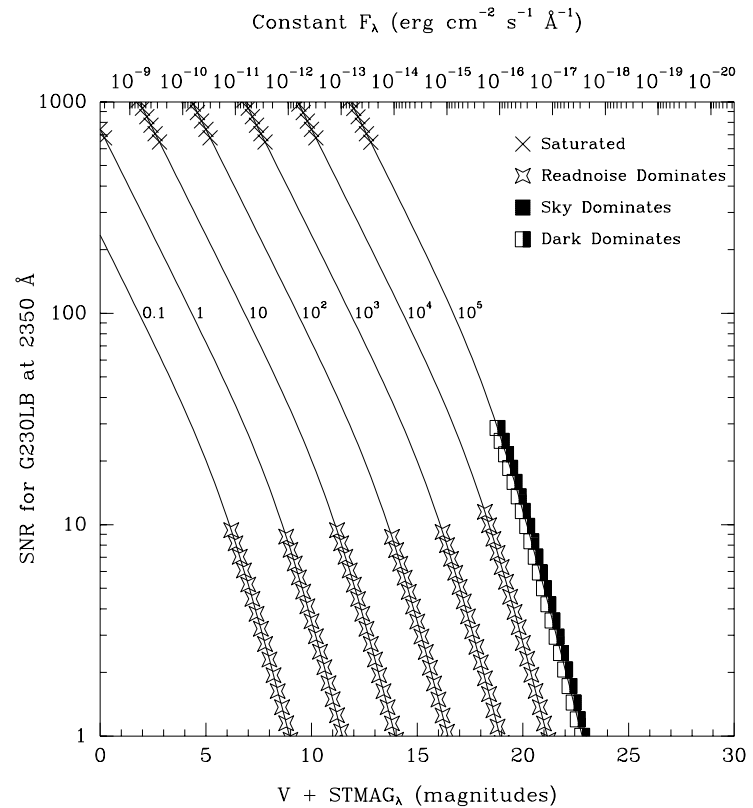


Figure 13.21: Point Source Signal-to-Noise as a Function of STMAG for G230LB

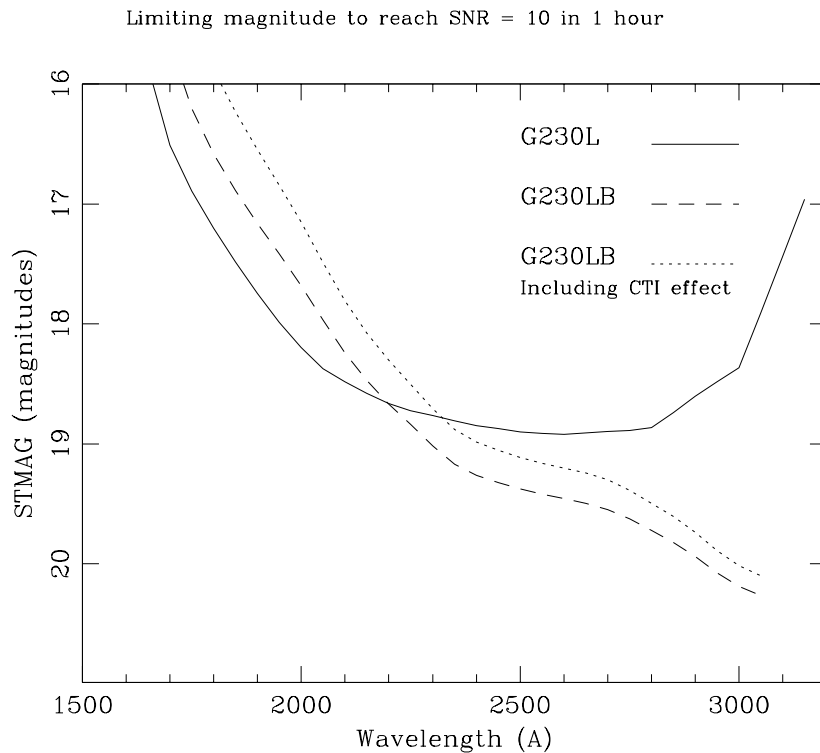


Comparison of G230LB and G230L

The trade-off between using the G230LB or the G230L (which uses the NUV-MAMA), depends sensitively on the science goals and your source properties.

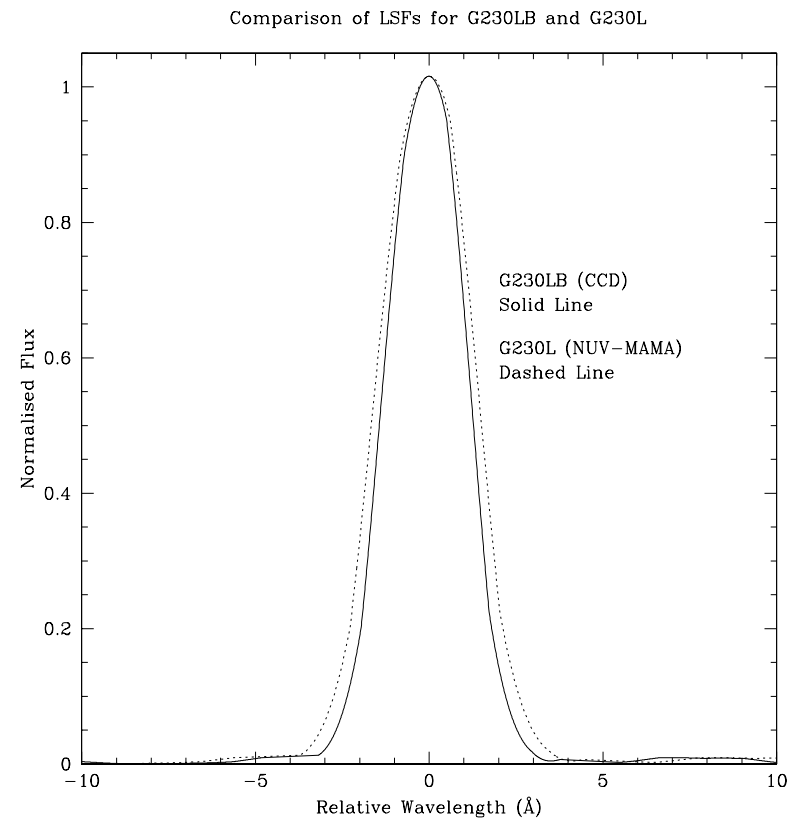
- The CCD has read noise, whereas the MAMA does not.
- The CCD suffers from charge transfer inefficiency (CTI), whereas the NUV-MAMA does not

Figure 13.22: Comparison of Limiting Magnitudes and Fluxes for G230LB and G230L. Plotted are the limiting source magnitudes and fluxes for G230LB and G230L to achieve a signal-to-noise ratio of 10 per 2-pixel spectral resolution element integrated across the PSF, in 1 hour. The prediction due to the Charge Transfer Inefficiency (CTI) effect, expected in the year 2005, is also shown.



- The CCD does not have bright object limits, whereas the MAMA does.
- The NUV-MAMA is solar insensitive, whereas the CCD is not.
- The spatial sampling of the MAMA is better than that of the CCD.
- The CCD does not enable high time resolution ($\Delta t < 10$ seconds), whereas the MAMA does.
- For red objects, CCD data can suffer from scattered light problems. The detector PSF of the CCD is much cleaner than that of the NUV-MAMA.

Figure 13.23: Comparison of LSFs for G230LB and G230L



First-Order Grating G230MB

Description

The G230MB grating mode uses an intermediate resolution grating originally designed for use with the NUV-MAMA which has been redirected for use with the CCD to provide R~6000 spectroscopy in the near-UV which takes advantage of the CCD's higher throughput longward of $\lambda=2500 \text{ \AA}$. The G230MB grating mode has a spectral range from 1640-3190 \AA .

As a single exposure with this grating covers only 150 \AA , the grating must be scanned with a series of exposures taken at 11 distinct settings to cover the full spectral range of the grating.

Recommended Uses

The G230MB grating is designed for programs that require the highest available sensitivity in the near-UV from ~2500 to 3100 \AA or more generally to allow observations of sources too bright for the MAMAs in near-UV.

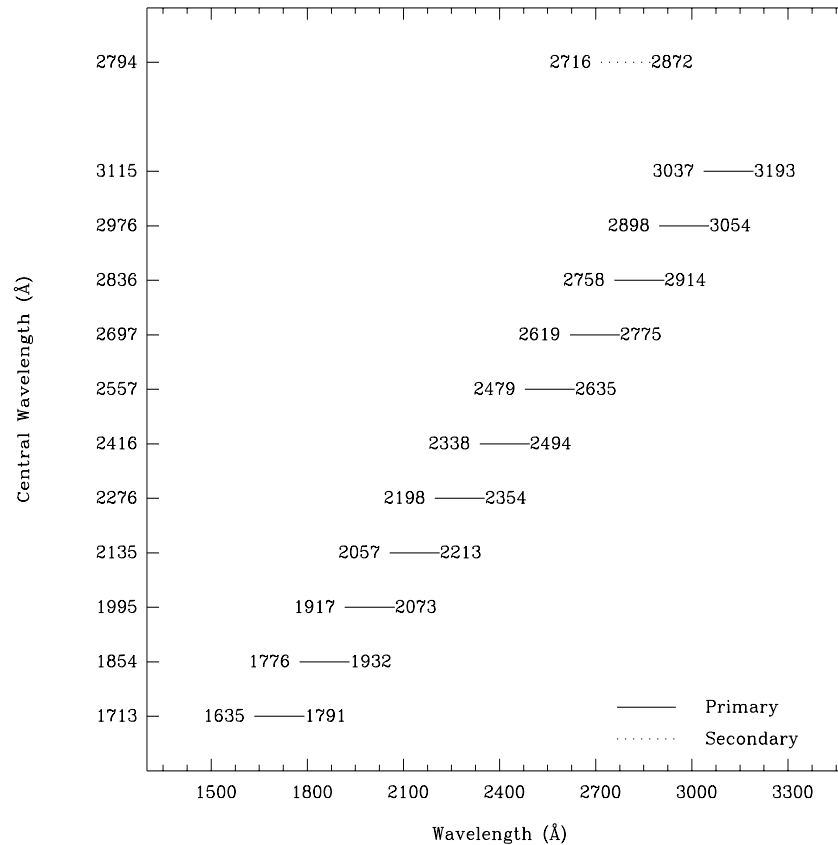
Special Considerations

In making the plots for the G230MB grating mode, we assumed that the CCD is subject to a change in the effective quantum yield resulting in the creation of multiple electron-hole pairs per photon for $\lambda < 3400 \text{ \AA}$.

Also, because of the high sensitivity of the CCD to red light, observations of red stars with G230MB are more likely be affected by scatter than those using the MAMA G230M mode.

Grating	Spectral Range		Average Dispersion (\AA per Pixel)	Plate Scale (arcsec / pixel)	Tilts	Central Wavelengths
	Complete	Per Tilt				
G230MB	1640-3190	155	0.15	0.05	Prime	1713, 1854, 1995, 2135, 2276, 2416, 2557, 2697, 2836, 2976, 3115
					Secondary	2794

Figure 13.24: Wavelength Ranges for the G230MB Grating Settings

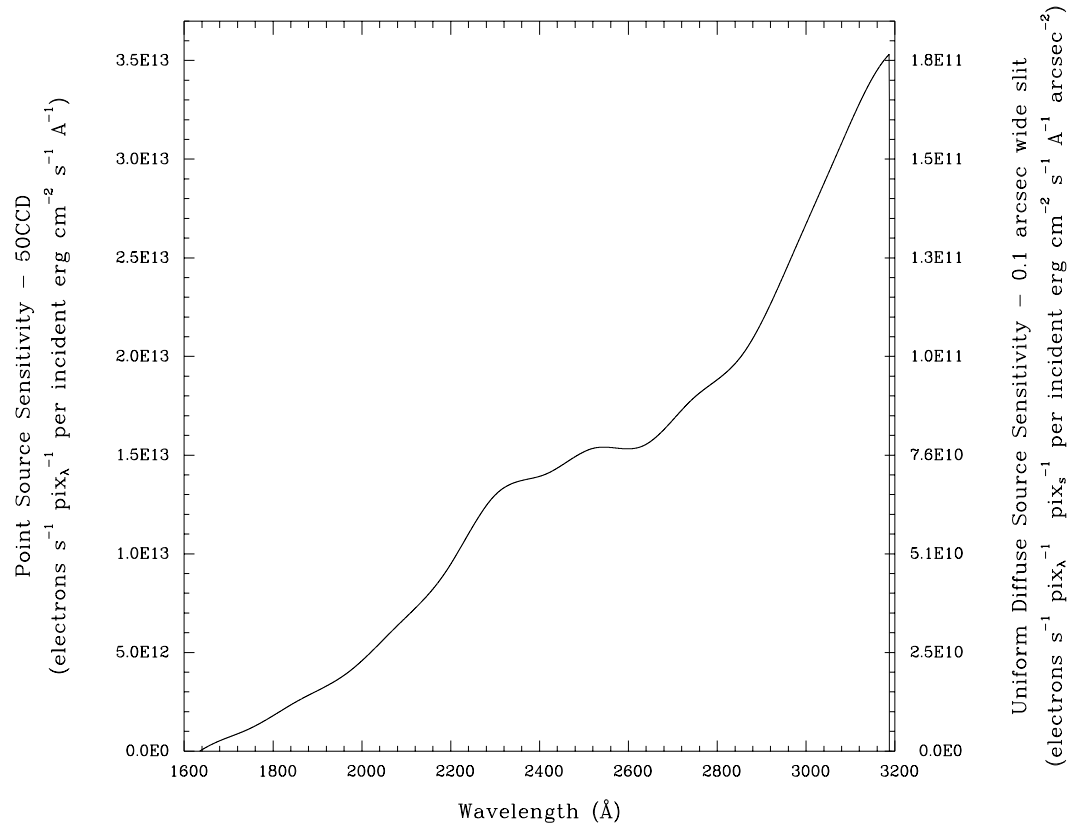


G230MB Sensitivities

Table 13.8: G230MB Throughputs & Sensitivities for a Point Source

λ	Sensitivity	% Throughput
1700	7.0E11	0.1
1800	1.8E12	0.3
1900	3.1E12	0.5
2000	4.6E12	0.7
2100	6.8E12	0.9
2200	9.5E12	1.3
2300	1.3E13	1.6
2400	1.4E13	1.7
2500	1.5E13	1.8
2600	1.5E13	1.7
2700	1.7E13	1.8
2800	1.9E13	2.0
2900	2.2E13	2.2
3000	2.7E13	2.6
3100	3.2E13	3.0

Figure 13.25: G230MB Point Source (left axis), and Diffuse Source (right axis) Sensitivities.



Note

Point source sensitivity assumes full transmission (zero slit losses). Diffuse source sensitivity assumes a 0.1" wide slit. To convert point source sensitivities to diffuse source sensitivities multiply the point source values by the grating spatial (cross dispersion) plate scale in units of arcseconds per pixel and by the width of the desired slit in units of arcseconds.

G230MB Signal-to-Noise

Note:

The top axis displays constant F_λ values corresponding to the STMAG units ($V+STMAG_\lambda$) on the bottom axis. Recall that $STMAG=0$ is equivalent to $F_\lambda = 3.63E-9 \text{ erg cm}^{-2} \text{ s}^{-1} \text{ \AA}^{-1}$. The curves are labeled with exposure times in seconds.

Figure 13.26: Diffuse Source Signal-to-Noise as a Function of STMAG for G230MB

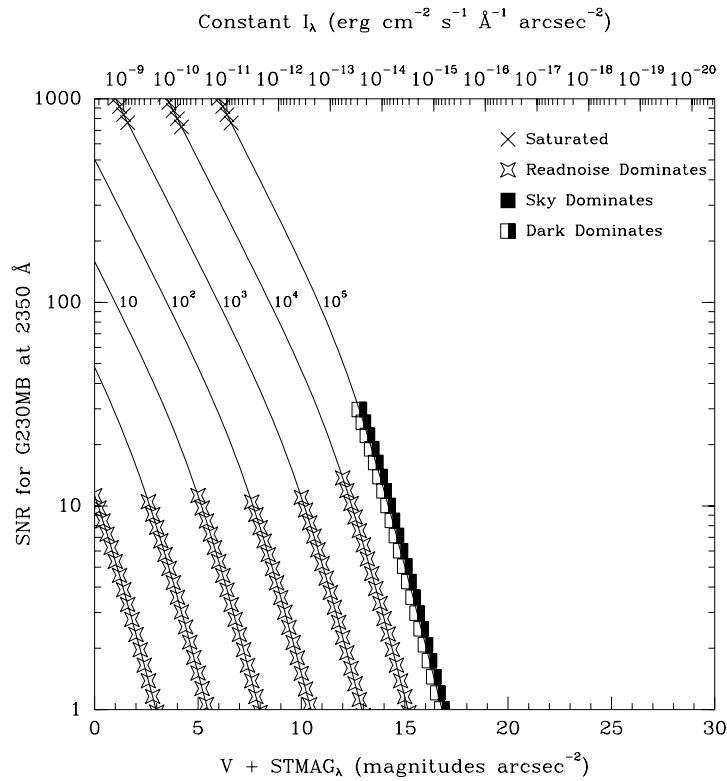
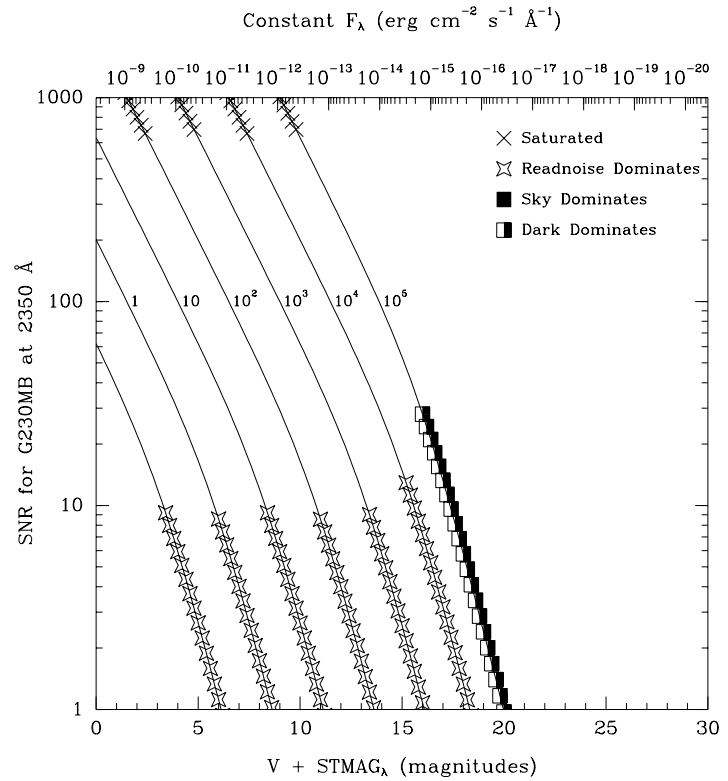


Figure 13.27: Point Source Signal-to-Noise as a Function of STMAG for G230MB



Comparison of G230MB and G230M

The trade-off between using the G230MB or the G230M (which uses the NUV-MAMA) grating modes, depends sensitively on the science goals and your source properties. Figures below show a direct comparison of some of the properties of the G230MB and G230M modes. See also “Comparison of G230LB and G230L” on page 305.

Figure 13.28: Comparison of Limiting Magnitudes and Fluxes for G230MB and G230M. Plotted are the limiting source magnitudes and fluxes for G230MB and G230M to achieve a signal-to-noise ratio of 10 per 2-pixel spectral resolution element integrated across the PSF, in 1 hour. The prediction due to the Charge Transfer Inefficiency (CTI) effect, expected in the year 2005, is also shown.

Limiting magnitude to reach SNR = 10 in 1 hour

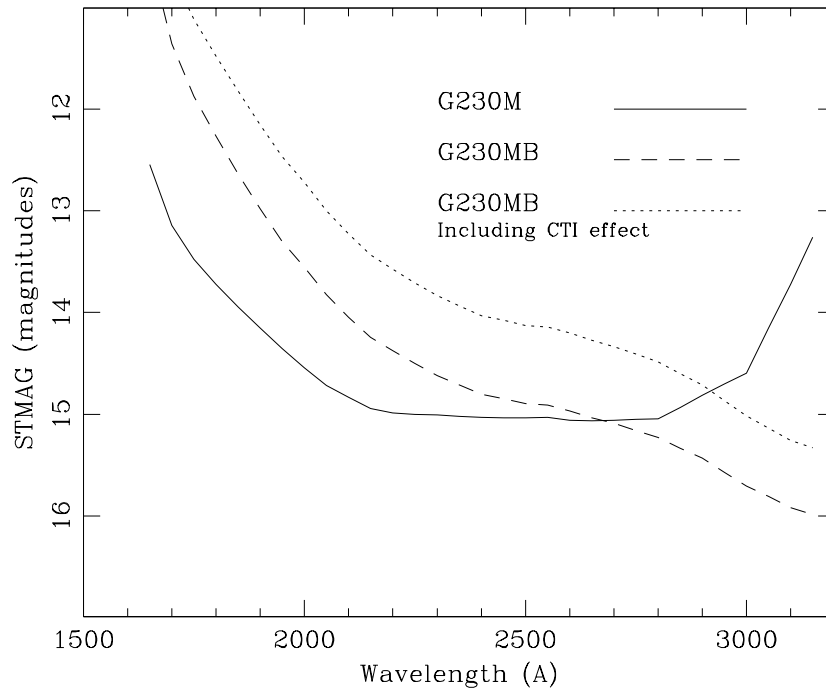
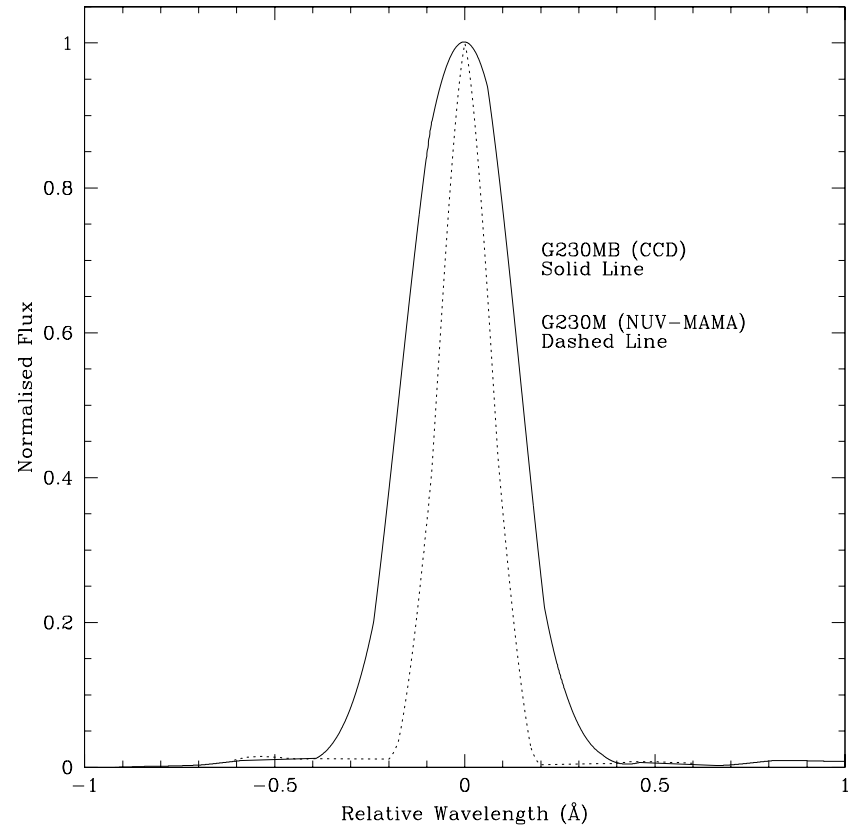


Figure 13.29: Comparison of LSFs for G230MB and G230M



First-Order Grating G230L

Description

The G230L grating is used with the NUV-MAMA and has a relatively high throughput and a resolving power of ~ 500 .

Recommended Uses

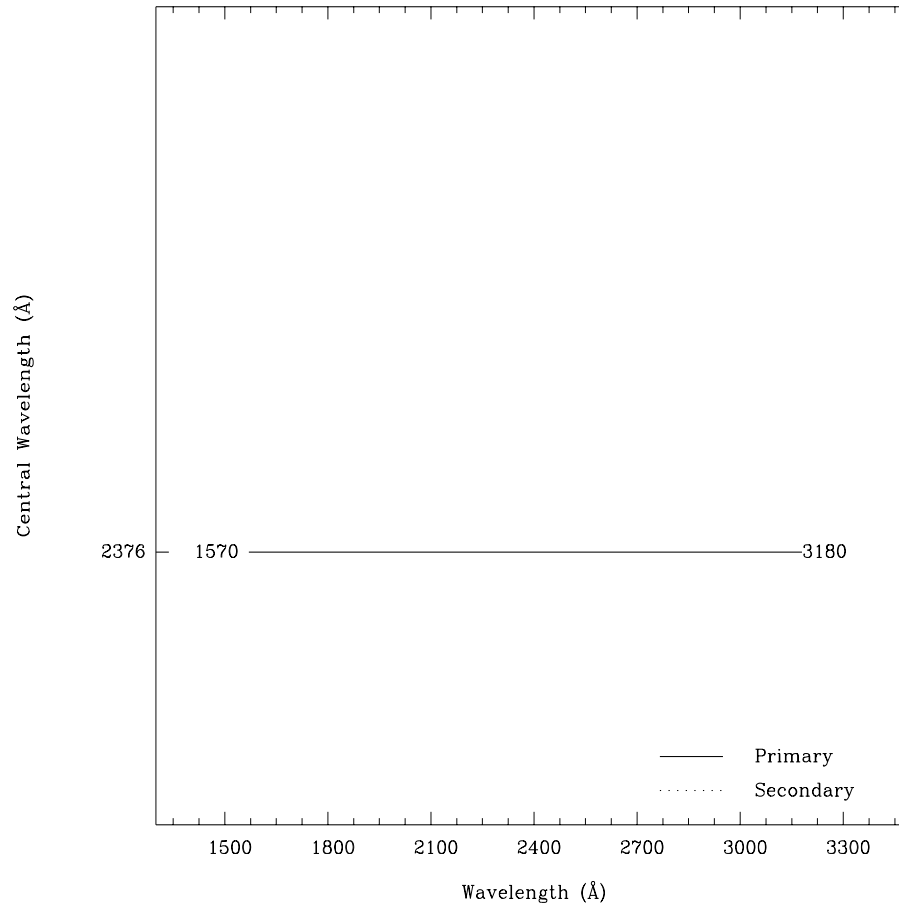
G230L is designed for observations where high spectral resolution is not required, but efficient, spatially resolved spectroscopy with full spectral coverage in the near-ultraviolet is desired.

Special Considerations

Notice that the CCD G230LB grating mode also covers the near-ultraviolet with comparable resolution; see “Comparison of G230LB and G230L” on page 305 for a detailed comparison of these two grating modes in that wavelength regime.

Grating	Spectral Range		Average Dispersion (\AA per Pixel)	Plate Scale (arcsec / pixel)	Tilts	Central Wavelengths
	Complete	Per Tilt				
G230L	1570-3180	1610	1.58	0.025	Prime	2376

Figure 13.30: Wavelength Range for the G230L Grating Settings

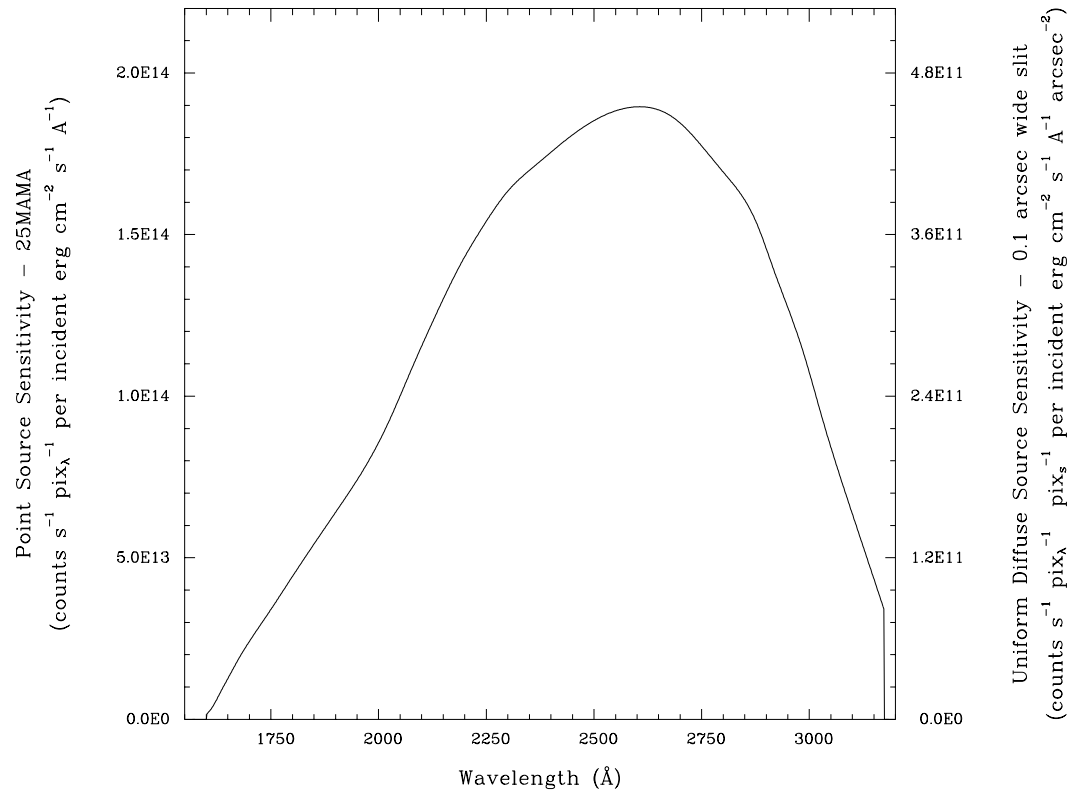


G230L Sensitivities

Table 13.9: G230L Throughputs and Sensitivities for a Point Source

λ	Sensitivity	% Throughput
1600	2.5E12	0.0
1700	2.4E13	0.4
1800	4.4E13	0.7
1900	6.4E13	0.9
2000	8.6E13	1.2
2100	1.2E14	1.5
2200	1.4E14	1.8
2300	1.6E14	1.9
2400	1.8E14	2.0
2500	1.9E14	2.0
2600	1.9E14	2.0
2700	1.8E14	1.9
2800	1.7E14	1.7
2900	1.5E14	1.4
3000	1.1E14	1.0
3100	6.4E13	0.6

Figure 13.31: G230L Point Source (left axis), and Diffuse Source (right axis) Sensitivities.



Note

Point source sensitivity assumes full transmission (zero slit losses). Diffuse source sensitivity assumes a 0.1" wide slit. To convert point source sensitivities to diffuse source sensitivities multiply the point source values by the grating spatial plate scale in units of arcseconds per pixel and by the width of the desired slit in units of arcseconds.

G230L Signal-to-Noise

Note:

The top axis displays constant F_λ values corresponding to the STMAG units ($V+STMAG_\lambda$) on the bottom axis. Recall that $STMAG=0$ is equivalent to $F_\lambda = 3.63E-9 \text{ erg cm}^{-2} \text{ s}^{-1} \text{ \AA}^{-1}$. The curves are labeled with exposure times in seconds.

Figure 13.32: Diffuse Source Signal-to-Noise as a function of STMAG for G230L

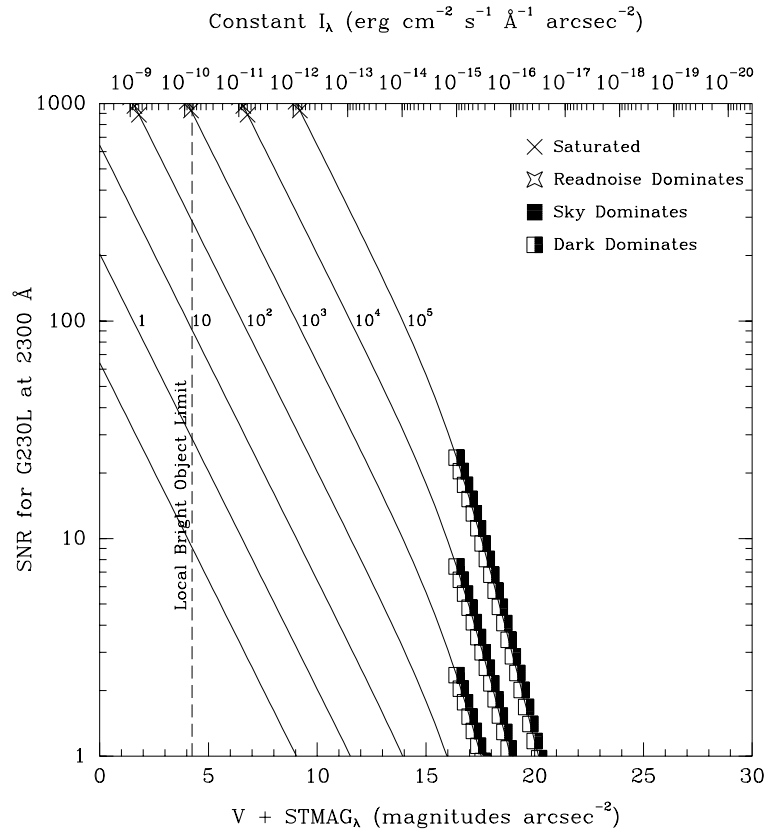
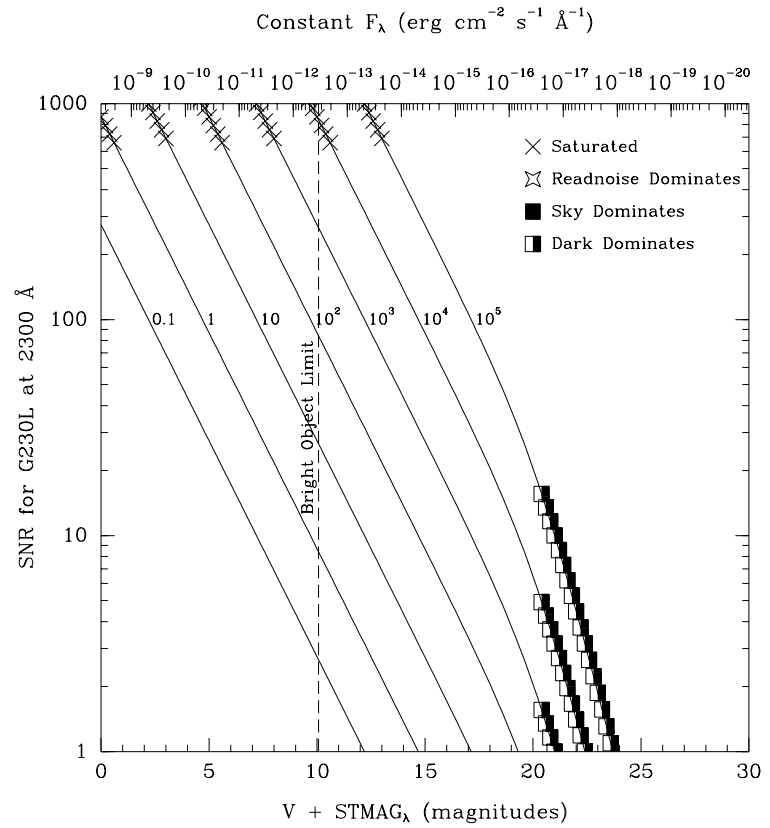


Figure 13.33: Point Source Signal-to-Noise as a Function of STMAG for G230L



First-Order Grating G230M

Description

Like the G230L grating, the G230M grating is used with the NUV-MAMA; it has a spectral range from 1650-3100 Å, however, with a resolving power $R \sim 10,000$ a single exposure with the G230M grating covers only 90 Å, and the grating must be scanned, with a series of exposures taken at 18 distinct settings to cover the full spectral range.

Recommended Uses

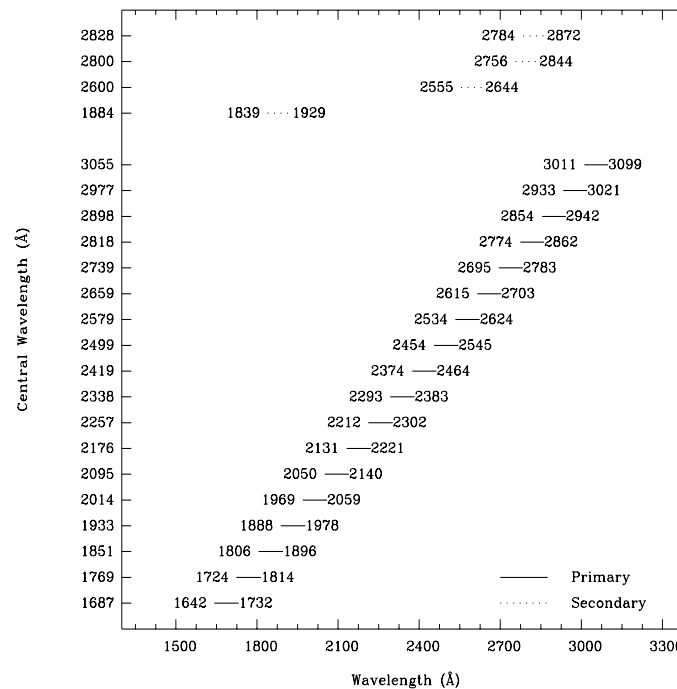
The G230M grating mode is designed for observations where spatially resolved, long slit, spectroscopy is desired at relatively high spectral resolution covering a limited region of the near-ultraviolet spectrum.

Special Considerations

Notice that the CCD G230MB grating mode also covers the near-ultraviolet with comparable resolution. See “Comparison of G230MB and G230M” on page 309 for a detailed comparison of these two grating modes in that wavelength regime.

Grating	Spectral Range		Average Dispersion (Å per Pixel)	Plate Scale (arcsec / pixel)	Tilts	Central Wavelengths
	Complete	Per Tilt				
G230M	1640-3100	90	0.09	0.029	Prime	1687, 1769, 1851, 1933, 2014, 2095, 2176, 2257, 2338, 2419, 2499, 2579, 2659, 2739, 2818, 2898, 2977, 3055
					Secondary	1884, 2600, 2800, 2828

Figure 13.34: Wavelength Ranges for the G230M Grating Settings

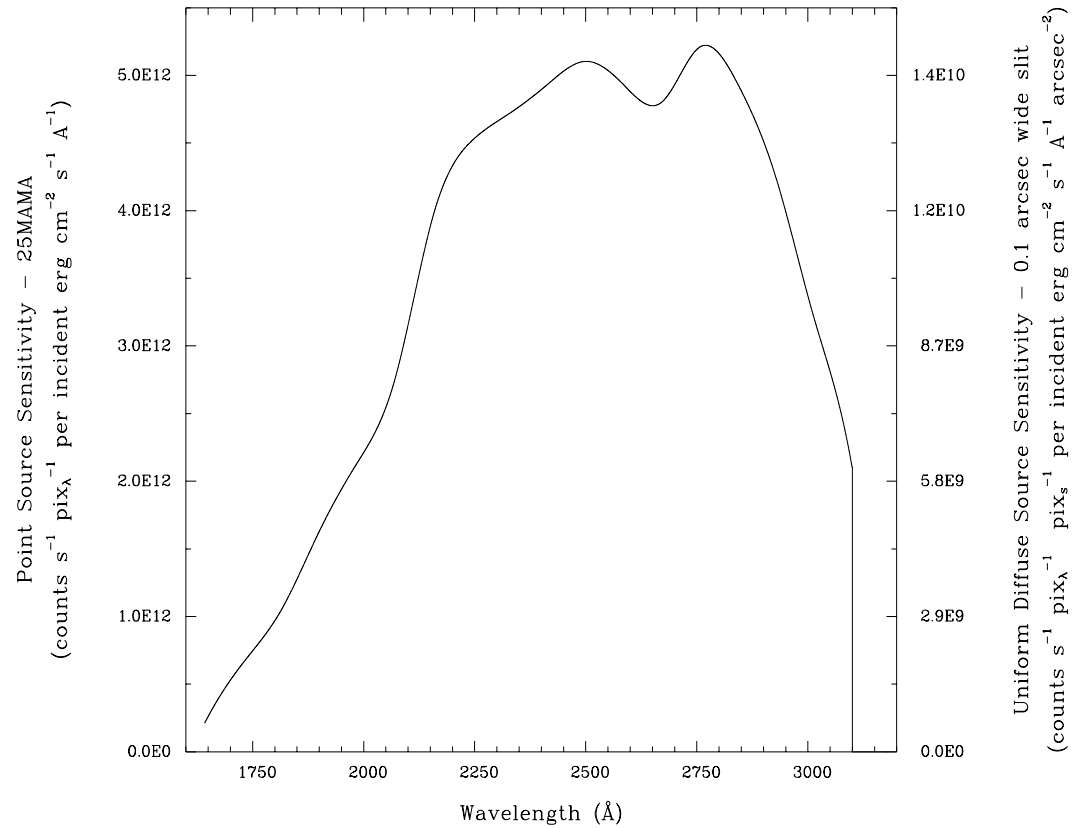


G230M Sensitivities

Table 13.10: G230M Throughputs & Sensitivities for a Point Source

λ	Sensitivity	% Throughput
1700	5.2E11	0.1
1800	9.8E11	0.3
1900	1.6E12	0.4
2000	2.2E12	0.5
2100	3.2E12	0.7
2200	4.3E12	1.0
2300	4.7E12	1.0
2400	4.9E12	1.0
2500	5.1E12	1.0
2600	4.9E12	0.9
2700	5.0E12	0.9
2800	5.1E12	0.9
2900	4.5E12	0.8
3000	3.4E12	0.6
3100	1.2E12	0.2

Figure 13.35: G230M Point Source (left axis), and Diffuse Source (right axis) Sensitivities.



Note

Point source sensitivity assumes full transmission (zero slit losses). Diffuse source sensitivity assumes a 0.1" wide slit. To convert point source sensitivities to diffuse source sensitivities multiply the point source values by the grating spatial (cross dispersion) plate scale in units of arcseconds per pixel and by the width of the desired slit in units of arcseconds.

G230M Signal-to-Noise

Note:

The top axis displays constant F_λ values corresponding to the STMAG units ($V+STMAG_\lambda$) on the bottom axis. Recall that $STMAG=0$ is equivalent to $F_\lambda = 3.63E-9 \text{ erg cm}^{-2} \text{ s}^{-1} \text{ \AA}^{-1}$. The curves are labeled with exposure times in seconds.

Figure 13.36: Diffuse Source Signal-to-Noise as a Function of STMAG for G230M

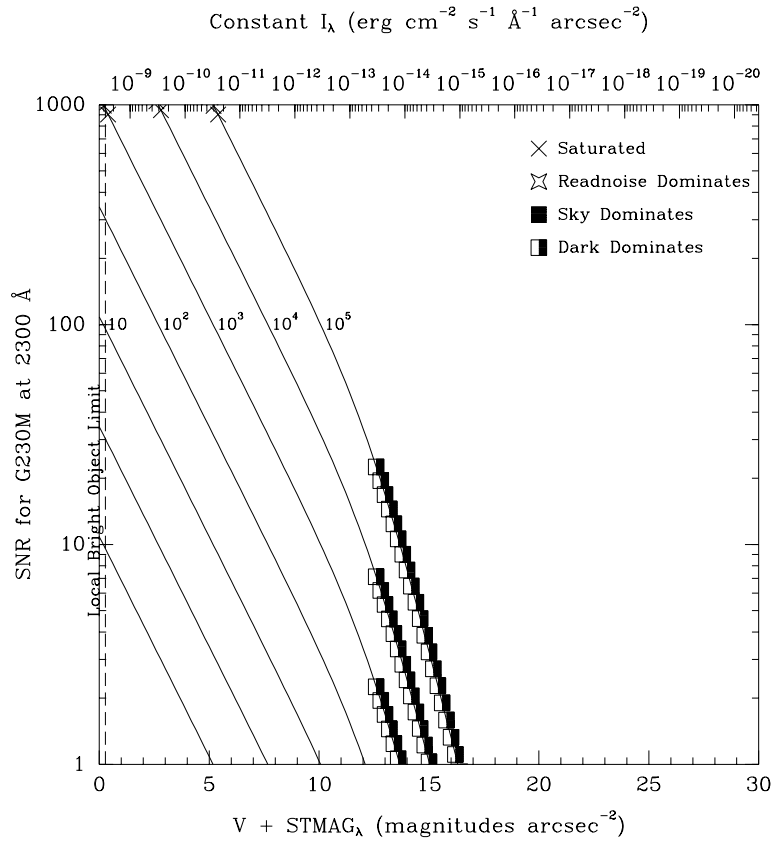
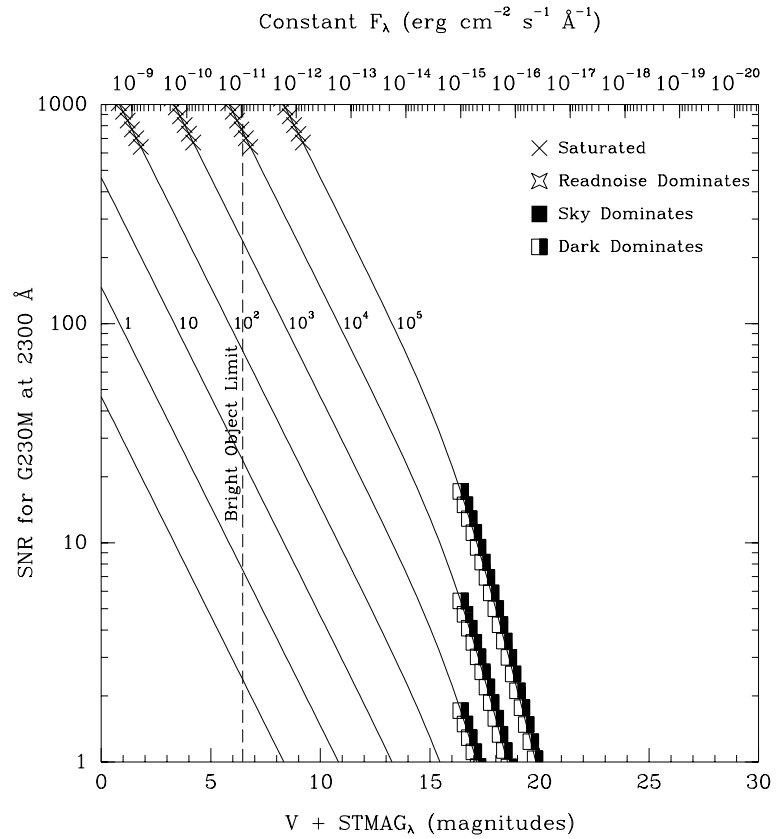


Figure 13.37: Point Source Signal-to-Noise as a Function of STMAG for G230M



First-Order Grating G140L

Description

The G140L grating mode is used with the FUV-MAMA, has a resolving power $R \sim 1000$, and covers a spectral range from 1150 to 1700 Å in a single exposure.

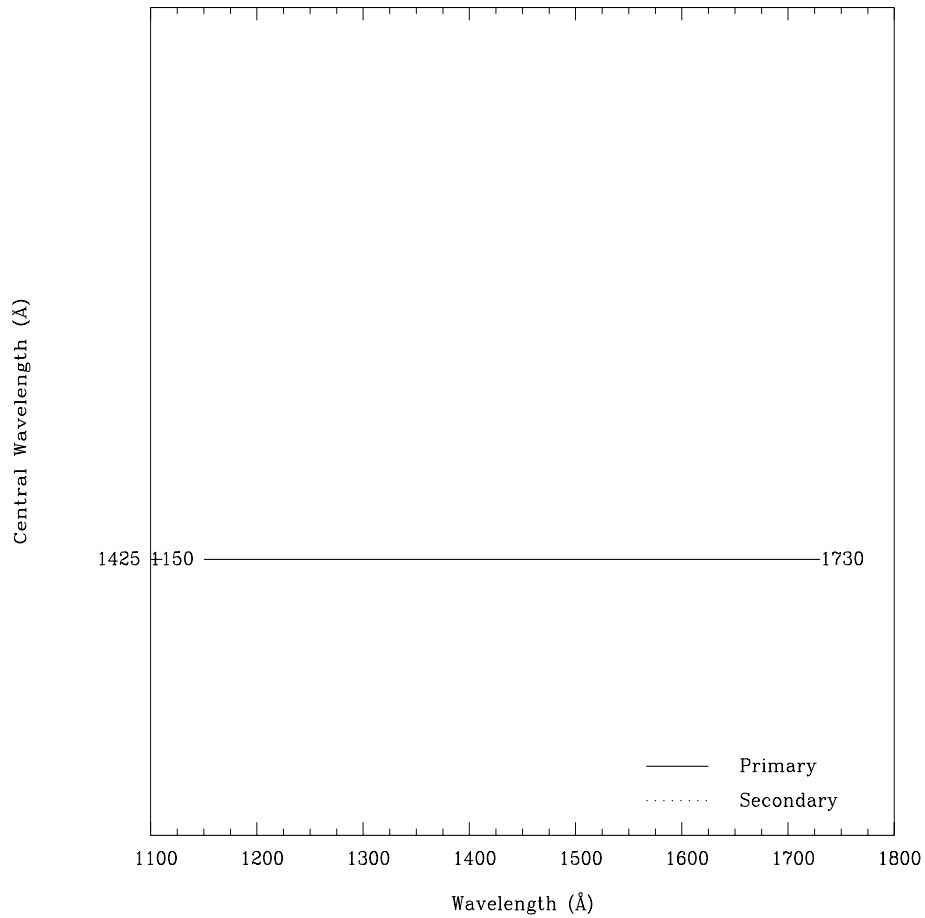
Notice, that with two observations, one with G140L and one with G230L, the full spectral region, from 1150 to 3100 Å can be efficiently observed at an $R \sim 1000$.

Recommended Uses

The G140L grating mode is designed for observations where high spectral resolution is not required, but efficient, spatially resolved spectroscopy providing wide spectral coverage in the ultraviolet is desired.

Grating	Spectral Range		Average Dispersion (Å per Pixel)	Plate Scale (arcsec / pixel)	Tilts	Central Wavelengths
	Complete	Per Tilt				
G140L	1150-1730	610	0.6	0.025	Prime	1425

Figure 13.38: Wavelength Range for the G140L Grating Setting

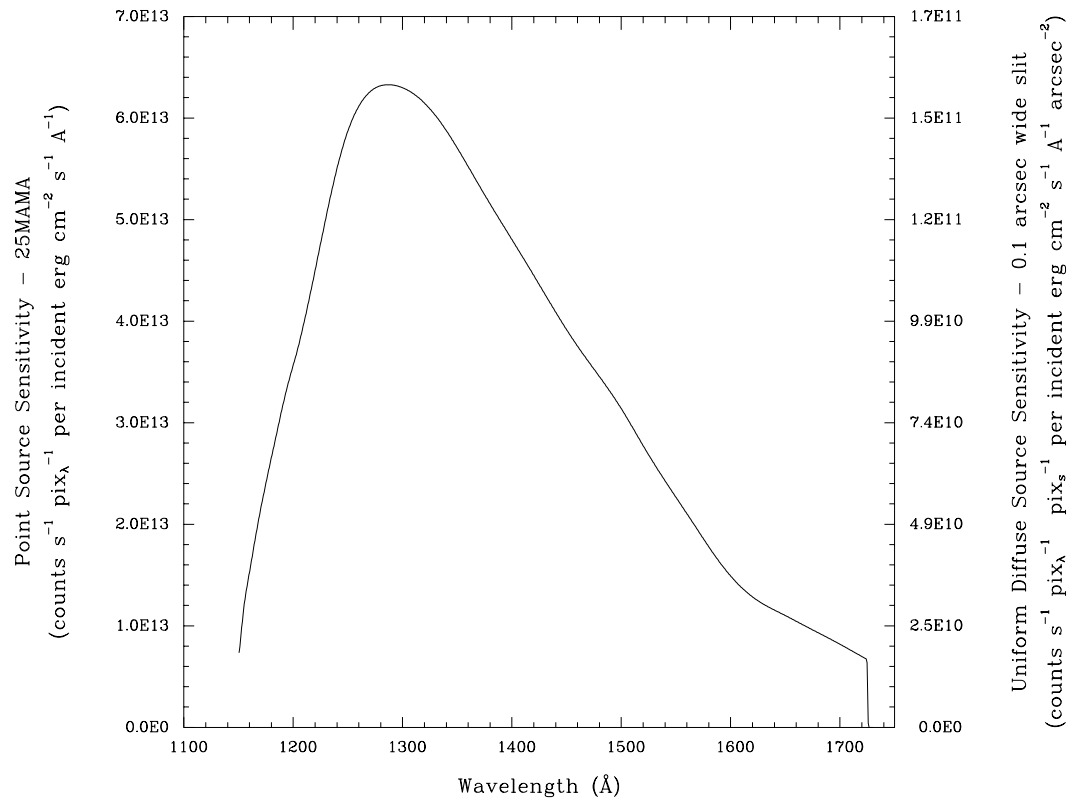


G140L Sensitivity

Table 13.11: G140L Throughputs & Sensitivities for a Point Source

λ	Sensitivity	% Throughput
1200	3.6E13	2.2
1250	5.8E13	3.4
1300	6.3E13	3.5
1350	5.7E13	3.1
1400	4.8E13	2.5
1450	3.9E13	2.0
1500	3.1E13	1.5
1550	2.3E13	1.1
1600	1.5E13	0.7
1650	1.1E13	0.5
1700	8.2E12	0.4

Figure 13.39: G140L Point Source (left axis) and Diffuse Source (right axis) Sensitivities.



Note

Point source sensitivity assumes full transmission (zero slit losses). Diffuse source sensitivity assumes a 0.1" wide slit. To convert point source sensitivities to diffuse source sensitivities multiply the point source values by the grating spatial plate scale in units of arcseconds per pixel and by the width of the desired slit in units of arcseconds.

G140L Signal-to-Noise

Note:

The top axis displays constant F_λ values corresponding to the STMAG units ($V+STMAG_\lambda$) on the bottom axis. Recall that $STMAG=0$ is equivalent to $F_\lambda = 3.63E-9 \text{ erg cm}^{-2} \text{ s}^{-1} \text{ \AA}^{-1}$. The curves are labeled with exposure times in seconds.

Figure 13.40: Diffuse Source Signal-to-Noise as a Function of STMAG for G140L

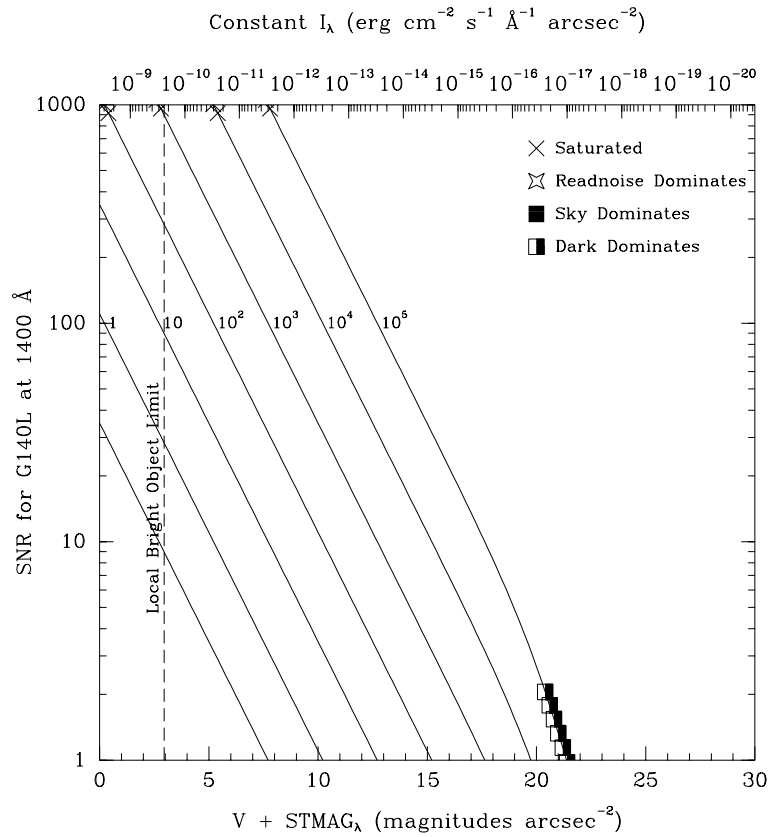
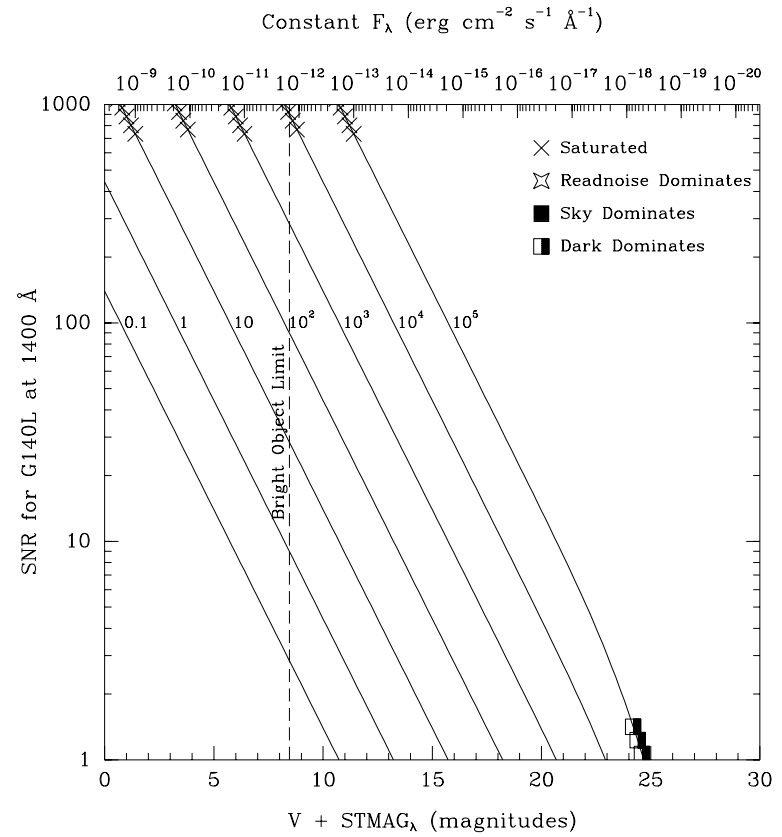


Figure 13.41: Point Source Signal-to-Noise as a Function of STMAG for G140L



First-Order Grating G140M

Description

The G140M grating mode is used with the FUV-MAMA and has a spectral range from 1150 to 1700 Å.

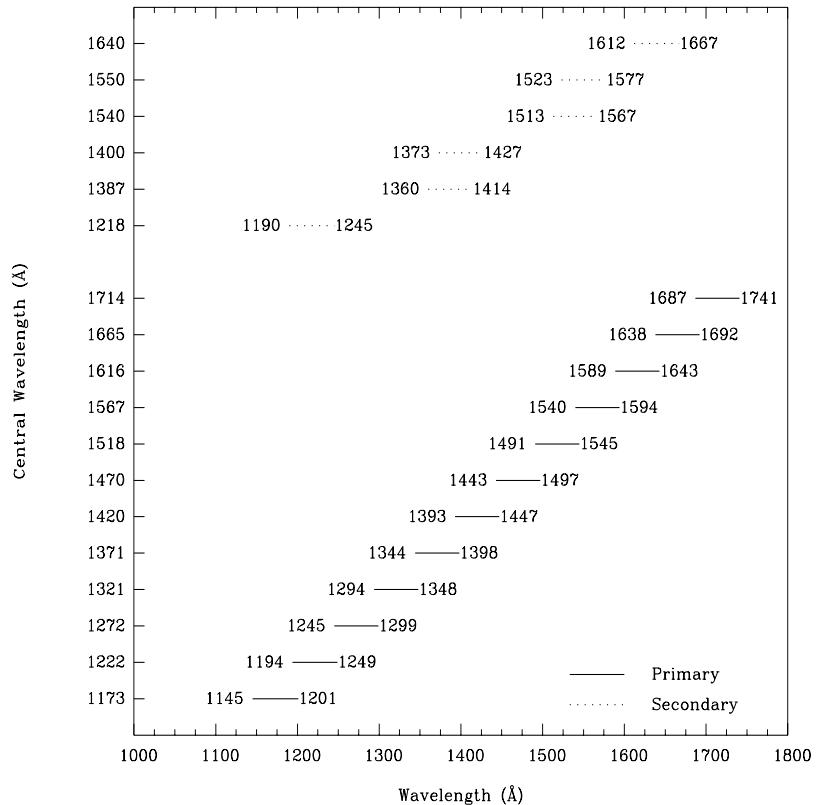
With a resolving power $R \sim 10,000$, a single exposure with this grating covers only 55 Å. The grating must be scanned, with a series of exposures taken at 12 distinct settings to cover the full spectral range.

Recommended Uses

The G140M grating mode is designed for observations where spatially resolved, long slit, spectroscopy is desired at relatively high spectral resolution over a limited region of the ultraviolet spectrum.

Grating	Spectral Range		Average Dispersion (Å per Pixel)	Plate Scale (arcsec / pixel)	Tilts	Central Wavelengths
	Complete	Per Tilt				
G140M	1140-1740	55	0.05	0.029	Prime	1173, 1222, 1272, 1321, 1371, 1420, 1470, 1518, 1567, 1616, 1665, 1714
					Secondary	1218, 1387, 1400, 1540, 1550, 1640

Figure 13.42: Wavelength Ranges for the G140M Grating Settings

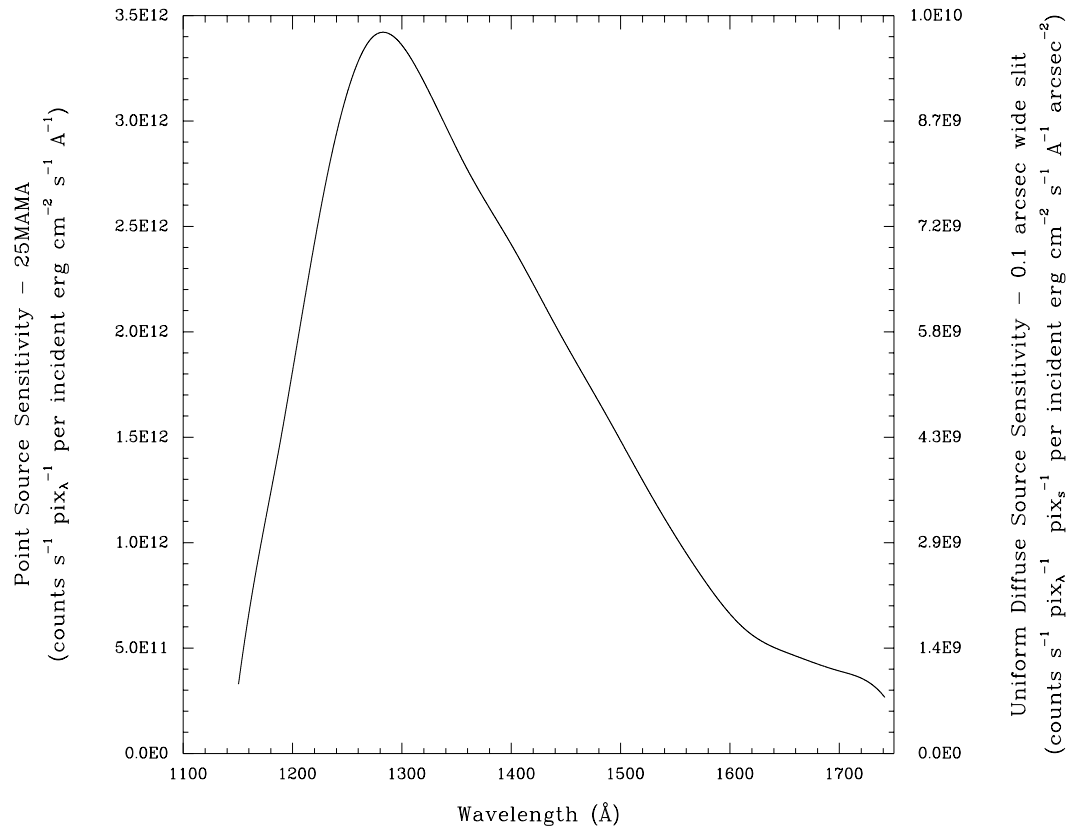


G140M Sensitivities

Table 13.12: G140M Throughputs & Sensitivities for a Point Source

λ	Sensitivity	% Throughput
1200	1.8E12	1.3
1250	3.1E12	2.2
1300	3.3E12	2.3
1350	2.9E12	1.9
1400	2.4E12	1.5
1450	1.9E12	1.2
1500	1.5E12	0.9
1550	1.0E11	0.6
1600	6.7E11	0.4
1650	4.8E11	0.3
1700	3.9E11	0.2

Figure 13.43: G140M Point Source (left axis), and Diffuse Source (right axis) Sensitivities.



Note

Point source sensitivity assumes full transmission (zero slit losses). Diffuse source sensitivity assumes a 0.1" wide slit. To convert point source sensitivities to diffuse source sensitivities multiply the point source values by the grating spatial plate scale in units of arcseconds per pixel and by the width of the desired slit in units of arcseconds.

G140M Signal-to-Noise

Note:

The top axis displays constant F_λ values corresponding to the STMAG units ($V+STMAG_\lambda$) on the bottom axis. Recall that $STMAG=0$ is equivalent to $F_\lambda = 3.63E-9 \text{ erg cm}^{-2} \text{ s}^{-1} \text{ \AA}^{-1}$. The curves are labeled with exposure times in seconds.

Figure 13.44: Diffuse Source Signal-to-Noise as a Function of STMAG for G140M

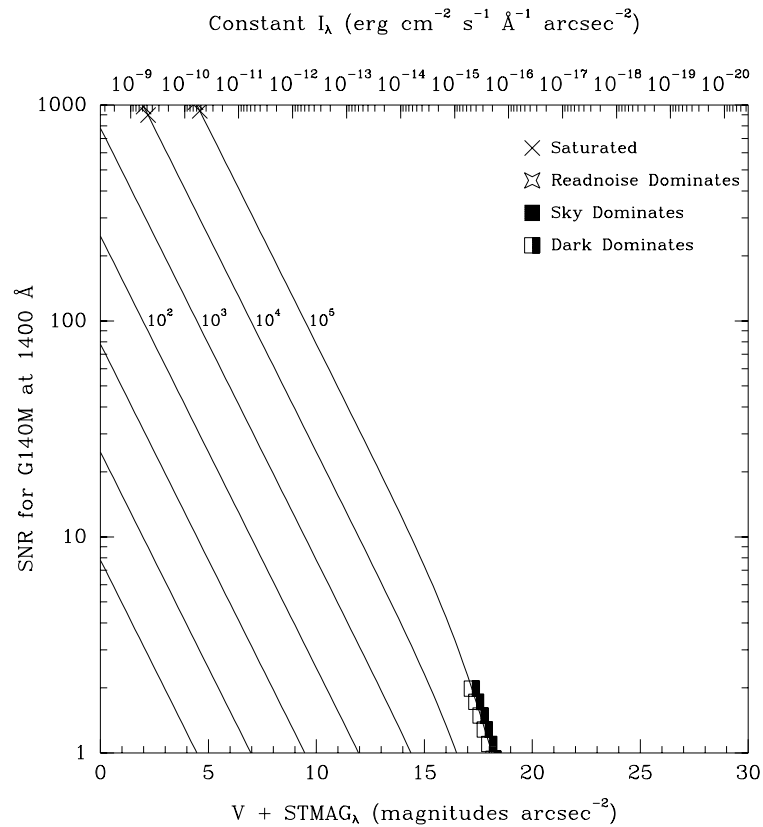
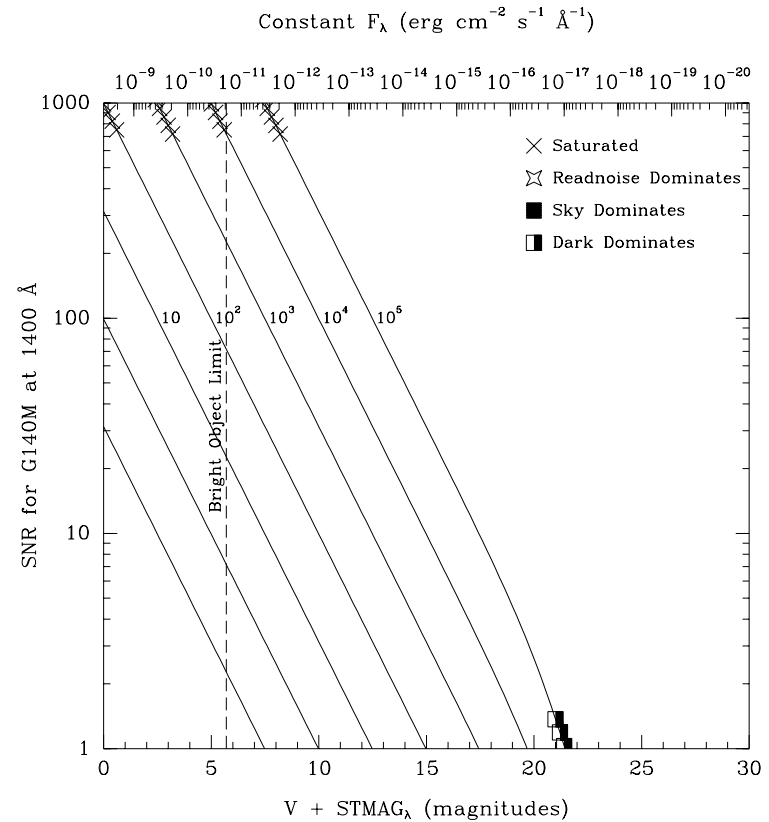


Figure 13.45: Point Source Signal-to-Noise as a Function of STMAG for G140M



Echelle Grating E230M

Description

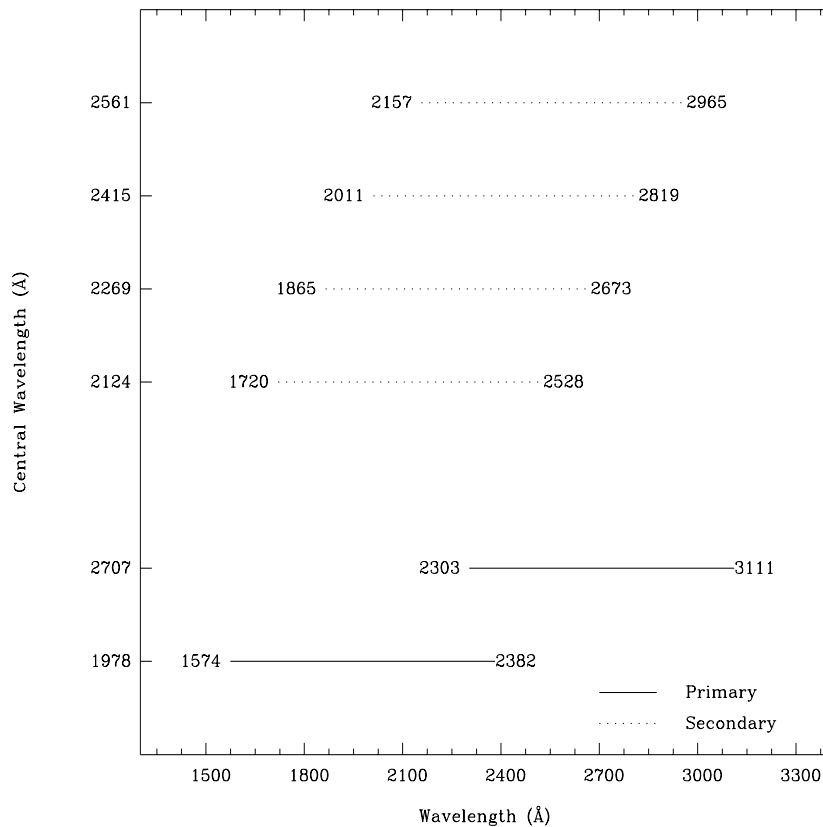
The E230M grating is used with the NUV-MAMA and provides echelle spectra at a resolving power of 30,000 from 1570 to 3100 Å.

Special Considerations

A single exposure with this grating covers 800 Å over ~20-40 orders. The interorder separation is ~18 pixels (0.52 arcseconds) at 1650 Å and 62.5 pixels (~1.8 arcseconds) at 3100 Å. The grating must be scanned, with exposures taken at two distinct settings to cover the full spectral range of the grating.

Grating	Spectral Range		Average Dispersion (Å per Pixel)	Dispersion, Cross Dispersion Plate Scales (arcsec / pixel)	Tilts	Central Wavelengths
	Complete	Per Tilt				
E230M	1570-3110	~800	~60,000	0.035, 0.029	Prime	1978, 2707
					Secondary	2124, 2269, 2415, 2561

Figure 13.46: Wavelength Ranges for the E230M Grating Settings

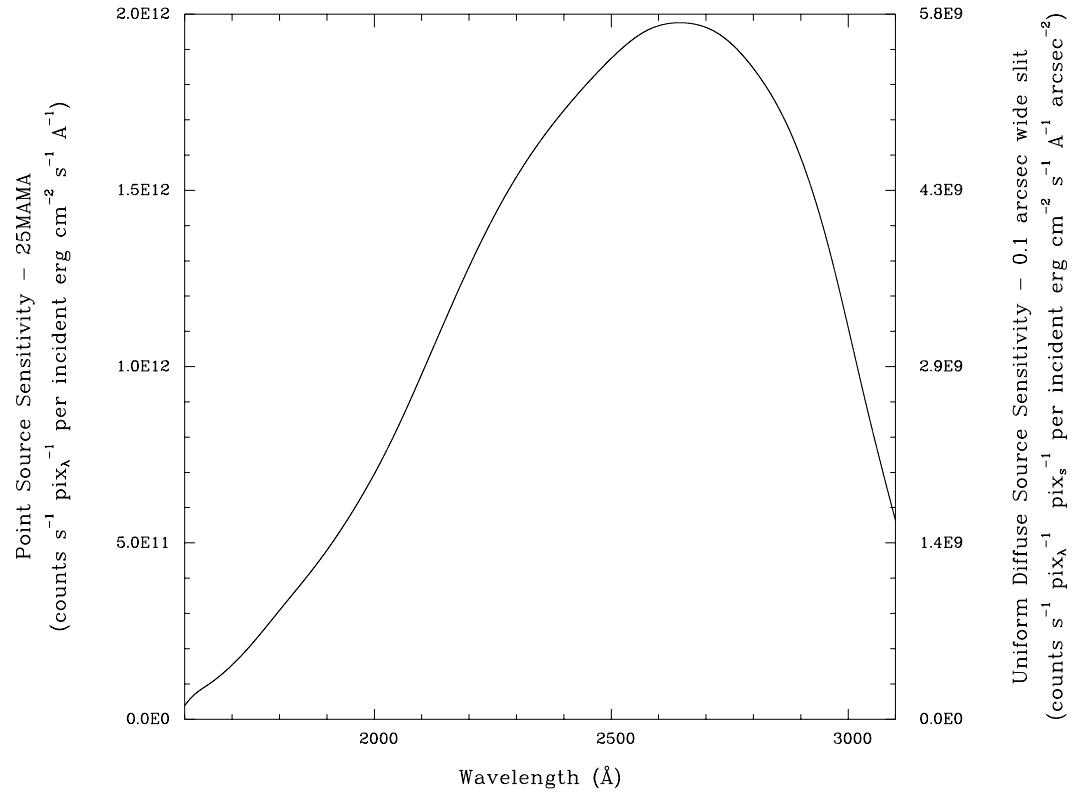


E230M Sensitivities

Table 13.13: E230M Throughputs & Sensitivities for a Point Source

λ	Sensitivity	% Throughput
1700	1.6E11	0.1
1800	3.1E11	0.2
1900	4.8E11	0.3
2000	7.0E11	0.4
2100	9.8E11	0.6
2200	1.3E12	0.7
2300	1.5E12	0.8
2400	1.7E12	0.9
2500	1.9E12	0.9
2600	2.0E12	0.9
2700	2.0E12	0.8
2800	1.8E12	0.7
2900	1.6E12	0.6
3000	1.1E12	0.4

Figure 13.47: E230M Point Source (left axis), and Diffuse Source (right axis) Sensitivities. Throughput curve traces the peaks of the blaze function for each order.



Note

Point source sensitivity assumes full transmission (zero slit losses). Diffuse source sensitivity assumes a 0.1" wide slit. To convert point source sensitivities to diffuse source sensitivities multiply the point source values by the grating spatial (cross dispersion) plate scale in units of arcseconds per pixel and by the width of the desired slit in units of arcseconds.

E230M Signal-to-Noise

Note:

The top axis displays constant F_λ values corresponding to the STMAG units ($V+STMAG_\lambda$) on the bottom axis. Recall that $STMAG=0$ is equivalent to $F_\lambda = 3.63E-9 \text{ erg cm}^{-2} \text{ s}^{-1} \text{ \AA}^{-1}$. The curves are labeled with exposure times in seconds.

Figure 13.48: Diffuse Source Signal-to-Noise as a function of STMAG for E230M

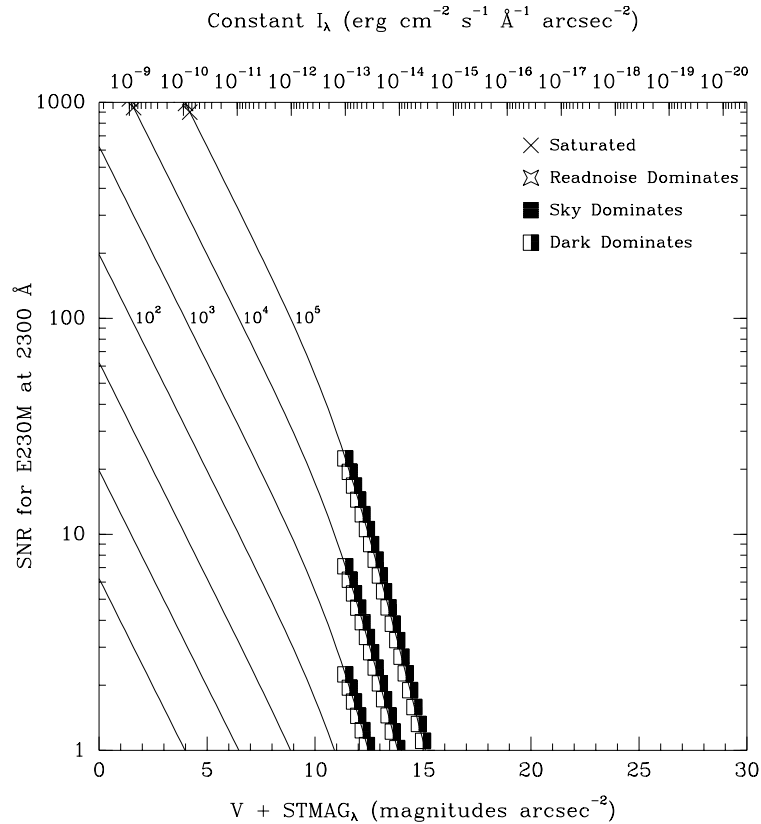
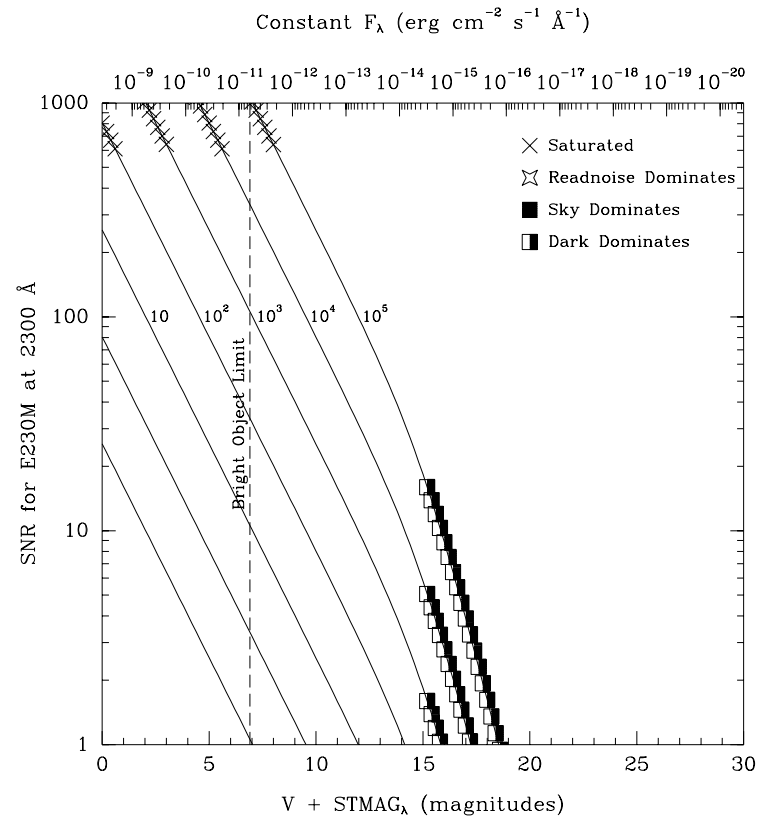


Figure 13.49: Point Source Signal-to-Noise as a Function of STMAG for E230M



Echelle Grating E230H

Description

The E230H grating is used with the NUV-MAMA and provides echelle spectra at a resolving power of $\sim 110,000$ from 1620 to 3100 Å.

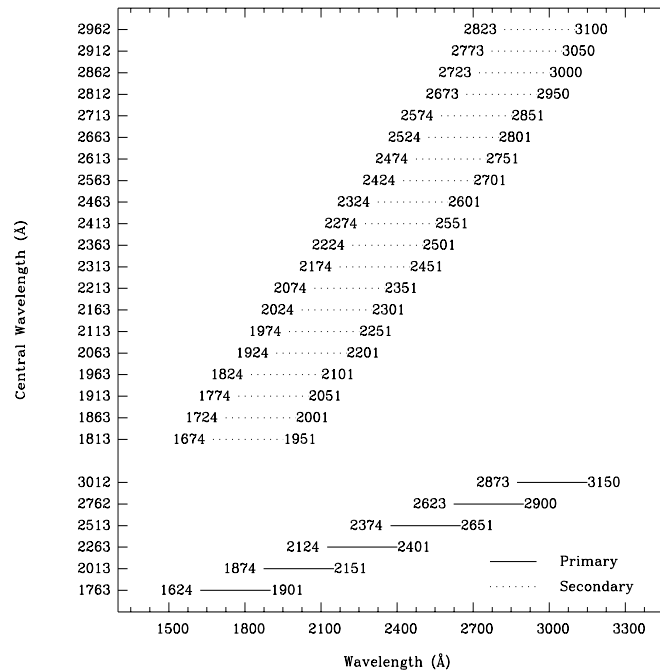
Special Considerations

A single E230H echellogram covers ~ 267 Å, over ~ 20 -70 orders. The orders are spaced by only ~ 12.7 pixels (0.37 arcseconds) at 1650 Å and 47.2 pixels (~ 1.38 arcseconds) at 3100 Å. The grating must be scanned, with exposures taken at six distinct settings to cover the full spectral range of the grating.

The secondary central wavelength at 2812 Å has had direct sensitivity calibrations performed during Cycle 7 to support the large number of observations using that position.

Grating	Spectral Range		Average Dispersion (Å per Pixel)	Dispersion, Cross Dispersion Plate Scale (arcsec / pixel)	Tilts	Central Wavelengths
	Complete	Per Tilt				
E230H	1620-3150	~ 267	$\lambda/228,000$	0.047,0.029	Prime	1763, 2013, 2263, 2513, 2762, 3012
					Secondary	1813, 1863, 1913, 1963, 2063, 2113, 2163, 2213, 2313, 2363, 2413, 2463, 2563, 2613, 2663, 2713, 2812, 2862, 2912, 2962

Figure 13.50: Wavelength Ranges for the E230H Grating Settings

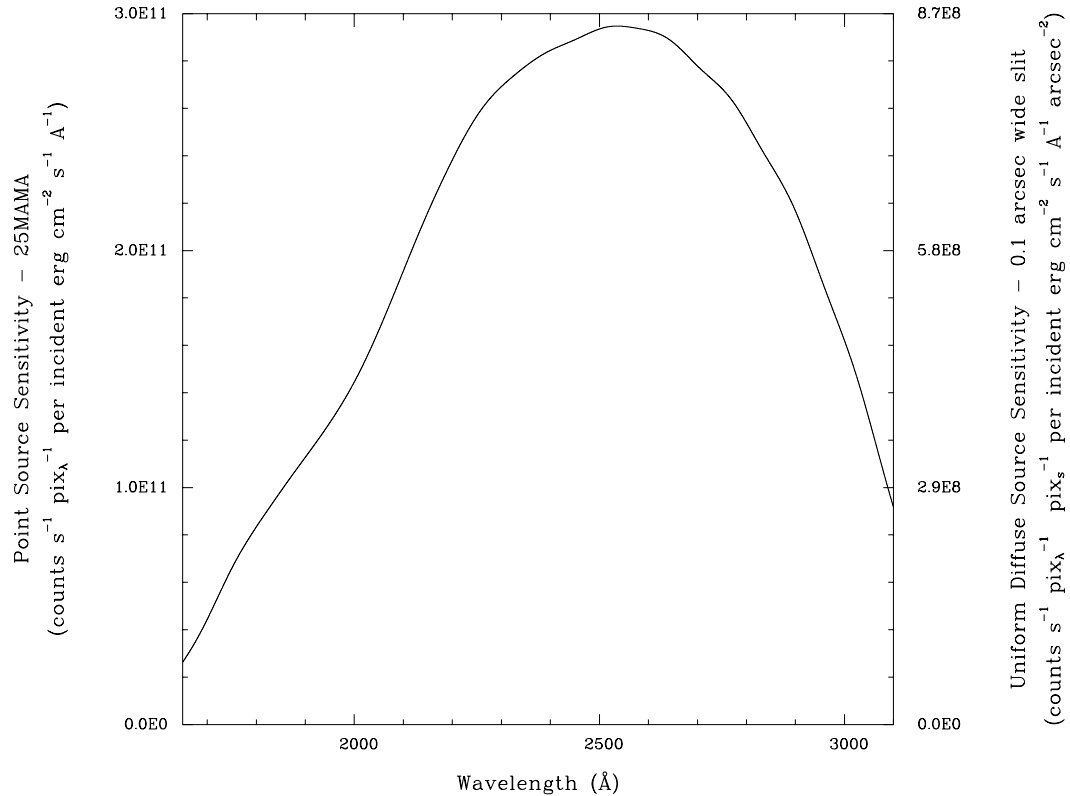


E230H Sensitivities

Table 13.14: E230H Throughputs and Sensitivities for a Point Source

λ	Sensitivity	% Throughput
1700	4.5E10	0.2
1800	8.3E10	0.3
1900	1.1E11	0.4
2000	1.5E11	0.4
2100	1.9E11	0.5
2200	2.4E11	0.6
2300	2.7E11	0.7
2400	2.8E11	0.7
2500	2.9E11	0.7
2600	2.9E11	0.6
2700	2.8E11	0.6
2800	2.5E11	0.5
2900	2.2E11	0.4
3000	1.6E11	0.3

Figure 13.51: E230H Point Source (left axis), and Diffuse Source (right axis) Sensitivities. Throughput curve traces the peaks of the blaze function for each order.



Note

Point source sensitivity assumes full transmission (zero slit losses). Diffuse source sensitivity assumes a 0.1" wide slit. To convert point source sensitivities to diffuse source sensitivities multiply the point source values by the grating spatial (cross dispersion) plate scale in units of arcseconds per pixel and by the width of the desired slit in units of arcseconds.

E230H Signal-to-Noise

Note:

The top axis displays constant F_λ values corresponding to the STMAG units ($V+STMAG_\lambda$) on the bottom axis. Recall that $STMAG=0$ is equivalent to $F_\lambda = 3.63E-9 \text{ erg cm}^{-2} \text{ s}^{-1} \text{ \AA}^{-1}$. The curves are labeled with exposure times in seconds.

Figure 13.52: Diffuse Source Signal-to-Noise as a Function of STMAG for E230H

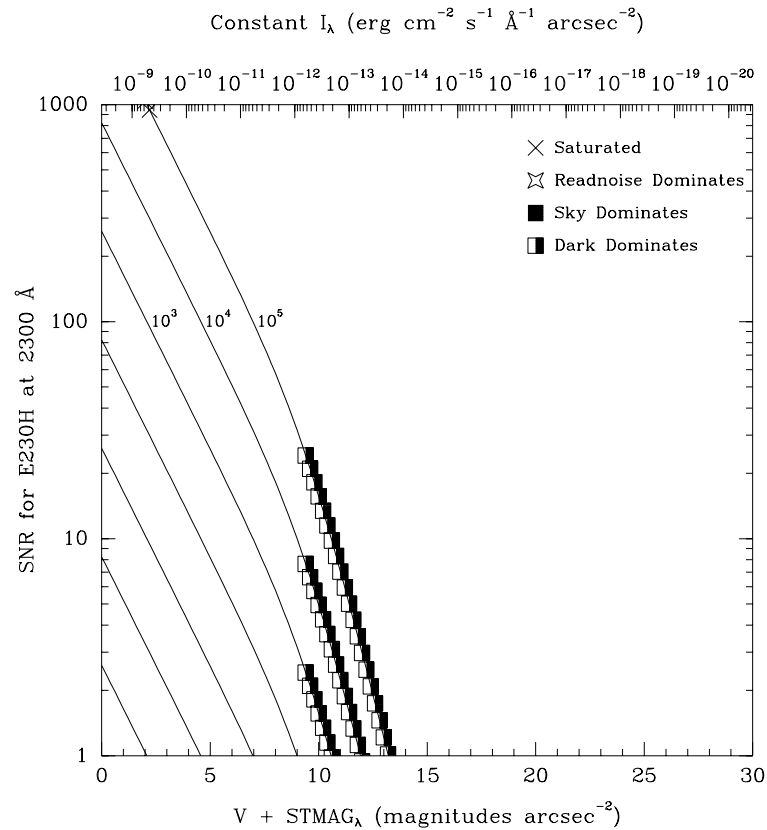
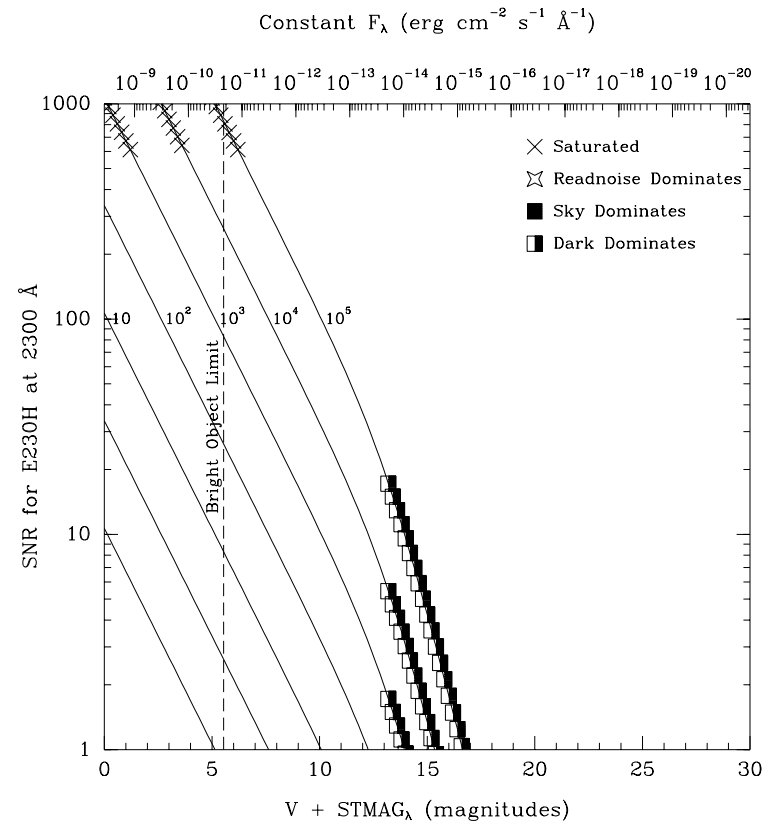


Figure 13.53: Point Source Signal-to-Noise as a Function of STMAG for E230H



Echelle Grating E140M

Description

The E140M grating is used with the FUV-MAMA and provides echelle spectra at a resolving power of 45,800 from 1123–1710 Å.

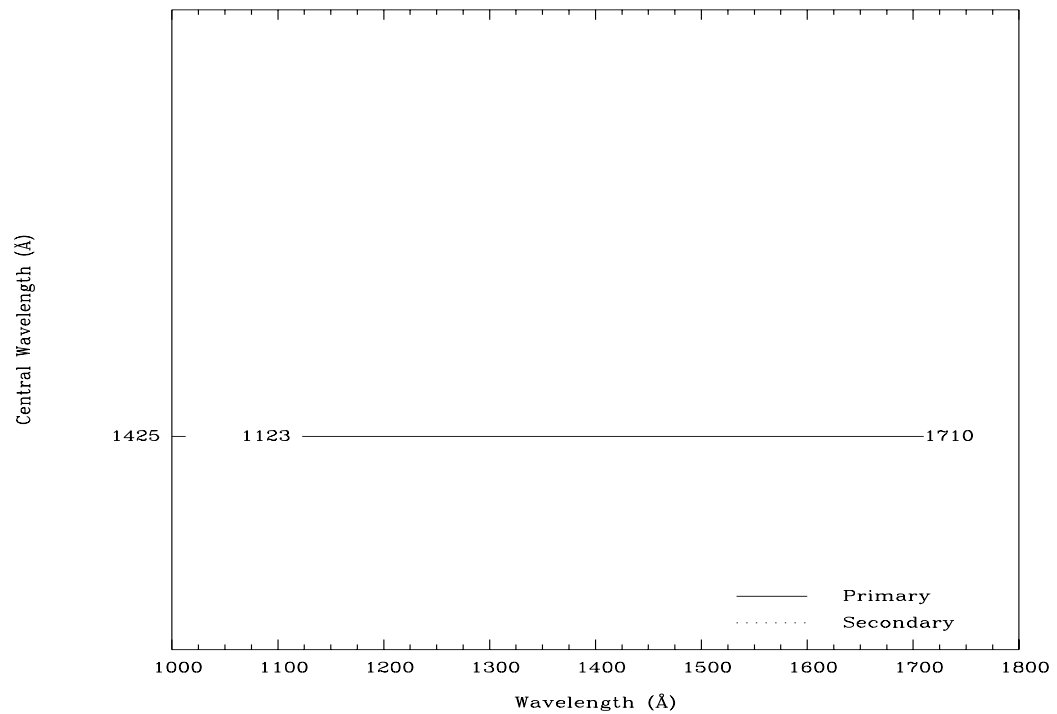
Special Considerations

A single E140M echellogram covers ~ 600 Å, however at wavelengths longward of 1649 Å, the echelle orders overrun the width of the detector in the dispersion direction, so there will be three small gaps in the wavelength coverage. One gap of ~ 0.2 Å, one of ~ 0.4 Å, and one of ~ 0.7 Å occur between 1649 and 1700 Å.

The separation between orders is ~ 15 pixels (or 0.44 arcseconds) at 1150 Å and ~ 33 (0.96 arcseconds) at 1700 Å.

Grating	Spectral Range		Average Dispersion (Å per Pixel)	Dispersion, Cross Dispersion Plate Scale (arcsec / pixel)	Tilts	Central Wavelengths
	Complete	Per Tilt				
E140M	1123–1710	620	$\sim 91,700$	0.036,0.029	Prime	1425

Figure 13.54: Wavelength Range for the E140M Grating Setting



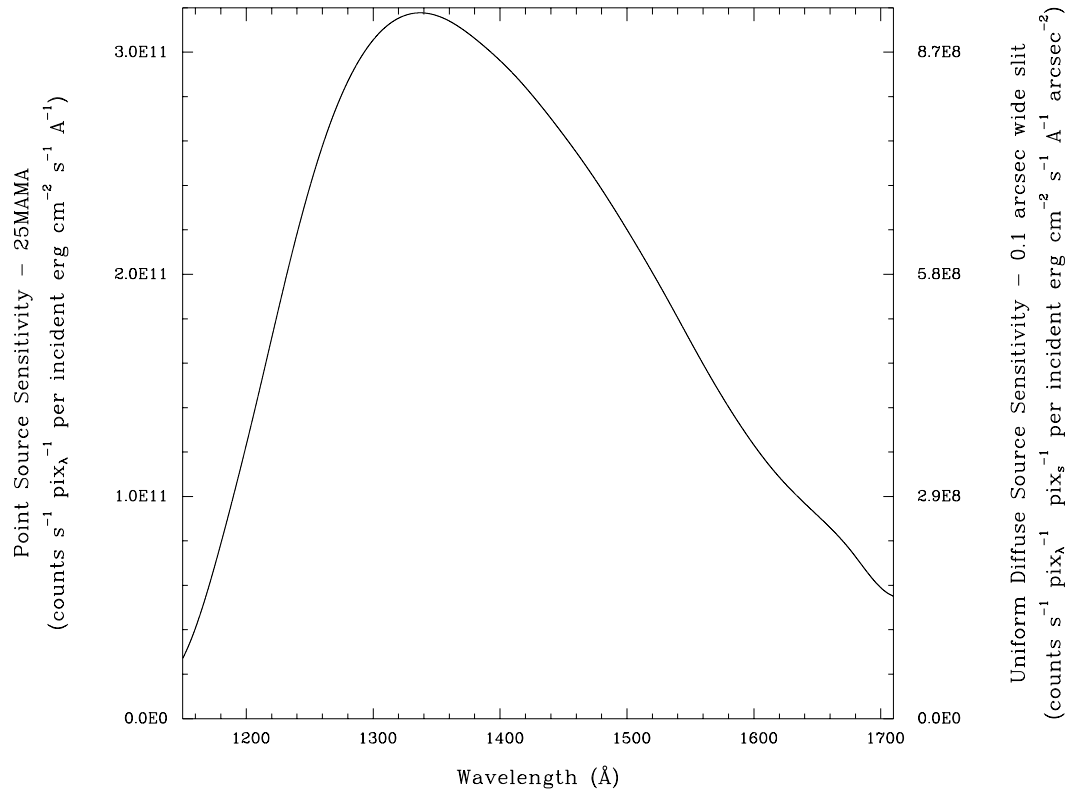
E140M Sensitivity

Table 13.15: E140M Throughputs & Sensitivities for a Point Source

λ	Sensitivity	% Throughput
1200	1.2E11	0.3
1250	2.4E11	0.6
1300	3.0E11	0.7
1350	3.2E11	0.7
1400	3.0E11	0.6
1450	2.6E11	0.5
1500	2.2E11	0.4
1550	1.7E11	0.3
1600	1.2E11	0.2
1650	9.1E10	0.1
1700	5.9E10	0.1

Figure 13.55: E140M Point Source (left axis), and Diffuse Source (right axis) Sensitivities.

Throughput curve traces the peaks of the blaze function for each order.



Note

Point source sensitivity assumes full transmission (zero slit losses). Diffuse source sensitivity assumes a 0.1" wide slit. To convert point source sensitivities to diffuse source sensitivities multiply the point source values by the grating spatial (cross dispersion) plate scale in units of arcseconds per pixel and by the width of the desired slit in units of arcseconds.

E140M Signal-to-Noise

Note:

The top axis displays constant F_λ values corresponding to the STMAG units ($V+STMAG_\lambda$) on the bottom axis. Recall that $STMAG=0$ is equivalent to $F_\lambda = 3.63E-9 \text{ erg cm}^{-2} \text{ s}^{-1} \text{ \AA}^{-1}$. The curves are labeled with exposure times in seconds.

Figure 13.56: Diffuse Source Signal-to-Noise as a Function of STMAG for E140M

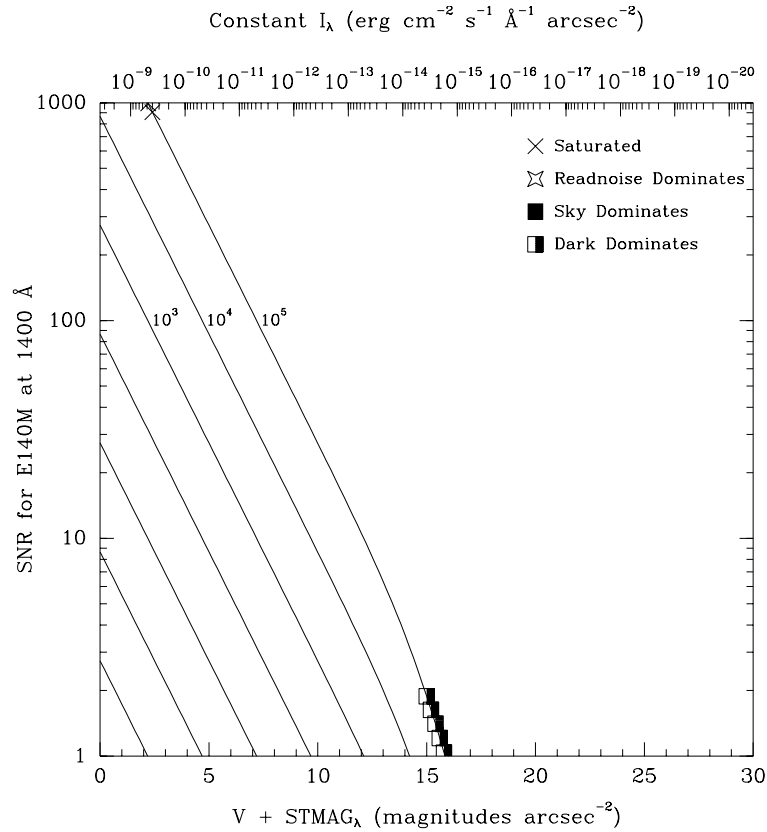
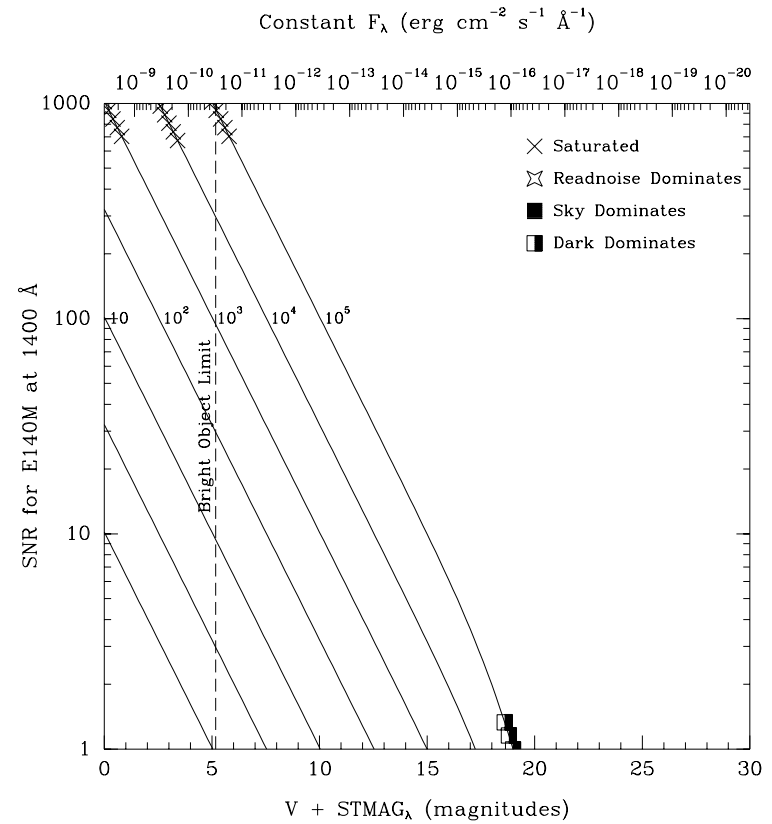


Figure 13.57: Point Source Signal-to-Noise as a Function of STMAG for E140M



Echelle Grating E140H

Description

The E140H grating is used with the FUV-MAMA and provides echelle spectra at a resolving power of $\sim 110,000$ from 1140 to 1700 Å

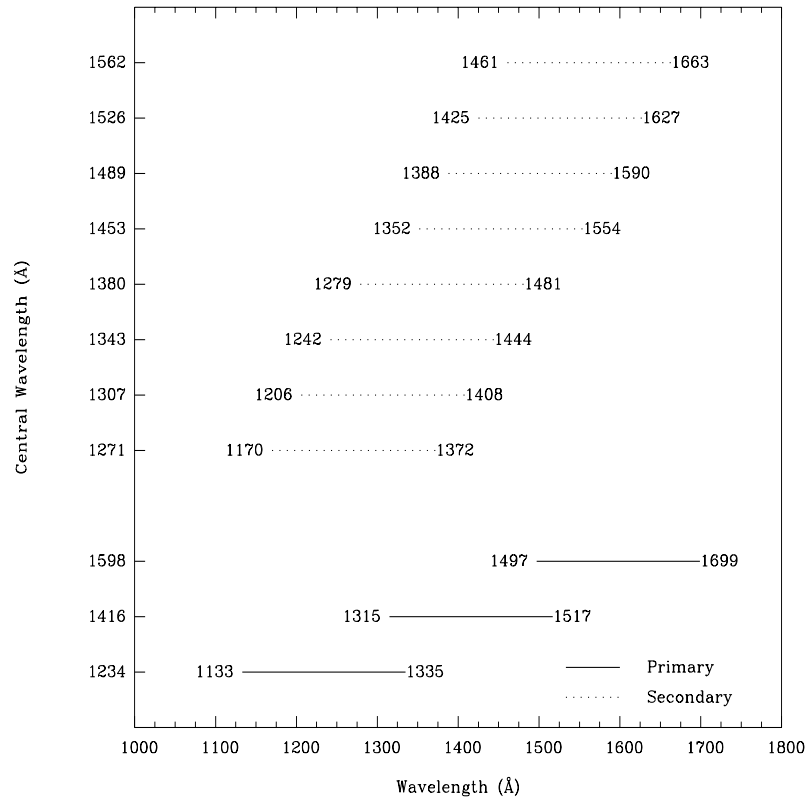
Special Considerations

A single E140H echellogram covers 210 Å over ~ 50 orders. The order separation is ~ 16 pixels (0.47 arcseconds) at 1150 Å and ~ 36 pixels (1.05 arcseconds) at 1700 Å. The grating must be scanned, with exposures taken at three distinct settings to cover the full spectral range of the grating.

The secondary central wavelength at 1271 Å has had direct sensitivity and wavelength calibrations performed during Cycle 7 to support the large number of observations using these positions.

Grating	Spectral Range		Average Dispersion (Å per Pixel)	Dispersion, Cross Dispersion Plate Scale (arcsec / pixel)	Tilts	Central Wavelengths
	Complete	Per Tilt				
E140H	1140-1700	~ 210	$\lambda/228,000$	0.047,0.029	Prime	1234, 1416, 1598
					Secondary	1271, 1307, 1343, 1380, 1453, 1489, 1526, 1562

Figure 13.58: Wavelength Ranges for the E140H Grating Settings

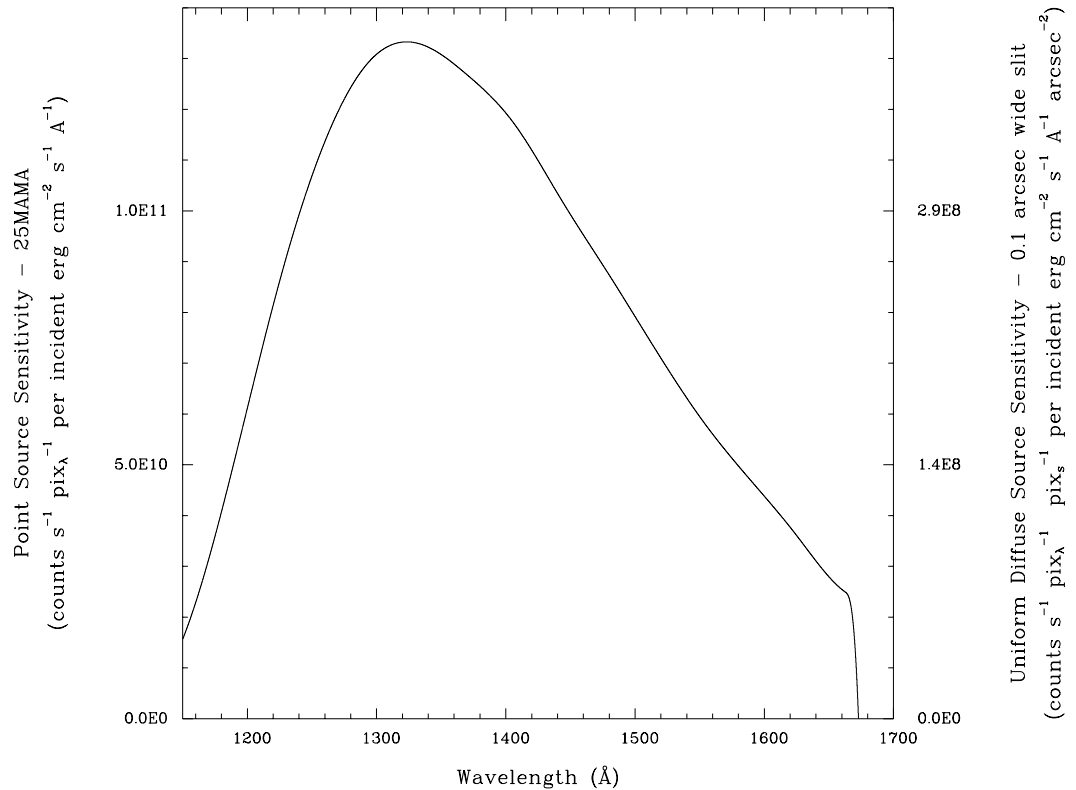


E140H Sensitivity

Table 13.16: E140H Throughputs & Sensitivities for a Point Source

λ	Sensitivity	% Throughput
1200	6.1E10	0.4
1250	1.1E11	0.7
1300	1.3E11	0.8
1350	1.3E11	0.8
1400	1.2E11	0.7
1450	9.9E10	0.5
1500	7.9E10	0.4
1550	6.0E10	0.3
1600	4.4E10	0.2
1650	2.8E10	0.1

Figure 13.59: E140H Point Source (left axis), and Diffuse Source (right axis) Sensitivities. Throughput curve traces the peaks of the blaze function for each order.



Note

Point source sensitivity assumes full transmission (zero slit losses). Diffuse source sensitivity assumes a 0.1" wide slit. To convert point source sensitivities to diffuse source sensitivities multiply the point source values by the grating spatial (cross dispersion) plate scale in units of arcseconds per pixel and by the width of the desired slit in units of arcseconds.

E140H Signal-to-Noise

Note:

The top axis displays constant F_λ values corresponding to the STMAG units ($V+STMAG_\lambda$) on the bottom axis. Recall that $STMAG=0$ is equivalent to $F_\lambda = 3.63E-9 \text{ erg cm}^{-2} \text{ s}^{-1} \text{ \AA}^{-1}$. The curves are labeled with exposure times in seconds.

Figure 13.60: Diffuse Source Signal-to-Noise as a Function of STMAG for E140H

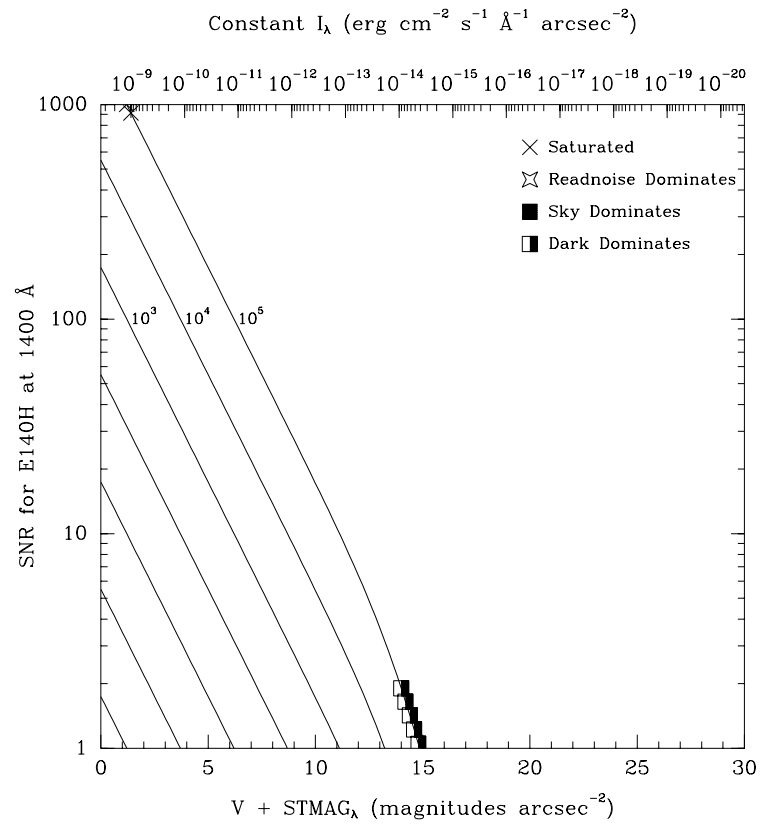
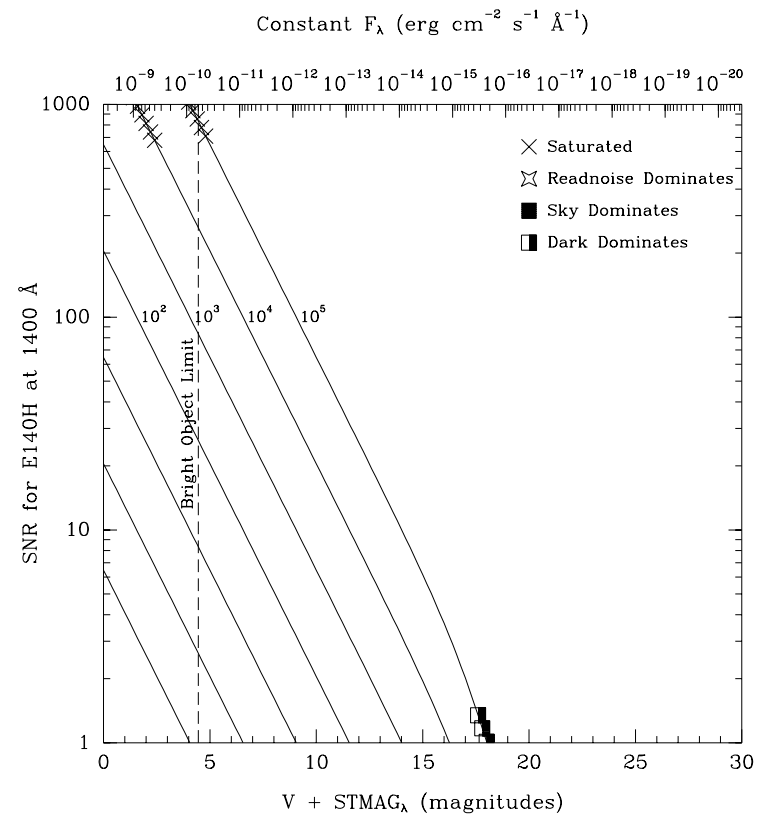


Figure 13.61: Point Source Signal-to-Noise as a Function of STMAG for E140H



PRISM

Description

The PRISM has two central wavelength settings optimized to cover the optical through the far-UV tail down to 1150 Å. It is used with the NUV-MAMA detector.

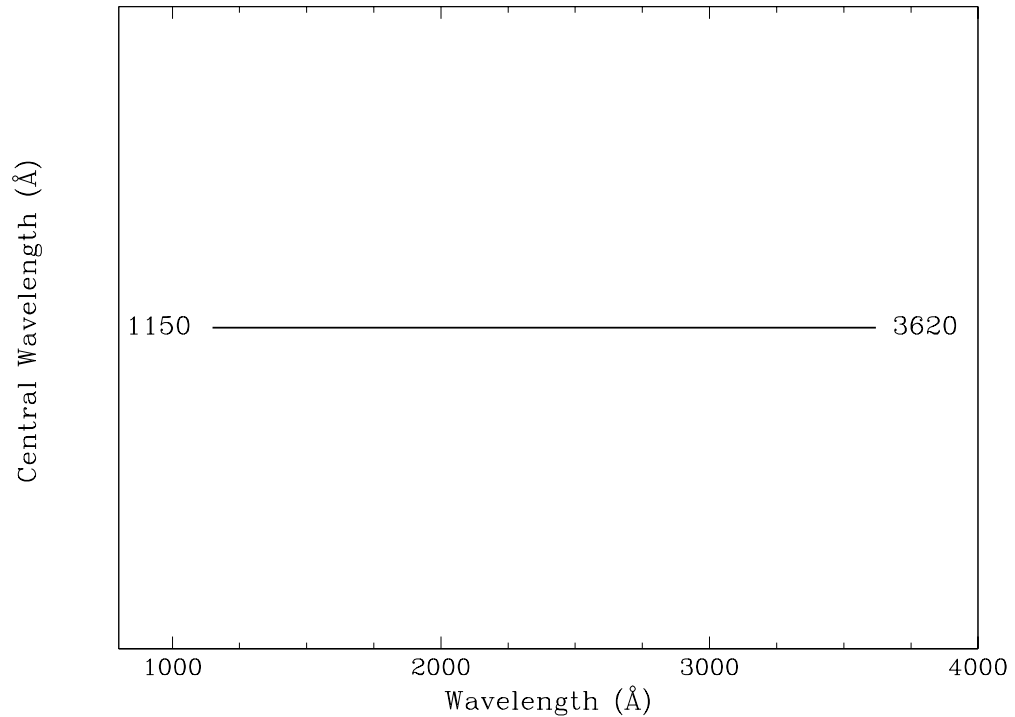
Special Considerations

The full dispersion spreads over ~450 pixels with dispersion as shown in Figure 13.64; thus if you have sources covering the field of view in the dispersion direction, the red tail will be lost for some targets with this setting. For a plot of wavelength vs. pixel no., see Figure 4.13.

We note that the dispersion of the PRISM at wavelengths longer than ~2600 Å is very poorly known at this time.

Grating	Spectral Range		Average Dispersion (Å per Pixel)	Plate Scale (arcsec / pixel)	Tilts	Central Wavelength
	Complete	Per Tilt				
PRISM	1150-3620	2470	0.2-72	0.029	Prime	1200/2125

Figure 13.62: Wavelength Range for the Prism Setting

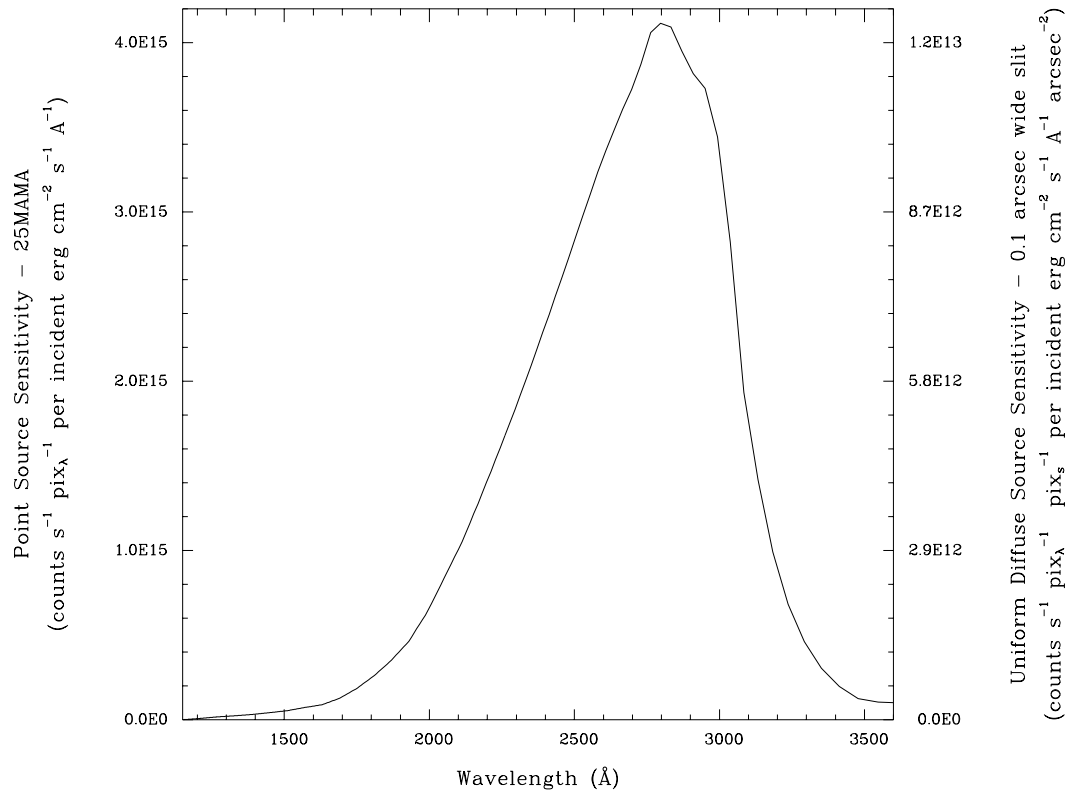


PRISM Sensitivities

Table 13.17: PRISM Throughputs & Sensitivities for a Point Source

λ	Sensitivity	% Throughput
1200	6.2E12	0.4
1400	3.4E13	0.6
1600	8.4E13	0.6
1800	2.6E14	0.9
2000	6.8E14	1.4
2200	1.4E15	1.8
2400	2.3E15	2.0
2600	3.3E15	2.0
2800	4.0E15	1.8
3000	3.1E15	1.1
3200	9.6E14	0.3
3400	2.3E14	0.0
3600	1.0E14	0.0

Figure 13.63: Prism Point Source (left axis), and Diffuse Source (right axis) Sensitivities.



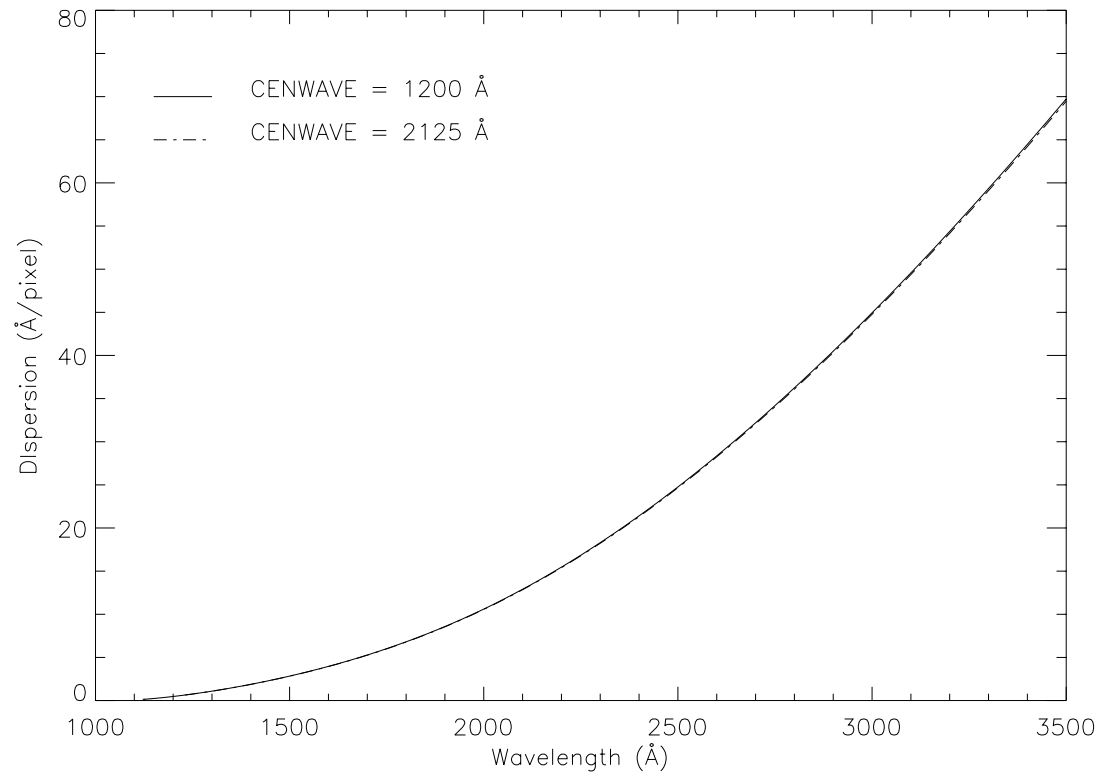
Note

Point source sensitivity assumes full transmission (zero slit losses). Diffuse source sensitivity assumes a 0.1" wide slit. To convert point source sensitivities to diffuse source sensitivities multiply the point source values by the grating spatial (cross dispersion) plate scale in units of arcseconds per pixel and by the width of the desired slit in units of arcseconds.

Prism Wavelength Relationship

The relationship between dispersion and wavelength for the PRISM is shown in Figure 13.64. The relationships between the wavelength and the pixel number for the two wavelength settings are given in Figure 4.13.

Figure 13.64: PRISM dispersion-wavelength relationship.



13.4 Apertures

On the following pages we provide, for each supported aperture, a description of the aperture, the wavelength dependent point source throughput of the aperture, and some advice on its use.

Wavelengths in this handbook and in STIS data products are always measured in vacuum conditions.

- “52X0.05 Aperture,” page 338.
- “52X0.05E1 and 52X0.05D1 Pseudo-apertures” on page 339.
- “52X0.1 Aperture,” page 340.
- “52X0.1E1 and 52X0.1D1 Pseudo-apertures” on page 341.
- “52X0.2 Aperture,” page 342.
- “52X0.2E1, 52X0.2E2, and 52X0.2D1 Pseudo-apertures” on page 343.
- “52X0.5 Aperture,” page 344.
- “52X0.5E1, 52X0.5E2, and 52X0.5D1 Pseudo-apertures” on page 345.
- “52X2 Aperture,” page 346.
- “52X2E1, 52X2E2, and 52X2D1 Pseudo-apertures” on page 347.
- “52X0.2F1 Aperture,” page 348.
- “0.2X0.06 Aperture,” page 349.
- “0.2X0.2 Aperture,” page 350.
- “0.2X0.09 Aperture,” page 351.
- “6X0.2 Aperture,” page 352.
- “0.1X0.03 Aperture” on page 353.
- “FP-SPLIT Slits 0.2X0.06FP(A-E) Apertures” on page 354.
- “FP-SPLIT Slits 0.2X0.2FP(A-E) Apertures” on page 356.
- “0.2X0.05ND Aperture” on page 358.
- “0.3X0.05ND Aperture” on page 359.
- “F25NDQ Aperture” on page 360.

52X0.05 Aperture

Description

This slit is supported with use of the first-order gratings and prism and provides the best spatial and spectral resolution of the long slits. This aperture is the 2 pixel wide slit in the dispersion direction for the MAMA first-order modes.

Special Considerations

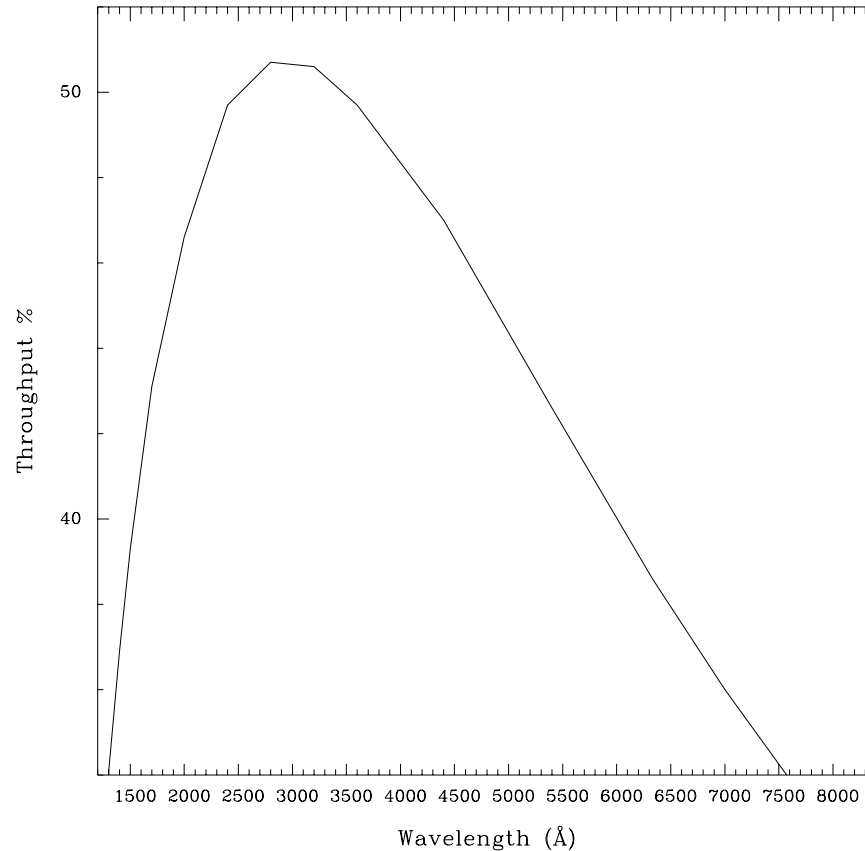
Observations with this slit require a PEAKUP prior to science observations. The actual width of this aperture is 34 milliarcsec instead of 50 milliarcsec, the value suggested by its name. Special pseudo-apertures have been defined to minimize detector effects such as background and CTE. See next page for more information.

Table 13.18: 52X0.05 Throughputs

λ	% Throughput
1200	31.0
1600	41.2
2000	46.6
2400	49.7
2800	50.7
3200	50.6
3600	49.7
4000	48.3
4400	47.0
4800	45.2
5200	43.5
5600	41.7
6000	40.0
6400	38.3
6800	36.8
7200	35.3
7600	33.9
8000	32.8
8400	31.7

Aperture	Projected Length (arcsec)			Width (arcsec)
	CCD	MAMA (M-modes)	MAMA (L-modes)	
52X0.05	52.0	28.0	25.0	0.034

Figure 13.65: 52X0.05 Aperture Throughput as a Function of Wavelength.



52X0.05E1 and 52X0.05D1 Pseudo-apertures

Description

These pseudo-apertures are the same physical aperture as the 52X0.05 aperture, but are used to place the target at different locations on the detectors to reduce CTE loss or FUV-MAMA background. The throughputs of the E1 and D1 apertures as a function of wavelength are similar to those of the corresponding regular positions. However, there is some vignetting of the gratings that changes the overall system throughput slightly with varying position along the slit. At the E1 positions, the overall low dispersion throughputs are decreased by 2 to 3%, while at the D1 position the G140L throughput is increased by 2 to 7%. Throughput changes for the medium resolution gratings are not well characterized, but should be similar. Since these throughput changes depend on the grating and the position on the detector, they are handled in the pipeline calibration by the use of low-order flat fields (lfl files) rather than by a change in aperture throughput curve. The usage of these slits is supported only for certain modes, as listed in the table below.

Special Considerations

Same special considerations as for the 52X0.05 aperture apply to these pseudo-apertures. See reference information on previous page.

Aperture	Detector	Allowed Gratings	Usage
52X0.05E1	CCD	All CCD gratings	Places the target at row ~900 to minimize CTE effects
52X0.05D1	FUV-MAMA	G140L and G140M	Places the target 2 ± 1 " (G140L) or 4 ± 1 " (G140M) above the bottom edge of FUV-MAMA; intended for observations of very faint targets where dark current contribution should be minimized

52X0.1 Aperture

Description

This slit is supported with the first-order gratings and prism. This aperture is the 2 pixel wide slit in the dispersion direction for the CCD first-order modes.

Special Considerations

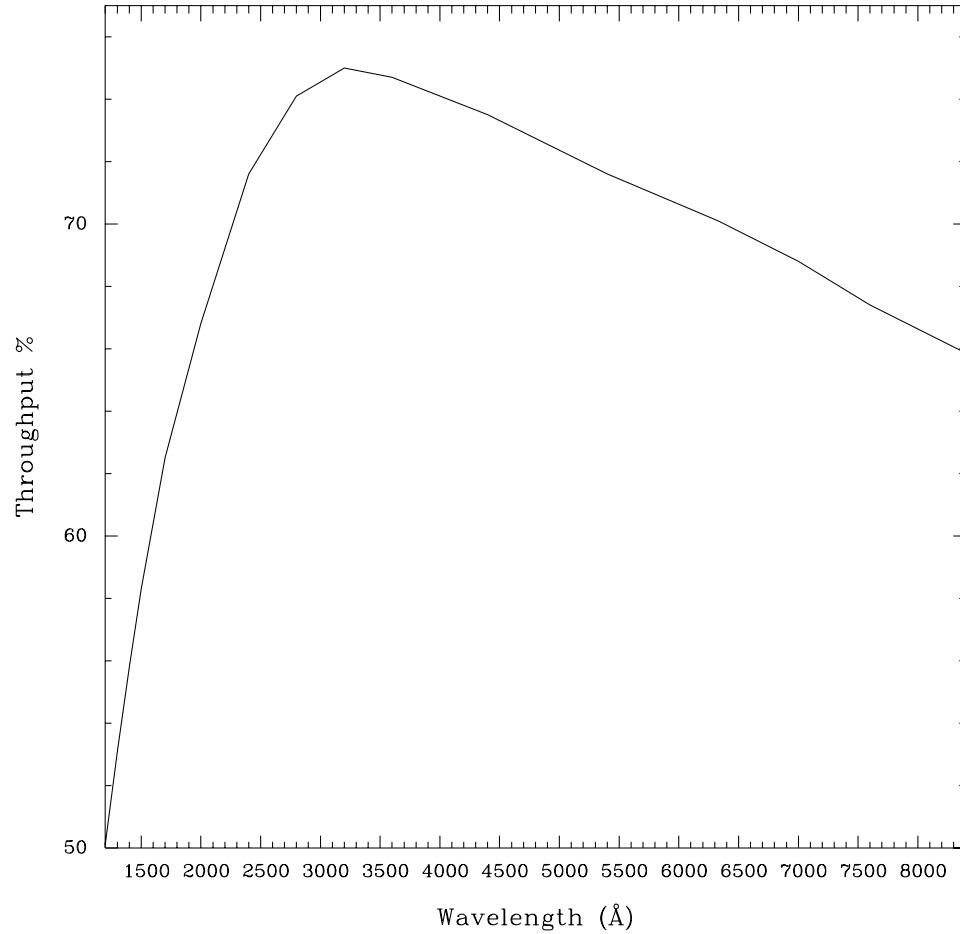
Observations with this slit require a PEAKUP prior to scientific observations.

Table 13.19: 52X0.1 Throughputs

λ	% Throughput
1200	50.1
1600	60.4
2000	66.8
2400	71.6
2800	74.1
3200	75.0
3600	74.7
4000	74.1
4400	73.5
4800	72.7
5200	72.0
5600	71.3
6000	70.6
6400	70.0
6800	69.2
7200	68.3
7600	67.4
8000	66.6
8400	65.9

Aperture	Projected Length (arcsec)			Width (arcsec)
	CCD	MAMA (M-modes)	MAMA (L-modes)	
52X0.1	52.0	28.0	25.0	0.1

Figure 13.66: 52X0.1 Aperture Throughput as a Function of Wavelength.



52X0.1E1 and 52X0.1D1 Pseudo-apertures

Description

These pseudo-apertures are the same physical aperture as the 52X0.1 aperture, but are used to place the target at different locations on the detectors to reduce CTE loss or FUV-MAMA background. The throughputs of the E1 and D1 apertures as a function of wavelength are similar to those of the corresponding regular positions. However, there is some vignetting of the gratings that changes the overall system throughput slightly with varying position along the slit. At the E1 positions, the overall low dispersion throughputs are decreased by 2 to 3%, while at the D1 position the G140L throughput is increased by 2 to 7%. Throughput changes for the medium resolution gratings are not well characterized, but should be similar. Since these throughput changes depend on the grating and the position on the detector, they are handled in the pipeline calibration by the use of low-order flat fields (lfl files) rather than by a change in aperture throughput curve. The usage of these slits is supported only for certain modes, as listed in the table below.

Special Considerations

Same special considerations as for the 52X0.1 aperture apply to these pseudo-apertures. See reference information on previous page.

Aperture	Detector	Allowed Gratings	Usage
52X0.1E1	CCD	All CCD gratings	Places the target at row ~900 to minimize CTE effects
52X0.1D1	FUV-MAMA	G140L and G140M	Places the target 2 ± 1 " (G140L) or 4 ± 1 " (G140M) above the bottom edge of FUV-MAMA; intended for observations of very faint targets where dark current contribution should be minimized

52X0.2 Aperture

Description

This is the “utility” slit used with first-order gratings and the prism. It provides a good compromise between spectral resolution and photometric throughput.

Special Considerations

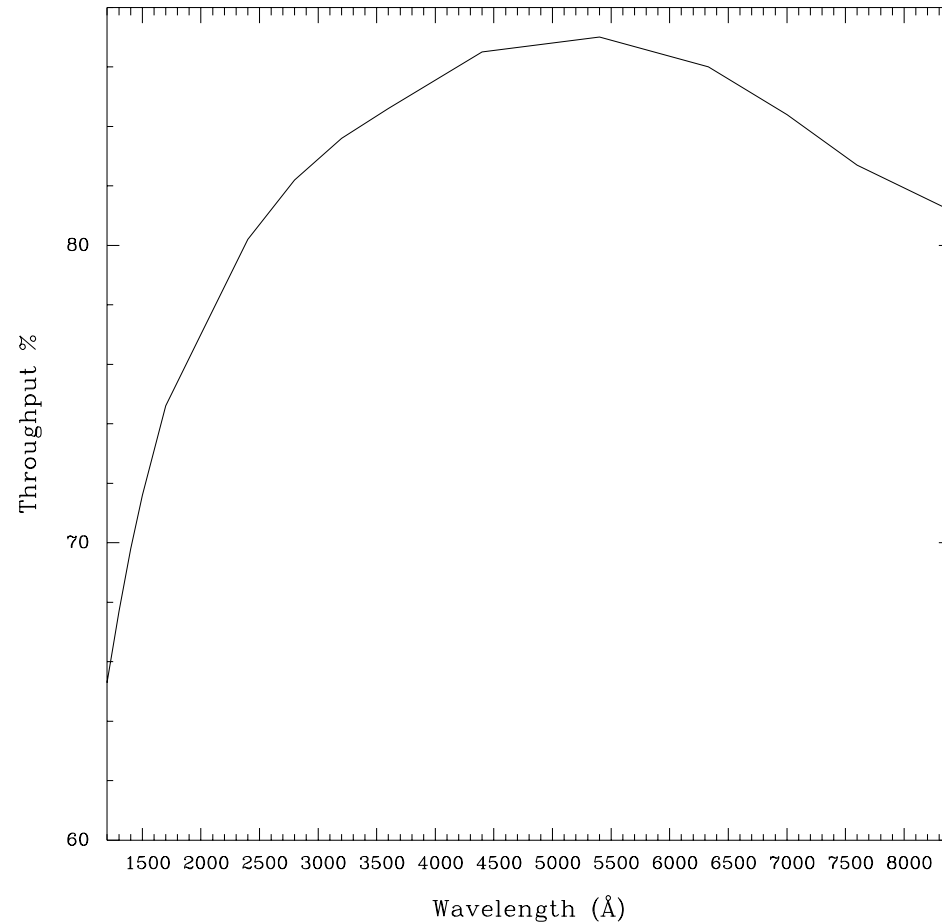
Observations using this slit do not need to be preceded by a PEAKUP.

Table 13.20: 52X0.2 Throughputs

λ	% Throughput
1200	65.3
1800	75.4
2400	80.2
3000	82.9
3600	84.6
4200	86.0
4800	86.7
5400	87.0
6000	86.4
6600	85.4
7200	83.8
7800	82.3
8400	81.2

Aperture	Projected Length (arcsec)			
	CCD	MAMA (M-modes)	MAMA (L-modes)	Width (arcsec)
52X0.2	52.0	28.0	25.0	0.2

Figure 13.67: 52X0.2 Aperture Throughput as a Function of Wavelength



52X0.2E1, 52X0.2E2, and 52X0.2D1 Pseudo-apertures

Description

These pseudo-apertures are the same physical aperture as the 52X0.2 aperture, but are used to place the target at different locations on the detectors to reduce CTE loss or FUV-MAMA background. The throughputs of the E1 and D1 apertures as a function of wavelength are similar to those of the corresponding regular positions. However, there is some vignetting of the gratings that changes the overall system throughput slightly with varying position along the slit. At the E1 positions, the overall low dispersion throughputs are decreased by 2 to 3%, while at the D1 position the G140L throughput is increased by 2 to 7%. Throughput changes for the medium resolution gratings are not well characterized, but should be similar. Since these throughput changes depend on the grating and the position on the detector, they are handled in the pipeline calibration by the use of low-order flat fields (lfl files) rather than by a change in aperture throughput curve. Throughput at the 52X0.2E2 position is about 20% lower than that at the 52X0.2E1 position. The usage of these slits is supported only for certain modes, as listed in the table below.

Special Considerations

Same special considerations as for the 52X0.2 aperture apply to these pseudo-apertures. See reference information on previous page.

Aperture	Detector	Allowed Gratings	Usage
52X0.2E1	CCD	All CCD gratings	Places the target at row ~900 to minimize CTE effects
52X0.2E2	CCD	G750L and G750M	Places the target at row ~900 to minimize CTE effects; positions are offset from the physical aperture, to give better alignment with fringe flats done using 52X0.1 aperture
52X0.2D1	FUV-MAMA	G140L and G140M	Places the target $2\pm 1''$ (G140L) or $4\pm 1''$ (G140M) above the bottom edge of FUV-MAMA; intended for observations of very faint targets where dark current contribution should be minimized

52X0.5 Aperture

Description

This slit is designated for use with the first-order gratings and prism and is a good slit for spectrophotometric observations of point sources.

Special Considerations

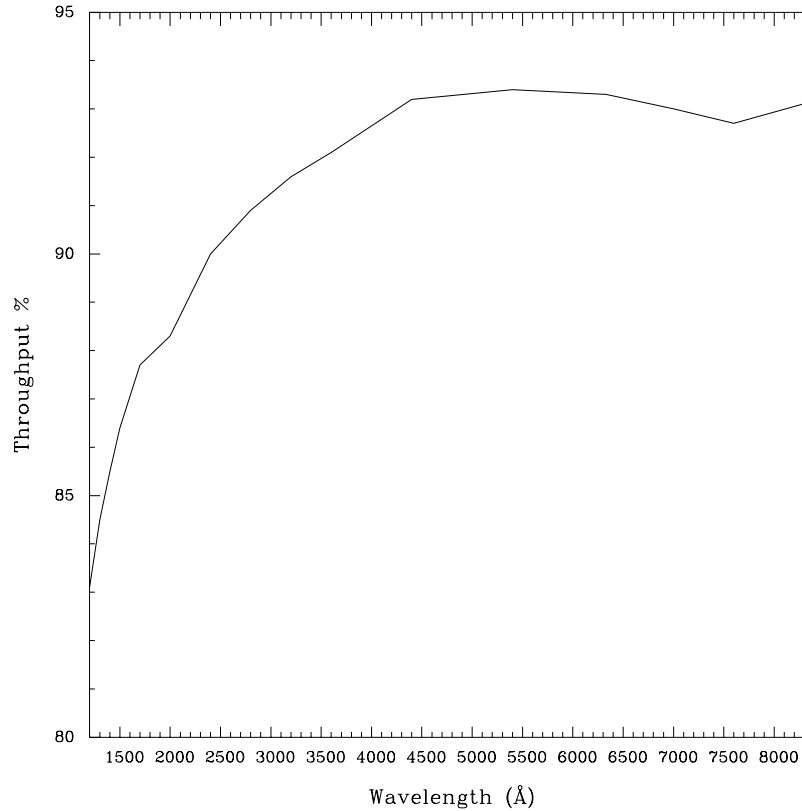
Observations with this slit do not need to be preceded by a PEAKUP. Be aware of effects of OTA scatter on the line profiles when observing point sources in wide slits (see Section 13.7). Targets not centered on the slit along the spatial direction can experience significant shifts in wavelength.

Table 13.21: 52X0.5 Throughputs.

λ	% Throughput
1200	83.1
1800	87.9
2400	90.0
3000	91.3
3600	92.1
4200	92.9
4800	93.3
5400	93.4
6000	93.3
6600	93.2
7200	92.9
7800	92.8
8400	93.2

Aperture	Projected Length (arcsec)			Width (arcsec)
	CCD	MAMA (M-modes)	MAMA (L-modes)	
52X0.5	52.0	28.0	25.0	0.5

Figure 13.68: 52X0.5 Aperture Throughput as a Function of Wavelength



52X0.5E1, 52X0.5E2, and 52X0.5D1 Pseudo-apertures

Description

These pseudo-apertures are the same physical aperture as the 52X0.5 aperture, but are used to place the target at different locations on the detectors to reduce CTE loss or FUV-MAMA background. The throughputs of the E1 and D1 apertures as a function of wavelength are similar to those of the corresponding regular positions. However, there is some vignetting of the gratings that changes the overall system throughput slightly with varying position along the slit. At the E1 positions, the overall low dispersion throughputs are decreased by 2 to 3%, while at the D1 position the G140L throughput is increased by 2 to 7%. Throughput changes for the medium resolution gratings are not well characterized, but should be similar. Since these throughput changes depend on the grating and the position on the detector, they are handled in the pipeline calibration by the use of low-order flat fields (lfl files) rather than by a change in aperture throughput curve. Throughput at the 52X0.5E2 position is very similar to that at the 52X0.5E1 position. The usage of these slits is supported only for certain modes, as listed in the table below.

Special Considerations

Same special considerations as for the 52X0.5 aperture apply to these pseudo-apertures. See reference information on previous page.

Aperture	Detector	Allowed Gratings	Usage
52X0.5E1	CCD	All CCD gratings	Places the target at row ~900 to minimize CTE effects
52X0.5E2	CCD	G750L and G750M	Places the target at row ~900 to minimize CTE effects; positions are offset from the physical aperture, to give better alignment with fringe flats done using 52X0.1 aperture
52X0.5D1	FUV-MAMA	G140L and G140M	Places the target $2\pm 1''$ (G140L) or $4\pm 1''$ (G140M) above the bottom edge of FUV-MAMA; intended for observations of very faint targets where dark current contribution should be minimized

52X2 Aperture

Description

The last in the series of supported long slits used with the first-order gratings and prism and is a good slit for spectrophotometric observations of point sources. The small dip seen at 2000Å is likely due to uncertainties in the numerical calculation, and will not affect the absolute flux calibration.

Special Consideration

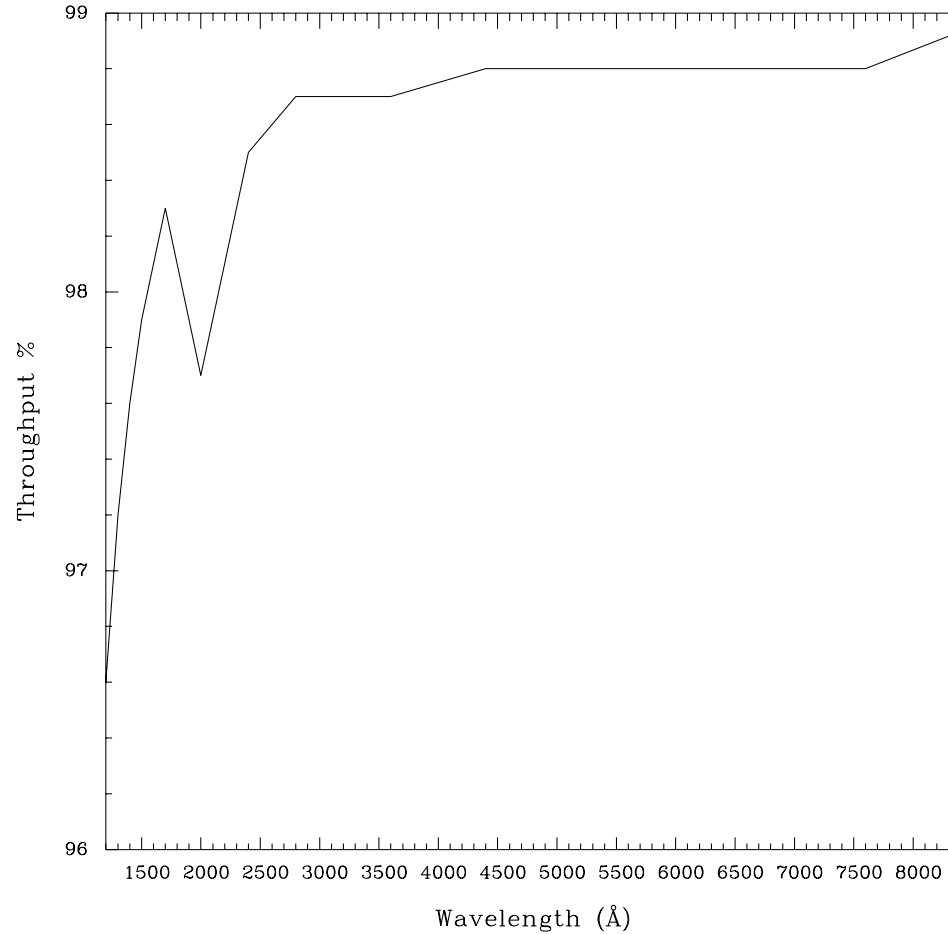
Observations using this slit do not need to be preceded by a PEAKUP. Be aware of effects of OTA scatter on the line profiles when observing point sources in the wide slits (see Section 13.7). Targets not centered on the slit along the spatial direction can experience significant shifts in wavelength.

Table 13.22: 52X2 Throughputs.

λ	% Throughput
1200	96.6
1800	98.1
2400	98.5
3000	98.7
3600	98.7
4200	98.8
4800	98.8
5400	98.8
6000	98.8
6600	98.8
7200	98.8
7800	98.8
8400	98.9

Projected Length (arcsec)				
Aperture	CCD	MAMA (M-modes)	MAMA (L-modes)	Width (arcsec)
52X2	52.0	28.0	25.0	2.0

Figure 13.69: 52X2 Aperture Throughput as a Function of Wavelength



52X2E1, 52X2E2, and 52X2D1 Pseudo-apertures

Description

These pseudo-apertures are the same physical aperture as the 52X2 aperture, but are used to place the target at different locations on the detectors to reduce CTE loss or FUV-MAMA background.

The throughputs of the E1 and D1 apertures as a function of wavelength are similar to those of the corresponding regular positions. However, there is some vignetting of the gratings that changes the overall system throughput slightly with varying position along the slit. At the E1 positions, the overall low dispersion throughputs are decreased by 2 to 3%, while at the D1 position the G140L throughput is increased by 2 to 7%.

Throughput changes for the medium resolution gratings are not well characterized, but should be similar. Since these throughput changes depend on the grating and the position on the detector, they are handled in the pipeline calibration by the use of low-order flat fields (lfl files) rather than by a change in aperture throughput curve. Throughput at the 52X2E2 position is very similar to that at the 52X2E1 position. The usage of these slits is supported only for certain modes, as listed in the table below.

Special Considerations

Same special considerations as for the 52X2 aperture apply to these pseudo-apertures. See reference information on previous page.

Aperture	Detector	Allowed Gratings	Usage
52X2E1	CCD	All CCD gratings	Places the target at row ~900 to minimize CTE effects
52X2E2	CCD	G750L and G750M	Places the target at row ~900 to minimize CTE effects; positions are offset from the physical aperture, to give better alignment with fringe flats done using 52X0.1 aperture
52X2D1	FUV-MAMA	G140L and G140M	Places the target 2 ± 1 " (G140L) or 4 ± 1 " (G140M) above the bottom edge of FUV-MAMA; intended for observations of very faint targets where dark current contribution should be minimized

52X0.2F1 Aperture

Description

The same physical aperture as the 52X0.2 but used at the position of the smaller of the two fiducials. The fiducial bar can be used for spectroscopic coronagraphic observations. The throughput for the unocculted 52X0.2 aperture is given below.

Special Considerations

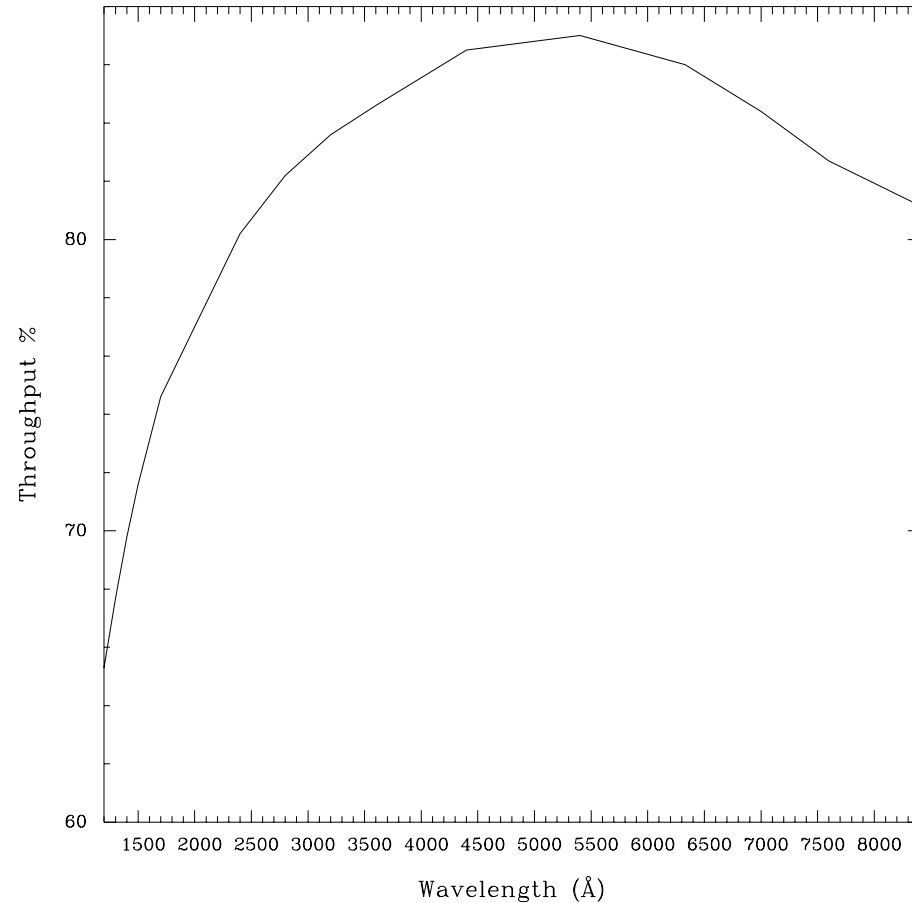
Observations using this slit do not need to be preceded by a PEAKUP.

Table 13.23: 52X0.2 Throughputs

λ	% Throughput
1200	65.3
1600	73.1
2000	77.0
2400	80.2
2800	82.2
3200	83.6
3600	84.6
4000	85.6
4400	86.5
4800	86.7
5200	86.9
5600	86.8
6000	86.4
6400	85.8
6800	84.9
7200	83.8
7600	82.7
8000	81.9
8400	81.2

Aperture	Projected Length (arcsec)			Width (arcsec)
	CCD	MAMA (M-modes)	MAMA (L-modes)	
52X0.2F1	52.0	28.0	25.0	0.2
Fiducial	0.5	0.5	0.5	0.2

Figure 13.70: 52X0.2 Aperture Throughput as a Function of Wavelength



0.2X0.06 Aperture

Description

Supported slit for use with the medium resolution echelle gratings. This slit is two pixels wide in dispersion for these gratings, providing optimal spectral resolution and line profiles.

Special Considerations

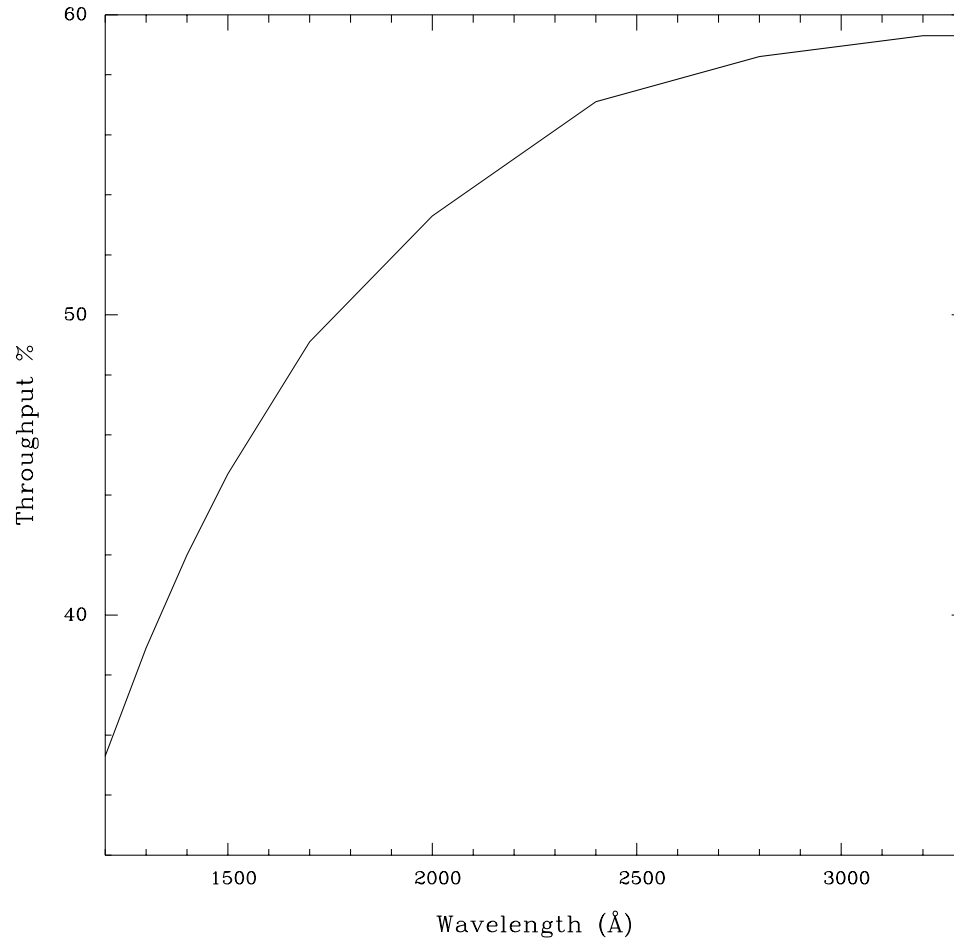
Used with E230M and E140M gratings. Observations with this slit require a prior PEAKUP.

Table 13.24: 0.2X0.06 Throughputs

λ	% Throughput
1200	35.3
1800	50.5
2400	57.1
3000	59.0
3600	59.3
6000	52.4

Aperture	Projected Length (arcsec) (MAMA E-modes)	Width (arcsec)
0.2X0.06	0.2	0.06

Figure 13.71: 0.2X0.06 Aperture Throughput as a Function of Wavelength



0.2X0.2 Aperture

Description

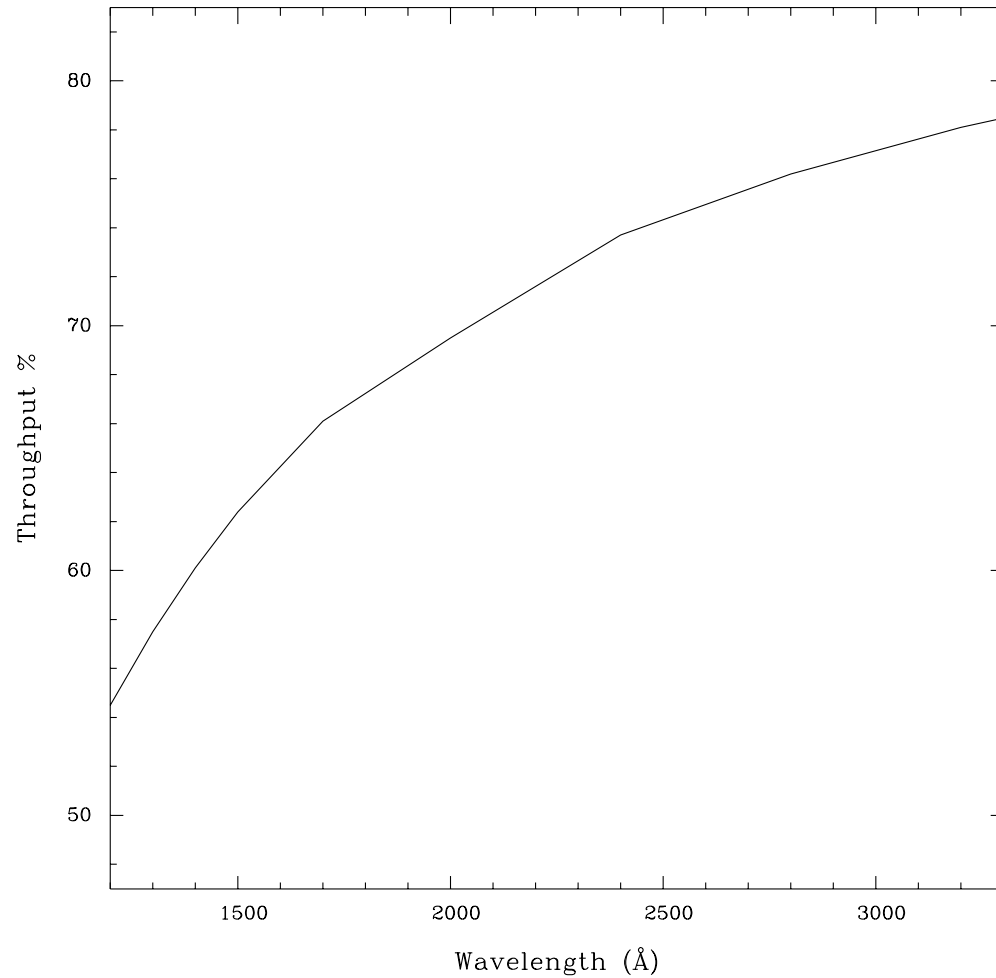
The “utility” slit for the echelle gratings. This slit is the most photometric of the supported echelle slits and has the highest throughput for photon statistics. Starting in Cycle 12, this slit is also supported for use with the first order gratings, and it is the recommended aperture for first order MAMA snapshot programs that do not have a scientific need for a long-slit (see Section 2.8 “STIS Snapshot Policies”).

Table 13.25: 0.2X0.2 Throughputs

λ	% Throughput
1200	54.5
1800	67.2
2400	73.7
3000	77.2
3600	79.6
6000	81.7

Aperture	Projected Length (arcsec) (MAMA E-modes)	Width (arcsec)
0.2X0.2	0.2	0.2

Figure 13.72: 0.2X0.2 Aperture Throughput as a Function of Wavelength



0.2X0.09 Aperture

Description

This slit is used with high resolution echelle gratings. This slit is two pixels wide in dispersion for these gratings, providing optimal spectral resolution and line profiles.

Special Considerations

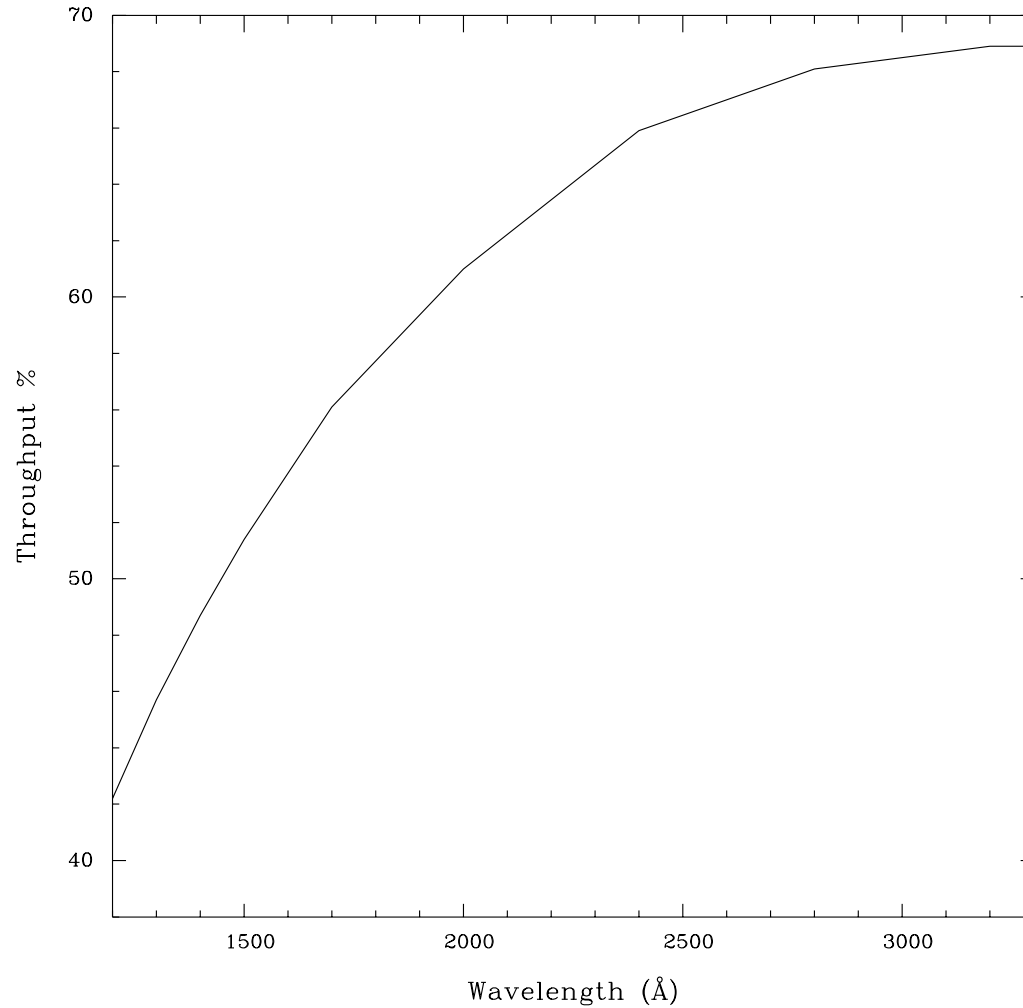
Used with E140H and E230H grating only. Observations with this slit require a prior PEAKUP.

Table 13.26: 0.2X0.09 Throughputs

λ	% Throughput
1200	42.2
1800	57.7
2400	65.9
3000	68.5
3600	68.9
6000	64.9

Aperture	Projected Length (arcsec) (MAMA E-modes)	Width (arcsec)
0.2X0.09	0.2	0.09

Figure 13.73: 0.2X0.09 Aperture Throughput as a Function of Wavelength



6X0.2 Aperture

Description

This slit is used with echelle gratings.

Recommended Uses

A good slit for echelle observations of extended sources with isolated emission lines.

Special Considerations

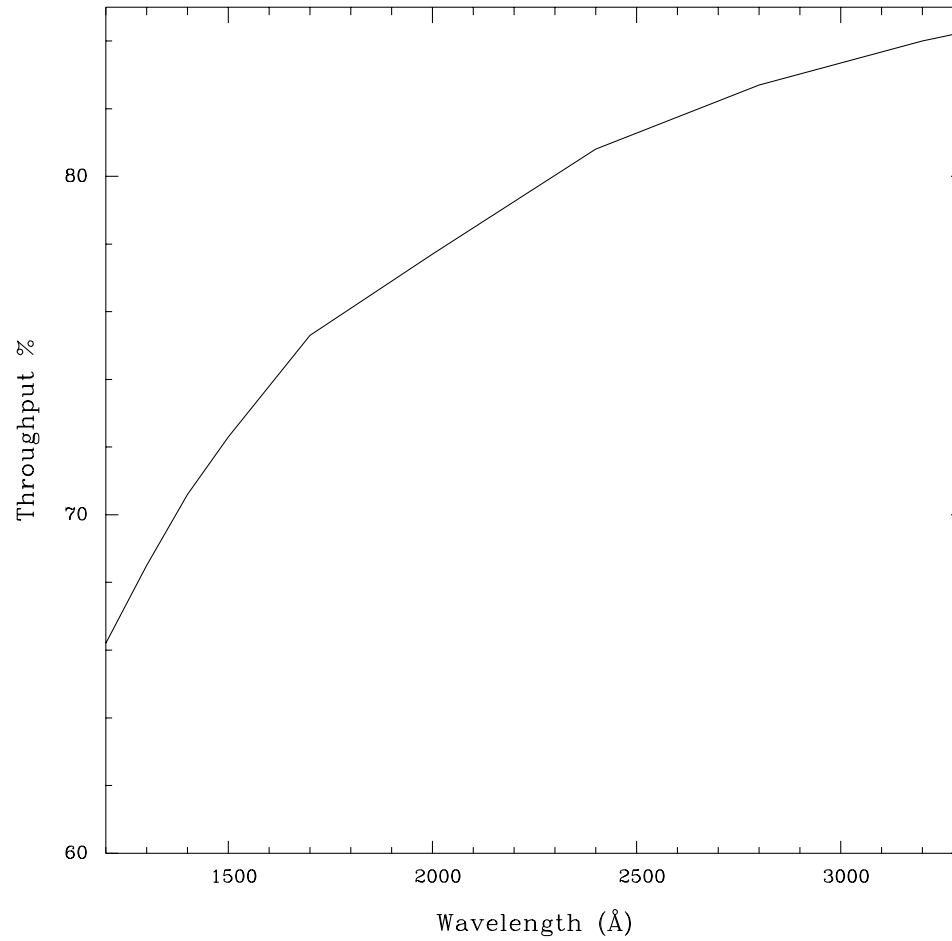
This slit can be used with all echelle gratings. Please note that use of this slit with an extended source will produce order overlap and may make analysis difficult (see also Section 13.7).

Aperture	Projected Length (arcsec) (MAMA E-modes)	Width (arcsec)
6X0.2	6.0	0.2

Table 13.27: 6X0.2 Aperture Throughputs

λ	% Throughput
1200	66.2
1400	70.6
1600	73.8
1800	76.1
2000	77.7
2200	79.3
2400	80.8
2600	81.8
2800	82.7
3000	83.4
3200	84.0
3400	84.5

Figure 13.74: 6X0.2 Aperture Throughput as a Function of Wavelength



0.1X0.03 Aperture

Description

This slit provides the highest spectral resolution of any STIS slit and is restricted to use with the MAMA echelle gratings. Tests during ground calibration with this slit to obtain MAMA exposures of a mono-isotopic platinum lamp source produced resolving powers in excess of 200,000.

Special Considerations

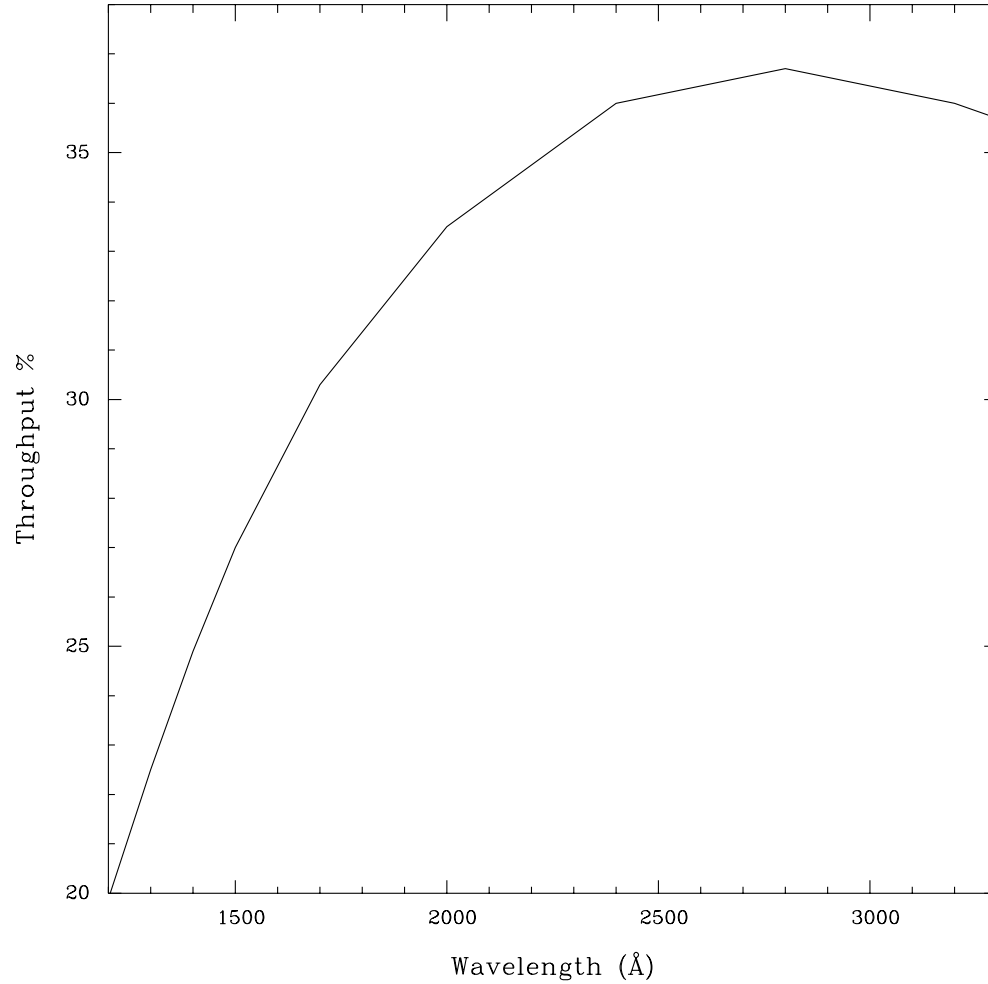
Observations with this slit require a prior PEAKUP. The peakup is performed in two stages - first with the 0.2X0.09 aperture (or one of the small neutral density apertures), and then with the 0.1X0.03 aperture.

Table 13.28: 0.1X0.03 Throughputs

λ	% Throughput
1200	19.9
1800	31.4
2400	36.0
3000	36.3
6000	27.0

Aperture	Projected Length (arcsec)	Width (arcsec)
0.1X0.03	0.1	0.025

Figure 13.75: 0.1X0.03 Aperture Throughput as a Function of Wavelength



FP-SPLIT Slits 0.2X0.06FP(A-E) Apertures

Description

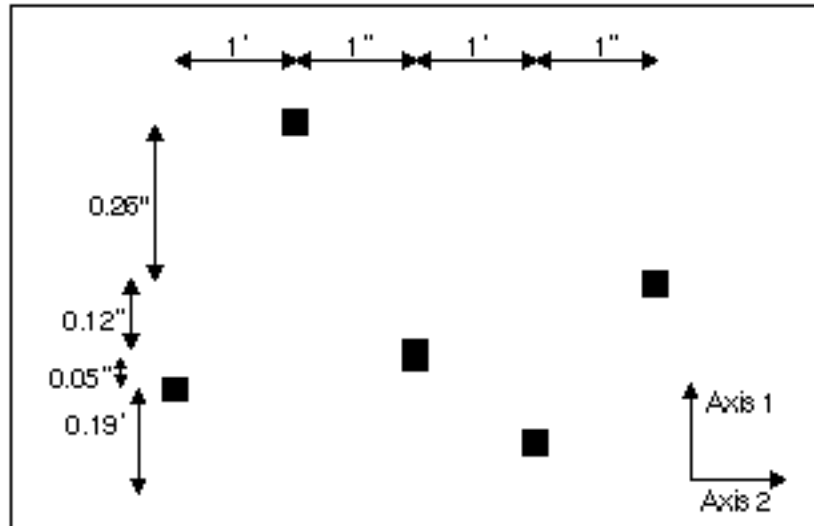
The FP-SPLIT slits consist of two sets of five slits; in each set the slits are all the same size. They are for use with the MAMA echelle gratings. It is possible to achieve high S/N data for bright targets, independently of the quality of the flat-field, by means of a special observing strategy wherein multiple spectrograms are obtained through these slits.

Special Considerations

See Chapter 12 for more details on obtaining high S/N spectral data. Observations with this slit require a prior PEAKUP.

Aperture	Projected Length (arcsec)	Width (arcsec)
0.2X0.06FPA	0.2	0.06
0.2X0.06FPB	0.2	0.06
0.2X0.06FPC	0.2	0.06
0.2X0.06FPD	0.2	0.06
0.2X0.06FPE	0.2	0.06

Figure 13.76: Schematic of the STIS Fixed-Pattern Slit Configuration. AXIS1 corresponds to the dispersion direction, and AXIS2 to the spatial direction. Dimensions are not to scale.

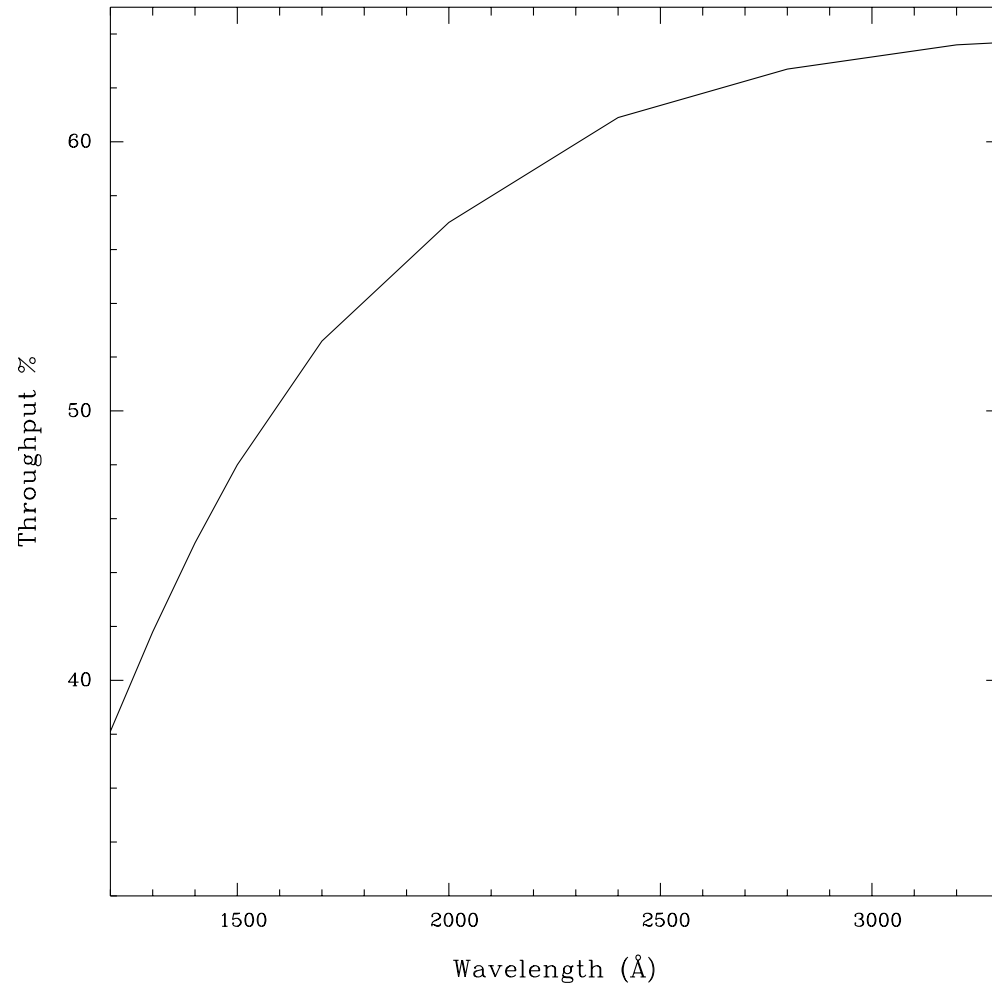


FP-SPLIT Throughputs

Table 13.29: Throughput for 0.2X0.06FP(A-E)

λ	% Throughput
1200	38.1
1800	54.1
2400	60.9
3000	63.1
3600	63.9
6000	58.0

Figure 13.77: 0.2X0.06FP(A-E) Aperture Throughput as a Function of Wavelength



FP-SPLIT Slits 0.2X0.2FP(A-E) Apertures

Description

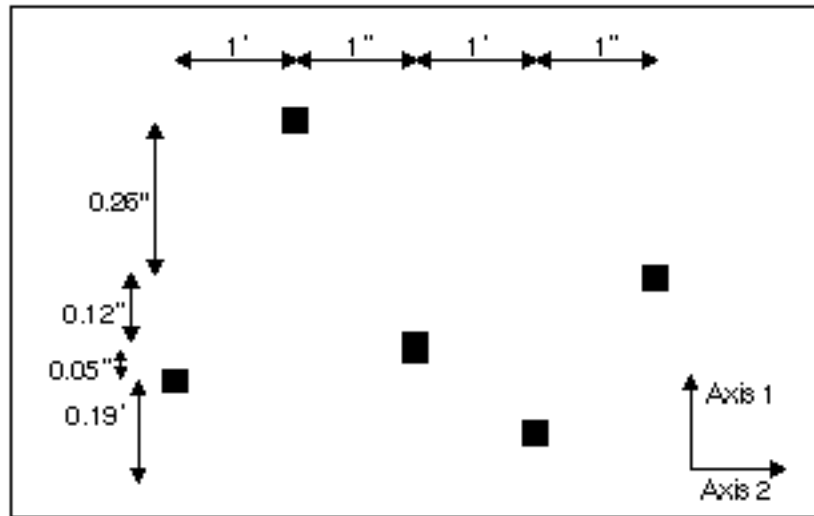
The FP-SPLIT slits consist of two sets of five slits—in each set the slits are all the same size. They are for use with the MAMA echelle gratings. It is possible to achieve high S/N data for bright targets, independently of the quality of the flat-field, by means of a special observing strategy wherein multiple spectrograms are obtained through these slits.

Special Considerations

See Chapter 12 for more details on obtaining high S/N spectral data.

Aperture	Projected Length (arcsec)	Width (arcsec)
0.2X0.2FPA	0.2	0.2
0.2X0.2FPB	0.2	0.2
0.2X0.2FPC	0.2	0.2
0.2X0.2FPD	0.2	0.2
0.2X0.2FPE	0.2	0.2

Figure 13.78: Schematic of the STIS Fixed-Pattern Slit Configuration. AXIS1 corresponds to the dispersion direction, and AXIS2 to the spatial direction. Dimensions are not to scale.

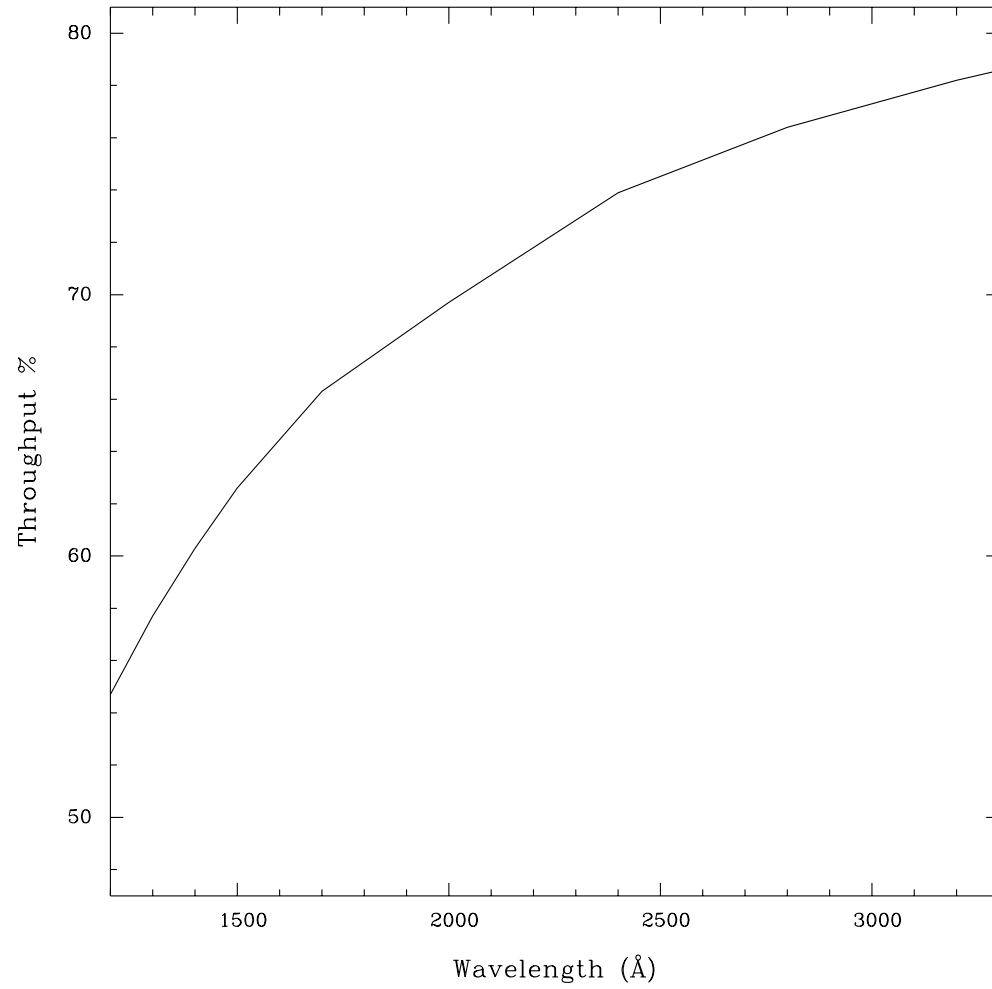


FP-SPLIT Throughputs

Table 13.30: 0.2X0.2FP(A-E) Slit Throughputs

λ	% Throughput
1200	54.7
1800	67.4
2400	73.9
3000	77.3
3600	79.7
6000	82.0

Figure 13.79: 0.2X0.2FP(A-E) Aperture Throughput as a Function of Wavelength



0.2X0.05ND Aperture

Description

Supported neutral-density-filtered slit for use with bright objects with the echelle gratings. The dex ND factor is 2.0.

Special Considerations

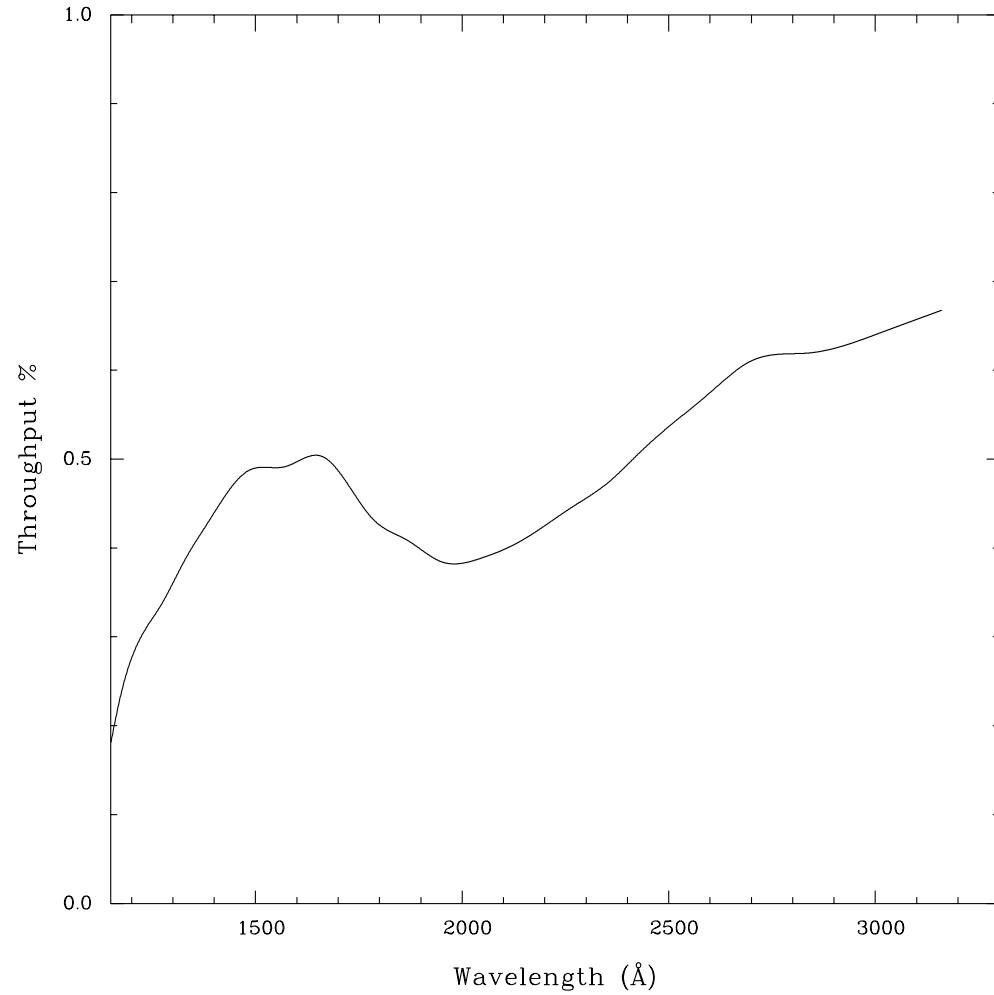
Observations with this slit require a prior PEAKUP. This aperture can also be used with the CCD for ACQ/PEAKs.

Aperture	Projected Length (arcsec) (MAMA E-modes)	Width (arcsec)
0.2X0.05ND	0.2	0.05

Table 13.31: 0.2X0.05ND Throughputs

λ	% Throughput
1150	0.18
1350	0.40
1550	0.49
1750	0.45
1950	0.38
2150	0.41
2350	0.47
2550	0.56
2750	0.62
2950	0.63
3150	0.67

Figure 13.80: 0.2X0.05ND Aperture Throughput as a Function of Wavelength



0.3X0.05ND Aperture

Description

Supported neutral-density-filtered slit for use with bright objects with the echelle gratings. The dex ND factor is 3.0.

Special Considerations

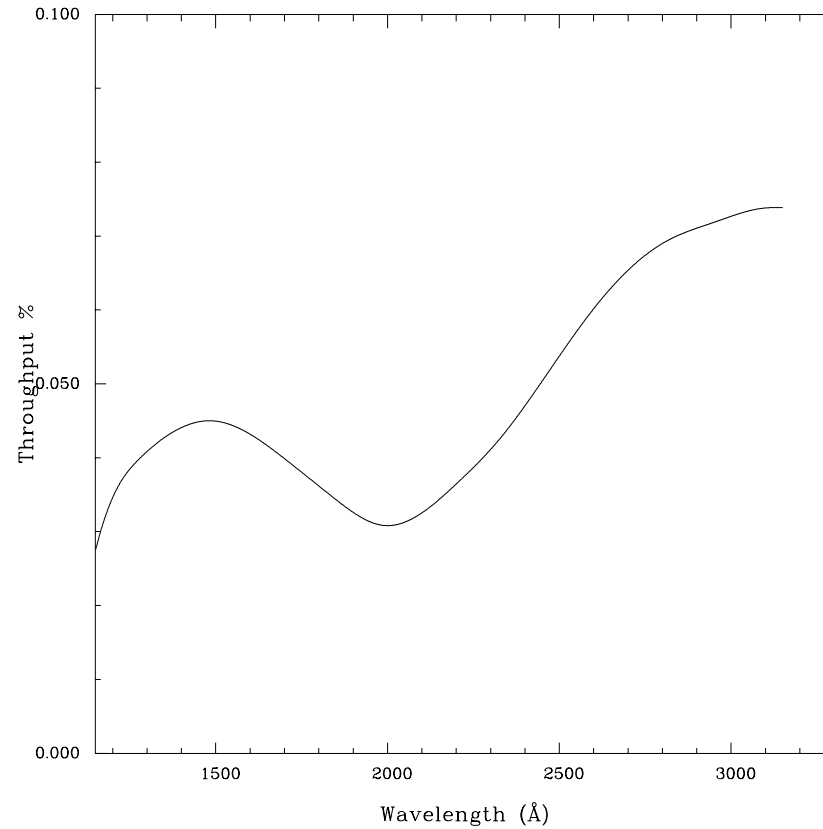
Observations with this slit require a prior PEAKUP. This aperture can also be used with the CCD for ACQ/PEAKs.

Table 13.32: 0.3X0.05ND Throughputs

λ	% Throughput
1150	0.028
1350	0.043
1550	0.044
1750	0.038
1950	0.031
2150	0.034
2350	0.044
2550	0.057
2750	0.067
2950	0.072
3150	0.074

Aperture	Projected Length (arcsec) (MAMA E-modes)	Width (arcsec)
0.3X0.05ND	0.3	0.05

Figure 13.81: 0.3X0.05ND Aperture Throughput as a Function of Wavelength



F25NDQ Aperture

Description

Supported neutral-density-filtered aperture for slitless 1st order MAMA spectroscopy of targets too bright to be observed with a clear aperture. The F25NDQ filter is unique in that it is divided into four quadrants, each having a different neutral density factor. In clockwise order starting from the upper left these are F25NDQ1, F25NDQ2, F25NDQ3, and F25NDQ4, where the number appended to each name is the approximate dex ND factor. Approximate dimensions of each quadrant and the default location of an external target in each quadrant are given in Table 13.33.

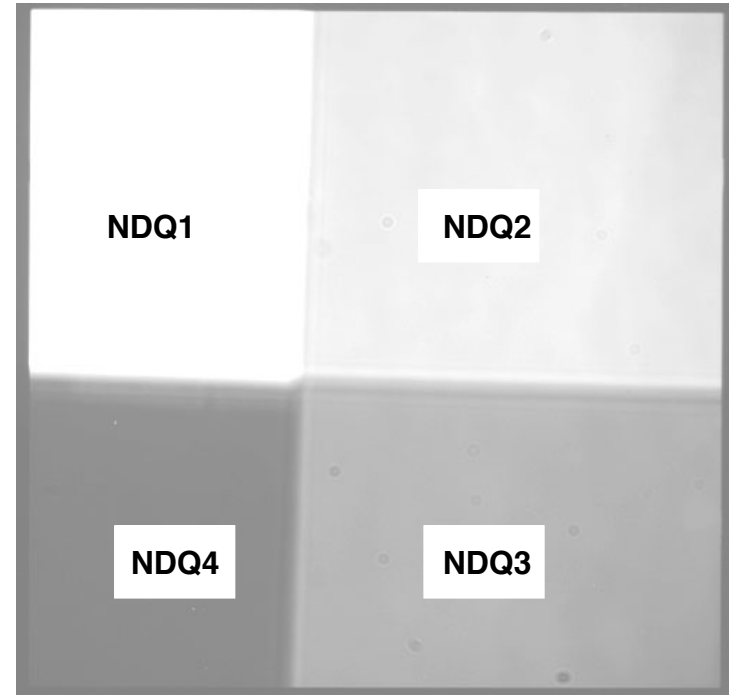
Special Considerations

The default aperture locations where the target is placed in each quadrant are significantly offset from the center of the detector in both the spatial and the dispersion directions. For observations at these nominal aperture locations this will cause a significant shift in the wavelength coverage for any given grating setting. For example, when observing with G140L in F25NDQ1, wavelengths shorter than about 1330 Å will fall off the detector. Users may wish to use a POS-TARG to bring the target back closer to the center line of the detector. However, if the target would violate BOP restrictions in any quadrant of the aperture, the restrictions regarding pointing close to objects violating safety limits discussed in Chapter 7 and STIS ISR 2000-01 will apply. This latter rule renders the F25NDQ4 quadrant mostly useless, and the F25NDQ3 quadrant is redundant with the full field F25ND3 aperture, so in practice only the F25NDQ1 and F25NDQ2 quadrants are commonly used. Also the dividing lines between the quadrants are somewhat displaced from the center of the detector and are not quite parallel to the detector edges (see Figure 13.82), so observers for whom the exact locations of the quadrant boundaries are important should consult help@stsci.edu.

Table 13.33: NDQ quadrant dimensions and the default locations at which a target is placed in each quadrant.

Aperture	Projected Length (arc-sec)	Projected Width (arc-sec)	Target X location (pixels)	Target Y location (pixels)
F25NDQ1	13.4	9.7	198	756
F25NDQ2	13.8	15.1	712	753
F25NDQ3	11.4	15.3	686	254
F25NDQ4	11.8	9.5	195	248

Figure 13.82: A CCD lamp image taken through the NDQ filter. Note the unequal sizes of the four quadrants.

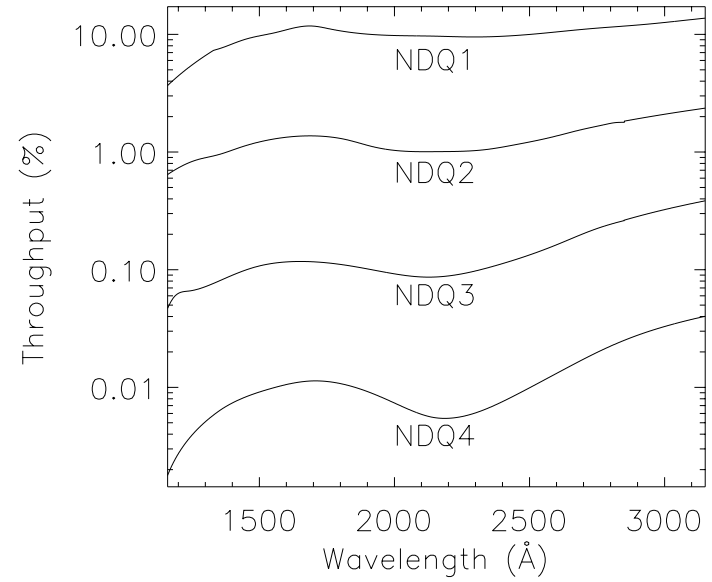


■ Table 13.34: F25NDQ Throughputs (%)

λ	F25NDQ1	F25NDQ2	F25NDQ3	F25NDQ4
1150	3.48	0.62	0.04	0.002
1350	7.54	0.95	0.08	0.006
1550	10.24	1.29	0.11	0.010
1750	11.26	1.35	0.11	0.011
1950	9.88	1.07	0.10	0.008
2150	9.66	1.01	0.09	0.006
2350	9.54	1.06	0.10	0.007
2550	10.22	1.29	0.15	0.011
2750	11.30	1.66	0.22	0.020
2950	12.29	2.01	0.30	0.030

Note: Aperture throughputs values for NDQ1 and NDQ4 at $\lambda < 1330$ Angstroms and for NDQ2 and NDQ3 at $\lambda > 2850$ Angstroms are extrapolated.

Figure 13.83: F25NDQ Aperture Throughputs vs. Wavelength.



13.5 Spatial Profiles

Below we provide encircled energy tables for each grating mode. Included are the values for the fraction of the total flux contained in the default point source extraction aperture (not the same as the physical aperture) during pipeline processing. **calstis**, the pipeline code, sums a number of pixels to obtain the spectral flux^o; this number of pixels is given by the “Extraction Height.” These tables also give the fractional flux in the peak pixels. Accompanying figures show sample spatial profiles (i.e., in the direction perpendicular to the dispersion).

First-Order Spatial Profiles

Table 13.35: Encircled Energies for G140L, G140M, G230L, G230M

Grating ¹	λ	Slit ²	Extraction Height (pixels)	Flux in Center Pixel	Flux in Extraction Aperture
G140L & G140M	1200	52X0.2	11	0.2049	0.8197
	1400			0.2655	0.8850
	1700			0.2703	0.9009
G230L & G230M	2000	52X0.2	11	0.2838	0.9009
	2500			0.3272	0.9091
	3000			0.3182	0.9091

1. M mode profiles are assumed to be identical to L mode profiles.
2. Values are only weakly dependent on observing slit.

Figure 13.84: G140L, G140M, G230L, G230M Spatial Profiles

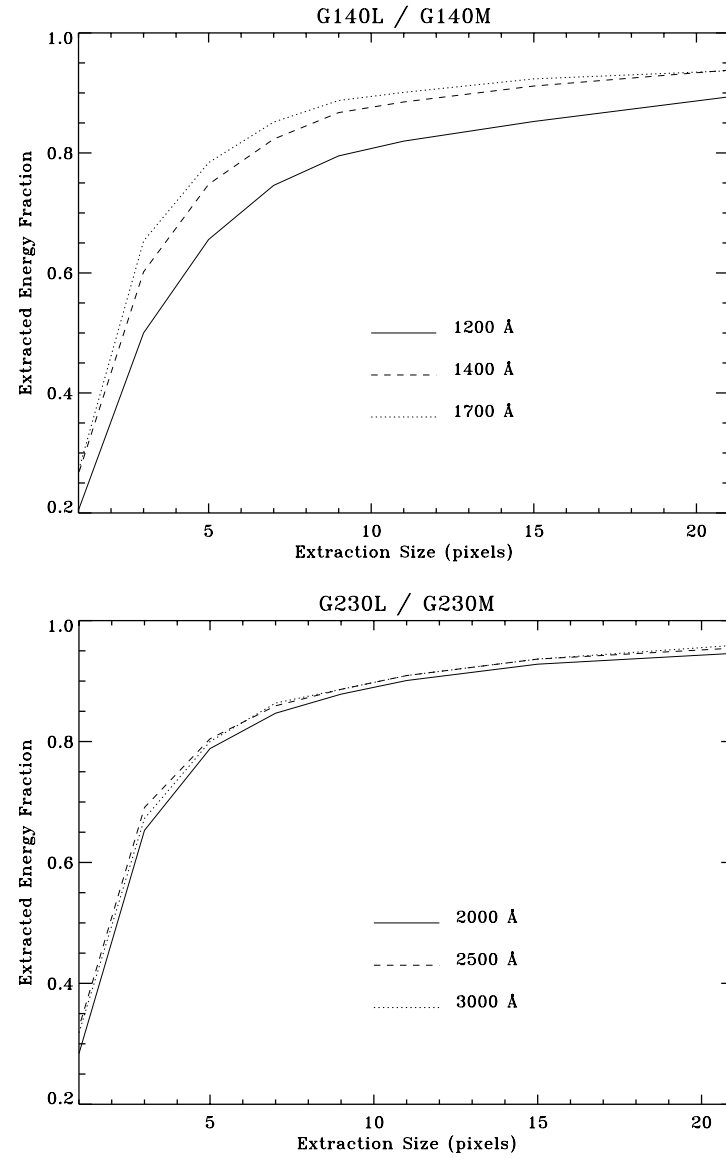


Table 13.36: Encircled Energies for G230LB and G230MB

Grating ¹	λ	Slit ²	Extraction Height (pixels)	Flux in Center Pixel	Flux in Extraction Aperture
G230LB & G230MB	2000	52x2	7	0.3008	0.8130
	2500			0.3390	0.8475
	3000			0.3017	0.8621

1. M mode profiles are assumed to be identical to L mode profiles.
2. Values are only weakly dependent on observing slit.

Figure 13.85: G230LB and G230MB Spatial Profiles

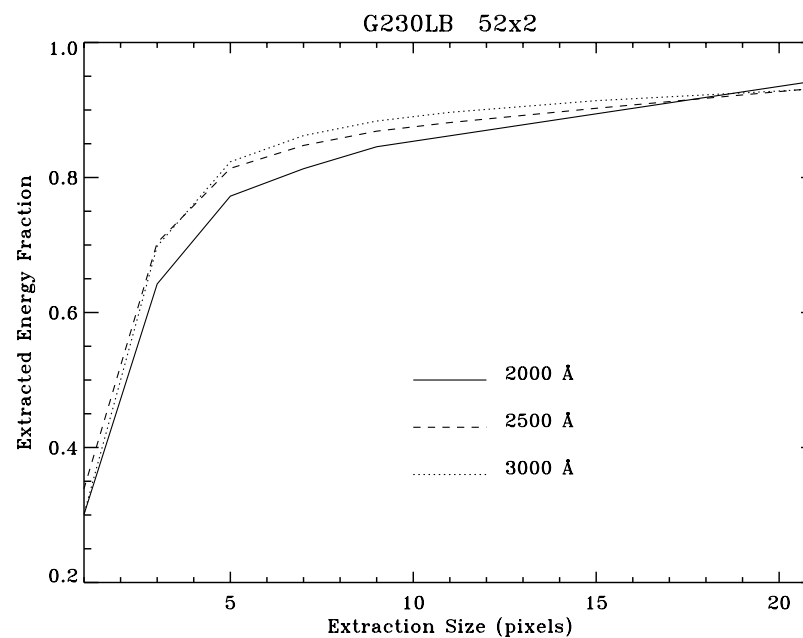
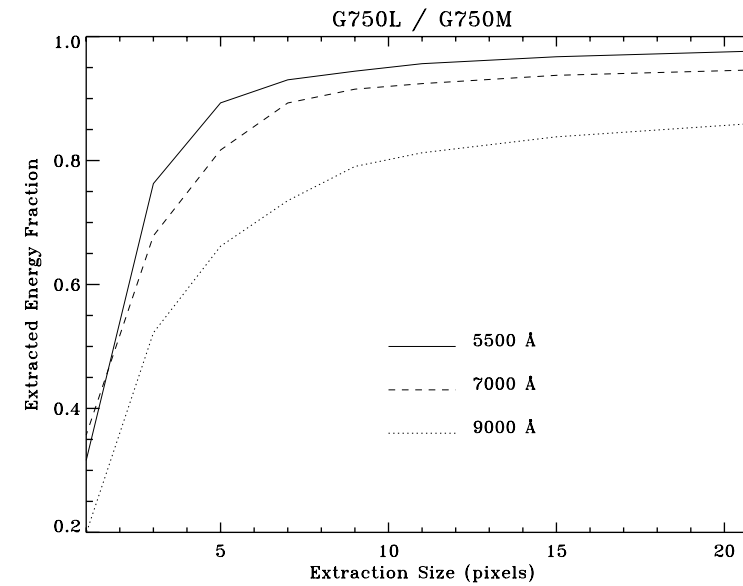
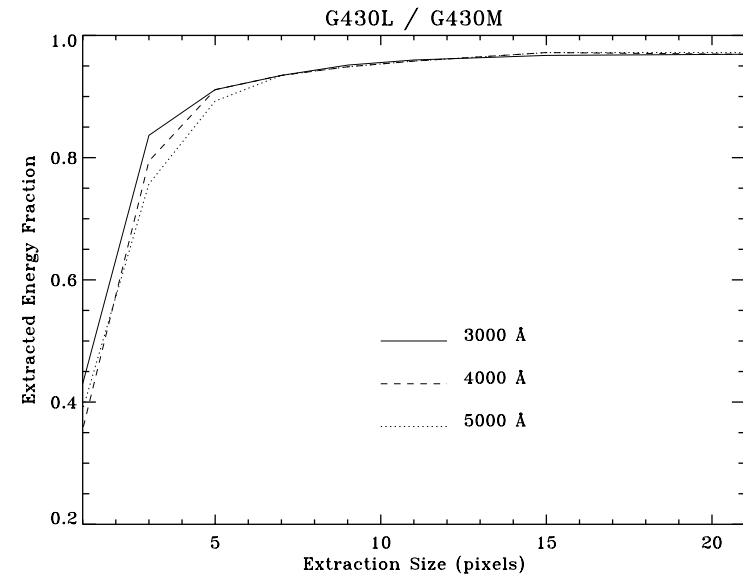


Figure 13.86: G430L, G430M, G750L, and G750M Spatial Profiles

Table 13.37: Encircled Energies for G430L, G430M, G750L, G750M

Grating ¹	λ	Slit ²	Extraction Height (pixels)	Flux in Center Pixel	Flux in Extraction Aperture
G430L & G430M	3000	52X0.2	7	0.4299	0.9348
	4000			0.3551	0.9346
	5000			0.3879	0.9346
G750L & G750M	5500	52X0.2	7	0.3163	0.9302
	7000			0.3571	0.8929
	9000			0.1985	0.7353

1. M mode profiles are assumed to be identical to L mode profiles.
2. Values are only weakly dependent on observing slit.



Echelle Spatial Profiles

Table 13.38: Encircled Energies for Echelle M Modes

Grating	λ	Slit	Extraction Height (pixels)	Flux in Center Pixel	Flux in Extraction Aperture
E140M	1170	0.2X0.2 ¹	7	0.274	0.944
	1400			0.308	0.959
	1600			0.331	0.961
E230M	1900	0.2X0.2	7	0.347	0.973
	2550			0.359	0.947
	3000			0.391	0.949

1. Values are only weakly dependent on observing slit.

Figure 13.87: Echelle M Modes Spatial Profiles

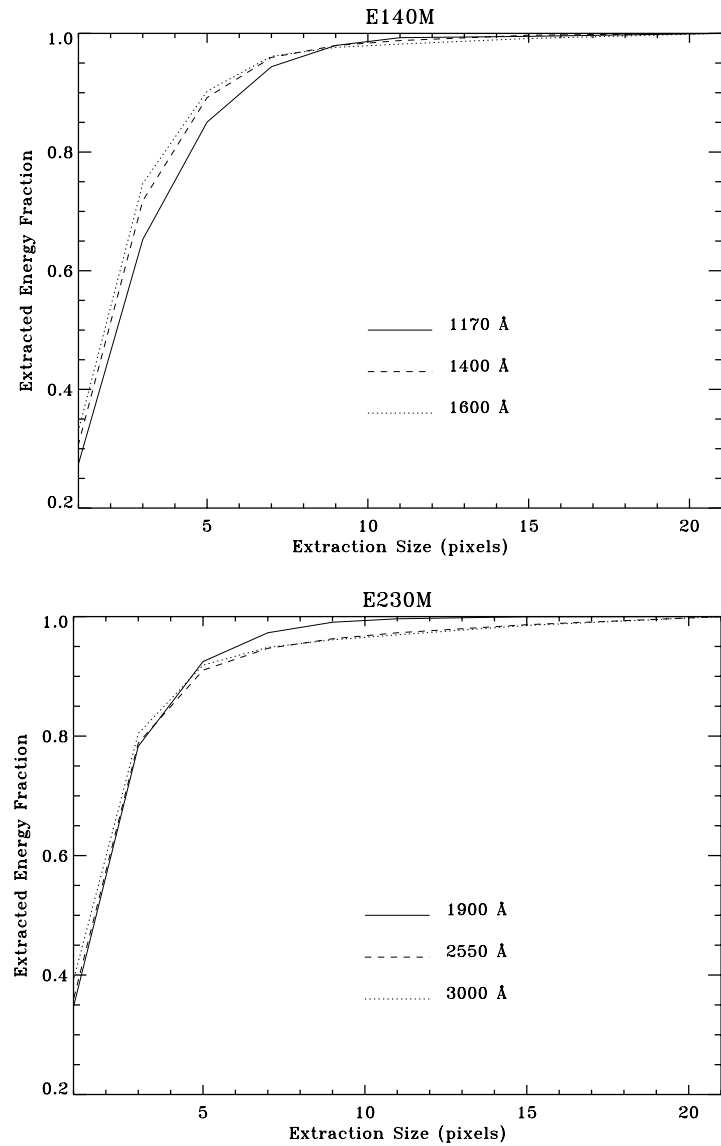
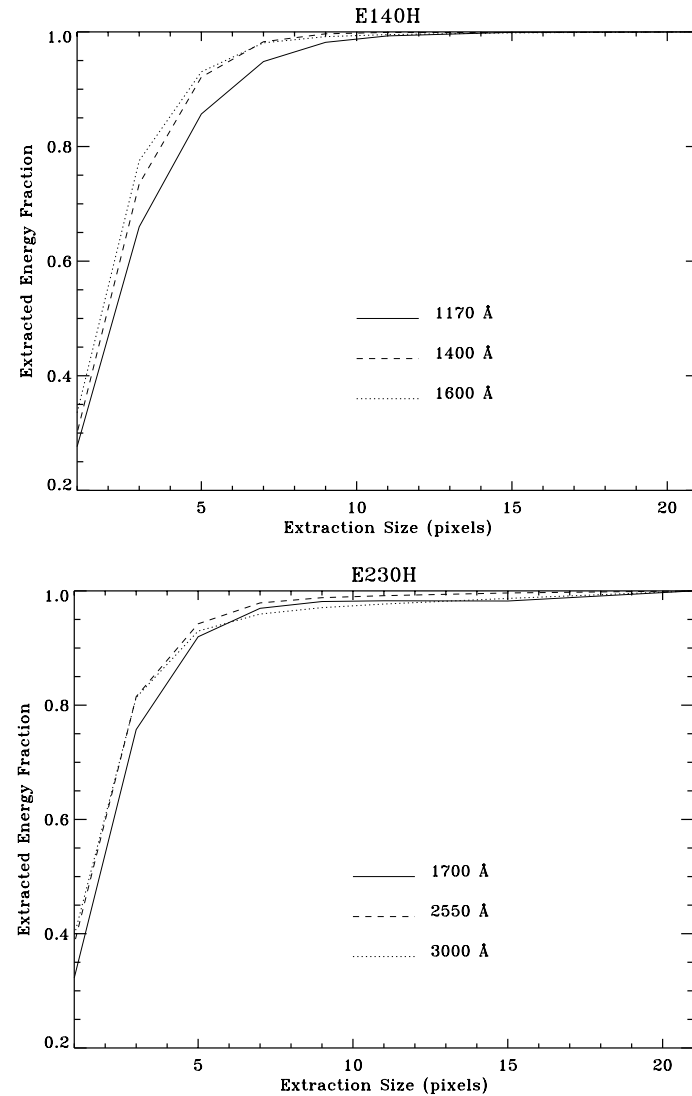


Table 13.39: Encircled Energies Echelle H Modes

Grating	λ	Slit	Extraction Height (pixels)	Flux in Center Pixel	Flux in Extraction Aperture
E140H	1170	0.2x0.2 ¹	7	0.276	0.948
	1400			0.300	0.983
	1600			0.335	0.981
E230H	1700	0.2x0.2	7	0.323	0.970
	2550			0.382	0.979
	2700			0.342	0.968

1. Values are only weakly dependent on observing slit.

Figure 13.88: Echelle H Mode Spatial Profiles



13.6 Line-Spread Functions

Below we provide model line spread functions (i.e., instrumental profiles) for point source observations through a sample of supported slits in first-order and echelle modes as a function of observing wavelength. Internal lamp observations and on-orbit data for external targets have been used to confirm and revise the original pre-flight models of the STIS LSFs.

These plots and the derived FWHM presented below in tabular form show that increasing the slit width for point source observations has very little effect on the FWHM of the observed lines but does broaden the wings of the LSFs. This occurs because a wider aperture allows more of the wings of the HST Optical Telescope Assembly PSF to enter but does not change the shape of the inner part of the PSF which is quite narrow. The implications of the LSF wings on line profile and equivalent width measures are discussed in more detail in Section 13.7. For diffuse source observations, don't forget that widening the slit, while it allows more light to enter, also will degrade the spectral resolution obtained.

First-Order Line Spread Functions

Table 13.40: Spectral Resolution for CCD First-Order Modes

Slit	Spectral Resolution (FWHM in pixels)				
	Point Source				Extended Source
	3200 Å	5500 Å	7000 Å	10000 Å	
52X0.05	1.3	1.4	1.5	1.7	2
52X0.1	1.3	1.4	1.5	1.7	~2-3
52X0.2	1.3	1.5	1.6	2.0	~4
52X0.5	1.3	1.5	1.6	2.0	~10
52X2	1.3	1.5	1.6	2.0	~40

Figure 13.89: CCD First-Order L-Mode Line Spread Functions

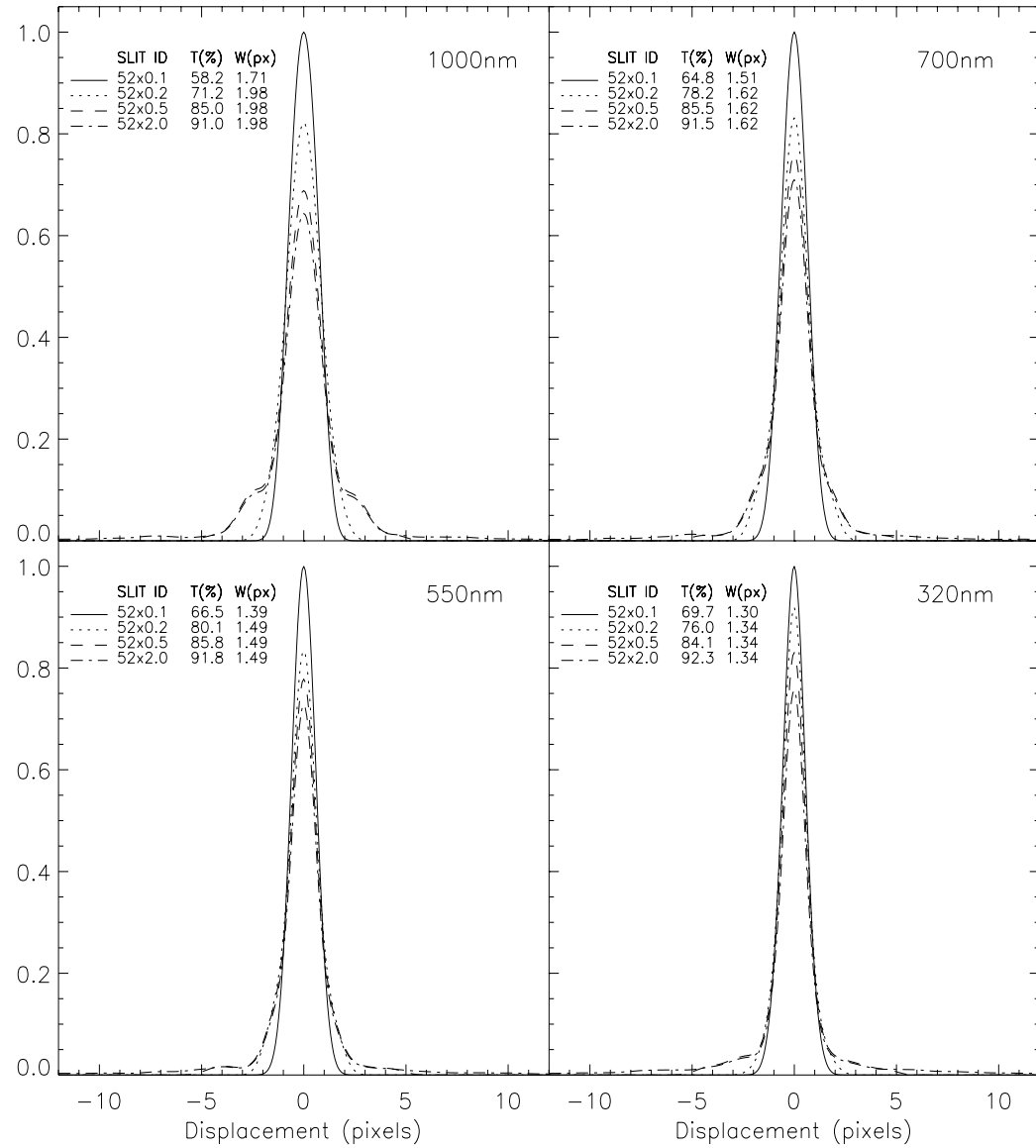
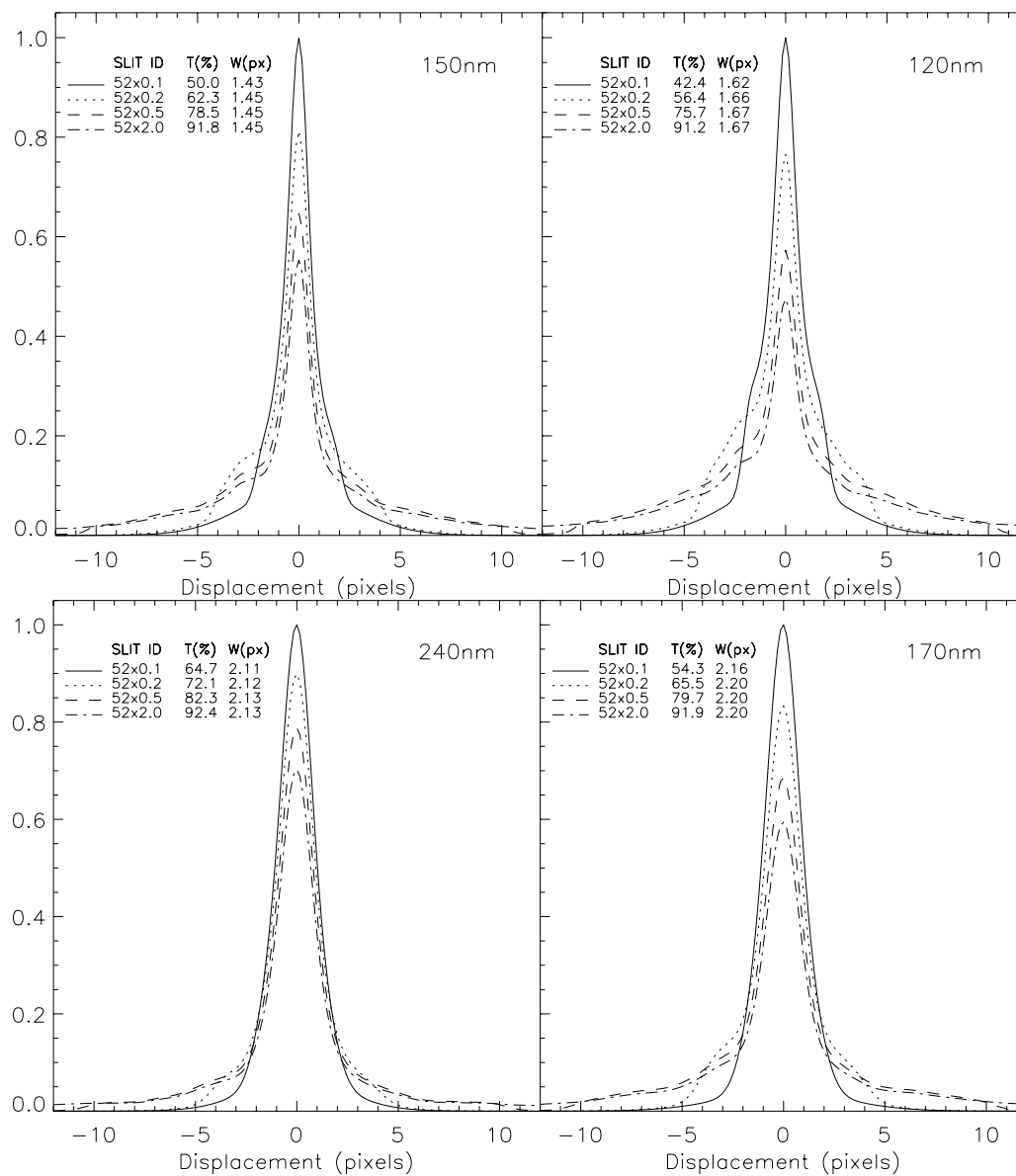


Table 13.41: Spectral Resolution for MAMA First Order Modes

Slit	Spectral Resolution (FWHM in pixels)				Extended Source
	Point Source				
	1200 Å	1500 Å	1700 Å	2400 Å	
52X0.05	1.6	1.5	1.4 ¹ 2.2 ²	2.1	-2
52X0.1	1.6	1.5	1.4 ¹ 2.2 ²	2.1	~4
52X0.2	1.7	1.5	1.4 ¹ 2.2 ²	2.1	~8
52X0.5	1.7	1.5	1.4 ¹ 2.2 ²	2.1	~20
52X2	1.7	1.5	1.4 ¹ 2.2 ²	2.1	~80

1. FWHM with FUV-MAMA (G140L, G140M).
2. FWHM with NUV-MAMA (G230L, G230M).

Figure 13.90: MAMA First-Order Line Spread Functions. Top G140L and G140M, bottom G230L and G230M



Echelle Line Spread Functions

Table 13.42: Spectral Resolution for Echelle Medium-Resolution Modes (E230M, E140M)

Slit	Spectral Resolution (FWHM in pixels)				Extended Source
	Point Source				
	1200 Å	1500 Å	1700 Å	2400 Å	
0.1X0.03	0.9	0.9	1.0 ¹ , 1.6 ²	1.6	~1
0.2X0.2	1.4	1.3	1.1 ¹ , 2.0 ²	1.9	~6
0.2X0.06	1.3	1.2	1.1 ¹ , 1.8 ²	1.7	~2
6X0.2	1.6	1.4	1.2 ¹ , 2 ²	1.9	~6

1. FWHM with FUV-MAMA (E140M).
2. FWHM with NUV-MAMA (E230M).

Figure 13.91: Echelle Line Spread Functions, E140M (top) and E230M (bottom)

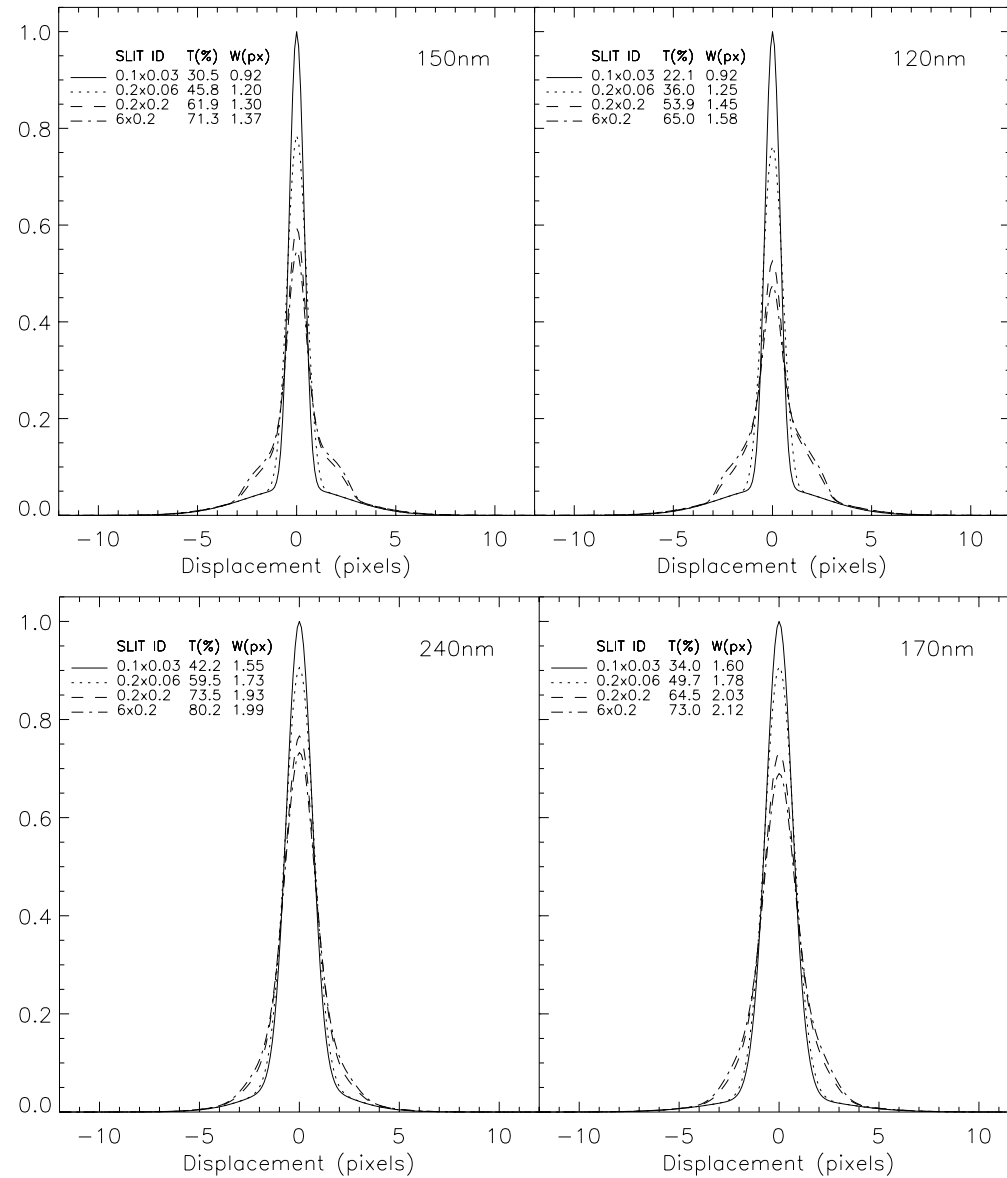
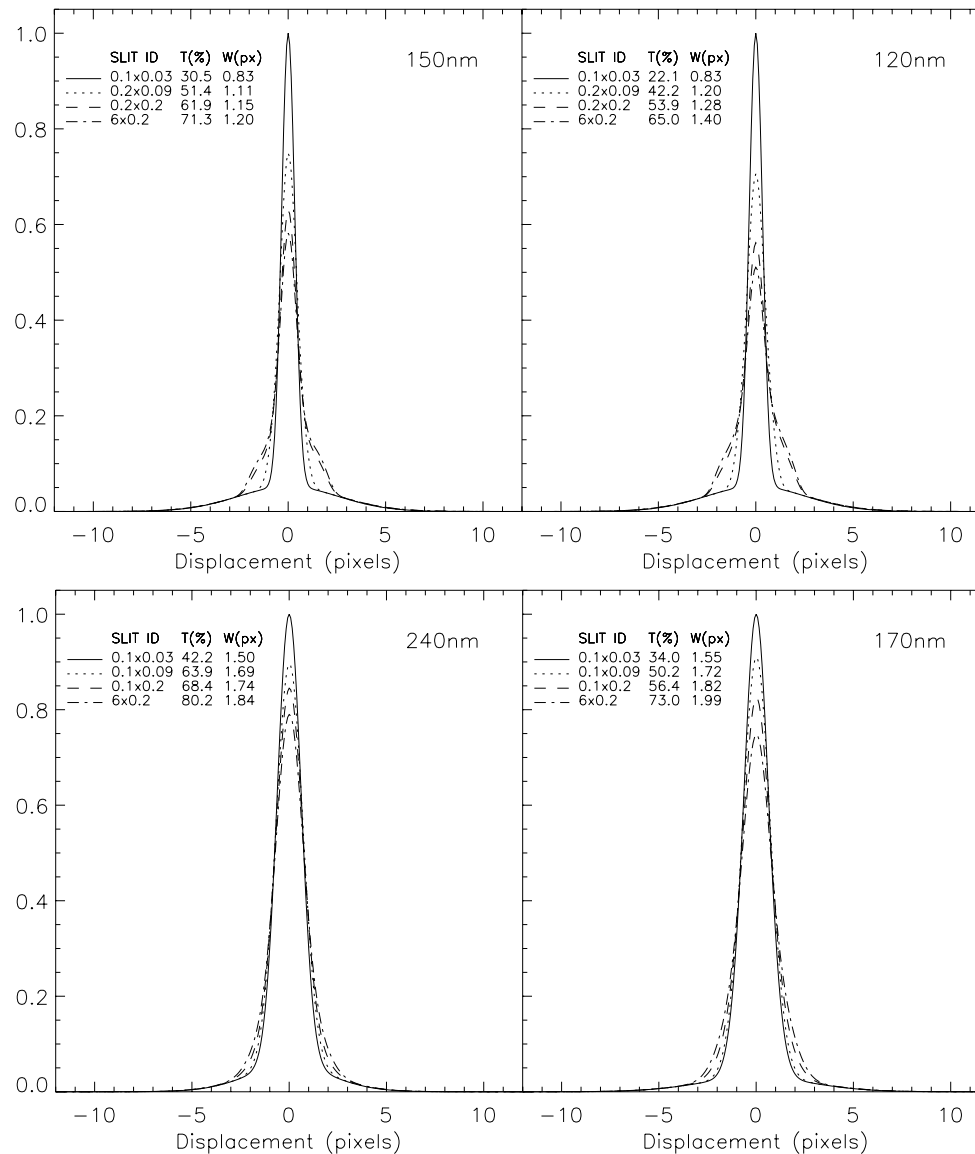


Table 13.43: Spectral Resolution for Echelle High Resolution Modes (E140H, E230H)

Slit	Spectral Resolution (FWHM in pixels)				Extended Source
	Point Source				
	1200 Å	1500 Å	1700 Å	2400 Å	
0.1X0.03	0.8	0.8	1 ¹ , 1.5 ²	1.5	~1
0.2X0.2	1.3	1.1	1 ¹ , 1.8 ²	1.7	~6
0.2X0.09	1.2	1.1	1 ¹ , 1.7 ²	1.7	~2
6X0.2	1.4	1.2	1.2 ¹ , 2 ²	1.8	~5

1. FWHM with FUV-MAMA (E140H).
2. FWHM with NUV-MAMA (E230H).

Figure 13.92: Echelle Line Spread Functions, E140H (top) and E230H (bottom). LSFs for E230H were derived using the 0.1X0.2 and 0.1X0.09 apertures, but results for 0.2X0.2 and 0.2X0.09 should be similar.



13.7 Spectral Purity, Order Confusion, and Peculiarities

If the PSF had an infinitely small FWHM and no extended wings, a point source would produce a spectrogram with infinitesimal extension in the spatial direction. Furthermore, the spectral resolution would be essentially the theoretical limit of the spectrograph, independent of the entrance slit. In practice, the Optical Telescope Assembly PSF is wider and more complex, and there is scattered light from both the gratings and the detector itself, leading to decreased spectral resolution and spectral purity.

In Figure 13.93 we have plotted $H\beta$ in the white dwarf Feige 110 observed with the G430L grating and five entrance slits with widths between $2''$ and $0''.05$. The spectrum observed through the $0''.05$ and $0''.1$ slits can be considered spectrally pure (remember $0''.1$ maps to 2 pixels on the CCD and $0''.05$ maps to 2 pixels on the MAMAs). Observations with the $0''.2$ slits are still reasonably pure but larger slit widths lead to significant impurity. This becomes evident from the increasing flux in the line core with increasing slit width. The maximum spectral purity is achieved with entrance slits of $0''.2$ width or smaller. Similar results can be seen in Figure 13.94 which shows the calcium triplet regions. Observers wishing to study spectral lines of continuum sources should always consider using small entrance slits.

Figure 13.93: $H\beta$ in the White Dwarf Feige 110 Observed with G430L and 5 Entrance Slits

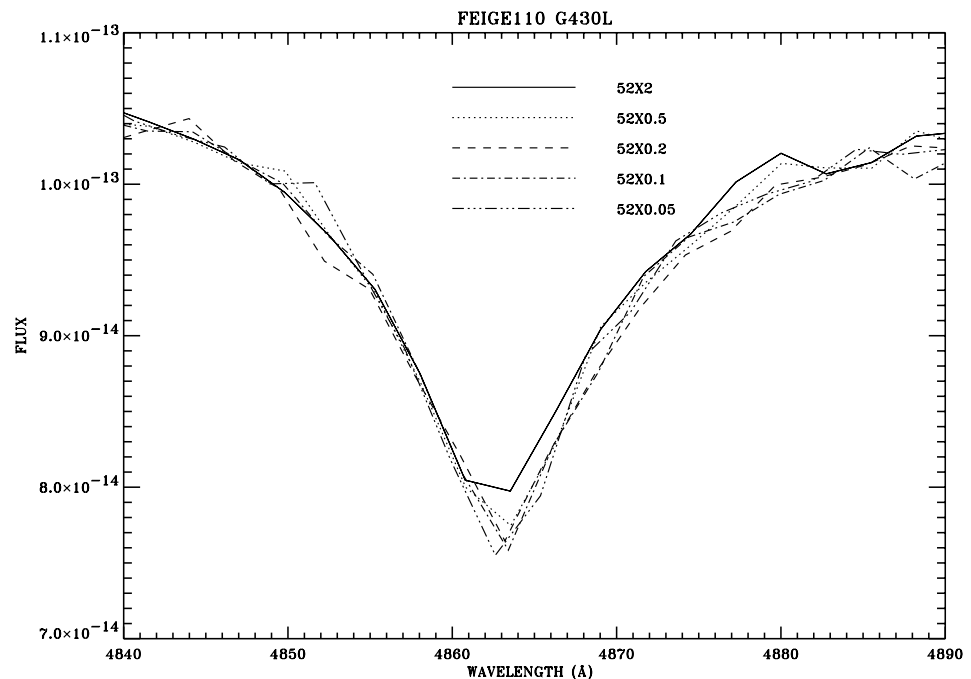
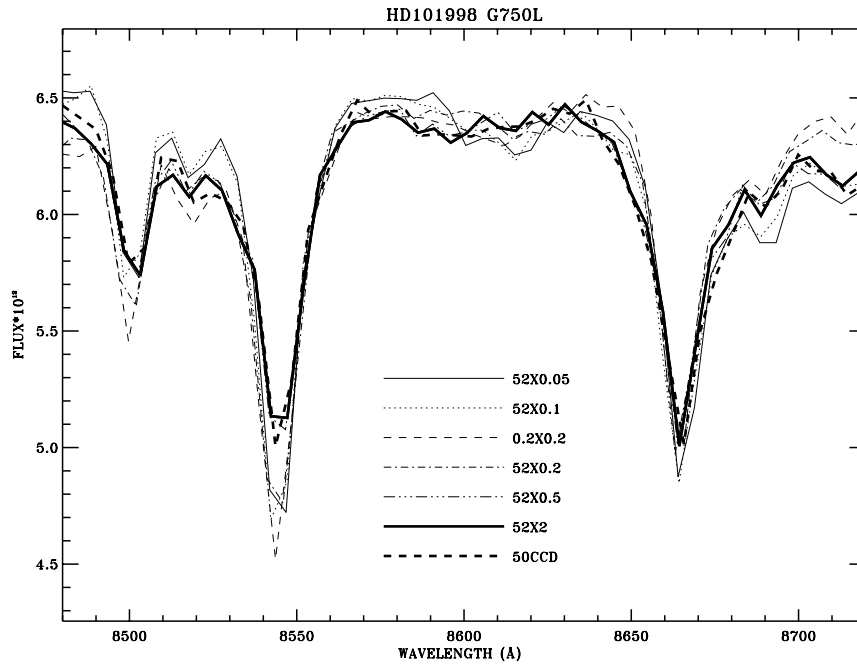


Figure 13.94: Calcium Triplet Observed with G750L and 7 Entrance Slits



13.7.1 Recommendations for stellar observations with narrow slits

In assessing the trade between the better spectral purity of small slits and the higher throughput and photometric precision of larger slits, the following should be kept in mind:

1. Choose a slit that meets your requirements for photometric precision.
2. Avoid the 52X0.05 slit with the G750 modes, since the Airy core of the point spread function is much larger than the slit size and the resulting light losses may exceed a factor of 5 in comparison with the 52X2 slit. Furthermore, the nominal resolution of 2 pixels is a match to a 0.1 arcsec slit width for the CCD modes.
3. Longer wavelength observations require wider slits to avoid light loss problems as the point spread function enlarges. Beyond ~ 5000 Å, a rapid loss of light is possible even when a 52X0.1 slit is used. In a test of medium dispersion modes, a loss of 10% was found near 4000 Å, but this increased to 25% by 8500 Å.
4. As a stellar target may not be perfectly centered, pipeline fluxes may, in general, be treated as lower limits. Exceptions are the CCD G230LB, G430L, and G750L modes which utilize a Lyot stop to improve small aperture transmission.

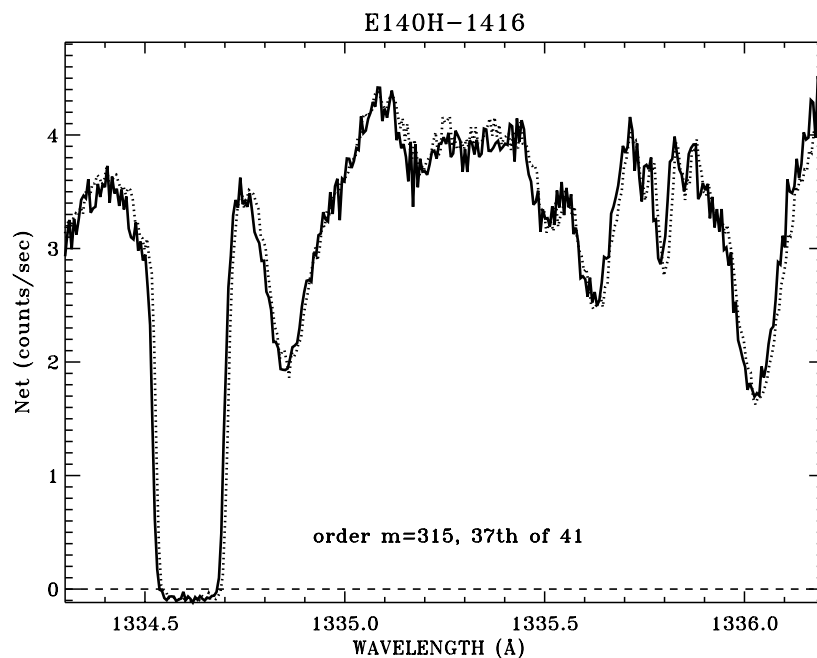
More complete details on these points can be found in [ISR 1998-20](#) by R. Bohlin and G. Hartig.

13.7.2 Order Overlap and Scattered Light for Echelle Gratings

As with most other echelle spectrographs, STIS echelle data are affected by spectral order overlap at the shortest wavelengths where adjacent spectral orders are not well separated. Echelle observations of continuum sources taken slitless or with a 2X2 entrance slit suffer from severe order overlap. Therefore, an entrance slit of 0.2 or smaller height should be used.

Figure 13.95 demonstrates the difference in resolution for a narrow absorption line for BD+75°325 observed in the 0.2X0.2 slit vs. a 0.2X0.09 slit. Any difference in the effect of impure light on the depth of the line profiles is less than ~1% of the continuum. An extraction height of 7 pixels is used; and the 0.2X0.09 aperture spectrum is multiplied by 1.28 to compensate for the lower transmission. A slight wavelength shift is maintained to improve visibility.

Figure 13.95: Comparison Between 0.2X0.2 (solid line) and 0.2X0.09 (dotted line) Aperture Spectra of BD+75°325 in the E140H-1416 Mode



Note the “oversubtraction” of the black line. This is a ramification of oversubtraction of the background; light which is scattered from the echelle, the OTA PSF, and the detector into the interorder area is being oversubtracted from the science spectrum in the straightforward

background subtraction procedure used. The E230M and E230H gratings are only a little affected by this scatter (7% of the light is scattered at $\sim 2000 \text{ \AA}$, 4% at 2500 \AA). However, the E140M and E140H modes do have appreciable scatter; 33% of the light scattered at 1235 \AA for E140M and 15% for E140H; at 1600 \AA this drops to $\sim 12\%$ and 8% , respectively. The STScI provides an exposure time calculator (ETC), which predicts global and net countrates to sufficient accuracy for planning purposes. An estimate of the *net S/N* and the *net + scattered light* in an echelle observation are produced for a specified input spectrum, including an approximation to the scattered component.

An “algorithm” parameter has been added to the **x1d** spectral extraction task in **calstis**. Changing this parameter from “unweighted” to **sc2d** enables a new two-dimensional background subtraction algorithm that was designed by Don Lindler (Sigma Space Corporation) and Chuck Bowers (Goddard Space Flight Center). Figure 13.96 shows the dramatic improvement achieved with the use of this new algorithm. Figure 13.97 summarizes the fractional error in saturated line cores as a function of wavelength and grating for both algorithms. Errors for the medium resolution gratings are comparable to errors for the high resolution gratings.

Figure 13.96: Comparison between the standard 1-D and the new 2-D background subtraction.

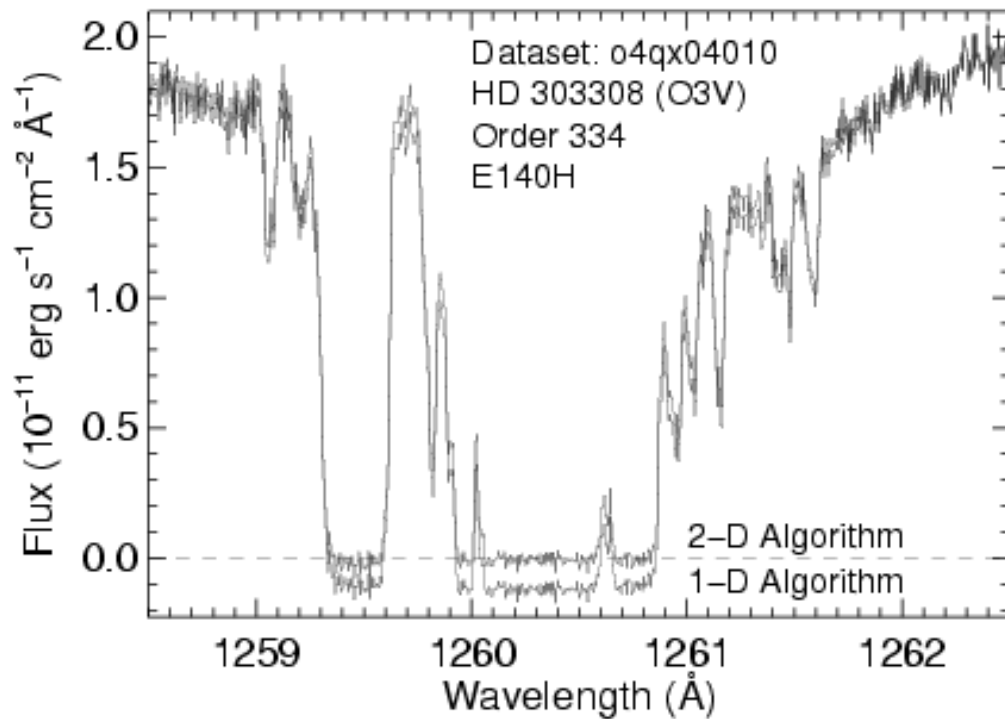
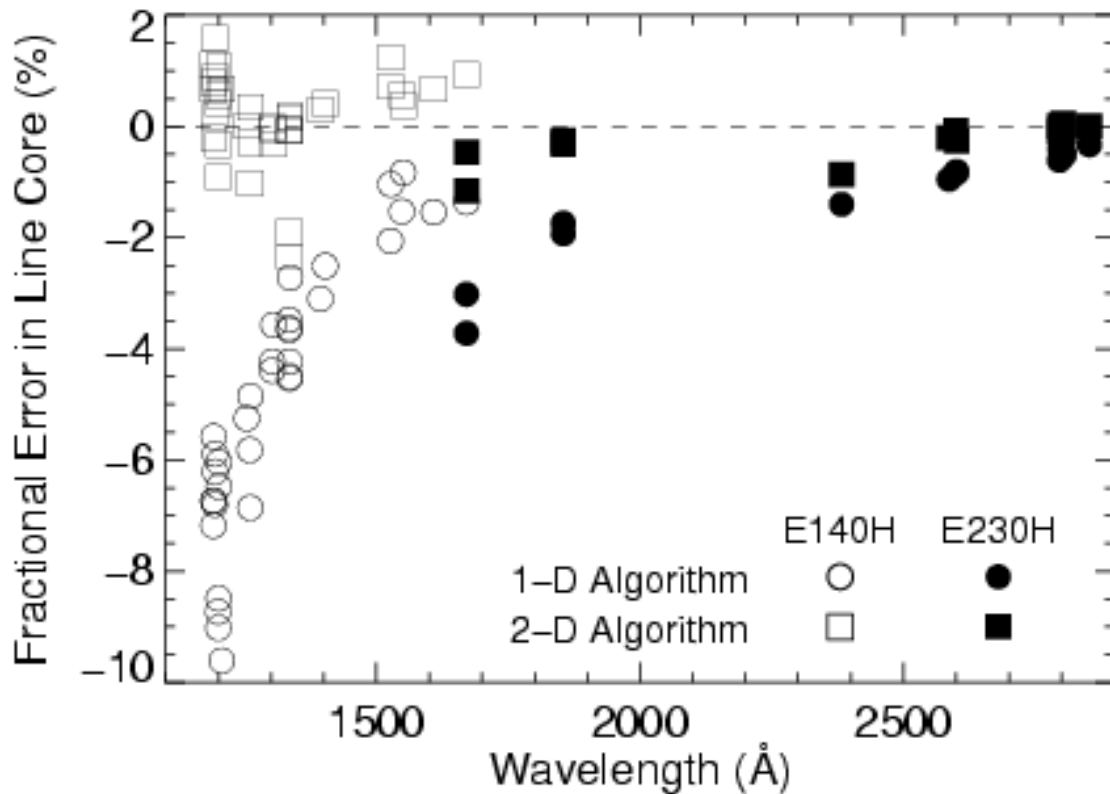


Figure 13.97: Comparison between the errors of the two methods.



Since early 2001, all archive requests for STIS echelle data are reprocessed automatically, using the new two-dimensional background subtraction algorithm.

Briefly, the new algorithm works as follows: a 2-D raw image is fit with a 2-D model, reconstructed at each iteration from the best current estimate of the extracted spectrum folded through a semi-empirical simulation of STIS optical properties. Self-consistency between the 2-D model and the extracted spectrum is achieved via iteration. An analogous model containing only scattered light is then constructed using only the echelle scatter outside an 11 pixel wide vertical window centered on each order. This 2-D scattered light model is subtracted from the raw data and the final spectrum is obtained using standard 1-D extraction.

Construction of the 2-D model during each iteration involves several steps. Counts in the 1-D extracted spectrum are mapped back to their idealized origin in hypothetical echelle orders that extend beyond the edge of the physical detector. Echelle scatter is modelled by redistributing extracted counts along diagonal lines of constant wavelength, using echelle line spread functions. Post-echelle smearing along columns is modelled by independently convolving each column with a smoothing kernel. Scattering due to the aperture truncated telescope PSF, isotropic detector halo, and

pre-echelle scattering by the cross-disperser are treated by 2-D convolution with a kernel constructed from these components.

13.7.3 Spectroscopic Mode Peculiarities

During the original SMOV and initial observations, a number of first-order mode spectra have been obtained which show additional features which may affect the scientific goals of the observations. One class of spectroscopic images shows diffraction structure of the PSF re-imaged at the various STIS detectors. A second class, commonly referred to as railroad tracks, displays additional “spectra” displaced and parallel to the primary spectrum. Some examples and impacts are presented below.

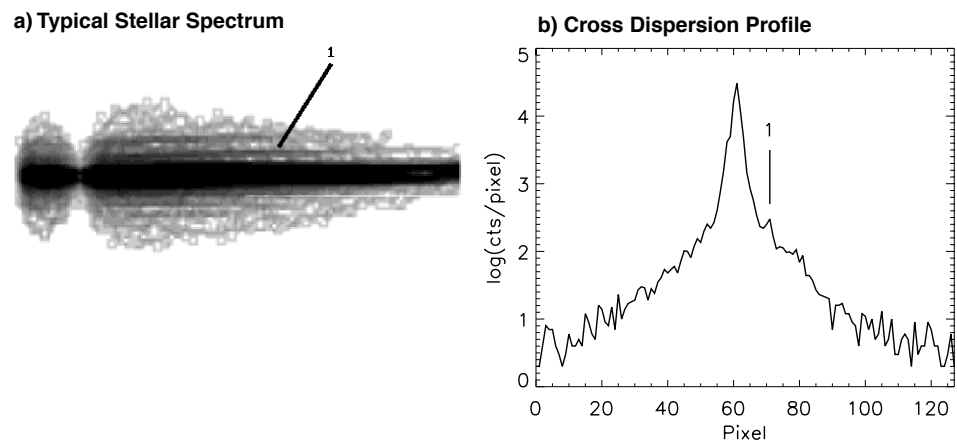
PSF Re-imaging

The STIS corrector mirrors re-image the OTA PSF at an intermediate focus within STIS at the location of the slit wheel. This intermediate image is re-imaged to one of the detectors via the selected mode, either imaging or spectroscopic. Any PSF structure present in the slit plane image will be re-imaged at the detectors; however, its appearance in a final spectrum or image depends on the selected mode and the slit or aperture used.

In the imaging modes, little PSF diffraction structure is apparent, since the available filters are typically relatively broad band, smoothing out any structure. The spectroscopic modes, however, create a series of near monochromatic images at the detector plane and the PSF diffraction structure can be detected with the two dimensional STIS detectors.

Point Source: Figure 13.98 shows the spectrum of a point source target, using G140L and slit 52X0.05.

Figure 13.98: Spectrum of a Point Source (Stellar) Target

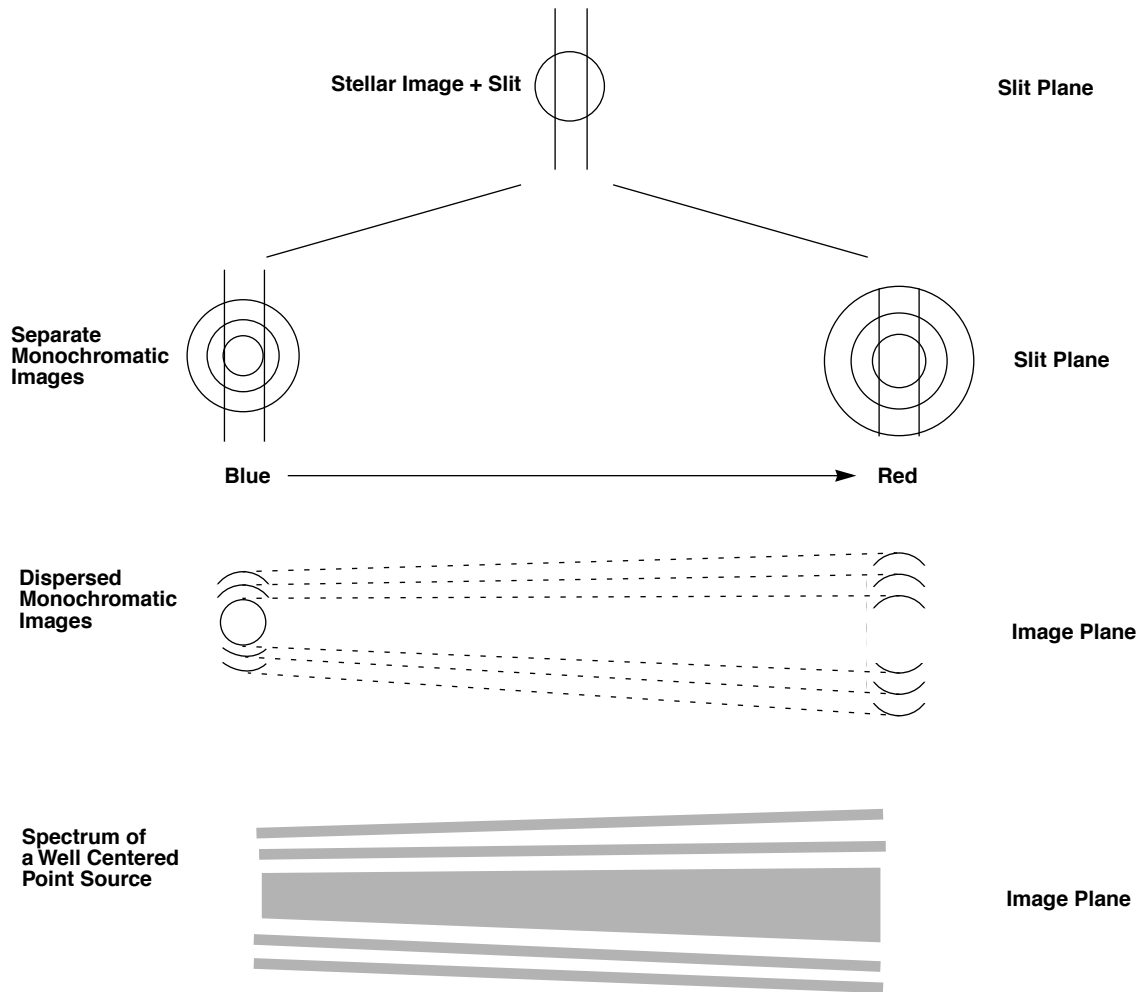


This typical stellar spectrum (1150–1700 Å) shown in panel a, was of a white dwarf for instrument calibration. The Lyman- α absorption feature is apparent near the left end. This image was processed and log stretched to enhance the “fringes” seen above and below the stellar spectrum. These

fringes are weak, diverge from the spectrum proportionally to wavelength, and are not present in the Lyman- α gap, indicating they are connected with the source at the slit plane and are not the result of STIS internal scatter. Panel b shows a cross dispersion profile of the original image, cut near the center of the spectrum at about 1430 Å. The brightest fringe (labelled “1”) is indicated; the peak of the fringe is roughly 0.005 times the peak of the stellar spectrum.

Figure 13.99 illustrates how such fringes are created at the detector. At each wavelength, the portion of the PSF at the slit plane which passes the slit is re-imaged onto the detector. The envelope of all such PSF portions forms the complete image at the detector, as shown. The characteristic fringe separation, proportional to wavelength, is expected as the diffraction structure in the PSF increases with wavelength as shown. In the medium resolution modes, with much less bandpass than the low resolution modes, the tilt of the fringes is much less—they are nearly parallel to the primary spectrum.

Figure 13.99: How Fringes are Created



The fringe visibility is decreased with increasing slit width. Figure 13.99 illustrates this—as the slit broadens, more of a curved portion of the diffraction rings is transmitted. The envelope of these more curved sections is broader with lower contrast compared to the sharp segments visible with a narrow slit.

Out of slit point source: Figure 13.100 shows the spectrum (G140L) of a stellar source, in which the target was mis-located and not nominally in the 52X0.05 slit. While the target center was not located in the slit, the extended PSF structure did cover the slit opening and was transmitted and re-imaged at the detector plane. This image has been processed and log stretched to enhance the faint fringe structure which is apparent.

Figure 13.100: Mis-Located Target—Stellar Source

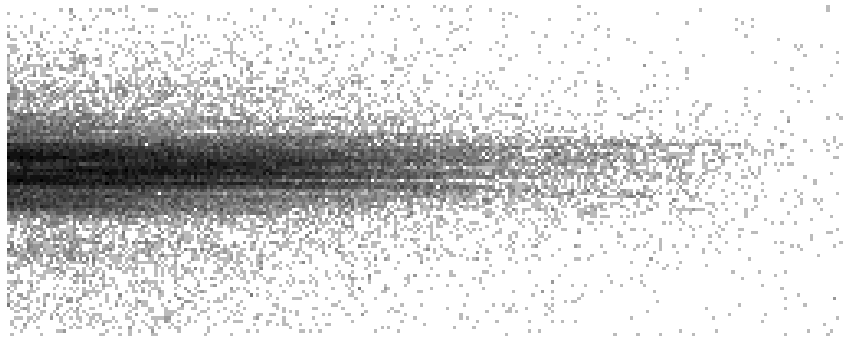
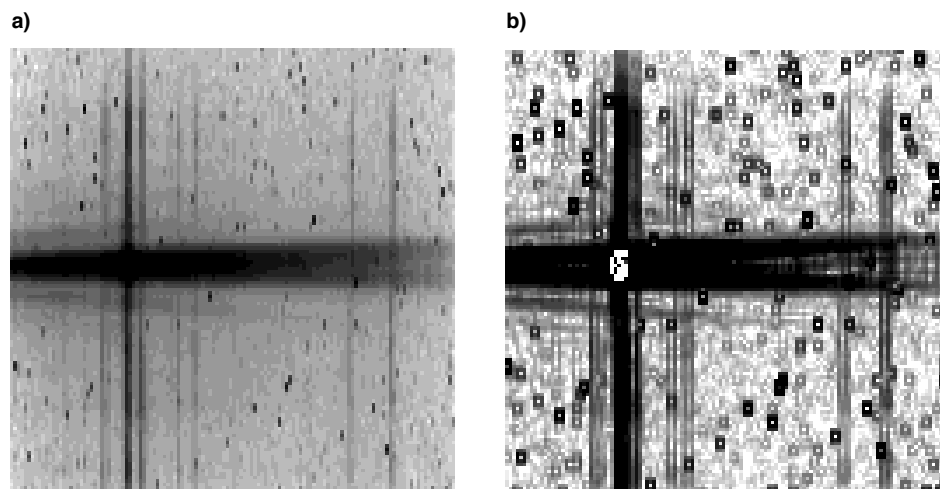


Figure 13.101 shows a similar case in which the spectrum of a galaxy with a very bright core was obtained with the core located roughly 0.1" from the center of the 0.1" wide slit in the visible mode G750L. The images were processed and log stretched to enhance the fringe appearance. Divergent fringes are apparent above and below the spectrum. A principal component of the “spectrum” consists of the upper and lower portions of the offset, first Airy ring, seen clearly separated at the long wavelength end of the spectrum. These two fringes converge at shorter wavelengths forming a single fringe which overlies the much fainter, off-core portion of the galaxy. The evident blueness of the core spectrum in this particular source makes the combined blue fringes much brighter than the combination of the separated red fringes.

Figure 13.101: Mis-Centered Spectrum of Galaxy with Bright Core



Impact

Diffraction structure in the PSF will set a limit to extracting spectra near a bright source. Blocking the bright source, either by using a coronagraphic

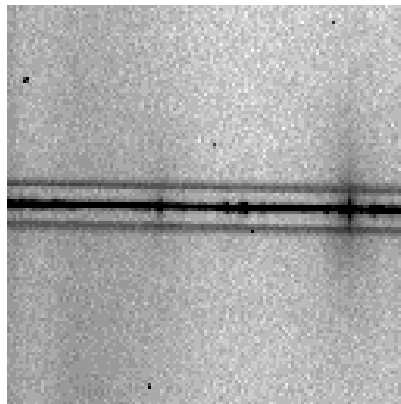
aperture or by moving the bright source out of the slit does not remove the inherent, adjacent PSF or diffraction structure. In the case of a faint companion adjacent to a bright, primary source, note that the spectra of the primary and companion will be parallel while the PSF fringes will be tilted. This is especially true in the low resolution modes and may allow the unambiguous identification of a faint companion even in the presence of comparably bright PSF structure.

13.7.4 Railroad Tracks

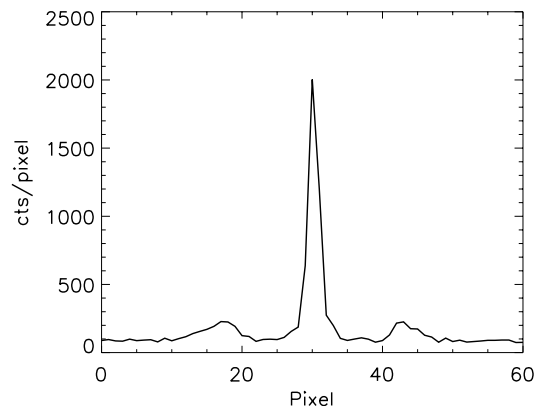
Figure 13.102 (panel a) shows a processed spectrum of a continuum lamp in mode G750M, $\lambda_C = 10,363$ and slit 0.1×0.2 obtained during ground testing. Beside the spectrum, two adjacent, parallel, secondary spectra are seen symmetrically displaced about 13 pixels from the lamp spectrum. Panel b shows a cross dispersion profile illustrating the magnitude and shape of the spectra. The secondary spectra have peak intensities about 8% of the primary spectrum but are broader and asymmetric. This was the only example of this peculiar condition noticed during ground testing; however, subsequent review showed one additional example also obtained during ground testing. This second case was a similar continuum lamp spectrum using G750M, $\lambda_C = 7795$, with the same slit. Secondary spectra were $\sim 8\%$ and 3% (peak intensity) of the primary peak intensity.

Figure 13.102: Railroad Tracks

a) Processed Spectrum from Ground Testing



b) Cross Dispersion Profile



One similar example has been obtained in flight to date, with the UV mode G230LB and the CCD. The target was a very red star. The parallel, secondary spectra are visible at a level of about 8% of peak intensity.

The cause of these secondary spectra in these three observations is not known. The three cases observed have all been with the CCD; no MAMA

examples have been obtained. Other observations in these modes under similar conditions have not shown such effects. In all cases, a red source was observed. The broad profile and relatively bright intensity of the secondary spectra suggest a multiple reflection instead of a diffraction origin, but no way of producing dual, symmetric features has yet been proposed which is consistent with these observations.

13.8 MAMA Spectroscopic Bright-Object Limits

As described in Section 7.6, the MAMAs are subject to absolute brightness limits, above which sources cannot be observed or they would potentially damage the detectors. In Table 13.44, we present the complete set of absolute bright object point source spectroscopic screening magnitudes and fluxes for the MAMA spectroscopic modes. These screening magnitudes are presented as a *guide*. Whether an individual source can be observed is ultimately determined by whether, in the desired configuration, the spectrum of that source is predicted to exceed the global and local observing count rate limits, as described in Chapter 7. The information presented here should be used in conjunction with the material presented in Chapter 7. Remember, sources cannot be observed in configurations where they exceed the absolute bright object limits. A few important points to note are:

- The screening limits are given either as V magnitude or CGS units as indicated.
- The screening limits in this table have been calculated assuming zero slit losses. To determine if your source will violate the limits in this table, you must first correct the magnitude limit for the aperture throughput for your chosen slit. The maximum magnitude correction achieved without use of a neutral density filter using a supported slit is ~ 0.75 magnitudes. An exception to this are the values for the local surface brightness limits in row 1 of Table 13.44. They were calculated for a 52X2 slit.
- The screening limits in the tables assume zero extinction. To determine if your source will violate the limits in this table, correct the magnitude limit for the extinction of your source.
- The peak flux from an emission line or from the continuum from your source must be less than the flux limit given in row two (for point sources—remember to correct for your aperture throughput) and row one for diffuse sources (remember to correct for the width of your source by scaling by your slit width in arcseconds divided by 2.0).
 - For echelle observations, the global limit of $200,000 \text{ counts sec}^{-1}$ over the detector sets the magnitude limits, but you must also

assure that your source does not violate the local limit, e.g., if it had a bright emission line.

- If you are observing a source which has high equivalent width line emission (i.e., whose flux is dominated by line emission), you must assure that the *line emission* does not exceed the limits. This may be a concern for stars with strong emission lines, such as Wolf-Rayet or T Tauri stars.
- If you plan to place multiple bright stars in the long slit, or observe slitless, you must also assure that the sum from all targets imaged on the detector does not exceed the applicable global limit.
- The limits in this table are the worst case limits for the scanned gratings; use of a less sensitive central wavelength may have a brighter true limit, allowing you to observe your target. The STIS Exposure Time Calculator should always be used to verify the safety of your detailed target and configuration specifications.

Table 13.44: Approximate MAMA Spectroscopic Bright-Object Limits (V magnitudes and cgs units). V magnitudes include an additional safety factor of 3 in flux to account for extrapolation uncertainties from the optical to the UV spectral range.

Spectral Type	G140L	G140M	E140M	E140H	G230L	G230M	E230M	E230H	PRISM
Local limit surface brightness ¹	2.6×10^{-11}	4.2×10^{-10}	3.9×10^{-8}	8.4×10^{-8}	8.4×10^{-12}	2.6×10^{-10}	5.4×10^{-9}	2.9×10^{-8}	7.5×10^{-13}
Local limit point source flux ²	5.1×10^{-12}	9.6×10^{-11}	1.4×10^{-9}	3.6×10^{-9}	1.4×10^{-12}	5.2×10^{-11}	1.2×10^{-10}	8.4×10^{-10}	6.0×10^{-14}
O5 V ³	15.2	13.0	11.3	10.5	14.7	11.4	10.9	10.0	15.2
B1 V	14.3	12.2	10.4	9.6	14.2	10.9	10.5	9.5	14.6
B3 V	13.5	11.3	9.6	8.8	13.6	10.3	10.0	8.9	14.0
B5 V	12.8	10.6	8.9	8.2	13.2	9.8	9.6	8.4	13.5
B8 V	11.6	9.3	7.8	7.2	12.4	9.0	8.8	7.6	12.7
A1 V	9.2	6.8	5.6	4.9	11.5	8.0	7.9	6.6	11.7
A3 V	7.8	5.4	4.3	3.6	11.2	7.8	7.7	6.3	11.4
A5 V	6.0	4.3	2.5	2.1	11.0	7.7	7.5	6.1	11.2
F0 V	3.0	2.2	-0.5	-1.5	10.5	7.5	7.1	5.8	10.6
F2 V	1.9	1.2	-1.5	-2.0	10.2	7.3	6.9	5.6	10.4
F5 V	-0.3	-1.1	<-2.0		9.8	7.1	6.6	5.2	10.0
F8 V	-1.5	<-2.0			9.5	6.9	6.3	5.0	9.7
G2 V	-3.1				9.1	6.6	5.9	4.6	9.3
G5 V	<-3.5				9.0	6.5	5.8	4.5	9.2
G8 V					8.7	6.2	5.5	4.1	8.9
K0 V					8.0	5.7	4.9	3.4	8.2
K4 V					5.9	3.6	2.6	1.0	6.4
K7 V					4.5	2.3	1.2	-0.3	5.1
M2 V					3.9	1.7	0.6	-1.0	4.6
T \sim 50,000 K ⁴	15.1	12.9	11.2	10.3	14.7	11.3	10.9	10.0	15.1
(λ^{-1}) ⁵	11.6	9.3	7.7	6.9	12.4	8.9	8.9	7.6	12.6

1. Peak surface brightness in $\text{ergs sec}^{-1} \text{cm}^{-2} \text{\AA}^{-1} \text{arcsec}^{-2}$ of the continuum or of an emission line from a diffuse source. For first-order and PRISM spectra, the calculation was done assuming use of the 52X2 aperture, while for echelle modes, the 6X0.2 aperture was used.

2. Peak flux in $\text{ergs sec}^{-1} \text{cm}^{-2} \text{\AA}^{-1}$ of an emission line from a point source.

3. Limits are V magnitudes, assuming zero reddening. Results for first-order gratings assume slitless spectra but neglect geocoronal lines. For echelles, the 0.2X0.2 aperture throughput is assumed.

4. Limits for a black body with a temperature of 50,000 K.

5. Limits for a source with a spectrum F_{λ} proportional to λ^{-1} .



CHAPTER 14:

Imaging Reference Material

In this chapter. . .

14.1 Introduction / 387
14.2 Using the Information in this Chapter / 388
14.3 CCD / 394
14.4 NUV MAMA / 408
14.5 FUV MAMA / 435
14.6 Image-Mode Geometric Distortion / 457
14.7 Spatial Dependence of the STIS PSF / 458
14.8 MAMA Imaging Bright Object Limits / 461



In this chapter, we provide imaging reference material, in support of the information presented in Chapter 5.

14.1 Introduction

This chapter provides reference material to help you select your filter and detector configuration and determine your observing plan (e.g., total required exposure time, and number of exposures). This chapter is, for the most part, organized by *filter and detector*. For each imaging mode the following are provided:

- A table of integrated system efficiencies and zeropoints for all the modes.
- Plots and tables of throughput and sensitivity as a function of wavelength.

- Where useful, plots of throughput on a logarithmic scale to show out-of band throughput (red leak or blue leak) for the different filters.
- Plots of the time needed to achieve a desired signal-to-noise ratio vs. magnitude for broadband filters and vs. line flux for narrowband filters.
- Plots of the PSF and encircled energies, along with a logarithmic-scale image of the PSF.

In addition, we provide the following sections:

- Section 14.8 presents screening tables of bright object magnitudes for sources of different spectral type, for use in deciding if a MAMA imaging observation is safe.
- Section 14.6 presents information on the geometry of the MAMA and CCD imaging modes.
- Section 14.7 presents information on the changes of the PSF with position in the STIS field of view.

14.2 Using the Information in this Chapter

14.2.1 Sensitivity Units and Conversions

This chapter contains plots of throughputs and tables of sensitivities and throughputs for each grating mode. Section 6.2 explains how to use these sensitivities to calculate expected counts rates from your source.

The first table for each filter provides the following quantities:

Pivot wavelength¹ Source-independent measure of the characteristic wavelength of the bandpass, defined such that it is the same if the input spectrum is in units of f_λ or f_ν :

$$\lambda_p = \sqrt{\frac{\int T(\lambda) d\lambda}{\int T(\lambda) ((d\lambda)/\lambda)}}$$

FWHM^a Full-width at half-maximum of the throughput $T(\lambda)$.

AB mag zeropoint AB magnitude of a source that produces a flux of one count per second.

S_{peak}^P Peak sensitivity (electrons $\text{s}^{-1} \text{\AA}^{-1}$ per incident $\text{erg cm}^{-2} \text{s}^{-1} \text{\AA}^{-1}$)

B_λ	Equivalent bandpass of filter, defined such that $\int S_\lambda^p d\lambda = S_{peak}^p B_\lambda$ (see Chapter 6). For filters with red leaks this integration includes only the primary bandpass.
R_{80}	Radius in arcseconds of an aperture that encloses 80% of the flux of a point source.
% flux in central pixel	Percentage of the flux of a point source that falls within the central pixel (this estimate is accurate to about 10%).

1. For filters with red leaks, the pivot wavelength and FWHM correspond to the “in-band” region, and do not include the red leak.

The first figure for each imaging mode gives the integrated system throughput. This is the combination of the efficiencies of the detector and of the optical elements in the light path. The bottom section of the throughput figures includes wavelengths beyond the nominal passband of that mode, showing any red or blue “leak” on a log scale (dotted sections are manufacturer’s lab measurements). The throughput is defined as the number of detected counts per second per cm^2 of telescope area relative to the incident flux in photons per cm^2 per second. For the CCD “counts” is the number of electrons detected. For the MAMA, “counts” is the number of valid events processed by the detector electronics after passing through the various pulse-shape and anti-coincidence filters. In both cases the detected counts obey Poisson statistics. The throughput includes all obscuration effects in the optical train (e.g., due to the HST secondary and due to the STIS CCD Lyot stops). The “effective area” of the mode can be computed from the throughput by multiplying by the physical area of the HST primary mirror (45238.93416 cm^2). This is shown on the ordinate label on the right side of each plot.

The table for each mode gives the throughput and the point-source sensitivity as a function of wavelength. Throughput has the meaning described above. The *imaging point-source sensitivity* S_λ^p has units of counts $\text{sec}^{-1} \text{Å}^{-1}$ per incident $\text{erg cm}^{-2} \text{s}^{-1} \text{Å}^{-1}$ for the MAMAs, and electrons $\text{sec}^{-1} \text{Å}^{-1}$ per incident $\text{erg cm}^{-2} \text{s}^{-1} \text{Å}^{-1}$ for the CCDs. Counts and electrons refer to the total counts from the point source integrated over the PSF.

The *imaging diffuse source sensitivity*, S_λ^d , has the units: counts $\text{sec}^{-1} \text{pix}^{-1}$ per incident dimensional $\text{erg cm}^{-2} \text{sec}^{-1} \text{Å}^{-1} \text{arcsec}^{-2}$ for the MAMAs and electrons $\text{sec}^{-1} \text{pix}^{-1}$ per incident dimensional $\text{erg cm}^{-2} \text{sec}^{-1} \text{Å}^{-1} \text{arcsec}^{-2}$ for the CCDs.

Thus S_λ^p and S_λ^d are related through the relation:

$$S_\lambda^d \equiv (S_\lambda^p \times m^2)$$

Where m is the plate-scale in arcsec per pixel. Here, we have assumed that the diffuse source has a uniform brightness over the area of interest.

The sensitivities and throughputs listed in this chapter have not been corrected for time-dependent changes in the sensitivity (see Section 13.2.2), but rather are the values as originally measured in 1997-1998. In many cases they are therefore higher than the current sensitivities by a few-to-several percent.

14.2.2 Signal-To-Noise

For each imaging mode, plots are provided to estimate the signal-to-noise (S/N) for a representative source. The first figure shows S/N for point sources (for two different gains for the CCD). The second figure shows S/N for uniform extended sources of area 1 arcsec^2 and 0.2 arcsec^2 .

The different line styles in the S/N figures delineate regions where different sources of noise dominate. A particular source of noise (read noise for example) is presumed to dominate if it contributes more than half the total noise in the observations.

To the left of the vertical line in the S/N plots, the count rate from the source exceeds the $100 \text{ counts sec}^{-1} \text{ pix}^{-1}$ local count rate limit. This is computed from the on-orbit measured PSF, which gives 6 to 14% of the flux in the central pixel. The bright-object screening limits in Table 14.39 use the more conservative (for this purpose) estimate of 25% of the flux in the central pixel.

The point-source S/N figures are shown for average sky levels (i.e., the ‘average zodiacal+average earthshine’ background level used in the STIS ETC), and for sky levels during orbital night (i.e., average zodiacal + low earth). For the CCD the read noise has been computed assuming a number of readouts $\text{NREAD} = \text{integer}(t / 1000 \text{ s})$, where t is the exposure time, with a minimum $\text{NREAD}=2$. That is, each exposure has a minimum $\text{CR-SPLIT}=2$. Different line styles in the figures are used to indicate which source of noise dominates.

For the CCD, the dominant sources of sky background are zodiacal light and scattered earthshine. The **LOW-SKY** requirement can be used to ensure that these backgrounds are kept as low or lower than the rates assumed for these plots. If your source falls within the sky-dominated portion of the figures, you may want to consider imposing the **LOW-SKY** requirement.

For the **NUV-MAMA** the sky background has different contributions which can dominate depending on the filter used and on whether the observation takes place on the day or night sides of the orbit. The FUV geocoronal lines dominate on the day side if **CLEAR**, **F25SRF2**, or a neutral-density filter are used due to the strength of those lines (see Table 6.6) and to the significant sensitivity of the detector at FUV wavelengths (see Figure 14.23 and Figure 14.41). The NUV [O II] 2471 Å geocoronal line is the second most important contribution and dominates on the day side of the orbit if **F25QTZ** is used. Zodiacal light provides the largest contribution for the rest of the filters on the day side of the orbit and for

most of them on the night side, where geocoronal emission is greatly reduced. The dark current is larger than the sky background in all cases except for CLEAR observations in the day side of the orbit.

For the FUV–MAMA, the dominant source of background is geocoronal emission (see Table 6.4 and Table 6.5). The lines vary strongly from the day to night side of the orbit. For broad-band the contribution from the geocoronal lines can be minimized by using the F25QTZ filter, or observing with the DARKTIME special requirement.

In situations requiring more detailed calculations (non-stellar spectra, extended sources, other sky background levels, unknown target V magnitude, etc.), the [STIS Exposure-Time Calculator](#) should be used.

Follow these steps to use the signal-to-noise plots:

1. Determine the AB magnitude of your source at the wavelength of interest. There are several ways to do this.
 - Examine Table 14.1 and find AB_V for the desired temperature and filter. Sum the V magnitude of the target and AB_V .
 - Alternatively, compute $ABMAG (=V+AB_V)$ from the source flux, using the relation:

$$ABMAG = -2.5 \log f_V - 48.60$$

or

$$ABMAG = -2.5 \log f_\lambda - 5 \log \lambda - 2.406$$

2. Find the appropriate plot for the filter in question, and locate $V+AB_V$ on the horizontal axis. Then read off the signal-to-noise ratio for the desired exposure time, or vice-versa.

The “x” characters at the top of each plot indicate the onset of saturation, in the case of the CCD. The “x” shows where the total number of counts exceeds the 16-bit buffer size of 65,535.

We now give a sample S/N calculation using these plots. Consider a $V=27$ star of spectral class G2V, for which we want to obtain $S/N = 20$ with F28X50LP observing with the CCD. From Table 14.1 we find a correction $AB_V = -0.21$ to go from V magnitude to AB magnitude near the center of the F28X50LP bandpass. We thus have $V+AB_V=26.79$. We look at Figure 14.8 and find this value on the horizontal axis and read up to find the curve that intersects the desired S/N. We find $\sim 10,000$ seconds are needed to reach $S/N = 20$ in conditions of low sky background.

14.2.3 Point Spread Functions

The final figures and table for each imaging mode contain information on the point-spread function. The encircled energy plots and tables are normalized to 1 at a radius of 1 arcsecond. In actuality about 10% of the light from a point source falls beyond this radius; however high S/N

observations extending out to large radius exist for only a few modes from on-orbit data. The intensity vs. radius plots are normalized to a total integrated flux of 1. The PSF image is shown on a logarithmic intensity scale to enhance faint features in the wings of the PSF. Note the stellar like ‘ghost’ at approximately 45 pixels left of the peak pixel in all NUV-MAMA+Filter images. The ghost is a few tenths of a percent of the psf peak intensity. See [Bowers \(1997 HST Calibration Workshop\)](#) for a discussion of HST “breathing” effects on the PSF. Updated information about the STIS PSF and color dependent aperture corrections can be found in [STIS ISR 2003-01](#).

Table 14.1: Color Corrections AB_V to convert from Johnson V Magnitude to AB Magnitude. Values were calculated using solar metallicity Lejeune models with $\log g = 5.0$.

Temp (K)	CCD				FUV-MAMA					
	F28x50LP	50CCD	F28X50OIII	F28X50OII	25MAMA	F25ND3	F25ND5	F25QTZ	F25SRF2	F25LYA
5000	0.48	-0.29	-0.01	-0.64	-2.16	-2.15	-2.15	-1.98	-2.09	-2.25
3000	0.47	-0.17	0.01	-0.42	-1.67	-1.67	-1.66	-1.46	-1.64	-1.68
2000	0.41	0.00	0.02	-0.08	-0.61	-0.62	-0.61	-0.60	-0.68	-0.43
1500	0.38	0.11	0.02	0.22	0.42	0.41	0.41	0.17	0.20	0.98
1000	0.30	0.26	0.03	0.88	2.86	2.84	2.80	1.96	2.35	4.70
900	0.23	0.27	0.04	0.99	4.61	4.63	4.49	3.07	4.03	7.34
800	0.13	0.27	0.07	1.01	7.10	7.21	6.98	5.26	6.49	10.50
700	0.02	0.26	0.11	1.03	9.19	9.34	9.12	7.29	8.57	12.83
600	-0.15	0.23	0.13	1.31	13.49	13.65	13.44	11.59	12.86	17.26
500	-0.37	0.17	0.14	2.38	18.09	18.09	17.35	16.15	17.44	22.24
400	-0.90	-0.19	-0.01	3.36	21.70	21.41	20.01	19.72	21.01	26.81
300	-2.28	-1.42	-1.99	4.26	23.08	22.68	20.89	21.07	22.36	29.95

Temp (K)	NUV-MAMA								
	25MAMA	F25ND3	F25ND5	F25QTZ	F25SRF2	F25CN182	F25CIII	F25CN270	F25MGII
5000	-1.62	-1.57	-1.40	-1.53	-1.58	-1.73	-1.71	-1.24	-1.16
3000	-1.23	-1.19	-1.06	-1.16	-1.20	-1.32	-1.28	-0.95	-0.89
2000	-0.49	-0.47	-0.41	-0.46	-0.48	-0.54	-0.52	-0.38	-0.35
1500	0.18	0.18	0.16	0.16	0.17	0.15	0.12	0.16	0.18
1000	1.54	1.50	1.34	1.45	1.50	1.58	1.50	1.32	1.33
900	1.98	1.91	1.66	1.85	1.93	2.08	1.95	1.64	1.65
800	2.56	2.41	1.99	2.42	2.50	3.00	2.87	2.04	2.01
700	3.12	2.90	2.31	2.97	3.05	3.91	3.88	2.51	2.43
600	4.06	3.73	2.93	3.91	3.99	5.62	5.90	3.33	3.10
500	5.92	5.53	4.49	5.76	5.84	8.36	7.60	5.17	4.04
400	7.63	7.25	6.03	7.47	7.55	10.95	8.55	6.44	4.53
300	8.19	7.80	6.49	8.03	8.10	12.23	9.14	6.83	4.80
300	23.08	22.68	20.89	21.07	22.36	29.95			

14.3 CCD

Below, for each filter used with the CCD detector, we provide the basic properties of the mode, sensitivities, throughputs and the radial profiles in the imaging mode. dispersions and plate scales.

- “CCD Clear Imaging—50CCD,” page 395.
- “CCD Long-Pass Imaging F28X50LP,” page 398.
- “F28X50OIII—CCD,” page 401.
- “F28X50OII—CCD,” page 404.
- “50CORON—Clear CCD,” page 407.

CCD Clear Imaging—50CCD

Description

The 50CCD mode is very sensitive for broad-band optical imaging. For a fixed exposure time, it can detect point sources roughly 0.8 mag fainter than with WFPC2 with the F606W filter. However, the ACS WFC with the F606W or F814W will be a better choice for most users.

Recommended Uses.

Recommended for deep imaging where detailed color information is not needed. In most cases the ACS WFC will be a better choice.

Special Considerations

Very red sources may show significant wings from detector halo (see Section 7.1.7)

Pivot λ (\AA)	FWHM (\AA)	AB mag zeropoint	S_{peak}	B_{λ}	R_{80} (arcsec)	Flux in central pixel
5751.9	4410.3	26.386	2.30×10^{15}	4898.9	0.16	14%

Figure 14.1: Throughput for 50CCD

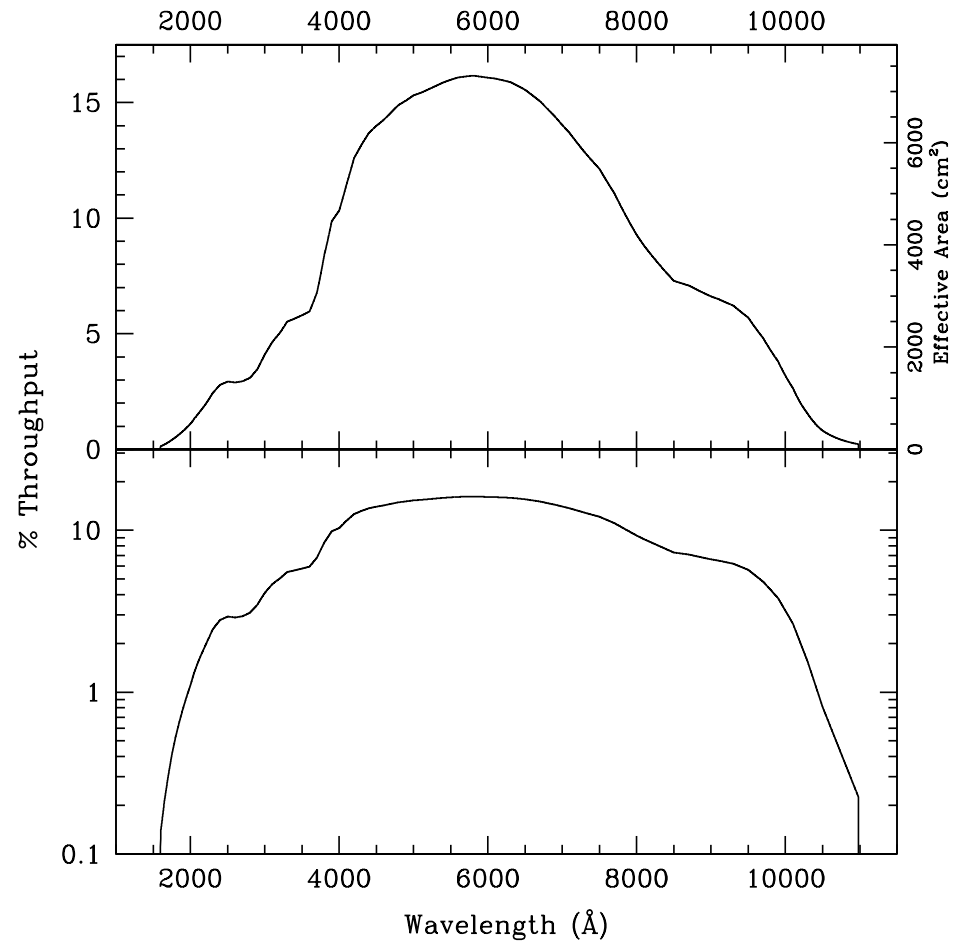


Table 14.2: Throughputs and Sensitivities for 50CCD

λ	Sensitivity	Throughput %
2500.	1.69E14	2.97
3000.	2.85E14	4.17
3500.	4.70E14	5.89
4000.	9.43E14	10.34
4500.	1.39E15	13.58
5000.	1.64E15	14.41
5500.	1.85E15	14.74
6000.	1.99E15	14.52
6500.	2.04E15	13.75
7000.	1.94E15	12.18
7500.	1.78E15	10.40
8000.	1.43E15	7.85
8500.	1.18E15	6.09
9000.	1.13E15	5.50
9500.	1.02E15	4.72
10000.	6.00E14	2.63
10500.	1.60E14	0.67

Figure 14.2: Point Source S/N vs. $V+AB_V$ for the 50CCD filter. Top curves are for low sky; bottom curves are for average sky. Curves are labeled by required exposure time (sec).

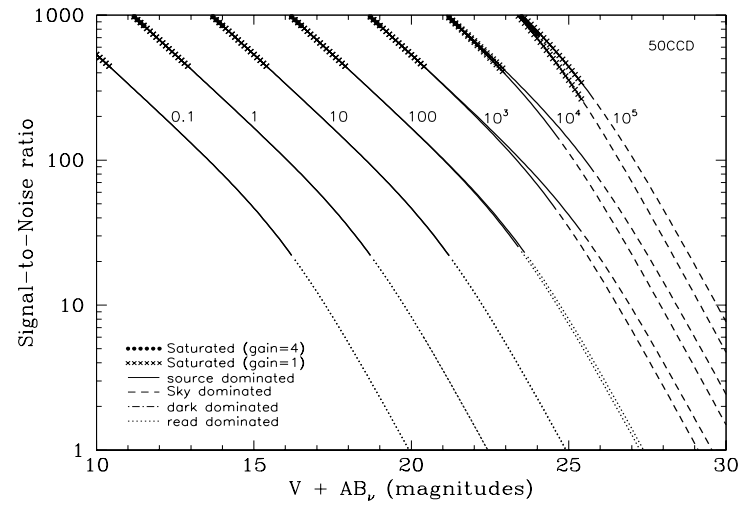


Figure 14.3: Extended Source S/N vs. $V+AB_V$ for the 50CCD filter for gain=1. Top curves are for a source area of 0.2 arcsec²; bottom curves are for 1 arcsec². Average sky assumed. Curves are labeled by required exposure time (sec).

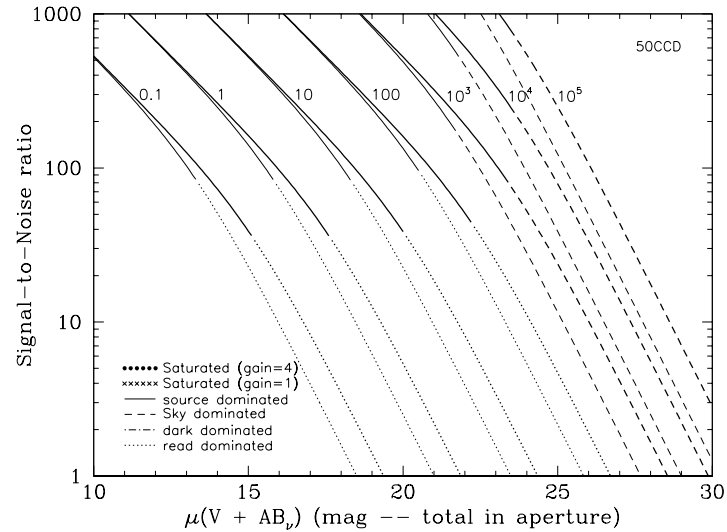


Table 14.3: Radial Profile for 50CCD

Radius		Intensity	Fraction of Energy Encircled
Pixels	Arcsec		
1	0.050	1.614e-02	0.321
2	0.075	7.765e-03	0.495
2	0.100	4.320e-03	0.621
3	0.150	1.629e-03	0.787
4	0.200	4.904e-04	0.868
5	0.250	1.978e-04	0.902
10	0.500	2.499e-05	0.964
15	0.750	7.654e-06	0.986
20	1.000	2.687e-06	0.996

Figure 14.4: Point Source PSF for 50CCD, 7."5 square (at pixel 518,517, log scaled, B-V=-0.25).

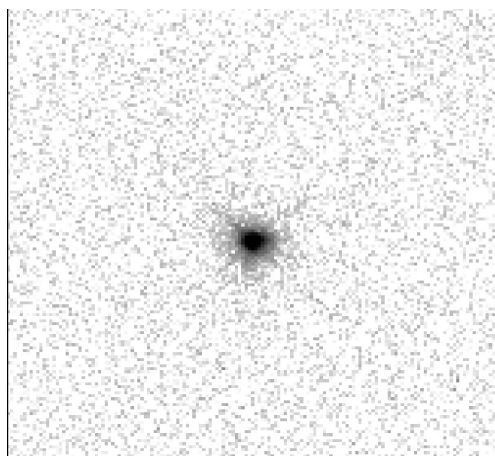


Figure 14.5: Point Source Encircled Energy for 50CCD

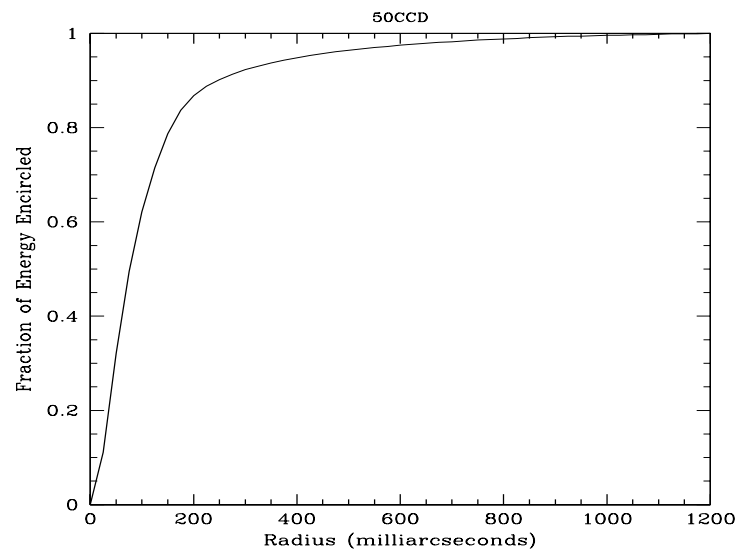
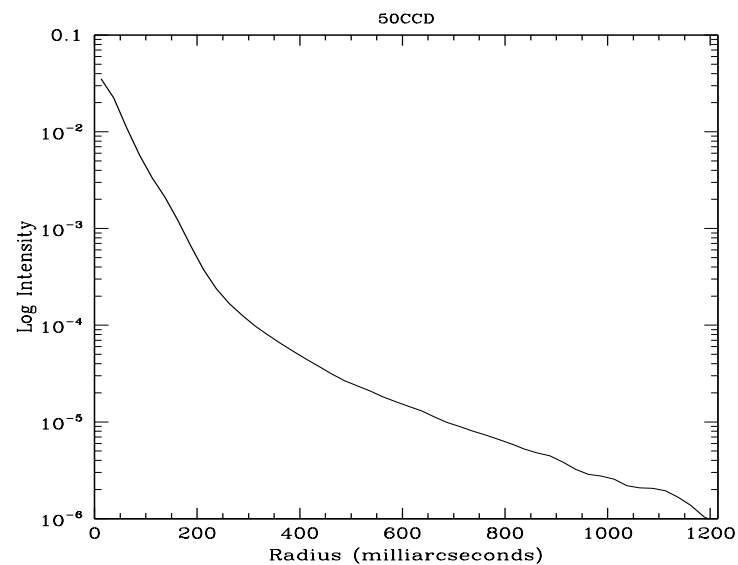


Figure 14.6: Point Source Intensity vs. Radius for 50CCD



CCD Long-Pass Imaging F28X50LP

Description

The F28X50LP mode is useful for deep imaging longward of 5500 Å. For a fixed exposure time it can detect point sources roughly as faint as with WFPC2 with the F606W filter, but with higher spatial resolution. The field of view is 28x50". The ACS/WFC with the F814W filter will be more appropriate for most programs.

Recommended Uses

Recommended for deep high-resolution imaging between 5500 Å and 10,000 Å. Default aperture for target acquisitions.

Special Considerations

Very red sources may show significant wings from detector halo (see Section 7.1.7).

Pivot λ (Å)	FWHM (Å)	AB mag zeropoint	S_{peak}	B_{λ}	R_{80} (arcsec)	Flux in central pixel
7218.9	2721.6	25.191	1.64e+15	3495.7	0.15	14%

Figure 14.7: Throughput for F28x50LP

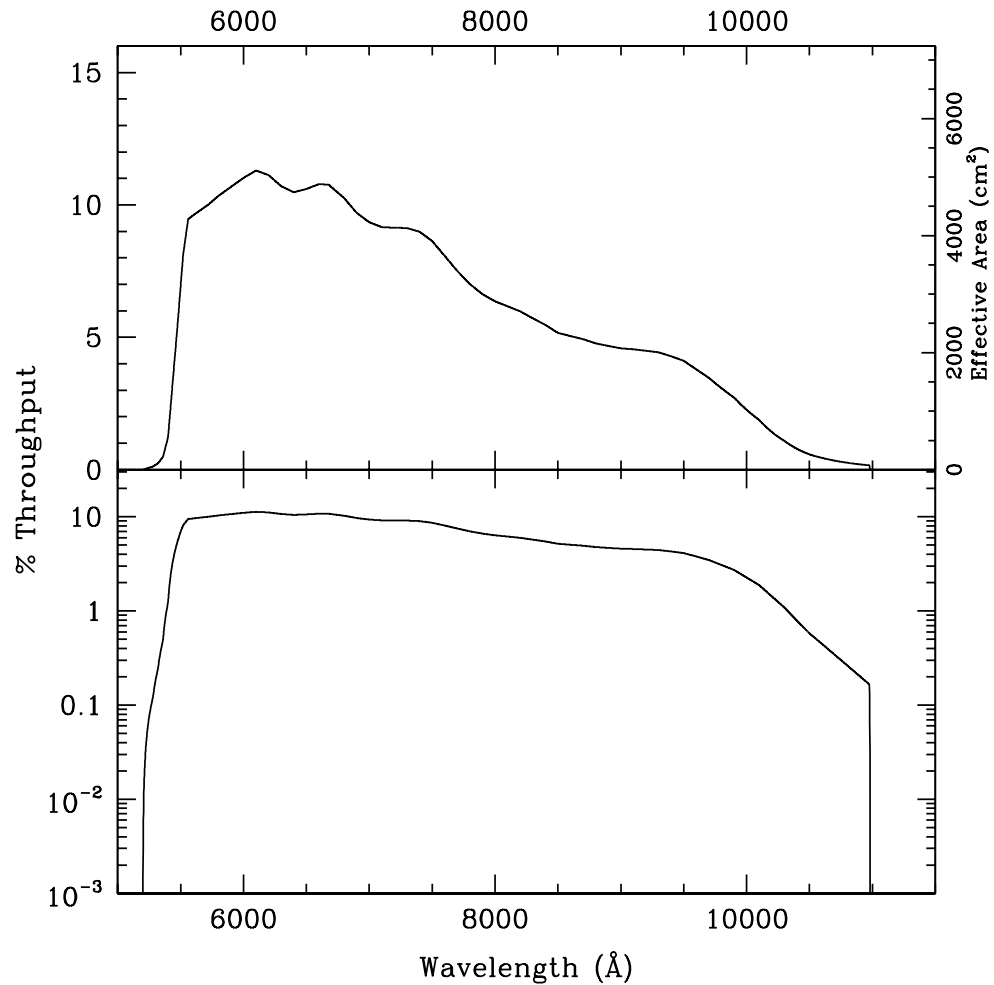


Table 14.4: Throughputs and Sensitivities for F28X50LP

λ	Sensitivity	Throughput %
5400.	1.54E14	1.25
5600.	1.24E15	9.69
5800.	1.49E15	11.27
6000.	1.70E15	12.39
6200.	1.70E15	12.04
6400.	1.75E15	11.98
6600.	1.75E15	11.66
6800.	1.65E15	10.64
7000.	1.70E15	10.66
7200.	1.63E15	9.95
7400.	1.61E15	9.55
7600.	1.42E15	8.22
7800.	1.39E15	7.82
8000.	1.27E15	6.97
8400.	1.11E15	5.78
8800.	1.01E15	5.03
9200.	9.68E14	4.61
9400.	9.42E14	4.39
9600.	8.75E14	4.00
9800.	7.18E14	3.21
10000.	5.20E14	2.28

Figure 14.8: Point Source S/N vs. $V+AB_v$ for the F28X50LP filter. Top curves are for low sky; bottom curves are for average sky. Curves are labeled by required exposure time (sec).

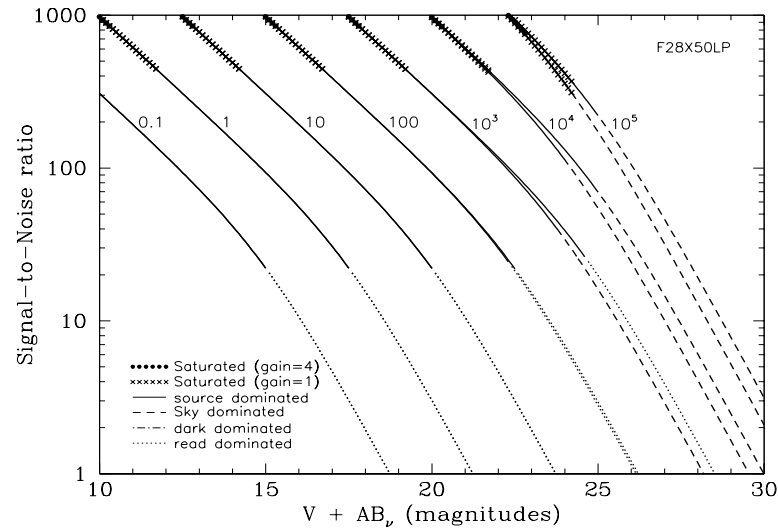


Figure 14.9: Extended Source S/N vs. $V+AB_v$ for the F28X50LP filter for gain=1. Top curves are for a source area of 0.2 arcsec²; bottom curves are for 1 arcsec². Average sky assumed. Curves are labeled by required exposure time (sec).

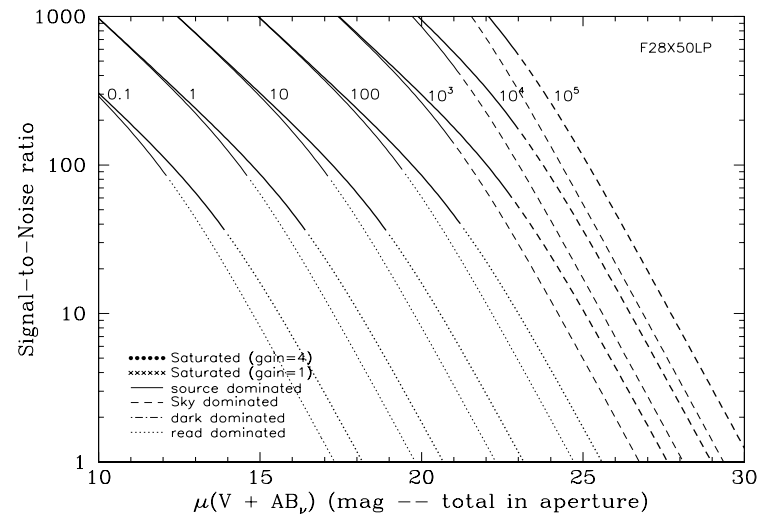


Table 14.5: Radial Profile for F28X50LP

Radius		Intensity	Fraction of Energy Encircled
Pixels	Arcsec		
1	0.050	1.703e-02	0.337
2	0.075	7.468e-03	0.512
2	0.100	4.196e-03	0.632
3	0.150	1.733e-03	0.804
4	0.200	4.246e-04	0.883
5	0.250	1.660e-04	0.911
10	0.500	2.469e-05	0.976
15	0.750	5.360e-06	0.996
19.25	0.963	3.333e-07	1.000

Figure 14.10: Point Source Encircled Energy for F28X50LP

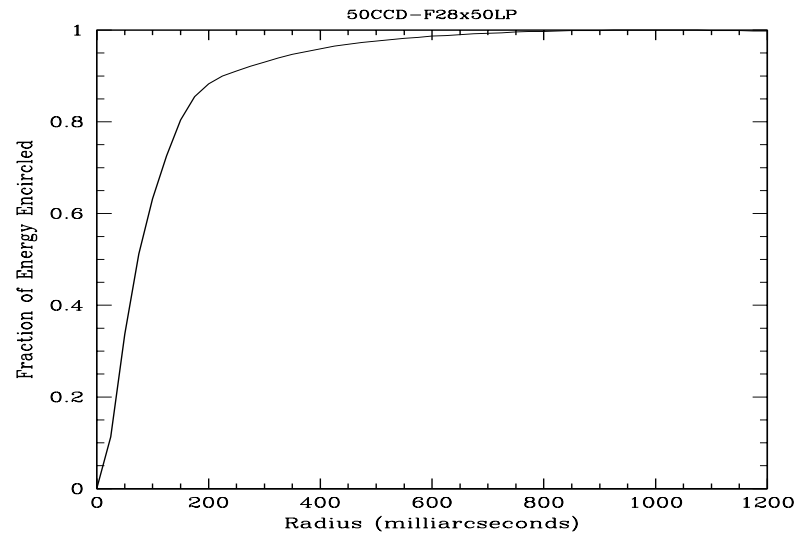
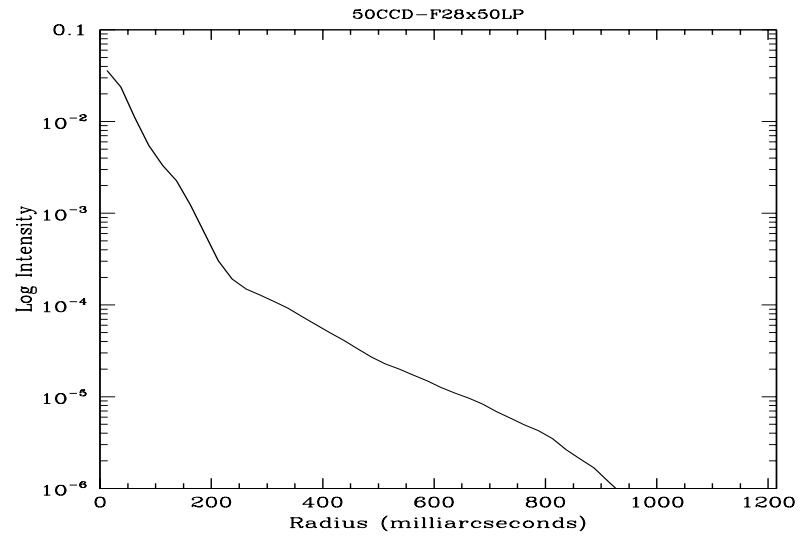


Figure 14.11: Point Source Intensity vs. Radius for F28X50LP



F28X50OIII— CCD

Description

The F28X50OIII mode is useful for narrow-band imaging of O III 5007 Å. The narrow bandpass and high spatial resolution provides some advantages over WFPC2 with the F502N filter, although the spatial resolution is not as high as that of ACS/HRC with its F502N filter.

Recommended Uses

Recommended for deep high-resolution O III imaging.

Special Considerations

This filter has a significant red leak longward of 1 micron. Depending on the source spectrum, the contribution from redleak may swamp the contribution from line emission.

Pivot λ (Å)	FWHM (Å)	AB mag zeropoint	S_{peak}	B_{λ}	R_{80} (arcsec)	Flux in central pixel
5005.8	6.2	18.846	1.26e+15	6.3	0.13	17%

Figure 14.12: Throughput for F28x50OIII.

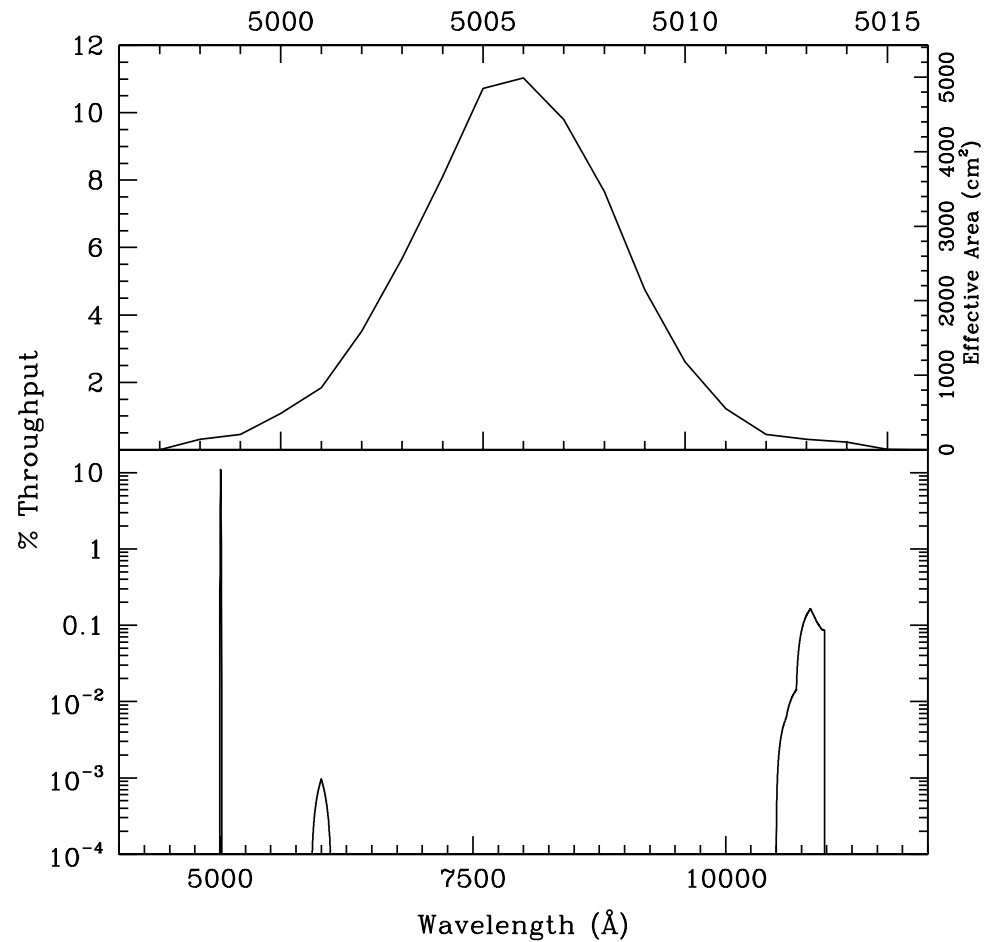


Table 14.6: Throughput and Sensitivity for F28X50OIII

I	Sensitivity	Throughput %
4999.	5.23E13	0.46
5000.	1.22E14	1.07
5001.	2.09E14	1.84
5002.	4.01E14	3.52
5003.	6.46E14	5.67
5004.	9.25E14	8.12
5005.	1.22E15	10.72
5006.	1.26E15	11.03
5007.	1.12E15	9.80
5008.	8.74E14	7.66
5009.	5.42E14	4.75
5010.	2.97E14	2.60
5011.	1.40E14	1.23
5012.	5.25E13	0.46

Figure 14.13: Point Source S/N vs. $V+AB_v$ for the F28X50OIII filter. Top curves are for low sky; bottom curves are for average sky. Curves are labeled by required exposure time (sec).

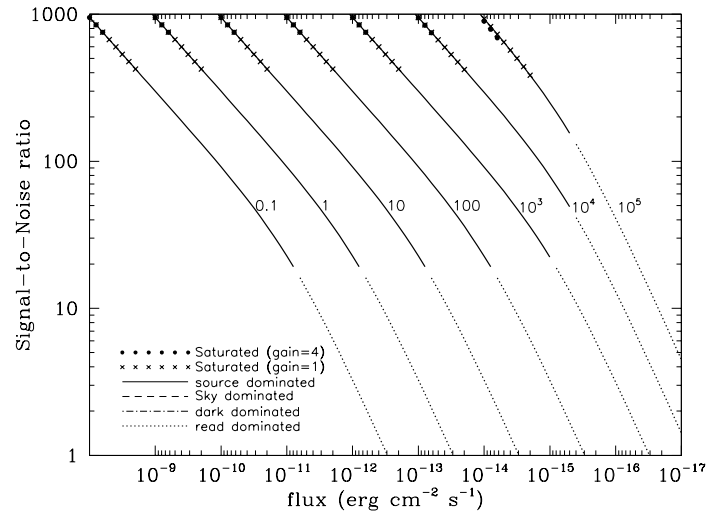


Figure 14.14: Extended Source S/N vs. $V+AB_v$ for the F28X50OIII for gain=1. Top curves are for a source area of 0.2 arcsec²; bottom curves are for 1 arcsec². Average sky assumed. Curves are labeled by required exposure time (sec).

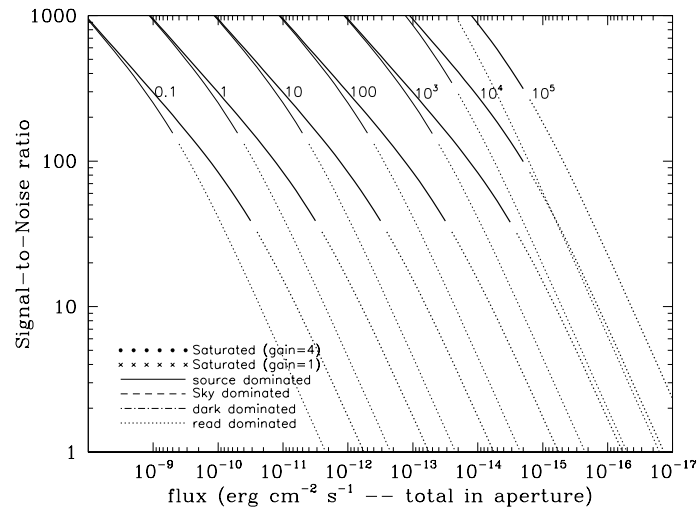


Table 14.7: Radial Profile for F28X50OIII

Radius		Intensity	Fraction of Energy Encircled
Pixels	Arcsec		
1	0.050	1.750e-02	0.358
2	0.075	9.783e-03	0.574
2	0.100	4.193e-03	0.711
3	0.150	8.194e-04	0.844
4	0.200	3.245e-04	0.884
5	0.250	2.403e-04	0.916
10	0.500	2.049e-05	0.979
15	0.750	4.391e-06	0.995
20	1.000	8.462e-07	1.000

Figure 14.15: Point Source PSF for F28X50OIII, 7."5 square (pixel 493,542, log scaled, B-V=-0.34)

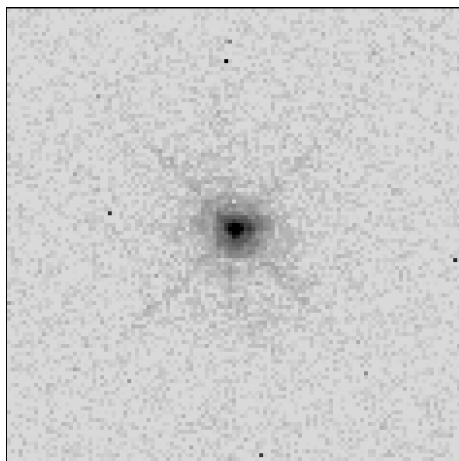


Figure 14.16: Point Source Encircled Energy for F28X50OIII

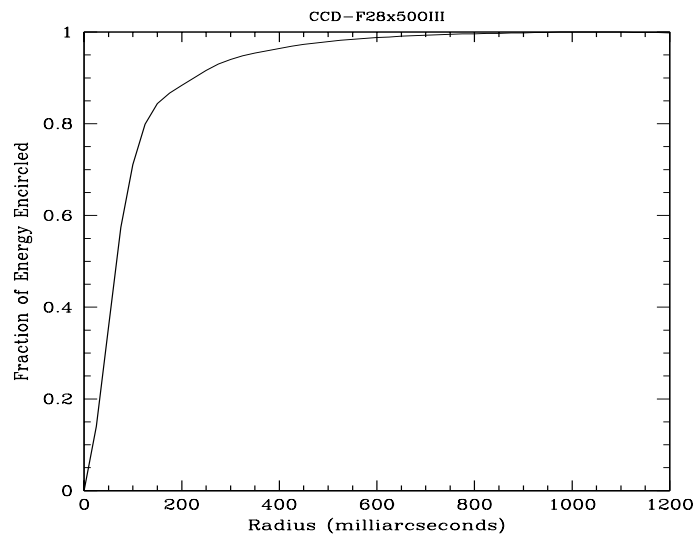
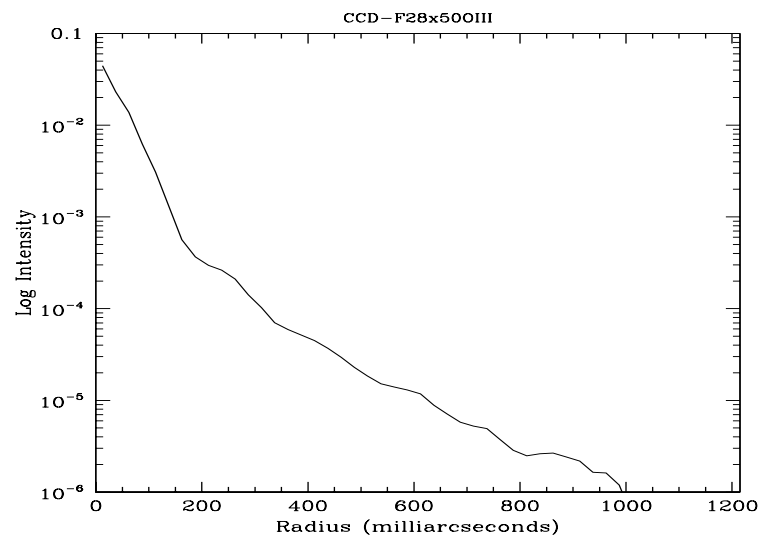


Figure 14.17: Point Source Intensity vs. Radius for F28X50OIII



F28X50OII—CCD

Description

The F28X50OII mode is useful for narrow-band imaging of OII 3727 Å. The high throughput and high spatial resolution provide a significant advantage over WFPC2 imaging with the F375N filter for some purposes. The narrow bandpass may offer some advantages over ACS and either the HRC or WFC with the [O II] ramp filter.

Recommended Uses

Recommended for deep high-resolution O II imaging.

Special Considerations

This filter does not have a significant red leak. Flat field images taken through this filter show scattered light at the top and bottom of the frame. This is not expected to be a problem for astronomical targets

Pivot λ (Å)	FWHM (Å)	AB mag zeropoint	S_{peak}	B_{λ}	R_{80} (arcsec)	Flux in central pixel
3738.1	62.0	20.534	$3.47\text{e}+14$	60.5	0.12	17%

Figure 14.18: Throughput for F28x50OII

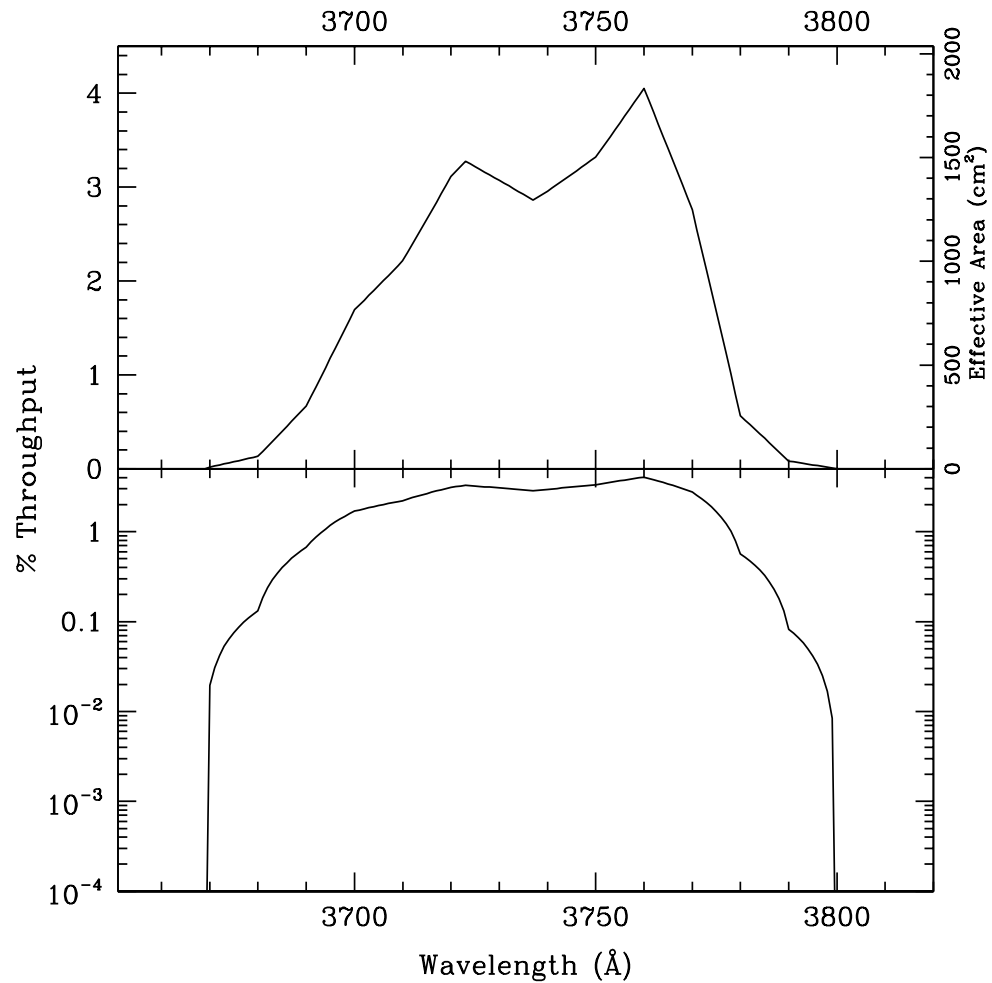


Table 14.8: Throughput and Sensitivity for F28X50OII

I	Sensitivity	Throughput %
3675.	6.32E12	0.08
3685.	3.35E13	0.40
3695.	9.91E13	1.18
3705.	1.65E14	1.95
3715.	2.25E14	2.66
3725.	2.73E14	3.22
3735.	2.49E14	2.92
3745.	2.68E14	3.14
3755.	3.15E14	3.68
3765.	2.93E14	3.41
3775.	1.44E14	1.67
3785.	2.81E13	0.33

Figure 14.19: Point Source S/N vs. Line Flux for the F28X50OII filter. Top curves are for low sky; bottom curves are for average sky. Curves are labeled by required exposure time (sec).

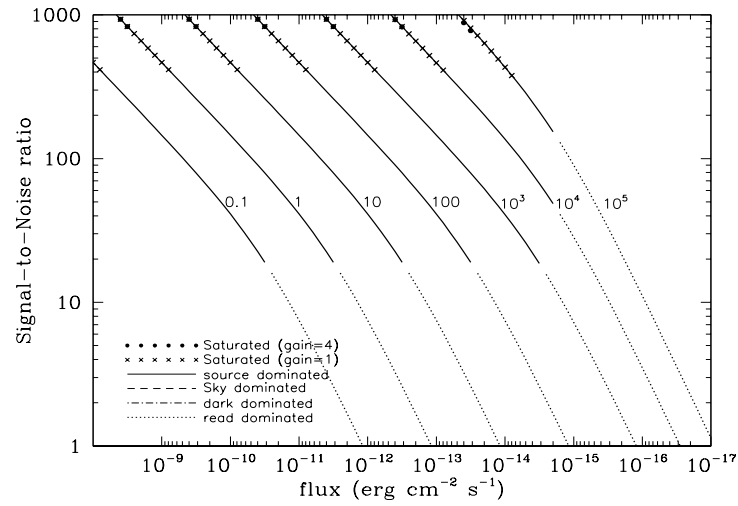


Figure 14.20: Extended Source S/N vs. $V+AB_V$ for the F28X50OII for gain =1. Top curves are for an area of 0.2 arcsec²; bottom curves are for 1 arcsec². Average sky assumed. Curves are labeled by required exposure time (sec).

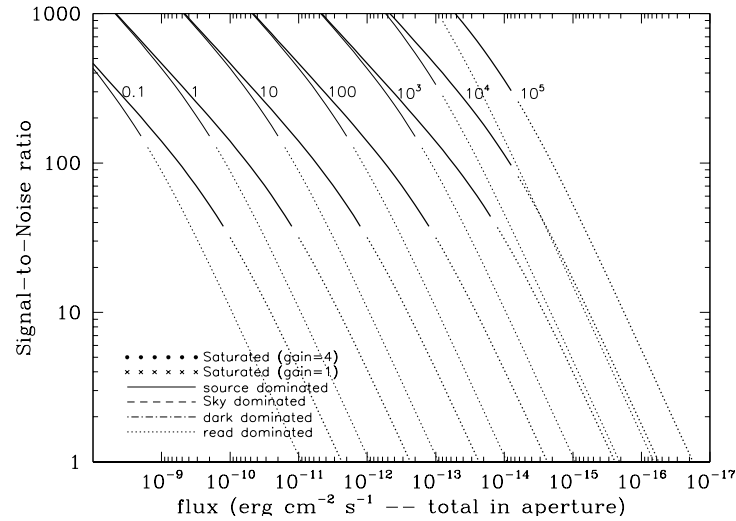


Table 14.9: Radial Profile for F28X500II

Radius		Intensity	Fraction of Energy Encircled
Pixels	Arcsec		
1	0.050	1.945e-02	0.405
2	0.075	9.266e-03	0.622
2	0.100	3.589e-03	0.750
3	0.150	7.742e-04	0.849
4	0.200	3.628e-04	0.895
5	0.250	1.826e-04	0.924
10	0.500	1.966e-05	0.982
15	0.750	4.876e-06	0.997
20	1.000	5.800e-07	1.000

Figure 14.21: Point Source Encircled Energy for F28X500II

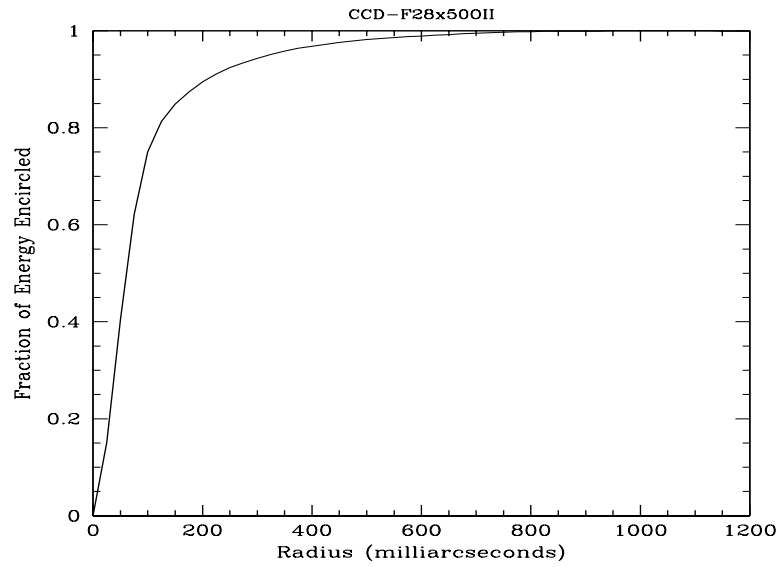
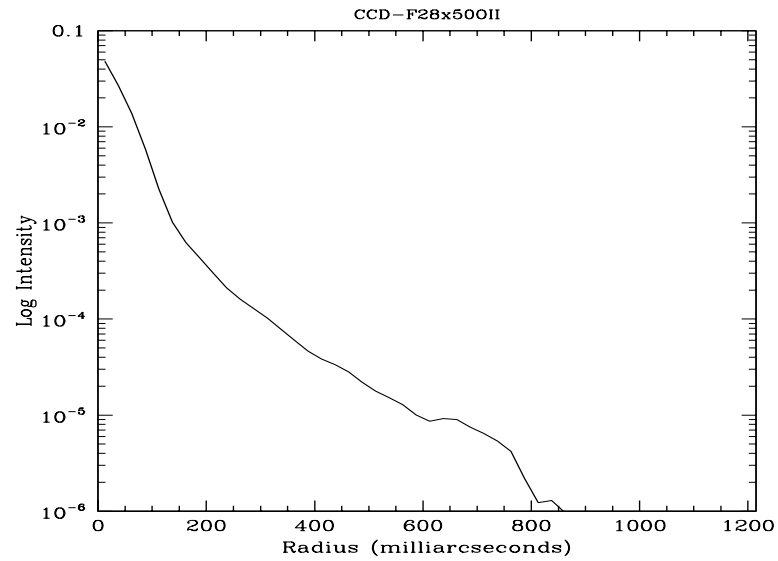


Figure 14.22: Point Source Intensity vs. Radius for F28X500II



50CORON—Clear CCD

Description

The 50CORON imaging mode is useful for imaging of faint targets next to bright ones. The STIS CCD optics include a Lyot stop, which suppresses the wings of the PSF. See “CCD Clear Imaging—50CCD” on page 395 for sensitivities, throughputs, and encircled energies. See Section 12.10 for the PSF and for a discussion of coronagraphic imaging. A diagram showing the layout of the 50CORON aperture and the wedge positions, can be seen in Figure 12.8

Recommended Uses

Recommended for broad-band coronagraphic imaging. Observers considering use of this mode may also want to investigate ACS coronagraphic imaging.

Pivot λ (Å)	FWHM (Å)	AB mag zeropoint	S_{peak}	B_{λ}	R_{80} (arcsec)	Flux in central pixel
5751.9	4410.3	26.386	2.30×10^{15}	4898.9	0.16	14%

14.4 NUV MAMA

Below, for each filter used with the NUV MAMA detector, we provide the basic properties of the mode, sensitivities, throughputs and radial profiles for the imaging mode.

Users should also consider whether the ACS HRC or SBC detector with a UV filter might be better for their particular imaging needs.

- “25MAMA—NUV-MAMA, Clear,” page 409.
- “F25ND3—NUV-MAMA” on page 412
- “F25ND5—NUV-MAMA,” page 414.
- “F25NDQ - NUV-MAMA,” page 416.
- “F25QTZ—NUV-MAMA, Longpass,” page 418.
- “F25SRF2—NUV-MAMA, Longpass,” page 421.
- “F25MGII—NUV-MAMA,” page 423.
- “F25CN270—NUV-MAMA,” page 426.
- “F25CIII—NUV-MAMA,” page 429.
- “F25CN182—NUV-MAMA,” page 432.

25MAMA—NUV-MAMA, Clear

Description

The 25MAMA mode with the NUV-MAMA provides high-throughput broad-band near-UV imaging with excellent pixel sampling and very high throughput at $\sim 2500 \text{ \AA}$. The field of view is $25 \times 25 \text{ arcsec}$.

Recommended Uses

Available (but not recommended, see below) for broad-band near-UV imaging.

Special Considerations

NUV-MAMA clear images will be somewhat out of focus because the mirror optimally focuses for use of a filter. Whenever possible, use F25SRF2 or F25QTZ instead of 25MAMA for NUV-MAMA imaging.

For long exposures of faint targets, sky background is likely to be a limiting factor. Observers should consider the use of DARKTIME or (preferably) use the F25QTZ filter, which has nearly the same throughput but rejects geocoronal Lyman- α and [O I] $1302+1306 \text{ \AA}$ air glow.

Users should also consider whether the ACS HRC with the F220W or the F250W filter might be a better choice for their science goals.

Pivot λ (\AA)	FWHM (\AA)	AB mag zeropoint	S_{peak}	B_{λ}	R_{80} (arcsec)	Flux in central pixel
2265.0	1201.9	24.085	1.76×10^{14}	11605	0.32	8%

Figure 14.23: 25MAMA NUV-MAMA Integrated System Throughput and Redleak

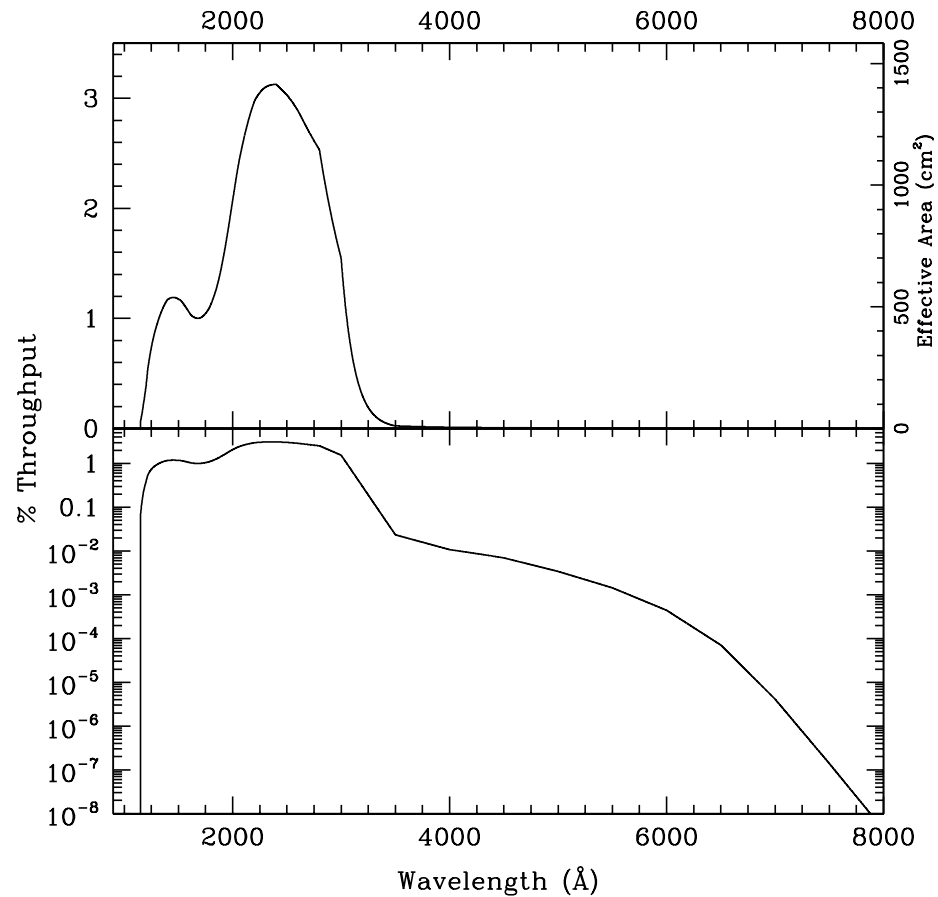


Table 14.10: Throughput and Sensitivity for 25MAMA NUV-MAMA

I	Sensitivity	Throughput %
1200.	1.07E13	0.39
1300.	2.75E13	0.93
1400.	3.69E13	1.16
1500.	4.00E13	1.17
1600.	3.86E13	1.06
1700.	3.92E13	1.01
1800.	4.67E13	1.14
1900.	6.46E13	1.49
2000.	9.43E13	2.07
2100.	1.25E14	2.61
2200.	1.48E14	2.96
2300.	1.62E14	3.09
2400.	1.70E14	3.11
2500.	1.72E14	3.03
2600.	1.71E14	2.89
2700.	1.66E14	2.70
2800.	1.58E14	2.48
2900.	1.31E14	1.98
3000.	9.95E13	1.46
3100.	4.87E13	0.69

Figure 14.24: Point Source S/N vs. $V+AB_v$ for the 25MAMA NUV-MAMA mode. Top curves are for DARKTIME. Bottom curves are for average sky. Top curves are for DARKTIME. Bottom curves are for average sky. Curves are labeled by required exposure time (sec).

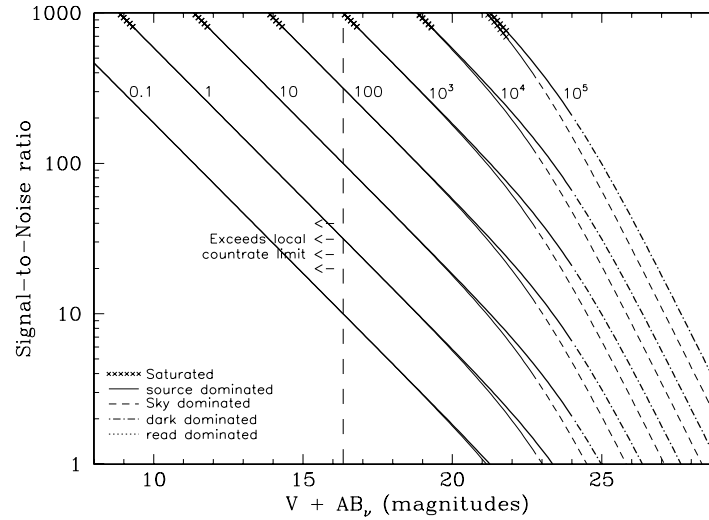


Figure 14.25: Extended Source S/N vs. $V+AB_v$ for the 25MAMA NUV-MAMA mode. Top curves are for an area of 0.2 arcsec^2 ; bottom curves are for 1 arcsec^2 . Average sky assumed. Curves are labeled by required exposure time (sec).

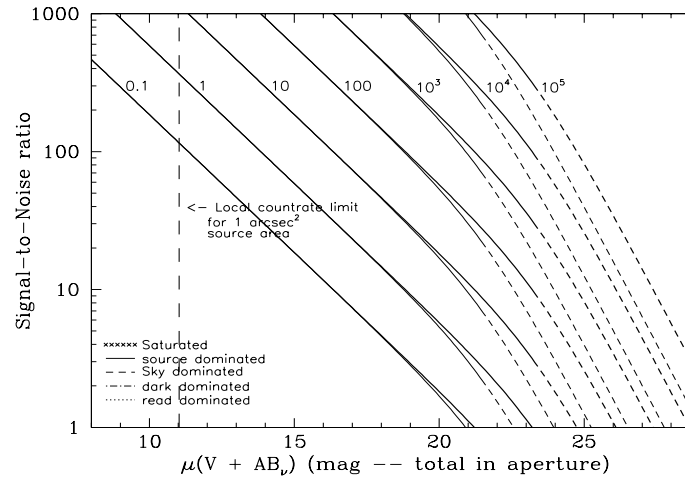


Table 14.11: Radial Profile for 25MAMA*

Radius			Fraction of Energy Encircled
Pix	arcsec	intensity	
1	0.024	3.267e-02	0.141
2	0.037	2.107e-02	0.236
2	0.049	1.345e-02	0.331
3	0.073	6.141e-03	0.467
4	0.098	2.981e-03	0.557
5	0.122	1.485e-03	0.614
10	0.245	3.377e-04	0.746
15	0.367	1.676e-04	0.834
20	0.490	9.542e-05	0.900
25	0.613	4.543e-05	0.947
30	0.735	2.065e-05	0.972
40	0.980	5.088e-06	0.994

*See [STIS ISR 2003-01](#).

Figure 14.26: Point Source Encircled Energy for 25MAMA NUV-MAMA

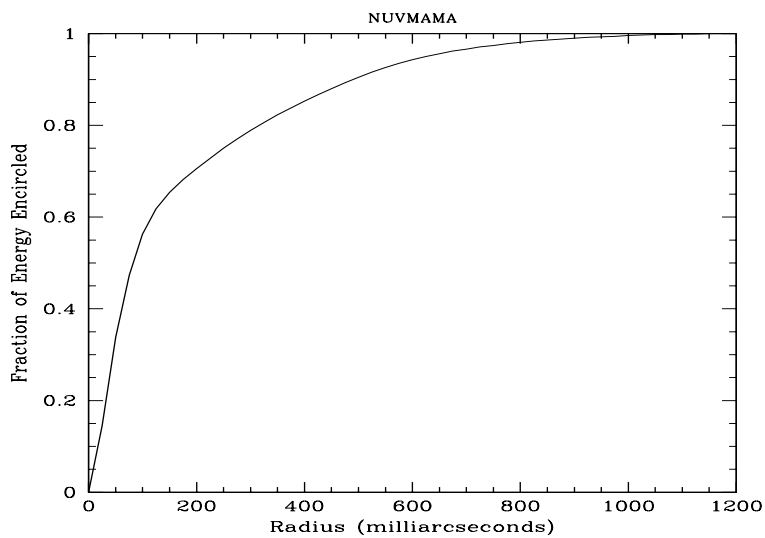
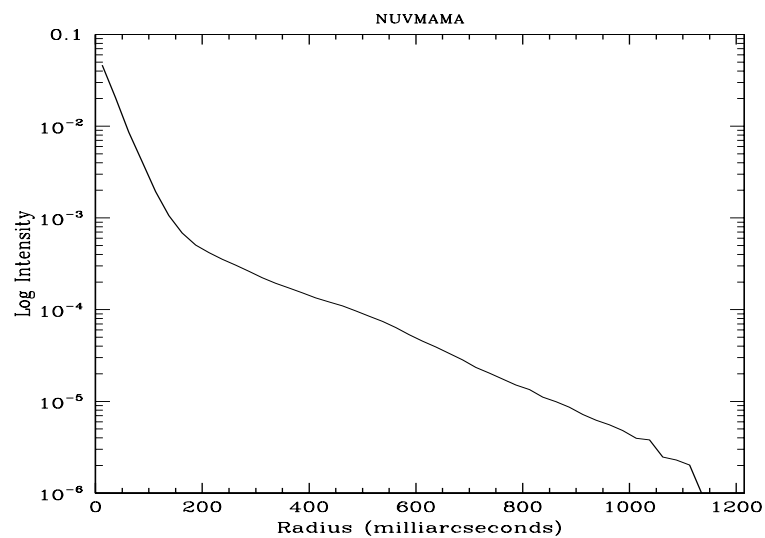


Figure 14.27: Point Source Intensity vs. Radius for 25MAMA NUV-MAMA



F25ND3—NUV-MAMA

Description

The F25ND3mode with the NUV-MAMA provides broad band imaging with an attenuation of 10^{-3} . The field of view is 25×25 arcsec. The value of R_{80} and the central pixel flux are unmeasured but assumed to be approximately the same as produced by the F25QTZ filter.

Recommended Uses

Recommended for broad-band near-UV imaging of objects too bright by 10^3 for clear mode.

Pivot λ (Å)	FWHM (Å)	AB mag zeropoint	S_{peak}	B_{λ}	R_{80} (arcsec)	Flux in central pixel
2360.7	1344.5	16.62	$2.38\text{e}+11$	942.0	0.32	8%

Figure 14.28: F25ND3 NUV-MAMA Integrated System Throughput and Redleak

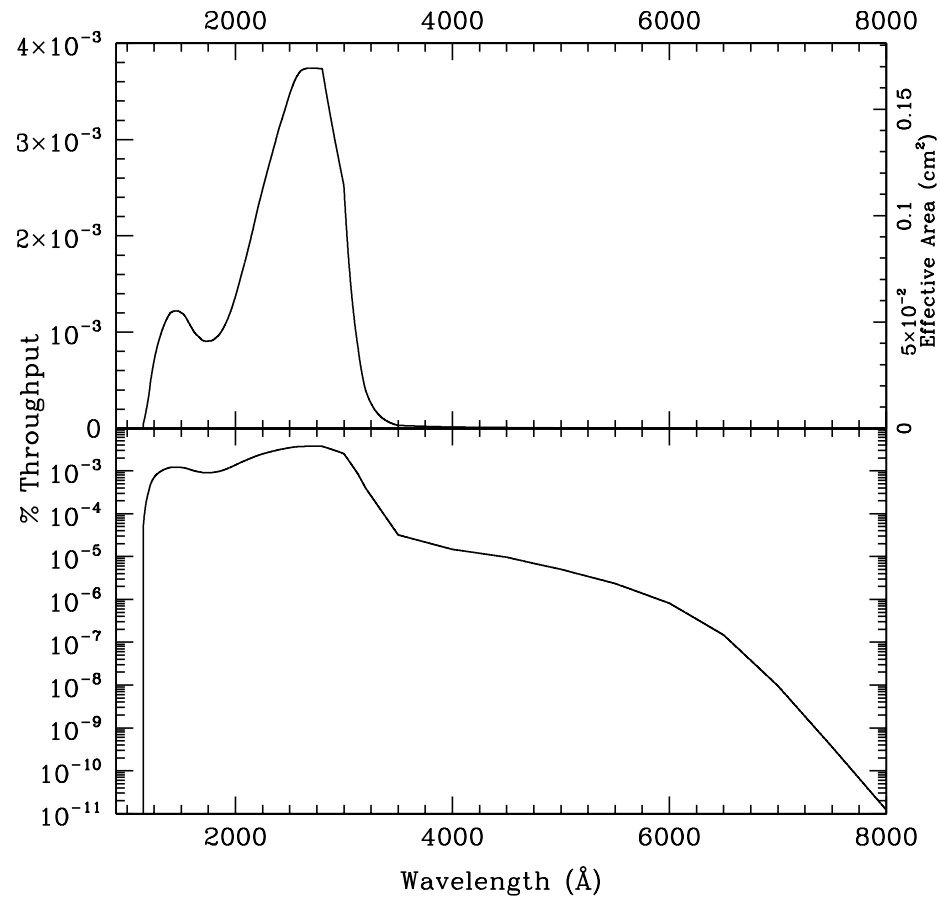


Table 14.12: Throughput and Sensitivity for F25ND3 NUV-MAMA

I	Sensitivity	Throughput %
1200.	9.75E9	4.0e-4
1300.	2.74E10	9.0e-4
1400.	3.77E10	1.2e-3
1500.	4.09E10	1.2e-3
1600.	3.80E10	1.0e-3
1700.	3.57E10	9.0e-4
1800.	3.81E10	9.0e-4
1900.	4.65E10	1.1e-3
2000.	6.27E10	1.4e-3
2100.	8.56E10	1.8e-3
2200.	1.13E11	2.3e-3
2300.	1.41E11	2.7e-3
2400.	1.70E11	3.1e-3
2500.	1.97E11	3.5e-3
2600.	2.19E11	3.7e-3
2700.	2.30E11	3.7e-3
2800.	2.33E11	3.7e-3
2900.	2.05E11	3.1e-3
3000.	1.61E11	2.4e-3
3100.	7.87E10	1.1e-3

Figure 14.29: Point Source S/N vs. $V+AB_V$ for the F25ND3 NUV-MAMA mode. Top curves are for DARKTIME. Bottom curves are for average sky. Top curves are for DARKTIME. Bottom curves are for average sky. Curves are labeled by required exposure time (sec).

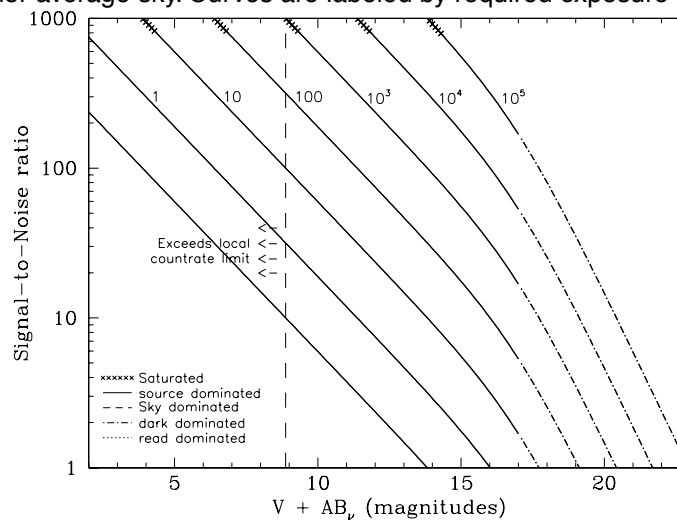
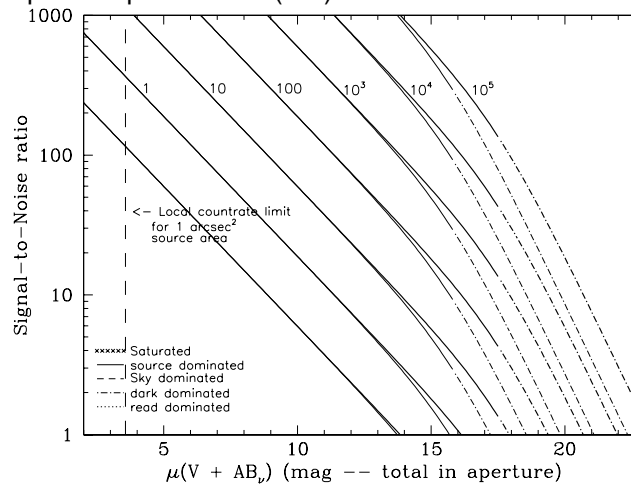


Figure 14.30: Extended Source S/N vs. $V+AB_V$ for the F25ND3 NUV-MAMA mode. Top curves are for an area of 0.2 arcsec^2 ; bottom curves are for 1 arcsec^2 . Average sky assumed. Curves are labeled by required exposure time (sec).



F25ND5—NUV-MAMA

Description

The F25ND5 mode with the NUV-MAMA provides broad band imaging with an attenuation of 5×10^{-6} . The field of view is 25×25 arcsec. The value of R_{80} and the central pixel flux are unmeasured but assumed to be approximately the same as produced by the F25QTZ filter.

Recommended Uses

Recommended for broad-band near-UV imaging of objects too bright by 2×10^5 for clear mode.

Special Considerations

The throughput of the ND5 filter and NUV-MAMA combination relative to the unfiltered NUV-MAMA varies strongly as a function of wavelength. At wavelengths between 3000 and 5000 Å the attenuation factor is close to 5×10^6 . At shorter wavelengths the relative throughput can be a factor of ten or more smaller, while at longer wavelengths it is considerably larger, so special care should be taken for red sources. To make an accurate prediction of the expected count rate, observers should use a good approximation of the source spectrum as input for the STIS ETC.

Pivot λ (Å)	FWHM (Å)	AB mag zeropoint	S_{peak}	B_{λ}	R_{80} (arcsec)	Flux in central pixel
2633.8	1514.7	9.185	5.01×10^8	594.3	0.32	8%

Figure 14.31: F25ND5 NUV-MAMA Integrated System Throughput and Redleak

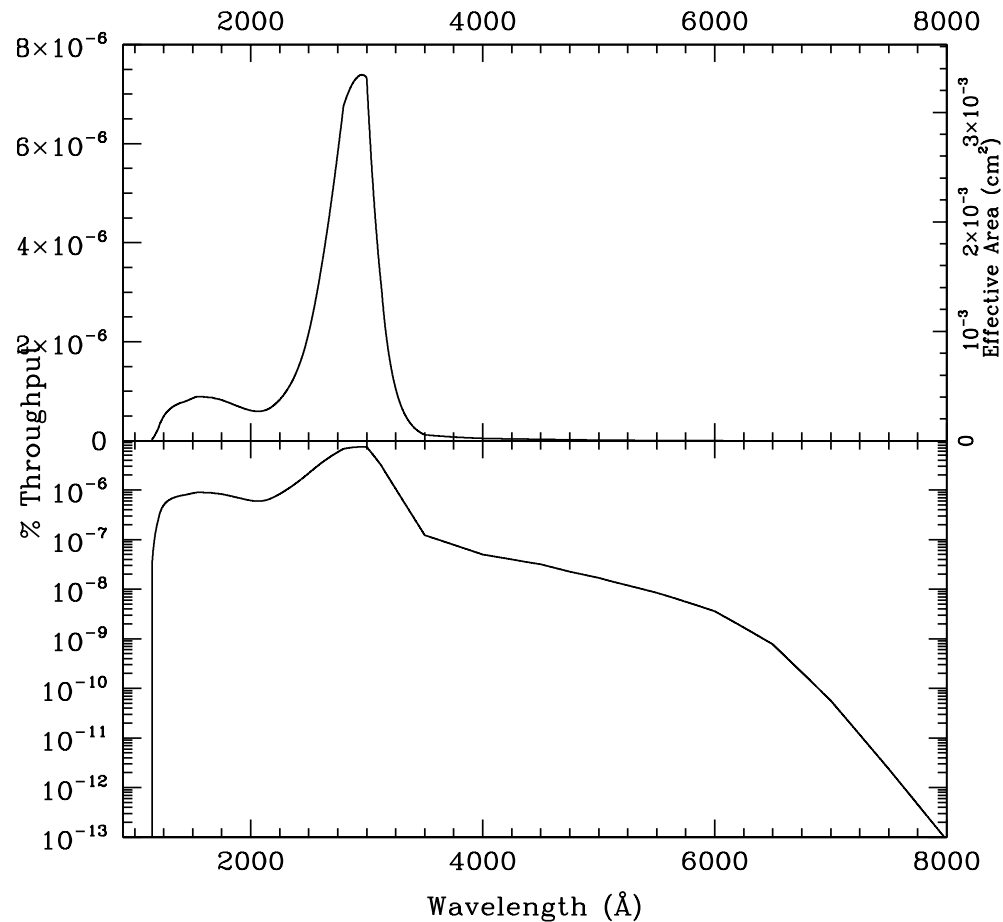


Table 14.13: Throughput and Sensitivity for F25ND5 NUV-MAMA

λ	Sensitivity	Throughput %
1200.	6.83E6	2.50e-7
1300.	1.86E7	6.27e-7
1400.	2.45E7	7.68e-7
1500.	2.94E7	8.59e-7
1600.	3.23E7	8.87e-7
1700.	3.31E7	8.54e-7
1800.	3.20E7	7.82e-7
1900.	2.99E7	6.91e-7
2000.	2.81E7	6.17e-7
2100.	2.91E7	6.09e-7
2200.	3.63E7	7.25e-7
2300.	5.17E7	9.87e-7
2400.	7.84E7	1.43e-6
2500.	1.25E8	2.20e-6
2600.	2.01E8	3.39e-6
2700.	3.03E8	4.93e-6
2800.	4.21E8	6.60e-6
2900.	4.80E8	7.27e-6
3000.	4.66E8	6.82e-6
3100.	2.68E8	3.80e-6

Figure 14.32: Point Source S/N vs. $V+AB_V$ for the F25ND5 NUV-MAMA mode. Top curves are for DARKTIME. Bottom curves are for average sky. Curves are labeled by required exposure time (sec).

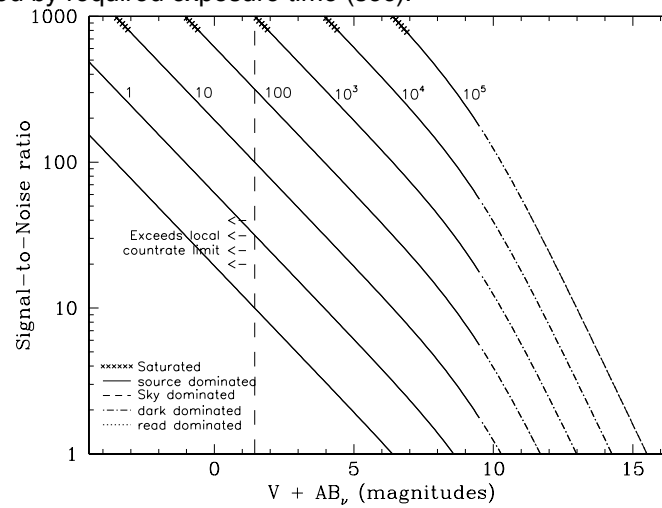
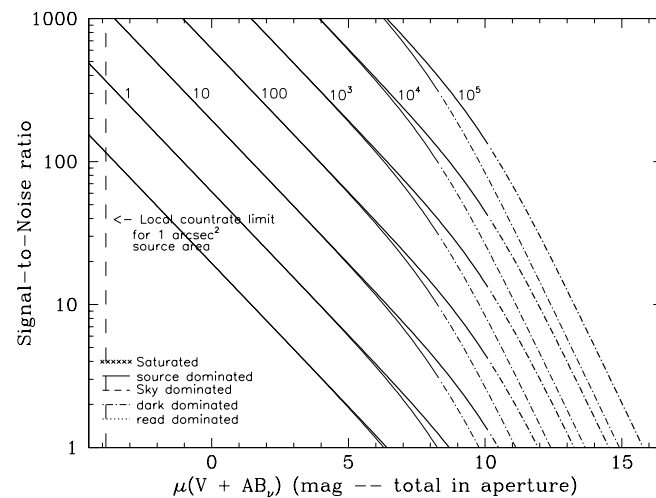


Figure 14.33: Extended Source S/N vs. $V+AB_V$ for the F25ND5 NUV-MAMA mode. Top curves are for an area of 0.2 arcsec²; bottom curves are for 1 arcsec². Average sky assumed. Curves are labeled by required exposure time (sec).



F25NDQ - NUV-MAMA

Description

The F25NDQ mode with the NUV-MAMA detector provides broad band imaging with attenuation factors varying between 10^{-1} and 10^{-4} . The full field of view is 25 X 25 arcsec, but the F25NDQ filter is unique in that it is divided into four quadrants, each having a different neutral

density factor. In clockwise order starting from the upper left these are F25NDQ1, F25NDQ2, F25NDQ3, and F25NDQ4, where the number appended to each name is the approximate dex ND factor. The R_{80} and central pixel flux are unmeasured but assumed to be approximately the same as produced by the F25SRF2 filter.

Recommended Uses

Recommended for broad-band imaging of bright objects which require attenuation of between 10^{-1} and 10^{-4} to meet NUV-MAMA bright-object limits.

Special Considerations

If a target would violate BOP restrictions in any quadrant of the F25NDQ aperture, the restrictions regarding pointing close to objects violating safety limits discussed in Chapter 7 and [STIS ISR 2000-01](#) will apply. Also the dividing lines between the quadrants are somewhat displaced from the center of the detector and are not quite parallel to the detector edges (see Figure 13.82), so observers for whom the exact locations of the quadrant boundaries are important should consult help@stsci.edu.

Aperture	pivot λ	FWHM	AB mag zeropoint	S_{peak}	B λ	R80	Flux central pixel
F25NDQ1	2277.46	1126	21.583	1.86e+13	1263	0.32	8%
F25NDQ2	2318.08	1036	19.326	2.82e+12	1098	0.32	8%
F25NDQ3	2417.84	756	16.906	3.92e+11	889	0.32	8%
F25NDQ4	2450.14	607	14.207	3.63e+10	814	0.32	8%

Figure 14.34: F25NDQ Integrated System Throughputs.

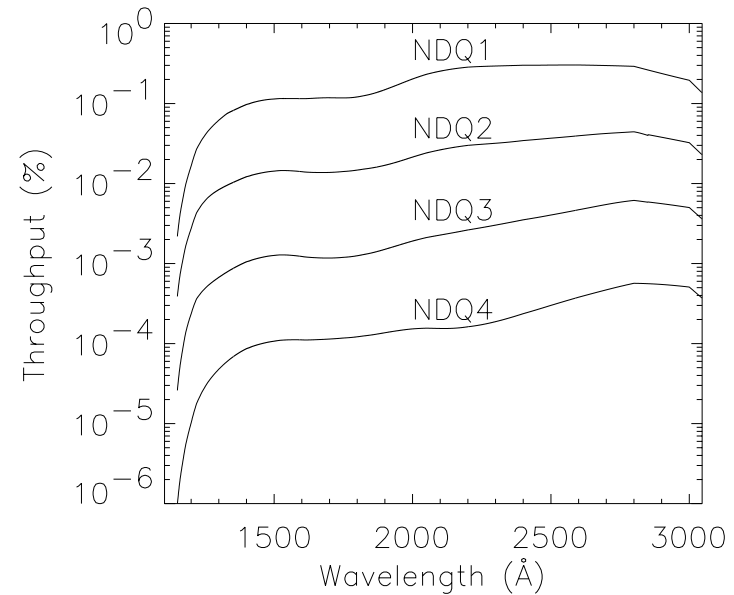


Table 14.14: Throughputs and Sensitivities for F25NDQ NUV-MAMA quadrants.

λ	Sensitivities				Throughputs			
	F25NDQ1	F25NDQ2	F25NDQ3	F25NDQ4	F25NDQ1	F25NDQ2	F25NDQ3	F25NDQ4
1200	4.51e+11	7.44e+10	6.39e+09	2.77e+08	1.65e-02	2.73e-03	2.34e-04	1.02e-05
1300	1.83e+12	2.48e+11	1.99e+10	1.41e+09	6.19e-02	8.39e-03	6.73e-04	4.79e-05
1400	3.10e+12	3.87e+11	3.35e+10	2.75e+09	9.73e-02	1.22e-02	1.05e-03	8.65e-05
1500	3.88e+12	4.88e+11	4.31e+10	3.65e+09	1.14e-01	1.43e-02	1.26e-03	1.07e-04
1600	4.19e+12	5.12e+11	4.46e+10	4.05e+09	1.15e-01	1.41e-02	1.23e-03	1.11e-04
1700	4.56e+12	5.32e+11	4.53e+10	4.40e+09	1.18e-01	1.38e-02	1.17e-03	1.14e-04
1800	4.95e+12	6.03e+11	5.12e+10	4.97e+09	1.21e-01	1.47e-02	1.25e-03	1.22e-04
1900	6.43e+12	7.30e+11	6.50e+10	5.90e+09	1.49e-01	1.69e-02	1.51e-03	1.37e-04
2000	9.21e+12	9.73e+11	8.69e+10	6.94e+09	2.03e-01	2.14e-02	1.91e-03	1.53e-04
2100	1.21e+13	1.26e+12	1.08e+11	7.38e+09	2.54e-01	2.64e-02	2.27e-03	1.55e-04
2200	1.43e+13	1.50e+12	1.32e+11	8.11e+09	2.85e-01	3.00e-02	2.63e-03	1.62e-04
2300	1.54e+13	1.67e+12	1.58e+11	9.83e+09	2.95e-01	3.19e-02	3.02e-03	1.88e-04
2400	1.64e+13	1.88e+12	1.92e+11	1.29e+10	3.01e-01	3.45e-02	3.52e-03	2.37e-04
2500	1.72e+13	2.10e+12	2.30e+11	1.71e+10	3.03e-01	3.69e-02	4.05e-03	3.00e-04
2600	1.79e+13	2.34e+12	2.78e+11	2.24e+10	3.03e-01	3.96e-02	4.71e-03	3.80e-04
2700	1.83e+13	2.59e+12	3.36e+11	2.88e+10	2.98e-01	4.23e-02	5.47e-03	4.69e-04
2800	1.86e+13	2.82e+12	3.92e+11	3.61e+10	2.92e-01	4.44e-02	6.16e-03	5.67e-04
2900	1.56e+13	2.50e+12	3.70e+11	3.61e+10	2.37e-01	3.79e-02	5.61e-03	5.48e-04
3000	1.33e+13	2.21e+12	3.41e+11	3.47e+10	1.95e-01	3.24e-02	5.01e-03	5.08e-04
3100	6.31e+12	1.07e+12	1.72e+11	1.78e+10	8.95e-02	1.52e-02	2.44e-03	2.53e-04

F25QTZ—NUV-MAMA, Longpass

Description

The F25QTZ filter with the NUV-MAMA provides high-throughput broad-band near-UV imaging with better rejection of geocoronal emission than the F25MAMA or F25SRF2 modes, the same field of view, and the same high spatial resolution.

Recommended Uses

Recommended for broad-band near-UV imaging of faint targets.

Special Considerations

Sky background on the day side of the orbit contains a significant contribution from [O II] air glow emission at 2471 Å. In high-background conditions, the sky background can dominate the detector background. In average day-side observing conditions about half the background will be from the sky and half from detector dark current. Observers can limit the background (with some cost to the total amount of observing time per orbit) by using the DARKTIME special requirement.

Users should also consider whether the ACS HRC with the F220W or the F250W filter might be a better choice for their science goals.

Pivot λ (Å)	FWHM (Å)	AB mag zeropoint	S_{peak}	B_{λ}	R_{80} (arcsec)	Flux in central pixel
2364.8	995.1	23.781	1.54e+14	1089.1	0.32	8%

Figure 14.35: F25QTZ NUV-MAMA Integrated System Throughput and Redleak

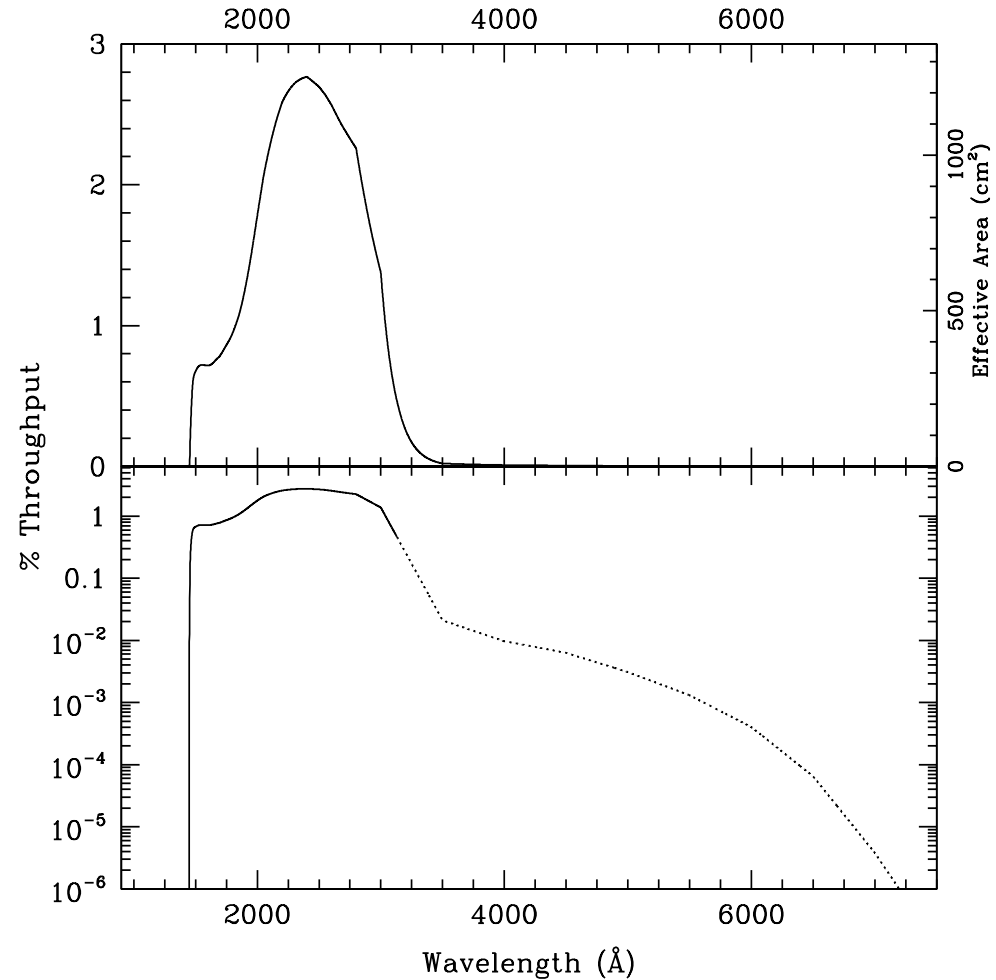


Table 14.15: Throughput and Sensitivity for F25QTZ NUV-MAMA

I	Sensitivity	Throughput %
1500.	2.01E13	0.59
1600.	2.63E13	0.72
1700.	3.08E13	0.79
1800.	3.91E13	0.95
1900.	5.48E13	1.27
2000.	8.10E13	1.78
2100.	1.08E14	2.26
2200.	1.29E14	2.57
2300.	1.42E14	2.71
2400.	1.51E14	2.76
2500.	1.53E14	2.69
2600.	1.52E14	2.56
2700.	1.48E14	2.40
2800.	1.41E14	2.21
2900.	1.17E14	1.77
3000.	8.85E13	1.30

Figure 14.36: Point Source S/N vs. $V+AB_V$ for the F25QTZ NUV-MAMA mode. Top curves are for DARKTIME. Bottom curves are for average sky. Curves are labeled by required exposure time (sec).

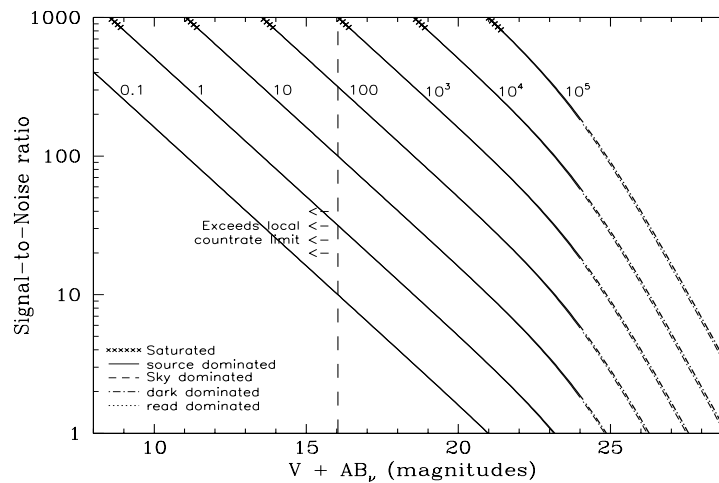


Figure 14.37: Extended Source S/N vs. $V+AB_V$ for the F25QTZ NUV-MAMA mode. Top curves are for an area of 0.2 arcsec^2 ; bottom curves are for 1 arcsec^2 . Average sky assumed. Curves are labeled by required exposure time (sec).

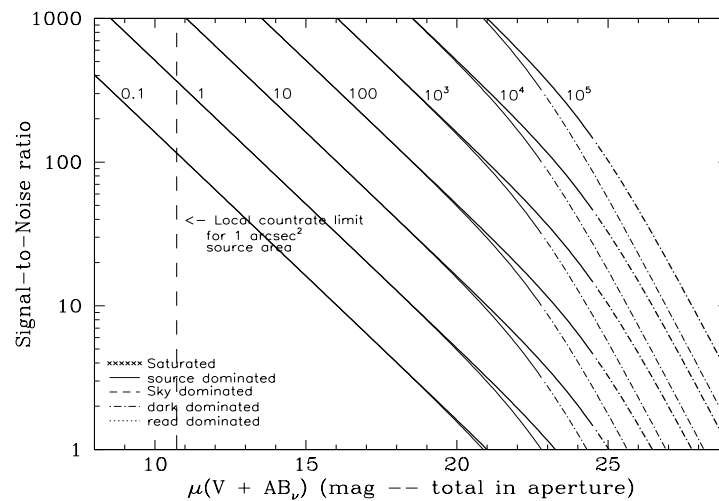


Table 14.16: Radial Profile for F25QTZ*

Radius			Fraction of Energy Encircled
Pixel	Arcsec	Intensity	
1	0.024	6.046e-02	0.210
2	0.037	4.292e-02	0.328
2	0.049	2.825e-02	0.440
3	0.073	1.036e-02	0.591
4	0.098	4.085e-03	0.667
5	0.122	1.839e-03	0.718
10	0.245	2.099e-04	0.820
15	0.367	9.929e-05	0.874
20	0.490	4.775e-05	0.911
25	0.613	2.706e-05	0.934
30	0.735	1.876e-05	0.953
40	0.980	8.441e-06	0.983

* See [STIS ISR 2003-01](#).

Figure 14.38: Point Source PSF for F25QTZ NUV-MAMA, 7."5 square (at pixel 606,649, log scaled). Note PSF ghost ~45 pixels left of peak pixel and a few 10^{-3} of the peak.

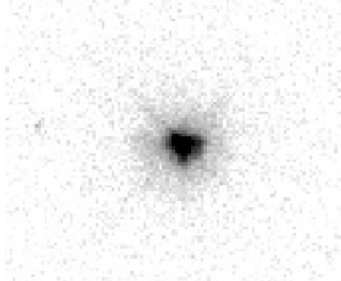


Figure 14.39: Point Source Encircled Energy for F25QTZ NUV-MAMA

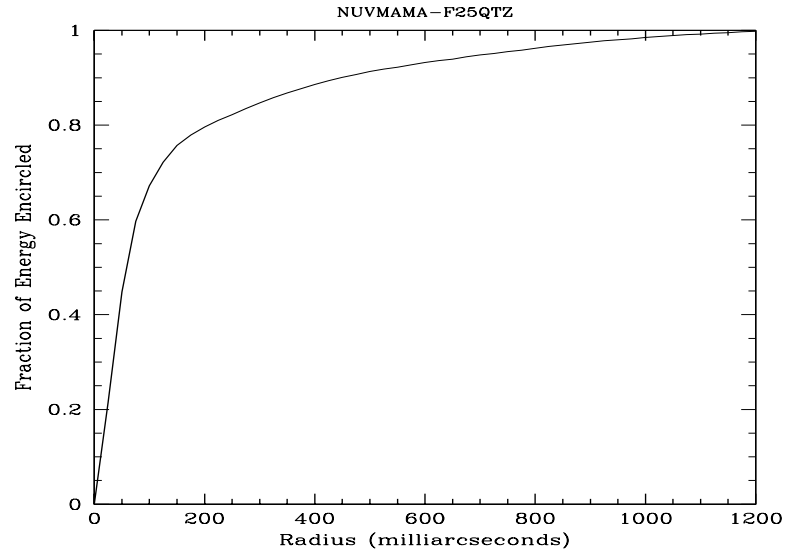
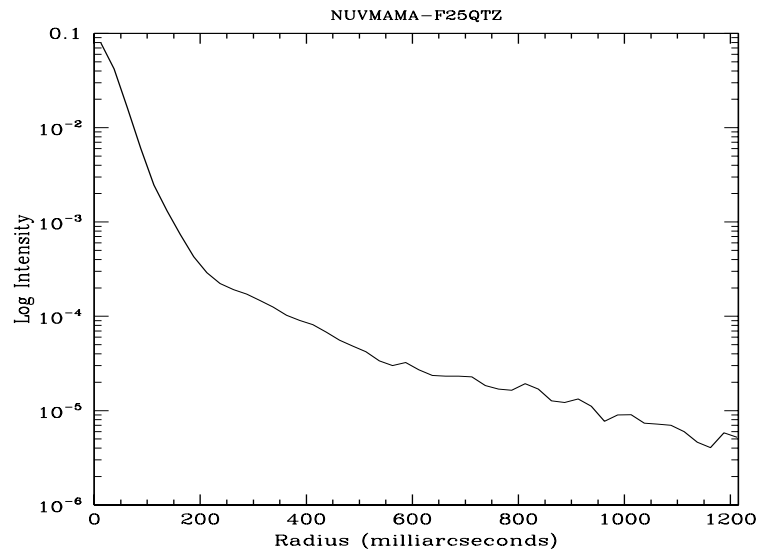


Figure 14.40: Point Source Intensity vs. Radius for F25QTZ NUV-MAMA



F25SRF2—NUV-MAMA, Longpass

Description

The F25SRF2 filter with the NUV-MAMA provides high-throughput broad-band near-UV imaging with better rejection of geocoronal emission than the F25MAMA but worse than or F25QTZ modes. It provides the same field of view and high spatial resolution.

Recommended Uses

This filter has slightly higher throughput than F25QTZ, but lets in geocoronal [O I] 1302 + 1306 Å. In most cases the sky background will still be lower than the detector background.

Special Considerations

Sky background on the day side of the orbit contains a significant contributions from [OII] air glow emission at 2471 Å and [O I] air glow at 1302 + 1306 Å. In high-background conditions, the sky background can dominate the detector background. In average day-side observing conditions about half the background will be from the sky and half from detector dark current. Also, the background through F25SRF2 will be about 10% higher than through F25QTZ. Observers can limit the background by using the DARKTIME special requirement.

Users should also consider whether the ACS HRC with the F220W or the F250W filter might be a better choice for their science goals.

Pivot λ (Å)	FWHM (Å)	AB mag zeropoint	S_{peak}	B_{λ}	R_{80} (arcsec)	Flux in central pixel
2299.3	1127.7	23.915	1.59e+14	1126.5	0.32	8%

Figure 14.41: F25SRF2 NUV-MAMA Integrated System Throughput and Redleak

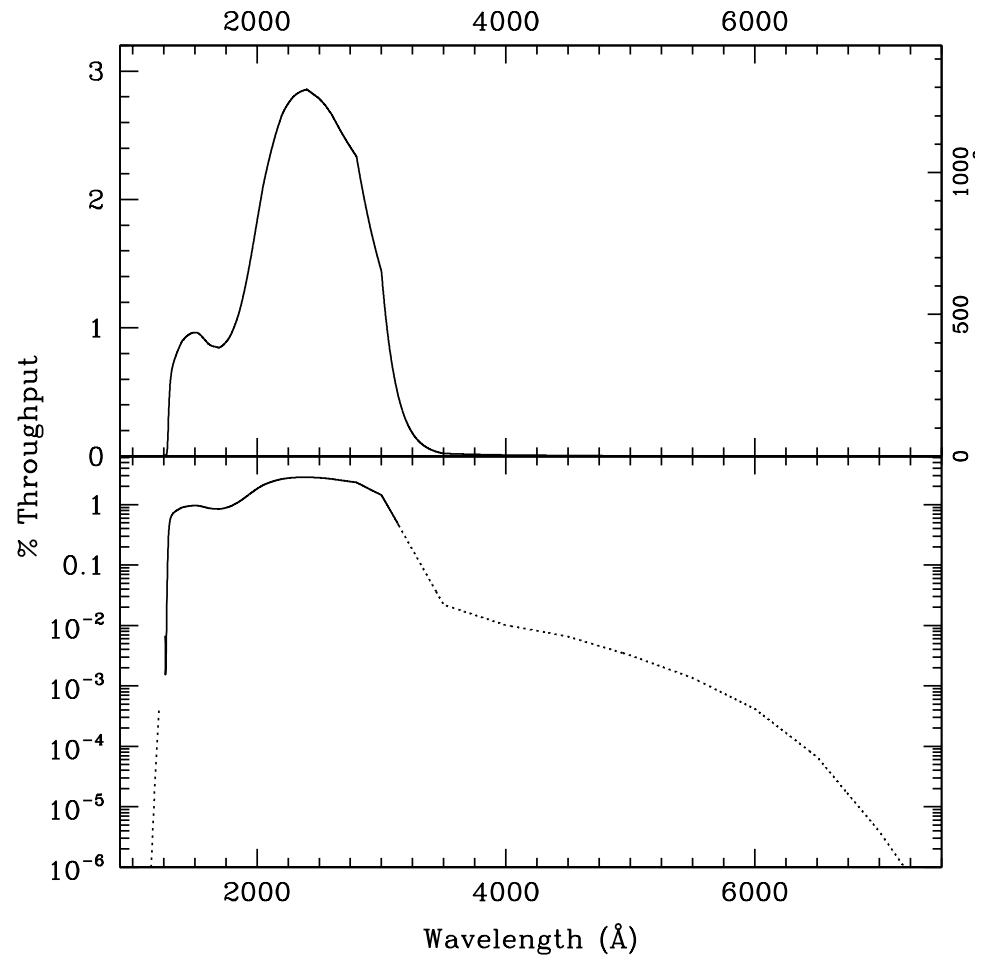


Table 14.17: Throughput and Sensitivity for F25SRF2 NUV-MAMA

I	Sensitivity	Throughput %
1300.	1.23E13	0.42
1400.	2.83E13	0.89
1500.	3.27E13	0.96
1600.	3.25E13	0.89
1700.	3.32E13	0.86
1800.	4.01E13	0.98
1900.	5.64E13	1.30
2000.	8.32E13	1.83
2100.	1.11E14	2.32
2200.	1.33E14	2.64
2300.	1.47E14	2.80
2400.	1.56E14	2.84
2500.	1.58E14	2.78
2600.	1.57E14	2.66
2700.	1.53E14	2.49
2800.	1.46E14	2.28
2900.	1.21E14	1.83
3000.	9.26E13	1.36
3100.	4.58E13	0.65
3200.	2.04E13	0.28

Figure 14.42: Point Source S/N vs. $V+AB_V$ for the F25SRF2 NUV-MAMA mode. Top curves are for DARKTIME. Bottom curves are for average sky. Curves are labeled by required exposure time (sec).

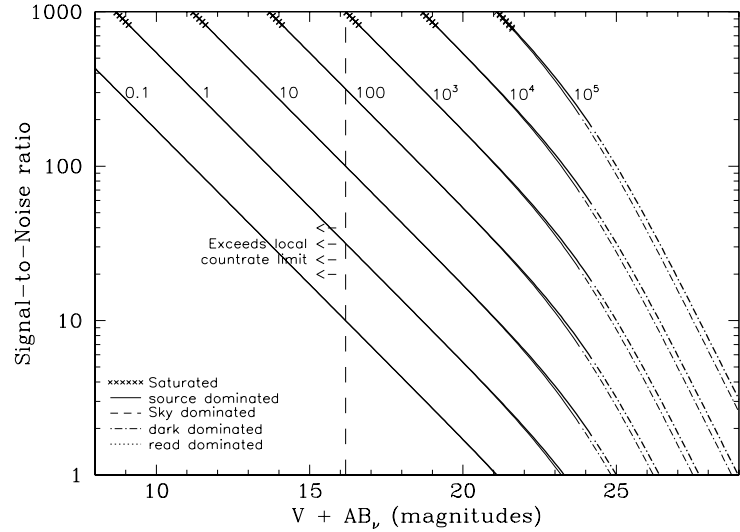
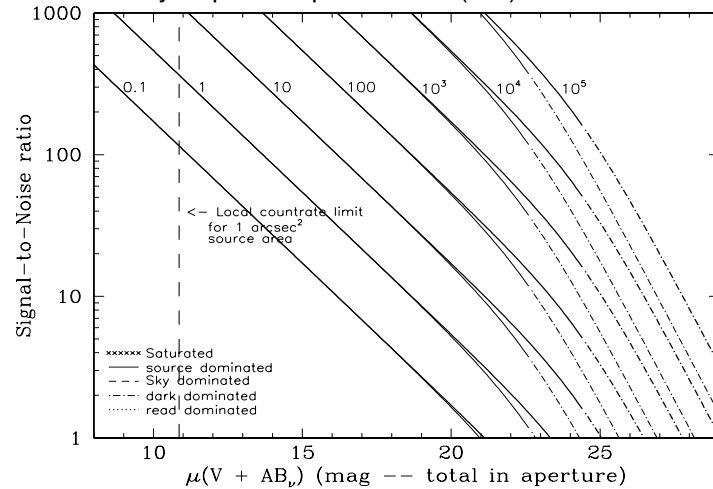


Figure 14.43: Extended Source S/N vs. $V+AB_V$ for the F25SRF2 NUV-MAMA mode. Top curves are for an area of 0.2 arcsec^2 ; bottom curves are for 1 arcsec^2 . Average sky assumed. Curves are labeled by required exposure time (sec).



F25MGII—NUV-MAMA

Description

The F25MGII filter with the NUV-MAMA provides narrow-band imaging centered on the 2798 Å Mg II feature.

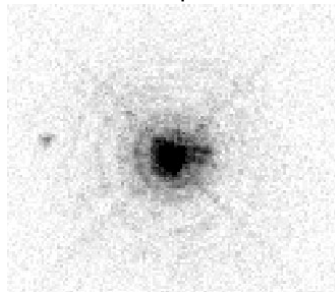
Recommended Uses

Narrowband imaging.

Special Considerations

There is a substantial redleak in this filter. Sources with a red underlying continuum may be difficult to observe. Users should be careful to take into account the underlying continuum in estimating whether the observation will fall within the bright-object protection limits. This filter also has a complex PSF and exhibits several ghosts.

Figure 14.44: Point Source PSF for F25MGII NUV-MAMA 7."5 square (at pixel 316,658, log scaled, B-V=-0.04). Note psf ghost ~45 pixels left of peak pixel and a few 10^{-3} of the peak, as well as the much more complex ghost about 10 pixels to the right of the central pixel.



Pivot λ (Å)	FWHM (Å)	AB mag zeropoint	S_{peak}	B_{λ}	R_{80} (arcsec)	Flux in central pixel
2801.8	45.0	19.463	8.22+13	55.9	0.18	14%

Figure 14.45: F25MGII NUV-MAMA Integrated System Throughput and Redleak

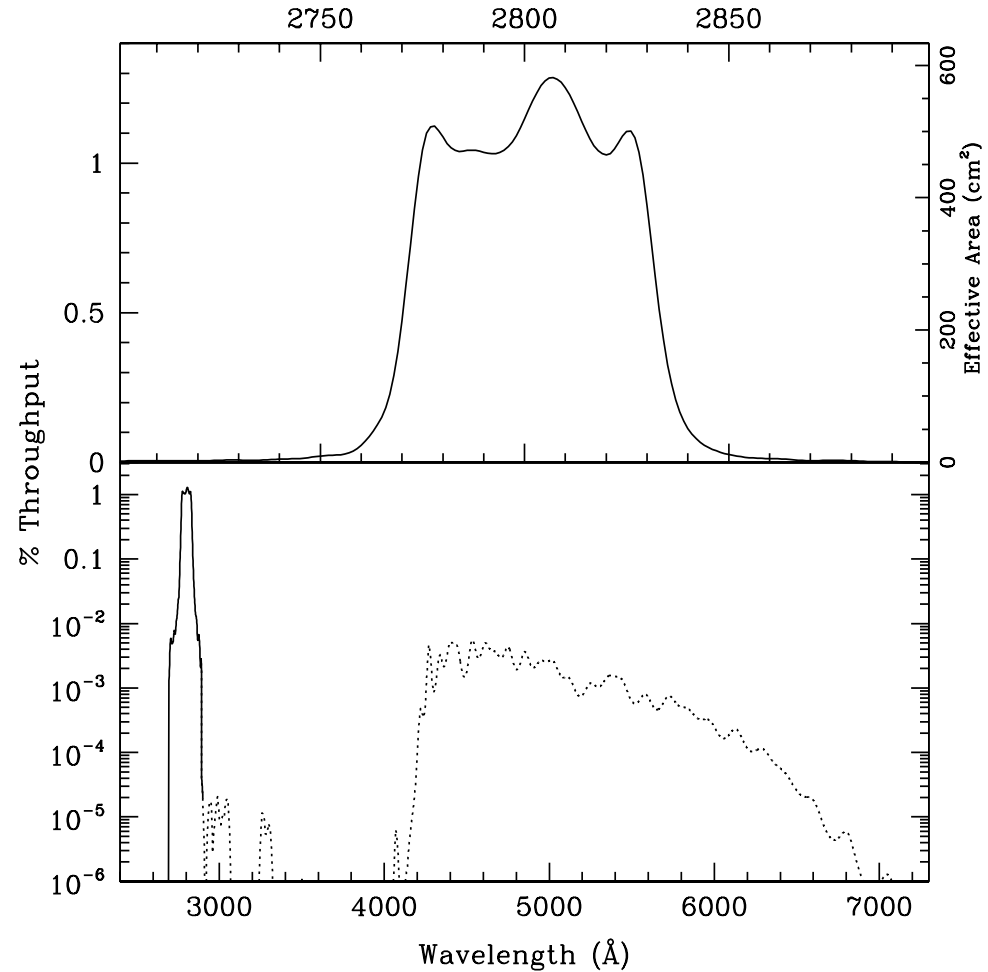


Table 14.18: Throughput and Sensitivity for F25MGII NUV-MAMA

I	Sensitivity	Throughput %
2765.	9.94E12	0.16
2770.	3.09E13	0.49
2775.	6.41E13	1.01
2780.	6.88E13	1.09
2785.	6.61E13	1.04
2790.	6.59E13	1.04
2795.	6.67E13	1.05
2800.	7.32E13	1.15
2805.	8.10E13	1.27
2810.	7.98E13	1.25
2815.	7.13E13	1.11
2820.	6.65E13	1.04
2825.	7.02E13	1.09
2830.	5.44E13	0.84
2835.	2.22E13	0.34
2840.	7.68E12	0.12
2845.	3.32E12	0.05
2850.	1.74E12	0.03

Figure 14.46: Point Source S/N vs. $V+AB_v$ for the F25MGII NUV-MAMA mode. Curves are labeled by required exposure time (sec).

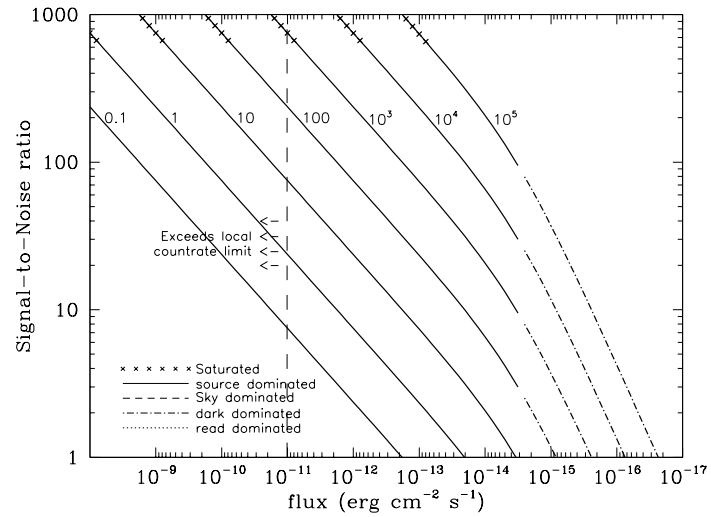


Figure 14.47: Extended Source S/N vs. $V+AB_v$ for the F25MGII NUV-MAMA mode. Top curves are for an area of 0.2 arcsec²; bottom curves are for 1 arcsec². Average sky assumed. Curves are labeled by required exposure time (sec).

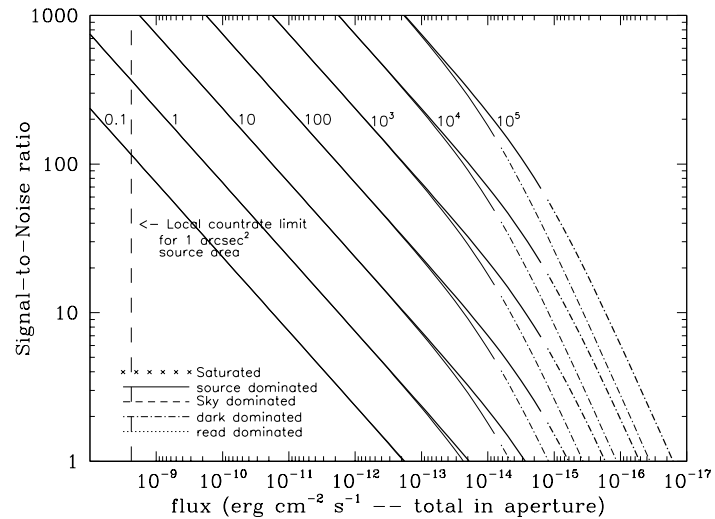


Table 14.19: Radial Profile for F25MGII*

Radius		Intensity	Fraction of Energy Encircled
Pixels	Arcsec		
1	0.024	5.302e-02	0.257
2	0.037	2.834e-02	0.391
2	0.049	1.466e-02	0.510
3	0.073	4.989e-03	0.641
4	0.098	1.739e-03	0.697
5	0.122	1.302e-03	0.738
10	0.245	2.035e-04	0.843
15	0.367	1.119e-04	0.899
20	0.490	3.763e-05	0.932
25	0.613	2.057e-05	0.949
30	0.735	1.692e-05	0.965
40	0.980	6.931e-06	0.988

* See [STIS ISR 2003-01](#).

Figure 14.48: Point Source Encircled Energy for F25MGII NUV-MAMA

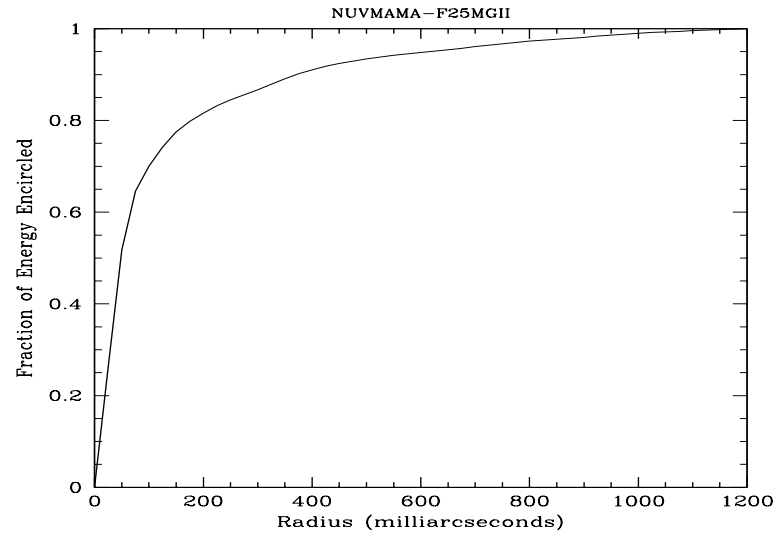
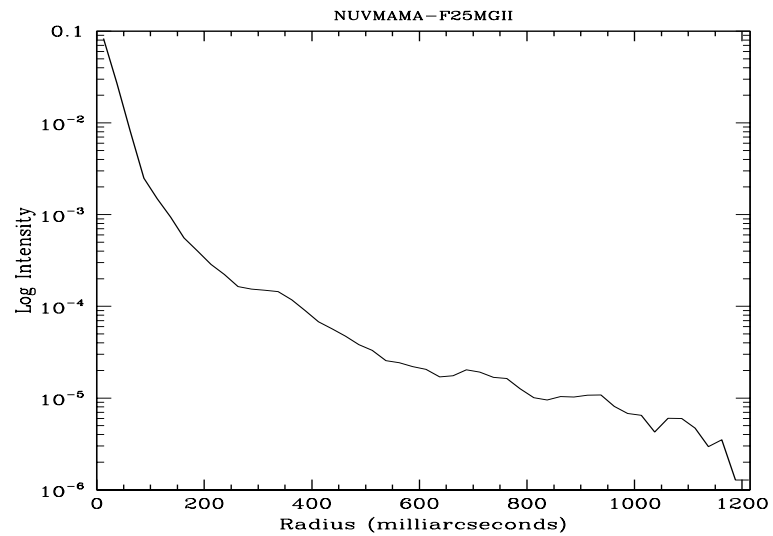


Figure 14.49: Point Source Intensity vs. Radius for F25MGII NUV-MAMA



F25CN270—NUV-MAMA

Description

The F25CN270 filter with the NUV-MAMA provides medium bandwidth imaging near the 2798 Å MgII feature.

Recommended Uses

Continuum filter for MgII imaging.

Special Considerations

There is a substantial redleak in this filter. Sources with a red underlying continuum may be difficult to observe. Users should be careful to take into account the underlying continuum in estimating whether the observation will fall within the bright-object protection limits.

Pivot λ (Å)	FWHM (Å)	AB mag zeropoint	S_{peak}	B_{λ}	R_{80} (arcsec)	Flux in central pixel
2709.2	155.1	21.361	1.24e+14	202.3	0.17	14%

Figure 14.50: F25CN270 NUV-MAMA Integrated System Throughput and Redleak

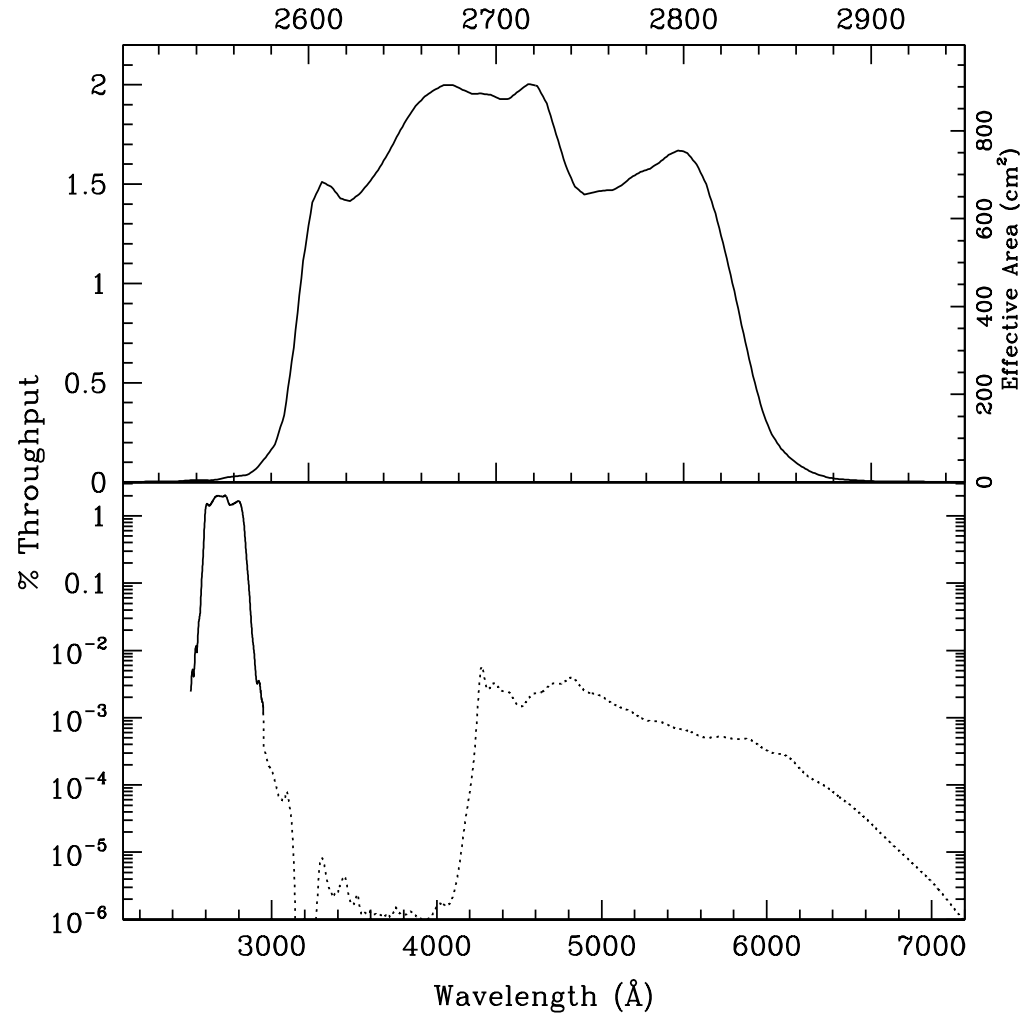


Table 14.20: Throughput and Sensitivity for F25CN270 NUV-MAMA

I	Sensitivity	Throughput %
2575.	7.44E12	0.13
2600.	6.80E13	1.15
2625.	8.77E13	1.47
2650.	1.07E14	1.78
2675.	1.21E14	1.98
2700.	1.20E14	1.94
2725.	1.17E14	1.88
2750.	9.25E13	1.48
2775.	9.76E13	1.54
2800.	1.04E14	1.62
2825.	6.63E13	1.03
2850.	1.50E13	0.23

Figure 14.51: Point Source S/N vs. $V+AB_V$ for the F25CN270 NUV-MAMA mode. Curves are labeled by required exposure time (sec).

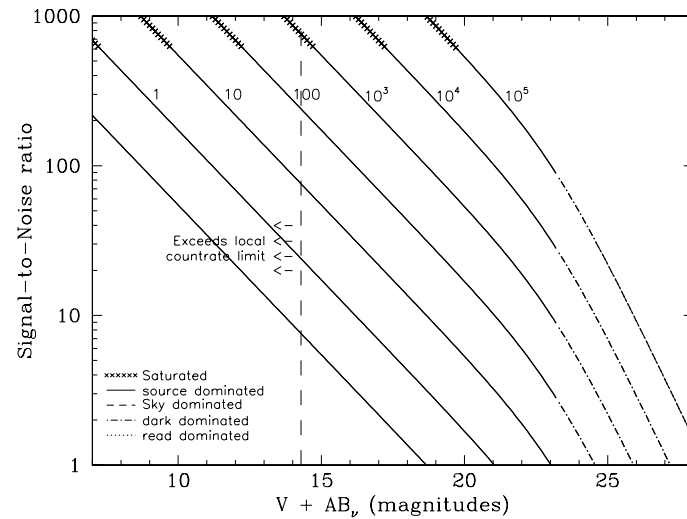


Figure 14.52: Extended Source S/N vs. $V+AB_V$ for the F25CN270 NUV-MAMA mode. Top curves are for an area of 0.2 arcsec^2 ; bottom curves are for 1 arcsec^2 . Average sky assumed. Curves are labeled by required exposure time (sec).

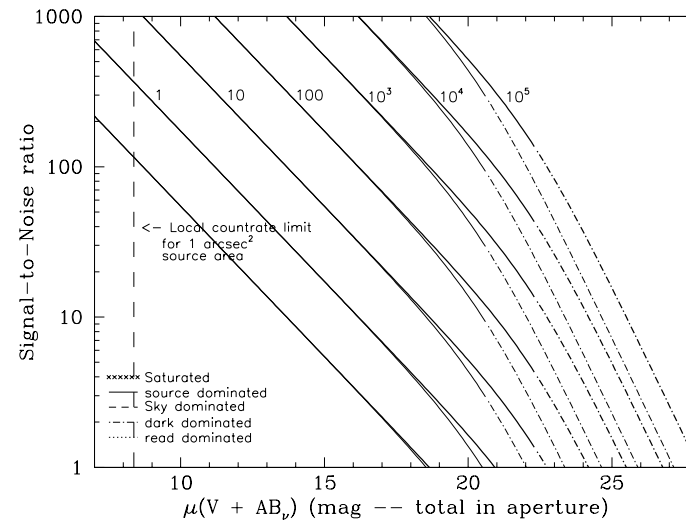


Table 14.21: Radial Profile for F25CN270*

Radius		intensity	Fraction of Energy Encircled
Pixels	Arcsec		
1	0.024	5.158e-02	0.240
2	0.037	2.953e-02	0.378
2	0.049	1.608e-02	0.504
3	0.073	5.260e-03	0.643
4	0.098	2.022e-03	0.708
5	0.122	1.215e-03	0.750
10	0.245	2.048e-04	0.854
15	0.367	9.848e-05	0.908
20	0.490	4.138e-05	0.942
25	0.613	1.817e-05	0.960
30	0.735	1.440e-05	0.974
40	0.980	4.656e-06	0.994

* See [STIS ISR 2003-01](#).

Figure 14.53: Point Source Encircled Energy for F25CN270 NUV-MAMA

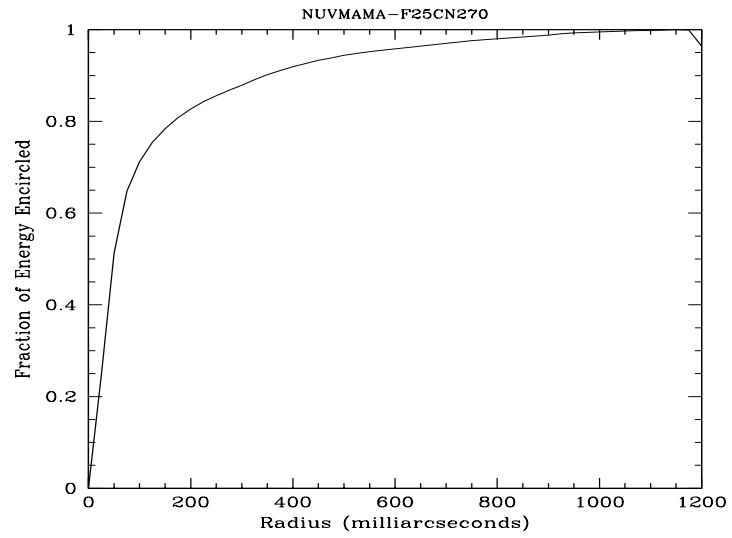
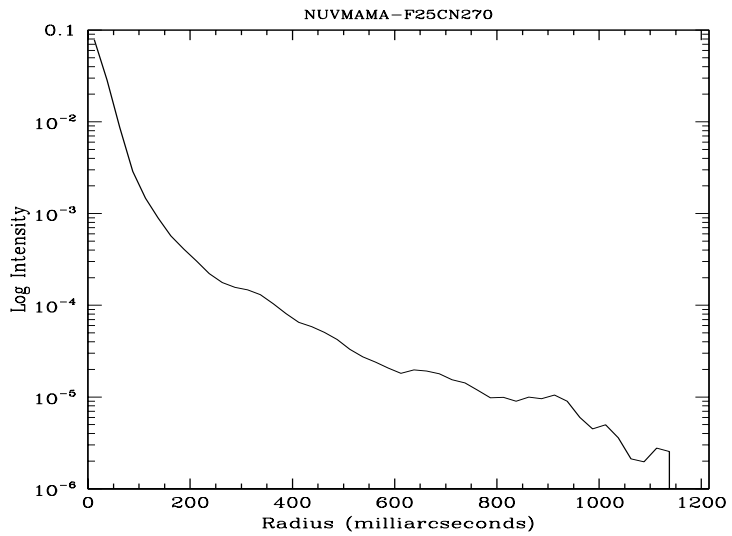


Figure 14.54: Point Source Intensity vs. Radius for F25CN270 NUV-MAMA



F25CIII—NUV-MAMA

Description

The F25CIII filter with the NUV-MAMA provides narrow band imaging of the C III] 1907 + 1909 Å feature.

Recommended Uses

C III] imaging.

Pivot λ (Å)	FWHM (Å)	AB mag zeropoint	S_{peak}	B_{λ}	R_{80} (arcsec)	Flux in central pixel
1989.5	173.5	19.313	1.05×10^{13}	207.6	0.23	10%

Figure 14.55: F25CIII NUV-MAMA Integrated System Throughput and Redleak

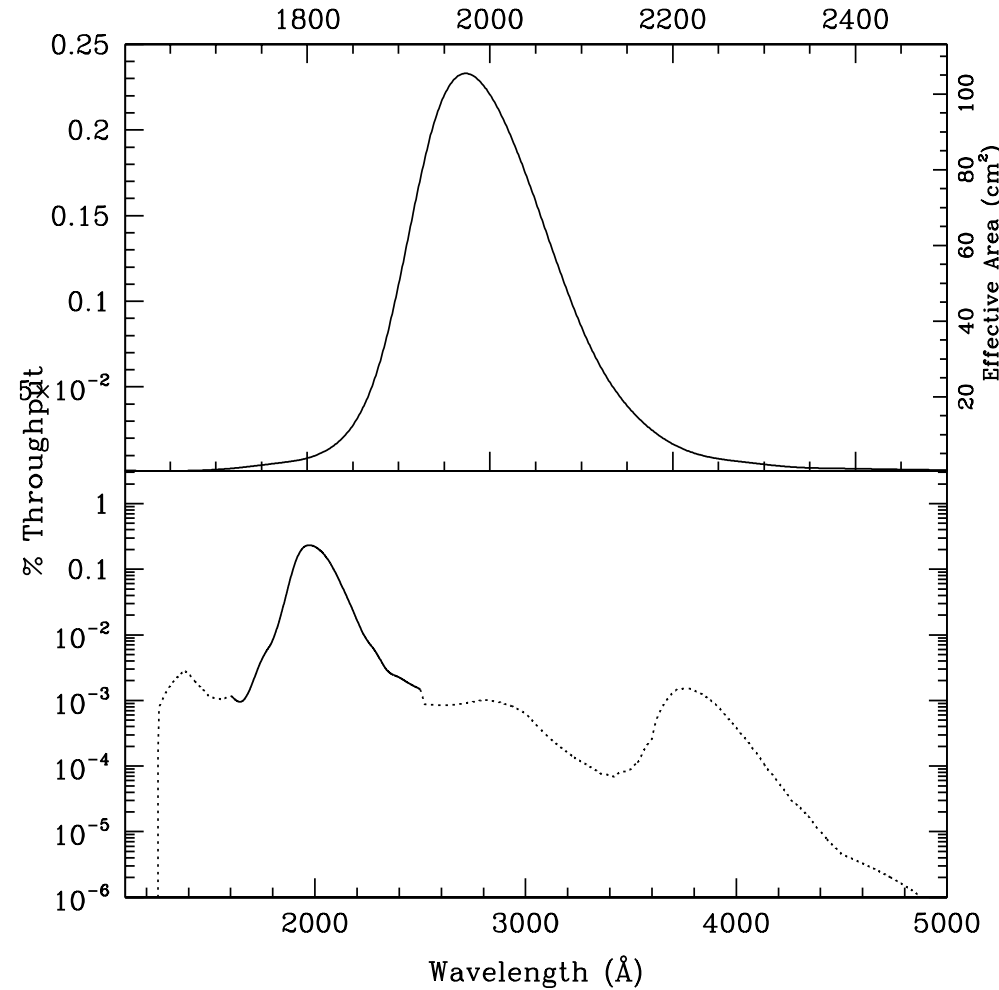


Table 14.22: Throughput and Sensitivity for F25CIII NUV-MAMA

I	Sensitivity	Throughput %
1750.	1.74E11	0.00
1800.	3.68E11	0.01
1850.	1.27E12	0.03
1900.	4.84E12	0.11
1950.	9.54E13	0.21
2000.	9.94E13	0.22
2050.	7.36E12	0.16
2100.	4.14E12	0.09
2150.	1.96E12	0.04
2200.	8.65E11	0.02
2250.	4.25E11	0.01

Figure 14.56: Point Source S/N vs. $V+AB_V$ for the F25CIII NUV-MAMA mode. Curves are labeled by required exposure time (sec).

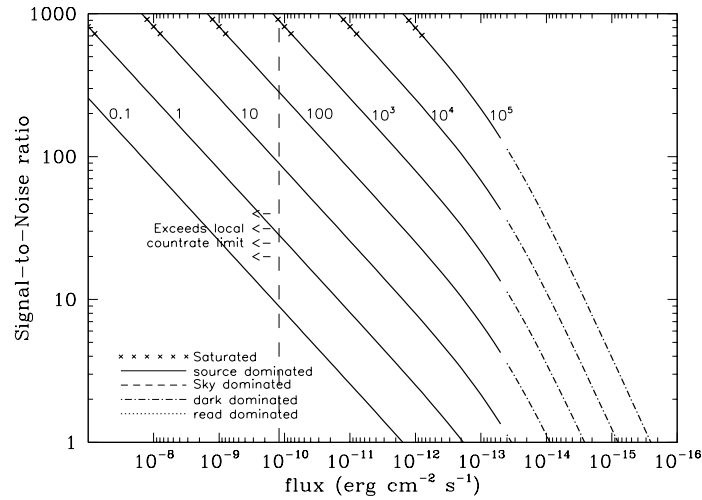


Figure 14.57: Extended Source S/N vs. $V+AB_V$ for the F25CIII NUV-MAMA mode. Top curves are for an area of 0.2 arcsec²; bottom curves are for 1 arcsec². Average sky assumed. Curves are labeled by required exposure time (sec).

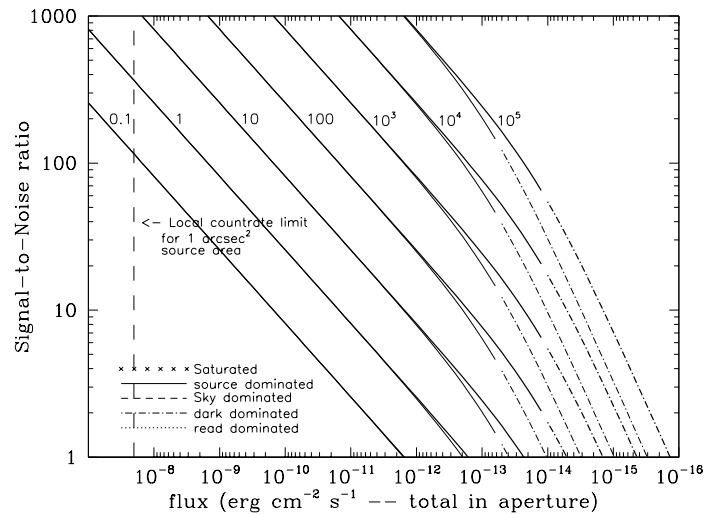


Table 14.23: Radial Profile for F25CIII*

Radius			Fraction of Energy Encircled
Pixels	Arcsec	intensity	
1	0.024	4.859e-02	0.173
2	0.037	3.660e-02	0.284
2	0.049	2.557e-02	0.392
3	0.073	9.899e-03	0.528
4	0.098	3.609e-03	0.598
5	0.122	1.832e-03	0.649
10	0.245	2.759e-04	0.753
15	0.367	1.339e-04	0.822
20	0.490	7.056e-05	0.873
25	0.613	4.358e-05	0.911
30	0.735	3.353e-05	0.944
40	0.980	1.002e-05	0.981

* See [STIS ISR 2003-01](#).

Figure 14.58: Point Source PSF for F25CIII NUV-MAMA, 7."5 square (at pixel 741,402, log scaled, B-V=-0.04). Note PSF ghost ~45 pixels left of peak pixel and a few 10^{-3} of the peak

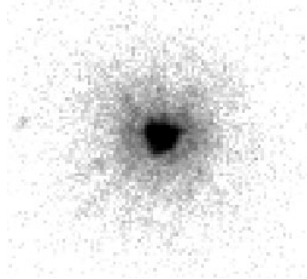


Figure 14.59: Point Source Encircled Energy for F25CIII NUV-MAMA

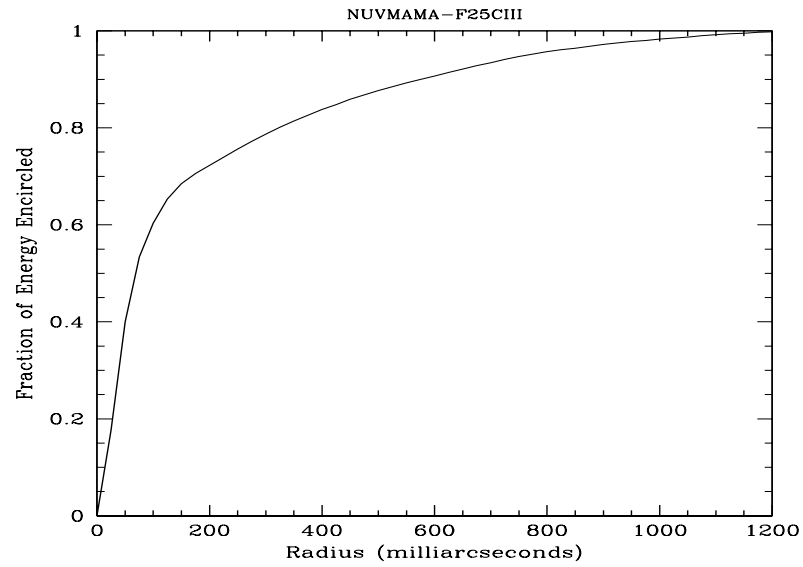
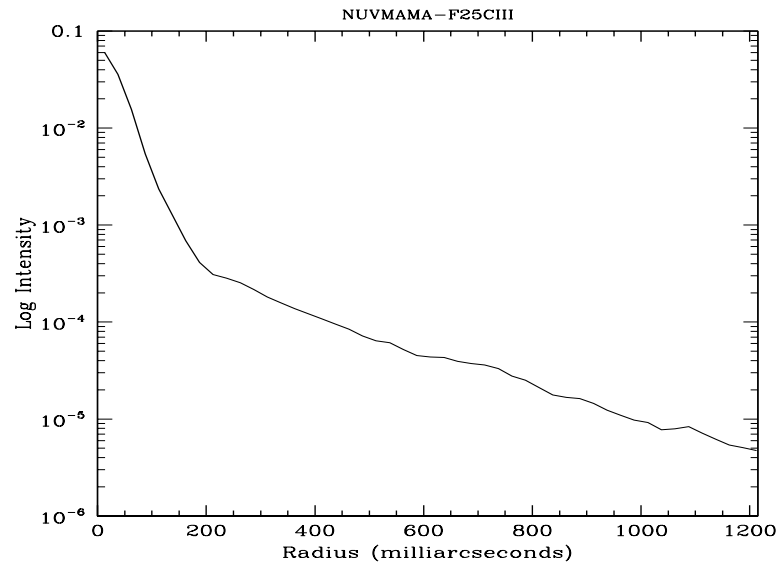


Figure 14.60: Point Source Intensity vs. Radius for F25CIII NUV-MAMA



F25CN182—NUV-MAMA

Description

The F25CN182 filter with the NUV-MAMA provides medium bandwidth imaging of the continuum near 1900 Å.

Recommended Uses

Continuum filter for C III].

Pivot λ (Å)	FWHM (Å)	AB mag zeropoint	S_{peak}	B_{λ}	R_{80} (arcsec)	Flux in central pixel
1982.0	514.2	21.478	$2.59\text{e}+13$	627.6	0.23	10%

Figure 14.61: F25CN182 NUV-MAMA Integrated System Throughput and Redleak

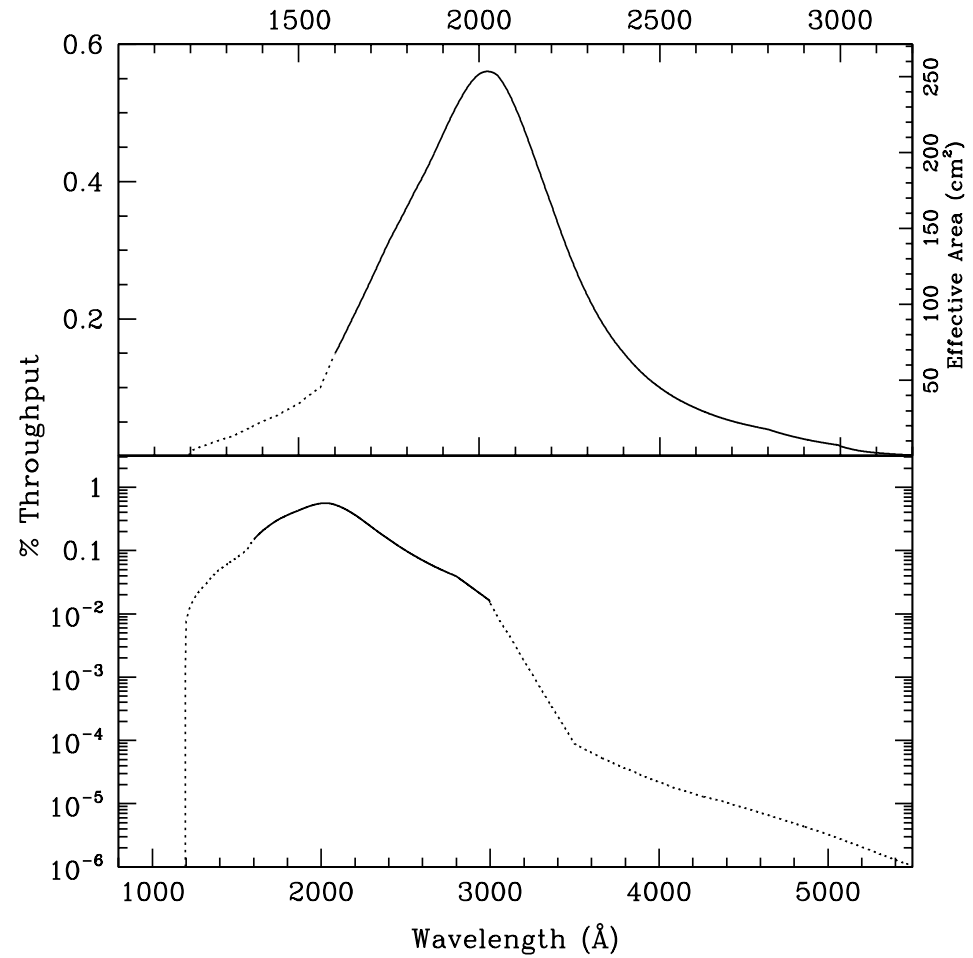


Table 14.24: Throughput and Sensitivity for F25CN182 NUV-MAMA

I	Sensitivity	Throughput %
1300.	7.97E11	0.03
1400.	1.60E12	0.05
1500.	2.68E12	0.08
1600.	5.37E12	0.15
1700.	9.95E12	0.26
1800.	1.49E13	0.36
1900.	2.03E13	0.47
2000.	2.51E13	0.55
2100.	2.41E13	0.50
2200.	1.83E13	0.37
2300.	1.24E13	0.24
2400.	8.29E12	0.15
2500.	5.74E12	0.10
2600.	4.18E12	0.07
2700.	3.17E12	0.05
2800.	2.46E12	0.04

Figure 14.62: Point Source S/N vs. $V+AB_V$ for the F25CN182 NUV-MAMA mode. Curves are labeled by required exposure time (sec).

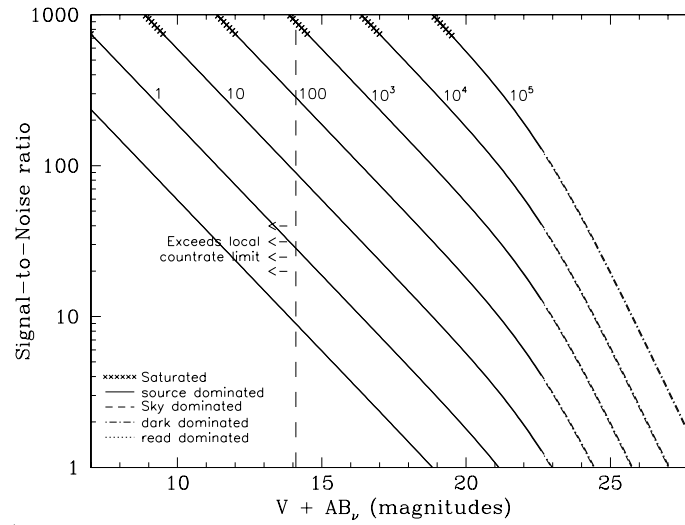


Figure 14.63: Extended Source S/N vs. $V+AB_V$ for the F25CN182 NUV-MAMA mode. Top curves are for an area of 0.2 arcsec^2 ; bottom curves are for 1 arcsec^2 . Average sky assumed. Curves are labeled by required exposure time (sec).

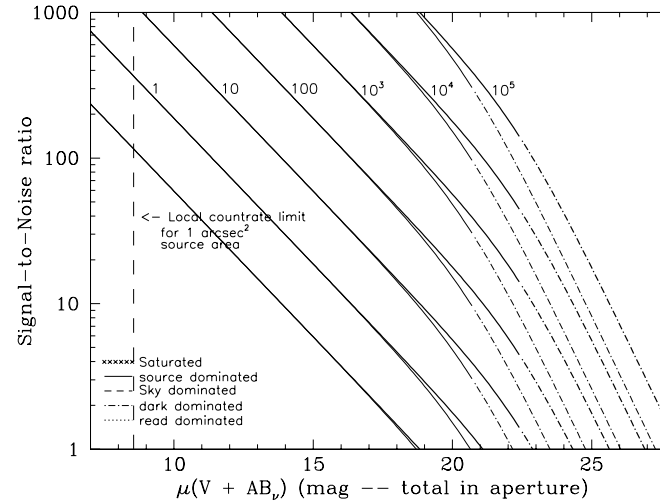


Table 14.25: Radial Profile for F25CN182*

Radius		Intensity	Fraction of Energy Encircled
Pixels	Arcsec		
1	0.024	4.177e-02	0.179
2	0.037	2.686e-02	0.302
2	0.049	1.620e-02	0.422
3	0.073	5.757e-03	0.565
4	0.098	2.720e-03	0.647
5	0.122	1.425e-03	0.700
10	0.245	2.600e-04	0.810
15	0.367	1.234e-04	0.876
20	0.490	6.357e-05	0.925
25	0.613	3.483e-05	0.956
30	0.735	2.099e-05	0.979
40	0.980	2.113e-06	0.999

* See [STIS ISR 2003-01](#).

Figure 14.64: Point Source Encircled Energy for F25CN182 NUV-MAMA

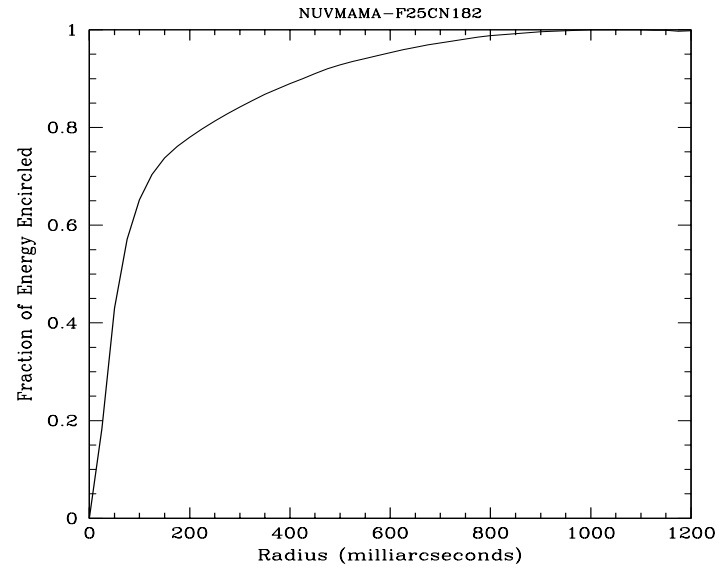
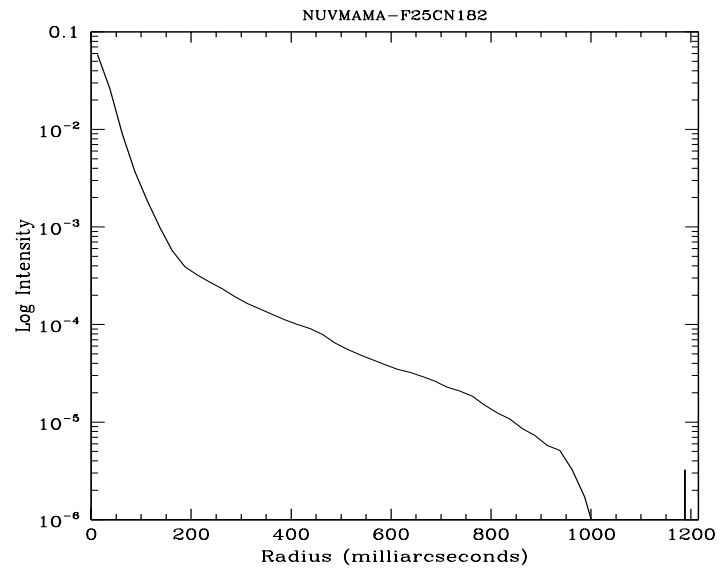


Figure 14.65: Point Source Intensity vs. Radius for F25CN182 NUV-MAMA



14.5 FUV MAMA

Below, for each used with the FUV MAMA detector, we provide the basic properties of the mode, sensitivities, throughputs and radial profiles for imaging mode. Note the FUV imaging sensitivity has been decreasing with time, with a time dependence very similar to that seen for the G140L mode (see Figure 7.12). The throughputs presented in this section represent the original 1997 values.

Users may also want to consider whether the ACS SBC detector might be better for their observing program. The SBC has a slightly larger field-of-view, a wider selection of filters, and better throughput at most wavelengths, while the STIS FUV MAMA detector may have a lower dark current.

- “25MAMA—FUV-MAMA Clear,” page 436.
- “25MAMAD1—FUV-MAMA Pseudo-aperture,” page 439.
- “F25ND3—FUV-MAMA,” page 440.
- “F25ND5—FUV-MAMA,” page 442.
- “F25NDQ - FUV-MAMA,” page 444.
- “F25QTZ—FUV-MAMA, Longpass,” page 446.
- “F25QTZD1—FUV-MAMA, Longpass Pseudo-aperture,” page 449.
- “F25SRF2—FUV-MAMA, Longpass,” page 450.
- “F25SRF2D1—FUV-MAMA, Longpass Pseudo-aperture,” page 453.
- “F25LYA—FUV-MAMA, Lyman- α ,” page 454.

25MAMA—FUV-MAMA Clear

Description

The 25MAMA mode with the FUV-MAMA detector provides high-throughput broad-band far-UV imaging with the highest available throughput at $\sim 1500 \text{ \AA}$ and the highest possible spatial resolution. The field of view is 25×25 arcsec.

Recommended Uses

Recommended for broad-band near-UV imaging of sources where sky background is not a consideration.

Special Considerations

For long exposures of faint targets, sky background is likely to be a limiting factor. Observers should consider the use of DARKTIME or (preferably) use the F25Q7Z filter, which has nearly the same throughput but rejects geocoronal Lyman- α and [O I] 1302 + 1306 \AA air glow.

Users may also want to consider whether the ACS SBC detector might be better for their observing program.

Pivot λ (\AA)	FWHM (\AA)	AB mag zeropoint	S_{peak}	B_{λ}	R_{80} (arcsec)	Flux in central pixel
1374.3	324.1	23.595	1.30×10^{14}	366.9	0.32	8%

Figure 14.66: 25MAMA FUV-MAMA Integrated System Throughput and Redleak

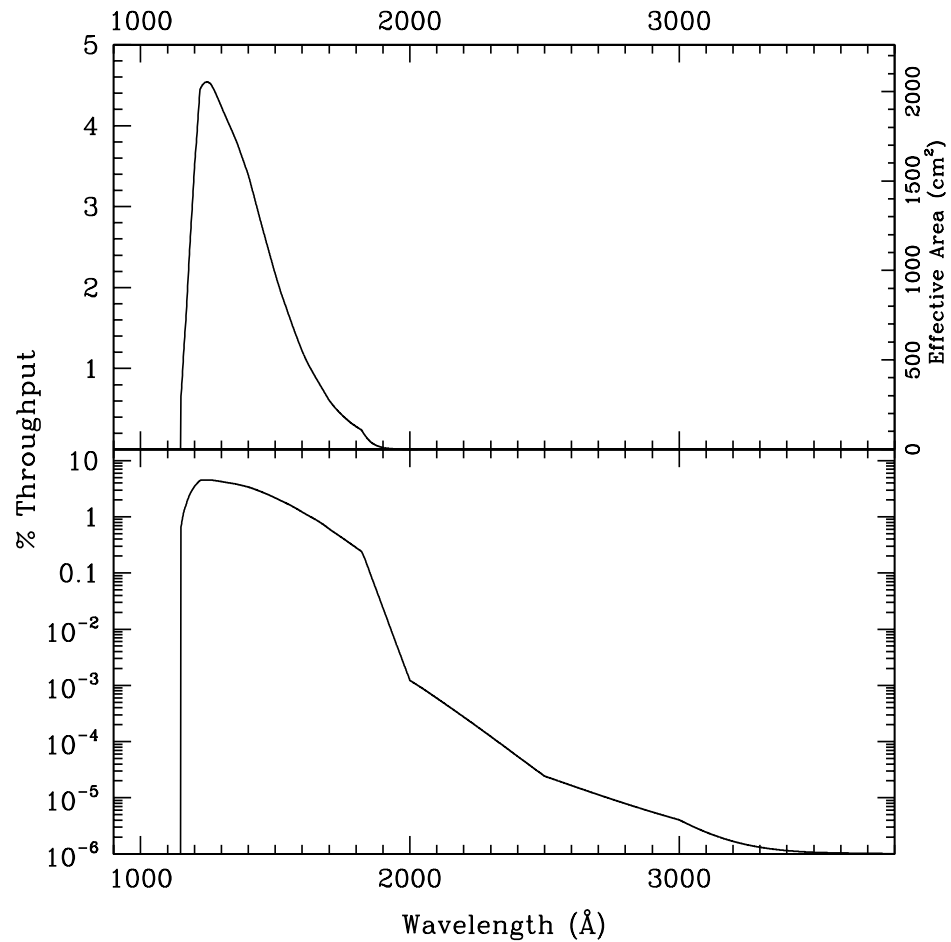


Table 14.26: Throughput and Sensitivity for 25MAMA FUV-MAMA

I	Sensitivity	Throughput %
1150.	1.72E13	0.66
1175.	5.41E13	2.02
1200.	9.51E13	3.48
1225.	1.25E14	4.48
1250.	1.29E14	4.54
1300.	1.25E14	4.23
1350.	1.18E14	3.85
1375.	1.14E14	3.63
1400.	1.08E14	3.39
1425.	9.99E13	3.08
1450.	9.14E13	2.77
1475.	8.28E13	2.46
1500.	7.41E13	2.17
1550.	5.87E13	1.66
1600.	4.43E13	1.21
1650.	3.34E13	0.89
1700.	2.36E13	0.61
1750.	1.67E13	0.42
1800.	1.16E13	0.28
1850.	4.45E12	0.11
1875.	2.17E12	0.05

Figure 14.67: Point Source S/N vs. $V+AB_v$ for the 25MAMA FUV-MAMA mode. Curves are labeled by required exposure time (sec).

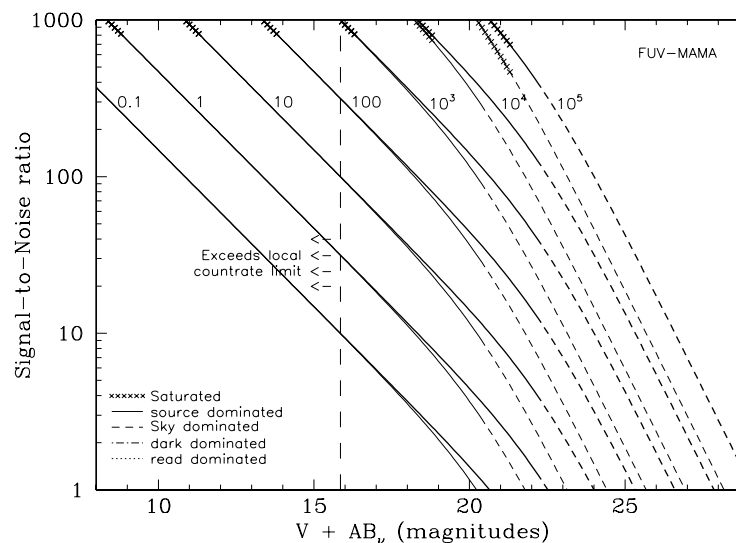


Figure 14.68: Extended Source S/N vs. $V+AB_v$ for the 25MAMA FUV-MAMA mode. Top curves are for an area of 0.2 arcsec^2 ; bottom curves are for 1 arcsec^2 . Average sky assumed. Curves are labeled by required exposure time (sec).

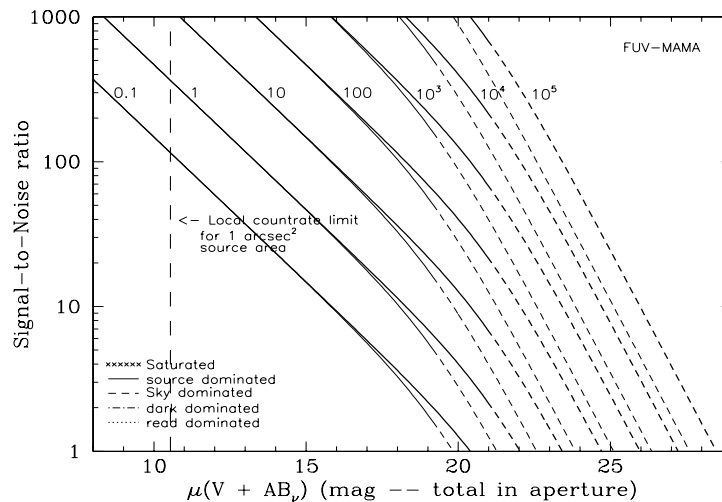


Table 14.27: Radial Profile for 25MAMA*

Radius		Intensity	Fraction of Energy Encircled
Pixels	Arcsec		
1	0.024	3.267e-02	0.141
2	0.037	2.107e-02	0.236
2	0.049	1.345e-02	0.331
3	0.073	6.141e-03	0.467
4	0.098	2.981e-03	0.557
5	0.122	1.485e-03	0.614
10	0.245	3.377e-04	0.746
15	0.367	1.676e-04	0.834
20	0.490	9.542e-05	0.900
25	0.613	4.543e-05	0.947
30	0.735	2.065e-05	0.972
40	0.980	5.088e-06	0.994

* See [STIS ISR 2003-01](#).

Figure 14.69: Point Source Encircled Energy for 25MAMA FUV-MAMA

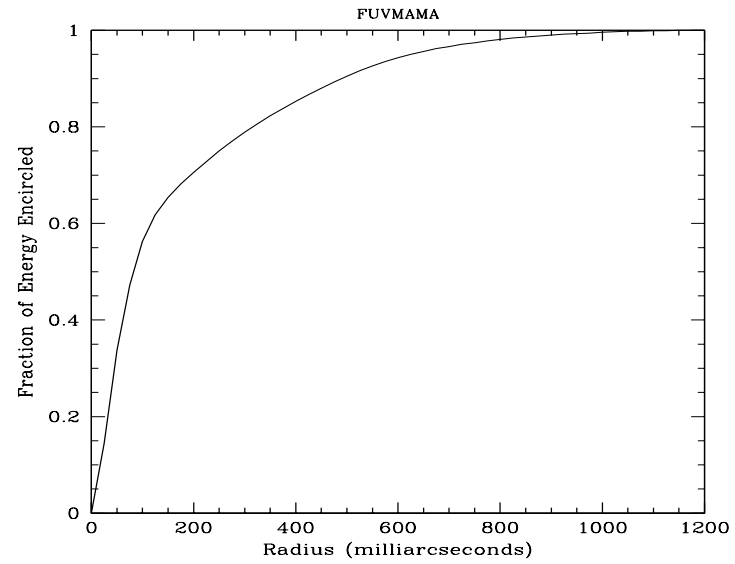
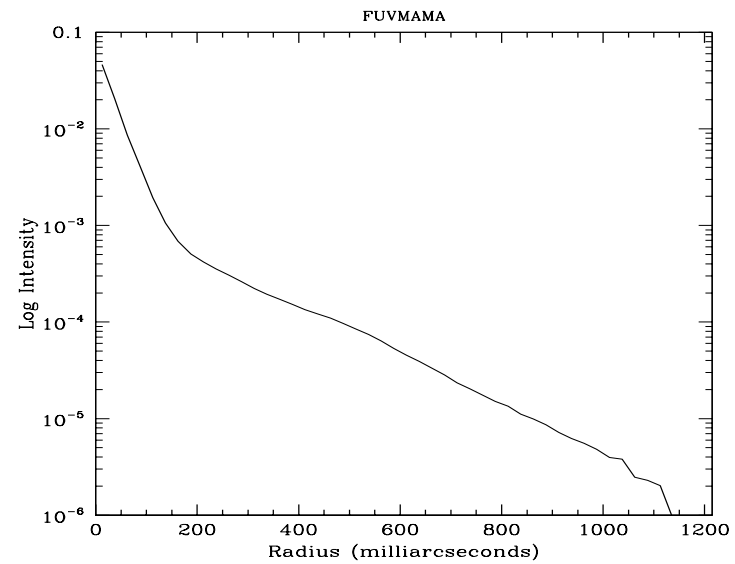


Figure 14.70: Point Source Intensity vs. Radius for 25MAMA FUV-MAMA



25MAMAD1 — FUV-MAMA Pseudo-aperture

Description

This is the same physical aperture as the 25MAMA aperture and has become available for use with the FUV-MAMA detector to minimize the contribution from the dark current when observing very faint targets. This aperture moves the target 2 arcseconds above the bottom edge of the FUV-MAMA. It is yet to be determined if the throughput for a target at this position is significantly different from that obtained at the standard position.

Special Considerations

■ Usage of this aperture is only allowed with the G140L and G140M gratings. For more information on throughputs, encircled energy, etc, please refer to the information for “25MAMA — FUV-MAMA Clear” on page 436.

F25ND3—FUV-MAMA

Description

The F25ND3mode with the FUV-MAMA detector provides broad band imaging with an attenuation of 10^{-3} . The field of view is 25x25 arcsec. The R_{80} and central pixel flux are unmeasured but assumed to be approximately the same as produced by the F25QTZ filter

Recommended Uses

Recommended for broad-band imaging of bright objects requiring 10^{-3} attenuation to meet FUV-MAMA bright-object protection limits.

Pivot λ (\AA)	FWHM (\AA)	AB mag zeropoint	S_{peak}	B_{λ}	R_{80} (arcsec)	Flux in central pixel
1376.0	316.2	16.070	$1.26\text{e}+11$	368.9	0.28	10%

Figure 14.71: F25ND3 FUV-MAMA Integrated System Throughput and Redleak

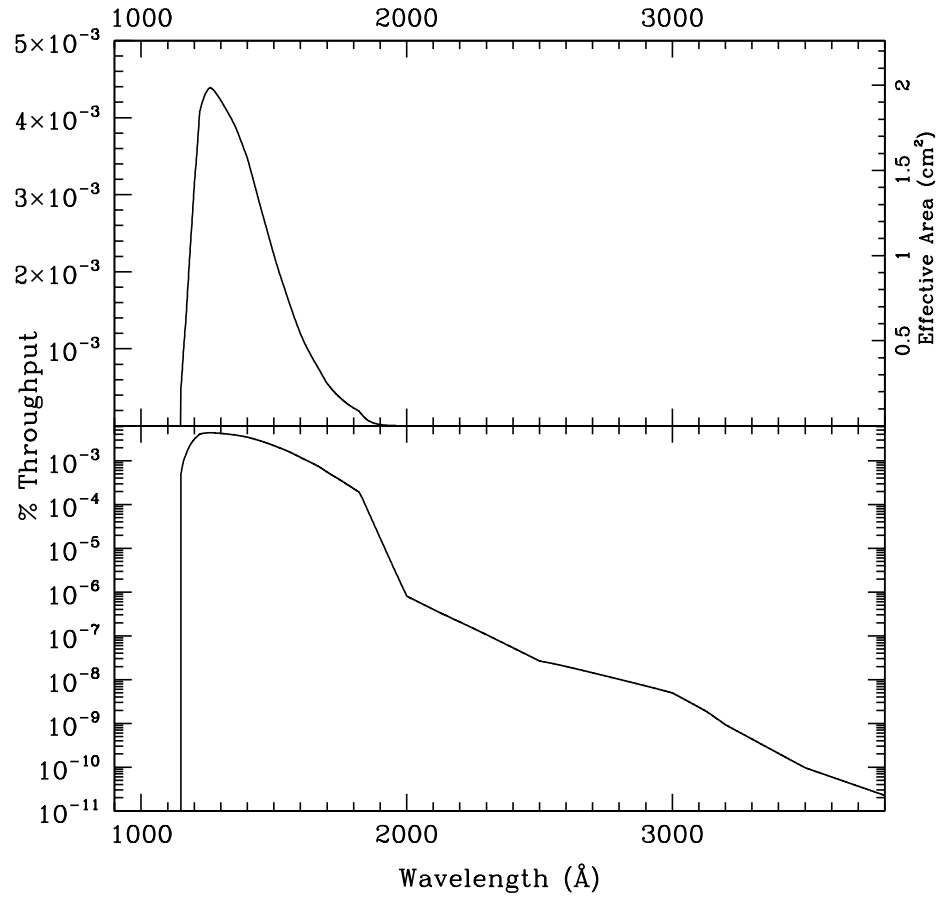


Table 14.28: Throughput and Sensitivity for F25ND3 FUV-MAMA

I	Sensitivity	Throughput %
1150.	1.07E10	0.41e-3
1175.	4.69E10	1.75e-3
1200.	8.42E10	3.08e-3
1225.	1.14E11	4.08e-3
1250.	1.24E11	4.35e-3
1300.	1.25E11	4.22e-3
1350.	1.20E11	3.91e-3
1375.	1.16E11	3.71e-3
1400.	1.10E11	3.46e-3
1425.	1.03E11	3.16e-3
1450.	9.37E10	2.84e-3
1475.	8.49E10	2.53e-3
1500.	7.59E10	2.22e-3
1550.	5.93E10	1.68e-3
1600.	4.37E10	1.20e-3
1650.	3.20E10	0.85e-3
1700.	2.16E10	0.56e-3
1750.	1.45E10	0.36e-3
1800.	9.53E9	0.23e-3
1850.	3.53E9	0.08e-3
1875.	1.64E9	0.04e-3

Figure 14.72: Point Source S/N vs. $V+AB_v$ for the F25ND3 FUV-MAMA mode. Curves are labeled by required exposure time (sec).

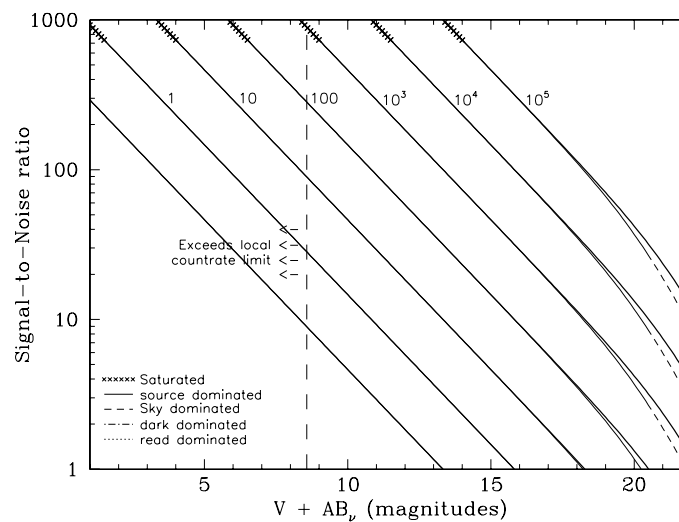
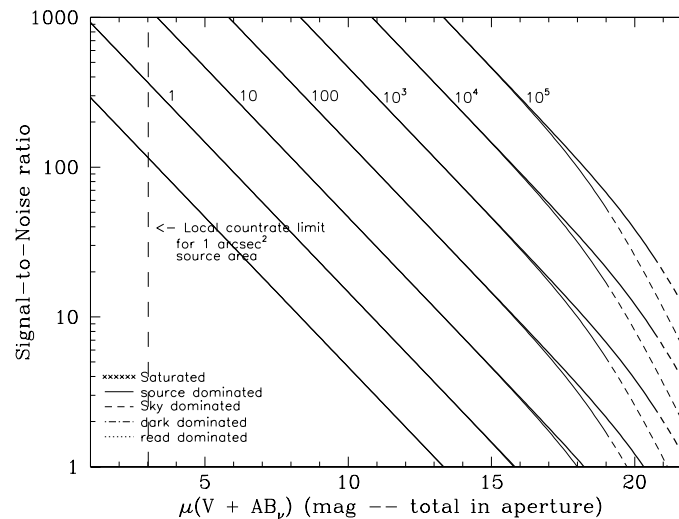


Figure 14.73: Extended Source S/N vs. $V+AB_v$ for the F25ND3 FUV-MAMA mode. Top curves are for an area of 0.2 arcsec^2 ; bottom curves are for 1 arcsec^2 . Average sky assumed. Curves are labeled by required exposure time (sec).



F25ND5—FUV-MAMA

Description

The F25ND5 mode with the FUV-MAMA detector provides broad band imaging with an attenuation of 7×10^{-7} . The field of view is 25×25 arcsec. The R_{80} and central pixel flux are unmeasured but assumed to be approximately the same as produced by the F25QTZ filter.

Recommended Uses

Recommended for broad-band imaging of objects too bright by about a factor of 10^6 to meet FUV-MAMA BOP limits.

Special Considerations

At FUV wavelengths the attenuation is closer to a factor of 10^6 rather than the nominal 10^5 , but the attenuation factor decreases at longer wavelengths, so special care should be taken for red sources. To make an accurate prediction of the expected count rate, observers should use a good approximation of the source spectrum as input for the STIS ETC.

Pivot λ (\AA)	FWHM (\AA)	AB mag zeropoint	S_{peak}	B_{λ}	R_{80} (arcsec)	Flux in central pixel
1385.1	333.6	8.188	$8.81\text{e}7$	377.2	0.28	10%

Figure 14.74: F25ND5 FUV-MAMA Integrated System Throughput and Redleak

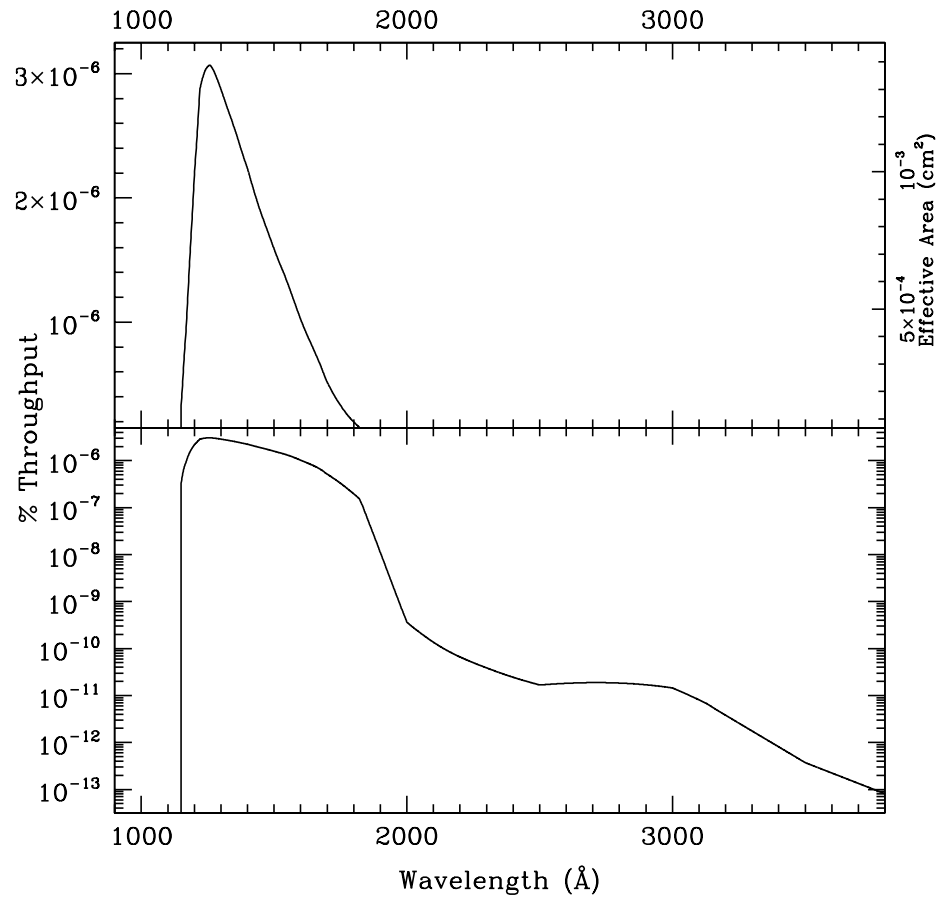


Table 14.29: Throughput and Sensitivity for F25ND5 FUV-MAMA

I	Sensitivity	Throughput %
1150.	7.19E6	2.75e-7
1175.	3.23E7	1.21e-6
1200.	5.90E7	2.16e-6
1225.	8.03E7	2.88e-6
1250.	8.69E7	3.05e-6
1300.	8.51E7	2.87e-6
1350.	7.89E7	2.56e-6
1375.	7.51E7	2.40e-6
1400.	7.12E7	2.23e-6
1425.	6.66E7	2.05e-6
1450.	6.23E7	1.88e-6
1475.	5.83E7	1.74e-6
1500.	5.43E7	1.59e-6
1550.	4.65E7	1.32e-6
1600.	3.73E7	1.02e-6
1650.	2.91E7	7.75e-7
1700.	2.01E7	5.19e-7
1750.	1.32E7	3.31e-7
1800.	8.07E6	1.97e-7
1850.	2.67E6	6.34e-7
1875.	1.16E6	2.71e-8

Figure 14.75: Point Source S/N vs. $V+AB_V$ for the F25ND5 FUV-MAMA mode. Curves are labeled by required exposure time (sec).

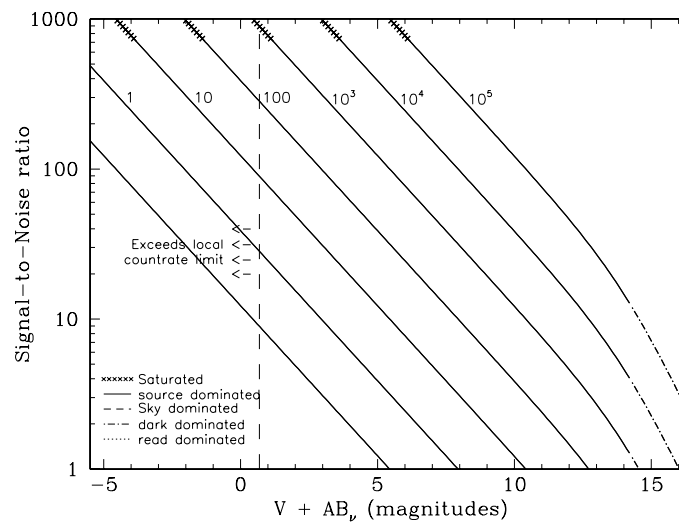
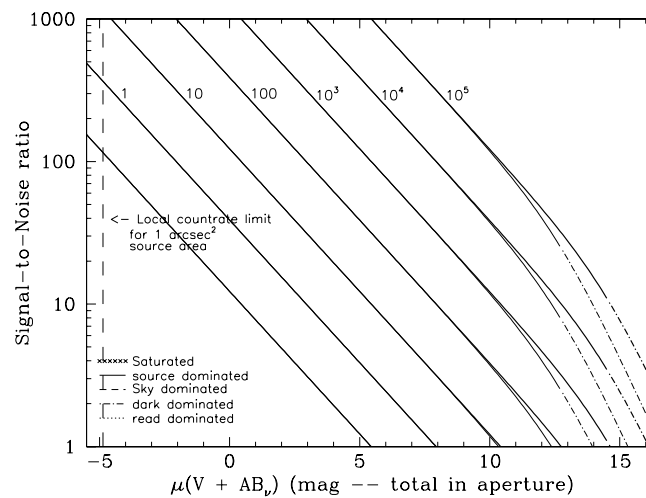


Figure 14.76: Extended Source S/N vs. $V+AB_V$ for the F25ND5 FUV-MAMA mode. Top curves are for an area of 0.2 arcsec^2 ; bottom curves are for 1 arcsec^2 . Average sky assumed. Curves are labeled by required exposure time (sec).



F25NDQ - FUV-MAMA

Description

The F25NDQ mode with the FUV-MAMA detector provides broad band imaging with attenuation factors varying between 10^{-1} and 10^{-4} . The full field of view is 25×25 arcsec, but the F25NDQ filter is unique in that it is divided into four quadrants, each having a different neutral density factor. In clockwise order starting from the upper left these are F25NDQ1, F25NDQ2, F25NDQ3, and F25NDQ4, where the number appended to each name is the approximate dex ND factor. The R_{80} and central pixel flux are unmeasured but assumed to be approximately the same as produced by the F25SRF2 filter. Approximate dimensions of each quadrant and the default target location in each quadrant are given in Table 14.30.

Recommended Uses

Recommended for broad-band imaging of bright objects which require attenuation of between 10^{-1} and 10^{-4} to meet FUV-MAMA bright-object limits.

Special Considerations

If a target would violate BOP restrictions in any quadrant of the F25NDQ aperture, the restrictions regarding pointing close to objects violating safety limits discussed in Chapter 7 and STIS ISR 2000-01 will apply. This rule renders the F25NDQ4 quadrant rather useless, and the F25NDQ3 quadrant is redundant with the full field F25ND3 aperture. Also the dividing lines between the quadrants are somewhat displaced

from the center of the detector and are not quite parallel to the detector edges (see Figure 13.82 for a lamp image taken through this filter), so observers for whom the exact locations of the quadrant boundaries are important should consult help@stsci.edu.

Table 14.30: NDQ quadrant dimensions and the default locations at which a target is placed in each quadrant

Aperture	pivot λ	FWHM	AB mag zeropoint	S_{peak}	$B\lambda$	R_{80}	Flux cen pixel
F25NDQ1	1416.0	384	20.775	8.95×10^{12}	393	0.3	9%
F25NDQ2	1403.9	384	18.580	1.13×10^{12}	394	0.3	9%
F25NDQ3	1407.3	401	15.898	9.68×10^{10}	415	0.3	9%
F25NDQ4	1433.7	391	13.091	7.95×10^9	393	0.3	9%

Figure 14.77: Integrated System Throughputs for F25NDQ FUV-MAMA.

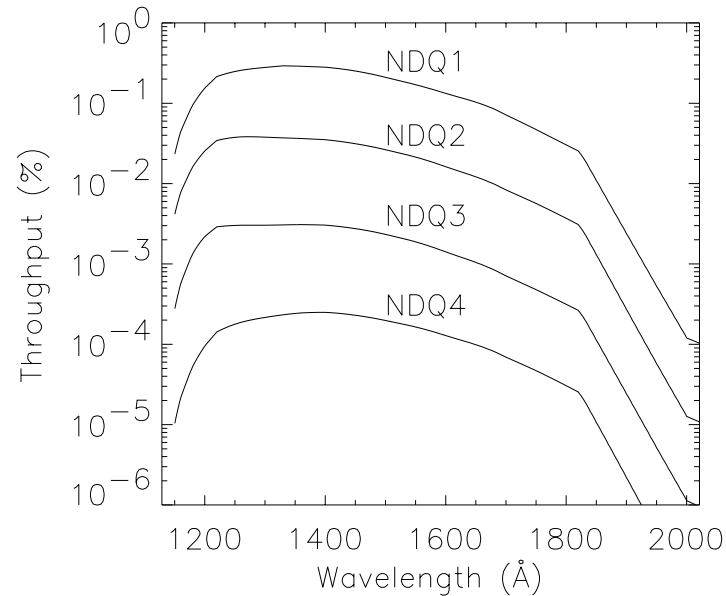


Table 14.31: Sensitivities and Throughputs for F25NDQ aperture with FUV-MAMA.

λ	Sensitivities				Throughputs (%)			
	F25NDQ1	F25NDQ2	F25NDQ3	F25NDQ4	F25NDQ1	F25NDQ2	F25NDQ3	F25NDQ4
1150	5.99e+11	1.07e+11	7.10e+09	2.65e+08	2.29e-02	4.08e-03	2.72e-04	1.02e-05
1175	2.13e+12	3.65e+11	2.95e+10	1.15e+09	7.99e-02	1.37e-02	1.10e-03	4.32e-05
1200	4.21e+12	6.95e+11	5.96e+10	2.59e+09	1.54e-01	2.55e-02	2.19e-03	9.49e-05
1225	6.16e+12	9.77e+11	8.14e+10	4.14e+09	2.21e-01	3.51e-02	2.93e-03	1.49e-04
1250	7.06e+12	1.07e+12	8.57e+10	5.05e+09	2.49e-01	3.77e-02	3.02e-03	1.78e-04
1300	8.25e+12	1.12e+12	8.97e+10	6.38e+09	2.79e-01	3.79e-02	3.04e-03	2.16e-04
1350	8.90e+12	1.12e+12	9.45e+10	7.42e+09	2.90e-01	3.67e-02	3.08e-03	2.42e-04
1400	8.95e+12	1.12e+12	9.68e+10	7.95e+09	2.81e-01	3.52e-02	3.04e-03	2.50e-04
1450	8.30e+12	1.03e+12	9.06e+10	7.57e+09	2.52e-01	3.14e-02	2.75e-03	2.30e-04
1500	7.17e+12	9.00e+11	7.95e+10	6.74e+09	2.10e-01	2.64e-02	2.33e-03	1.98e-04
1550	5.99e+12	7.53e+11	6.63e+10	5.78e+09	1.70e-01	2.14e-02	1.88e-03	1.64e-04
1600	4.83e+12	5.90e+11	5.14e+10	4.67e+09	1.33e-01	1.62e-02	1.41e-03	1.28e-04
1650	3.86e+12	4.55e+11	3.92e+10	3.70e+09	1.03e-01	1.21e-02	1.04e-03	9.87e-05
1700	2.76e+12	3.23e+11	2.74e+10	2.67e+09	7.16e-02	8.35e-03	7.11e-04	6.91e-05
1750	1.87e+12	2.25e+11	1.90e+10	1.87e+09	4.71e-02	5.66e-03	4.79e-04	4.70e-05
1800	1.24e+12	1.51e+11	1.29e+10	1.25e+09	3.04e-02	3.70e-03	3.14e-04	3.05e-05
1850	4.58e+11	5.46e+10	4.73e+09	4.47e+08	1.09e-02	1.30e-03	1.13e-04	1.06e-05

F25QTZ—FUV-MAMA, Longpass

Description

The F25QTZ filter with the FUV-MAMA provides high-throughput broad-band far-UV imaging with better rejection of geocoronal emission than the F25MAMA or F25SRF2 modes and the same field of view and spatial resolution.

Recommended Uses

Recommended filter for broad-band far-UV imaging of faint targets.

Special Considerations

With this filter the background is dominated by detector dark current. The dark current is not constant across the detector and not constant in time. This could limit the sensitivity for very extended faint targets, however, note that the FUV-MAMA dark is extremely low.

Users may also want to consider whether the ACS SBC detector might be better for their observing program.

Pivot λ (Å)	FWHM (Å)	AB mag zeropoint	S_{peak}	$B\lambda$	R_{80} (arcsec)	Flux in central pixel
1595.1	227.8	21.539	4.29e+13	225.0	0.28	10%

Figure 14.78: F25QTZ FUV-MAMA Integrated System Throughput and Redleak

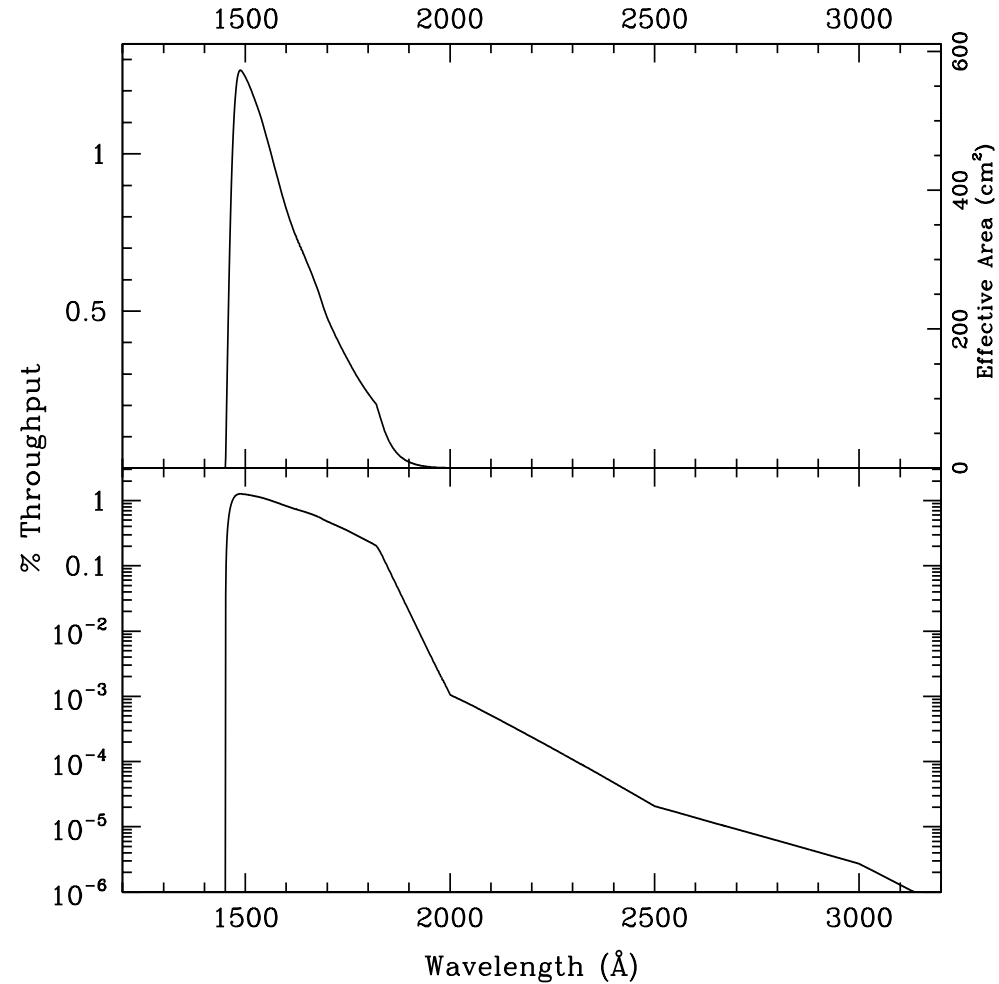


Table 14.32: Throughput and Sensitivity for F25QTZ FUV-MAMA

I	Sensitivity	Throughput %
1475.	3.93E13	1.17
1500.	4.25E13	1.24
1525.	4.05E13	1.17
1550.	3.75E13	1.06
1575.	3.38E13	0.94
1600.	3.01E13	0.83
1625.	2.72E13	0.73
1650.	2.46E13	0.65
1675.	2.19E13	0.57
1700.	1.85E13	0.48
1725.	1.60E13	0.41
1750.	1.38E13	0.35
1775.	1.16E13	0.29
1800.	9.75E12	0.24
1825.	7.59E12	0.18
1850.	3.75E12	0.09
1875.	1.83E12	0.04
1900.	8.71E11	0.02

Figure 14.79: Point source S/N vs. $V+AB_V$ for the F25QTZ FUV-MAMA mode. Curves are labeled by required exposure time (sec).

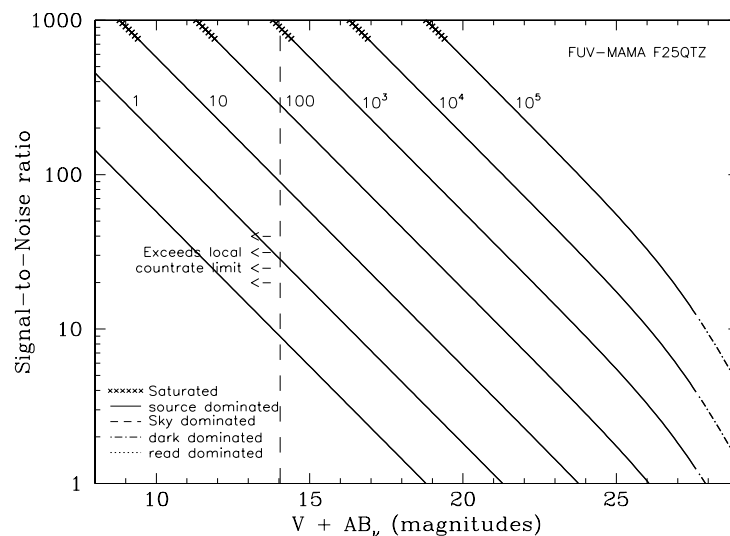


Figure 14.80: Extended source S/N vs. $V+AB_V$ for the F25QTZ FUV-MAMA mode. Top curves are for an area of 0.2 arcsec^2 ; bottom curves are for 1 arcsec^2 . Average sky assumed. Curves are labeled by required exposure time (sec).

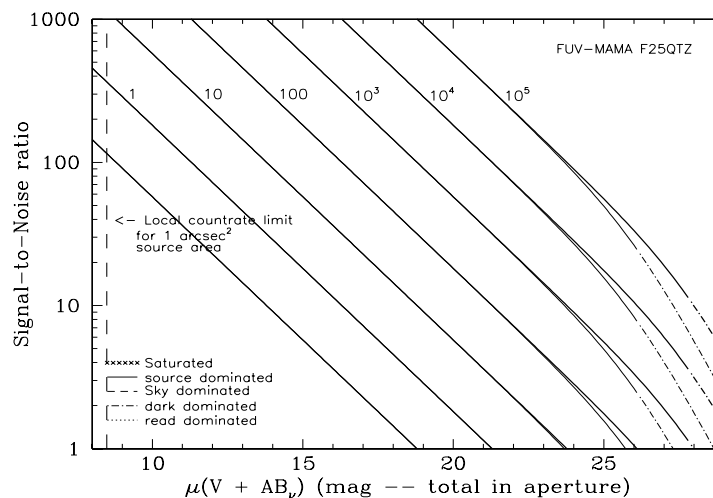


Table 14.33: Radial Profile for F25QTZ*

Radius		intensity	Fraction of Energy Encircled
Pix	arcsec		
1	0.024	3.961e-02	0.172
2	0.037	2.515e-02	0.287
2	0.049	1.505e-02	0.398
3	0.073	5.412e-03	0.532
4	0.098	2.570e-03	0.609
5	0.122	1.373e-03	0.659
10	0.245	2.735e-04	0.778
15	0.367	1.447e-04	0.851
20	0.490	7.887e-05	0.909
25	0.613	4.703e-05	0.953
30	0.735	2.117e-05	0.980
40	0.980	1.135e-05	1.000

* See [STIS ISR 2003-01](#).

Figure 14.81: Point Source Encircled Energy for F25QTZ FUV-MAMA

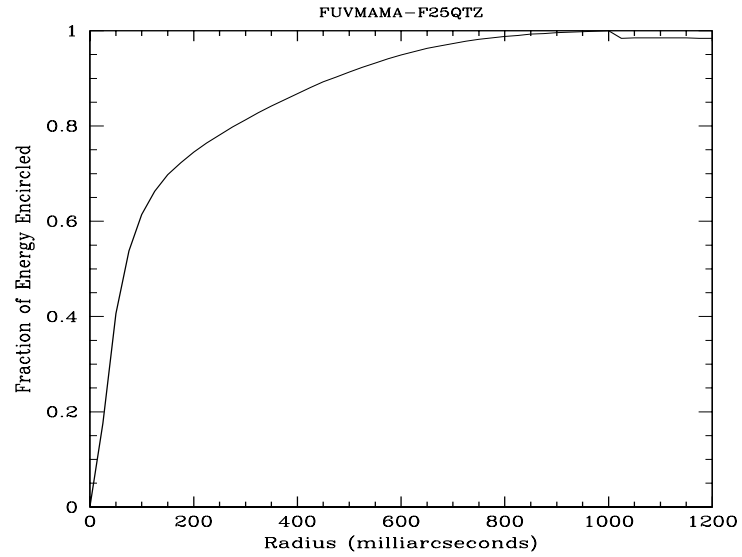
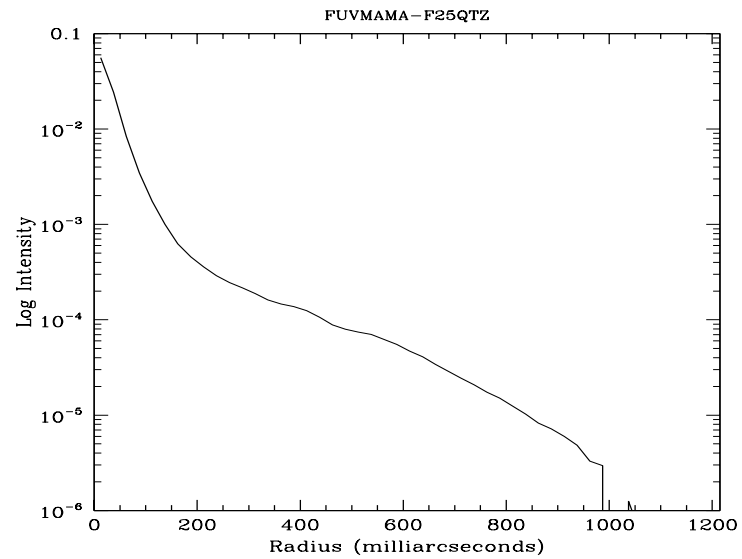


Figure 14.82: Point Source Intensity vs. Radius for F25QTZ FUV-MAMA



F25QTZD1 — FUV-MAMA, Longpass Pseudo-aperture

Description

This is the same physical aperture as the F25QTZ aperture and has become available for use with the FUV-MAMA detector to minimize the contribution from the dark current when observing very faint targets. This aperture moves the target 2 arcseconds above the bottom edge of the FUV-MAMA. It is yet to be determined if the throughput for a target at this position is significantly different from that obtained at the standard position.

Special Considerations

Usage of this slit is only allowed with the G140L and G140M gratings. For more information on throughputs, encircled energy, etc, please refer to the information for “F25QTZ—FUV-MAMA, Longpass” on page 446.

F25SRF2—FUV-MAMA, Longpass

Description

The F25SRF2 filter with the FUV-MAMA provides high-throughput broad-band far-UV imaging with better rejection of geocoronal emission than the F25MAMA but worse than F25QTZ modes. It provides the same field of view and spatial resolution as these modes.

Recommended Uses

This filter has slightly higher throughput than F25QTZ, but lets in geocoronal [O I] 1302 + 1306 Å. For sky-limited imaging F25QTZ is usually a better choice.

Special Considerations

Sky background on the day side of the orbit contains a significant contributions from [O I]/O I air glow emission at 1356 Å and at 1302 + 1306 Å. In high-background conditions, the sky background can dominate the detector background. In average day-side observing conditions the sky background through this filter will be about a factor of 100 higher than for F25QTZ. Observers can limit the background (with some cost to the total amount of observing time per orbit) by using the DARKTIME special requirement.

Users may also want to consider whether the ACS SBC detector might be better for their observing program.

Pivot λ (Å)	FWHM (Å)	AB mag zeropoint	S_{peak}	$B\lambda$	R_{80} (arcsec)	Flux in central pixel
1457.4	283.7	22.825	$8.67e+13$	303.5	0.30	9%

Figure 14.83: F25SRF2 FUV-MAMA Integrated System Throughput and Redleak

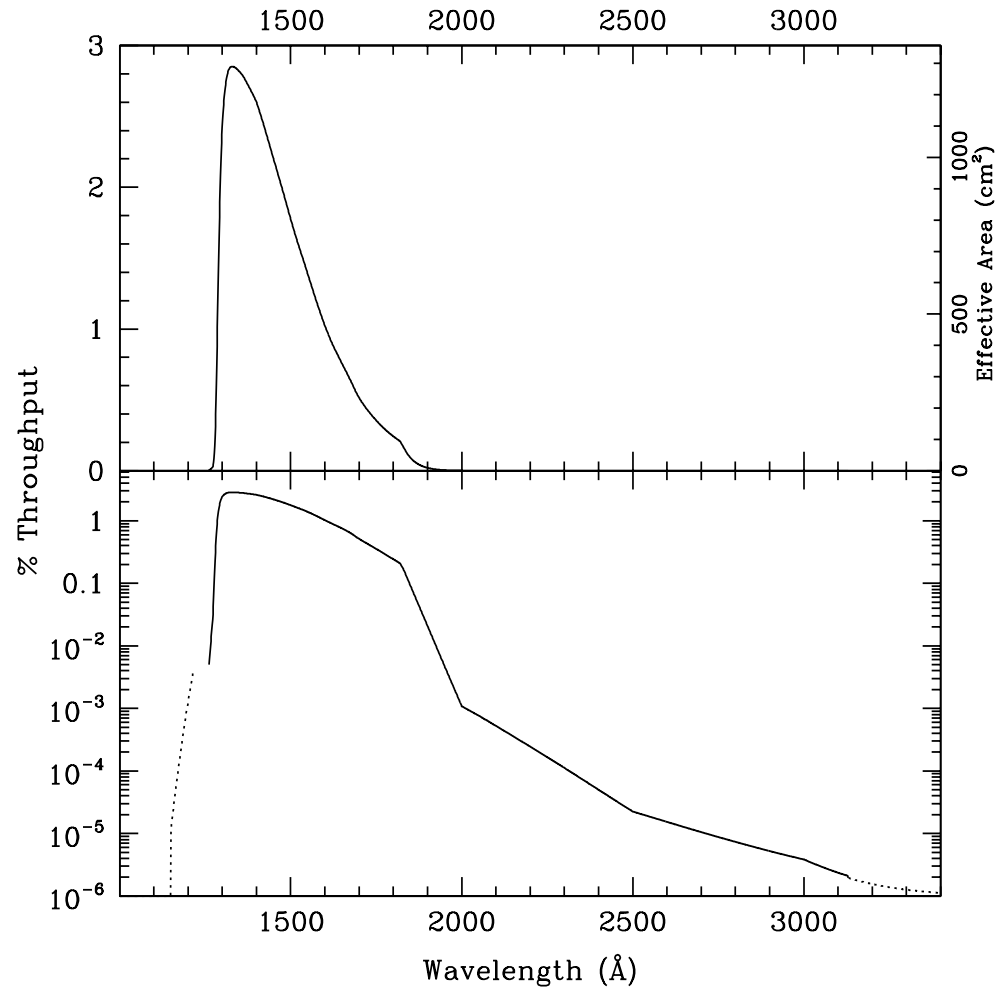


Table 14.34: Throughput and Sensitivity for F25SRF2 FUV-MAMA

I	Sensitivity	Throughput %
1300.	7.18E13	2.42
1325.	8.60E13	2.85
1350.	8.66E13	2.82
1375.	8.53E13	2.72
1400.	8.30E13	2.60
1425.	7.82E13	2.41
1450.	7.27E13	2.20
1475.	6.69E13	1.99
1500.	6.07E13	1.78
1525.	5.47E13	1.58
1550.	4.90E13	1.39
1575.	4.30E13	1.20
1600.	3.73E13	1.02
1625.	3.25E13	0.88
1650.	2.84E13	0.76
1675.	2.43E13	0.64
1700.	1.99E13	0.51
1725.	1.68E13	0.43
1750.	1.42E13	0.36
1775.	1.19E13	0.29
1800.	9.96E12	0.24

Figure 14.84: Point Source S/N vs. $V+AB_v$ for the F25SRF2 FUV-MAMA mode. Curves are labeled by required exposure time (sec).

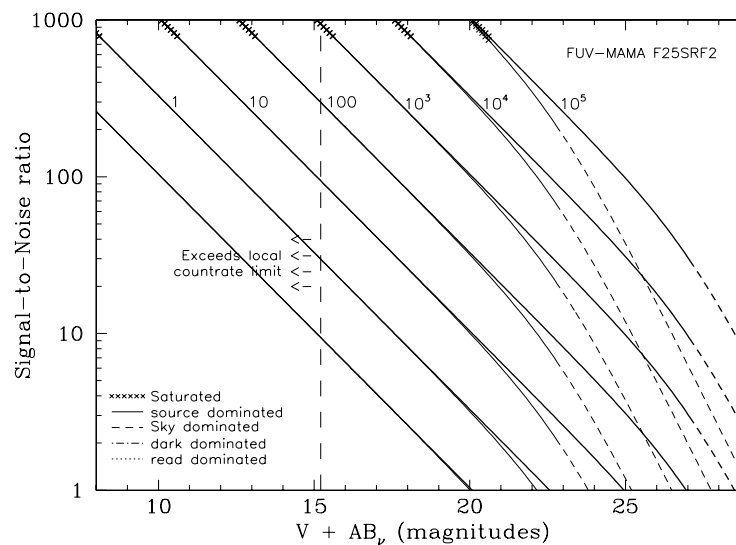


Figure 14.85: Extended Source S/N vs. $V+AB_v$ for the F25SRF2 FUV-MAMA mode. Top curves are for an area of 0.2 arcsec^2 ; bottom curves are for 1 arcsec^2 . Average sky assumed. Curves are labeled by required exposure time (sec).

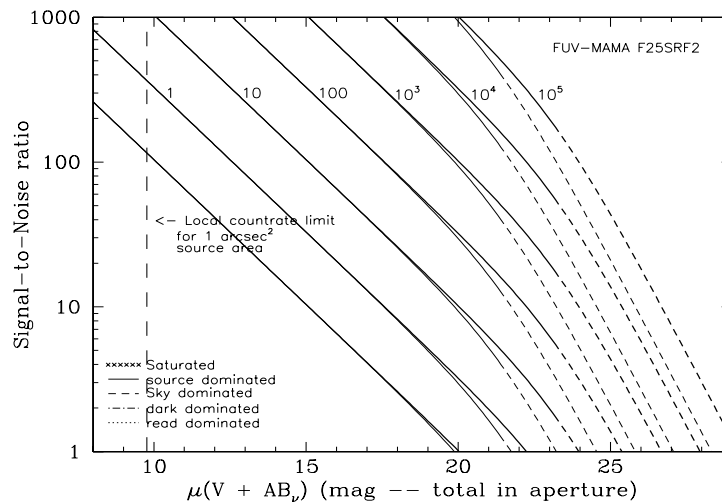


Table 14.35: Radial Profile for F25SRF2*

Radius		Intensity	Fraction of Energy Encircled
Pixels	Arcsec		
1	0.024	3.544e-02	0.154
2	0.037	2.268e-02	0.256
2	0.049	1.408e-02	0.358
3	0.073	5.787e-03	0.493
4	0.098	2.765e-03	0.576
5	0.122	1.514e-03	0.630
10	0.245	3.098e-04	0.762
15	0.367	1.677e-04	0.847
20	0.490	8.854e-05	0.910
25	0.613	4.487e-05	0.954
30	0.735	2.080e-05	0.980
40	0.980	1.510e-06	0.999

* See [STIS ISR 2003-01](#).

Figure 14.86: Point Source Encircled Energy for F25SRF2 FUV-MAMA

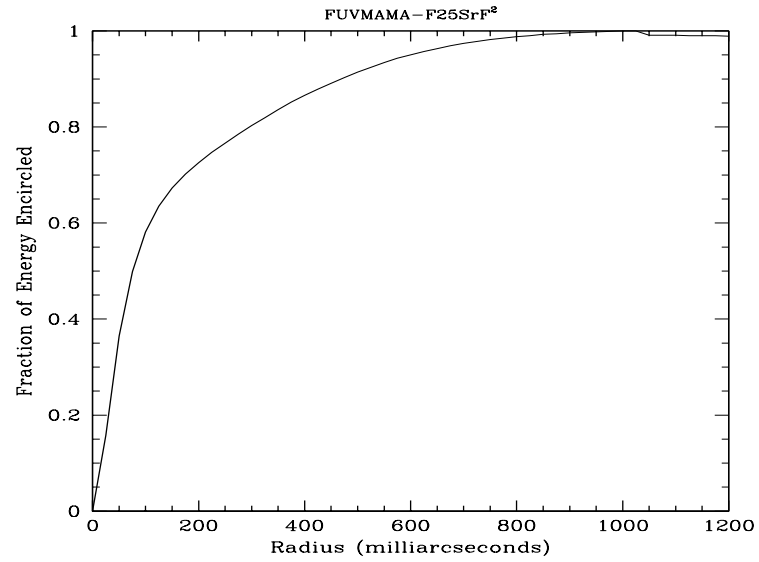
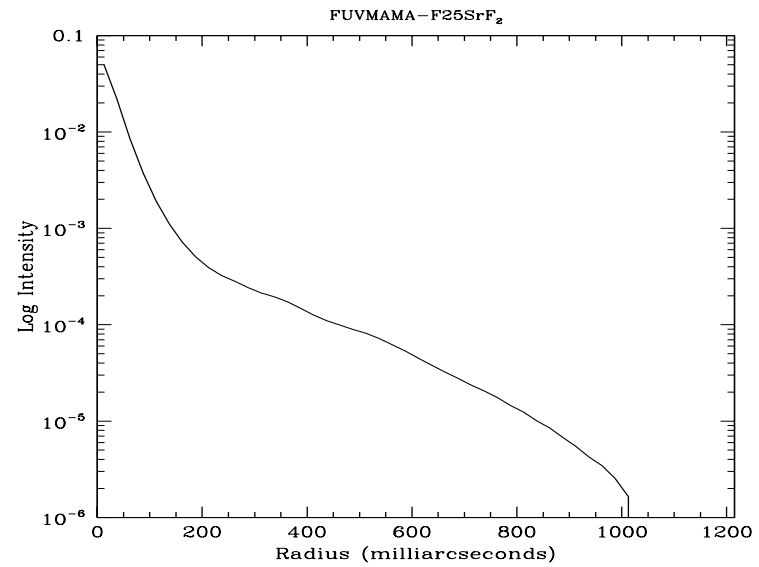


Figure 14.87: Point Source Intensity vs. Radius for F25SRF2 FUV-MAMA



F25SRF2D1 — FUV-MAMA, Longpass Pseudo-aperture

Description

This is the same physical aperture as the F25SRF2 aperture and has become available for use with the FUV-MAMA detector to minimize the contribution from the dark current when observing very faint targets. This aperture moves the target 2 arcseconds above the bottom edge of the FUV-MAMA. It is yet to be determined if the throughput for a target at this position is significantly different from that obtained at the standard position.

Special Considerations

Usage of this slit is only allowed with the G140L and G140M gratings. For more information on throughputs, encircled energy, etc, please refer to the information for “F25SRF2—FUV-MAMA, Longpass” on page 450.

F25LYA — FUV-MAMA, Lyman- α

Description

The F25LYA filter with the FUV-MAMA provides narrowband imaging of the HI 1216 Å Lyman- α line.

Recommended Uses

Lyman- α imaging. Differencing two images taken with 25MAMA and F25SRF2 is another option.

Special Considerations

Sensitivity is limited by geocoronal Lyman- α . Observers can limit the background (with some cost to the total amount of observing time per orbit) by using the DARKTIME special requirement.

Users may also want to consider whether the ACS SBC detector with the F122M filter might be a better choice for their observing program.

Pivot λ (Å)	FWHM (Å)	AB mag zeropoint	S_{peak}	B_{λ}	R_{80} (arcsec)	Flux in central pixel
1220.5	71.9	19.303	9.44e+12	101.1	0.35	6%

Figure 14.88: F25LYA FUV-MAMA Integrated System Throughput and Redleak

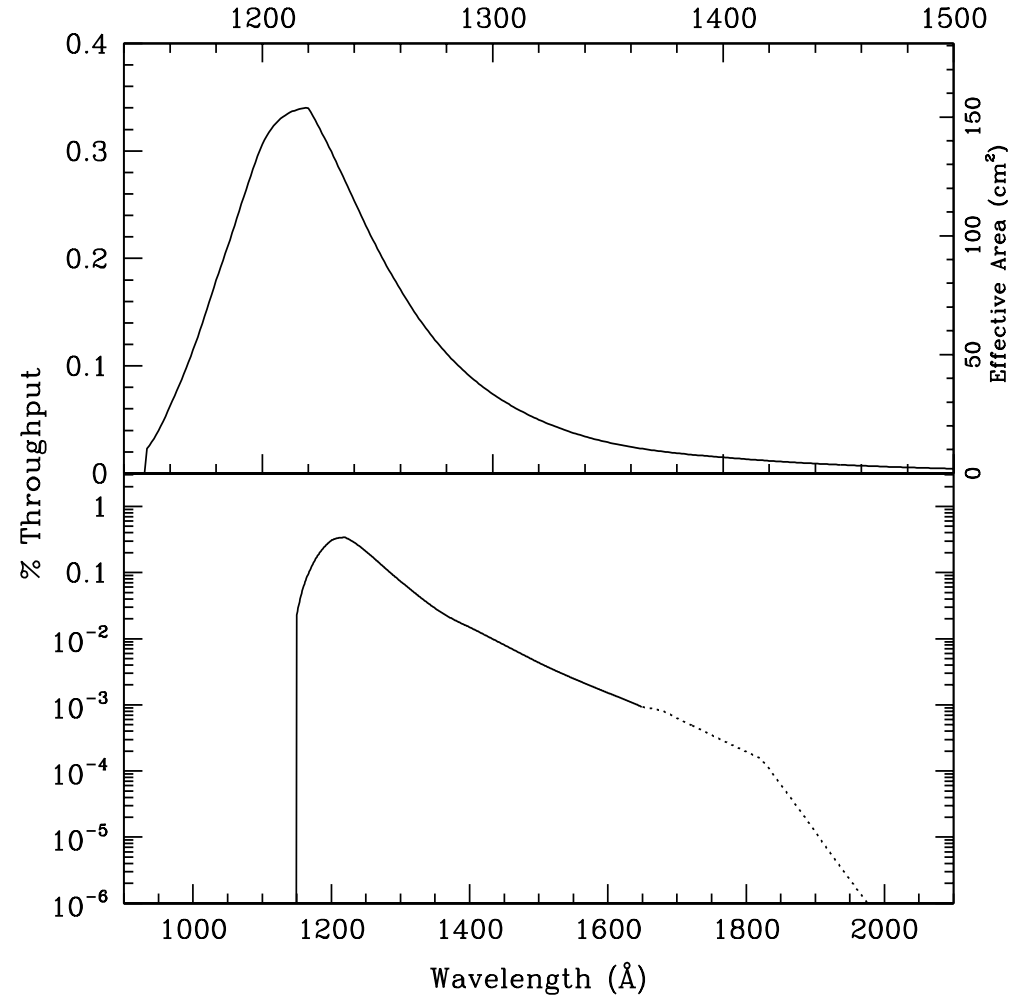


Table 14.36: Throughput and Sensitivity for F25LYA FUV-MAMA

I	Sensitivity	Throughput %
1150.	6.01E11	0.02
1175.	3.91E12	0.15
1200.	8.37E12	0.31
1225.	8.94E12	0.32
1250.	5.95E12	0.21
1275.	3.60E12	0.12
1300.	2.19E12	0.07
1325.	1.37E12	0.05
1350.	8.90E11	0.03
1375.	6.26E11	0.02

Figure 14.89: Point Source S/N vs. flux for the F25LYA FUV-MAMA mode. Curves are labeled by required exposure time (sec).

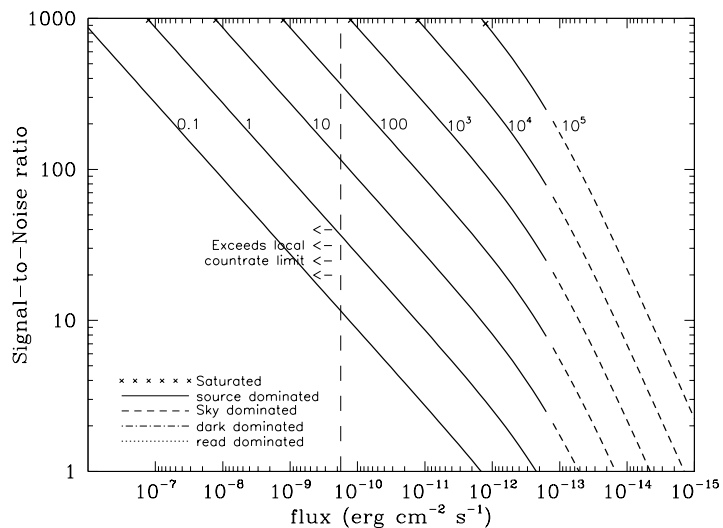


Figure 14.90: Extended Source S/N vs. flux for the F25LYA FUV-MAMA mode. Top curves are for an area of 0.2 arcsec²; bottom curves are for 1 arcsec². Average sky assumed. Curves are labeled by required exposure time (sec).

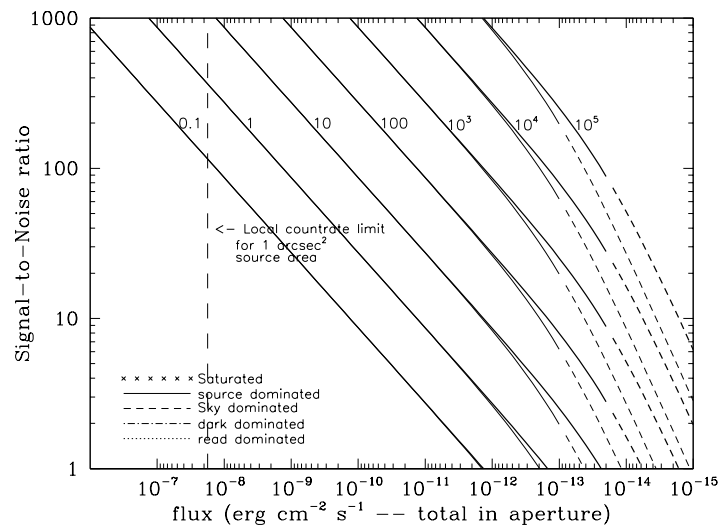


Table 14.37: Radial Profile for F25LYA*

Radius			Fraction of Energy Encircled
Pix	arcsec	intensity	
1	0.024	2.440e-02	0.100
2	0.037	1.702e-02	0.174
2	0.049	1.199e-02	0.254
3	0.073	6.423e-03	0.387
4	0.098	3.326e-03	0.485
5	0.122	1.718e-03	0.549
10	0.245	3.888e-04	0.712
15	0.367	2.140e-04	0.816
20	0.490	1.044e-04	0.895
25	0.613	4.910e-05	0.943
30	0.735	1.741e-05	0.968
40	0.980	8.124e-06	0.994

* See [STIS ISR 2003-01](#).

Figure 14.91: Point Source PSF for F25LYA FUV-MAMA, 7."5 square (at pixel 739, 368, log scaled, B-V=-0.04)

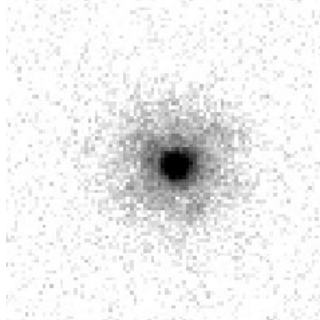


Figure 14.92: Point Source Encircled Energy for F25LYA FUV-MAMA

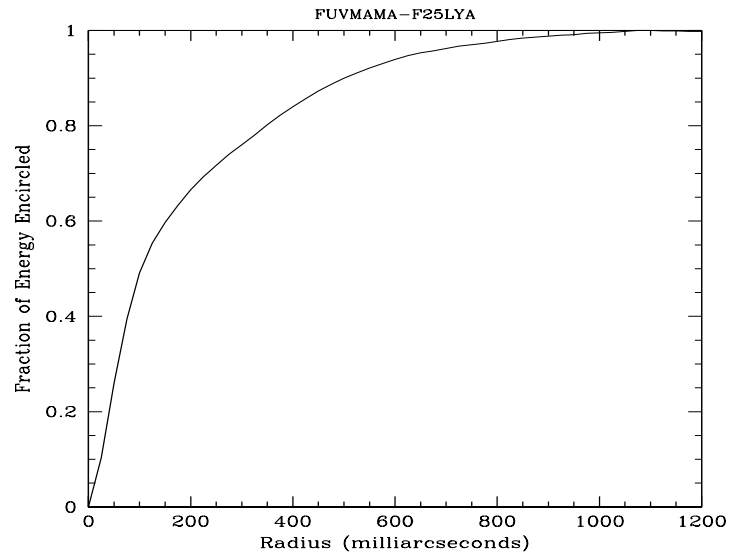
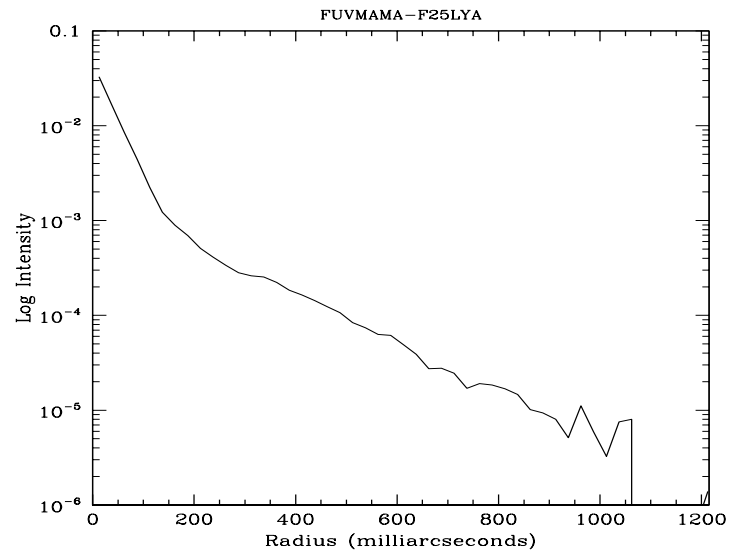


Figure 14.93: Point Source Intensity vs. Radius for F25LYA FUV-MAMA



14.6 Image-Mode Geometric Distortion

The STIS cameras have significant geometric distortion that not only affects astrometry, but also in principle affects photometry (because the extended sources used to generate flat fields have an induced change in the apparent surface brightness). In the CCD the image distortions are less than one pixel across the whole detector, and can often be ignored. For the MAMA the distortions are larger, approaching 3 pixels at the corners of cameras.

Geometric distortion and plate scales for the STIS imaging configurations have been measured on-orbit by observing star fields shifted to different positions in the field, following a procedure similar to that used for WFPC-2 (Holtzman et al., PASP, 107, 156). The geometric distortion data also allowed a determination of the mean plate scale at the center of the field for each detector. These plate scales are given in Table 14.38.

Table 14.38: Mean pixel scales for STIS detectors.

Detector	X scale (arcsec/pix)	X error (arcsec/pix)	Y scale (arcsec/pix)	Y error (arcsec/pix)	Corrected mean scale
CCD	0.050716	0.000072	0.050735	0.000087	0.050725
FUV-MAMA	0.024328	0.000025	0.024608	0.000086	0.024468
NUV-MAMA	0.024526	0.000120	0.024829	0.000126	0.024677

The MAMA plate scales given here only apply to filtered imaging. For the unfiltered (25MAMA) imaging configuration, the FUV plate scale is 1.0031 times larger (more arcsec per pixel) and the NUV plate scale is 1.0008 times smaller (less arcsec per pixel). The quoted errors are formal random errors derived from the uncertainties in measuring the positions of the sources.

The geometric distortion equations given below account for the plate scale differences along rows and columns, as well as higher-order distortions. Application of these equations (e.g., using the STSDAS **drizzle** task) will rectify the CCD, NUV-MAMA, and filtered FUV-MAMA images to the corrected mean pixel scales given in Table 14.38. For the MAMA unfiltered configurations, the adopted scales are larger by a factor of 1.0031 for the FUV detector and smaller by a factor of 1.0008 for the NUV detector.

The geometric distortion for the STIS cameras has been characterized in a similar way to that used for WFPC2, with a cubic or quartic distortion solution, which relates the true x_i, y_i positions of the stars with the observed positions x, y using:

$$x_i - x_r = \sum_{i=0}^k \sum_{j=0}^i c_{x,i,j} (x - x_r)^j (y - y_r)^{i-j}$$

$$y_i - y_r = \sum_{i=0}^k \sum_{j=0}^i c_{y,i,j} (x - x_r)^j (y - y_r)^{i-j}$$

where x_r and y_r are the coordinates of the central pixel.

The values of the original distortion coefficients and the full analysis used to derive them can be found in Walsh, Goudfrooij, and Malumuth (STIS ISR 2001-02). Maíz-Apellániz and Úbeda (STIS ISR 2004-01) discovered that the coefficients for the NUV-MAMA had been incorrectly implemented into the IDCTAB reference file and produced a revised analysis which is the one currently used for that detector. A similar re-analysis for the FUV-MAMA and the CCD is planned using calibration data that will be acquired in Cycle 13.

14.7 Spatial Dependence of the STIS PSF

The STIS PSF varies across the field of view. Observations of Omega Cen and NGC 6681 have been used to study the PSF variations, and confirm the behavior expected from the optics. One way of characterizing the spatial variation is to measure the flux in a fixed aperture. Figure 14.94 through Figure 14.97 show the fraction of the flux enclosed within a 0.05 arcsec radius aperture. This parameter is relatively constant for the CCD, but is more pronounced for the MAMA detectors. For example, the 0.05" encircled energy varies from 47% to 31% across the NUV-MAMA with the F25CN182 filter.

See Bowers (1997 HST Calibration Workshop) for a discussion of HST "breathing" effects on the PSF.

Figure 14.94: Fraction of the total flux of a point source that passes through an aperture of $0.05''$ radius for the CCD and a clear aperture (50CCD). The data were obtained from observations of the Omega Cen star cluster. Crosses represent stars that have little or no contamination from other sources, while triangles are sources that were marginally contaminated in the region outside the PSF core. No objects were used that had contamination within $0.15''$ of the center.

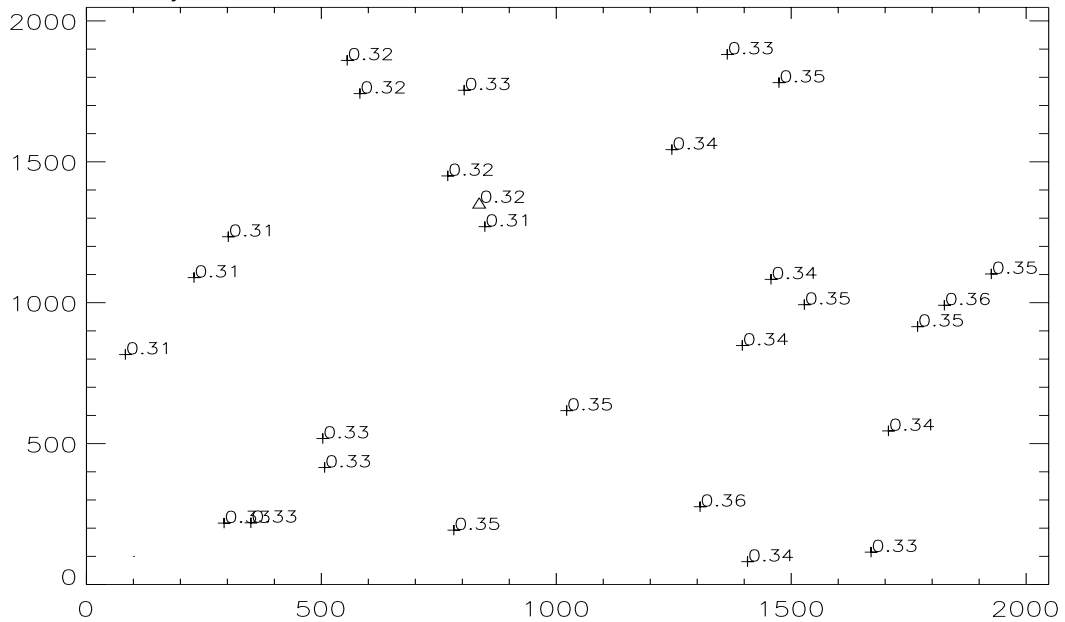


Figure 14.95: Fraction of the total flux of a point source that passes through an aperture of $0.05''$ radius for the NUV-MAMA with the F25CN182. The data were obtained from observations of the star cluster NGC 6881. Crosses represent stars that have little or no contamination from other sources, while triangles are sources that were marginally contaminated in the region outside the PSF core. No objects were used that had contamination within $0.15''$ of the center.

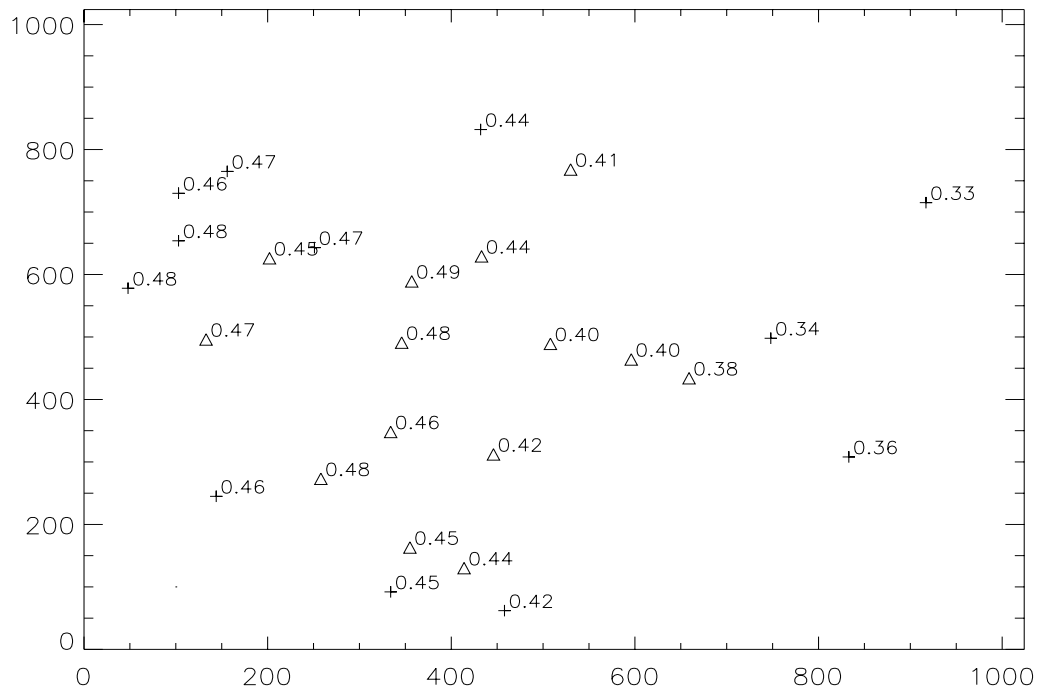


Figure 14.96: Fraction of the total flux of a point source that passes through an aperture of $0.05''$ radius for the NUV-MAMA with the F25CN270 filter. The data were obtained from observations of the star cluster NGC 6881. Crosses represent stars that have little or no contamination from other sources, while triangles are sources that were marginally contaminated in the region outside the PSF core. No objects were used that had contamination within $0.15''$ of the center.

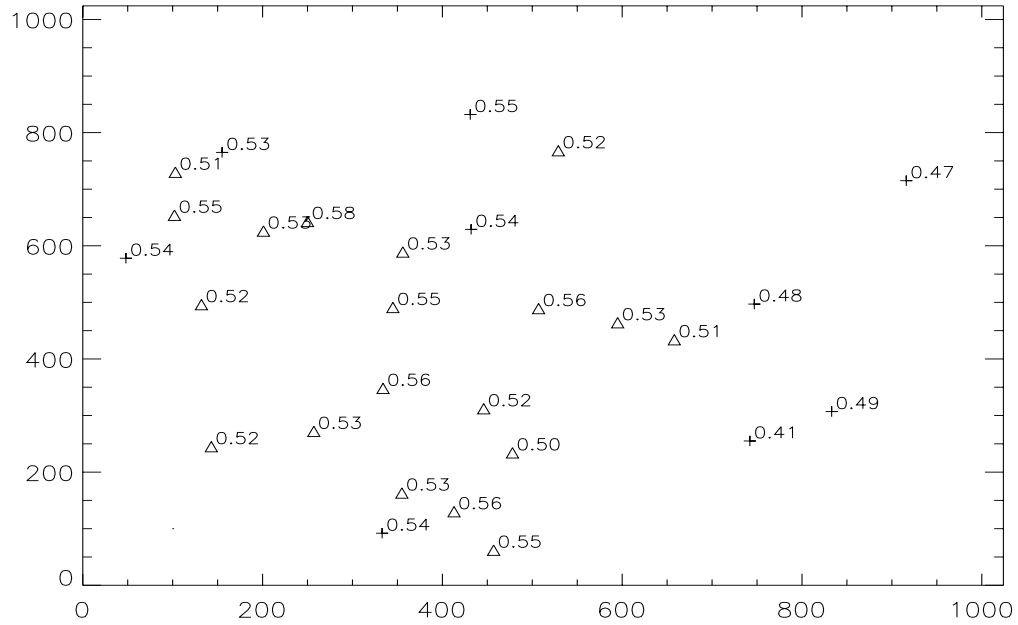
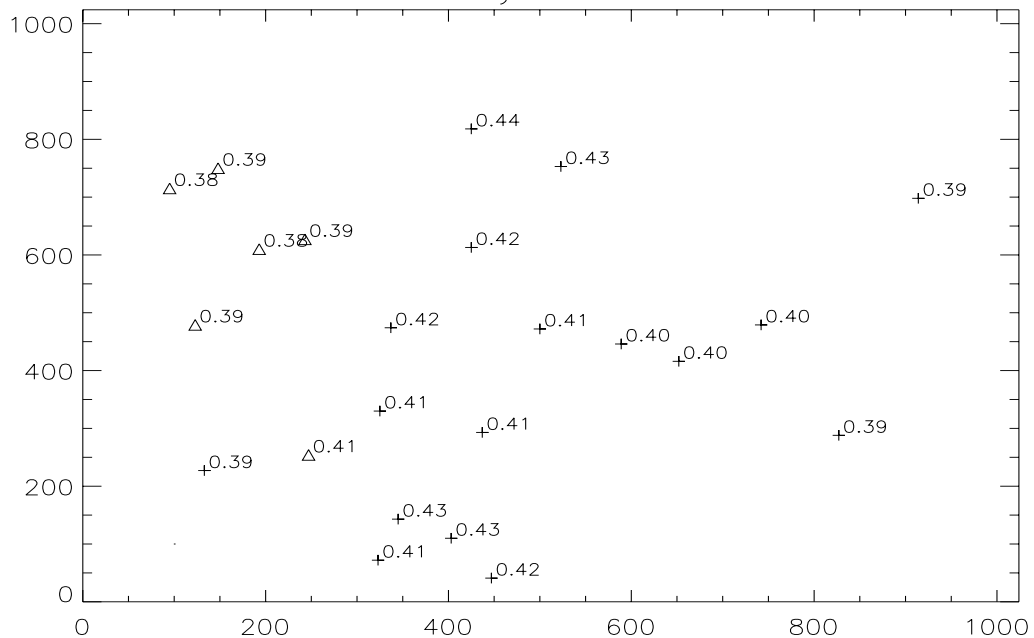


Figure 14.97: Fraction of the total flux of a point source that passes through an aperture of $0.05''$ radius for the FUV-MAMA with the F25QTZ filter. The data were obtained from observations of the star cluster NGC 6881. Crosses represent stars that have little or no contamination from other sources, while triangles are sources that were marginally contaminated in the region outside the PSF core. No objects were used that had contamination within $0.15''$ of the center.



14.8 MAMA Imaging Bright Object Limits

As described in Section 7.6, the MAMA's are subject to absolute brightness limits, above which sources cannot be observed or they would potentially damage the detectors. In Table 14.39, we present the complete set of bright object point source and integrated magnitude screening limits for the MAMA imaging modes. These screening magnitudes are presented as a *guide*. Whether or not an individual source can be observed is determined by whether the desired configuration and the spectrum of that source is predicted to exceed the global and local absolute observing count rate limits, as described in Chapter 7. Remember, sources cannot be observed in configurations where they exceed the absolute bright object limits. The information presented here should be used in conjunction with the material presented in Chapter 7.

A few important points to note.

- Limits are given as V magnitudes, $\text{ergs sec}^{-1} \text{cm}^{-2} \text{\AA}^{-1}$, $\text{ergs sec}^{-1} \text{cm}^{-2} \text{\AA}^{-1} \text{arcsec}^{-2}$.
- The limits were derived assuming zero slit loss.
- The imaging table includes a single point source limit. No single source in the field of view can exceed this limit.
- The limits in the tables assume zero extinction. If your source, when corrected for Galactic extinction, does not exceed the absolute limits, then you will be allowed to observe your source.
- The imaging table also includes an integrated magnitude limit. Remember that the global limit of $200,000 \text{ counts sec}^{-1}$ applies to all sources imaged onto the MAMA detector. The integrated magnitude limit gives the total magnitude from all stars (or galaxies, or diffuse objects) of spectral type O which can appear in the MAMA field of view. Initial screening of all MAMA imaging observations will be done assuming all stars are O stars, however, ultimately for the final decision, the colors of the stars are taken into account whenever such information is available (see Chapter 7).
- Be aware of the additional limitations that exist for crowded fields and slightly-resolved stellar clusters (see Section 7.6.3).

Table 14.39: MAMA Bright-Object limits (V magnitudes and cgs units). V magnitudes include an additional safety factor of 3 in flux to account for extrapolation uncertainties from the optical to the UV spectral range.

Spectral Type	FUV-MAMA				NUV-MAMA							
	25MAMA	F25SRF2	F25QTZ	F25LYA	25MAMA	F25SRF2	F25QTZ	F25CN182	F25CIII	F25CN270	F25MGII	
Flat, point source ¹	9.4x10 ⁻¹⁵	1.7x10 ⁻¹⁴	4.8x10 ⁻¹⁴	4.6x10 ⁻¹³	2.0x10 ⁻¹⁵	2.2x10 ⁻¹⁵	2.4x10 ⁻¹⁵	2.6x10 ⁻¹⁴	1.9x10 ⁻¹³	1.7x10 ⁻¹⁴	8.4x10 ⁻¹⁴	
Flat, extended, peak ²	4.0x10 ⁻¹²	7.2x10 ⁻¹²	2.0x10 ⁻¹¹	1.9x10 ⁻¹⁰	8.8x10 ⁻¹³	9.8x10 ⁻¹³	1.0x10 ⁻¹²	1.1x10 ⁻¹¹	7.8x10 ⁻¹¹	6.8x10 ⁻¹²	3.4x10 ⁻¹¹	
O5 V ³	20.2	19.4	17.9	16.3	20.3	20.1	19.9	17.9	15.7	17.3	15.3	
O7 V	20.0	19.2	17.8	16.1	20.2	20.0	19.8	17.8	15.6	17.2	15.3	
O9 V	19.8	19.0	17.6	15.8	20.0	19.9	19.7	17.7	15.5	17.1	15.2	
B0 V	19.7	18.9	17.5	15.7	19.9	19.8	19.6	17.6	15.4	17.1	15.1	
B1 V	19.4	18.6	17.1	15.4	19.7	19.5	19.3	17.3	15.1	16.9	14.9	
B3 V	18.5	17.8	16.4	14.4	19.0	18.9	18.8	16.6	14.4	16.4	14.5	
B5 V	17.8	17.2	15.9	13.4	18.6	18.4	18.3	16.2	14.0	16.0	14.1	
B8 V	16.7	16.2	15.0	11.7	17.8	17.7	17.6	15.4	13.2	15.3	13.4	
A1 V	14.4	14.2	13.4	8.3	16.7	16.6	16.6	14.2	12.1	14.4	12.6	
A3 V	13.2	13.0	12.7	6.5	16.5	16.4	16.3	13.9	11.9	14.2	12.4	
A5 V	11.9	11.7	11.6	4.5	16.2	16.1	16.1	13.5	11.5	14.0	12.2	
F0 V	9.6	9.4	9.4	2.0	15.7	15.6	15.5	12.6	10.5	13.6	11.8	
F2 V	8.8	8.6	8.5	1.1	15.4	15.3	15.3	12.2	10.0	13.4	11.7	
F5 V	6.8	6.7	6.6	-0.9	15.0	14.9	14.9	11.4	9.1	13.1	11.4	
F8 V	5.6	5.4	5.4	<-2.0	14.8	14.7	14.6	10.9	8.5	12.8	11.2	
G2 V	4.0	3.9	3.8	<-2.0	14.3	14.3	14.2	10.2	7.8	12.4	10.9	
G5 V	3.5	3.4	3.3	<-2.0	14.2	14.1	14.1	10.0	7.6	12.3	10.8	
G8 V	2.8	2.6	2.5	<-2.0	13.9	13.8	13.8	9.5	7.3	12.1	10.6	
K0 V	1.2	1.0	1.0	<-2.0	13.3	13.3	13.2	8.6	6.8	11.5	10.3	
K4 V	<-2.0	<-2.0	<-2.0	<-2.0	11.8	11.7	11.7	6.4	6.0	10.0	9.9	
K7 V	<-2.0	<-2.0	<-2.0	<-2.0	11.1	11.0	10.9	5.2	5.5	9.7	9.7	
M2 V	<-2.0	<-2.0	<-2.0	<-2.0	10.8	10.7	10.7	4.7	5.4	9.5	9.6	
F0 I	10.6	10.4	10.3	3.1	15.3	15.2	15.2	12.5	10.6	13.2	11.5	
G5 I	-1.8	-1.9	-1.9	<-2.0	12.1	12.0	12.0	7.0	6.0	10.2	9.9	
M2 I	<-2.0	<-2.0	<-2.0	<-2.0	10.2	10.1	10.0	3.1	4.0	9.3	9.4	
Integrated V magnitude ⁴	13.4	12.6	11.2	9.6	13.5	13.3	13.1	11.2	8.9	10.5	8.5	
Flat, extended, all detector ⁵	7.4x10 ⁻¹⁵	1.4x10 ⁻¹⁴	4.0x10 ⁻¹⁴	3.6x10 ⁻¹⁷	1.7x10 ⁻¹⁵	1.9x10 ⁻¹⁵	2.0x10 ⁻¹⁵	2.0x10 ⁻¹⁴	1.5x10 ⁻¹³	1.3x10 ⁻¹⁴	6.6x10 ⁻¹⁴	

1. Maximum allowed flux for a point source in $\text{erg s}^{-1} \text{cm}^{-2} \text{\AA}^{-1}$.
2. Maximum peak allowed flux for an extended source in $\text{erg s}^{-1} \text{cm}^{-2} \text{\AA}^{-1} \text{arcsec}^{-2}$.
3. V magnitude limit for unreddened single stars.
4. Maximum integrated V magnitude for stars in the field assuming all are of O5 V spectral type.
5. Maximum allowed flux for an extended source which covers the full detector in $\text{erg s}^{-1} \text{cm}^{-2} \text{\AA}^{-1} \text{arcsec}^{-2}$.



PART IV:

Calibration

The chapters in this part describe the calibration of STIS. These chapters include an overview of the calibration pipeline process, expected accuracies for data, and plans for calibrating and verifying the instrument's performance.

Overview of Pipeline Calibration

In this chapter. . .

15.1 Pipeline Processing Overview / 465

15.2 How Phase II parameter choices affect calibration / 471

15.3 More Detailed Information / 472

In this chapter we summarize briefly the basic reductions and calibrations that are performed in the STScI STIS pipeline, and summarize the effects that particular Phase II proposal parameter choices have on calibration. The material in this chapter is intended to provide only enough background to develop robust observing proposals. A recent series of [STIS Instrument Science Reports](#) and the STIS chapters in the [HST Data Handbook](#) provide the more detailed information needed for analyzing your data.

15.1 Pipeline Processing Overview

Science data taken by STIS are received from the Space Telescope Data Capture Facility and sent to the STScI pipeline, where the data are unpacked, keywords extracted from the telemetry stream, and the science data reformatted and repackaged into raw (uncalibrated) FITS¹ files by the generic conversion process. All STIS data products are FITS files. The vast majority of the STIS data products are two-dimensional images that are

1. Flexible Image Transport System.

stored in FITS image extension files as triplets of science, error, and data quality arrays. FITS image extensions offer great flexibility in data storage and allow us to package related science data that are processed through calibration as a single unit together into one file. The uncalibrated FITS files are passed through **calstis**, the software code that calibrates the data, producing *calibrated* FITS files. For more details on STIS data structure and the naming conventions for the uncalibrated and calibrated data products, see [Chapter 2 in Part II of the STIS Data Handbook](#).

Calstis performs the following basic science data calibrations:

- Basic, two-dimensional image reduction producing a flat-fielded output image (*rootname_flat.fits*), which, depending on whether the data are from the MAMA or the CCD and whether they are imaging or spectroscopic data, includes the following: data quality initialization, dark subtraction, bias subtraction, non-linearity flagging, flat fielding, and photometric calibration.
- Two-dimensional spectral extraction producing a flux-calibrated, rectified spectroscopic image (usually *rootname_x2d.fits* for MAMA data, *_sx2.fits* for CCD) with distance along the slit running linearly along the Y axis and wavelength running linearly along the X axis, for spectroscopic first-order mode data.
- One-dimensional spectral extraction producing a one-dimensional spectrum of flux versus wavelength (usually *rootname_x1d.fits* for MAMA data, *_sx1.fits* for CCD), uninterpolated in wavelength space, but integrated across an extraction aperture in the spatial direction, for first-order and echelle spectroscopic data.
- Data taken in TIME-TAG mode are corrected for the Doppler shift from the spacecraft motion and output as an uncalibrated event stream by the pipeline in a FITS binary table (*rootname_tag.fits*). The time-tag data stream is also integrated in time to produce an uncalibrated ACCUM mode image (*rootname_raw.fits*) which is then passed through standard calibration. The **odelaytime** task in STSDAS can be used off-line to correct the TIME-TAG spacecraft times to heliocentric times.

In addition, **calstis** performs two types of *contemporaneous calibrations*:

- For CCD exposures which have been CR-SPLIT or when multiple exposures have been taken, **calstis** combines the exposures, producing a cosmic-ray rejected image (*rootname_crj.fits*) which is then passed through subsequent calibration (e.g., spectral extraction).
- For spectroscopic exposures, **calstis** processes the associated wavecal exposure (see “Routine Wavecals” on page 28) to determine the zero point offset of the wavelength and spatial scales in the science image,

thereby correcting for thermal drifts and the lack of repeatability of the mode select mechanism. Whereas the uncalibrated science data are stored in the *rootname_raw.fits* file, the accompanying wavecal observations are stored in the file *rootname_wav.fits*.²

Figure 15.1 through Figure 15.3 show example output from the **calstis** pipeline. The **calstis** program propagates statistical errors and tracks data quality flags through the calibration process. **calstis** is available to users in STSDAS, so they can recalibrate their data as needed.³ Recalibration may be performed in its entirety in a manner identical to the pipeline calibration by using **calstis**, or modular components of **calstis**, such as basic two-dimensional image reduction (**basic2d**), two-dimensional spectral extraction (**x2d**), one-dimensional spectral extraction (**x1d**), or cosmic ray rejection (**ocrreject**). The calibration step that **calstis** performs on a given set of science observations depends on the nature of those observations.⁴

Since the spring of 2001, calibrated data products for STIS have been available through On-the-fly-reprocessing (OTFR), which replaces On-the-fly-calibration (OTFC). The OTFR systems starts with raw telemetry products and converts these to FITS files and adds the latest instrument calibrations. This change is transparent to the user.

Some changes have been made to **calstis**, and propagated to OTFR, to handle temporal changes in instrument performance, more changes will be implemented during Cycle 12.

- In July 2001, STIS operation was resumed with side 2 electronics after failure of the side 1 electronics in May. A wider range in the operating temperature of the CCD detector with the side 2 electronics has made it necessary to include a temperature-dependent scaling factor when producing and applying side 2 CCD dark reference files. This is discussed more fully in [STIS ISR 2001-03](#).
- Since September 2002, **calstis** has used epoch-selected darks for the NUV-MAMA, which are scaled by a factor depending on the time and detector temperature of the science data.
- Gradual changes in spectroscopic and imaging sensitivity have been measured over the lifetime of the STIS detectors. See [STIS ISR 2001-01](#) for full details. Currently, 1-D spectral fluxes (FLUX column in *rootname_sx1.fits* and *rootname_x1d.fits* files) extracted from data taken with the first-order low and medium resolu-

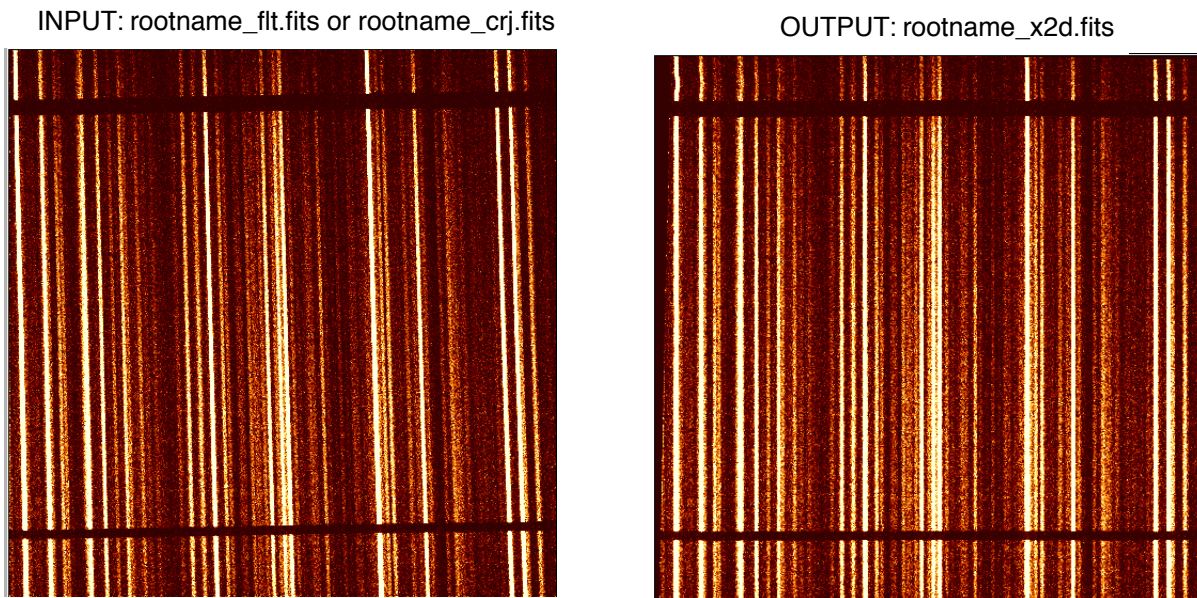
2. Unassociated wavecal observations (e.g., GO added wavecals) are stored in *rootname_raw.fits*, where *rootname* is different for the science and wavecal exposures.

3. The **calstis** software is written in C and uses open IRAF in conjunction with a specially written I/O interface to the FITS data file.

4. Available-but-unsupported-mode data are calibrated only through flat-fielding in the pipeline.

tion CCD and MAMA gratings are calibrated with a time-dependent sensitivity (TDS) factor to correct for these changes. Temporal changes in CCD spectroscopic count rates are dominated by the steadily increasing charge transfer inefficiency (CTI), whose dependence on the structure and count level of the source and background is complex. See Section 7.2.6 and Section 7.2.7 and [STIS ISR 2003-03](#) for additional discussion. Correction of extracted CCD spectral fluxes for these CTI effects is also implemented in the standard pipeline software. TDS corrections were implemented in the pipeline for first-order MAMA spectra in September 2002 (**calstis 2.13b**). TDS and CTE corrections for CCD spectra were implemented in December 2003 (**calstis 2.15b**). Users who have data calibrated with earlier versions of the **calstis** pipeline software may wish to obtain new copies from the MAST archive. Corrections for time-dependent changes of extracted echelle fluxes and for the PHOTFLAM keyword values in imaging data are currently being implemented.

Figure 15.1: Two-Dimensional Rectification



Observers can retrieve HST data by using StarView (<http://starview.stsci.edu/>) or the HST archive WWW interface (<http://archive.stsci.edu/hst/>) to select specific datasets. One can choose where and how the data are delivered: on the archive computer staging disk for copy using anonymous FTP, directly sent to a home computer via FTP or SFTP, or for very large requests, sent on a medium of your choice (CDs, DVDs or tapes). One must be a registered archive user to be able to retrieve HST data (see http://archive.stsci.edu/hst/getting_started.html).

Figure 15.2: Cosmic Ray Rejection

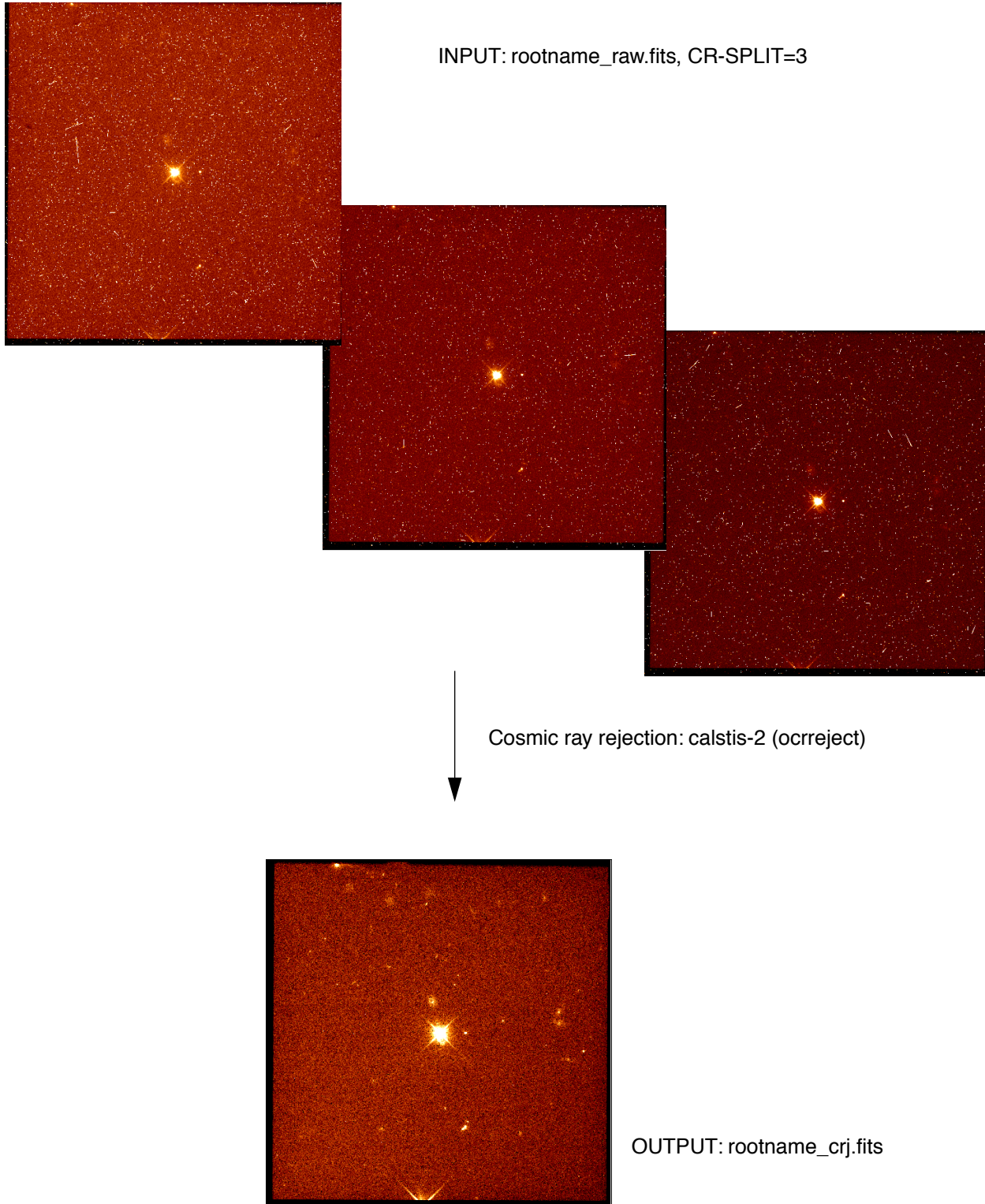
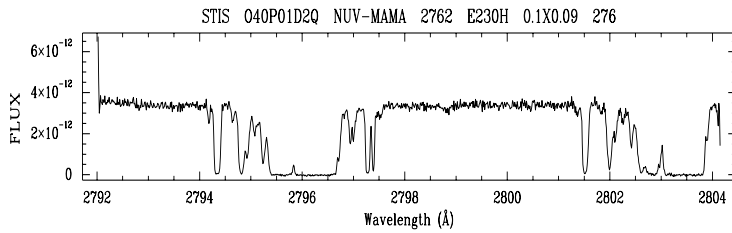
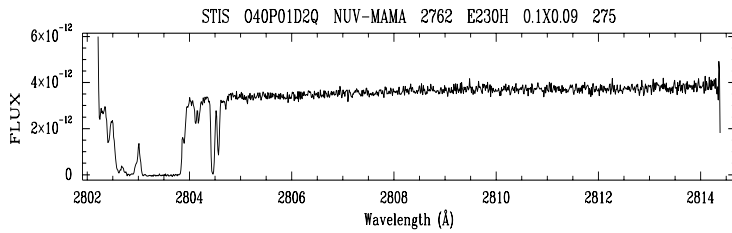
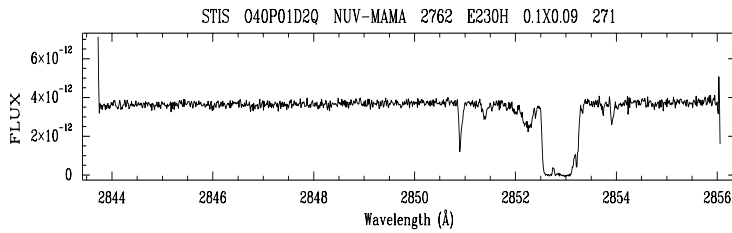
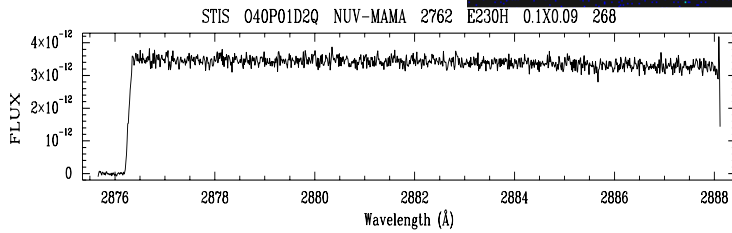
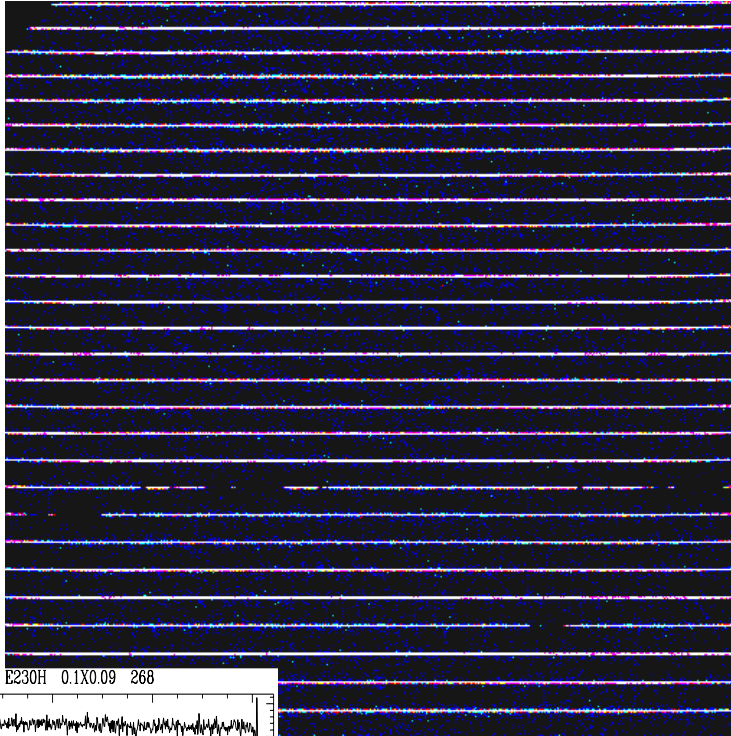


Figure 15.3: One-Dimensional Spectral Extraction

INPUT: rootname_raw.fits,
NUV-MAMA, E230H, cenwave=2762



OUTPUT: rootname_x1d.fits, plotted
by echplot (only a few spectral
orders are plotted)

15.2 How Phase II parameter choices affect calibration

Table 15.1: Calibration dependencies on Phase II parameter choices.

Parameter	Effect in pipeline calibration
Engineering MODE	Not calibrated; receive raw data files only.
Available-but-unsupported MODE	Calibrated through flat-fielding only; no 2-D rectification, cosmic-ray rejection (if applicable), flux calibration, or 1-D extraction.
MODE=ACQ or ACQ/PEAK	Not calibrated; receive raw data files only.
MODE=TIME-TAG	Data events are tabulated in <i>rootname_tag.fits</i> file with one binary table extension for each buffer read (determined by exposure time and BUFFER-TIME parameters). All raw data events are gathered into a single image, <i>rootname_raw.fits</i> , which is then passed through the normal calibration steps.
CCD only CR-SPLIT > 1 or Number_of_Iterations > 1	The number of imsets in the raw file equals CR-SPLIT or Number_of_Iterations. Raw file imsets are cosmic-ray rejected and summed before the bias, dark, and flat-fielding corrections are made, producing a <i>rootname_crj.fits</i> file. The individual imsets are also flagged for cosmic rays and processed without summing to produce a <i>rootnameflt.fits</i> file.
MAMA only Number_of_Iterations > 1	The raw file contains Number_of_Iterations imsets, as do the flat-fielded and 2-D rectified files; the 1-D extracted files contain Number_of_Iterations tables. Repeat exposure imsets are summed after flat-fielding and 2-D rectification producing files <i>rootname_sfl.fits</i> and <i>rootname_x2d.fits</i> respectively (this is also true for imaging data). Note that for the MAMA detectors, 1-D spectral extraction data are not summed even when there are repeat exposures.
POS-TARG	Normal calibration processing.
PATTERN	Separate PATTERN step exposures are not associated with each other. Each PATTERN step exposure is processed through calibration independently.
WAVECAL=NO	No 1-D extraction or 2-D rectification of spectral data will be done, because the associated wavelengths would be incorrect and therefore misleading.
Target_Name=CCDFLAT	An internal STIS CCD flat-field lamp exposure useful in post-pipeline processing to correct for fringing above ~7000 Å with gratings G750L and G750M.

15.3 More Detailed Information

More detailed descriptions of the **calstis** software and its modular components are available in [Chapter 3 of the STIS Data Handbook](#), and in a series of [Instrument Science Reports \(ISRs\)](#) accessible via the [STIS WWW pages](#).

- [STIS ISR 1998-10](#): “Calstis0: Pipeline Calibration of STIS Data—A Detailed View”
- [STIS ISR 1998-26](#): “Calstis1: Basic Two-Dimensional Image Reduction”
- [STIS ISR 1998-11](#): “Calstis2: Cosmic Ray Rejection in the STIS Calibration Pipeline”
- [STIS ISR 1998-22](#): “Cosmic Ray Rejection in STIS CCD Images”
- [STIS ISR 1998-12](#): “Calstis4, calstis11, calstis12: Wavecal Processing in the STIS Calibration Pipeline”
- [STIS ISR 1999-03](#): “Calstis6: “Extraction of 1_d Spectra in the STIS Calibration Pipeline”
- [STIS ISR 1998-13](#): “Calstis7: Two-dimensional rectification of spectroscopic data in the STIS Calibration Pipeline”
- [STIS ISR 1998-28](#): “The STIS Pipeline - Determination of Calibration Switch Settings”
- [STIS ISR 2002-01](#): “2-D Algorithm for Removing Scattered Light from STIS Echelle Data”
- [STIS ISR 2003-03](#): “An Algorithm for Correcting CTE Loss in Spectrophotometry of Point Sources with the STIS CCD”

The ISRs currently contain the most up-to-date descriptions of the calibration software. New releases of **calstis** are accompanied by updates under the “[Software Tools](#)” page on the [STIS](#) web site.

Accuracies

In this chapter. . .

16.1 Summary of Accuracies / 473

In this chapter we describe the accuracies for STIS photometric, spectral, and astrometric calibration we plan to achieve through Cycle 13 and the expectation for Cycle 14.

16.1 Summary of Accuracies

In Table 16.1 through Table 16.5, the accuracies are listed for each of STIS's basic observation modes: CCD spectroscopy, MAMA spectroscopy, CCD imaging, MAMA imaging, and target acquisition. The pixels in these tables are low-resolution pixels. All accuracies quoted are 2σ limits. The accuracies reflect our current understanding of STIS as of June 2004 and are those we expect the pipeline calibration or recalibration of archive data to achieve during Cycle 13.

The accuracies quoted below do not include the effects of time-dependent changes in sensitivity (see Section 7.1.4 and Section 7.3.3). Over that last two years, we have modified our calibration software to take those changes into account. Likewise, the effects of CTE losses on accuracies are not included in the estimates in this chapter (see Section 7.2.6). Correction of extracted CCD spectra for CTE and time-dependent sensitivity was implemented during Cycle 12.

The flux calibration of the echelle modes is adversely affected by the monthly offsetting of the spectrum on the MAMA detectors (see Section 7.5), and this can cause wavelength dependant flux errors of as much as 15%. Software changes to minimize these effects on the flux calibration of

extracted spectra have been implemented for the primary echelle wavelength settings. Note that starting early in Cycle 11, the monthly offsetting of all echelle modes was stopped. For data obtained after this date, this change will ameliorate the uncertainties in flux and wavelength calibration that resulted from the offsetting. Implementation of improvements in the calibration software to correct earlier data for this effect will continue.

We remind you that calibration data are immediately non-proprietary and should you have need for extreme accuracy or urgent results, you may wish to consider direct analysis of the calibration data for your particular observing mode (see also Chapter 17 for a description of our on-orbit calibration program).

Table 16.1: CCD Spectroscopic Accuracies

Attribute	Accuracy ¹	Limiting Factors
Relative wavelengths—within an exposure	0.1–0.3 pixel	<ul style="list-style-type: none"> • Stability of optical distortion • Accuracy of dispersion solutions
Absolute wavelengths—across exposures	0.2–0.5 pixel	<ul style="list-style-type: none"> • Thermal stability • Derivation of wavecal zero point • Accuracy of dispersion solutions
Absolute photometry ^{2,3,4}		Instrument stability, evolution of charge transfer efficiency, and photometric calibration
L modes	5%	
M modes	5%	
Relative photometry ^{2,3} (within an exposure)		Instrument stability, evolution of charge transfer efficiency, and photometric calibration
L modes	2%	
M modes	2%	

1. All accuracies refer to prime wavelength settings and directly calibrated special secondary settings. Intermediate settings have roughly a factor of two less accuracy.
2. Assumes star is well-centered in slit. See the *HST Data Handbook* for a more complete description of the impact of centering on accuracies.
3. Assumes use of a 2'' wide photometric slit. See the *HST Data Handbook* for a fuller description of the impact of slit width on photometric accuracy.
4. Photometric accuracies referenced are for continuum sources; equivalent width and line profile measures are subject to other uncertainties (such as spectral purity and background subtraction).

Table 16.2: MAMA Spectroscopic Accuracies

Attribute	Accuracy ¹	Limiting Factors
Relative wavelengths—within an exposure	0.25–0.5 pixel	<ul style="list-style-type: none"> Stability of small-scale geometric distortion Optical distortion Accuracy of dispersion solutions
Absolute wavelengths ¹	0.5–1.0 pixel	<ul style="list-style-type: none"> Thermal stability Derivation of wavecal zero point Accuracy of dispersion solutions
Absolute photometry ^{1,2,3}		Instrument stability and photometric calibration
L modes	4%	
M modes	5%	
Echelle modes ⁴	8%	
Relative photometry (within an exposure) ^{2,3}		Instrument stability and flat fields
L modes	2%	
M modes	2%	
Echelle modes ⁴	5%	Ripple correction accuracy, scattered light subtraction

1. All accuracies refer to prime wavelength settings and directly calibrated special secondary settings. Intermediate settings have roughly a factor of two less accuracy.
2. Assumes star is well-centered in slit. See the *HST Data Handbook* for a more complete description of the impact of centering on accuracies.
3. Assumes use of a wide photometric slit. See the *HST Data Handbook* for a fuller description of the impact of slit width on photometric accuracy.
4. For 0.2 × 0.2 arcsecond slit. These are typical accuracies which can be 2 to 3 times better or worse as a function of wavelength (see *STIS ISR 1998-18* for details).

Table 16.3: CCD Imaging Accuracies

Attribute	Accuracy	Limiting Factors
Relative astrometry within an image	0.1 pixel	Stability of optical distortion
Absolute photometry	5%	Instrument stability
Relative photometry within an image	5%	External illumination pattern

Table 16.4: MAMA Imaging Accuracies

Attribute	Accuracy	Limiting Factors
Relative astrometry within an image	0.25 pixel	Small scale distortion stability
Absolute photometry	5%	Instrument stability and calibration
Relative photometry within an image	5%	Flat fields and external illumination

Table 16.5: Target Acquisition Accuracies

Attribute	Accuracy	Limiting Factors
Guide star acquisition	1–2 arcseconds	Catalog uncertainties
Following target acquisition exposure		Centering accuracy plus plate scale accuracy to convert pixels to arcseconds
Point sources	0.01 arcsecond	
Diffuse sources	0.01–0.1 arcsecond	See Chapter 8
Following peakup acquisition exposure	5% of the slit width	Number of steps in scan and PSF

16.1.1 Flats

We are in the process of updating all library flats to a signal-to-noise of at least 100:1 per pixel.¹ The CCD flats have temporal variation of < 1% per year. The MAMA flats have shown some evidence for variation at the 1–2% per resolution element level over roughly year timescales. Due to the limited calibration-lamp lifetimes, we expect to take MAMA flats once per year per detector. As our knowledge grows, we will provide updates on the web pages.

1. A “pixel” for the MAMA refers to 1024 x 1024 native format pixels.

Calibration Status and Plans

In this chapter. . .

17.1 Introduction / 477
17.2 Ground Testing and Calibration / 478
17.3 SMOV2 Testing and Calibration / 478
17.4 Cycle 7 Calibration / 480
17.5 Cycle 8 Calibration / 482
17.6 Cycle 9 Calibration / 483
17.7 Cycle 10 Calibration / 484
17.8 Cycle 11 Calibration / 484
17.9 Cycle 12 Calibration / 485
17.10 Cycle 13 Calibration / 486

17.1 Introduction

In this chapter we describe the current status of STIS calibration and the plans for future calibration in Cycle 13. At the time this Handbook is being written, Cycle 12 calibration is nearly complete. Detailed planning for Cycle 13 calibration is approaching completion. The calibration observing cycle starts 2-3 months after the scientific program observing cycle to allow time for development. Below we give a brief guide to the calibrations obtained during ground testing, the original period of Servicing Mission Orbital Verification (SMOV2), and Cycles 7 to 12, as well as the plans for Cycle 13. Further information on calibration, including detailed descriptions of the proposals, can be found on the [STIS “Monitoring” page](#).

STIS provides a large number of available-but-unsupported capabilities (Appendix A) beyond those which are routinely supported. Observers

should remember that *STScI will not normally undertake additional calibrations for these available-but-unsupported instrument configurations*. Observers wishing to use non-standard instrument configurations should assess their specific calibration needs and include time in their Phase I proposal for any additional calibrations that are required. Proposers who believe that more extensive calibration observations or analysis may be of benefit to users of STIS, should consider submitting a Cycle 14 Calibration Outsourcing Proposal (see the Cycle 14 “Call for Proposals” for details).

17.2 Ground Testing and Calibration

The STIS Investigation Definition Team (Principal Investigator, Bruce Woodgate, GSFC) was responsible for the ground testing and ground calibration of STIS. Most of the ground test data were obtained in late 1996, during thermal vacuum testing at Ball Aerospace in Colorado, and during subsequent testing in a dry-nitrogen environment at GSFC. These tests characterized the basic properties of the optics, the detectors, and the mechanisms. Certain measurements (e.g., measurements of the quantum efficiency of the STIS detectors vs. wavelength) cannot be repeated in orbit. However, most of the ground test data have been superseded by on-orbit measurements.

17.3 SMOV2 Testing and Calibration

The primary goal of the Second Servicing Mission’s Orbital Verification (SMOV2) was the timely commissioning of the HST observatory for normal science operations. For STIS, just installed at this time, this included testing the focus (internal and external), verifying the target acquisition procedures, monitoring instrument stability (both in terms of image motions and sensitivity), and measuring selected characteristics: plate scales, slit throughputs, line spread functions, etc. SMOV2 observations were complete by the summer of 1997. Most of the results of the calibrations were presented in the [1997 HST Calibration Workshop](#). A high level summary was provided in the Kimble et al. (1998, *ApJ*, 492, L83) paper on STIS on-orbit performance. For an update including early Cycle 7 calibration, see also Baum et al., 1998, *SPIE*, 3356, 271. Brief descriptions of the SMOV2 proposals are given in Table 17.1. Data from

calibration proposals are non-proprietary, and can be obtained from the archive with the proposal IDs listed in the table.

Table 17.1: STIS SMOV2 Proposals

ID	Title
7058	STIS Memory Load and Dump
7059	Science Data Buffer Check with Self-Test
7061	CCD Functional
7062	CCD Temperature Set Point Determination
7063, 7064	STIS SMOV Contamination Monitor
7065	STIS to FGS Alignment
7066	STIS Acquisition Aperture and Slit Location
7067	STIS CCD Point Source Acquisition
7068	STIS CCD Diffuse Source Acquisition
7070	STIS CCD Coronagraphic Acquisition
7071	CCD Target Centering
7073	CCD Peakdowns for Coronagraphic Acquisition
7075	STIS Corrector Alignment, Coarse
7076	STIS Corrector Alignment, Fine
7077, 7078	Spectroscopic Mode Image Quality
7079, 7080	Camera Mode Image Quality
7081, 7082	Repeatability of Image Positions for STIS Modes
7083, 7084	Verification of Optical Format of STIS Modes
7085, 7086	STIS Slit to Detector Internal Stability
7087	OTA-STIS Pointing and Throughput Stability
7088, 7089	Occulting Bar Scattered Light
7090	PSF measurement for MAMAs
7091	STIS Pixel-To-Pixel Response Stability
7092	CCD Dark Rate and Read Noise
7093	Dark Measurement for MAMAs
7094, 7096	STIS Sensitivity On-Axis
7095, 7097	STIS Sensitivity (Vignetting)
7098	MAMA Flat Field Uniformity
7099	CCD Flat Field Stability

Table 17.1: STIS SMOV2 Proposals (Continued)

ID	Title
7100	SMOV Slit Transmission
7101	SMOV Slit Transmission
7103	STIS Mechanism Mini-Functional
7104	STIS Onboard Doppler Processing Checkout
7105	MAMA Turn-On
7106	STIS MAMA Fold Distribution
7107	STIS CCD Hot Pixel Annealing
7108	STIS MAMA Time Tag Mode
7131, 7132	STIS Imaging Mode Geometric Distortion
7133	STIS to FGS alignment
7142	CCD Flat Field Monitoring
7143	CCD Internal Image stability with LVPS cycling
7144	STIS Thermal Stability with LVPS cycling
7147	STIS Fine Corrector Alignment with CCD
7148	STIS CCD Target Acquisition Workout
7151	STIS CCD V2V3 Aperture Verification
7159	NUV MAMA Dark Current vs. Time from SAA
7160	CCD Reconfiguration Effects

17.4 Cycle 7 Calibration

The [STIS Cycle 7 calibration plan](#) included additional characterization of STIS performance, along with periodic monitoring of sensitivity, flat fields, dark current, gain, etc. Because it is not feasible to calibrate the instrument in all possible observing modes, the calibration emphasizes measurements in all the *supported* modes.

The results of all Cycle 7 calibration programs are presented in the close-out report [STIS ISR 2000-04](#).

17.4.1 Calibration Priorities

The task of calibrating STIS involved a number of important trade-offs. HST calibration observations are planned to use a limited number of orbits

(no more than about 10% of the total science time allocated in the cycle), and to stretch out through each cycle so that the observing schedule is not too heavily front-loaded with calibrations. The allocation of spacecraft and staff resources to the calibration effort for STIS has followed roughly the following set of priorities:

1. *Monitor the health and safety of STIS.* Carry out the necessary periodic monitoring of STIS to ensure that it is operating correctly. Revise operations as necessary to ensure that it will maintain its scientific performance over its (anticipated 13 year) lifetime.
2. *Update and Maintain Pipeline Reference files.* This includes such things as darks, biases, flats, and sensitivities. Information on newly released files is announced via the [Space Telescope Analysis Newsletters \(STANs\)](#), and posted to the [STIS WWW pages](#). As new reference files are incorporated into the pipeline, the “recommended reference files” are updated as appropriate for each dataset in the HST Archive.
3. *Basic sensitivity calibration of spectroscopic modes.* The majority of STIS science observations use the spectroscopic modes. Sensitivity calibration is important for instrument safety, science optimization, and data analysis. The sensitivity calibration includes basic measurements of on-orbit throughput, and monitoring of time variations either due to contamination or due to gain variations in the detectors.
4. *Characterization of optical performance.* This includes point-spread functions, line-spread functions, aperture throughputs, enclosed energy for different spectral extraction heights, and imaging and spectroscopic geometric distortion calibrations. Detailed characterization of scattering (e.g., in wavelength in the gratings, or in the far wings of the imaging PSF) is included, but is orbit-intensive and therefore will be carried out over a longer time scale.
5. *Characterization of detector and observation specific peculiarities.* This includes detector nonlinearities, charge transfer effects, fringing, long-wavelength scattering within the CCD, grating scatter and extended PSF wings, etc.
6. *Calibration and testing of future observing mode strategies.* The original goals to test cross-dispersed gratings and other operating modes were scaled back through the course of Cycle 7 due to the press of the higher priority calibrations.

Within each of these priority groups, calibration priority is in the following order by observing mode:

1. First order prime L grating modes (G140L, G230L, G430L, G750L).

2. Echelle spectroscopy.
3. First- order M-mode gratings.
4. CCD imaging (broad band first, then narrow band).
5. MAMA imaging (broad band first, then narrow band).
6. G230LB and G230MB backup modes, including analysis of scattered red light.

In addition, on-axis calibrations have higher priority than off-axis calibrations. That is, we sought first to establish the calibrations at the field/slit center and thereafter, to expand the calibration to two dimensions.

17.4.2 Calibration Status

The overall status of STIS calibration was summarized in the STScI Newsletter in October 1998 and in the Cycle 7 Calibration Close-out Report (STIS ISR 2000-04). Many reference files were updated with new calibrations from on-orbit data. The HISTORY and PEDIGREE fields of the calibration reference files should be consulted if you are in doubt about the origin of the calibration. HISTORY keywords contain commentary on the file's creation. The PEDIGREE keyword describes the type of data (GROUND, INFLIGHT) and gives the date range over which the calibration data were taken.

17.5 Cycle 8 Calibration

The [Cycle 8 calibration plan](#) was modeled closely on the Cycle 7 calibration plan. Once again, *supported* modes were monitored for such things as sensitivity changes, flat field evolution, and dispersion solutions. No additional calibrations were taken for most *available-but-unsupported* configurations.

In addition to monitoring instrument health and safety and maintaining the overall calibration of STIS supported modes, our special goals were as follows:

1. to improve the imaging throughput calibration accuracy (to better than the current 5% systematic uncertainty);
2. to improve PSF characterization in imaging mode and in coronagraphic mode;
3. to improve CCD hot-pixel and bias subtraction;
4. to improve the CCD charge transfer efficiency (CTE) characterization for sparse fields at low count levels;

5. to calibrate the dispersion as a function of position for MAMA slitless spectroscopy with the L-mode gratings;
6. to characterize observations with the FUV-MAMA repeller wire turned off, with the aim of possibly making this available for Cycle 10. This should improve the spectral resolution at the expense of a ~35% loss of sensitivity.

The results of all the Cycle 8 calibration programs are presented in the close-out report [STIS ISR 2001-04](#).

17.6 Cycle 9 Calibration

The [STIS Cycle 9 calibration plan](#) was modeled closely on the Cycle 8 calibration plan. *Supported* modes were monitored for items such as sensitivity changes, flat field evolution, and dispersion solutions.

In addition to monitoring instrument health and safety and maintaining the overall calibration of STIS supported modes at the accuracies as established during Cycles 7 and 8, a few special calibration programs were added for Cycle 9, with the following goals:

1. To improve the Charge Transfer Efficiency (CTE) characterization for the CCD, i.e., its dependences on time, source intensity, source nature (point source vs. extended source), and sky background;
2. To quantify the remanence intensity level after over-illumination of the CCD as a function of time after saturation and of number of read-outs after saturation. The remanence level may well have increased since STIS was installed on HST due to the degraded CTE;
3. To improve PSF characterization for the CCD in imaging mode, coronagraphic mode, and spectroscopic mode as a function of source color;
4. To improve the dispersion solutions for the reddest settings of the G750M grating;
5. To model the ghosts (which are caused by multiple reflections in the CCD window) in the G750M grating mode.

The results of all the Cycle 9 calibration programs are presented in the close-out report [STIS ISR 2003-02](#).

17.7 Cycle 10 Calibration

The [STIS Cycle 10 calibration plan](#) was in turn very similar to the Cycle 9 calibration program. Supported modes continued to be monitored for items such as sensitivity changes, flat field evolution, dispersion solutions, and evolution of charge transfer efficiency of the CCD detector.

In addition to monitoring instrument health and safety and maintaining the overall calibration of STIS supported modes at the accuracies as established during Cycles 7 through 9, a few new calibration programs were added for Cycle 10, with the following goals.

1. To obtain exposures of primary spectrophotometric standard stars in *every single* supported spectroscopic mode of STIS, including the echelle and first-order medium-resolution modes;
2. To characterize the effect of the presence of bright stars outside the field of view of the STIS CCD on the amount of scattered light;
3. To further improve PSF characterization for the CCD in imaging and coronagraphic mode as a function of source color;
4. To finalize the accurate determination of the throughput curve of the Long-Pass filter used for CCD imaging;
5. To monitor the throughput curves of the broad-band and medium-band imaging filters used with the MAMA's and the CCD;
6. To characterize STIS spectroscopic performance at the recently defined, "pseudo-apertures" located near row 900 of the CCD (see Section 7.2.7) that have been defined to ameliorate losses due to the decreasing charge transfer efficiency of the CCD with time. Spectroscopic sensitivity, PSFs, and LSFs will be measured at the pseudo-apertures using all supported long slits.

17.8 Cycle 11 Calibration

The [Cycle 11 calibration plan](#) closely follows the plans for previous cycles. Supported modes continue to be monitored for sensitivity changes, flat field evolution, dispersion solutions, and the evolution of charge transfer efficiency of the CCD detector. Existing monitor programs have been expanded to include routine sensitivity measurements at the E1 aperture positions, to include an annual NUV-PRISM flux monitor observation, and to more thoroughly check the adopted STIS dispersion solutions. The frequency of some other monitors has been decreased, as our improved understanding of STIS allows us to predict future trends with greater confidence.

In addition to monitoring instrument health and safety and maintaining the overall calibration of STIS supported modes at the accuracies established during cycles 7 through 10, a few special calibration programs have been added for Cycle 11, with the following goals:

1. To improve the calibration of detector sensitivity, aperture throughputs, and the PSF at the E1 positions that were defined to mitigate CTI effects;
2. To better test the effects of the monthly MSM offsetting on echelle sensitivity;
3. To verify models the PSF for first order G750L and G750M observations that are critical for many programs targeted at determining rotation curves of galaxies and black hole masses;
4. To remeasure, with improved accuracy, the ratio between CCD-GAIN=1 and CCDGAIN=4 observations;
5. To define additional faint spectroscopic flux standards to support calibration of ACS (especially the ACS Sloan filters), and COS.

17.9 Cycle 12 Calibration

The [Cycle 12 calibration plan](#) continues the routine monitoring programs of Cycle 11, with reductions in observing time where less data or less frequent monitoring are now sufficient. As before, much of the program is devoted to producing timely darks, biases, flats, and sensitivity corrections, and to monitoring basic instrument characteristics and performance. Characterization of CTE remains a high priority, to support upcoming CTE correction of fluxes in extracted CCD spectra in the pipeline.

Additional or modified observations were made to meet specific needs in some continuing programs, and some new observations were made, as follows:

1. CCD spectroscopic sensitivity was monitored somewhat more frequently so that dependence on detector temperature can be modelled more accurately, along with tracking temporal dependence.
2. Deeper MAMA wavecal exposures were made to support physical modelling that will lead to better dispersion solutions.
3. Spectroscopic observations were made of a star stepped along slit, achieving low signal and background levels, to improve our characterization of the large CTE losses that occur at these low levels.

4. New “apertures” (target locations in existing apertures) were defined to improve observations high on the CCD detector (where CTE losses are less) and low on the FUV-MAMA detector (where dark current is less), and to provide a new coronagraphic aperture (see Section 12.10). The locations of the new apertures were verified.

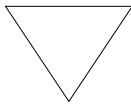
17.10 Cycle 13 Calibration

The Cycle 13 calibration plan largely continues the routine monitoring programs of Cycle 12. These programs were trimmed in Cycle 12 where the stability of instrument performance and the completeness of prior calibration permitted. Much of the calibration plan is devoted to producing timely darks, biases, flats, sensitivity corrections, and corrections for the steady degradation of charge transfer efficiency (CTE). Testing is under way to apply time-dependent sensitivity corrections to images and to echelle spectra; corrections are already being applied to first-order spectra. Extracted CCD spectra are now being corrected for CTE losses as well as sensitivity changes (see [STIS ISR 2003-03](#)), based on a combination of programs to characterize the CTE losses at different signal and background levels and on iterative analysis of sensitivity changes and CTE losses.

New or additional observations are planned in the following areas:

1. Additional observations are needed to characterize throughput for a few configurations using detector-centered and E1 apertures. More exposures will also be taken to support the production of flats for E1 apertures.
2. The HITM1 calibration lamp is used to produce wavecalcs for many configurations, and to illuminate the reference aperture during the STIS target acquisition procedure. After a few instances of late or failed lamp turn-ons in these observing modes, a program was added in Cycle 12 to characterize the performance of the alternate HITM2 calibration lamp. More HITM2 observations will be made in Cycle 13, including MAMA observations as well as additional CCD observations.
3. A new geometric distortion solution was recently produced for the NUV-MAMA ([STIS ISR 2004-01](#)). Observations will be made in Cycle 13 to support the production of new geometric distortion solutions for the FUV-MAMA and the CCD.
4. The effects on spectral images of mis-centering a target in the slit will be investigated. This program will supplement GO observations for a limited set of configurations and calibration program observations of a source placed beyond the edge of the slit.

5. In Cycle 12, members of the HST European Coordinating Facility (ECF) collaborated with STScI staff to take deep wavecal in the echelle modes to support their production of improved dispersion solutions. In Cycle 13, a GO program will take echelle wavecal at a variety of time intervals to test the stability of the wavelength scales over periods of days to months. As a supplement to this program, ECF and STScI staff will conduct an echelle wavecal program that samples the sub-orbital time-scale to characterize the effects of bright/shadow transition, thermal cycling, and potential geomagnetic influence.



If your program requires unique calibrations beyond those that are planned (use the Cycle 7-13 Calibration Programs as a guide) and that are of direct benefit to other STIS users, then you should apply directly for this calibration in your Phase I proposal.

Available-But-Unsupported Spectroscopic Capabilities

In this appendix. . .

A.1 Introduction / 489

A.2 Full Aperture Complement / 490

A.3 Central Wavelength Settings / 494

A.1 Introduction

STIS provides additional *available-but-unsupported* capabilities beyond those which will be routinely *supported*. Section 2.4 describes the distinction between supported and available-but-unsupported modes, and the policy with regard to the use of the latter.

This appendix to the *STIS Instrument Handbook* provides information about the additional available-but-unsupported capabilities of STIS. Since all of the imaging capabilities are supported, it contains information relevant to spectroscopic observations only. Briefly, these comprise the use of numerous additional entrance slits or apertures beyond those which are currently supported, and a small number of central wavelength settings which have been removed from the set of supported settings due to difficulties with them (e.g., order overlap).

A.2 Full Aperture Complement

The STIS aperture wheel has 65 positions, several of which correspond to multiple slits or masks. Only a small fraction of the full complement of spectroscopic apertures are currently supported. Table A.1 provides a complete list of STIS apertures for spectroscopy, together with comments regarding their characteristics or purposes. Schematics of three complex apertures are given in Figure A.1, Figure A.2, and Figure A.3.

Table A.1: STIS Spectroscopic Apertures. Supported apertures are in boldface. For most apertures, the name gives the length by the width in arcseconds.

Apertures	Comments
<i>Apertures that can be used with the First-Order Gratings and the NUV-PRISM</i>	
52X0.05 52X0.1 52X0.2 52X0.5 52X2	Long slits; the names give the length in the spatial direction by the width in the dispersion direction in arcseconds.
52X0.05E1 52X0.1E1 52X0.2E1 52X0.5E1 52X2E1	Long slits centered at 19.7 arcsec in +Y position. (Places compact target at row ~900 on the CCD to reduce CTE losses.). Supported with all CCD gratings. Use with the MAMAs is not allowed.
52X0.2E2 52X0.5E2 52X2E2	These CTE aperture positions are also centered near row 900 on the STIS CCD detector. However, the positions are offset from the physical aperture centers to give better alignment with fringe flats done using the 52X0.1 aperture. The E2 positions are supported for the G750L and G750M gratings only.
52X0.05D1 52X0.1D1 52X0.2D1 52X0.5D1 52X2D1	These aperture positions put a target near the bottom edge of the FUV-MAMA and are intended for observation of very faint targets where it is necessary to minimize the contribution of the FUV-MAMA dark current. They are all supported with the G140L and G140M gratings. 52X0.05D1 and 52X0.1D1 are also supported for CCD peakups.
52X0.05F1 52X0.05F2 52X0.1F1 52X0.1F2 52X0.2F1 52X0.2F2 52X0.5F1 52X0.5F2 52X2F1 52X2F2	Fiducial bars on the long slits which can be used for coronagraphic spectroscopy. The 52X0.2F1 is supported for all first-order gratings and is available-but-unsupported for the PRISM. The other fiducial bars are available-but-unsupported with all gratings and the PRISM. The F1 and F2 bars are 0.5" and 0.86" long, respectively (see Figure 13.1).
52X0.1B0.5 52X0.1B1.0 52X0.1B3.0	A long slit with 3 fiducial bars where the bar length in arcseconds is given by the third dimension. See Figure A.1.
31X0.05NDA 31X0.05NDB 31X0.05NDC	Neutral-density-filtered long slits of the given dimensions in arcsec, which may be used for bright objects or flat-field calibration. The dex ND factors are 0.4, 0.8, and 1.2, respectively.
0.5x0.5 2X2 6X6	Square apertures of the given dimensions in arcsec.
0.1X0.03 0.1X0.06 0.1X0.09 0.1X0.2 0.2X0.06 0.2X0.09 0.2X0.2 0.2X0.5 0.3X0.06 0.3X0.09 0.3X0.2 1X0.06 1X0.2 6X0.06 6X0.2 6X0.5 0.2X0.05ND 0.3X0.05ND	As of Cycle 12, the 0.2X0.2 aperture is supported for use with all first-order gratings; it is available-but-unsupported with the PRISM. While not supported for first-order observations, the other echelle apertures can be used in first order as available-but-unsupported apertures. This includes the echelle neutral-density slits 0.2X0.05ND and 0.3X0.05ND with dex ND factors of 2.0 and 3.0, respectively.

Table A.1: STIS Spectroscopic Apertures. Supported apertures are in boldface. For most apertures, the name gives the length by the width in arcseconds.

Apertures	Comments
25MAMA 50CCD	Supported full-field clear apertures.
F25QTZ F25SRF2	F25QTZ and F25SRF2 are supported for all MAMA gratings and PRISM, but are unavailable with the CCD.
25MAMAD1 F25SRF2D1 F25QTZD1	These aperture positions put a target near the bottom edge of the FUV-MAMA and are intended for observation of very faint targets where it is necessary to minimize the contribution of the FUV-MAMA dark current. They are all supported with the G140L and G140M gratings.
F25ND3 F25ND5 F25NDQ1 F25NDQ2 F25NDQ3 F25NDQ4	Supported neutral-density filters for MAMA detectors. Can be used as available-but-unsupported apertures with the CCD gratings. The numbers give the dex ND factors.
F25MGII F25CN270 F25CIII F25CN182	F25MGII is supported and these other filters are available -but-unsupported with the NUV-MAMA gratings and PRISM only.
F25LYA	The F25LYA filter is available-but-unsupported with the G140L, G140M, E140H, and E140M gratings only.
F28X50LP F28X50OII F28X50OIII	These CCD imaging filters are available-but-unsupported with the CCD gratings, but are unavailable with the MAMA detectors.
36X0.05P45 36X0.05N45 36X0.6P45 36X0.6N45	Long slits of the given dimensions in arcsec which are inclined at $\pm 45^\circ$ to facilitate observations of moving targets at off-nominal rolls. See Figure A.1.
<i>Apertures that can be used with the Echelle Gratings</i>	
0.1X0.03 0.1X0.06 0.1X0.09 0.1X0.2	The latter two are supported with E230H only. The 0.1x0.03 is supported with all echelle gratings.
0.2X0.06 0.2X0.09 0.2X0.2 0.2X0.5	0.2X0.06 and 0.2X0.2 are supported with E230M and E140M, while 0.2X0.09 and 0.2X0.2 are supported with E230H and E140H.
0.2X0.06FP 0.2X0.2FP	Masks with five apertures, suffixed A through E, for reduction of fixed-pattern noise; see Figure A.3.
0.2X0.05ND 0.3X0.05ND	Neutral-density slits. Dex ND factors are 2.0 and 3.0, respectively.
0.3X0.06 0.3X0.09 0.3X0.2 0.5X0.5 1X0.06 1X0.2	Miscellaneous available-but-unsupported echelle apertures.
2X2 6X0.06 6X0.2 6X0.5 6X6	The 6X0.2 long slit is supported with the echelles.
52X0.05 52X0.1 52X0.2 52x0.5 52X2	Long slits for use with the echelles. 52X0.05 is supported, and the others are available-but-unsupported with the echelle gratings.
52X0.05F1 52X0.05F2 52X0.1F1 52X0.1F2 52X0.2F1 52X0.2F2 52X0.5F1 52X0.5F2 52X2F1 52X2F2	The fiducial bar slits are available-but-unsupported with the echelle gratings.
52X0.1B0.5 52x0.1B1.0 52x0.1B3.0	A long slit with 3 fiducial bars. The bar length in arcseconds is given by the third dimension. See Figure A.1.

Table A.1: STIS Spectroscopic Apertures. Supported apertures are in boldface. For most apertures, the name gives the length by the width in arcseconds.

Apertures	Comments
31X0.05NDA 31X0.05NDB 31X0.05NDC	Neutral-density-filtered long slits, which may be used for bright objects. The dex ND factors are 0.4, 0.8, and 1.2, respectively.
25MAMA	Full-field clear aperture.
F25QTZ F25SRF2	Supported long-pass filters, with all echelles.
F25ND3 F25ND5 F25NDQ1 F25NDQ2 F25NDQ3 F25NDQ4	Supported neutral-density filters for MAMA detectors. The numbers give the dex ND factors.
F25MGII F25CN270 F25CIII F25CN182	Narrow-band filters. F25MGII is supported for E230H and E230M. Others are available with the NUV-MAMA only.
F25LYA	Available-but-unsupported with the FUV-MAMA only.
36X0.05P45 36X0.05N45 36X0.6P45 36X0.6N45	Long slits which are inclined at $\pm 45^\circ$ to facilitate observations of moving targets at off-nominal rolls. See Figure A.2.

Figure A.1: Schematic Showing the 52x 0.1" Long Slit with 3 Occulting Bars.

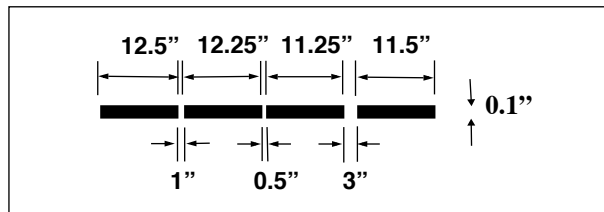


Figure A.2: Schematic Showing the STIS 45° Slits Design. A second pair has the same morphology but widths of 0.6" (central) and 2.0" (peripheral).

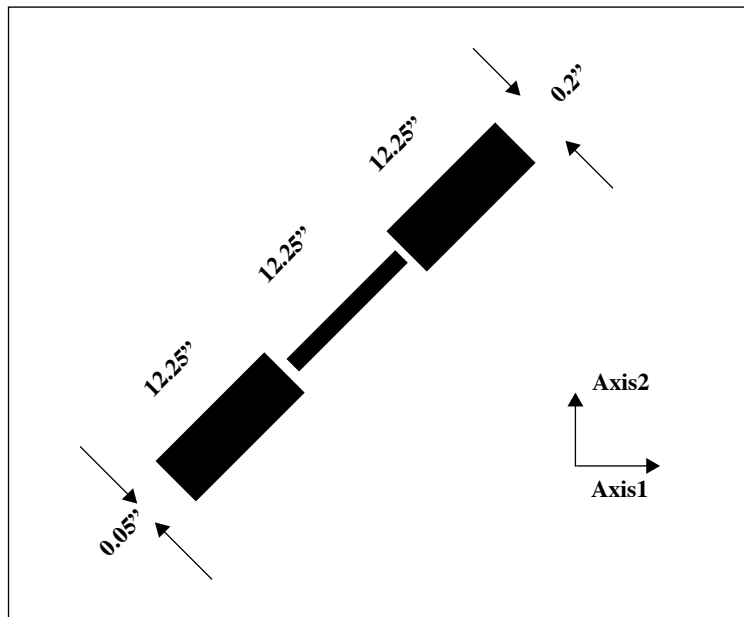
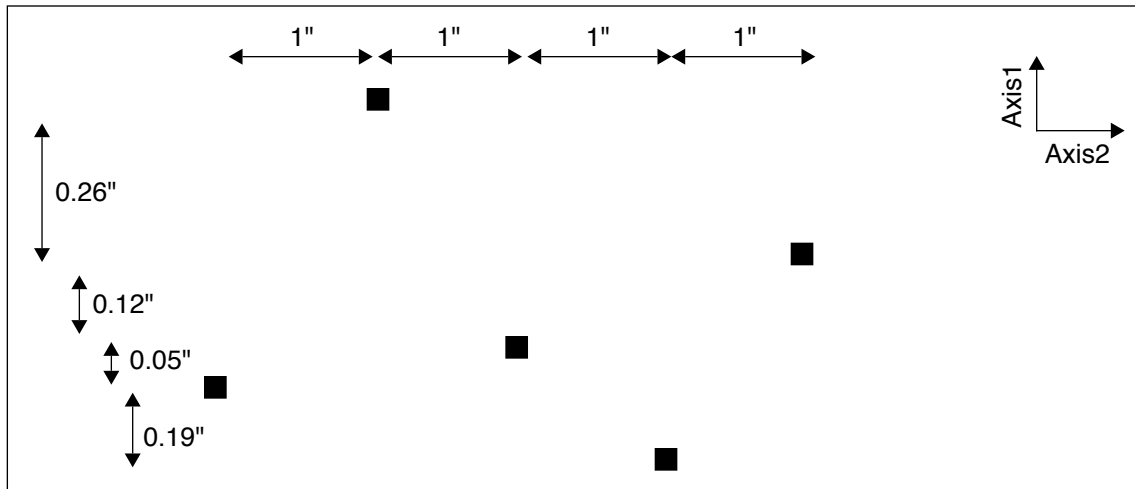


Figure A.3: Schematic Showing the Configuration of the Fixed-Pattern Slits. There are two sets with slit widths of 0.06" and 0.2", and lengths of 0.2" in both cases. Axis1 corresponds to the dispersion direction.



The 45° slits (Figure A.2) are nominally inclined at plus or minus that angle with respect to the dispersion and normal long slit, in order to increase the scheduling flexibility for moving-target observations with specified position angles. Otherwise, the HST roll angle constraints severely limit the windows for such observations. These slits have different widths in their central and outer segments, and there are two pairs with different dimensions.

The fixed-pattern slits (Figure A.3) comprise two masks with five apertures each, which are spaced to place the spectrum at different detector locations designed to optimize the reduction of fixed-pattern noise. The target is moved from one aperture to another, and the slit wheel is repositioned, with the intention that the spectrum shifts along the dispersion direction only. See Section 12.5.2 for further details.

It is not feasible to provide detailed transmission properties of all of the unsupported apertures at this time. They can in many cases be estimated from the data provided for similar supported apertures in Chapter 13, and from the imaging data in Table 14.38.

A.3 Central Wavelength Settings

The following central wavelength settings are available-but-unsupported.

Table A.2: Unsupported Central Wavelength Settings

Grating	Central Wavelength (Å)	Why Unsupported
G750L	8975	Confused by second order
G750M	10363	Confused by second order

Additionally, two central wavelength settings originally offered in the Cycle 7 Handbook were found not to be achievable with STIS, and these have been removed from the available-but-unsupported complement. They are:

Table A.3: Unavailable Central Wavelength Settings

Grating	Central Wavelength (Å)	Why Unavailable
G750M	10871	Not reachable
G230M	3134	Not reachable

Glossary

The following terms and acronyms are used in this Handbook.

A-D: Analog to Digital

ACS: Advanced Camera for Surveys

ABMAG: $-2.5 \log (F_{\nu}) - 48.60$ where F_{ν} is the flux from the source in $\text{erg cm}^{-2} \text{sec}^{-1} \text{hz}^{-1}$

APT: Astronomer's Proposal Tool

BOP: Bright-Object Protection

CALSTIS: STIS calibration pipeline software

CCD: Charge Coupled Device. Solid-state, light detecting device

CDBS: Calibration Data Base. System for maintaining reference files and tables used to calibrate HST observational datasets.

CIM: Calibration insert mechanism

CP: Call for Proposals

CR: Cosmic ray

CR-SPLIT: Division of a CCD exposure into shorter exposures to be used for cosmic ray rejection

CTE: Charge Transfer Efficiency

CTI: Charge Transfer Inefficiency

CVZ: Continuous Viewing Zone

DQ: Data Quality

DN: Data Number

ETC: Exposure Time Calculator. ETCs are web-based tools which can be accessed through the STIS web pages.

ERO: Early Release Observations

FAQ: Frequently Asked Questions

FGS: Fine Guidance Sensors

FITS: Flexible Image Transport System. A generic IEEE and NASA defined standard file format used for storing image data.

FOC: Faint Object Camera

foible: Peculiarities in the STIS data, usually caused by the data processing software. Data foibles are posted on the STIS web pages.

FOS: Faint Object Spectrograph

FOV: Field of View

FSW: Flight Software

FTP: File Transfer Protocol. Basic tool used to retrieve files from a remote system. Ask your system manager for information about using FTP.

FUV: Far Ultraviolet (~912-2000 Å)

FWHM: Full Width at Half Maximum

GEIS: Generic Edited Information Set. Multigroup format used by STSDAS for storing some HST image data.

GHR: Goddard High-Resolution Spectrograph

GO: General Observer

GSC: Guide Star Catalog

GTO: Guaranteed Time Observer

HDA: Hubble Data Archive

Help Desk: Facility for getting help on HST related topics via email. help@stsci.edu.

HITM: Hole in the Mirror

HSP: High-Speed Photometer

HST: Hubble Space Telescope

HUT: Hopkins Ultraviolet Telescope

ICD: Interface control document. Defines data structures used between software or systems to ensure compatibility.

IDT: Investigation Development Team

IHB: Instrument Handbook

IR: Infrared

IRAF: Image Reduction and Analysis System. The environment in which STSDAS operates.

IS: Instrument Scientist

ISR: Instrument Science Report

IUE: International Ultraviolet Explorer

K: Degree Kelvin

LMC: Large Magellanic Cloud

LSF: Line-spread function

MAMA: Multi-Anode Microchannel Array

MCP: Microchannel Plate

- MSM:** Mode-Selection Mechanism
- ND:** Neutral density
- NICMOS:** Near-Infrared Camera and Multi-Object Spectrograph
- NUV:** Near ultraviolet (~2000-4000 Å)
- OSS:** Observation Support System
- OTA:** Optical Telescope Assembly
- OTFR:** On-the-Fly Re-processing
- PC:** Program Coordinator
- Phase I:** A proposal for observing time on HST
- Phase II:** An approved HST proposal; includes precise detail of how program is to be executed
- PI:** Principal investigator
- PSF:** Point-spread function.
- QE:** Quantum efficiency
- QEH:** Quantum efficiency hysteresis
- QPOE:** Quick Position-Oriented Event (IRAF data format for x-ray data)
- QSO:** Quasi-stellar object
- RA:** Right ascension
- reference file:** Data file containing STIS parameters or calibration information which is used by the pipeline
- rms:** Root mean square
- SAA:** South Atlantic anomaly
- SIM:** Space Interferometry Mission
- SITe:** Scientific Image Technologies; company that designed the STIS CCD
- SMOV:** Servicing Mission Orbital Verification
- S/N:** Signal-to-noise ratio
- ST-ECF:** Space Telescope European Coordinating Facility
- STAN:** Space Telescope Analysis Newsletter
- STIS:** Space Telescope Imaging Spectrograph
- STMAG:** STScI magnitude system; $-2.5 \log (F_\lambda) - 21.10$ where F_λ is the flux from the source in $\text{erg cm}^{-2} \text{sec}^{-1} \text{Å}^{-1}$
- STScI:** Space Telescope Science Institute
- STSDAS:** Space Telescope Science Data Analysis System. The complete suite of IRAF data analysis and calibration routines used to process HST data.

SV: Science verification. Process of taking observations that can be used for HST instrument calibration.

synphot: STSDAS synthetic photometry (IRAF) software package

TAC: Telescope Allocation Committee

TAS: Target Acquisitions Simulator; software available on the web

TDS: Time-dependent Sensitivity

TIR: Technical Instrument Report

URL: Uniform resource locator. Address for WWW.

UV: Ultraviolet

WF/PC: Wide Field/Planetary Camera

WFPC2: Wide Field Planetary Camera-2. Replacement for WF/PC installed during first servicing mission of December 1993.

WWW: World Wide Web.

Index

Numerics

0.1X0.03 Aperture 353
0.2X0.05ND Aperture 358
0.2X0.06 Aperture 349
0.2X0.06FP(A-E) Apertures 354
0.2X0.09 Aperture 351
0.2X0.2 Aperture 52, 350
0.2X0.2FP(A-E) Apertures 356
0.3X0.05ND Aperture 359
52X0.05 Aperture 338
52X0.05D1 Aperture 339
52X0.05E1 Aperture 139, 236, 339, 348
52X0.1 Aperture 340
52X0.1D1 Aperture 341
52X0.1E1 Aperture 139, 236, 341, 348
52X0.2 Aperture 342
52X0.2D1 Aperture 343
52X0.2E1 Aperture 139, 236, 343, 348
52X0.2E2 Aperture 236, 343
52X0.2F1 Aperture 236, 270, 285, 348
52X0.5 Aperture 344
52X0.5D1 Aperture 345
52X0.5E1 Aperture 139, 236, 345
52X0.5E2 Aperture 236, 345
52X2 Aperture 346
52X2D1 Aperture 347
52X2E1 Aperture 139, 236, 347
52X2E2 Aperture 236, 347
6X0.2 Aperture 352

A

ACCUM mode 222, 223, 225, 226, 227
accuracy 473

Advanced Camera for Surveys (ACS) 65
annealing 131
aperture 337, **490**
 see also "filter" 387
 slit wheel 63, 178, 234, 270, 378, 493
auto-wavecalcs 233
available-but-unsupported apertures 490

B

background 96
bandpass 76, 93, 113, 120, 194, 273, 379, 389, 401
bars 277
 52X0.2F1 236, 270, 271
 coronagraphic mask 270, 273, 277
 fiducials 66, 187, 285
bias 127, 133, 169, 183, 222, 225, 482
 overscan 133, 134, 222, 225
binning 152, 238
breathing 392
bright object limits 154, 259
 imaging 461
 spectroscopic 383
buffer 29, 229
BUFFER-TIME 230

C

calibration
 exposures 232
 ground testing 478
 pipeline 465
 SMOV 478
calibration lamp 26, 28

- also see flat fields for krypton and deuterium 28, 35, 122, 123, 234, 235, 353, 368, 382, 471
 - calstis 465
 - CCD
 - ACCUM 222
 - bias 133
 - binning 223
 - charge transfer efficiency 134
 - cosmic rays 25, 30, 71, 113, 130, 131, 188, 232, 235, 246, 471
 - CR-SPLIT 235, 283, 284
 - CTE 117, 134
 - detector 25, 115
 - fringe flat fields 235
 - fringing 120
 - gain 90, 95, 96, 127, 129, 130, 222, 283, 405, 481
 - ghost images 124, 392
 - hot pixel 132, 169, 246
 - performance 116
 - plate scale 116, 125
 - saturation 127, 129
 - sensitivity 117
 - shutter 28, 130, 158, 169
 - spectral response 117
 - subarrays 224
 - CCDGAIN 127
 - charge transfer efficiency 134
 - checkbox 164
 - conventions
 - nomenclature 4
 - coronagraph
 - wedge 187
 - coronagraphic
 - imaging 273
 - observations 270
 - count rate
 - determination 88
 - global 112, 160
 - local 390
 - MAMA 20
 - cross-dispersers 233
 - cross-dispersion 280
 - cross-dispersion profiles 286
 - CR-SPLIT 235
 - CTE 117, 134
 - CVZ (Continuous Viewing Zone) 205, 207, 208, 210, 211, 264
- ## D
- D1 aperture positions 54, 337, 435
 - dark current 55, 65, 71, 95, 97, 108, 112, 113, **116**, 131, 139, **147**, 149, 150, 151, 283, 446
 - darks
 - daily dark 134
 - superdark 131, 134
 - Data Number (DN) 127, 133, 222
 - data storage 29
 - detector
 - background 96
 - CCD 25, 115
 - MAMA 25
 - detectors 25
 - CCD 115
 - parallel operation 216, 218, 223, 225, 378, 379
 - diffraction 274, 275, 378, 380, 382
 - diffuse acquisition 172
 - distortion 247, 475
 - dither 152, 232, 244, 246, 247, **262**
 - dithering 239, 262
 - Doppler Correction 229
 - drift rates 166, 203
 - dynamic-range 34
- ## E
- E1 aperture positions 53, 137, 237, 282, 337
 - E140H grating **331**, 332, 333, 351, 367, 372, 375, 376, 385
 - E140M grating 186, **328**, 329, 330, 349, 366, 371, 372, 376, 385
 - E2 aperture positions 53, 237, 337
 - E230H grating 56, 186, 206, **325**, 326, 327, 367, 385
 - E230M grating 186, **322**, 323, 324, 349, 366, 371, 372, 385
 - earthshine 97

echelle
 order overlap 375
 scattered light 375
 efficiency 18, 24
 encircled energy 88, 362, 391, 458
 Exposure Time Calculator (ETC) 34, 87
 exposure times 87
 extended source 106, 109, 172
 extinction 105, 111, 155, 383

F

fiducials 40, 285, 348
 field of view
 HST 29
 filter
 25MAMA 411, 438
 25MAMAD1 439
 50CCD 395
 50CORON 273, **407**
 F25CIII 431
 F25CN182 84, **434**
 F25CN270 83, **428**
 F25LYA 454
 F25MGII 425
 F25ND3 86, **412**
 F25ND5 414, **442**
 F25QTZ 79, 82, 412, 414, **419**, 420, **447**,
 460
 F25QTZD1 449
 F25SRF2 422, **452**
 F25SRF2D1 453
 F28X50LP 398
 F28X50OII 405
 F28X50OIII 402
 neutral density 35, 61, 86, 159, 176, 177,
 178, 198, 199, 260, 353, 491, 492

FITS
 data files 17, 465, 466, 467
 fixed-pattern 262, 264, 491, 493
 flat field
 krypton and deuterium 153, 237, 272
 flat field calibration 232
 focus 70, 478
 FP-SPLIT 262
 apertures 152, 218, 264, 265

fringe amplitudes 121
 fringe flat 53, 120, 205, 209, 235, 236, 237,
 238, 290, 293
 fringing 120, 235, 238, 271, 272, 471
 full well
 CCD saturation 25, 29, 129, 177, 216, 222
 FUV-MAMA 28, 51, 69, 71, 73, 78, 80, 81, 86,
 141, 142, 147, 149, 150, 152, 153, 316,
 319, 328, 331, 436, 440, 442, 446, 449,
 450, 453, 454, 483

G

G140L grating 52, 153, 210, 259, **316**, 317,
 318, 363, 370, 380, 385
 G140M grating 52, 110, 113, 153, **319**, 320,
 321, 363, 385
 G230L grating 48, 289, 302, 303, 304, 305,
 310, 311, 312, 313, 316, 363, 364, 370,
 385
 G230LB grating 48, 49, 123, 159, **302**
 G230M grating 48, 289, 306, 307, 308, 309,
 313, 314, 315, 363, 364, 385
 G230MB grating 48, 49, 123, 159, **306**
 G430L grating 123, 124, 244, 284, **296**, 297,
 298, 299, 365, 373, 374
 G430M grating 123, 210, **299**, 300, 301, 365
 G750L grating 123, 209, 218, 270, 272, **290**,
 291, 292, 296, 365, 374, 381, 471
 G750M grating 49, 51, 123, 218, 238, **293**, 294,
 295, 365
 geocoronal emission 82, 97, 102, 105, 255
 geometric distortion 457
 ghost image 125, 392
 GO wavecalcs 234
 grating wheel 27, 121
 ground testing 147, 382, 478
 guide stars 189

H

help desk 9, 10
 highres 228
 sampling 152, 263, 264, 266
 high-time-resolution 221, 229
 HITM 28

calibration 28, 169
hot pixels 131

I

imaging 63
 central wavelength 63
 coronagraphic 273
 filters 63
 FWHM 63
 limiting magnitudes 71
 overview 63
 red leak 80
 sensitivity limits 71
interstellar extinction 105

J

Jupiter 161, 162

L

light path 26
linearity
 also see non-linearity 111, 114, 140
line-spread function 88, 239, 265, 286, **368**
long-slit echelle 256
LOW-SKY 98
Lyman- α geocoronal 97

M

MAMA
 ACCUM 226
 bright object limits 154, 383, 461
 BUFFER-TIME 230
 dark current 55, 147
 detector 25
 highres 228
 non-linearity 152
 parallel observations 19
 performance 140
 plate scale 140
 read time 224
 saturation 147
 sensitivity 142
 spectral offset 153
 spectral response 142
 Time-Tag 229

mask

 also see coronagraph 270, 273, 275
 coronagraphic 381
memory 29, 74, 147, 222, 479
microchannel 141, 153, 154, 280
moving targets 266
MSM (mode selection mechanism) 28, 80, 207,
 210, 233

N

non-linearity
 MAMA 133, 152, 153, 259, 466
nonuniformity 129, 130, 153, 262
NUV-MAMA 28, 65, 69, 71, 72, 78, 79, 80, 81,
 117, **140**, 141, 142, 147, 149, 152, 302,
 305, 306, 309, 310, 313, 322, 325, 334,
 370, 409, 410, 412, 413, 414, 415, 418,
 421, 423, 424, 426, 427, 429, 432, 433,
 458, 459, 460

O

occultation 238
occulting 66, 187, 270
occulting bar
 see fiducial or coronagraph 236, 273
operating modes 221
optical design 26
orbits
 CCD/MAMA 19
 maximum number 18
orbit-time determination 201
ORIENT 18, 166, 248, 251, 272
orientation 20, 35, 217, 221, 229, 248, 255,
 268, 272, 275
 roll angle 493
overheads 36, 202
overillumination 139
overlight 159, 169

P

paper products 200
parallel observations 19, 29, 69, 248, 267
 CCD 74
 coordinated 216, 218
 pure 217, 268

pattern 71, 120, 127, 133, 152, 185, 200, 228,
 232, **239**, 242, 243, 244
 patterns 239
 generic
 LINE 240
 SPIRAL 240
 imaging
 STIS-CCD-BOX 240
 STIS-MAMA-BOX 240
 STIS-SPIRAL-DITH 240
 spectroscopic
 STIS-ALONG-SLIT 240
 STIS-PERP-TO-SLIT 240
 pickup 28, 183
 exposure time 188
 Phase I 201, 215
 preparation 8
 Phase II 217
 preparation 8
 photocathode 140, 142
 pipeline calibration 465
 planetary targets 175, **266**
 plate scales 284
 PLATE-ID 189, 190
 point source 28, 36, 74, 89, 90, 92, 108, 112,
 153, **171**, 236, 281, 285, 311, 317, 320,
 373, 378, 385, 389, 391
 point source acquisitions 171
 point spread function 45, 65, 69, 71, 73, 74, 75,
 79, 89, **124**, 141, **144**, 235, 244, 256,
 276, 286, 368, 373, 374, 382, 388, **391**,
 397, 403, 407, 420, 423, 431, 458, 459,
 460
 position angle 248
 POS-TARG 204
 precision 473
 prism 59, 61, 82, 218, **334**, 335, 336
 proposal
 observing sequence 31
 overheads 36, 163, 179, 188, **201**, 202, 203,
 211, 216, 228, 235
 parallel observations 29, 248
 Phase II 202
 pseudo-apertures 52, 337
 D1 apertures 54, 435

E1 CTE positions 53, 137, 237, 282
 E2 CTE positions 53, 237

Q

quantum efficiency (QE) 24, 25, 80, 116

R

read noise 35, 71, 74, 94, 95, 96, 97, 107, 108,
 109, 116, 127, 131, 147, 223, 246
 readout 127, 203, 222, 228
 red leak 48, 76, 83, 84, 177, 401, 423, 426
 reflection 125
 repeatability 233, 234, 467
 repeller wire 52, 71, 141, 145, 153, 226
 resolution 24, 31, 33, **40**, 45, 50, 57, 58, 66, 70,
 88, 90, 91, 106, 109, 145, 151, 152, 157,
 175, 176, 223, 226, 228, 229, 239, 247,
 254, 261, 262, 266, 296, 299, 302, 306,
 310, 313, 319, 374, 375, 404, 450, 483

S

SAA

see South Atlantic Anomaly 148

saturation 31, 34, 35, 46, 74, 76, 77, 83, 84, 85,
 127, 129, 179, 188, 222, 284

Saturn 161, 162

scattered light 373, 376, 404, 475

scheduling policies 19

sensitivity 281

time dependence 118, 143, 282, 468

units 281, 388

shadow 51, 71, 102, 153

signal-to-noise 26, 30, 31, 33, 34, 36, 73, 74,
 76, 77, 81, 84, 85, 87, 88, 94, 95, 96,
 106, 107, 109, 111, 112, 120, 130, 147,
 151, 152, 177, 179, 206, 207, 216, 218,
 223, 234, 235, 238, 255, 261, 264, **280**,
 283, 290, 293, 305, 309, **388**, 391, 476

determination 88

high 34, 218, 261

sky background 96, 103

slit

see aperture 337, **490**, **491**

slit wheel 27

slitless spectroscopy 253
 SMOV 478
 solar system targets 266
 solar-blind 3, 24, 25, 48, 78, 142, 266
 solar-system
 target acquisition 182
 South Atlantic Anomaly 19, 36
 spatial profiles 286, 362
 spectral purity 50, 58, 373
 spectroscopy 39
 echelle 56
 first-order 49
 gratings 39
 limiting magnitudes 45
 objective-prism 58
 overview 39
 sensitivity limits 45
 slitless 34, 40, 131, 218, 268, 269
 spatially resolved 23, 24, 310
 spectral range 39
 spectral resolution 39
 stability 26, 261, 474, 475, 478, 480
 STMAG system 283, 284, 287, 288, 292, 295,
 298, 301, 304, 308, 312, 315, 318, 321,
 324, 327, 330, 333
 STSDAS 78, 200, 245, 466
 supported apertures 490

T

target acquisition 19, 28, 35, 86, 88, **163**, 216,
 476, 478
 ACQ 177, 180, 358, 359
 centering 28, 51, 61, 164, 165, 166, 171,
 174, 175, 187, 188, 200, 216, 237,
 247, 474, 475
 checkbox 164, 171, 172, 173, 174, 176,
 177, 178, 193, 204, 207
 diffuse 172
 dwell point 211
 exposure time 177
 flux-weighted centroid 171, 172
 moving targets 182
 offset 175, 183
 peakdown 188
 pickup 183

 point 171
 target-of-opportunity 20, 216
 TAS (Target Acquisition Simulator) 164, 200
 tastis 200
 TDS 118, 143
 throughput
 spectroscopy 42
 tilt
 primary 47
 secondary 47
 see scan 27, 28, 29, 47, 153, 233, 244, 270,
 280, 290, 379, 382
 time-resolved observations 8, 34, 221, 224,
 239, 257, 258
 TIME-TAG 102, 229, 230, 258
 transmission 90, 374, 493
 Two-Gyro Mode 14

U

undersampling 244, 265
 user support
 help desk ii

W

wavecal 29, 31, 203, 204, 205, 207, 210, 212,
 216, 218, 233, 234, 466, 467, 474, 475
 automatic 203, 204, 207, 210
 zero-points 29, 35, 61, 203, 233, 387
 wavelength calibration 28, 232
 web pages 10

Z

zodiacal light 97, 98, 99, 390